Hashemite Kingdom of Jordan

Jordan Journal of Biological Sciences

An International Peer-Reviewed Scientific Journal

Financed by the Scientific Research and Innovation Support Fund

This title is indexed in Scopus

http://jjbs.hu.edu.jo/

المجلة الأردنية للعلوم الحياتية
Jordan Journal of Biological Sciences (JJBS)
http://jjbs.hu.edu.jo

Jordan Journal of Biological Sciences (JJBS) (ISSN: 1995–6673 (Print); 2307-7166 (Online)): An International Peer- Reviewed Open Access Research Journal financed by the Scientific Research and Innovation Support Fund, Ministry of Higher Education and Scientific Research, Jordan and published quarterly by the Deanship of Scientific Research , The Hashemite University, Jordan.

Editor-in-Chief
Professor Wedyan, Mohammed A.
Environmental Biochemistry,
The Hashemite University

Assistant Editor
Professor Muhannad, Massadeh I.
Microbial Biotechnology,
The Hashemite University

Editorial Board (Arranged alphabetically)

Professor Al-Eitan, Laith
Biotechnology and Genetic Engineering
Jordan University of Science and Technology

Professor Al-Khateeb , Wesam M.
Plant Genetics and Biotechnology
Yarmouk University

Professor Al-Ghzawi , Abdul Latief A.
Plant biotechnology
The Hashemite University

Professor Al-Najjar , Tariq Hasan Ahmad.
Marine Biology
The University of Jordan/ Aqaba

Professor Khleifat, Khaled M.
Microbiology and Biotechnology
Mutah University

Professor Odat , Nidal
Plant biodiversity
Al Balqa Applied University

Associate Editorial Board

Professor Al-Hindi, Adnan I.
Parasitology
The Islamic University of Gaza, Faculty of Health Sciences, Palestine

Dr Gammoh, Noor
Tumor Virology
Cancer Research UK Edinburgh Centre, University of Edinburgh, U.K.

Professor Kasparek, Max
Natural Sciences
Editor-in-Chief, Journal Zoology in the Middle East, Germany

Professor Krystufek, Boris
Conservation Biology
Slovenian Museum of Natural History, Slovenia

Dr Rabei, Sami H.
Plant Ecology and Taxonomy
Botany and Microbiology Department, Faculty of Science, Damietta University,Egypt

Professor Simerly, Calvin R.
Reproductive Biology
Department of Obstetrics/Gynecology and Reproductive Sciences, University of Pittsburgh, USA

Editorial Board Support Team

Language Editor
Professor Shadi Neimneh

Publishing Layout
Eng.Mohannad Oqdeh

Submission Address
Professor Wedyan, Mohammed A.
The Hashemite Universit y
P.O. Box 330127, Zarqa, 13115, Jordan
Phone: +962-5-3903333 ext.4147
E-Mail: jjbs@hu.edu.jo

المجلة الاردنية للعلوم الحياتية
Jordan Journal of Biological Sciences (JJBS)
http://jjbs.hu.edu.jo

International Advisory Board (Arranged alphabetically)

Professor Abdelaziz M. Hussein
Mansoura University, Egypt

Professor Abhik Gupta
School of Environmental Sciences, Assam University, India

Professor Adnan Bashir Al- lahham
German Jordanian University, Jordan

Professor Ahmed Deaf Allah Telfah
Leibniz-Institut für Analytische Wissenschaften- ,Germany

Professor Ahmed Amri
genetic resources ICARDA in Morocco, Morocco

Dr. Amalia A Tsiami
University of West London, London

Professor Amir Menwer Al-Hroob
Al-Hussein Bin Talal University, Jordan

Professor David Modry
Masaryk University, Science Department, Czech

Professor Elif Demirkan
Bursa Uludag University Turkey, Turkey

Professor Emad Hussein Malkawi
Yarmouk University, Jordan

Professor Erhan Nurettin ÜNLÜ
Turkey Dicle University,Turkey

Professor Gottfried Hartmut Richard Jetschke
Friedrich-Schiller-University of Jena, Germany

Professor Hassan Mohammed M. Abd El-Rahman Awad
National Research Centre, Egypt

Professor Ihsan Ali Mahasneh
Al al-Bayt University, Jordan

Professor Khalid M. Al-Batayneh
Yarmouk University, Jordan

Professor Khalid Majid Hameed
Dept. of Biological Sciences, Duke University, USA

Professor Laith Abd Jalil Jawad
School of Environmental and Animal Sciences, Unitec Institute of Technology Auckland ,New Zealand

Professor Maizirwan Bin Muhammad Mel
International Islamic University Malaysia, Malaysia

Professor Maroof A. Khalaf
Jordan University/ Aqaba , Jordan

Professor Mohamed Emara
Chartered Management Institute, UK

Professor Mohammed H. Abu-Dieyeh
Biological and Environmental Sciences, Qatar University, Qatar

Professor Nabil Joseph Awadalla Girgis
King Khalid University, Saudi Arabia

Professor Nour Shafik Emam El-Gendy
Egyptian Petroleum Research Institute, Egypt

Professor Olga Anne
Marine Technology and Natural Sciences of Klaipėda University, Lithuania

Professor Omar F. Khabour
Jordan University of Science and Technology, Jordan

Professor Roy Hendroko Setyobudi
University of Muhammadiyah, Indonesia

Professor Saleem Hmood Aladaileh
Al-Hussein Bin Talal University, Jordan

Dr. Salem M Akel
St, Jude's Children's Research Hospital, USA

Professor Walid Al Zyoud
German Jordanian University, Jordan

Professor Yacob Hassan Yacob
Al al-Bayt University, Jordan

Instructions to Authors

Scopes

Study areas include cell biology, genomics, microbiology, immunology, molecular biology, biochemistry, embryology, immunogenetics, cell and tissue culture, molecular ecology, genetic engineering and biological engineering, bioremediation and biodegradation, bioinformatics, biotechnology regulations, gene therapy, organismal biology, microbial and environmental biotechnology, marine sciences. The JJBS welcomes the submission of manuscript that meets the general criteria of significance and academic excellence. All articles published in JJBS are peer-reviewed. Papers will be published approximately one to two months after acceptance.

Type of Papers

The journal publishes high-quality original scientific papers, short communications, correspondence and case studies. Review articles are usually by invitation only. However, Review articles of current interest and high standard will be considered.

Submission of Manuscript

Manuscript, or the essence of their content, must be previously unpublished and should not be under simultaneous consideration by another journal. The authors should also declare if any similar work has been submitted to or published by another journal. They should also declare that it has not been submitted/ published elsewhere in the same form, in English or in any other language, without the written consent of the Publisher. The authors should also declare that the paper is the original work of the author(s) and not copied (in whole or in part) from any other work. All papers will be automatically checked for duplicate publication and plagiarism. If detected, appropriate action will be taken in accordance with International Ethical Guideline. By virtue of the submitted manuscript, the corresponding author acknowledges that all the co-authors have seen and approved the final version of the manuscript. The corresponding author should provide all co-authors with information regarding the manuscript, and obtain their approval before submitting any revisions. Electronic submission of manuscripts is strongly recommended, provided that the text, tables and figures are included in a single Microsoft Word file. Submit manuscript as e-mail attachment to the Editorial Office at: JJBS@hu.edu.jo. After submission, a manuscript number will be communicated to the corresponding author within 48 hours.

Peer-review Process

It is requested to submit, with the manuscript, the names, addresses and e-mail addresses of at least 4 potential reviewers. It is the sole right of the editor to decide whether or not the suggested reviewers to be used. The reviewers' comments will be sent to authors within 6-8 weeks after submission.
Manuscripts and figures for review will not be returned to authors whether the editorial decision is to accept, revise, or reject. All Case Reports and Short Communication must include at least one table and/ or one figure.

Preparation of Manuscript

The manuscript should be written in English with simple lay out. The text should be prepared in single column format. Bold face, italics, subscripts, superscripts etc. can be used. Pages should be numbered consecutively, beginning with the title page and continuing through the last page of typewritten material.

The text can be divided into numbered sections with brief headings. Starting from introduction with section 1. Subsections should be numbered (for example 2.1 (then 2.1.1, 2.1.2, 2.2, etc.), up to three levels. Manuscripts in general should be organized in the following manner:

Title Page

The title page should contain a brief title, correct first name, middle initial and family name of each author and name and address of the department(s) and institution(s) from where the research was carried out for each author. The title should be without any abbreviations and it should enlighten the contents of the paper. All affiliations should be provided with a lower-case superscript number just after the author's name and in front of the appropriate address.
The name of the corresponding author should be indicated along with telephone and fax numbers (with country and area code) along with full postal address and e-mail address.

Abstract

The abstract should be concise and informative. It should not exceed **350 words** in length for full manuscript and Review article and **150 words** in case of Case Report and/ or Short Communication. It should briefly describe the purpose of the work, techniques and methods used, major findings with important data and conclusions. No references should be cited in this part. Generally non-standard abbreviations should not be used, if necessary they should be clearly defined in the abstract, at first use.

Keywords

Immediately after the abstract, **about 4-8 keywords** should be given. Use of abbreviations should be avoided, only standard abbreviations, well known in the established area may be used, if appropriate. These keywords will be used for indexing.

Abbreviations

Non-standard abbreviations should be listed and full form of each abbreviation should be given in parentheses at first use in the text.

Introduction

Provide a factual background, clearly defined problem, proposed solution, a brief literature survey and the scope and justification of the work done.

Materials and Methods

Give adequate information to allow the experiment to be reproduced. Already published methods should be mentioned with references. Significant modifications of published methods and new methods should be described in detail. Capitalize trade names and include the manufacturer's name and address. Subheading should be used.

Results

Results should be clearly described in a concise manner. Results for different parameters should be described under subheadings or in separate paragraph. Results should be explained, but largely without referring to the literature. Table or figure numbers should be mentioned in parentheses for better understanding.

Discussion

The discussion should not repeat the results, but provide detailed interpretation of data. This should interpret the significance of the findings of the work. Citations should be given in support of the findings. The results and discussion part can also be described as separate, if appropriate. The Results and Discussion sections can include subheadings, and when appropriate, both sections can be combined

Conclusions

This should briefly state the major findings of the study.

Acknowledgment

A brief acknowledgment section may be given after the conclusion section just before the references. The acknowledgment of people who provided assistance in manuscript preparation, funding for research, etc. should be listed in this section.

Tables and Figures

Tables and figures should be presented as per their appearance in the text. It is suggested that the discussion about the tables and figures should appear in the text before the appearance of the respective tables and figures. No tables or figures should be given without discussion or reference inside the text.

Tables should be explanatory enough to be understandable without any text reference. Double spacing should be maintained throughout the table, including table headings and footnotes. Table headings should be placed above the table. Footnotes should be placed below the table with superscript lowercase letters. Each table should be on a separate page, numbered consecutively in Arabic numerals.

Each figure should have a caption. The caption should be concise and typed separately, not on the figure area. Figures should be self-explanatory. Information presented in the figure should not be repeated in the table. All symbols and abbreviations used in the illustrations should be defined clearly. Figure legends should be given below the figures.

References

References should be listed alphabetically at the end of the manuscript. Every reference referred in the text must be also present in the reference list and vice versa. In the text, a reference identified by means of an author's name should be followed by the year of publication in parentheses (e.g.(Brown,2009)). For two authors, both authors' names followed by the year of publication (e.g.(Nelson and Brown, 2007)). When there are more than two authors, only the first author's name followed by "*et al*." and the year of publication (e.g. (Abu-Elteen *et al*., 2010)). When two or more works of an author has been published during the same year, the reference should be identified by the letters "a", "b", "c", etc., placed after the year of publication. This should be followed both in the text and reference list. e.g., Hilly, (2002a, 2002b); Hilly, and Nelson, (2004). Articles in preparation or submitted for publication, unpublished observations, personal communications, etc. should not be included in the reference list but should only be mentioned in the article text (e.g., Shtyawy,A., University of Jordan, personal communication). Journal titles should be abbreviated according to the system adopted in Biological Abstract and Index Medicus, if not included in Biological Abstract or Index Medicus journal title should be given in full. The author is responsible for the sccuracy and completeness of the references and for their correct textual citation. Failure to do so may result in the paper being withdraw from the evaluation process. Example of correct reference form is given as follows:-

Reference to a journal publication:

Bloch BK. 2002. Econazole nitrate in the treatment of *Candida vaginitis*. *S Afr Med J.* , **58**:314-323.

Ogunseitan OA and Ndoye IL. 2006. Protein method for investigating mercuric reductase gene expression in aquatic environments. *Appl Environ Microbiol.*, **64**: 695-702.

Hilly MO, Adams MN and Nelson SC. 2009. Potential fly-ash utilization in agriculture. *Progress in Natural Sci.*, **19**: 1173-1186.

Reference to a book:

Brown WY and White SR.1985. **The Elements of Style**, third ed. MacMillan, New York.

Reference to a chapter in an edited book:

Mettam GR and Adams LB. 2010. How to prepare an electronic version of your article. In: Jones BS and Smith RZ (Eds.), **Introduction to the Electronic Age**. Kluwer Academic Publishers, Netherlands, pp. 281–304.

Conferences and Meetings:

Embabi NS. 1990. Environmental aspects of distribution of mangrove in the United Arab Emirates. Proceedings of the First ASWAS Conference. University of the United Arab Emirates. Al-Ain, United Arab Emirates.

Theses and Dissertations:

El-Labadi SN. 2002. Intestinal digenetic trematodes of some marine fishes from the Gulf of Aqaba. MSc dissertation, The Hashemite University, Zarqa, Jordan.

Nomenclature and Units

Internationally accepted rules and the international system of units (SI) should be used. If other units are mentioned, please give their equivalent in SI.

For biological nomenclature, the conventions of the *International Code of Botanical Nomenclature, the International Code of Nomenclature of Bacteria,* and the *International Code of Zoological Nomenclature* should be followed.

Scientific names of all biological creatures (crops, plants, insects, birds, mammals, etc.) should be mentioned in parentheses at first use of their English term.

Chemical nomenclature, as laid down in the *International Union of Pure and Applied Chemistry* and the official recommendations of the *IUPAC-IUB Combined Commission on Biochemical Nomenclature* should be followed. All biocides and other organic compounds must be identified by their Geneva names when first used in the text. Active ingredients of all formulations should be likewise identified.

Math formulae

All equations referred to in the text should be numbered serially at the right-hand side in parentheses. Meaning of all symbols should be given immediately after the equation at first use. Instead of root signs fractional powers should be used. Subscripts and superscripts should be presented clearly. Variables should be presented in italics. Greek letters and non-Roman symbols should be described in the margin at their first use.

To avoid any misunderstanding zero (0) and the letter O, and one (1) and the letter l should be clearly differentiated. For simple fractions use of the solidus (/) instead of a horizontal line is recommended. Levels of statistical significance such as: $^{*}P < 0.05$, $^{**}P < 0.01$ and $^{***}P < 0.001$ do not require any further explanation.

Copyright

Submission of a manuscript clearly indicates that: the study has not been published before or is not under consideration for publication elsewhere (except as an abstract or as part of a published lecture or academic thesis); its publication is permitted by all authors and after accepted for publication it will not be submitted for publication anywhere else, in English or in any other language, without the written approval of the copyright-holder. The journal may consider manuscripts that are translations of articles originally published in another language. In this case, the consent of the journal in which the article was originally published must be obtained and the fact that the article has already been published must be made clear on submission and stated in the abstract. It is compulsory for the authors to ensure that no material submitted as part of a manuscript infringes existing copyrights, or the rights of a third party.

Ethical Consent

All manuscripts reporting the results of experimental investigation involving human subjects should include a statement confirming that each subject or subject's guardian obtains an informed consent, after the approval of the experimental protocol by a local human ethics committee or IRB. When reporting experiments on animals, authors should indicate whether the institutional and national guide for the care and use of laboratory animals was followed.

Plagiarism

The JJBS hold no responsibility for plagiarism. If a published paper is found later to be extensively plagiarized and is found to be a duplicate or redundant publication, a note of retraction will be published, and copies of the correspondence will be sent to the authors' head of institute.

Galley Proofs

The Editorial Office will send proofs of the manuscript to the corresponding author as an e-mail attachment for final proof reading and it will be the responsibility of the corresponding author to return the galley proof materials appropriately corrected within the stipulated time. Authors will be asked to check any typographical or minor clerical errors in the manuscript at this stage. No other major alteration in the manuscript is allowed. After publication authors can freely access the full text of the article as well as can download and print the PDF file.

Publication Charges

There are no page charges for publication in Jordan Journal of Biological Sciences, except for color illustrations,

Reprints

Ten (10) reprints are provided to corresponding author free of charge within two weeks after the printed journal date. For orders of more reprints, a reprint order form and prices will be sent with article proofs, which should be returned directly to the Editor for processing.

Disclaimer

Articles, communication, or editorials published by JJBS represent the sole opinions of the authors. The publisher shoulders no responsibility or liability what so ever for the use or misuse of the information published by JJBS.

Indexing

JJBS is indexed and abstracted by:

DOAJ (Directory of Open Access Journals)	CABI
Google Scholar	EBSCO
Journal Seek	CAS (Chemical Abstract Service)
HINARI	ETH- Citations
Index Copernicus	Open J-Gat
NDL Japanese Periodicals Index	SCImago
SCIRUS	Clarivate Analytics (Zoological Abstract)
OAJSE	Scopus
ISC (Islamic World Science Citation Center)	AGORA (United Nation's FAO database)
Directory of Research Journal Indexing (DRJI)	SHERPA/RoMEO (UK)
Ulrich's	

المجلة الأردنية للعلوم الحياتية
Jordan Journal of Biological Sciences (JJBS)
ISSN 1995- 6673 (Print), 2307- 7166 (Online)
http://jjbs.hu.edu.jo

The Hashemite University

Deanship of Scientific Research

TRANSFER OF COPYRIGHT AGREEMENT

Journal publishers and authors share a common interest in the protection of copyright: authors principally because they want their creative works to be protected from plagiarism and other unlawful uses, publishers because they need to protect their work and investment in the production, marketing and distribution of the published version of the article. In order to do so effectively, publishers request a formal written transfer of copyright from the author(s) for each article published. Publishers and authors are also concerned that the integrity of the official record of publication of an article (once refereed and published) be maintained, and in order to protect that reference value and validation process, we ask that authors recognize that distribution (including through the Internet/WWW or other on-line means) of the authoritative version of the article as published is best administered by the Publisher.

To avoid any delay in the publication of your article, please read the terms of this agreement, sign in the space provided and return the complete form to us at the address below as quickly as possible.

Article entitled:----------

Corresponding author: ----------

To be published in the journal: Jordan Journal of Biological Sciences (JJBS)

I hereby assign to the Hashemite University the copyright in the manuscript identified above and any supplemental tables, illustrations or other information submitted therewith (the "article") in all forms and media (whether now known or hereafter developed), throughout the world, in all languages, for the full term of copyright and all extensions and renewals thereof, effective when and if the article is accepted for publication. This transfer includes the right to adapt the presentation of the article for use in conjunction with computer systems and programs, including reproduction or publication in machine-readable form and incorporation in electronic retrieval systems.
Authors retain or are hereby granted (without the need to obtain further permission) rights to use the article for traditional scholarship communications, for teaching, and for distribution within their institution.

☐ **I am the sole author of the manuscript**

☐ **I am signing on behalf of all co-authors of the manuscript**

☐ **The article is a 'work made for hire' and I am signing as an authorized representative of the employing company/institution**

Please mark one or more of the above boxes (as appropriate) and then sign and date the document in black ink.

Signed:_____ **Name printed:** _____
Title and Company (if employer representative) : _____
Date: _____

Data Protection: By submitting this form you are consenting that the personal information provided herein may be used by the Hashemite University and its affiliated institutions worldwide to contact you concerning the publishing of your article.

Please return the completed and signed original of this form by mail or fax, or a scanned copy of the signed original by e-mail, retaining a copy for your files, to:

Hashemite University
Jordan Journal of Biological Sciences
Zarqa 13115 Jordan
Fax: +962 5 3903338
Email: jjbs@hu.edu.jo

Editorial Preface

Jordan Journal of Biological Sciences (JJBS) is a refereed, quarterly international journal financed by the Scientific Research and Innovation Support Fund, Ministry of Higher Education and Scientific Research in cooperation with the Hashemite University, Jordan. JJBS celebrated its 12th commencement this past January, 2020. JJBS was founded in 2008 to create a peer-reviewed journal that publishes high-quality research articles, reviews and short communications on novel and innovative aspects of a wide variety of biological sciences such as cell biology, developmental biology, structural biology, microbiology, entomology, molecular biology, biochemistry, medical biotechnology, biodiversity, ecology, marine biology, plant and animal biology, plant and animal physiology, genomics and bioinformatics.

We have watched the growth and success of JJBS over the years. JJBS has published 14 volumes, 60 issues and 800 articles. JJBS has been indexed by SCOPUS, CABI's Full-Text Repository, EBSCO, Clarivate Analytics- Zoological Record and recently has been included in the UGC India approved journals. JJBS Cite Score has improved from 0.7 in 2019 to 1.4 in 2021 (Last updated on 6 March, 2022) and with Scimago Institution Ranking (SJR) 0.22 (Q3) in 2021.

A group of highly valuable scholars have agreed to serve on the editorial board and this places JJBS in a position of most authoritative on biological sciences. I am honored to have six eminent associate editors from various countries. I am also delighted with our group of international advisory board members coming from 15 countries worldwide for their continuous support of JJBS. With our editorial board's cumulative experience in various fields of biological sciences, this journal brings a substantial representation of biological sciences in different disciplines. Without the service and dedication of our editorial; associate editorial and international advisory board members, JJBS would have never existed.

In the coming year, we hope that JJBS will be indexed in Clarivate Analytics and MEDLINE (the U.S. National Library of Medicine database) and others. As you read throughout this volume of JJBS, I would like to remind you that the success of our journal depends on the number of quality articles submitted for review. Accordingly, I would like to request your participation and colleagues by submitting quality manuscripts for review. One of the great benefits we can provide to our prospective authors, regardless of acceptance of their manuscripts or not, is the feedback of our review process. JJBS provides authors with high quality, helpful reviews to improve their manuscripts.

Finally, JJBS would not have succeeded without the collaboration of authors and referees. Their work is greatly appreciated. Furthermore, my thanks are also extended to The Hashemite University and the Scientific Research and Innovation Support Fund, Ministry of Higher Education and Scientific Research for their continuous financial and administrative support to JJBS.

Professor Wedyan ,Mohammed A.
March, 2024

JJBS

Volume 17, Number 1, March 2024
ISSN 1995-6673

Jordan Journal of Biological Sciences

CONTENTS(no final)

Original Articles

© 2023 Jordan Journal of Biological Sciences. All rights reserved - Volume 16, Number 1

JJBS

Volume 17, Number 1,March 2024
ISSN 1995-6673
Pages 1 – 7
https://doi.org/10.54319/jjbs/170101

Jordan Journal of Biological Sciences

Data on heavy metals (Pb, Ni, Zn) in soil and biota (common nettle and Roman snail) around the power plant TC Kosova A in Obiliq (Kosovo)

Mentor Bici[1], Hazbije Sahiti[1], Muhamet Zogaj[2], Jeton Halili[3], Kemajl Bislimi[1,*]

[1]University of Prishtina "Hasan Prishtina", Faculty of Natural Sciences and Mathematics, Department of Biology, str. Nene Tereza, no. 5, 10000 Prishtine, Kosovo; [2]University of Prishtina "Hasan Prishtina", Faculty of Natural Sciences and Mathematics, Department of Chemistry, str. Nene Tereza, no. 5, 10000 Prishtine, Kosovo; [3]University of Prishtina, Faculty of Agriculture and Veterinary, St. "Bill Clinton" n.n. 10 000 Prishtinë, Kosovo.

Received: December 31, 2022; Revised: May 5, 2023; Accepted: June 16, 2023

Abstract

The heavy metal content of Pb, Zn, and Ni in soil, nettle plants (rhizomes, stems, and leaves), and snail shells was investigated in this study. Samples were collected during the summer-autumn period of 2020 from the vicinity of the TC Kosova A power plant in Obiliq (Prishtina), Kosovo, and compared to samples from the control site, Brezne-Opoja. Soil samples were dried at 105°C for 48 hours and treated with a mixture of 69% HNO3 and HClcc in a 1:3 ratio. Similarly, biota samples were dried at 105°C for 48 hours and treated with a mixture of 69% HNO3 and H2O2cc in a 1:3 ratio. All sample types were digested in the microwave at 200°C for 45 minutes and analyzed using a flame type absorber (Analyticyena Contra AAA).

The results indicate significantly higher concentrations of Pb, Ni, and Zn in the Obiliq area compared to Opoja, in both soil and biota (nettle and snail shells), suggesting potential environmental impact from the nearby coal-burning plant, heavy traffic, or other urban services. The average values generally fell below the limits specified by the UK (1989) or Germany (1992) standards (Directive 2008/50/EC). However, the Zn content in all soil samples exceeded the German standard. Pb and Zn were found to be extensively absorbed by nettle plants (U. dioica) and garden snails (H. pomatia), whereas Ni showed no significant bioaccumulation in either species, despite its high concentration in the soil. Nettle plants exhibited heavy bioaccumulation of Pb, reaching levels up to 105.6 mg/kg dw, surpassing the German standard limit. Nettle plants show promise in the phytoremediation and soil amendment processes for heavy metal pollution, particularly for Pb and Zn, but not for Ni. Garden snails can serve as bioindicators for assessing heavy metal pollution and its impact on transfer processes within the food chain, as well as the resulting effects on biochemical and physiological processes in living organisms, specifically in relation to oxidative stress. The contamination of soil and biota with heavy metals in the Obiliq area should be regarded as a significant concern. Therefore, regular monitoring of heavy metal content in agricultural, garden, livestock, and poultry activities is necessary to mitigate the associated health risks to humans.

Keywords: TC Kosova A, heavy metals, stinging nettle, snail, bioaccumulation

1. Introduction

The electricity sector in Kosovo heavily relies on coal-fired power plants, particularly Kosova A and Kosova B, which have been operational since 1983. Located in Kastriot (Obilić), just 13 km away from Prishtina, the capital of Kosovo, these power plants are known to be major sources of pollution in Europe, emitting significant amounts of particulate matter and sulphur dioxide. The nearby lignite mines in Bardh and Mirash villages supply the fuel for these plants. As the harmful effects of heavy metals (HM) as environmental pollutants become more apparent and present a growing concern for their presence in soil and their potential to penetrate the food chain, leading to bioaccumulation in plants, animals and ultimately to humans. Various human activities, including mining, traffic, and intensive agriculture, can contribute to the contamination of soil and air with particulate matter, especially during dry and windy weather conditions. The concentrations of heavy metals in the soil are influenced by factors such as the chemical properties of the soil and the distance from the contamination source. The amount of heavy metals absorbed by biota depends on the type and concentration of the metals, as well as the specific plant and animal species involved.

Nettle plants (*Urtica dioica L.)* and land snails (*Helix pomatia L.)* are examples of organisms that naturally accumulate heavy metals, particularly Pb, Zn, and Ni. In industrial areas and along urban settlements and roads, these metals tend to accumulate in snail shells and tissues. Nettle plants, characterized by their erect green stems and stinging hairs, are herbaceous perennials that grow up to 2 meters tall during the summer and die off in winter. They are commonly found in Kosovo, particularly in moist and nutrient-rich soils near human settlements. The young

* Corresponding author. e-mail: kemajl.bislimi@uni-pr.edu

shoots of nettle plants are traditionally valued for their medicinal properties and as a food source.

The Roman or garden snail, on the other hand, is a large land gastropod mollusk that prefers habitats with calcareous substrate, high humidity, lower temperatures, and soft soil for egg-laying and hibernation. Feeding primarily on fresh green plant parts, garden snails can live up to 8 years in controlled environments but have a shorter lifespan in the wild. Both nettle plants and garden snails are considered Least Concern species on the IUCN Red List, although habitat disturbance and unsustainable harvesting pose threats to their populations.

The Obiliq area, where the TC Kosova A power plant is located, has long been exposed to industrial operations, making it susceptible to heavy metal pollution. The landscape has been significantly altered due to open-cast mining activities, resulting in large dumps of overburden and solid wastes such as ash and sludge. These industrial activities contribute to high levels of dust, sulphur dioxide, and nitrogen oxides, with lead, cadmium, mercury, and arsenic being prevalent contaminants in the area.

In this study, we aim to investigate the impact and distribution of heavy metals (Pb, Zn, Ni) in soil, nettle plant parts (rhizomes, stems, and leaves), and snail shells collected around the TC Kosova A power plant in Obiliq, Kosovo. A comparison will be made with samples collected from Brezne-Opoja, serving as a control site. The goal is to provide an updated assessment of the environmental conditions in the vicinity of TC Kosova A, specifically focusing on heavy metal concentrations in the soil and their potential mobility to different parts of nettle plants and snail shells.

2. Materials and methods

Soil samples, as well as samples of common nettle (U. dioica) and Roman or garden snail (H. pomatia) (Fig. 3), were collected for the purpose of analyzing heavy metal concentrations, specifically Pb, Zn, and Ni. The sampling took place during the summer-autumn period of 2020 in two locations: around the TC Kosova A power plant in Obiliq, Kosovo, and in Brezne-Opoja, a mountainous plain in the south of Kosovo situated at an elevation of 1380 m above sea level, which is considered an unpolluted control site (Fig. 1).

The area surrounding TC Kosova A was divided into four geographical regions: northwest, northeast, southeast, and southwest, each encompassing imaginary circles at 1 km, 2 km, and 5 km radii. A total of 12 sampling stations were selected, with three stations in each region (Fig. 2 above). At each sampling site, 10 material samples were collected, including soil, nettle plants, and snails, resulting in a total of 120 samples. Additionally, in the control site of Brezne-Opoja, which was also divided into four geographical regions mirroring those in Obiliq (Fig. 2 below), 10 samples of soil, nettle plants, and snails were collected separately, amounting to 30 samples in total.

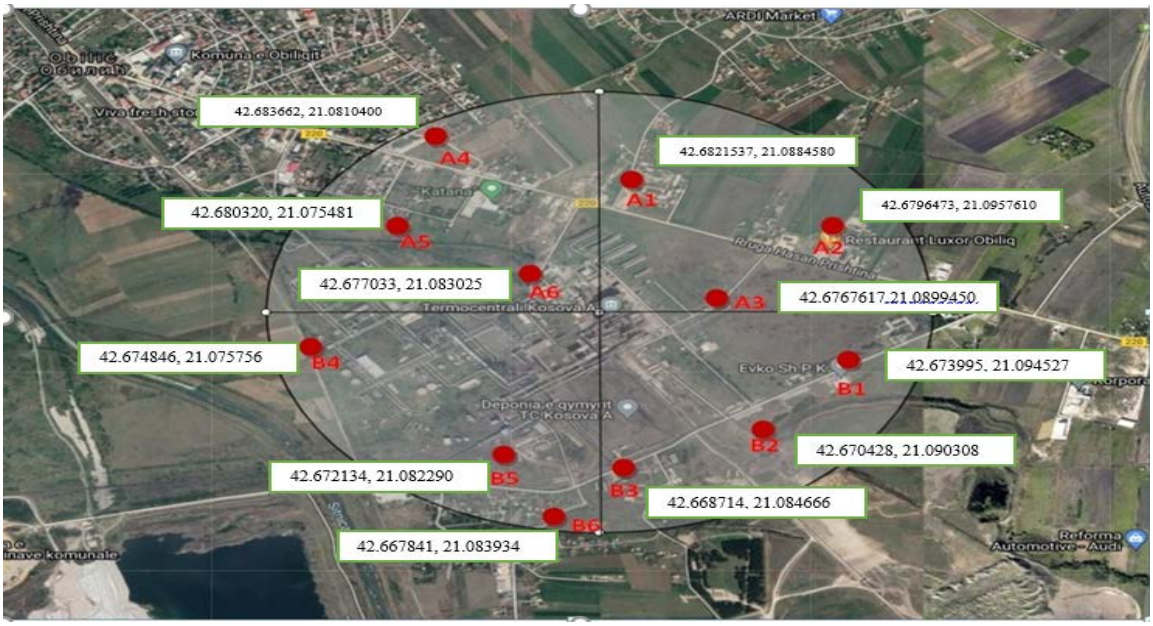

Figure 1.Kosovo map where the two sampling places are shown: TC Kosova A in Obiliq and Brezne-Opoja (control site) (elaborated in Google Earth 2015).

Figure 2. Schematic representation of the sample collection at locality TC Kosova A, Obiliq (above) and at the unpolluted locality Brezne-Opoja (below).

Figure 3. Photo of common nettle (U. dioica) from Obiliq: vegetative shoots and an individual of garden snail (H. pomatia) (white arrow) in it (© M. Bici).

Soil samples were collected manually using a hand probe at a depth of 15 cm from undisturbed areas, following the methods described by Kluge and Wessolek (2012) and ISO11466 (1995). The collected soil samples were then ground using a soil mill and placed in glass cups, after which they were dried in a thermostat at 105°C for 48 hours to eliminate moisture. A 0.3 g portion of the dried soil sample (based on dry weight) was subjected to treatment with a mixture of 69% HNO_3 and HClcc (Merck Millipore) in a 2:6 ratio, using Teflon columns. The samples were digested in a microwave instrument (Analyticyena TOPwave) at 200°C for 45 minutes. After filtration, the contents were transferred to 50 ml glass containers using distilled water. Analysis of metals Pb, Zn, and Ni was conducted using a flame type absorber (Analyticyena Contra AAA) with the application of Merck Millipore ICP multi-element standard solution 111355.

Samples of nettle plants and snails (4-6 years old) were collected from the same habitats. The vegetative parts of the nettle plants (rhizomes, stalks, and leaves) were separated and washed with distilled water. They were then dried at 105°C for 24-48 hours and ground using a Philips kitchen mixer. A 0.5 g portion of the sample was treated with ultra-pure nitric acid (HNO_3) of 69% purity and Lachner hydrogen peroxide (H_2O_2) of 30% purity in a 1:3 ratio. The samples were digested in a microwave instrument at 200°C for 45 minutes. After filtration, the contents were transferred to 50 ml glass containers and normalized with distilled water. Analysis of metals Pb, Zn, and Ni in the samples was performed using a flame absorber (Analyticyena Contra AAA).

Bioaccumulation factor (BCF) and transfer factor (TF) calculations were carried out to assess the movement of heavy metals from the soil to different plant parts (rhizomes, stems, and leaves), as well as from leaves to snail shells in the Obiliq area at distances of 1 km, 2 km, and 5 km. The BCF was determined using the formula: BCF = Cbiota / Csoil, where Cbiota represents the concentration of the metal in plant or animal tissues (dry weight) and Csoil represents the concentration of the metal in the soil (mg/kg dry weight). The TF within plant parts, such as from rhizomes to stems or leaves, and from leaves to snail shells, was calculated using the formulas: TF = Cshoot/leave / Crhizome and Cshells / Cleaves, respectively. Here, Cshoot, Cleave, Crhizome, and Cshells represent the concentrations of heavy metals in the plant shoot, leaves, rhizomes, and snail shells, respectively (Galal and Shehata, 2015).

The statistical analysis of the results was performed using Minitab® 19 software, including the Tukey-Kramer Test and ANOVA software for Excel.

3. Results

Table 2 presents the average concentrations of heavy metals (Pb in mg/kg, Ni in µg/kg, and Zn in mg/kg) reported as dry weight values for all sample types, including soil, nettle parts (rhizomes, stems, and leaves), the overall nettle plant, and snail shells collected from Obiliq and Opoja. The data is also visually represented in Figures 4 and 5. Due to the low levels of nickel observed in the vegetative organs, the concentration is reported in µg/kg for both nettle and shell samples in all cases.

Additionally, Table 2 provides information on the concentrations, bioaccumulation factors (BCFs), and transfer factors (TFs) of heavy metals from the soil to rhizomes, from rhizomes to stems and leaves, and from leaves to shells in the Obiliq area at distances of 1 km, 2 km, and 5 km.

Table 1. Average data of heavy metals (Pb, mg/kg, Ni, µg/kg, Zn, mg/kg), reported as dry weight values, in all sample types: soil, nettle parts (rhizomes, stems and leaves), overall nettle plant, and snail shells from Obiliq and Opoja.

HMs / Sample	Soil	SD	Rhizome	SD	Stem	SD	Leave	SD	Nettle	Snail	SD
Obiliq 1 km											
Pb, mg/kg	32.6	0.4	22.5	1.9	16.8	2.72	15.4	2.3	18.23	11.6	1.4
Ni, µg/kg	186.7	5.1	0.06	5.1	0.093	5.2	0.015	1.2	0.06	2.8	2.4
Zn, mg/kg	161.5	3.3	44.7	10.9	13.9	6.27	11.4	1.3	23.33	44.5	5.6
Obiliq 2 km											
Pb, mg/kg	77.3	1.3	17.7	6.65	10.8	2.48	12.7	2.2	13.73	11.1	1.38
Ni, µg/kg	214.9	0.4	0.065	0.95	0.084	4.1	0.017	1.3	0.06	1.58	2.5
Zn, mg/kg	230.8	13.2	25.3	12.3	16.1	9.15	6.6	1.1	16.00	40.7	4.3
Obiliq 5 km											
Pb, mg/kg	90.4	1.4	56.1	0.46	99.3	5.25	105.6	5.4	87.00	10.3	1.29
Ni, µg/kg	252.2	0.5	0.06	3.05	0.014	2.3	0.032	2.5	0.04	2.3	2.1
Zn, mg/kg	290.9	9.6	33.5	3.05	19.8	9.71	23.5	1.4	25.60	40.9	6.34
Obiliq area, overall average											
Pb, mg/kg	66.77	1.03	32.10	3.00	42.30	3.48	44.57	3.30	39.66	11.00	1.36
Ni, µg/kg	217.93	2.00	0.06	3.03	0.06	3.87	0.02	1.67	0.05	2.23	2.33
Zn, mg/kg	227.73	8.70	34.50	8.75	16.60	8.38	13.83	1.27	21.64	42.03	5.41
Opoja											
Pb, mg/kg	9.23	0.9	0.16	0.12	0.078	0.035	0.012	0.09	0.08	0.09	0.02
Ni, µg/kg	25.1	1.3	0.021	0.019	0.034	0.013	0.054	0.026	0.04	0.011	0.05
Zn, mg/kg	46.2	0.62	0.042	0.021	0.026	0.018	0.045	0.017	0.04	0.025	0.09

Table 2. Concentration, bioaccumulation factor (BCF), transfer factor (TF) of heavy metals from soil to rhizomes, from rhizomes to stems and leaves, and from leaves to shells in Obiliq (1 km, 2 km and 5 km).

Sample	C	BCF	TF	C	BCF	TF	C	BCF	TF
Obiliq 1 km				Obiliq 2 km			Obiliq 5 km		
Pb (mg/kg)									
Soil	32.6			90.3			77.4		
Rhizome	22.5	0.69		17.7	0.2		56.06	0.72	
Stem	16.8	0.52	0.75	10.8	0.12	0.61	99.25	1.28	1.77
Leaf	15.3	0.47	0.68	12.7	0.14	0.71	105.6	1.36	1.88
Shell	11.7	0.36	0.76	11.1	0.12	0.87	10.33	0.13	0.1
Zn (mg/kg)									
Soil	162			231			290.9		
Rhizome	44.7	0.28		25.3	0.82		33.51	0.12	
Stalk	14	0.08	0.31	16.1	0.07	0.64	19.84	0.07	0.59
Leaf	11.4	0.07	0.25	6.62	0.03	0.26	23.47	0.08	0.7
Shell	44.5	0.28	3.89	40.7	0.18	6.15	40.92	0.14	1.74
Ni (µg/kg)									
Soil	187			215			252.2		
Rhizome	0.08	0.04		0.06	0.03		0.05	0.02	
Stalk	0.09	0.05	0.01	0.08	0.04	0.01	0.014	0.05	0.03
Leaf	0.02	0.08	0.02	0.02	0.08	0.03	0.032	0.01	0.06
Shell	8.17	0.04	0.06	1.58	0.07	0.94	2.3	0.09	7.2

Significant differences were observed between the samples collected from Opoja (Op) and those from Obiliq ($p<0.001$; $n=10$) as depicted in Figures 4 and 5. Table 1 and Figures 3a, c, and e demonstrate that the heavy metal (HM) content in the soil was generally higher compared to the biota. Nettle plants showed a greater affinity for absorbing Pb compared to Ni or Zn. On the other hand, the garden snail exhibited a higher bioaccumulation of Ni and Zn in its shell than Pb (Figures 4b, d, and f). Notably, higher HM values were recorded at a distance of 5 km, followed by lower values at 2 km, and the lowest values at 1 km in the Obiliq area. While the HM content in the soil increased with the distance from TC Kosova A, this trend was not consistently observed in plant and shell samples. For instance, Ni content in plant vegetative organs and shell did not show a similar increase with distance (Figure 5).

Overall, the concentrations of HMs in both soil and biota were generally below the limits set by the UK (1989) and Germany (1992) standards (Directive 2008/50/EC).

However, the average Zn content in the soil samples from Obiliq at 2 km , 5 km , and Obiliq itself exceeded the German standard (highlighted in red in Table 1). Lead, which is bioaccumulated in nettle plants up to 105.6 mg/kg dry weight, surpassed the limit set by the German standard. Furthermore, when compared to the control site in Opoja, both soil and biota samples consistently exhibited higher HM content (Table 1), indicating pollution in the area, possibly resulting from the coal-burning plant, heavy traffic, or other urban activities.

The relatively high content of Pb absorbed by nettles raises concerns for animal health, particularly for grazing animals and human consumption. The young shoots of nettle plants are traditionally harvested and used in various food preparations, such as 'burek,' 'lakror,' or ' pispilit.' Additionally, nettle leaves are commonly traded as medicinal plants. Similar considerations apply to garden snails, as their preferential bioaccumulation of Ni and Zn can have detrimental effects on other biota higher up in the food chain (e.g., birds and mammals) as well as on human health. Garden snails are often harvested and consumed as food, and they are also traded in the pharmaceutical and cosmetic industries.

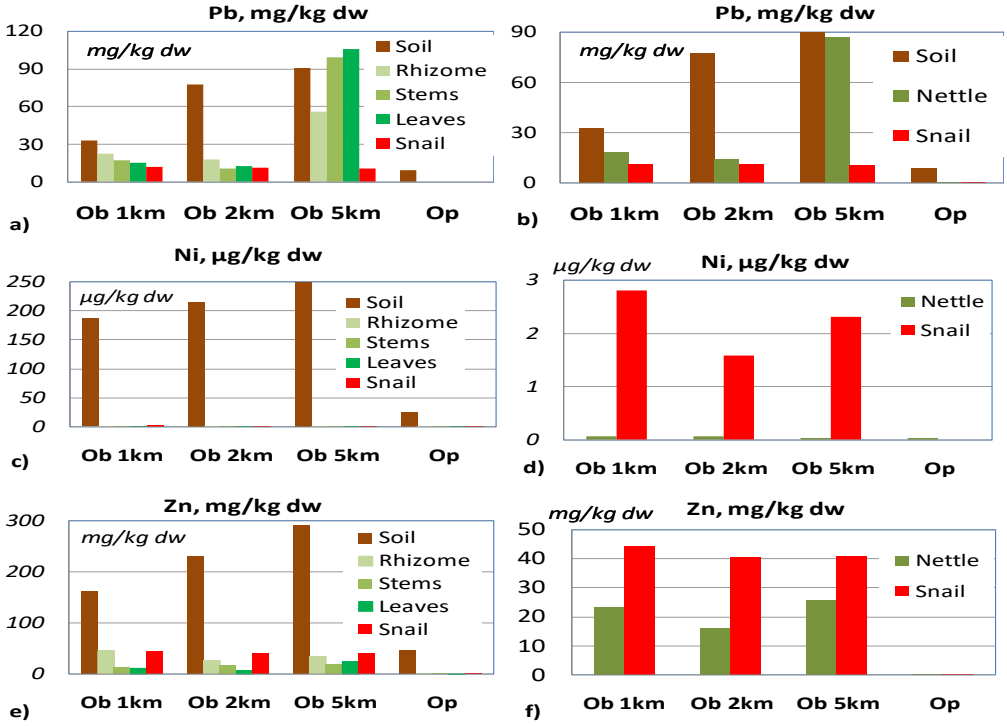

Figure 4. Average content of heavy metals considering the distance from TC Kosova A (1 km, 2 km dhe 5 km) and Opoja, in all sample types (soil, rhizomes, stems, leaves, snail shells) (a, c, e), and in soil, whole plant (nettle) and snail shells (b), and only nettle and snail (d, f). Ob, Obiliq; Op, Opoja.

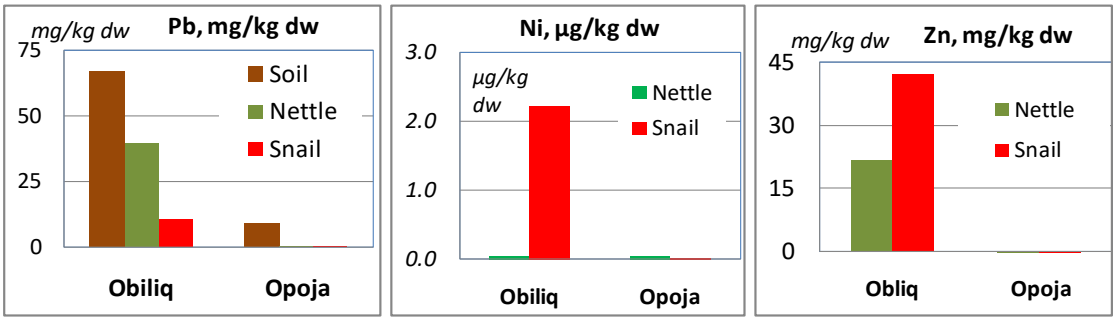

Figure 5. Average content of heavy metals in Obiliq and Opoja; for Pb in soil, whole plant (nettle) and snail shells; and for Ni and Zn in nettle plant and snail shells.

4. Discussion

The overall contamination of h eavy metals (HMs) in Obiliq poses a serious threat not only to the indicated species but also to other biota, plants, animals, and human life itself. Similar to the nettle and snail, other plants and animals living in the area, including cultivated vegetables, crops, fruit orchards, and livestock and their products, may be affected. Bislimi et al. (2013) reported data on hemocyanin (Hc) and transaminase activity (AST and ALT) in garden snails (H. pomatia) from the Obiliq Power Plant area. Bislimi et al. (2021) provided data on heavy metal concentrations (Pb, Ni, Cd, Cu, Fe) in soils and plants (U. dioica) around the Kishnica mineral deposit. Additionally, Çarkaj et al. (2022) reported data on heavy metals (Pb, Zn, Cu, Cd) in garden snails collected around the Trepça smelter and Vernica village (control area) in

Mitrovica. Demaku et al. (2022) presented data on heavy metals (Pb, Fe, Cd, Zn, Ni, Al, Cu, Mn, Cr) in water, sediment, and soil around the Sitnica River, which flows through the Kosovo A landfill, during April, July, and October of 2018. According to their findings, the order of HMs in almost all soil samples was Pb > Fe > Ni > Cd > Mn > Al > Cu > Zn and > Cr, which is consistent with our results from soil samples in Obiliq: Pb 0.7 mg/kg > Ni 0.17 mg/kg > Zn 0.25 mg/kg.

The relatively high nickel content in Obiliq, particularly at a distance of 5 km in the southern area, indicates the polluted state of the zone. The source of nickel, lead, and zinc is likely the power plants, resulting from the combustion of lignite and substandard oil during turbine ignition for energy production, as well as from industrial and municipal waste. Factors such as ash dumps, wind rosettes, and heavy coal-carrying vehicles likely contribute to their distribution in the southwest part of the area. The Pb content in soil samples at 1 km was 38.5 mg/kg in the southern part and 26.8 mg/kg in the northern part. The Ni content was 162.2 µg/kg in the northern part and 211.2 µg/kg in the southern part, while the Zn content was 151 mg/kg in the northern part and 179.9 mg/kg in the southern part. At a distance of 2 km, the soil content was: Pb 35.4 mg/kg in the northern samples and 52.9 mg/kg in the southern part; Ni was 213.5 µg/kg in the north and 216.3 µg/kg in the south; Zn was 162.3 mg/kg in the north and 188.1 mg/kg in the southern samples. At a distance of 5 km, the respective average values were: Pb 58.6 mg/kg, Ni 215 µg/kg, Zn 218.3 mg/kg in the north soil samples, whereas Pb 96.3 mg/kg, Ni 288.7 µg/kg, Zn 280.1 mg/kg in the south soil samples in the polluted area (Table 1).

These findings align with the fact that nickel is a widely dispersed transition element present in the environment, including air, water, and soil. It can originate from both anthropogenic activities and natural sources (Genchi et al., 2020). Altıkulaç et al. (2022) confirmed that the concentrations of Ti, V, Cr, Mn, Fe, Cu, Zn, As, Sr, Hg, and Pb in fly ash are higher compared to those in slag. Furthermore, highly toxic heavy metals such as As and Hg are significantly enriched in coal compared to the average Earth's crust. Some heavy metals may leach from ash and slag heaps, contaminating agricultural areas, soil, surface water, and groundwater.

Table 2 displays the bioaccumulation values of heavy metals from soil to plants or animals. In some cases, such as different parts of the nettle plant (rhizomes, stems, leaves) and shells, the bioconcentration factor (BCF) for Pb and Zn is <1, indicating biomagnification along the food chain. These results are consistent with those of other studies (Nica et al., 2012; Salih et al., 2021). In other cases, BCF is close to 1, while very low translocation values were recorded for Ni.

The concentration of heavy metals in soil and plant species is influenced by various factors such as bioavailability, cation exchange capacity, pH, vegetation season, climatic conditions, age, and nutrition of animals like snails, mammals, and humans (Gardiner et al., 1995). Our data challenges the claim by Bislimi et al. (2013) that snails (H. pomatia) are super bioindicators of environmental degradation due to their sensitivity to heavy metals and other pollutants. Çarkaj et al. (2022) also emphasizes that garden snails can accumulate relatively high concentrations of heavy metals and survive, making them a good model for biomonitoring heavy metals in the environment.

The mining industry, including soil, groundwater, and air pollution, is often responsible for ecological and environmental problems (Zhang et al., 2019). Heavy metal contamination has become a significant environmental issue in mining regions, affecting the quality of agricultural goods and ultimately impacting human health. Therefore, soil and water-related environmental challenges play a crucial role in agriculture (Linhua and Songbao, 2019). HMs, such as Cd, Pb, Ni, and Cr, may have long-term effects on human health through the consumption of apple fruit and other plants, with the possibility of these elements entering the food chain (Imeri et al., 2019). Pb and Zn frequently exceed the maximum permissible limits set by various countries and are responsible for most of the potential ecological impact in the studied sites (98.64%) (Yahya et al., 2021).

Pb, Cd, and Ni are examples of non-essential elements that tend to accumulate in vegetative parts and biomagnify from roots to stems and leaves with translocation factor values >1 (Bislimi et al., 2021). Furthermore, their potential bioavailability in products near contaminated soils is found to be extremely high (Zogaj et al., 2014). The nettle plant (U. dioica) has been shown to bioaccumulate and translocate heavy metals, making it a potential candidate for phytoremediation and soil amendment processes, particularly for Pb (Bislimi et al., 2021). Heavy metals, particularly Pb, Zn, and Ni, bioaccumulate in the shells and tissues of snails, and this bioaccumulation is more common in industrial areas and along urban highways (Salih et al., 2021). To fully understand the human risks associated with heavy metal pollution, further research is needed on other plant species (cereals, fruits, vegetables), different locations, and routes of metal exposure, such as the consumption of animal foods (meat, milk, eggs), drinking water, or air contact (Filimon et al., 2021).

Our results demonstrate that the heavy metal content (Pb, Ni, and Zn) in the Obiliq area is significantly higher compared to Opoja, both in soil and biota (nettle and snail shells), indicating the environmental impact likely from coal-burning plants, heavy traffic, or other urban services. While the average values generally fall below the limits set by standards like those of the UK (1989) or Germany (1992) (Directive 2008/50/EC), Zn content in all soil samples exceeds the German standard, and Pb is heavily absorbed by nettle from the soil, with concentrations as high as 105.6 mg/kg dw in its leaves, surpassing the limit of the German standard.

5. Conclusions

The observed soil pollution by heavy metals (HMs) in Obiliq is likely attributed to the emissions from the chimneys of the Kosovo A power plant, as well as the dispersion of ash and its widespread distribution across the area. The presence of wind rosettes contributes to a higher dispersion in the southern part compared to the northern part.

Pb and Zn show a higher affinity for uptake by both the nettle plant (U. dioica) and the garden snail (H. pomatia), whereas Ni does not exhibit significant bioaccumulation in either species despite its high concentration in the soil. The

nettle plant shows potential for effective phytoremediation and soil amendment processes to address heavy metal pollution, particularly for Pb and Zn, but not for Ni. The garden snail can serve as a valuable bioindicator for assessing heavy metal pollution and its impact on transfer processes within the food chain, as well as its effects on the biochemical and physiological processes of living organisms.

The contamination of soil and biota with HMs in the Obiliq area is a matter of serious concern. It is crucial to regularly monitor the HM content in agricultural, garden, livestock, and poultry products from this region to prevent potential risks to human health.

6. References

Altıkulaç A, Turhan S, Kurnaz A, Gören E, Duran C, Hançerlioğulları A and Uğur FA. 2022. Assessment of the Enrichment of Heavy Metals in Coal and Its Combustion Residues. *ACS omega*, **7(24):** 21239-21245.

AnimalBase. 2009. Species summary for *Helix pomatia*. AnimalBase, last modified 5 March 2009, accessed 6 September 2010.

Bislimi K, Behluli A, Halili J, Mazreku I and Halili F. 2013. Impact of pollution from Kosova's power plant in Obiliqon some biochemical parameters of the local populationof garden snail (*Helix pomatia* L.). *Resour Environ*, **3(2): 15-19.** DOI: 10.5923/j.re.20130302.01

Bislimi K, Halili J, Sahiti H, Bici M and Mazreku I. 2021. Effect of mining activity in accumulation of heavy metals in soil and plant (*Urtica dioica* L). *J. Ecol. Eng.*, **22(1): 1–7.** DOI: https://doi.org/10.12911/22998993/128691

Bislimi K, Halili J, Sahiti H, Bici M and Mazreku I. 2021. Effect of mining activity in accumulation of heavy metals in soil and plant (*Urtica dioica* L)., *J. Ecol. Eng,* **22(1): 1–7.**

Çarkaj L, Selimi Q, Ismaili M and Milaimi AP. 2022. Roman Snail (*Helix pomatia* L.) as bioindicator of heavy metals pollution in Mitrovica town, Kosovo. *Ecol. Engineering & Environ. Technology,* **23(3): 64-71.**

https://doi.org/10.12912/27197050/147149

Demaku S, Kastrati G and Halili J, 2022. Contamination with heavy metals of water, sediment and soil around Kosovo power plants. *Environ. Protection Engineering,* **48/2: 15-27.** DOI: 10.37190/epe220202

Directive 008/50/EC of the European Parliament and of the Council of 21 May 2008 on ambient air quality and cleaner air for Europe.

Galal TM and Shehata HS. 2015. Bioaccumulation and translocation of heavy metals by *Plantago major* L. grown in contaminated soils under the effect of traffic pollution. *Ecol. Ind.*, **48: 244–251.**

Gardiner DT, Miller RW, Badamchian B, Azzari AS and Sisson DR. 1995. Effects of repeated sewage sludge applications on plant accumulation of heavy metals. *Agri. Ecos & Environ,* **55(1): 1–6.**

Genchi G, Carocci A, Lauria G, Sinicropi MS and Catalano A. 2020. Nickel: Human health and environmental toxicology. *Int. J. Environ. Res. Public Health,* **17(3): 679.**

https://doi.org/10.3390/ijerph17030679.

Imeri R, Kullaj E, Duhani E and, Millaku L. 2019. Impact of rootstock on heavy metal bioaccumulation in apple plant grown near an industrial source in Obiliq, Kosovo. *Agronomy Research*, **17(1): 100–110.** https://doi.org/10.15159/AR.19.012

IQAir. 2019. Tiny Kosovo is one of Europe's big polluters. *IQAir Staff Writers*. Last updated Sep 3, 2019. https://www.iqair.com/newsroom/tiny-kosovo-is-one-of-europe-s-big-polluters .

ISO 11466:1995. Soil quality — Extraction of trace elements soluble in aqua regia. https://www.iso.org/standard/19418.html .

Jolly YN, Islam A and Akbar S. 2013. Transfer of metals from soil to vegetables and possible health risk assessment. *SpringerPlus* **2, 385.**

https://doi.org/10.1186/2193-1801-2-385 .

Kluge B and Wessolek G. 2012. Heavy metal pattern and solute concentration in soils along the oldest highway of the world–the AVUS Autobahn. *Environ. Monit. and Assessment*, **184: 6469-6481.**

Linhua S and Songbao F. 2019. Heavy metals in the surface soil around a coalmine: pollution assessment and source identification. *Polish J. of Environ. Studies*, **28(4): 2717-2724.**

Maiz-Tome L. 2016. *Urtica dioica*. **The IUCN Red List of Threatened Species** 2016: e.T167815A78457212. https://dx.doi.org/10.2305/IUCN.UK.2016-1.RLTS.T167815A78457212 en. Accessed on 17 April 2023.

MolluscaBase eds. 2021. **MolluscaBase.** *Helix pomatia* Linnaeus, 1758. Accessed through: World Register of Marine Species at: http://marinespecies.org/aphia.php?p=taxdetails&id=1050286 on 2021-02-19

Nica DV, Bura M, Gergen I, Harmanescu M and Bordean D-M. 2012. Bioaccumulative and conchological assessment of heavy metal transfer in a soil-plant-snail food chain. *Chemistry Central Journal*, **6(1): 1–15.**

Olayinka KO, Aderonke O and Fausat OB. (2011). Uptake of potentially toxic metals by vegetable plants grown on contaminated soil and their potential bioavailability using sequential extraction. *Journal of Soil Science and Environ. Management*, **2: 220-227.**

Reilly C. 2002. Metal contamination of Food. Its Significance for Food Quality and Human Health. **Blackwell Science Ltd, Oxford, UK, 288 pp.**

Rizaj M, Beqiri E, McBow I, O'Brien EZ and Kongoli F. 2008. The mineral base and productive capacities of metals and non-metals of Kosovo. *JOM*, **60: 18-22.**

Salih AHSH, Hama AA, Hawrami KAM and Ditta A. 2021. The Land Snail, *Eobania vermiculata*, as a bioindicator of the heavy metal pollution in the urban areas of Sulaimani, Iraq. *Sustainability*, **13(24): 13719.**

SOT. 2018. Hithra "mbretëresha" e mjekësisë popullore, përdoret si kurues dhe si agjent kozmetik. From ***SOT.COM.AL***, in 28 August 2018.

WB, 2014. **Electrical energy in Kosovo**. Projekti Energjetik i Kosovës (PDF). World Bank. Retrieved 2 March 2014. https://en.wikipedia.org/wiki/Electrical_energy_in_Kosovo#cite_ref-2 .

Yahaya SM, Abubakar F and Abdu N. 2021. Ecological risk assessment of heavy metal-contaminated soils of selected villages in Zamfara State, Nigeria. *SN Applied Sciences*, **3: 1-13.**

Young J. 2016. **Why Kosovo needs climate friendly energy alternatives**. https://rs.boell.org/en/2016/08/11/why-kosovo-needs-climate-friendly-energy-alternatives.

Zhang H-J, Zhao K-L, Ye Z-Q, Xu B, Zhao W-M, Gu X-B and Zhang H-F. 2018. Spatial variation of heavy metals in soils and its ecological risk evaluation in a typical Caryacathayensis production area. *Huan Jing KeXue* **39(6): 2893–2903.**

Zogaj M, Pacarizi M and Duering RA. 2014. Spatial distribution of heavy metals and assessment of their bioavailability in agricultural soils of Kosovo. *Carpathian J. of Earth and Environ. Sciences,* **9(1): 221-230.**

JJBS

Volume 17, Number 1,March 2024
ISSN 1995-6673
Pages 9 – 19
https://doi.org/10.54319/jjbs/170102

Jordan Journal of Biological Sciences

Comparative Profiling of Volatile Compositions of Fresh and Dehydrated Rinds and Leaves of Different Indian *Citrus* Species

Susmita Das[1,*], Rinku Saha[2], Moumita Biswas[1], Sritopa Mondal[2], Gargi Mahapatra[2]

[1]*Phytochemistry and Pharmacognosy Research Laboratory, Department of Botany, University of Calcutta, 35, Ballygunge Circular Road, Kolkata - 700 019, West Bengal, India;* [2]*Lady Brabourne College, Beniapukur, Kolkata, West Bengal, 700017*

Received: February 4, 2023; Revised: May 20, 2023; Accepted: June 16, 2023

Abstract

Citrus is an essentially important fruit that grows in diverse parts of the world. India is one of the chief producers of *Citrus* species. The most important varieties cultivated in West Bengal, India are: Paati, Gondhoraaj, Kaghchi, Batapi, Rangpur, Kamala and Musambi. This research aimed at profiling the volatile organic compositions of the essential oils (EOs) of a few popularly cultivated *Citrus* sps, isolated, in their fresh and dehydrated conditions, both from leaves as well as from fruit rinds. GC-MS (Gas Chromatography - Mass Spectrometry) analyzed a total of 78 metabolites belonging to different classes. This study has established a comprehensive volatile profile of *Citrus* species. The essential oils (EOs) isolated using hydro-distillation method from the discarded rinds and leaves can be used as a potential source of aroma and flavour compounds for the emerging nutritional market. The PLS-DA (Partial Least Squares – Discriminant Analysis) and HCA (Hierarchical Cluster Analysis) showed distinct clusters for dehydrated and fresh rind and leaf samples of all the studied species.

Keywords: volatile organic compounds, fruit rind, GC-MS, PLS-DA, HCA

1. Introduction

Among the different horticultural fruit crops, Lemon (*Citrus* sp.) is one of the chief fruit crops cultivated around the globe, with universal agricultural produce exceeding 80 million tons / year (Marin et al., 2007), and is the largest genus belonging to the family Rutaceae with approximately 70 species (Mahato et al., 2020). The *Citrus* sps and varieties are a prospective source of essential oils worldwide, utilised in flavour industries of alcoholic and non-alcoholic beverages, confectionaries, cookies, desserts and also in perfumery, cosmeceutical and nutraceutical industries. In the pharmaceutical industry, the volatile essential components play a major role in masking the disagreeable bitter tastes of medicines (Steuer et al., 2001; Nguyen et al. 2009). EOs may improve the olfactory properties viz., flavour, odour and colour when added to food substances (Maroid, 2016). The rinds (flavedo) of the fruits contain oil glands that contain essential oil fractions composed of several important volatile and semi-volatile compounds (Dugo and Mondello, 2011; Tranchida et al., 2012; Sarrou et al., 2013). The *Citrus* essential oils are mostly obtained from the flavedo or fruit rinds, but flowers and foliages are also exploited. The most studied *Citrus* EO compositions from rinds, leaves and flowers of *Citrus* sp. comprise *C.* x *sinensis* (L.) Osb. (Sweet orange), *C. reticulata* Bl. (Mandarin), *C. paradise* Macfad. (Grapefruit), *C. grandis* (L.) Osb. (*C. maxima* Burm. pummelo), *C. limon* (L.) Burm.f. (Lemon), *C. medica* L. (Citron), *C.* x *aurantifolia* (Christm.) Swingle (Lime), *C. aurantium* (Bitter orange), *C. bergamia* Rissoet Poit. (Bergamot orange) and *C. junos* Sieb. ex. Tanaka (yuzu) (Gonzalez-Mas et al., 2019).

The different species of *Citrus* fruits are cheaply available throughout India and they are very popular fruits because of the economical source of nutritive juices, rich in vitamins and minerals. After consumption of the edible parts of *Citrus* fruits, the fruit rinds are discarded as waste. The discarded rinds could be a source of essential oils needed for various industrial purposes. Massive amounts of *Citrus* waste, especially rinds, are generated internationally, and these are an ecological menace in several areas of the globe. Moreover, essential oils present in the rinds of oranges are fatal to yeasts (Murdock and Allen, 1960) and deter the progress of yeasts, molds and bacterial growth (Subba et al., 1967). Various studies have shown that incorporating *Citrus* rinds as powder or as EOs into food products may enhance the food's quality without negatively affecting the sensory attributes when added at the right amount (Ademosun, 2022). So, it is noteworthy to use *Citrus* wastes scientifically in food-nutrients industries and other areas (Tripodo et al., 2004; De Gregorio et al., 2002; Lo Curto et al., 1992).

The EOs present in oil glands are found at diverse layers in the rinds and cuticles of *Citrus* fruits and leaves. The EOs are released when oil glands are squashed, smashed or broken. These essential oils are used for flavouring ingredients in drinks, ice creams and other food products, also used in the preparation of toilet soaps, perfumes, cosmetics and other home and health care products (Raeissi et al., 2008).

Some plants' essential oils (EOs) are ranked among the most bioactive EOs in the world (Gherairia et al., 2022) and *Citrus* EOs are very common around the world. The

* Corresponding author. e-mail: susouravipar@gmail.com.

isolation of EOs from *Citrus* vegetal materials (rinds and leaves) is based on h ydro-distillation principally in Clevenger-type hydro-distillation (Asikin et al., 2015; Fancello et al., 2016, Ben Hsouna et al., 2017). So for this purpose, fresh lemon rinds are used to obtain essential oils which possess the characteristic aroma and flavour (Fierascu et al., 2019). Many researchers have deciphered the volatile profile of e ssential oil from the lemon rinds, but information on the comparison of fresh and dehydrated rinds as well as their leaves of the studied *Citrus* samples is not yet reported.

Recently, the idea of valorization of agro-industrial bio-wastes following the recently developed extraction processes has been increasingly applied as an emerging tool to manage and recover value-added products (Zema, Calabro et al., 2018) including *Citrus* rinds and pulps (Zema, Folino et al., 2018; Forney and Song, 2017; Zhang et al., 2019). *Citrus* rinds and leaves are under-exploited owing to the availability of scant information for i ts recycling and valorization. These products deserve to be reconnoitred as a promising and valuable source of aroma and flavour compounds significant for t he flavour and fragrance, nutraceutical, cosmeceutical and functional food industries. So, the focus of t his study was to detect and quantify the volatile profiles of a few popularly cultivated species of *Citrus* from the essential oils (EOs) of t heir rinds and leaves using the hydro-distillation method under fresh and dehydrated conditions in order to compare the yield and their essential oil compositions. From this study, enough information could be assimilated about the chemical variability of the rinds and leaves of these *Citrus* species of West Bengal, India.

2. 2. Materials and Methods

2.1. Collection of samples and preparation

Healthy fully mature ripened fruits of 2. 5 to 3 kilograms each of the seven different species of *Citrus* (Fig.1) were used in the current study: *Citrus* x *aurantifolia* (Christm.) Swingle (Paati), *Citrus medica* L. (Bir-jara / Kaghchi), *Citrus* x *sinensis* (L.) Osbeck cv. *Mosambi* [Godhadi type (thick skinned)], *Citrus reticulata* Blanco (Darjeeling Mandarin), *Citrus limon* (L.) Osbeck (Gondhoraj), *Citrus* x *limonia* Osbeck (Rangpur/Gora), *Citrus maxima* Merr. (Batapi pomelo). *Citrus reticulata* Blanco and *Citrus* x *sinensis* (L.) Osbeck were collected from the local market in East Kolkata, West Bengal, India. The collected samples of *Citrus reticulata* (Darjeeling Mandarin) and *Citrus* x *sinensis* cv. *mosambi* were harvested from fruit farms in Darjeeling and West Medinipur district, West Bengal respectively, as confirmed by the vendor. All the other species viz., *Citrus* x *aurantifolia* (Paati), *Citrus medica* (Kaghchi), *Citrus limon* (Gondhoraaj), *Citrus maxima* (Batapi pomelo) were collected from the garden of Lady Brabourne College, South Kolkata, and *Citrus* x *limonia* (Gora) was collected from a l ocal garden in Salt Lake, East Kolkata, West Bengal. The collection of the fruits was done under the same climatic conditions. The climatic condition at the time of c ollection was mild winter, with temperatures ranging between 20 and 25° C. in the months of February and March. The *Citrus* fruit species were identified by Prof. Pinaki Acharya, Professor in the Department of Agriculture, University of Ca lcutta. After collection, the *Citrus* fruit species were washed thoroughly under tap water to remove the suspended particulate matters (SPMs) and dirt. The fruits were then peeled off manually, but very carefully. 100g of the lemon rinds were kept for drying at room temperature for 2 - 3 days and 50g of the rinds were kept fresh. Both dried and freshly scraped out rinds were recycled for t he isolation of E Os. The fresh rinds of *C.* x *aurantifolia* could not produce isolatable essential oil (but the oil droplets were found s uspended in the hydro-distilled water) and the dried rinds of *C. medica*, *C.* x *sinensis, C. limon* and *C.* x *limonia* could not be preserved for EO isolation. The fresh leaves of *Citrus* x *limonia* and *Citrus limon* were also collected, cleaned and torn into pieces before the extraction of essential oils. Some of t he fresh leaves were left at room temperature for 2-3 days to dehydrate. The leaves of ot her species could not be collected in appreciable amounts for E O isolation.

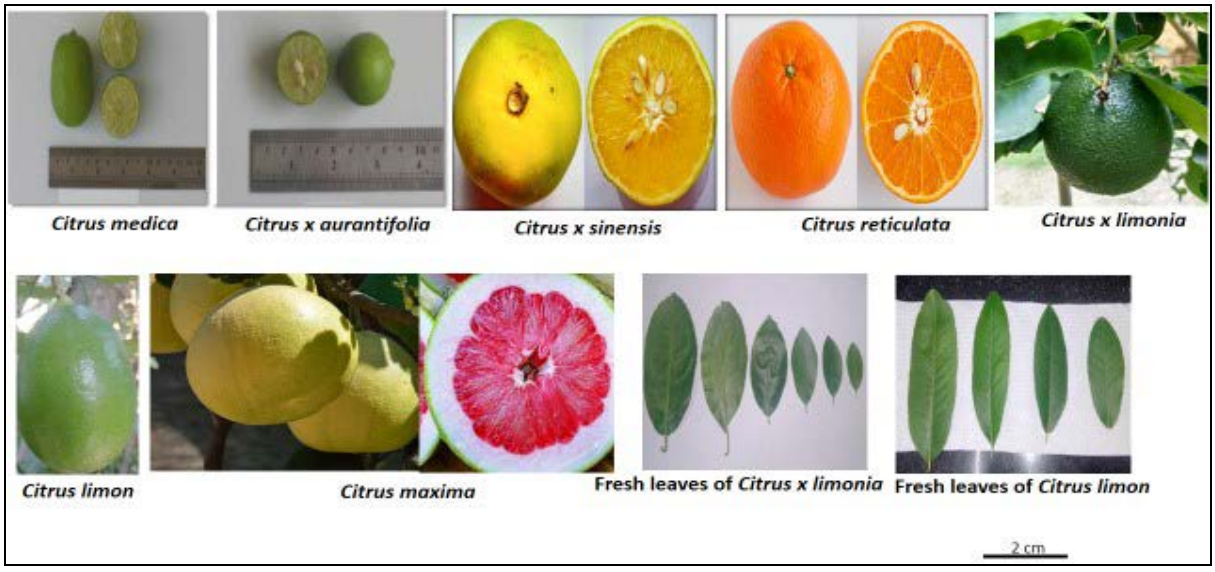

Figure 1. Fruits and leaves of the experimental samples

2.2. Isolation of essential oils

For the isolation of essential oils, 50g of fresh rinds and 25g of dry rinds of each *Citrus* fruit were taken separately in a 500 mL flask with 100 mL and 60 mL of double - distilled water respectively. Similarly, 60g of fresh leaves and 40g of dry leaves were taken separately with 200 mL and 150 mL of distilled water, respectively. The optimization of isolation as well as yield of volatile oils was done by several factors, including EO extraction time, temperature, water to plant material (rind / leaf) ratio and also the sample size. As per literature (Bardakei et al., 2019), the essential oils were isolated by the hydro-distillation method using a Clevenger-type apparatus for 3 hrs at 100° C. The time of EO isolation was determined by counting from the moment when the plant materials in the flask started to boil and the first drop was distilled. The hydro-distillation system was heated by a heating mantle, placed under the flask containing the plant material and distilled water. The condenser of the Clevenger was attached to a running tap water (Bardakei et al., 2019). Once the mixture started boiling, the steam-volatile components of the samples were condensed, and the insoluble, lighter than water, volatile oil was separated and collected on the surface of the water. The essential oils isolated were collected in 2 ml Eppendorff (EP) tubes, dehydrated over anhydrous sodium sulphate (Na_2SO_4). Thereafter, the essential oils were taken in fresh EP tubes and preserved in a -20° C. freezer (Bardakei et al., 2019) with proper sealing until GC/MS analyses were conducted. The EO extraction yields [average yields in mL/g, absolute yields in g and % yield (v/w)] were recorded. The percentage yield of EOs was computed using the below-mentioned equation:

$$y = x/z * 100 \quad \text{(i)}$$

Where y is the EO yield (mL/g), x is volume of the isolated EO (mL) and z is the mass of plant sample (g).

2.3. Identification of volatile compounds

For the detection of volatile components, the EOs were analyzed and identified using GC/MS. From each isolated anhydrous EO of fresh and dried lemon rinds and leaves, only 5 µL were diluted with 500 µL of *n*-hexane of HPLC grade. To it 1µL of 0. 66% methyl myristate (methyl tetradecanoate) mixed in *n*-hexane was used as an internal standard and injected into GC via split-less mode. The separation of EO components was done using a DB-5-MS capillary column (Agilent J & W; GC columns, USA) of 30 m length, 0.25 mm diameter and 0.25 mm narrow-bore film of an Agilent 7890A GC equipped with a 5795C inert MSD with Triple Axis Detector. The analysis was done under the temperature programme: the oven temperature ramp was set at 60° C (5 -minute hold time) to 220° C at the rate of 4° C / minute and held for 10 minutes, pressure 8.232 psi, purge flow 24 mL /minute, 55 minutes of run time. The injection temperature was set at 230° C, the MS transfer line at 280° C and the ion source at 250° C. Helium was used as the carrier gas at a constant flow rate of 1 mL /minute (carrier linear velocity of 36.623 cm/sec). Samples (1 µ L) were injected with a standard septum purge flow mode, maintaining 3 minutes of solvent delay to prevent sample overload. MS detector was operated on the Electron Ionization (EI) method at 70eV (Karak et al., 2016).

The constituents of EOs were detected by aligning the fragmentation configuration of the mass spectral data of samples with those of the G1033A NIST 2011 (National Institute of Standards and Technology, USA: Agilent PMB Search format) mass spectral library entries. Only the compound hit that showed the highest matching factor (MF) and reverse MF (RMF) (≥ 650) was considered (Wahyuni et al., 2013). Confirmation of identification was also done based on the minimum deviation from the Retention Index (RI) value entries in the NIST database. Once the retention times of the alkane standards were properly determined, the RI of each compound was calculated.

Metabolites were further confirmed by computing the Arithmetic Index (AI) value by comparing the AI relative to alkane standards (C_{11} to C_{28}) with reported literature (Adams, 2009). When temperature programming is done, an Arithmetic Index (AI) would be more appropriate than a logarithm-based index. The Arithmetic Index (AI) was computed exploiting the formula:

$$AI\ (unknown) = 100\ P_Z + 100\ [RT_{(unknown)} - RT\ (P_z)] / (RT\ (P_{z+1}) - RT\ (P_z)] \quad \text{(ii)}$$

Where, P_z = the no. of carbon atoms in the smaller alkane, $RT_{unknown}$ = the retention time of the unknown compound, RT (P_z) = the retention time of the smaller alkane, RT (P_{z+1}) = the retention time of the larger alkane. An RI deviation of < 50 units and AI deviation of < 20 units were considered as reliable for the identification of components. The quantitation of individual identified volatile components was determined as a percentage of peak area relative to the total peak area from the GC/MS study of the samples.

2.4. Hierarchical Cluster Analysis

In this study, the results reported are the average values of three biological replicates. The chemical compositions of the *Citrus* EOs obtained from fresh and dry rinds as well as leaves of different species were subjected to cluster analysis. The EO compositions could be used as operational taxonomic units (OTUs), and the relative responses of the components detected were used to define the chemical fingerprints between the volatile organic compounds (VOCs) of the EOs of different *Citrus* species using Hierarchical Cluster Analysis (HCA) using Metaboanalyst 5.0 version. Dissimilarities were measured using Euclidean distance and cluster analysis was done using Ward's method. PCA and PLS-DA were accomplished using the same software.

Multivariate analysis (MVA) approaches for example PCA and PLS are used to decipher the importance in metabolomics raw datasets, where spectral characters participating mostly for distinction or discrimination are acknowledged for additional analysis (Worley & Powers, 2015).

3. Results and Discussion

3.1. Variability in the EOs' yield

In this study, different species of *Citrus*, popularly cultivated and available in plentiful amounts in West Bengal, India were picked for evaluating the variability of yield and characterisation in their essential oils. The total volume (mL), absolute yield (g) and percentage yield (w/v) of 50g of fresh fruit rinds of *C. reticulata*, *C.* x

sinensis, *C. limon*, *C.* x *limonia*, *C. medica*, and *C. maxima*, 25g of dehydrated rinds of *C.* x *aurantifoila*, *C. reticulata* and *C. maxima*, 60g of fresh leaves of *C. limon* and *C.* x *limonia* and 40g of dry leaves of *C. limon* were compared correspondingly (Table 1).

Table 1. Variability of EOs' yield in various *Citrus* species

Plant materials (fresh / dry)		Weight of sample (g)	Total volume (mL)	Absolute yield (g)	Percentage yield (v/w) (%)
Fresh rinds	*C. reticulata*	50	5.48	4.658	9.316
	*C.*x *sinensis*	50	3.174	3.332	6.664
	C. limon	50	1.03	0.999	1.998
	*C.*x *limonia*	50	1.66	1.709	3.418
	C. medica	50	0.625	0.613	1.225
	C. maxima	50	0.3	0.261	0.522
Dehydrated rinds	*C.* x *aurantifoila*	25	0.945	0.926	3.704
	C. reticulata	25	3.67	3.927	15.708
	C. maxima	25	0.1	0.085	0.34
Fresh leaves	*Citrus limon*	60	0.63	0.611	1.108
	Citrus x *limonia*	60	0.49	0.505	0.841
Dry leaves	*C. limon*	40	0.879	0.835	2.087

3.2. Variability in VOCs

In this study, the variability of VOCs from the EOs obtained from the studied *Citrus* species was investigated by GC/MS study. A total number of 78 VOCs were recognised from the EOs of different *Citrus* species studied. The normalized data of the relative responses of individual compounds was deposited in Metaboanalyst 5.0. PCA (Fig. 2) and PLS-DA (Fig. 3) was performed and the metabolites responsible for their differentiation were determined based on VIP scores. Normalised values were also subjected to ANOVA and Tukey's HSD Post-hoc test, designated 74 significant metabolites ($p < 0.05$) out of the 78 identified compounds. A Dendrogram was produced based on generalized logarithm transformed dataset.

The volatile metabolites identified were 11 monoterpenes, 12 sesquiterpenes, 10 aldehydes, 25 alcohols, 8 ethers, 4 esters, 3 ketones, 2 hydrocarbons and 3 unknown compounds presented in Table 2.

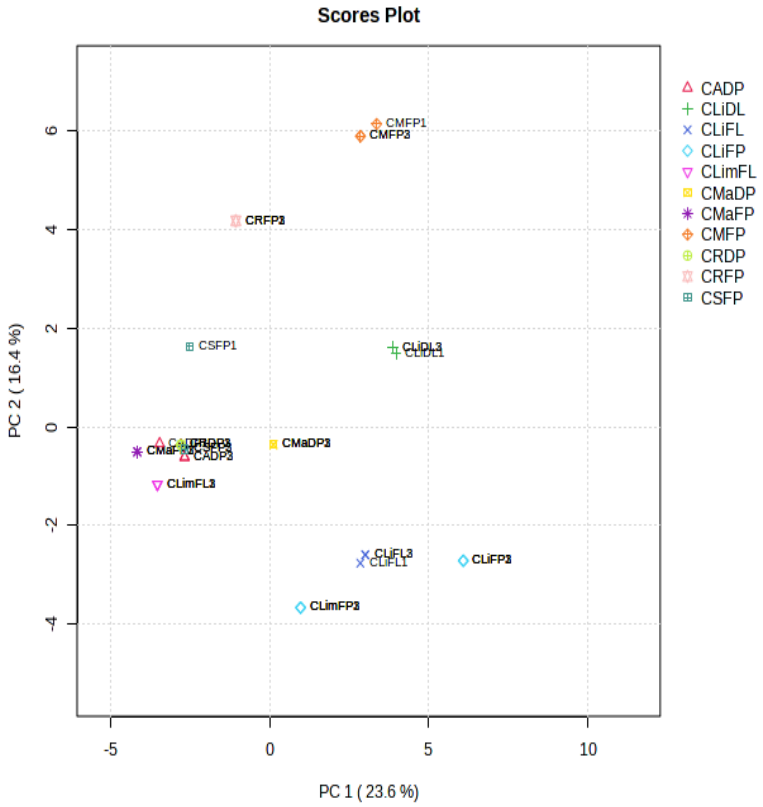

Figure 2. Principal Component Analysis (PCA) of the *Citrus* species studied; *C.* x *aurantifolia* dry peel (CADP); *C. limon* dry leaf (CLiDL); *C. limon* fresh leaf (CLiFL); *C.* x *limonia* fresh peel (CLiFP); *C.* x *limonia* fresh leaf (CLimFL); *C. maxima* dry peel (CMaDP); *C. maxima* fresh peel (CMaFP); *C. medica* fresh peel (CMFP); *C. reticulata* dry peel (CRDP); *C. reticulata* fresh peel (CRFP); *C.* x *sinensis* fresh peel (CSFP)

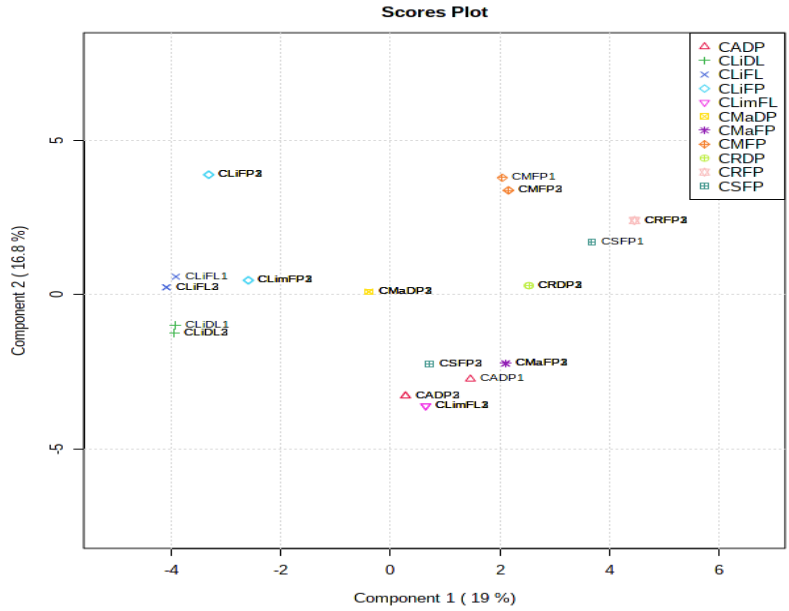

Figure 3. PLS-DA 2-D scores plot of the *Citrus* species studied; *C.* x *aurantofolia* dry peel (CADP); *C. limon* dry leaf (CLiDL); *C. limon* fresh leaf (CLiFL); *C.* x *limonia* fresh peel (CLiFP); *C.* x *limonia* fresh leaf (CLimFL); *C. maxima* dry peel (CMaDP); *C. maxima* fresh peel (CMaFP); *C. medica* fresh peel (CMFP); *C. reticulata* dry peel (CRDP); *C. reticulata* fresh peel (CRFP); *C.* x *sinensis* fresh peel (CSFP)

Table 2. List of volatile organic compounds identified in the seven *Citrus* species studied; RT = r etention time, AI calculated = experimental arithmetic index; Adam's AI = literature Adam's index, nd = not detected

					Area percentage					
					Orange *Citrus reticulata* dry peel	Orange *Citrus reticulata* fresh peel	Musambi *Citrus* x *sinensis* fresh peel	Kaghchi *Citrus* x *aurantifolia* dry peel	Paati *Citrus medica* fresh peel	Batapi pomelo *Citrus maxima* dry peel
Chemical classes	Metabolites	RT	AI calculated	Adam's AI	CRDP	CRFP	CSFP	CADP	CMFP	CMaDP
Monoterpene	α-Pinene	10.919	933	932	nd	0.31 ± 0.01	0.54 ± 0.01	0.21 ± 0.002	0.002 ± 0.01	0.23 ± 0.01
Bicyclic monoterpene	Sabinene	12.55	974	969	nd	nd	nd	0.17 ± 0.001	nd	nd
Monoterpene	β-Pinene	13.102	988	974	1.196 ±0.01	0.53 ± 0.02	1.09 ± 0.01	0.39 ± 0.00	0.09 ± 0.01	1.14 ± 0.001
Bicyclic monoterpene	delta-3-Carene	13.865	1007	1008	nd	nd	nd	0.40 ± 0.01	nd	nd
Cyclic monoterpene	D-Limonene	15.041	1036	1024	84.48 ± 0.001	88.40 ± 0.002	92.18 ± 0.001	97.30 ± 0.01	90.25 ± 0.00	89.89 ± 0.003
Monoterpene	trans-β-Ocimene	15.468	1047	1044	nd	nd	nd	nd	nd	nd
Monoterpene	α-Ocimene	16.292	1067		nd	nd	nd	nd	nd	nd
Aldehyde	Bergamal	16.379	1069	1051	nd	nd	nd	nd	nd	nd
Ether	α-Pinene oxide	16.824	1080	1099	nd	nd	nd	nd	nd	nd
Monoterpene	γ-Terpinene	17.093	1086	1054	nd	7.18 ± 0.003	3.09 ± 0.01	nd	nd	0.20 ± 0.02
Hydrocarbon	p-Mentha-1,4(8)-diene	17.286	1091	1080	8.05 ± 0.02	nd	nd	nd	nd	0.05 ± 0.002
Ketone	Chrysanthenone	17.433	1096	1124	nd	nd	nd	nd	nd	nd
Hydrocarbon	α-Terpinolene	17.618	1099	1086	nd	0.18 ± 0.001	0.12 ± 0.00	0.04 ± 0.01	nd	nd
Aldehyde	n-Nonanal	18.007	1109	1100	nd	nd	nd	nd	nd	nd
Ether	Rose oxide	18.027	1110	1106	nd	nd	nd	nd	nd	nd
Alcohol	β-Linalool	17.831	1105	1095	3.00 ± 0.01	1.13 ± 0.01	1.23 ± 0.02	0.74 ± 0.01	3.68 ± 0.01	0.89 ± 0.01
Monoterpene	p-Mentha-1,3,8-triene	18.541	1123	1108	nd	nd	0.02 ± 0.001	nd	nd	nd
Monoterpene	Allo-Ocimene	18.818	1130	1128	nd	nd	nd	nd	nd	nd
Monoterpene	Neo-allo-ocimene	18.844	1130	1140	nd	nd	nd	nd	nd	0.03 ± 0.001
Ethers	cis-Limonene oxide	19.088	1137	1132	nd	nd	nd	nd	nd	nd

Ethers	trans- Limonene oxide	19.339	1144	1137	nd	0.02 ± 0.001	nd	nd	nd	nd
Alcohol	trans-3(10)-Caren-2-ol	19.434	1146		nd	nd	nd	nd	nd	0.07 ± 0.01
Aldehydes	β-Citronellal / (R)-(+)-Citronellal	19.757	1155	1148	nd	0.052 ± 0.001	0.11 ± 0.01	0.05 ± 0.01	0.13 ±0.001	0.23 ± 0.001
Cyclic nonaromatic alcohol	L-isopulegol	19.882	1158	1145	0.16 ± 0.001	nd	nd	nd	nd	nd
Alcohol	cis-Verbenol	20.14	1165	1137	nd	nd	nd	nd	nd	0.17 ± 0.01
Ether	Limonene oxide, cis-	20.916	1185	1132	nd	nd	nd	nd	nd	0.52 ± 0.002
Alcohol	L-terpinen-4-ol	21.002	1187	1174	0.72 ± 0.001	0.13 ± 0.001	0.39 ± 0.01	0.26 ± 0.02	1.08 ± 0.001	nd
Aldehyde	1,3,4-Trimethyl-3-cyclohexenyl-1-carboxaldehyde	21.127	1190		nd	nd	nd	nd	nd	nd
Alcohol	cis-p-mentha-1(7),8-dien-2-ol	21.272	1194	1227	nd	nd	nd	nd	nd	nd
Alcohol	L-α-Terpineol	21.509	1200	1186	0.68 ± 0.002	0.16 ± 0.01	0.34 ± 0.001	0.11 ± 0.001	2.42 ± 0.001	0.12 ± 0.02
Aldehyde	n-Decanal	21.79	1208	1201	0.34 ± 0.001	0.16 ± 0.01	0.17 ± 0.01	0.10 ± 0.02	nd	0.16 ± 0.03
Ketone	D-Verbenone	22.075	1215	1204	nd	nd	nd	0.08 ± 0.002	nd	nd
Alcohol	cis-Carveol	22.447	1226	1226	0.41 ± 0.001	nd	0.23 ± 0.01	nd	nd	nd
Alcohol	Citronellol	22.522	1228	1223	nd	0.09 ± 0.001	nd	nd	nd	nd
Aldehyde	cis-Neral/ cis-Citral	22.946	1240	1235	0.10 ± 0.01	0.02 ± 0.001	0.07 ± 0.001	0.06 ± 0.001	0.95 ± 0.002	2.20 ± 0.002
Ketone	(-)-Carvone	23.229	1248	1239	nd	0.02 ± 0.002	nd	nd	0.33 ± 0.002	nd

					Area percentage					
					Batapi pomelo	Gora lebu	Gora lebu	Gondhoraj	Gondhoraj	Gondhoraj
					Citrus maxima	*Citrus* x *limonia*	*Citrus* x *limonia*	*Citrus limon*	*Citrus limon*	*Citrus limon*
					fresh peel	fresh peel	leaf fresh	dry leaf	fresh leaf	peel fresh
Chemical classes	Metabolites	RT	AI calculated	Adam's AI	CMaFP	CLiFP	CLimLF	CLiDL	CLiFL	CLiFP
Monoterpene	α-Pinene	10.919	933	932	nd	nd	nd	0.27 ± 0.002	nd	nd
Bicyclic monoterpene	Sabinene	12.55	974	969	nd	nd	6.77 ± 0.04	nd	nd	nd
Monoterpene	β-Pinene	13.102	988	974	0.35 ± 0.01	0.16 ± 0.001	nd	0.64 ± 0.02	0.21 ± 0.004	0.28 ± 0.002
Bicyclic monoterpene	delta-3-Carene	13.865	1007	1008	nd	nd	nd	nd	nd	nd
Cyclic monoterpene	D-Limonene	15.041	1036	1024	95.75 ± 0.002	9.49 ± 0.001	26.39 ±0.004	74.98 ± 0.04	17.41 ± 0.01	61.59 ± 0.003
Monoterpene	trans-β-Ocimene	15.468	1047	1044	nd	0.20 ± 0.04	0.29 ± 0.01	nd	nd	nd
Monoterpene	α-Ocimene	16.292	1067		nd	nd	nd	nd	nd	0.03 ± 0.02
Aldehyde	Bergamal	16.379	1069	1051	nd	nd	nd	nd	nd	0.01 ± 0.01
Ether	α-Pinene oxide	16.824	1080	1099	nd	nd	nd	nd	nd	0.03 ± 0.002
Monoterpene	γ-Terpinene	17.093	1086	1054	nd	nd	nd	nd	nd	nd
Hydrocarbon	p-Mentha-1,4(8)-diene	17.286	1091	1080	0.04 ± 0.02	nd	nd	nd	nd	nd
Ketone	Chrysanthenone	17.433	1096	1124	nd	nd	nd	nd	nd	0.02 ± 0.002
Hydrocarbon	α-Terpinolene	17.618	1099	1086	nd	nd	nd	nd	nd	nd
Aldehyde	n-Nonanal	18.007	1109	1100	nd	nd	nd	0.41 ± 0.02	nd	nd
Ether	Rose oxide	18.027	1110	1106	nd	0.05 ± 0.002	nd	nd	nd	nd
Alcohol	β-Linalool	17.831	1105	1095	2.97 ± 0.01	nd	6.09 ± 0.002	nd	nd	0.14 ± 0.002
Monoterpene	p-Mentha-1,3,8-triene	18.541	1123	1108	nd	nd	nd	nd	nd	nd
Monoterpene	Allo-Ocimene	18.818	1130	1128	nd	nd	nd	0.12 ± 0.02	nd	nd

Monoterpene	Neo-allo-ocimene	18.844	1130	1140	nd	nd	nd	nd	nd	0.07 ± 0.01
Ethers	cis-Limonene oxide	19.088	1137	1132	nd	nd	nd	0.09 ± 0.01	nd	0.20 ± 0.001
Ethers	trans- Limonene oxide	19.339	1144	1137	nd	nd	nd	nd	nd	nd
Alcohol	trans-3(10)-Caren-2-ol	19.434	1146		nd	nd	nd	nd	nd	nd
Aldehydes	β-Citronellal / (R)-(+)-Citronellal	19.757	1155	1148	0.08 ± 0.03	81.53 ± 0.04	55.51 ± 0.03	19.73 ± 0.001	72.76 ± 0.003	14.48 ± 0.02
Cyclic nonaromatic alcohol	L-isopulegol	19.882	1158	1145	nd	nd	nd	nd	nd	0.003 ± 0.00
Alcohol	cis-Verbenol	20.14	1165	1137	nd	nd	nd	0.05 ± 0.02	nd	nd
Ether	Limonene oxide, cis-	20.916	1185	1132	nd	nd	nd	nd	nd	nd
Alcohol	L-terpinen-4-ol	21.002	1187	1174	0.12 ± 0.03	nd	1.06 ± 0.002	0.07 ± 0.02	nd	nd
Aldehyde	1,3,4-Trimethyl-3-cyclohexenyl-1-carboxaldehyde	21.127	1190		nd	nd	nd	nd	nd	0.42 ± 0.02
Alcohol	cis-p-mentha-1(7),8-dien-2-ol	21.272	1194	1227	nd	nd	nd	nd	nd	0.08 ± 0.002
Alcohol	L-α-Terpineol	21.509	1200	1186	0.28 ± 0.003	nd	0.12 ± 0.002	nd	nd	0.12 ± 0.002
Aldehyde	n-Decanal	21.79	1208	1201	nd	0.25 ± 0.001	nd	0.28 ± 0.001	0.41 ± 0.002	0.30 ± 0.01
Ketone	D-Verbenone	22.075	1215	1204	nd	0.08 ± 0.02	nd	nd	nd	nd
Alcohol	cis-Carveol	22.447	1226	1226	nd	nd	nd	nd	nd	nd
Alcohol	Citronellol	22.522	1228	1223	0.15 ± 0.001	1.43 ± 0.001	3.03 ± 0.002	1.30 ± 0.001	2.63 ± 0.01	13.93 ± 0.003
Aldehyde	cis-Neral/ cis-Citral	22.946	1240	1235	0.08 ± 0.001	nd	0.32 ± 0.02	0.31 ± 0.03	nd	nd
Ketone	(-)-Carvone	23.229	1248	1239	nd	nd	nd	nd	nd	nd

To better understand the relationships among the VOCs present in the different *Citrus* samples (fresh as well as dehydrated rinds and leaves), PCA (Fig. 2) and PLS-DA (Fig. 3) were applied to the experimental results. It was very easy to understand that there was substantial variability in the chemical components of VOCs in the studied samples.

The HCA was performed on the VOCs of *Citrus* species and the dendrogram showed two main clusters (Fig. 4). Cluster II was constituted of six samples including *C.* x *sinensis* fresh rind, *C.* x *aurantifolia* dry rind, *C.* x *limonia* fresh leaf, *C. maxima* fresh rind, *C. reticulata* dry rind, and *C. maxima* dry peel. Cluster I was composed of six *Citrus* samples including *C. limon* fresh leaf, *C. limon* dry leaf, *C.* x *limonia* fresh rind, *C. maxima* fresh rind, *C. reticulata* fresh rind, and *C. limon* fresh rind.

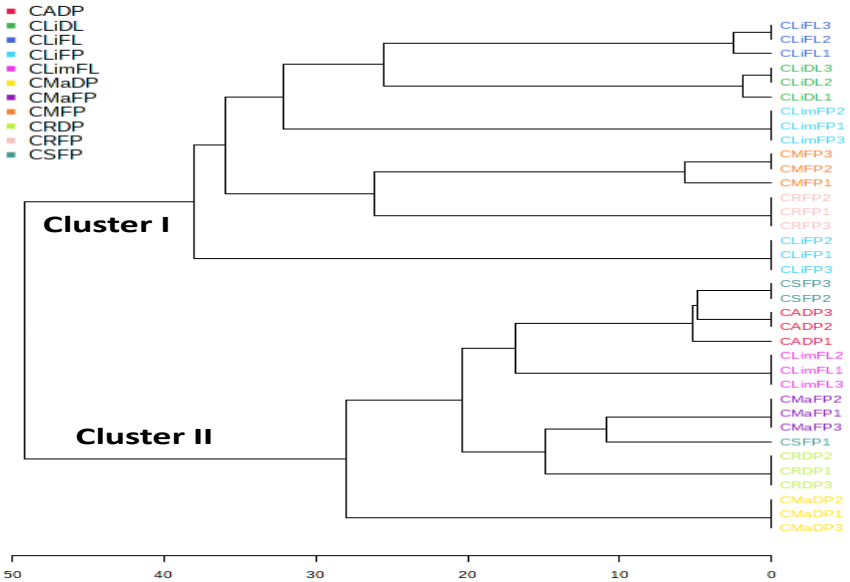

Figure 4. Dendogram obtained by hierarchical cluster analysis of VOCs of the *Citrus* species under study based on Ward's method using the Euclidean distances. *C.* x *aurantofolia* dry peel (CADP); *C. limon* dry leaf (CLiDL), *C. limon* fresh leaf (CLiFL), *C.* x *limonia* fresh peel (CLiFP), *C.* x *limonia* fresh leaf (CLimFL); *C. maxima* dry peel (CMaDP); *C. maxima* fresh peel (CMaFP); *C. medica* fresh peel (CMFP); *C. reticulata* dry peel (CRDP); *C. reticulata* fresh peel (CRFP); *C.* x *sinensis* fresh peel (CSFP); 1 - 4 depicted 4 biological replicates of same sample.

Based on Fig. 5, we could be able to identify the top 15 VOCs for which the different *Citrus* species and samples under study were different from each other. The top most 15 metabolites based on V IP (Variable importance of projection) scores of P LS-DA were: α-humulene, L-perillaldehyde, β-citronellal, α-bisabolol, caryophyllene, cedr-8-en-13-ol, isolongifolol, δ-elemene, n-dodecanol, α-terpinolene, cis-neral, α-bisabolene, (-)-carvone, cis-limonene-oxide, and trans-limonene oxide.

Based on this study, we find that α-humulene is present in the highest concentration in *C. limon* dry leaf, and then in *C. limon* fresh leaf and next in *C. limon* fresh peel. L-perillaldehyde is present in the highest relative concentration in *C. reticulata* fresh peel, followed by *C. reticulata* dry peel. β – citronellal was present in its highest concentration in *C. reticulata* fresh peel and next in *C. maxima* fresh peel. α-bisabolol, caryophyllene, cedr-8-en-13-ol, isolongifolol and α-bisabolene were present in the highest concentration in *C. limon* fresh leaf. δ-elemene was found its highest concentration in *C. limon* dry leaf. *n*-dodecanal was found in maximum amounts both in *C. medica* fresh peel and *C. reticulata* fresh peel. α-terpinolene was found t o be present in the highest concentration in *C.* x *sinensis* fresh peel. Cis-neral, (-) -carvone and trans-limonene oxide were found in the highest amounts in *C. reticulata* fresh peel.

Based upon percentage peak area calculated, the cyclic monoterpene, D-limonene was estimated as the chief volatile component in the EOs extracted, ranging from 97.302 ± 0.01% in dry peel of *C.* x *aurantifolia* > 95.747 ± 0.002% in *C. maxima* fresh peel > 90.251± 0.00% in *C. medica* fresh peel > 89.89 ± 0.003% in *C. medica* dry peel > 88.392 ± 0.002% in *C. reticulata* fresh peel > 88.392 ± 0.002% in *C. reticulata* fresh peel > 84.48 ± 0.001% in *C. reticulata* dry peel > 74.981 ± 0.04% in *C. limon* dry leaf > 61.489 ± 0.003% in *C. limon* fresh peel > 26.389 ± 0.004% *C.* x *limonia* fresh leaf > 17.412 ± 0.01% in *C. limon* fresh leaf > 9.494 ± 0.001% in *C.* x *limonia* fresh peel. It was the only compound found in all the studied samples, both in fresh and dehydrated conditions. The monoterpene, β -pinene was detected in all the experimental samples except in the EO of *C.* x *limonia* fresh leaf. The alcohol, β-linalool was found in all except in *C. limon* dehydrated as well as fresh leaf samples. The highest percentage of peak area of β-linalool was calculated in *C.* x *limonia* fresh leaf (6.092 ± 0.002%). *C. medica* fresh rind and *C. maxima* fresh rind also contained β-linalool in 3.675 ± 0.01% and 2.974 ± 0.01% respectively. *C. reticulata* dry and fresh peel contained 3.001 ± 0.01% and 1.131 ± 0.01 % of β-linalool. *C.* x *sinensis* contained 1.233 ± 0.02% of β-linalool in its EO. The aldehyde β-citronellal was present in a high percentage peak area in *C.* x *limonia* fresh rind (81.533 ± 0.004%) > in *C. limon* fresh leaf (72.757 ± 0.003%) > *C.* x *limonia* fresh leaf (55.51 ± 0.03%) > *C. limon* dry leaf (19.733 ± 0.001 %) > *C. limon* fresh rind (14.479 ± 0.02%).

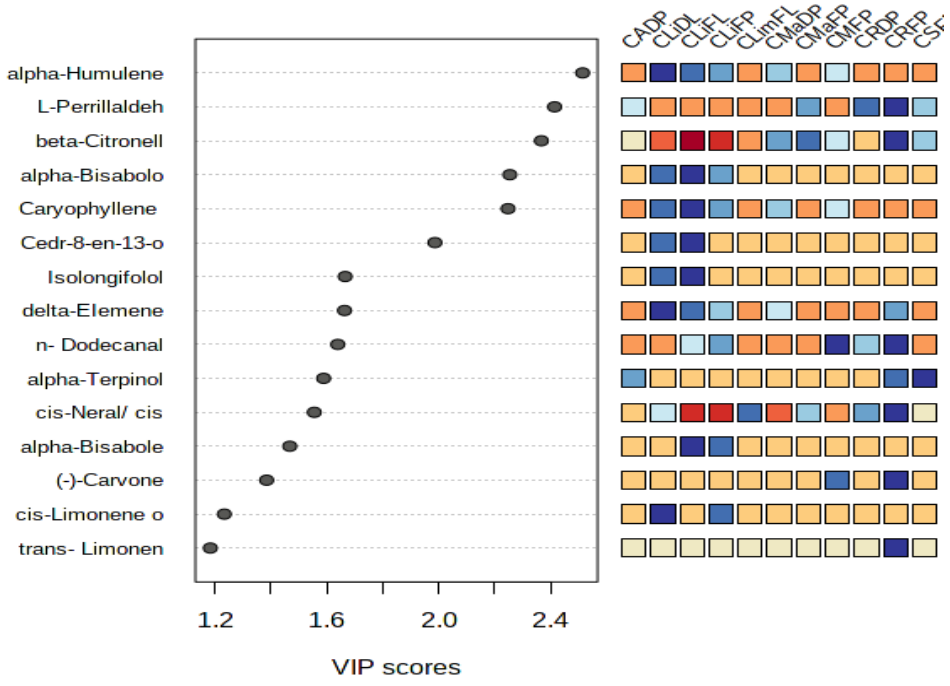

Figure 5. VIP scores of PLS-DA showing top 15 metabolites. The coloured boxes on the right indicate the relative concentrations of the corresponding metabolites in *Citrus* species under study. *C.* x *aurantifolia* dry peel (CADP), *C. limon* dry leaf (CLiDL), *C. limon* fresh leaf (CLiFL); *C.* x *limonia* fresh peel (CLiFP); *C.* x *limonia* fresh leaf (CLimFL); *C. maxima* dry peel (CMaDP); *C. maxima* fresh peel (CMaFP); *C. medica* fresh peel (CMFP); *C. reticulata* dry peel (CRDP); *C. reticulata* fresh peel (CRFP); *C.* x *sinensis* fresh peel (CSFP)

Previously EOs from the rinds of Malta (*C. limetta*, a cultivar of *C. limon*), Mousambi (*C.* x *sinensis*), Grapefruit (*C. paradisi*) and Eureka lemon (*C. limon*) were isolated employing the cold press method, and the chemical composition of the EOs of the species was investigated by GC/FID on a Carbowax 20 M packed glass column. It was reported that composition of t he EOs varied significantly among the species, which may be due to their variation in genetic makeup (Ahmad et al., 2006). The volatile aroma and flavour metabolies of fl ower, leaf, rind and "Page" mandarin juice were scrutinised and the compounds were separated by ultrasound water bath apparatus, water distillation method, by utilizing poly dimethyl siloxane membranes (PDMS) and cold press technique, respectively, and then eluted by *n*-pentane: diethylether

(1:2), *n*-hexane, pentane: dichloromethane (2:1) and *n*-hexane respectively and were analyzed by GC-FID and GC/MS, and it was reported that the percentage of flavour molecules was significantly different from organ to organ (Darjazi, 2011). The EO components from the leaf and fruit rinds of *C. reticulata* Blanco cv. Santra (Santra mandarin) cultivated in Egypt were assessed qualitatively and quantitatively using GLC and GLC/MS and 131 components were identified and quantified. The Egyptian Santra mandarin chemotype was discriminated for the presence of limonene in rind oil and sabinene and linalool in leaf oil (Hamdan et al., 2016). The difference in yield, chemical characteristics and detections in solvent-assisted oils extracted from the dehydrated rinds and seeds of the two different *Citrus* samples from Isinbode-Ekiti, Ekiti-State, Nigeria –*C. sinensis* var. Shamuti and *C. paradisi* var. Marsh planted in a cocoa farm was investigated, and it was found that the raw rinds and seeds have a lower yield and a higher percentage of metabolites that serve as compound detection for the *Citrus* family, whereas the dehydrated rinds and seeds have alcohol components like spathulenol, linalool, nerol, α-terpeniol and farnesol, which are not present in the fresh samples (Adebisi, 2014).

In a review report by Gonzales Mas et. al., 2019, based upon quantitative insight, the greatest copious metabolites in EO of *C. reticulata* were found monoterpene hydrocarbons. Among these, the chief pertinent is limonene, usually indicating about 95% of the total EO, but sometimes down to 60% in some analysis (Fanciullino et al., 2006; Tao et al., 2014). The following compounds in large quantity are γ-terpinene, sometimes accomplished above 15% (Mondello et al., 2003; Petretto et al., 2016), β-myrcene (7.43–0.1%) (Fanciullino et al., 2006; Tao et al., 2014), α-pinene (3.93–0.1%) (Fanciullino et al., 2006; Tao et al., 2014) or β-pinene (4% - traces) (Fanciullino et al., 2006). Linalool and β-citronellal were reported to contain up to 2.9% and 0.6%, respectively (Tao et al., 2014). Amongst minor metabolites with great quantities approximately between 0.7 and 0.1%, sesquiterpene α-sinensal, the non-terpene aliphatic compounds octanal and decanal, and the aromatic compound methyl N-methylanthranilate were reported (Gonzales Mas et. al., 2019).

As per Gonzales Mas et al., 2019; the VOCs of *C.* x *sinensis* peel EO is the most analyzed *Citrus* species along with those of *C. reticulata* and *C. limon*. This species seems to be higher in the diversity of sesquiterpene hydrocarbons such as aromadendrene (Njoroge et al., 2005; Hosni et al., 2010) and sesquiphellandrene (Ruberto and Rapisarda, 2002; Sawamura et al., 2005) than other species as *C. reticulata* or *C. limon*. The major VOCs in *C. sinensis* are very identical to that of *C. reticulata*, with analogous proportions. Limonene is generally affirmed between 90 and 97% in *C.* x *sinensis*, although this percentage decreased down to 64% in some analyses (Chen et al., 2014).

The most plentifully present compound in *C. medica* is limonene, but its % can drop down to 51% (Verzera et al., 2005), while other monoterpene compounds such as γ-terpinene, β-pinene or camphene are present at greater concentration, in comparison with species of *C. reticulata* cluster where these compounds are usually described in percentages below 1%. Thus, in *C. medica* oil, γ-terpinene, β-pinene or camphene can reach upto 31%, 9.7%, and 10%, respectively (Aliberti et al., 2016; Petretto et al., 2016). Also *C. medica* represents higher amounts of some sesquiterpenes, as is the case of (E)-α-bergamotene (Aliberti et al., 2016) or germacrene D (Petretto et al., 2016), although their copiousness is usually lower than 0.5%.

Many mono- and sesquiterpene hydrocarbons and oxygenated monoterpenes have been reported in *C. aurantifolia* rind. The % of limonene may decrease to 39.9% in the oil of *C. aurantifolia* (Lota et al., 2002), and the prevalence of other terpene compounds is improved, such as β-pinene, neryl acetate, geranyl acetate, β-bisabolene, (E)- α-bergamotene, germacrene D and β-caryophyllene (Lota et al., 2002; Minh Tu et al., 2002a).

Quantitatively, the chief compound of *C. limon* EO is limonene, at levels usually ranging between 70 and 48%. Geranial and neral are some of the more richly present compounds reported so far (Lota et al., 2002; Loizzo et al., 2016).

Our results substantiate the earlier studies on some species of the *Citrus* EOs, and still we report several other VOCs much more elaborately and also some marker metabolites for each of the studied species for the first time with the help of multivariate analytical approaches.

4. Conclusions

In conclusion, based on this study, it can be said that an increasing amount of fruit rinds and other agricultural wastes can be useful as a source of bioactive substances. This idea of utilizing agricultural wastes may increase the financial strength of farmers and decrease the problem of agricultural waste management. Moreover, in India, the organic wastes generated from food processing industries are highly hazardous to the environment and can be a potential source for extraction of bioactive compounds.

Citrus fruits have a very high-water content, making them difficult to dry through common conventional methods or industrial drying devices. Before disposing of the peel waste in and around landfills, extraction of EOs from peels is very important, because EOs adversely influence fermentation and bacterial degradation. Expulsion of waste into waterbodies may cause pollution and devastation of aquatic life. Wastes released into urban garbage or sewage structure can contaminate aquatic resources below the surface, cause impairment to pumps and piping, choke gravel beds, and produce froth in primary settling reservoirs. Thus, direct disposal of *Citrus* waste without proper processing causes environmental hazard.

In this study, we also find a clear understanding of the VOCs of *Citrus* rind and leaf wastes (both in fresh and dehydrated conditions), many of which are bioactive VOCs and may have medicinal benefits against various diseases. In this research we have determined different classes of VOCs, namely monoterpene (Cyclic, bicyclic), aldehyde, ketone, ether, alcohols, cyclic nonaromatic alcohols, hydrocarbons and their variation in content in the studied *Citrus* species. The present study also focused on the simple hydro-distillation extraction method of various beneficial value-added metabolites obtained from their EOs from these wastes, which are extremely costly and time-consuming to produce using typical chemical approaches. The EOs and their isolated components may be exploited in therapeutic implementation and as plant-based value-additives for functional foods.

This work also represents the identification of VOCs which are species specific biomarkers based on which the species could be useful for food, flavor, aroma and therapeutic industries. This research provides significant facts and figures in the selection of *Citrus* species for volatile chemicals for ph armaceutical, food, beverages, flavor, fragrances, cosmeceuticals and nutraceticals etc.

5. Author Contributions

SD and RS conceptualized the experimental design and SD performed the data analyses and wrote the manuscript. RS, collected the samples. SM, GM and MB performed the extraction and isolation of the EOs from different samples and injected the EOs in GC/MS. All authors contributed to the article and approved the submitted version.

Acknowledgements

GC-MS based work supported by DST-FIST Programme, Govt. of India [Grant Number: SR/FST/LS1-459/2010] is acknowledged.

References

Adebisi O. 2014. Comparative study of essential oil composition of fresh and dry peel and seed of Citrus sinensis (L) Osbeck var Shamuti and Citrus paradise Macfadyen var Marsh. *IJS.***16 (2)**: 211-217.

Adams RP. 2009. Identification of Essential Oil Components by Gas chromatography/Mass Spectrometry, 4th ed.; Allured Business Media: Illinois.

Ademosun AO. 2022. Citrus peels odyssey: From the waste bin to the lab bench to the dining table. *Appl. Food Res.* **2**: 100083.

Ahmad MM, Rehman SU, Anjum FM and Sultan JI. 2006. Genetic Variability to Essential Oil Composition in Four Citrus fruit species. *Pak. J. Bot.* **38 (2)**: 319-324.

Aliberti L, Caputo L, de Feo V, de Martino L, Nazzaro F. and Souza LF. 2016. Chemical composition and in vitro antimicrobial, cytotoxic, and central nervous system activities of the essential oils of Citrus medica L. cv. 'Liscia' and C. medica cv. 'Rugosa' cultivated in Southern Italy. *Molecules* **21**: E1244.

Asikin Y, Maeda G, Tamaki H, Mizu M, Oku H and Wada K. 2015. Cultivation line and fruit ripening discriminations of Shiikuwasha (*Citrus depressa* Hayata) peel oils using aroma compositional, electronic nose and antioxidant analyses. *Food Res. Int.* **67**: 102-110.

Bardakei H, Servi H and Polatoglu K. 2019. Essential oil composition of *Salvia candidissima* Vahl. *occidentalis* Hedge, *S. tomentosa* Miller and *S. heldreichiana* Boiss. Ex Benthum from Turkey. *J. Essent. Oil - Bear. Plants.* **22 (6)**: 1467-1480.

Ben Hsouna A, Ben Halima N, Smaoui S and Hamdi N. 2017. Citrus lemon essential oil: chemical composition, antioxidant and antimicrobial activities with its preservative effect against Listeria monocytogenes inoculated in minced beef meat. *Lipids Health Dis.***16**: 1-11.

Chen Y. Wu J, Xu Y, Fu M, and Xiao G. 2014. Effect of second cooling on the chemical components of essential oils from orange peel (Citrus sinensis). *J. Agric. Food Chem.* **62**: 8786–8790.

Darjazi BB. 2011. Comparison of volatile components of flower, leaf, peel and juice of 'Page' mandarin [(Citrus reticulate var 'Dancy' x Citrus paradise var 'Duncan') x Citrus clementina]. *Afr. J. Biotechnol.* **10 (51)**: 10437-10446.

De Gregorio A, Mandalari G, Arena N, Nucita F, Tripodo M M and Lo Curto, R B. 2002. SCP and crude pectinase production by slurry-state fermentation of lemon pulps. *Bioresour Technol.* **83**: 89–94.

Dugo P and Mondello L. 2011. Citrus Oils: Composition, Advanced Analytical Techniques, Contaminants, and Biological Activity, 49. Boca Raton, FL: CRC Press

Fancello F, Petretto G L, Zara S, Sanna M L, Addis R, Maldini M. et al. 2016. Chemical characterization, antioxidant capacity and antimicrobial activity against food related microorganisms of Citrus limon var. pompia leaf essential oil. *LWT Food Sci. Technol.* **69**: 579-585.

Fanciullino AL, Tomi F., Luro, F., Desjobert, J. M., and Casanova, J. (2006). Chemical variability of peel and leaf oils of mandarins. Flavour Frag. J. **21:** 359–367.

Fierascu RC, Fierascu I, Avramescu SM and Sieniawska E. 2019. Recovery of natural antioxidants from agro-industrial side streams through advanced extraction techniques. *Molecules*, **24**: 1-29.

Forney C and Song J. 2017. Flavors and aromas: chemistry and biological functions. In Fruit and Vegetable Phytochemicals; Wiley: Hoboken, NJ, USA,

Gherairia N, Boukerche S, Mustapha MA and Chefrour A. 2022. Effects of biotic and abiotic factors on the yield and chemical composition of essential oils from four Thymus species wild growing in Northeastern Algeria. *JJBS*, **15(2)**: 173 – 181.

Gonzalez-Mas MC, Rambla JL, Lopez-Gresa MP, Blazquez MA and Granell A. 2019. Volatile compounds in Citrus Essential oils: A comprehensive review. *Front. Plant Sci.* **10**: 1-18.

Hamdan DI, Mohamed ME and El-Shazly AM. 2016. Citrus reticulata Blanco cv. Santra leaf and fruit peel: A common waste products, volatile oils composition and biological activities. *J. Med. Plant res.* **10 (30)**: 457-467

Hosni K, Zahed N, Chrif R, Abid I., Medfei W, Kallel M, et al. (2010). Composition of peel essential oils from four selected Tunisian Citrus species: evidence for the genotypic influence. *Food Chem.* **123**: 1098–1104.

Karak S, Bhattacharya P, Nandy A, Saha A and De B . 2016. Metabolite Profiling and Chemometric Study for Varietal Difference in Piper Betle L. Leaf. *Curr. Metabolomics* **4(2)**: 129–140.

Lo Curto RB, Tripodo MM, Leuzzi U, Giuffre D and Vaccarino C.1992. Flavonoids recovery and SCP production from orange peel. *Bioresour Technol.* **42**: 83–87.

Loizzo MR, Tundis R, Bonesi M, Di San zo G, Verardi A, Lopresto CG, et al. (2016). Chemical profile and antioxidant properties of extracts and essential oils from Citrus x limon (L.) BURM. cv. Femminello comune. *Chem. Biodiversity* **13**: 571–581.

Lota ML, de Rocca Serra, D., Tomi, F., Jacquemond, C., and Casanova, J. (2002). Volatile components of peel and leaf oils of lemon and lime species. *J. Agric. Food Chem.* **50**: 796–805. doi: 10.1021/jf010924l

Mahato N, Sharma K, Sinha M, Baral E R, Koteswararao R. et al. 2020. Biosorbents, industrially important chemicals and novel materials from citrus processing waste as a s ustainable and renewable bioresource: A review. *J. Adv. Res.* **23**: 61-82.

Marin FR, Soler-Rivas C, Benavente-Garcia O, Castillo J and Perez-Alvarez J. 2007. By-products from different citrus processes as a source of customized functional fibres. *Food Chem.* **100 (2)**: 736-741.

Mariod AA. 2016. Effect of Essential oils on organoleptic (Smell, Taste and Texture) properties of food. Essential oils in food preservation, flavor and safety, Elsevier Inc., London UK, Academic Press, 131-137.

Minh Tu NT, Onishi Y, Choi HS, Kondo Y, Bassore SM, Ukeda H. et al. 2002. Characteristic odor components of Citrus sphaerocarpa Tanaka (Kabosu) cold-pressed peel oil. J. Agric. *Food Chem.* **50:** 2908–2913.

Mondello L, Casilli A, Tranchida PQ, Cicero L, Dugo P, and Dugo G. 2003. Comparison of fast and conventional GC analysis for Citrus essential oils. *J. Agric. Food Chem.* **51:** 5602–5606.

Murdock DI. and Allen WE. 1960. Germicidal effect of orange peel oil and d-limonene in water and orange juice: Fungicidal properties against yeast. *Food Technol.* **14**: 441–445.

Nguyen H, Campi E M, Roy Jackson W and Patti AF. 2009. Effect of oxidative deterioration on flavour and aroma components of lemon oil, *Food Chem.***112 (2)**: 388–393.

Njoroge SM, Koaze H, Karanja PN, and Sawamura M. (2005). Essential oil constituents of three varieties of Kenyan sweet oranges (Citrus sinensis). *Flavour Frag. J.* **20**: 80–85

Petretto GL, Sarais G, Maldini MT, Foddai M, Tirillini B, Rourke JP. et al. 2016. Citrus monstruosa discrimination among several Citrus species by multivariate analysis of volatiles: a metabolomic approach. *J. Food Process. Preserv.* **40**: 950–957.

Raeissi S, Diaz S, Espinosa S, Peters CJ and Brignole EA. 2008. Ethane as an alternative solvent for supercritical extraction of orange peel oils. *J. Supercrit. Fluid.* **45**: 306–313.

Ruberto G. and Rapisarda P. 2002. Essential oils of new pigmented citrus hybrids: Citrus sinensis L. Osbeck x C. clementina Hort. ex Tanaka. *J. Food Sci.* **67**: 2778–2780.

Sarrou E, Chatzopoulou P, Dimassi-Theriou K and Therios I. 2013. Volatile constituents and antioxidant activity of peel, flowers and leaf oils of Citrus aurantium L. growingin Greece. *Molecules.* **18**:10639–10647.

Sawamura M, Onishi Y, Ikemoto J, Minh Tu NT, and Lan Phi NT. 2006. Characteristic odour components of bergamot (Citrus bergamia Risso) essential oil. *Flavour Frag. J.* **21**: 609–615.

Subba MS, Soumithri TC and Suryanarayana R. 1967. Antimicrobial action of citrus oils. *J Food Sci.* **32**: 225–227.

Steuer B, Schulz H an d L¨ager E. 2 001. Classification and analysis of citrus oils by NIR spectroscopy. *Food Chem.***72 (1)**: 113–117.

Tranchida PQ, Bonaccorsi I, Dugo P, Mondello L and Dugo G. 2012. Analysis of Citrus essential oils: state of the art and future perspectives. A review. *Flavour Frag. J.* **27**: 98–123.

Tao N, Jia L, and Zhou H. (2014). Anti-fungal activity of Citrus reticulata Blanco essential oil against Penicillium italicum and Penicillium digitatum. *Food Chem.* **153**: 265–271.

Tripodo MM, Lanuzza F, Micali G, Coppolino R and Nucita F. 2004. Citrus waste recovery: a n ew environmentally friendly procedure to obtain animal feed. *Bioresour Technol.* **91**: 111–115.

Verzera A, Trozzi A, Zappalá M, Condurso C and Cotroneo A. 2005. Essential oil composition of Citrus meyerii Y. Tan. and Citrus medica L. cv. Diamante and their lemon hybrids. *J. Agric. Food Chem.* **53**: 4890–4894.

Worley B, and Powers R. 2013. Multivariate Analysis in Metabolomics. *Curr. Metabolomics.* **1(1)**: 92–107.

Wahyuni Y, Ballester AR, Tikunov Y, de Vos RCH, Pelgrom KTB, Maharijaya A, Sudarmonowati E, Bino RJ and Bovy AG. 2013. Metabolomics and Molecular Marker Analysis to Explore Pepper (Capsicum sp.) Biodiversity. *Metabolomics* **9**: 130–144.

Zema DA, Calabrò PS, Folino A, Tamburino V, Zappia G and Zimbone SM. 2018. Valorisation of citrus processing waste: A review. *Waste Manage.* **80**: 252-273.

Zema DA, Fòlino A, Zappia G, Calabrò PS, Tamburino V and Zimbone SM. 2018. Anaerobic digestion of orange peel in a semi-continuous pilot plant: An environmentally sound way of citrus waste management in agro-ecosystems. *Sci. Total Environ.* **630**: 401-408.

Zhang B, Chen J, He Z, Chen H and Kandasamy S. 2019. Hydrothermal liquefaction of fresh lemon-peel: parameter optimization and product chemistry. *Renew. Energy.***143**: 512–519.

JJBS

Volume 17, Number 1,March 2024
ISSN 1995-6673
Pages 21 – 27
https://doi.org/10.54319/jjbs/170103

Jordan Journal of Biological Sciences

Testing the Susceptibility of Some Potato Cultivars to Black Scurf Disease Caused by *Rhizoctonia solani* Kühn.

Sally Abo-Akel[1] , Walid Naffaa[2,*] Mohammed Jamal Mando[1]

[1]*General Commission for Scientific Agricultural Research (GCSAR), Damascus, Syria;*[2]*Damascus University, Faculty of Agriculture, Plant Protection Dept., 30621 Damascus, Syria.*

Received: February 20, 2023; Revised: June 5, 2023; Accepted: June 23, 2023

Abstract

Rhizoctonia stem canker and black scurf are among the most important diseases associated with potato (*Solanum tuberosum* L.) cultivation worldwide. Pathogenicity test of 19 isolates of *Rhizoctonia solani* Kühn obtained from four governorates in Syria revealed that isolates varied in their ability to cause disease with the isolate Rh15 being the most virulent in the development of the disease on potato plant under artificial infection. The relative susceptibility of seven commercial and local potato cultivars against *R. solani* was tested. The evaluation was based on black scurf severity and the negative impact of the disease on plant growth and expected effect on yield. The tested cultivars showed variable degrees of black scurf severity and consequent plant growth, but no completely immune cultivars were observed. Based on disease index (DI), potato varieties 'Agria', 'Ultra' and 'Labella' were highly susceptible to the disease; 'Spunta' was moderately resistant whereas 'Everest' was the most tolerant. Infection of the most susceptible cultivar "Afamia" resulted in the death of a large number of seedlings, large and deep canker on stems, with no formation of new tubers. Although 'Synergy' was moderately susceptible, and the black scurf incidence was higher than that of 'Everest' and 'Spunta', the loss of tubers weight was not significant compared to the previous two cultivars. The results suggested that use of tolerant and moderately resistant cultivars in Syria may help in reducing the development of black scurf on potatoes.

Keywords: Black scurf; cultivars; potato; *Rhizoctonia solani*; *Solanum tuberosum*; stem canker; susceptibility.

1. Introduction

Potato *Solanum tuberosum* L. is the third most important food crop in the world. In developing countries, potato production has greatly increased in the past two decades, and has now overtaken that in the developed world, indicating the increasing importance of potato as a main food crop to respond to the needs of increasing human populations (Birch *et al*., 2012). Potato cultivated area in the world reached more than 18 million hectares with a production of about 376.1 million tons (FAO, 2021). In Syria, potato production was estimated at 507,384 tons with a cultivated area of 22,369 hectares in 2016 (Annual Agricultural Statistical Group, 2016).

Stem canker and black scurf caused by *Rhizoctonia solani* Kühn. (telemorph *Thanatephorus cucumeris* (A.B. Frank) Donk is a serious disease of potato grown in cooler regions of the world (Yanar *et al*., 2005). *R. solani* causes appreciable yield losses each year, and losses caused by this pathogen have varied from 5% to 34% in different potato growing regions in the world (Carling and Leiner, 1990; Banville *et al*., 1996; Das *et al*., 2014). According to Keiser (2008), yield losses caused by black scurf disease reached 50%, resulting in important economic losses for potato growers. Abdo *et al*. (2012) confirmed the presence of the disease in most potato cultivation areas in Syria, where the infection rate of the disease was higher in the spring season than in autumn season with average incidence of 64.19% and 60.46% respectively.

Potato infection by Rhizoctonia diseases can occur at two different stages: infection of growing plants (Rhizoctonia stem canker) and infection of new tubers by sclerotia (black scurf). Either or both infection stages may be observed in potato crops (Banville *et al*., 1996; Ogoshi, 1987).

R. solani isolates can be classified into different anastomosis groups (AG), based on hyphal anastomosis in paired isolates grown in culture. Isolates belonging to the same AG are generally compatible and show a successful hyphal fusion, while isolates belonging to different AGs are usually incompatible and show unsuccessful anastomosis (Anderson, 1982; Carling, 1996; Carling *et al*., 2002; Kankam *et al*., 2021). Presently, 13 AGs are reported, several of which are divided into subgroups (Carling *et al*. 2002; Lees *et al*., 2002; Harikrishnan and Yang, 2004; Guleria *et al.*, 2007; Woodhall *et al*., 2007; Yang *et al*., 2015). Several studies confirm AG-3 as the main cause of both stem canker and black scurf of potato (Carling and Leiner, 1990; Moussa *et al.,* 2014). However, other AGs (AG-1, AG-2,1, AG-4, AG-5, AG-7, AG8, AG-9) have also been implicated in causing disease in potatoes (Okubara *et al*., 2008; Woodhall *et al*., 2007; Yanar *et al*., 2005; Campion *et al*., 2003; Lees *et al*., 2002; Sneh *et al*., 1996; Balali *et al*., 1995; Kankam *et al*., 2021). In Syria, two anastomosis groups (AGs) were identified: 47 isolates

* Corresponding author. e-mail: walid1851966@yahoo.com or ray-dya@scs-net.org.

(85.45%) belonged to AG3, only one isolate (1.81%) belonged to AG1, and 7 isolates (12.72%) remained unidentified (Abdo *et al*., 2012). A molecular study, using specific primers, showed that 78.95% of *R. solani* isolates belonged to the sub-group AG3- PT (Abo Akel *et al*., 2022).

Diseases caused by *R. solani* are traditionally controlled by the use of fungicides (Grosch *et al.,* 2005; Lahlali and Hijri, 2010). However, they have minor impact and may cause environmental pollution (Jiang *et al.,* 2005; Kurzawińska and Mazur, 2008). Consequently, a combination of crop rotation and resistant varieties offers the most practical and effective measure to control the disease (Scholten *et al*., 2001). Accordingly, the selection and cultivation of resistant potato cultivars has become one of the most economical and effective way to control tuber black scurf (Naz *et al.,* 2008).

The purpose of this study was to evaluate the susceptibility of some potato cultivars grown in Syria to *R. solani* under artificial infection.

2. Materials and Methods

2.1. Sample collection and pathogen isolation

Potato tubers showing typical symptoms of black scurf were collected from four different governorates (Homs, Aleppo, Daraa, Damascus countryside) in Syria. Samples were washed carefully under running tap water to remove the adjacent soil particles, surface sterilized with 1% sodium hypochlorite for 2 min, rinsed three times with sterile water and then were dried between two sterilized filter papers. Infected parts were cut using sterilized scalpel into small pieces (3-5 mm), transferred to plates of PDA supplemented with streptomycin sulfate (120 mg l^{-1}) to suppress bacterial growth, then incubated at 25 ± 1ºC for 7 days. Plates were daily observed for mycelial growth. Hyphal tips of mycelium emerging from the infected pieces were transferred to fresh plates of PDA (Sinclair and Dhingra, 2019; Naffaa *et al*., 2021). Pure cultures of *R. solani* isolates were identified microscopically on the basis described by Ogoshi (1996). The identified isolates were subcultured on PDA slants and kept at 4ºC for further studies.

2.2. Preliminary pathogenicity test

Nineteen isolates of *R. solani*, identified in another study as AG3 (Abo Akel *et al*., 2022), were used for pathogenicity tests. Potato tubers (cv. 'Spunta'), relatively similar in size with 6-7 buds, were surface sterilized by soaking in sodium hypochlorite (1%) for 3 min, then in ethanol 70% for one minute. After that, they were washed several times with sterilized water. Experimental layout Soil (clay, sand and peat 1: 1: 2 v) was sterilized twice in autoclave at 121ºC for 30 min. One tuber was planted at a depth of approximately 5 cm in a 50-cm plastic pot containing 6 kg of sterilized soil mixture. Each tuber was inoculated by adding 700 g of sterilized sand with 5 mycelial discs (5 mm) which were taken at the periphery of 7-day-old fungal colonies, then 500 ml of distilled water were added, and covered with the soil mixture (Simons and Gilligan, 1997). The same amount of autoclaved sand without mycelial discs was added to control. Three pots were used as replications for each isolate as well as for the control. The plants were grown in winter season at ambient temperature. The plants were harvested 5 weeks after planting. The average plant length was calculated. Since most plants did not form tubers, and some seedlings were killed (damping-off), a preliminary assessment of the pathogenicity was based on the percent of plant showing stem canker symptoms according to the following formula:

Disease incidence % = [(plant number in control – plant number in treatment) / plant number in control] × 100.

2.3. Susceptibility of potato cultivars to R. solani (Rh15)

Susceptibility of 7 commercial and local potato cultivars ['Spunta', 'Afamia', 'Benella', 'Everest', 'Ultra', 'Synergy', 'Agria', and 'Labella'] against the most virulent isolate *R. solani* (Rh15) was tested under greenhouse conditions. The isolate Rh15 was chosen based on the results of the preliminary pathogenicity test. Planting and inoculation methods were the same as described above for the pathogenicity test. Nine plots were used as replications for each cultivar as well as for the control. The plants were fertilized with a balanced NPK (2-3g/ liter of water), and watered when needed.

Average of plant lengths at the beginning of flowering stage, stem canker incidence (%), number and weight of tubers and the ratio of infected progeny tubers were noted 120 days after planting (Woodhall *et al*., 2008). The *tuber surface area covered with sclerotia* was used as a general method to evaluate potato black scurf severity based on the following rating scale: **0**: no sclerotia present, **1**: (< 1%), **2**: (2–10%), **3**: (11–20%), **4**: (21–50%), **5**: (≥ 51%) of tuber area covered. Disease index (DI) and relative resistance index (RRI) were calculated by the following formulas (Zhang *et al*., 2014).

$$DI = \frac{(n0 \times 0) + (n1 \times 1) + (n2 \times 2) + (n3 \times 3) + (n4 \times 4) + (n5 \times 5)}{y \times 5}$$

Where nx = number of tubers in severity class x,y = total number of tubers

$$PRI = 1 - \frac{DI_x}{DI_{\max}}$$

DI_x = disease index of the observed tuber, DI_{max} = the maximum disease index of all cultivars.

Black scurf resistance was measured with the relative resistance index (RRI) as follows: 0.00–0.39 = highly susceptible (HS), 0.40–0.59 = moderately susceptible (MS), 0.60–0.79 = moderately resistant (MR), 0.80–0.99 = highly resistant (HR), 1 = immune (I) (Zhang *et al*., 2014).

2.4. Statistical analysis:

One – way analysis of variance was carried out using SPSS15 statistical program at $P \leq 0.05$ (Gomez and Gomez, 1984).

3. Results and Discussion

3.1. Pathogen isolates

Nineteen fungal isolates were obtained from sclerotia of *R. solani* on potato tubers and identified based on their morphological characteristics (Table 1).

Table 1: *Rhizoctonia solani* isolates and their isolation sources

R. solani isolates	Isolates sources	
	Season	Area
Rh1, Rh2, Rh3, Rh4, Rh6, Rh7, Rh9, Rh11, Rh12, Rh13, Rh15, Rh17, Rh18	Spring (February, March, April)	Homs
Rh5, Rh19	Spring (February, March, April)	Aleppo
Rh10, Rh16	Summer (August, September)	Damascus countryside (Saasa)
Rh8, Rh14	Summer (August, September)	Daraa

3.2. Preliminary pathogenicity test

Nineteen *R. solani* isolates were tested for their pathogenicity to potato cultivar 'Spunta' in pots under artificial infection during winter season at ambient temperature. Isolates' pathogenicity was evaluated based on the percent of plants showing stem canker symptoms. It was not possible to assess the disease severity based on tuber surface area covered by sclerotia because a large number of plants did not form any new tubers, and this may be due to the prevailing environmental conditions during the experiment period, and also to the experiment duration. So, a preliminary evaluation of the isolates pathogenicity was based on their ability to cause stem cankers. Isolates showed significant differences of potato stem canker incidence (% plants showing stem canker). Isolates Rh4, Rh8, and Rh17 seemed to be non-pathogenic, whereas infection percentage varied between 2.26% for the isolates Rh14 and 38.64% for the isolates Rh2, Rh9 and Rh15 (Table 2).

The artificial infection with some *R. solani* isolates resulted in a significant reduction in plant height. The average plant heights ranged between 24.43 cm for the isolate Rh15 and 35.53 cm for the isolate Rh14 compared to the control (34 cm). In general, no correlation was observed between stem canker incidence and plant height. The disease did not negatively affect the plant growth for some isolates, whereas other isolates significantly reduced the plant growth. However, Rh15 isolated from Homs province, which led to the highest percentage of plants showing stem canker (38.64%) with significant reduction in plant growth (28.15%) compared to the control, was chosen for susceptibility test of some potato cultivars to *R. solani* infection.

Table 2: Pathogenicity of *Rhizoctonia solani* isolates on 'Spunta' potato cultivar under artificial infection

Isolates	Infection percentage %(1)	Average of plant heights (cm)	Isolates	Infection percentage %(1)	Average of plant heights (cm)
Rh1	31.82 ef	34.7 jk	Rh11	22.73 cd	27.5 bcd
Rh2	38.64 g	29.11cde	Rh12	13.64 b	25.92 ab
Rh3	22.73 cd	34.47 jk	Rh13	34.09 fg	30.67 efg
Rh4	0 a	27.51 bcd	Rh14	2.26 a	35.53 k
Rh5	34.09 fg	31.25 efghi	Rh15	38.64 g	24.43 a
Rh6	36.37 fg	26.33 abc	Rh16	27.28 de	32.67 ghijk
Rh7	18.18 bc	25.83 ab	Rh17	0 a	32.09 fghij
Rh8	0 a	34.1 ijk	Rh18	27.28 de	31.13 efgh
Rh9	38.64 g	31.44 efghi	Rh19	27.28 de	29.63 def
Rh10	20.46 c	26.33 abc	Control	-	34 hijk
LSD5%	6.72	2.9	LSD%	6.72	2.9

Values followed by the same letter do not differ significantly according to (LSD) least significant difference ($P \leq 0.05$).

These results are in according with other previous studies (Balkan and Wenham, 1973; Abdo *et al*., 2012). Pathogenicity test of 12 isolates showed significant differences between isolates where RS7 was the most virulent isolate in the development of the stem canker and black scurf disease on potato cv. 'Spunta' in Egypt (Abdel-Sattar *et al*., 2017). *R. solani* isolates, even under similar conditions, showed significant differences in infection severity and induced symptoms, suggesting the involvement of genetic factors in virulence differences (Rubio *et al*., 1996). Variance of isolates in pathogenicity was also attributed to difference between (AGs) where *R. solani* AGs, other than AG3, usually have low virulence against potato (Balkana and Wenham, 1973; Yanar *et al*., 2005; Khandaker *et al*., 2011; Abdel-Sattar *et al*., 2017). Jaradat *et al*. (2023) showed that *R. solani* AG-3PT was the primary pathogen associated with potato stem canker and black scurf diseases in Jordan. Carling and Leiner (1990) showed that virulence of *R. solani* isolates on potato may be affected by the source of isolates, where isolates recovered from lesions were more virulent than those obtained from sclerotia. Truter and Wehner (2004) found that isolates obtained from stem lesions or from sclerotia on tubers were more virulent than isolates obtained from asymptomatic tubers and soil.

3.3. Susceptibility of potato cultivars to Rhizoctonia solani infection

Based on the preliminary pathogenicity test results, the most virulent isolate (Rh15) was used for cultivar susceptibility test. Seven commercial and local potato cultivars were tested under artificial infection in pots. Tested cultivars showed variable degrees of black scurf

severity and subsequent plant growth and yield, but no completely immune cultivars were found.

Table 3 showed that 'Everest' cultivar had significantly lower black scurf incidence (31.15%), and lower percent of stem canker (11.1%) than the other six cultivars. Number and weight of tubers and plant length were also less affected by the infection. 'Spunta' showed black scurf incidence of 38.26%. Although the significant decrease in the number of tubers compared to the previous cultivar, no significant differences were observed between them in tuber weight loss and plant length reduction. This can be explained by the formation of few and relatively large tubers. A previous study reported that 'Spunta' was the most susceptible cultivar to this pathogen. However, 'Spunta' produced the highest progeny tuber weight but with a noticeable incidence of black scurf (Daami-Remadi *et al*., 2008). In contrast, according to Djébali and Belhassen (2010) investigation, 'Spunta' showed the least percentage of infection of progeny tubers by *R. solani* sclerotia at harvest.

Although the infected tubers incidence in 'Synergy' cultivar was relatively high (55.4%), this did not significantly affect the number and weight of the tubers, as the reduction in both was not significant compared to the less affected 'Everest' cultivar, and the stem canker incidence did not exceed 22.2%. Cultivars 'Labella', 'Agria' and 'Ultra' had a high rate of infected tubers and stem canker (76.67 and 67.8%, respectively in 'Agria'). The infection resulted in a significant yield loss.

Infection of the local variety 'Afamia' resulted in the death of a large number of seedlings, stem canker of all remaining plants, a relatively weak vegetative growth, and no formation of new tubers. Therefore, it was not possible to assess the effect of infection on plant growth and yield. This cultivar was ranked as highly susceptible to infection by *R. solani*.

Figure 1: Different degrees of covered area from the surface of potato tubers by *Rhizoctonia solani* sclerotia under artificial infection.

Table 3: Susceptibility of seven potato cultivars to the black scurf disease caused by *Rhizoctonia solani* Kühn (Rh15) under artificial infection

Cultivar		Percentage of progeny tubers infection (%)	Percentage of stem canker %	Number of tubers	Relative reduction in tubers Number %	Average weight of tubers (g)	Relative reduction in tubers weight %	Average length of plants (cm)	Relative reduction in plant length %
'Synergy'	*Infected*	55.4 c	22.2 b	9.56	22.47 a	425.36	23.34 a	46.9	13.47 ab
	Control	-	-	12.33	-	567.92	-	54.2	-
'Labella'	Infected	61.6 c	56.7 d	5.67	52.75 c	212	48.14 b	27.67	17.25 bc
	Control	-	-	12	-	408.83	-	33.44	-
'Spunta'	Infected	38.26 b	33.3 c	9.83	37.27 b	358.55	25.36 a	28.99	16.36 abc
	Control	-	-	15.67	-	480.35	-	34.66	-
'Agria'	Infected	76.67 d	67.8 e	3.67	63.3 d	179.3	56.93 c	38.39	17.64 c
	Control	-	-	10	-	416.33	-	46.61	-
'Ultra'	Infected	60 c	56.7 d	5.2	52.73 c	274.83	44.12 b	36.16	12.99 a
	Control	-	-	11	-	491.78	-	41.56	-
'Everest'	*Infected*	31.15 a	11.1 a	13	27.78 a	412.7	19.8 a	30.31	12.42 a
	Control	-	-	18	-	514.56	-	34.61	-
'Afamia'	*Infected*	-	100 f	-	-	-	-	22.9	40.22 d
	Control	-	-	16.67	-	245.11	-	38.31	-
LSD at 5%		6.73	10.12		7.99		7.07		4.1

Values followed by the same letter in the same column do not differ significantly according to LSD test (at $P \leq 0.05$).

Table 4 shows the evaluation of tuber black scurf resistance of the 7 tested potato cultivars. All cultivars were obviously infected, and black scurf severity induced by Rh15 varied significantly among cultivars tested. These results showed also that there were no immune cultivars, but that most were susceptible. 'Everest' was highly resistant (HR) with fewer and smaller sclerotia on tubers, and small superficial lesions scattered on stems. Only 'Spunta' showed moderate resistance. However, 'Agria', 'Ultra' and 'Labella' were highly susceptible to the disease, with disease index more than 34. The most susceptible cultivar 'Afamia' exhibited post-emergence stem death, large and deep canker on stems, without formation of new tubers. Although 'Synergy' was moderately susceptible (MS), and the black scurf incidence was higher than that of 'Everest' and 'Spunta', the loss of tubers weight was not significant compared to the previous two cultivars.

These results agree with other research. In fact, Bains *et al*. (2002) reported that potato cultivars showed variation in susceptibility to *R. solani*, but no cultivars were totally resistant to the black scurf disease. Yanar *et al*. (2005) showed that some of tested potato cultivars were highly susceptible to black scurf disease, but some cultivars had higher levels of resistance than the local susceptible cv. 'Batum' in Turkey. Potato cultivars showed different degrees of resistance to *R. solani,* but no completely resistant cultivars have been observed (Daami-Remadi *et al*., 2008; Djébali and Belhassen, 2010; Khandaker *et al*., 2011; Thangavel *et al*., 2014). In contrast, Singh *et al*. (2021) showed that out of eighteen potato varieties, three expressed immune response to stem canker and black scurf in India.

Otrysko and Banville (1992) suggested that range of susceptibilities may not indicate varying levels of resistance to *R. solani*, but may be due to the different levels of maturity of the cultivars. Bains *et al*. (2002) reported that cultivars with late maturity showed comparatively low levels of the disease, whereas, early and mid-maturing cultivars showed comparatively high levels of the disease, with some exceptions. The differences in cultivar susceptibility may be due to both inheritance and maturity levels of the cultivars. But these conclusions do not seem to be fully applicable to the cultivars tested in this study. The early-season cultivar 'Everest' showed a high level of resistance, while the early-season local cultivar 'Afamia' was in contrast highly susceptible. The other cultivars showed a range of susceptibility reactions to *R. solani*, and almost all of them are semi-early, except the early season cultivar 'Synergy'. This may indicate that the genotype of the variety is the most important factor in the resistance process.

Zhang *et al*. (2014) reported that the susceptibility was relatively stable across years, but some moderately resistant and susceptible cultivars may be changed from moderate resistance to moderate susceptibility or from moderate susceptibility to moderate resistance.

Some researchers have confirmed that the difference in susceptibility to infection is due to the nature of resistance in potato varieties (Zhang *et al*., 2016). Moreover, other factors, such as environment conditions, plant vigor, cuticular stricture, tuber maturity, genetic factors, and pathogenicity that affect the expression of potato resistance may also be the causes that affect potato resistance evaluation (Bains *et al*., 2002; Djébali and Belhassen, 2010; Leach and Webb, 1993; Otrysko *et al*., 1992).

Table 4: Assessment of susceptibility of seven potato cultivars to *Rhizoctonia solani* (Rh15) under artificial infection.

Cultivars	Disease Index (DI)	Relative Resistance Index (RRI)	Resistance evaluation
'*Synergy*'	26.81	0.41	MS
'Labella'	45.43	0	HS
'Spunta'	16.36	0.64	MR
'Agria'	35.85	0.21	HS
'Ultra'	34.02	0.25	HS
'*Everest*'	9.19	0.8	HR
'*Afamia*'	-	-	HS

4. Conclusion

The relative susceptibility test of seven commercial and local potato cultivars grown in Syria showed a range of susceptibility to the black scurf disease caused by *R. solani,* and no totally immune cultivars were found. Most of the tested cultivars were highly susceptible to the disease. 'Everest' was the most resistant cultivar whereas 'Spunta' was moderately resistant, and the local cultivar 'Afamia' was the most susceptible.

To our knowledge, this is the first study demonstrating the relative susceptibility of some potato cultivars grown in Syria to *R. solani*. In fact, it is very important to estimate the susceptibility degree to potato cultivars based on the density of the sclerotia formed on the tubers, which (in addition to the soil-borne inoculum) are considered important sources for the initiation of Rhizoctonia disease in potato plant. Further studies are needed to evaluate the susceptibility of other potato cultivars cultivated in Syria to stem canker and black scurf disease.

References

Abdel-Sattar MA, El-Marzouky H and Ibrahim EE. 2017. Pathogenicity test and anastomosis group of *Rhizoctonia solani* the causal organism of stem canker and black scurf disease of potato in Egypt. *J. Appl. Plant Prot*, **6**: 1-8. https://doi.org/10.21608/japp.2017.7494

Abdo RH, BayaaB and Abbas A. 2012. Determination of anastomosis groups within population of *Rhizoctonia* solani Kuhn in potato in Syria. *Arab J. Plant Prot*, **30:** 1-10. https://asplantprotection.org/wp-content/uploads/2018/07/1-10.pdf

Abo-Akel S, Naffaa W and Mando MJ. 2022. Morphological and molecular characterization of *Rhizoctonia solani* isolates causing black scurf disease to potato in some regions in Syria. *Syrian J. Agric. Res,* **9(1):** 352 – 368.

Anderson NA. 1982. The genetics and pathology of *Rhizoctonia solani. Annu. Rev. Phytopathol,* **20**:329-347. https://doi.org/10.1146/annurev.py.20.090182.0015 53

Annual Agricultural Statistical Collection. 2016. Agricultural Statistics Directorate, Ministry of Agriculture and Agrarian Reform, Damascus, Syria.

Bains PS, Bennypau HS, Lynch LDR, Kawchuk LM and Schaupmeyer CA. 2002. Rhizoctonia disease of potatoes *(Rhizoctonia solani):* fungicidal efficacy and cultivar susceptibility. *Am. J. Potato Res*, **79**: 99-106. https://doi.org/10.1007/BF02881518.

Balali G, Neate S, Scott E, Whisson D an d Wicks T. 1995. Anastomosis group and pathogenicity of isolates of *Rhizoctonia solani* from potato crops in South Australia. *Plant Pathol*, **44(6)**: 1050-1057. https://doi.org/10.1111/j.1365-3059.1995.tb02664.x.

Balkan H and Wenham H. 1973. Pathogenicity of potato sclerotial isolates of *Rhizoctonia solani* to potato shoots. *New Zealand J. Exp. Agr,* **1(4)**: 383-385. https://doi.org/10.1080/03015521.1973.10427931

Banville GJ, Carling DE and Otrysko BE. 1996. Rhizoctonia disease on potato. Pages: 321-330. [In:] **Rhizoctonia species. Taxonomy, Molecular Biology, Ecology, Pathology and Disease Control**.(Sneh, B.; S. Jabaji- Hare; S. Neate; G. Dijst [editor]). Dordrecht, Netherlands. Kluwer Academic.

Birch PRJ, Bryan G, Fenton B, Gilroy EM, Hein I, Jones JT, …Toth IK. 2012. Crops that feed the world 8: Potato: are trends of increased global production sustainable? *Food Secur*, **4**: 477-508. https://doi.org/10.1007/s12571-012-0220-1

Campion C, Chatot C, Perraton B and Andrivon D. 2003. Anastomosis groups, pathogenicity and sensitivity to fungicides of *Rhizoctonia solani* isolates collected on potato crops in France. *Eur. J. Plant Pathol*, **109(9)**: 983-992. https://doi.org/10.1023/B:EJPP.0000003829.83671.8f

Carling DE. 1996. Grouping in *Rhizoctonia solani* by hyphal anastomosis reaction. Pages: 37-47. [In:] **Rhizoctonia species taxonomy, molecular biology, ecology, pathology and disease control**. (Sneh, B.; S. Jabaji-Hare; S. Neate and G. Dijst [editor]). Dordrecht, Netherlands. Kluwer Academic Publishers.

Carling D andLeiner R. 1990. Virulence of isolates of *Rhizoctonia solani* AG-3 collected from potato plant organs and soil. *Plant Dis*, **74(11):** 901-903. https://doi.org/10.1094/PD-74-0901.

Carling D, Baird R, Gitaitis R, Brainard K and Kuninaga S. 2002. Characterization of AG-13, a newly reported anastomosis group of *Rhizoctonia solani*. *Phytopathol*, **92(8):** 893-899. https://doi.org/10.1094/PHYTO.2002.92.8.893.

Daami-Remadi M, Zammouri S and El Mahjoub M. 2008. Effect of the level of seed tuber infection by *Rhizoctonia solani* at planting on potato growth and disease severity. *African J. Plant Sci. Biotech*, **2:** 34-38. Corpus ID: 56245569.

Das S, Shah FA, Butler RC, Falloon RE, Stewart A, Raikar S and Pitman AR. 2014. Genetic variability and pathogenicity of *Rhizoctonia solani* associated with black scurf of potato in New Zealand. *Plant Pathol*, **63:** 651-666. https://doi.org/10.1111/ppa.12139.

Djébali N an d Belhassen T. 2010. Field study of the relative susceptibility of eleven potato (*Solanum tuberosum* L.) varieties and the efficacy of two fungicides against *Rhizoctonia solani* attack. *Crop Prot*, **29:** 998-1002. https://doi.org/10.1016/j.cropro.2010.06.012.

FAO. 2021. FAOSTAT. Food and Agriculture Organization of the United Nations.

Gomez KA and Gomez A. 1984. **Statistical Procedure for Agricultural Research**—Hand Book. John Wiley & Sons, New York.

Grosch R, Faltin F, Lottmann J, Kofoet A an d Berg G. 2005. Effectiveness of 3 antagonistic bacterial isolates to control *Rhizoctonia solani* Kühn on lettuce and potato. *Can. J. Microbiol*, **51:** 345-353. https://doi.org/ 10.1139/w05-002.

Guleria S, Aggarwal R, Thind TS and Sharma TR. 2007. Morphological and pathological variability in rice isolates of *Rhizoctonia solani* and molecular analysis of their genetic variability. *J. Phytopathol*, **155:** 654-661. https://doi.org/10.1111/j.14390434.2007.01291.x.

Harikrishnan R and Yang X. 2004. Recovery of anastomosis groups of *Rhizoctonia solani* from different latitudinal positions and influence of temperatures on their growth and survival. *Plant Dis*, **88:** 817-823. https://doi.org/10.1094/PDIS.2004.88.8.817.

Jaradat Z, Aldakil H, Tadros M, Alboom M and Khataybeh B. 2023. *Rhizoctonia solani* AG-3PT is the major pathogen associated with potato stem canker and black scurf in Jordan[J]. *AIMS Agric. Food*, **8(1)**: 119-136. https://doi: 10.3934/agrfood.2023006.

Jiang JZ, Wu SY and Zhao LK. 2005. Resistance of potato tuber slices against *Rhizoctonia solani* induced by abiotic factors. *J. Hebei Univ. (Nat. Sci. Ed)*, **25:** 167–172.

Kankam F, Larbi-Koranteng S and Adomako J. 2021. Rhizoctonia disease of potato: Epidemiology, toxin types and management. *Egypt. J. Phytopathol*, **49(1):** 197-209. https://doi:10.21608/ejp.2021.72057.1028.

Keiser A. 2008. *Rhizoctonia solani*—a fungal disease with multiple symptoms: means of preventive and curative control. *In*: Potato Research for a Pr oduction of Quality. Information Day, February 2008, Changins.

Khandaker MM, Khair A and Bhuiyan MKA. 2011. Disease reaction of potato germplasms and true potato seeds against *Rhizoctonia solani* Kuhn. *Bangladesh J. Bot*, **40:** 193–196. https://doi.org/10.3329/bjb.v40i2.9777.

Kurzawińska H and Mazur S. 2008.Biological control of potato against *Rhizoctonia solani* (Kühn). *Sodininkystė ir Daržininkystė*, **27:** 419–425. http://www.lsdi.lt/straipsniai/27-2/27(2)-43.pdf.

Lahlali R and Hijri M. 2010.Screening, identification and evaluation of potential biocontrol fungal endophytes against *Rhizoctonia solani* AG3 on potato plants. *FEMS Microbiol. Lett*, **311:** 152–159. https://doi.org/10.1111/j.1574-6968.2010.02084.x.

Leach SS and Webb RE. 1993.Evaluation of potato cultivars, clones and a tr ue seed population for resistance to *Rhizoctonia solani*. *Am. Potato J*, **70:** 317–328. https://doi.org/10.1007/BF02851425.

Lees AK, Cullen DW, Sullivan L and Nicolson KJ. 2002. Development of conventional and quantitative real-time PCR assays for the detection and identification of *Rhizoctonia solani* AG-3 in potato and soil. *Plant Pathol*, **51:** 293-302. https://doi.org/10.1046/j.1365-3059.2002.00712.x.

Moussa T, Khalil MS, Gomaa NM and Al-Hazzim RA. 2014. Biodiversity of *Rhizoctonia solani* AG3 and AG2-1 associated with potato diseases. *Life Sci. J*, **11:** 407-417.

Naffaa W, Al-Jaramany L, Elbenay A and Al-Mhethawi R. 2022. Biological control of tomato damping-off and potato black scurf by seed treatment with *Trichoderma harzianum*. *Jordan J. Biol. Sci*, **15 (3):** 373 – 380. https://doi.org/10.54319/jjbs/150305.

Naz F, Rauf CA, Abbasi NA, Haque I, AhmadI. 2008. Influence of inoculum levels of *Rhizoctonia solani* and susceptibility on new potato germplasm. *Pak. J. Bot*, **40:** 2199–2209.

Ogoshi A. 1987. Ecology and pathogenicity of anastomosis and intraspecific groups of *Rhizoctonia solani* Kühn. *Annu. Rev. Phytopathol*, **25:** 125–143. https://doi.org/10.1146/annurev.py.25.090187.001013.

Ogoshi A.1996. Introduction: The genus *Rhizoctonia*. Pages: 1-9 [In:] **Rhizoctonia Species. Taxonomy, Molecular Biology, Ecology, Pathology and Disease Control**.(Sneh, B.; S. Jabaji-Hare; S. Neate and G. Dijst [editor]).Kluwer Academic Dordrecht, Netherlands.

Okubara PA, Schroeder KL and Paulitz TC. 2008. Identification and quantification of *Rhizoctonia solani* and *R. oryzae* using real-time polymerase chain reaction. *Phytopathol*, **98:** 837-847. https://doi.org/10.1094/PHYTO-98-7-0837.

Otrysko BE and Banville GJ. 1992. Effect of infection by *Rhizoctonia solani* on the quality of tubers for processing. *Am. Potato J*, **69:**645-652.
https://doi.org/10.1007/BF02852677.

Rubio V, Tavantzis SM and Lakshman DK. 1996. Extrachromosomal Elements and Degree of Pathogenicity in *Rhizoctonia Solani*. In: Sneh B., Jabaji-Hare S., Neate S., Dijst G. (eds) **Rhizoctonia Species: Taxonomy, Molecular Biology, Ecology, Pathology and Disease Control**. Springer, Dordrecht. https://doi.org/10.1007/978-94-017-2901-7_11

Scholten OE, Panella L, de Bock TSM and Lange W. 2001. A greenhouse test for screening sugar beet (*Beta vulgaris*) for resistance to *Rhizoctonia solani*. *Eur. J. Plant Pathol*, **107(2)**: 161-166.
https://doi.org/10.1023/A:1011208903344.

Simons SA and Gilligan CA. 1997. Relationships between stem canker, stolon canker, black scurf (*Rhizoctonia solani*) and yield of potato (*Solanum tuberosum*) under different agronomic conditions. *Plant Pathol*, **46:** 651–658.
https://doi.org/10.1046/j.13653059.1997.d01-54.x

Sinclair JB and Dhingra OD. 2019. **Basic Plant Pathology Methods**, 2nd Ed. CRC Press, Boca Raton, 448 pp.

Singh PK, Patidar JK, Singh R and Roy S. 2021. Screening of potato varieties against black scurf caused by *Rhizoctonia solani* Kuhn. *Int. J. Curr. Microbiol. Appl. Sci*, **10(1):** 1444-1449.
https://doi.org/10.20546/ijcmas.2021.1001.171.

Sneh B, Hare SJ, Neate S an d Dijst G. 1996. ***Rhizoctonia* species.Taxonomy, Molecular, Biology, Ecology, Pathology and disease control**. Kluwer Academic Publishers, Dordrecht the Netherland: pp. 580.

Thangavel T, Tegg R and Wilson C. 2014. Resistance to multiple tuber diseases expressed in soma clonal variants of the potato cultivar Russet Burbank. *Sci. World J*, 417697. https://doi.org/10.1155/2014/417697.

Truter M and Wehner F. 2004. Anastomosis grouping of *Rhizoctonia solani* associated with black scurf and stem canker of potato in South Africa. *Plant Dis*, **88(1)**: 83-83. https://doi.org/10.1094/PDIS.2004.88.1.83B

Woodhall JW, Lees AK, Edwards SG and Jenkinson P. 2007. Characterization of *Rhizoctonia solani* from potato in Great Britain. *Plant Pathol*, **56:** 286–295.
https://doi.org/10.1111/j.1365-3059.2006.01545.x

Woodhall JW, Lees AK, Edwards SG and Jenkinson P. 2008. Infection of potato by *Rhizoctonia solani*: Effect of anastomosis group. *Plant Pathol*, **57:** 897–905.
https://doi.org/10.1111/j.1365-3059.2008.01889.x.

Yanar Y, Yilmaz G, Cesmeli I and Coskun S. 2005. Characterization of *Rhizoctonia solani* isolates from potatoes in Turkey and screening potato cultivars for resistance to AG-3 isolates. *Phytoparasitica*, **33:** 370-376.
https://doi.org/10.1007/BF02981304

Yang Y, Zhao C, Guo Z and Wu X. 2015. Anastomosis group and pathogenicity of *Rhizoctonia solani* associated with stem canker and black scurf of potato in China. *Eur. J. Plant Pathol*, **143(1):** 99-111. https://doi.org/10.1007/s12230-016-9535-3.

Zhang XY, Yu XX, Yu Z, Xue YF and Qi LP. 2014. A simple method based on laboratory inoculum and field inoculum for evaluating potato resistance to black scurf caused by *Rhizoctonia solani*. *Breed. Sci*, **64:** 156–163.
https://doi.org/10.1270/jsbbs.64.156.

Zhang XY, Huo HL, Xi XM, Liu LL, Yu Z and Hao JJ. 2016. Histological observation of potato in response to *Rhizoctonia solani* infection. *Eur. J. Plant Pathol*, **145(2):** 289-303. https://doi.org/10.1007/s10658-015-0842-1.

JJBS

Volume 17, Number 1,March 2024
ISSN 1995-6673
Pages 29 – 36
https://doi.org/10.54319/jjbs/170104

Jordan Journal of Biological Sciences

Expression, Significance, and Impact on Survival of Fatty Acid Binding Proteins 4 and 7 in Colorectal Cancer: A Tissue Microarray Study

Nisreen Abu Shahin[1,3,*], Ahmad Alhessa[1], Tasneem Alhusani[1], Akram Kilani[2], Dana Alqatawneh[2], Ahmad Qarajeh[2], Yousef Omar[2], Mohammad Al-Sanouri[2], Tamer Barakat[2], Bahaa Abdelrahim[2], Heyam Awad[1,3]

[1] *Department of Pathology, Microbiology, and Forensic Medicine/ Faculty of Medicine, University of Jordan, Amman 11942, Jordan;* [2] *Faculty of Medicine, University of Jordan, Amman 11942, Jordan;* [3] *Pathology Section, Department of laboratories, Jordan University Hospital, Amman 11942, Jordan*

Received: March 15, 2023; Revised: June 4, 2023; Accepted: July 3, 2023

Abstract.

Background. Colorectal cancer (CRC) remains a major cause of cancer-related morbidity and mortality worldwide. Recently, the pathogenesis of CRC among other cancer types has been linked to lipid metabolism. Fatty acid-binding proteins (FABPs) are a protein-family expressed in multiple tissues and play a crucial role in lipid metabolism. A few recent studies have examined FABPs role in CRC. Our aims are to explore the immunohistochemical expression of fatty acid binding proteins (FABP) 4 and 7 in colorectal cancer, and correlate their expression levels with clinical, histopathological features, and survival.

Methods. A retrospective review of colorectal cancer biopsies over a 5-year period was conducted in our institute. Clinical and histological data were collected. Immunohistochemical staining for FABP 4 and 7 was performed using microarray and their expression was evaluated using the Histologic score (HS). The correlations between the expression of FABP 4 and 7 and clinicopathological parameters were determined by Fisher's exact test**.** The impact of the expression on the overall survival was determined using Kaplan–Meier survival analysis.

Results. 125 CRC tissue biopsy blocks were included. Median follow-up time was 35 months. High FABP4 expression was observed in 107 (85.60%). For FABP7, only 8.8% of cases (11/125) showed high expression. Co-expression of FABP4 and FABP7 occurred in 11 cases (8.8%). FABP7 expression correlated with age (p = 0.001). The median overall survival of patients with high expression of FABP4 was 43.00 ± 3.01 months, whereas patients showing low/negative expression reported a survival of 24. 00 ± 6.24 months(p =0.041). No statistically significant association between FABP7 high expression and the overall survival was detected (Log-Rank test, p = 0.086).

Conclusion. FABP4 expression in CRC is higher than that of FABP7. FABP7 expression levels negatively correlate with the age of CRC patients. FABP4 expression is associated with a better survival in CRC. No significant association between FABP4 and 7 with tumor grade, stage, or other clinicopathological criteria has been found in this study.

Keywords: colorectal carcinoma; fatty acid-binding proteins; FABP4; FABP7; survival.

1. Introduction

CRC remains a major type of cancer in adults; and despite being studied for decades, it continues to be one of the leading causes of cancer mortality worldwide (Favoriti et al. 2016). In addition, about a third of CRC patients are diagnosed at an advanced stage, during which many cases are resistant to chemotherapy(Amiri et al. 2018)(Jaganathan et al. 2014)(Gupta et al. 2019). This dictates the need for novel treatments to manage CRC.

Understanding the molecular mechanisms involved in cancer development can aid in finding new treatment modalities. Some studies have found a relationship between the pathogenesis of certain cancers and lipid storage, uptake, and synthesis(Furuhashi M 2010)(Jung, Kim, and Koo 2015)(Amiri et al. 2018)(Kagawa et al. 2019). The effect of lipids on promoting tumor growth is mediated by inflammatory reactions and changes in the microenvironment, as well as by circulating inflammatory and metabolic mediators(H. Zhao et al. 2022). On the other hand, inhibition of lipid synthesis can suppress cancer development, as the inhibition of lipid storage may decrease the protection against reactive oxygen species toxicity, reduce cell survival exposed to hypoxia-reoxygenation in vitro, and hence may inhibit tumorigenesis in vivo (Bensaad et al. 2014)(McKillop, Girardi, and Thompson 2019).

Fatty acid-binding proteins (FABPs) belong to a protein family that exists in multiple tissues and plays a

* Corresponding author. e-mail: n.abushahin@ju.edu.jo .

** **Abbreviations**: FABP: fatty acid binding, proteinCRC: colorectal cancer,TMA: Tissue microarray

crucial role in lipid metabolism (Coe and Bernlohr 1998). FABP4 (adipocyte FABP (A-FABP) or aP2)(Furuhashi M 2010) is a gene located on chromosome 8q21 a nd expressed in adipose tissues and other tissues (Amiri et al. 2018; Jung, Kim, and Koo 2015; McKillop, Girardi, and Thompson 2019). FABP7 (Brain typed FABP; Brain Lipid Binding Protein),(Furuhashi M 2010) is mainly identified in brain neural tissues.(Liu et al. 2010)(Alshareeda et al. 2012)(Jung, Kim, and Koo 2015).

FABPs act as intracellular lipid chaperones that play a role in the intake, transference, signal transduction, and packing of long-chain fatty acids (Coe and Bernlohr 1998). Several studies investigated the link of F ABPs and lipid metabolism with neoplasia (Bensaad et al. 2014)

FABP 4 and 7 are expressed in several types of human malignancies, such as gliomas, renal cell carcinomas, breast cancers, and others (Mukherjee et al. 2020; Zeng, Sauter, and Li 2020; Sun and Zhao 2022)(Kagawa et al. 2019). The link between CRC and FABP4 and 7 expressions has not been adequately investigated. Few recent studies have shown that FABP4 and FABP7 may promote invasion and metastasis of CRC. The mechanism of promoting invasiveness maybe, in part, through improvingepithelial-mesenchymal transformation (EMT)of CRC cells, as documented by Tian et al withFABP4 overexpression leading to upregulation of S nail, matrix metalloproteinase (MMP-2 and MMP-9), and downregulation of E-cadherin. Moreover, Ma et al. have demonstrated that FABP7-overexpression activates CRC cell proliferation, and inhibits apoptosis, which are vital processes in cancer aggression and metastasis. On the contrary, FABP7 knockdown may negatively impact CRC cell proliferation and survival (Ma et al. 2018; Tian et al. 2020). FABP4 expression was found to be a risk factor for CRC progression , and it could be a biomarker for CRC diagnosis (Y. Zhang et al. 2019). Due to their role in tumor development, FABPs may become potential targets in cancer treatment (Sun and Zhao 2022).

The aims of t his work are to define the rate of immunohistochemical expression of FABP4 and FABP7 in CRC, and to inspect the link with the clinical and histopathological features of CRC as well as with survival. The current study is the first of its kind in our population, and its significance is to explore the relationship of FABP 4 & 7, if any, with patient's survival, clinical, and histological parameters like CRC tumordifferentiation, stage, and lymph node invasion.

2. Materials and methods

This study is retrospective and cross sectional covering the period from 1/7/2016 until 31/12/ 2021. It includes 125 tissue samples obtained from colorectal carcinoma cases. The Institutional Review Board (IRB) approves the study in its decision no. (55-2022).

2.1. Patients and tissues.

One hundred and twenty-five cases diagnosed with CRC are retrospectively selected from the electronic database of t he Department of P athology. Inclusion criteria are: (*i*) adults above 18 years old; (*ii*) confirmed pri mary colorectal adenocarcinoma (*iii*) Paraffin blocks from CRC tissue biopsies or s urgical resection specimens are available in our archives. Exclusion criteria are: (*i*) colon cancer other than adenocarcinoma (for e xample gastrointestinal stromal tumors and lymphomas), (*ii*) history of n eoadjuvant or adjuvant therapy and (*iii*) paraffin tissue blocks that are not available or insufficient.

2.2. Tissue microarray construction (TMA).

Eight TMA blocks are constructed from the 125 archival paraffin blocks using a manual tissue microarrayer (Array mold Kit A, Catalogue # IW-110, IHC World/ USA). Representative tumor area is recognized on Hematoxylin and Eosin-stained slides and discerned on the paraffin blocks by two pathologists (N.A. and H.A.). Following instructions that are previously used in literature(Fowler et al. 2011), two cylindrical cores of 2-mm diameter each are removed from the blocks using a dermal biopsy punch and transferred to the TMA recipient blocks. Then *4*-micrometers (µm) sections are cut from each TMA block using an automatic rotary microtome *(*Microm HM355 S, Thermo Fisher Scientific Inc., USA) and are stained using immunohistochemistry.

2.3. Immunohistochemistry (IHC).

A standardized IHC protocol is performed in accordance to literature(Walker 2006; Taylor and Levenson 2006) and manufacturer's instructions. 4-µm-thick paraffin-embedded tissue sections (PETS) are de-waxed with xylene (twice for 5 minutes) then rehydrated by descending alcohol series (100%, 95%, and70% alcohol, 5 minutes each). Antigen unmasking is performed using a water bath for 15 m inutes at 95°C i n Coplin jars containing sodium citrate buffer for FABP7 (pH=6.0) and Tris/ethylene diamine tetra-acetate buffer for FABP4 (pH=9.0). Next, PETS are rinsed with phosphate-buffered saline (PBS;pH=7.2) and with 3% hy drogen peroxide (H2O2) for 10 m inutes at room temperature to ablate endogenous peroxidase. Next, PETS are incubated with serum blocking reagent G (CTS005; R&D Systems, Minneapolis, MN) in PBS for 60 m inutes to prevent non-specific binding. The sections are incubated with rabbit polyclonal anti-FABP4 (1:750, NBP1-89218, Novus biological/ USA) and rabbit polyclonal anti-FABP7 (1:600, NBP1-88648, Novus biological/ USA) for 90 minutes at room temperature. After rinsing with PBS buffer, sections are then incubated for 30 m inutes with anti-rabbit HRP secondary antibody (ab236466, Abcam, Cambridge, UK). The chromogenic reaction is performed with 3-diaminobenzidine solution (CTS005; R&D Systems, Minneapolis, MN/USA) at room temperature in darkness for 7 min. After rinsing with PBS buffer, the sections are counterstained with Mayer's Hematoxylin solution, for 4 min at room temperature. Finally, the sections are dehydrated with ascending alcohol (70%, 95%, and 100%) and mounted with dibutyl phthalate in xylene mounting media (BCBX0183, Sigma/ Germany) and cover-slipped.

Thyroid cancer and nevus tissue samples are used as positive controls for FABP4 and FABP7, respectively(Coe and Bernlohr 1998)(Hewitt et al. 2014). PBS is utilized as a negative control.

2.4. IHC scoring.

Two pathologists using an Olympus CX41 upright light microscope (Olympus / Tokyo / Japan) evaluated the IHC results. Expression of F ABP4 and FABP7 is scored

according to cytoplasmic staining intensity (0 points = no staining, 1 = weak, 2 = moderate, and 3 = strong staining) and percentage of positive cells (0 points (0-25%), 1 point (26-50%), 2 points (51-75%), and 3 points (76-100%)). The total Histological Score (HS) is calculated by multiplying the staining intensity score and percentage score. Using comparable methodology to the previous studies, (Chen et al. 2021; Zang et al. 2021; C. Zhang et al. 2020) we considered HS scores of 3 or less as low expression, while HS that is equal to or greater than 4 as high expression.

2.5. Statistical analysis.

The relationship of FABP4/ FABP7 expression and the clinicopathological features is determined using Fisher's exact test (two-sided). Overall survival time is calculated from the date of surgical resection of CRC to the date of death from any cause or l ast follow-up date. Survival probabilities of pa tients based on t heexpression status of FABP4 and FABP7 are estimated using the Kaplan-Meier approach and compared with the log-rank test. Two-tailed P values ≤0.05 are considered statistically significant. Analyses are made using Statistical Package for Social Sciences (SPSS) version 26 software (SPSS Inc., Chicago, Illinois, United States).

3. Results

3.1. Demographical and clinicopathological characteristics of the study patients.

One hundred and twenty five CRC t issue samples belonging to 125 patients are included in this study. The median patients' age is 55.14 years (range: 18–85). 71 (56.8%) patients are males with a male-to-female ratio of 1.3:1. Pathological evaluation shows that 105 (84%) tumors are colorectal adenocarcinoma, and 20 (16%) tumors are mucinous colorectal adenocarcinoma. Both Demographical and clinicopathological characteristics are summarized in Table 1.

Table 1. Demographic and clinicopathological characteristics of study population.

Feature		Number	Percentage
Age (Years)	<50	52	41.6
	≥50	73	58.4
Gender	Female	54	43.2
	male	71	56.4
Histological type	Adenocarcinoma	105	84.0
	Mucinous carcinoma	20	16.0
Grade (differentiation)	Well	10	8.0
	moderate	104	83.2
	poor	11	8.8
Tumor T Stage	T1	1	0.8
	T2	17	13.6
	T3	75	60.0
	T4	32	25.6
Lymph node metastasis	Present	74	59.2
	Absent	51	40.8
Lymphovascular invasion	Present	46	36.8
	Absent	79	63.2
Perineural invasion	Present	19	15.2
	Absent	106	84.8

3.2. Expression of FABP4 and FABP7 in CRC.

Overall, high FABP4 immuno-expression in tumor cells is observed in 107/125 (85.60%) (Figure 1A). Low/negative FABP4 immuno-expression in tumor cells is observed in 18/125 (14.4%) (Figure 1B). On the other hand, only 8.8% of cases (11/125) show high expression of FABP7 (Figure 1C). Low/negative FABP7 expression in tumor cells is observed in 114/125 (91.2%) (Figure 1D). Co-expression of FABP4 and FABP7 proteins is ascertained in 11 cases (8.8%). Figure 2 demonstrates IHC staining intensity for FABP 4 and 7.

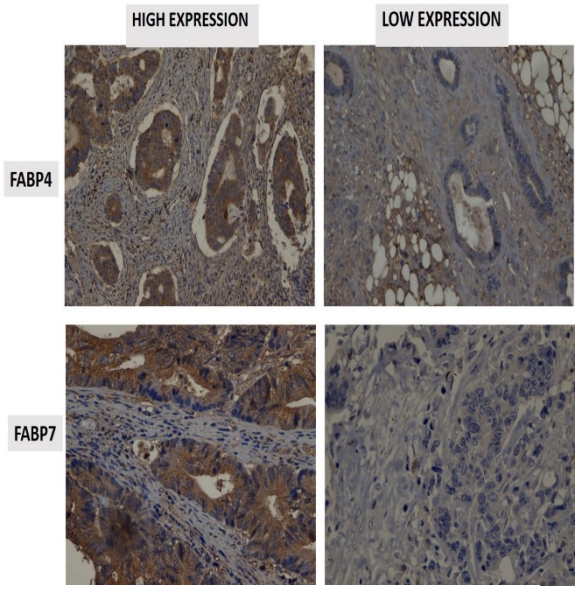

***Figure** 1.* Representative images of immunohistochemistry for FABP4 and FABP7 protein expression in colorectal cancer tissue samples. Light microscopy; original magnification upper panel 200X, and lower panel 400X.

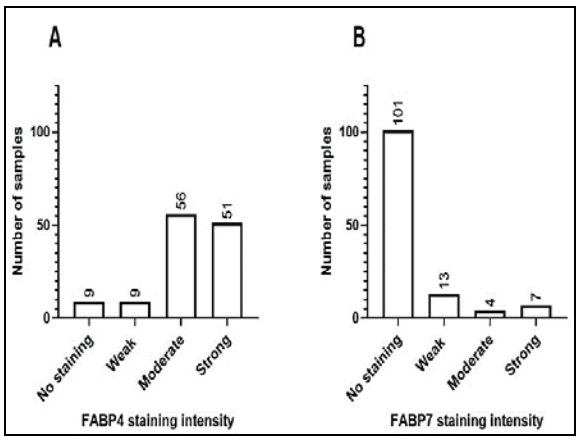

Figure 2. Staining intensity results for FABP4 and FABP7 protein in colorectal cancer cells.

3.3. Correlation between FABP4 and FABP7 expression with clinicopathological characteristics.

Table 2 details the correlation between FABP4 and FABP7 expression and the clinico-pathological features.

There is a significant difference of F ABP7 expression in patients below 50 years of age (19.2% high expression rate) and those aged fifty and above (1.4% high expression rate), ($p = 0.001$). However, there is no statistical significance of FABP7 expression with respect to gender, tumor grade, T stage, and lymph node metastasis or perineural or lymphovascular invasion.

There is no s ignificant correlation between FABP4 expression and any of the clinico-pathological variables.

Table 2. Clinicopathological variables and the expression of FABP4 and FABP7 in corresponding colorectal carcinoma tissue samples.

	FABP4			FABP7		
Variables	Low/no expression	High expression		Low/ no expression	High expression	
	n (%)	*n* (%)	*P Value*	*n* (%)	*n* (%)	*p Value*
Age (years)						
≦50	8 (15.4)	44 (84.6)	0.801	42 (80.8)	10 (19.2)	0.001*
>50	10 (13.7)	63 (86.3)		72 (98.6)	1 (1.4)	
Gender						
Female	5 (9.3)	49 (90.7)	0.201	50 (92.6)	4 (7.4)	0.756
Male	13 (18.3)	58 (81.7)		64 (90.1)	7 (9.9)	
Histologic type						
Adenocarcinoma	15 (14.3)	90 (85.7)	1.000	96 (91.4)	9 (8.6)	0.689
Mucinous	3 (15.0)	17 (85.0)		18 (90.0)	2 (10.0)	
Degree of differentiation						
Well	3 (30.0)	7 (70.0)	0.221	9 (90.0)	1 (10.0)	1.000
Moderate	13 (12.5)	91 (87.5)		95 (91.3)	9 (8.7)	
Poor	2 (18.2)	9 (81.8)		10 (90.9)	1 (9.1)	
Tumor T-Stage						
T1	0 (0.0)	1 (100.0)	0.677	1 (100.0)	0 (0.0)	0.345
T2	2 (11.8)	15 (88.2)		16 (94.1)	1 (5.9)	
T3	13 (17.3)	62 (82.7)		70 (93.3)	5 (6.7)	
T4	3 (9.4)	29 (90.6)		27 (84.4)	5 (15.6)	
Lymph node metastasis						
Absent	7 (13.7)	44 (86.3)	1.000	47 (92.2)	4 (7.8)	1.000
Present	11 (14.9)	63 (85.1)		67 (90.5)	7 (9.5)	
Lymphovascular invasion						
Absent	12 (15.2)	67 (84.8)	0.798	72 (91.1)	7 (8.9)	1.000
Present	6 (13.0)	40 (87.0)		42 (91.3)	4 (8.7)	
Perineural invasion						
Absent	14 (13.2)	92 (86.8)	0.475	97 (91.5)	9 (8.5)	0.674
Present	4 (21.1)	15 (78.9)		17 (89.5)	2 (10.5)	

3.4. Survival analysis.

The impact of FABP4/ FABP7 protein expression on overall survival is investigated using Kaplan–Meier survival analysis. The Median follow-up time after surgical resection is 35 months, and 16 deaths (12.8%) are documented. The median overall survival of patients with high expression of F ABP4 is 43.00 ± 3.01 months, which is significantly better than that of patients with low/negative expression of FABP4 (24.00 ± 6.24 months, p =0.041). On another hand, Kaplan–Meier analysis exposes no s ignificant association between FABP7 expression and overall survival (Log-Rank test, p = 0.086) (Figure 3).

Univariate and multivariate Cox proportional hazards regression are calculated to detect impact of FABP4 and 7 expression along with other variables on overall survival of CRC patients (Tables 3 and 4).

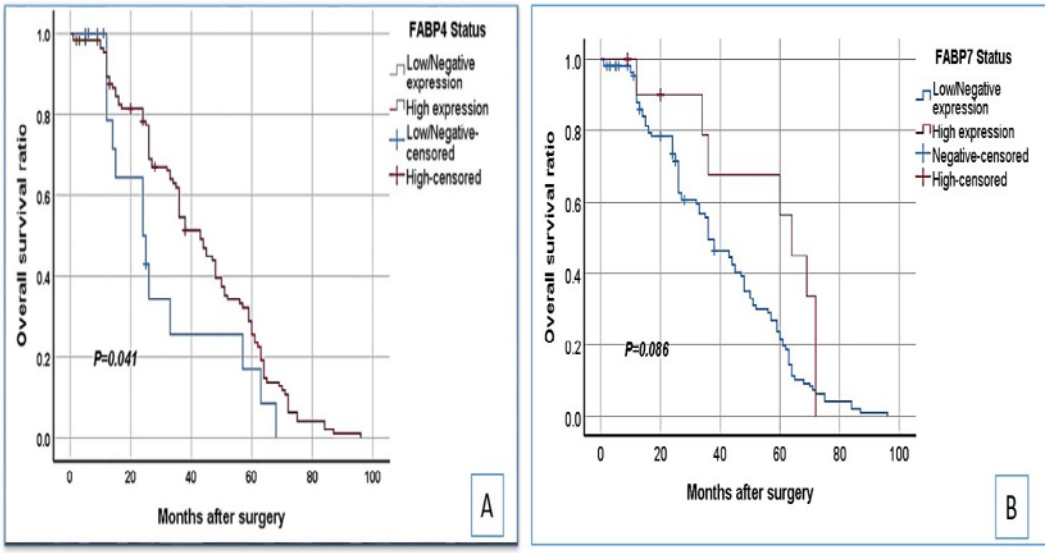

Figure 3. Kaplan-Meier survival analysis for patients with colorectal cancer according to FABP4 status (A) and FABP7 status (B).

Table 3. *Univariate Cox proportional hazards regression* to detect the influences *FABP4 and FABP7 expression and other variables on overall survival of CRC patients.*

Univariate Cox proportional hazards regression					
Variable		Odd ratio	95% C.I.		p
			Lower	Upper	
FABP4 expression	High vs Low	3.622	1.221	10.745	0.020
FABP7 expression	High vs Low	0.694	0.156	3.076	0.630
Age	< 50 vs ≥ 50	1.141	0.412	3.158	0.799
Gender	Female vs Male	0.624	0.226	1.721	0.362
Lymphovascular invasion	Present vs Absent	0.807	0.287	2.268	0.684
Perineural invasion	Present vs Absent	0.445	0.141	1.401	0.166
Lymph node metastasis	Present vs Absent	1.176	0.426	3.249	0.754
Degree of differentiation	Well vs Moderate vs Poor	1.392	0.414	4.683	0.593
Tumor T-Stage	T1 vs T2 vsT3 vsT4	2.589	1.092	6.137	0.031

Table 4. *Multivariate Cox proportional hazards regression* to detect influences *of FABP4, FABP7 protein expression and other variables on overall survival of colorectal cancer patients.*

Multivariate Cox proportional hazards regression					
Variables		Odd ratio	95.0% CI		p
			Lower	Upper	
FABP4 expression	High vs Low	0.176	0.053	0.586	0.005
FABP7 expression	High vs Low	1.880	0.318	11.105	0.486
Age	< 50 vs ≥ 50	1.994	0.684	5.818	0.206
Gender	Female vs Male	1.016	0.317	3.257	0.979
Lymphovascular invasion	Present vs Absent	1.328	0.428	4.121	0.623
Perineural invasion	Present vs Absent	1.665	0.505	5.495	0.402
Lymph node metastasis	Present vs Absent	0.451	0.141	1.443	0.180
Degree of differentiation	Well vs Moderate vs Poor	1.029	0.284	3.735	0.965
Tumor T-Stage	T1 vs T2 vsT3 vsT4	3.373	1.190	9.560	0.022

4. Discussion

The current work has utilized TMA(Camp, Neumeister, and Rimm 2008)(Hutchins and Grabsch 2018)as the method for tissue processing; and IHC for studying FABP 4/ 7 e xpression. This technique has been in use for 2 decades in oncology research. TMA proves to be a co st-effective and rapid scheme to examine large sample numbers. TMA has been utilized in colorectal cancer diagnostic and prognostic studies (Knösel et al. 2005).

This study proposes that 58.6% of CRC c ases show high FABP4 expression but only a minority (8.8%) exhibit high expression of F ABP7**.** It also demonstrates that expression of FABP7 correlates with younger patient's age (p = 0.001). Interestingly, the overall survival is

statistically longer with high expression compared to low expression of F ABP4 (p =0.041). We observe no association between FABP4 or FABP7 expression and other clinicopathological characteristics. No significant association is detected between FABP7 expression and overall survival (Log-Rank test p = 0.086).

Our results are compatible with those of Prayugo et al (Prayugo et al. 2021) who studied F ABPs' Gene expression analysis in CRC. They showed that, a mong other genes, FABP 4 gene has a higher expression levels in CRC tissues as matched to normal colon (Prayugo et al. 2021).Meanwhile, their results do not show statistical significance of FABP7 expression in CRC tissues compared to normal colon. Nevertheless, our re sults are the opposite of theirs regarding the relationship of FABP4 expression and overall survival. We have found the median overall survival to be statistically longer with high expression contrasted to low/negative expression of FABP4.On the other hand, our results contradict with other papers such as the one by Ma et al(Ma et al. 2018), since we observe negative/low expression of F ABP7 in the majority of our cases.(Ma et al. 2018; Tian et al. 2020)

It has been previously postulated that FABP4 has a role in the early development of CRC, as it activates the Wnt/-catenin pathway, which plays a chief role in CRC evolution. (H. Zhao et al. 2022; Oliveira, Predes, and Borges 2022; Prayugo et al. 2021) Moreover, a high blood level of F ABP4 has been detected in CRC pa tients (Y. Zhang et al. 2019). A recent study proposes that FABP4 overexpression can enhance invasiveness of CRC through activating lipid metabolism. (Ma et al. 2018; Tian et al. 2020)

FABP 4 is a gene that is located on chromosome 8q21 and it is expressed in adipose tissues and other tissues. EndogenousFABP4 acts as a tumor suppressor and exogenous FABP4 enhances cancer development. Fatty acids regulate FABP4 expression as its levels are higher in obese than in non-overweight patients (Hancke et al. 2010). FABP4 is found to be involved in lipid metabolism and pathogenesis in some cancers (McKillop, Girardi, and Thompson 2019).

Previous studies show that FABP4 expression plays an vital role in some cancers including breast cancer; where higher FABP4 serum levels indicate a worse prognosis (Xie et al. 2020). Moreover, FABP4 is increased in fatty tissue and is continually released in blood of obe se persons. Thus, inhibition of FABP4 activity may provide a new treatment strategy for obesity-associated breast cancer (Zeng, Sauter, and Li 2020).

FABP4 is documented to play a role in prostate cancer, (Huang et al. 2017; Amiri et al. 2018) bladder cancer, and lung cancer . FABP4 expression in lung cancer is found to be related to advanced lymph node metastasis (Tang et al. 2016).

FABP7 is identified mainly in evolving and mature neural tissues (brain astrocytes, cerebellar glial cells, and retinal cone photoreceptor cells)(Kagawa et al. 2019). It is also identified in liver Kupffer cells, reticular cells in lymph nodes and melanocytes. FABP7 seems to be expressed in several malignant tumors, such as gliomas, renal cell carcinomas, breast cancers, and others (Shi et al. 1997).

The role of FABP7 expression in carcinogenesis is the subject of several studies that show controversial results. For instance, De Rosa et al propose that FABP7 expression has a negative impact on prognosis in gliomas (De Rosa et al. 2012). Similarly, FABP7 expression correlates with unfavorable prognosis in Renal cell carcinoma.(Tan et al. 2014). However, contradictory results are found in breast cancer with better survival in cases with higher expression levels. A possible explanation of w orsened prognosis maybe because FABP7 overexpression leads to activated cell proliferation and migration of tumor cells (Kagawa et al. 2019). Some studies demonstrate that FABP7 shortage decreases cultured astrocytes proliferation (Sharifi et al. 2011).

Prayugo et al results do not show significant discrepancy of FABP7 gene expression between normal colon and CRC t issues (Prayugo et al. 2021). Moreover, the expression does not correlate with prognosis in CRC patients. The current study demonstrates similar findings on the protein expression level using IHC testing.

Adding to the controversy, Ma et al. (Ma et al. 2018) have found FABP7 expression to be stronger in CRC tissues in comparison to normal colon tissues, suggesting possible involvement in CRC carcinogenesis. Furthermore, their investigations display that FABP7 overexpression stimulates neoplastic proliferation and inhibits apoptosis. Moreover, FABP7 knockdown has a negative effect on cell proliferation (Ma et al. 2018).

Due to their role in tumor development, FABPs may become potential targets in cancer treatment (Sun and Zhao 2022). FABP4 has been embattled using several methods, such as small molecules like Polyphenols that are derivatives of natural plant sources and act as therapeutic substitutes for cancer therapy(Oliveira, Predes, and Borges 2022). These small molecules are synthesized by plants and are found i n multiple sources such as seeds, leaves, and roots. Small molecule inhibitors (siRNAs) and short hairpin RNAs are also recently examined as potential cancer therapy agents (Mukherjee et al. 2020). In t heir animal experiment, Mukherjee et al. utilizea small-molecule inhibitor (BMS309403), an antagonist of FABP4 that interacts with its lipid-binding pocket. Interestingly, they document substantial reduction in the number and size of m etastatic lesions in ovarian cancer with BMS309403 treatment. Similar trials have been performed in animal models of CRC. For example, it is proposed that miR-211 may reduce cell migration, invasiveness, and EMT via targeting FABP4 (D. Zhao et al. 2019).

Presently, however, no pub lished research on h uman subjects or clinical trials to evaluate the usefulness of FABP4 inhibition is so far available. Future studies and clinical trials are needed to prove that FABPs may become promising targets of cancer therapy.

5. Conclusions

This study shows high expression of F ABP4 in CRC, and that it may have an influence on survival. On the other hand, FABP7 is expressed in a minority of cases and high expression is not predictive of outcome.

The current work has several limitations including a relatively small sample size, and utilizing immunohistochemistry as a sole method to investigate FABP4 and FABP7 expression without molecular or genetic studies. Further studies and clinical trials are required to ascertain the relationship of F ABP and CRC.

The emphasis of such studies should be placed on the impact of FABPs on patient's outcome, along with the potential role of FABP inhibitors in targeted therapy for CRC patients, expanding the opportunities of therapeutic approaches in the clinical practice.

Acknowledgments

This work was supported by a grant from the Deanship of Scientific Research, the University of Jordan/ Amman, Jordan (Grant No.2434**).**

The authors would like to thank the lab technicians Mrs. Duaa Qattan and Mrs. Khloud Frehat for their skillful technical contributions.

References

Alshareeda, Alaa T, Emad A Rakha, Christopher C Nolan, Ian O Ellis, and Andrew R Green. 2012. Fatty Acid Binding Protein 7 Expression and Its Sub-Cellular Localization in Breast Cancer. *Breast Cancer Res Treat.,* 134 (2): 519–29. https://doi.org/10.1007/s10549-012-2083-8.

Amiri, Mina, Saghar Yousefnia, Farzad Seyed Forootan, Maryam Peymani, Kamran Ghaedi, and Mohammad Hossein Nasr Esfahani. 2018. Diverse Roles of Fatty Acid Binding Proteins (FABPs) in Development and Pathogenesis of Cancers. *Gene*., 676 (November): 171–83. https://doi.org/10.1016/j.gene.2018.07.035.

Bensaad, Karim, Elena Favaro, Caroline A Lewis, Barrie Peck, Simon Lord, Jennifer M Collins, Katherine E Pinnick, et al. 2014. Fatty Acid Uptake and Lipid Storage Induced by HIF-1α Contribute to Cell Growth and Survival after Hypoxia-Reoxygenation. *Cell Rep.,* 9 (1): 349–65. https://doi.org/10.1016/j.celrep.2014.08.056.

Camp, Robert L., Veronique Neumeister, and David L. Rimm. 2008. A Decade of Tissue Microarrays: Progress in the Discovery and Validation of Cancer Biomarkers. *J Clin Oncol*., https://doi.org/10.1200/JCO.2008.17.3567.

Chen, Xi, Shi-Liu Hu, Ying Feng, Peng Li, Qin-Sheng Mao, and Wan-Jiang Xue. 2021. Expression of Fatty Acid-Binding Protein-3 in Gastrointestinal Stromal Tumors and Its Significance for Prognosis. *J Surg Res.,* 260 (April): 462–66. https://doi.org/10.1016/j.jss.2020.11.003.

Coe, N R, and D A Bernlohr. 1998. Physiological Properties and Functions of Intracellular Fatty Acid-Binding Proteins. *Biochim Biophys Acta.,* 1391 (3): 287–306. https://doi.org/10.1016/s0005-2760(97)00205-1.

Favoriti, Pasqualino, Gabriele Carbone, Marco Greco, Felice Pirozzi, Raffaele Emmanuele Maria Pirozzi, and Francesco Corcione. 2016. Worldwide Burden of Colorectal Cancer: A Review. *Updates Surg.,* 68 (1): 7–11. https://doi.org/10.1007/s13304-016-0359-y.

Fowler, Carol B., Yan Gao Man, Shimin Zhang, Timothy J. O'Leary, Jeffrey T. Mason, and Robert E. Cunningham. 2011. Tissue Microarrays: Construction and Uses. In ***Methods in Molecular Biology***. https://doi.org/10.1007/978-1-61779-055-3_2.

Furuhashi M, Hotamisligil Gs. 2010. Fatty Acid-Binding Proteins: Role in Metabolic Diseases and Potential as Drug Targets. *Nat Rev Drug Discov*., 7, 489–503 (2008). https://doi.org/10.1038/nrd2589.

Gupta, Riya, Lokesh Kumar Bhatt, Thomas P Johnston, and Kedar S Prabhavalkar. 2019. Colon Cancer Stem Cells: Potential Target for the Treatment of Colorectal Cancer. *Cancer Biol Ther.,* 20 (8): 1068–82. https://doi.org/10.1080/15384047.2019.1599660.

Hancke, K, D Grubeck, N Hauser, R Kreienberg, and J M Weiss. 2010. Adipocyte Fatty Acid-Binding Protein as a Novel Prognostic Factor in Obese Breast Cancer Patients. *Breast Cancer Res Treat.,* 119 (2): 367. https://doi.org/10.1007/s10549-009-0577-9.

Hewitt, Stephen M., Denis G. Baskin, Charles W. Frevert, William L. Stahl, and Eduardo Rosa-Molinar. 2014. Controls for Immunohistochemistry: The Histochemical Society's Standards of Practice for Validation of Immunohistochemical Assays. *J Histochem Cytochem*., https://doi.org/10.1369/0022155414545224.

Huang, Mingguo, Shintaro Narita, Takamitsu Inoue, Atsushi Koizumi, Mitsuru Saito, Hiroshi Tsuruta, Kazuyuki Numakura, et al. 2017. Fatty Acid Binding Protein 4 Enhances Prostate Cancer Progression by Upregulating Matrix Metalloproteinases and Stromal Cell Cytokine Production. *Oncotarget.,* 8 (67): 111780–94. https://doi.org/10.18632/oncotarget.22908.

Hutchins, Gordon, and Heike I. Grabsch. 2018. How to Make Tissue Microarrays. *Diagnostic Histopathol.,* https://doi.org/10.1016/j.mpdhp.2018.02.008.

Jaganathan, Saravana Kumar, Muthu Vignesh Vellayappan, Gayathri Narasimhan, and Eko Supriyanto. 2014. Role of Pomegranate and Citrus Fruit Juices in Colon Cancer Prevention. *World J Gastroenterol.,* 20 (16): 4618–25. https://doi.org/10.3748/wjg.v20.i16.4618.

Jung, Yoon Yang, Hye Min Kim, and Ja Seung Koo. 2015. Expression of Lipid Metabolism-Related Proteins in Metastatic Breast Cancer. *PloS One* 10 (9): e0137204. https://doi.org/10.1371/journal.pone.0137204.

Kagawa, Yoshiteru, Banlanjo A Umaru, Islam Ariful, Subrata Kumar Shil, Hirofumi Miyazaki, Yui Yamamoto, Masaki Ogata, and Yuji Owada. 2019. Role of FABP7 in Tumor Cell Signaling. *Adv Biol Regul.,* 71 (January): 206–18. https://doi.org/10.1016/j.jbior.2018.09.006.

Knösel, Thomas, Anna Emde, Karsten Schlüns, Yuan Chen, Karsten Jürchott, Matthias Krause, Manfred Dietel, and Iver Petersen. 2005. Immunoprofiles of 11 Biomarkers Using Tissue Microarrays Identify Prognostic Subgroups in Colorectal Cancer. *Neoplasia*. https://doi.org/10.1593/neo.05178.

Liu, Rong-Zong, Raja Mita, Michael Beaulieu, Zhihua Gao, and Roseline Godbout. 2010. Fatty Acid Binding Proteins in Brain Development and Disease. *Int J Dev Biol.,* 54 (8–9): 1229–39. https://doi.org/10.1387/ijdb.092976rl.

Ma, Ran, Lan Wang, Fang Yuan, Shaoxuan Wang, Yingping Liu, Tingting Fan, and Fulai Wang. 2018. FABP7 Promotes Cell Proliferation and Survival in Colon Cancer through MEK/ERK Signaling Pathway. *Biomed Pharmacother.,* 108 (December): 119–29. https://doi.org/10.1016/j.biopha.2018.08.038.

McKillop, Iain H, Cara A Girardi, and Kyle J Thompson. 2019. Role of Fatty Acid Binding Proteins (FABPs) in Cancer Development and Progression. *Cell Signal.,* 62 (October): 109336. https://doi.org/10.1016/j.cellsig.2019.06.001.

Mukherjee, Abir, Chun-Yi Chiang, Helen A Daifotis, Kristin M Nieman, Johannes F Fahrmann, Ricardo R Lastra, Iris L Romero, Oliver Fiehn, and Ernst Lengyel. 2020. Adipocyte-Induced FABP4 Expression in Ovarian Cancer Cells Promotes Metastasis and Mediates Carboplatin Resistance. *Cancer Res.,* 80 (8): 1748–61. https://doi.org/10.1158/0008-5472.CAN-19-1999.

Oliveira, Luiz F S, Danilo Predes, and Helena L Borges. 2022. Therapeutic Potential of Naturally Occurring Small Molecules to Target the Wnt / β -Catenin Signaling Pathway in Colorectal Cancer.*Cancers.,* 14 (2): 403. https://doi.org/10.3390/cancers14020403.

Prayugo, Fidelia Berenice, Tzu-Jen Kao, Gangga Anuraga, Hoang Dang Khoa Ta, Jian-Ying Chuang, Li-Chia Lin, Yung-Fu Wu, Chih-Yang Wang, and Kuen-Haur Lee. 2021. Expression Profiles and Prognostic Value of FABPs in Colorectal Adenocarcinomas.*Biomedicines*., 9 (10). https://doi.org/10.3390/biomedicines9101460.

Rosa, Antonella De, Serena Pellegatta, Marco Rossi, Patrizia Tunici, Letizia Magnoni, Maria Carmela Speranza, Federico Malusa, et al. 2012. A R adial Glia Gene Marker, Fatty Acid Binding Protein 7 (FABP7), Is Involved in Proliferation and Invasion of Glioblastoma Cells. *PloS One* 7 (12): e52113. https://doi.org/10.1371/journal.pone.0052113.

Sharifi, Kazem, Yusuke Morihiro, Motoko Maekawa, Yuki Yasumoto, Hisae Hoshi, Yasuhiro Adachi, Tomoo Sawada, et al. 2011. FABP7 Expression in Normal and Stab-Injured Brain Cortex and Its Role in Astrocyte Proliferation. *Histochem Cell Biol.,* 136 (5): 501–13. https://doi.org/10.1007/s00418-011-0865-4.

Shi, Y E, J Ni, G Xiao, Y E Liu, A Fuchs, G Yu, J Su, et al. 1997. Antitumor Activity of the Novel Human Breast Cancer Growth Inhibitor, Mammary-Derived Growth Inhibitor-Related Gene, MRG. *Cancer Res.,* 57 (15): 3084–91.

Sun, Naihui, and Xing Zhao. 2022. Therapeutic Implications of FABP4 in Cancer: An Emerging Target to Tackle Cancer. *Front Pharmacol.,*13: 948610. https://doi.org/10.3389/fphar.2022.948610.

Tan, Cheng, Tatsuya Takayama, Naohisa Takaoka, Hiromi Fujita, Miki Miyazaki, Takayuki Sugiyama, and Seiichiro Ozono. 2014. Impact of Gender in Renal Cell Carcinoma: The Relationship of FABP7 and BRN2 Expression with Overall Survival. *Clin Med Insights Oncol.,* 8: 21–27. https://doi.org/10.4137/CMO.S13684.

Tang, Zhiyuan, Qin Shen, Hao Xie, Xiaoyu Zhou, Jun Li, Jian Feng, Hua Liu, Wei Wang, Shu Zhang, and Songshi Ni. 2016. Elevated Expression of FABP3 and FABP4 Cooperatively Correlates with Poor Prognosis in Non-Small Cell Lung Cancer (NSCLC). *Oncotarget*., 7 (29): 46253–62. https://doi.org/10.18632/oncotarget.10086.

Taylor, C. R., and R. M. Levenson. 2006. Quantification of Immunohistochemistry - Issues Concerning Methods, Utility and Semiquantitative Assessment II. *Histopathology*. https://doi.org/10.1111/j.1365-2559.2006.02513.x.

Tian, Wenying, Wenjia Zhang, Yan Zhang, Tianyue Zhu, Yuting Hua, Hui Li, Qinglin Zhang, and Min Xia. 2020. FABP4 Promotes Invasion and Metastasis of Colon Cancer by Regulating Fatty Acid Transport. *Cancer Cell Int.,* 20: 512. https://doi.org/10.1186/s12935-020-01582-4.

Walker, R. A. 2006. Quantification of Immunohistochemistry - Issues Concerning Methods, Utility and Semiquantitative Assessment I. *Histopathology*. https://doi.org/10.1111/j.1365-2559.2006.02514.x.

Xie, Qin, Ying-Sheng Xiao, Shi-Cheng Jia, Jie-Xuan Zheng, Zhen-Chao Du, Yi-Chun Chen, Mu-Tong Chen, Yuan-Ke Liang, Hao-Yu Lin, and De Zeng. 2020. FABP7 Is a Potential Biomarker to Predict Response to Neoadjuvant Chemotherapy f or Breast Cancer. *Cancer Cell Int.,* 20 (1): 562. https://doi.org/10.1186/s12935-020-01656-3.

Zang, Wei-Jie, Zi-Niu Wang, Yi-Lin Hu, Hua Huang, and Peng Ma. 2021. Expression of Fatty Acid-Binding Protein-4 in Gastrointestinal Stromal Tumors and Its Significance for Prognosis. *J Clin Lab Anal.,* 35 (11): e24017. https://doi.org/10.1002/jcla.24017.

Zeng, Jun, Edward R Sauter, and Bing Li. 2020. FABP4: A New Player in Obesity-Associated Breast Cancer. *Trends Mol Med.,* 26 (5): 437–40. https://doi.org/10.1016/j.molmed.2020.03.004.

Zhang, Chunyu, Yuandong Liao, Pan Liu, Qiqiao Du, Yanchun Liang, Shiyin Ooi, Shuhang Qin, Shanyang He, Shuzhong Yao, and Wei Wang. 2020. FABP5 Promotes Lymph Node Metastasis in Cervical Cancer by Reprogramming Fatty Aci d Metabolism.*Theranostics*., 10 (15): 6561–80. https://doi.org/10.7150/thno.44868.

Zhang, Yaqin, Xiaotong Zhao, Lili Deng, Xueting Li, Ganbiao Wang, Yongxing Li, and Mingwei Chen. 2019. High Expression of FABP4 and FABP6 in Patients with Colorectal Cancer. *World J Surg Oncol.,* 17 (1): 171. https://doi.org/10.1186/s12957-019-1714-5.

Zhao, Dongmei, Yanying Ma, Xu Li, and Xiaoyu Lu. 2019. MicroRNA-211 Promotes Invasion and Migration of Colorectal Cancer Cells by Targeting FABP4 via PPARγ. *J Cell Physiol*., https://doi.org/10.1002/jcp.28190.

Zhao, Hui, Tianqi Ming, Shun Tang, Shan Ren, Han Yang, Maolun Liu, Qiu Tao, and Haibo Xu. 2022. Wnt Signaling in Colorectal Cancer: Pathogenic Role and Therapeutic Target.*Mol Cancer.,* 21 (1): 144. https://doi.org/10.1186/s12943-022-01616-7.

JJBS

Volume 17, Number 1,March 2024
ISSN 1995-6673
Pages 37 – 66
https://doi.org/10.54319/jjbs/170105

Jordan Journal of Biological Sciences

Studying the Transcriptome Profiling of Banana Plantlets Exposed to Water Stress and the Alteration in Their Major Bioprocesses

Sri N. Widiyanto[1,*] , Fainmarinat S. Inabuy , Tyas Nugraheni , Simon Duve , Diky S. Diningrat[2] , John E. Carlson[3]

[1]*School of Life Sciences and Technology, Institut Teknologi Bandung, Bandung 40132, Indonesia ;* [2]*Department of Biology, Faculty of Mathematics and Natural Sciences, Medan State University, Medan 20221, Indonesia;* [3]*Department of Ecosystem Science and Management, Pennsylvania State University, University Park, PA 16802, US.*

Received: March 15, 2023; Revised: May 17, 2023; Accepted: July 4, 2023

Abstract

Water shortage has been one of the major problems that limit the production yield of banana. The molecular mechanisms by which banana plants thrive in drought are not completely understood. This study aimed to reveal the major bioprocesses affected by water shortage in banana plantlet using a transcriptomic analysis approach. *In vitro* shoot cultures of banana (*Musa acuminata*) cv Barangan Merah were established on water stress treatments with the addition of polyethylene glycol (PEG) in the culture medium. Banana plantlets generated from water stressed shoots from the control (BK), low 2.5% PEG), medium (7.5% PEG) and high (10% PEG) levels were utilized as the resource for total RNA samples. Four cDNA libraries were constructed and sequenced using the Illumina MiSeq™ 2000 platform. Transcriptome data analysis was conducted. From a pool of four transcriptome libraries, each consisting of about 3,500,000 paired-end raw reads, 147,811 contigs were assembled, from which 129,701 contigs were annotated with SwissProt reference and *Musa acuminata* gene model. A total of 101,406 high quality and non-redundant contigs were obtained for differential expressed genes (DEG) analyses. Gene ontology was performed using DAVID, followed by pathway prediction using KEGG. Statistical analysis identified 1,744 genes as DEGs under PEG treatment in which 1,046 genes (67%) of them were mapped to the reference genomes. These DEGs were distributed in 26 functional clusters. There were eight major biological processes that were highly affected by the drought stress in banana, including photosynthesis, cellular redox balance, cellular components stability, cellular energy preservation, metal ion homeostasis, hormonal-activated signaling pathways, organ development, and production of transcription factors (TFs). There 47 genes encoded for TFs were identified including five families that are typical for stress-responsive genes families (MYB, WRKY, bZIP, ABF, DRE), also auxin- and ethylene-activated TFs and WUSCHEL-related homeobox. Fifteen DEGs were selected for qRT-PCR validation and their expression results were confirmed.

Keywords: Drought stress, *Musa acuminata*, shoot cultures, transcriptome profile.

1. Introduction

Bananas (*Musa* spp.) are famously known as a commercial crop in tropical and subtropical countries, including Indonesia. For optimal growth, banana plants require a warm and humid climate. The existing commercial cultivars of banana are mostly parthenocarpy and generated from hybridization between one or two of the major diploid ancestors, *Musa acuminata* (A-genome) and *Musa balbisiana* (B-genome) that produce the three triploid hybrids, either with AAA, AAB, or ABB genome constitution (Nayar, 2010 and Davey *et al*., 2013). Naturally, banana plants are exposed to suboptimal field conditions throughout its life cycle. Drought is one of major abiotic stresses that is affecting banana production worldwide (Santos *et al.*, 2018) because insufficiency of water supply will reduce the growth of banana plants and cause a big loss of production yield of banana fruits (Nansamba *et al.,* 2020).

Drought refers to the condition of water deficit when water levels drop below a certain threshold. The water deficit condition occurs either when the water supply becomes limited or when the transpiration rate becomes intense. The effects of plant water stress vary between the plant species. The most common early symptom of plant water stress is when the leaves wither and dry. Recognition of water-stress symptoms can be critical to maintaining the growth of a crop (Bhattacharjee and Saha, 2014). When the plant encounters water stress, the osmotic pressure inside leaf cells decreases and causes the leaves to wilt. To get through with the drought, tolerant plants initiate defense strategies against water deficit that can be expressed at the phenotypic levels and the molecular levels (Ilyas *et al,* 2021). In response to water stress, changes occurred in the cellular level, including changes in metabolic pathway directions, changes in the nutrient and

* Corresponding author. e-mail: srinanan@itb.ac.id.

ion uptakes, synthesis of new proteins and modulation of free radical generation (Omprakash *et al*., 2017).

Drought has been known to cause morphological, physiological, biochemical, and molecular changes in banana. Water stress evidently changed morphological and physiological activity, that affected the growth and productivity of plants. Morphological characteristics of banana plants, such as the numbers of leaves, shape and color appearance of leaves, reduction of the greenness of leaves, and plant heights were significantly changed under drought conditions (Uwimana *et al*, 2021). It was found that the lack of sufficient water also affected the relative water content (RWC), soluble protein content, total chlorophyll, and photosynthetic pigment contents of various banana genotypes. Water deficiency also gave an impact on increasing the biosynthesis of epicuticular wax, proline, and free amino acid in banana plants (Surendar *et al.,* 2013). Nevertheless, studies showed that drought tolerance in banana plants was genotype-dependent. It was indicated that different cultivars of banana are varied in their tolerance levels to drought conditions. Among the three-triploid banana hybrids, i.e. the AAA, AAB, or ABB genomes, the cultivars with ABB genome constitution are known to be more tolerant to drought (Wang *et al*., 2020).

Understanding the molecular basis of how banana plants respond to water stress is the main key to developing drought tolerant banana plants in the future. Molecular studies showed that banana plants are capable of super-expressing genes related to resistance and defense response to abiotic stresses, including drought and salinity stresses (Hu *et al*., 2017). The molecular regulation mechanisms of banana in response to various abiotic stresses have been extensively studied using the next generation sequencing (NGS) technology. The NGS technology is known to be very useful in generating large amounts of expressed sequence tags (EST) which is adequate to cover the transcriptome of bananas (Lowe *et al.,* 2017). A draft genome of the wild *M. balbisiana* diploid variety, the 'Pisang Klutuk Wulung' ('PKW', B-genome) was successfully sequenced and assembled (Davey *et al*., 2013). The draft genome was used in comparative transcriptomics and genomics studies of interspecific triploid and tetraploid banana hybrids. The computational prediction, identification, and expression profiling of microRNAs had been used to identify drought-responsive miRNAs in the EST library of drought-stressed banana. The miRNAs are post-transcriptional gene regulators and implied to regulate gene expression during drought response (Muthusamy *et al*., 2014).

Based on NGS-technology, Backiyarani *et al.* (2015) accomplished the transcriptome analysis of banana (*Musa balbisiana*). The transcriptome sequencing was performed using the Ion Torrent platform and generated about 4.5 million paired-end reads. The RNA sequencing results provided transcriptomic information on the *Musa* sp. 'B' genome and led to the development of trait-specific markers and also the discovery of new genes and regulatory sequences that are involved in resistance mechanisms. Likewise, transcriptome analysis had been employed to identify and compare drought stress-responsive long non-coding RNAs (lncRNAs) from drought-tolerant and -susceptible banana (*Musa* spp) cultivars. The LncRNAs are known to be responsive to biotic and abiotic stresses and regulate genes to respond (Muthusamy *et al.,* 2015). Muthusamy *et al.* (2016) also discovered the transcriptomic changes of tolerant and sensitive banana cultivars exposed to drought stress. The differences in profiles were determined between drought-tolerant cv Saba (ABB genome) and the drought-susceptible cv. 'Grand Naine' (AAA genome) in tolerance mechanism to water deficiency. It was verified that comparative physiological and transcriptomic analyses were applicable to reveal the integrated insight into abiotic stress tolerance mechanisms in banana. Based on phenotypic and physiological analyses, it was confirmed that the ABB genotype banana had the strongest tolerance to abiotic stresses compare to the AAA and AAB genotypes (Wang *et al*., 2020).

Studies showed comparative transcriptomic analyses had confidently improved our understanding of the molecular mechanisms of defense occurred in *Musa* spp. when plants under drought stress. Transcriptome sequencing technologies successfully generate and provide a framework dataset that is needed to be further analyzed for transcriptome mapping, determining metabolic pathways, clarifying gene expression patterns, and identifying new genes (Rani and Sharm, 2017). Basically, the information contents of transcriptome data are recorded as a snapshot at the moment taken, hence the information contents will be very specific and will not be the same in different tissues or conditions, or at different times. Nevertheless, transcriptome data give us information on how genes are regulated and reveal details of biological processes occurring in cells, tissues, or organ parts of an organism at a certain time and in a specific condition; therefore, drought responsive gene expression profiles of banana remain unexplored thoroughly (Hu *et al*., 2017). Accordingly, it was emphasized that there is a need for more studies using the transcriptome sequencing technology to discover the molecular mechanisms of banana in response to water stress. A comprehensive transcriptome data will further enhance our understanding of the mechanisms regulating drought tolerance in banana and determine the play roles of expressed genes in stress regulation and post-translational mechanisms (Mattos-Moreira *et al*., 2018). This study aimed to unravel the mechanism of banana plantlets in response to water stress condition through morphological observation and transcriptional analysis. A reference transcriptome dataset was generated from cDNA libraries of banana plantlets, *Musa acuminata*, Colla cv Barangan Merah (AAA genome), which is known as a drought-susceptible cultivar (Sebayang *et al*., 2018). In this study, transcriptomic changes of the water stressed plantlets of Barangan Merah banana cultivar were analyzed to discover the gene expression profiles related to the major biological processes.

2. Materials and Methods

2.1. Plant Materials and Treatments

In vitro shoot cultures of banana (*M. acuminata*) cv Barangan Merah used in this study were obtained from SEAMEO BIOTROP, Bogor, Indonesia. Banana shoots were cultured on MS (Murashige and Skoog, 1962) basal medium (PhytoTech Lab. USA) supplemented 3 % (w/v) sucrose and 0.8 % (w/v) agar (Swallow Globe, Indonesia)

to solidify. Emerged axillary shoots were sub-cultured every four weeks and used as explants for water stress treatments. Polyethylene glycol (HiMedia Laboratories, India) was added to the culture medium to induce water deficiency. Three different PEG concentration levels used in experiments were 2.5% (coded as BP2), 7.5% (coded as BP7), and 10 % (coded as BP10), and those were equivalent to osmotic potential (OP) at -0.19, - 0.93, and - 1.48 bars (Michel and Kaufmann, 1973). Shoots grown on culture medium without the addition of PEG were used as the control treatment (coded as BK). After a four-week period of culturing, shoots were rooted and regenerated into plantlets on MS medium supplemented with 5 µM 6-Benzyl-aminopurine (Sigma-Aldrich, Singapore). All banana in vitro cultures were maintained in a culture room at 22 ± 2˚C under continuously-lighting at 2,000- 3,000 lux (Bharati *et al.*, 2018). Six replicates were made for each treatment. Three replicates of each sample were prepared for RNA extractions and three other replicates were used for subculturing and further experimental analyzing.

2.2. Morphological Observations

Morphological observations were carried out to evaluate the effects of water stress on the growth and morphological changes of banana plantlets. The physical appearances of the four groups of banana plantlets (BK, BP2, BP7, and BP10) were compared. The shoot lengths of plantlets (height in mm), number of leaves, and shoot multiplication rates were used as the growth parameters and measured after a four-week period of PEG exposures. Changes in the appearance of leaves, reduction of the greenness of foliage, and the evidence of necrotic, chlorosis, or browning tissues of plantlets were also monitored. For morphological observation, six replicates were made for each treatment, and the statistical analysis was determined by One-way ANOVA and Tukey test using the SPSS software version 23.0.

2.3. RNA Extraction

For transcriptome sequencing, tissue samples of the four groups of banana cv Barangan Merah plantlets (BK, BP2, BP7, and BP10) were collected and prepared for the RNA isolation. The total RNA of each group of treatment was extracted separately using the CTAB-LiCl protocol (Song *et al.*, 2011). Frozen tissues of banana plantlets were ground into fine power in liquid nitrogen using a pre-cooled mortar. The fine powder samples were then submerged into 0.1% (v/v) cethyl trimethyl ammonium bromide buffer (CTAB Merck, Singapore), and followed by two times extractions with chloroform. The RNAs were precipitated using lithium chloride (Merck, Singapore), and then extracted using chloroform again. The least RNAs were precipitated with ethanol, and the pellets were resuspended in 20-100 µL diethyl pyrocarbonate (DEPC) treated water (ThermoFisher Scientific, USA). The integrity of RNAs was assessed with the Agilent 6000 RNA Nano Chip Kit on 21 00 Bioanalyzer (Agilent Technologies), following the procedure described by Diningrat *et al.* (2015).

2.4. cDNA Library Construction and Transcriptome Sequencing

Two-paired-end cDNA libraries were developed according to the protocol of Two-Paired-End Sample Preparation Kit (Illumina Inc., USA). The four cDNA libraries were constructed and sequenced using the Illumina MiSeq^{TM} 2000 platform (Diningrat *et al.*, 2015). Only one transcriptome dataset was presented for each treatment group. Transcriptome raw data were generated from four cDNA libraries of banana plantlets, and coded as BP2, BP7, BP10, and BK as the control.

2.5. Transcriptome Data Analysis

Banana transcriptome data analysis was conducted through several steps as illustrated in the bioinformatics analysis flow chart (Figure 1). Quality assessment of all raw FASTQ reads was conducted using FastQC version 0.11.8 prior to *de novo* transcriptome assembly. *De novo* transcriptome assembly was performed using Trinity assembler package version 2.8.4 (commission no. 4539805) with a k-mer size of 25 and both sequencing adapter and bases with low quality scores were removed with Trimmomatic version 0.36 (Haas *et al.*, 2013). Transrate version 1.0.3 was used to assess the quality and filter the assembled contigs, retaining only contigs that have Transrate contig quality scores greater than or equal to 0.04776 (Smith-Unna *et al.*, 2016).

Contigs that passed the filtering step by Transrate were used as input for TransDecoder (version 5.5.0) for the detection of the putative open reading frame (ORF). Contigs were then annotated using Trinotate version 3.1.1 with all the contigs passing Transrate filtering step and ORFs predicted by TransDecoder as inputs. Contigs were annotated against Swiss-Prot database (The Uniprot Consortium, 2019), Pfam 32.0 (El-Gebali *et al.*, 2019) and *Musa acuminata* genome assembly and annotation-version (Martin *et al.* 2016). Contigs expression level for each treatment group was determined using the align_and_estimate_abundance.pl script as part of the Trinity package. Quality trimmed reads from each treatment were mapped using Bowtie2 version 2.3.5.1 (Langmead and Salzberg, 2012) read counts were estimated using RSEM version 1.3.2 (Li and Dewey, 2011).

Differential expression analysis was done in RStudio version 1.2.1335 (RStudio Team, 2018) using DESeq2 package (Love *et al.*, 2014). To reduce the probability of false positive error, we removed any contigs with an expression level less than the expression level at the 85th percentile across all contigs. For gene expression analysis, the number of expressed tags was calculated and normalized to the number of transcripts per million (TPM) tags. Each unigene was grouped based on the ratio of TPM to that of the control data. Unigenes were analyzed with a cut-off ratio of log10 > 2 to obtain a list of unigenes with multiples of more than 100 times compared to those of the control group (p-value ≤ 0.001). The differentially expressed tags were used for further mapping and annotation. To visually represent the similarities and differences of functional gene expressions among the three groups of treatments (BP2, BP7 and BP10), the Venn diagrams were made up and generated using a web-based tool by PSB Ugent (http://bioinformatics.psb.ugent.be/webtools/Venn/).

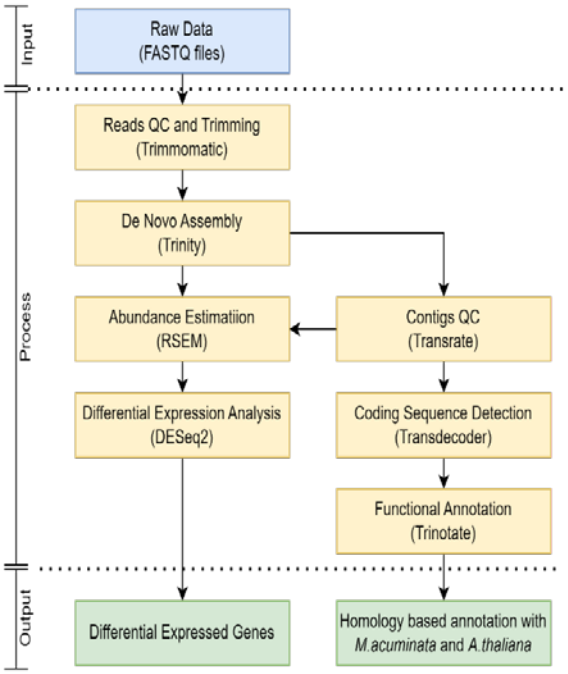

Figure 1. Bioinformatics analysis flow chart for transcriptome profiling of banana plantlets under drought stress.

2.6. Gene Ontology (GO) Enrichment Analysis

Further analysis of GO enrichment was accomplished only for the high concentration treatment, the 10% PEG (BP10 plantlet) as a representative of other treatments. The GO enrichment analysis of the differentially expressed genes was completed using the Database for Annotation, Visualization, and Integrated Discover (DAVID) at http://david.abcc.ncifcrf. gov/. The pathway analysis was performed based on *Arabidopsis thaliana* (TAIR) annotation and the Kyoto Encyclopedia of Genes by and Genomes (KEGG) http://www.genome.jp/kegg/.

2.7. Validation of Selected Gene Expressions by qRT-PCR Assay

To confirm the expressions of selected annotated DEGs, an independent experiment was carried out to replicate a similar experiment with previous experiments, except that for validation of gene expressions, the total RNA samples were extracted from banana cv Barangan Merah plantlets of the BK (control treatment without PEG) and the BP10 (with 10% PEG treatment) only. The total RNA samples were isolated from plantlets of the BK and the BP10 after four weeks of the PEG treatment. The RNA extractions were done using CTAB-LiCl method as described previously (Song *et al*., 2011). Three biological replicates were used for the validation. The quality and quantity of RNA were measured using Nanodrop™ Lite Spectrophotometer (Thermo Scientific, USA) and electrophoresis was confirmed in 1.5 % agarose (Kusdianti *et al*., 2016). The cDNA constructions were carried out with the GoScript™ Reverse Transcription System according to manufacture manual (Promega, USA). The cDNA synthesis reaction was done by incubation for 5 minutes at 25 °C, followed by incubation for 1 h at 42 °C and deactivated of reverse transcriptase for 15 minutes at 70 °C. The quantity of total RNA measured using nanodrops showed an average of 273.3 ng/µl (Amalia *et al*., 2016). Construction of cDNA with reverse transcriptase enzyme generated banana cDNA that can be used for qRT-PCR analysis.

Fifteen genes selected from annotated DEGs (Supplementary Table S.1) were subjected to quantitative real-time PCR (qRT-PCR) assay. Primer pairs were designed using the Primer3Plus package following the procedure described at https://www.bioinformatics.nl/cgi-bin/primer3plus/primer3plus.cgi. All designed primers were checked with the Primer Blaster (https://banana-genome-hub.southgeen.fr/primer blaster) and compared to the banana genome available at CIRAD to ensure the primers would hit with the *M. acuminata* (AAA genome). The primers had a specification of 18 -25 bases length (Macrogen, Singapore), 40-60% GC percent, the temperature of melting (Tm) between 55-65°C, and no self-complementary or di mer. Analysis with Primer Blaster software also showed the same amount of amplification with Primer3Plus software, thus the primers could amplify the target genes and used for gene expression analysis.

Quantitative Real-Time PCR (qRT-PCR) analyses were performed using QuantStudio 1 (Termo Scientific, USA). The qRT-PCR was performed using GoTaq® qPCR Master Mix according to the manufacturer manual (Promega, USA). The PCR reaction procedure (Amalia *et al*., 2016) was started with pre-denaturation at 95 °C for 15 minutes, followed by 40 cycles of polymerization (15 s at 95 °C, 30 s at 60 °C and 30 s at 72 °C). Three technical replicates were applied in the qRT-PCR assay. Relative fold expression values were normalized using *MaACT* (actin) and *MaBT* (betatubulin) as the housekeeping genes and calculated using the $2^{-\Delta\Delta Ct}$ method (Livak and Schmittgen, 2001). Statistical analyses are used to estimate the significance of statistical program and presented graphically (Hu *et al*., 2017).

3. Results

3.1. Morphological Evaluations

Visible morphological changes occurred in plantlets after four weeks of PEG exposure. Morphologically, plantlets of the BP2, BP7 and BP10 were very different in their appearance compared to plantlets of the control group (BK). Remarkable signs were noticed as the reduction in the greenness of foliage, changes in shoot colors, reduced size of leaves, and fewer leaves turgidity in plantlets (Figure 2.A-D). Some leaves of plantlets turned yellowish after four weeks cultured on a water shortage condition, particularly on medium with 10% PEG. Morphological changes might be related to the expression of specific genes related to the major biological process that occurred in plantlets as a response to water shortage. The lack of water may further reduce most downstream processes that require water, primarily photosynthesis but also increase the effectiveness of energy formation and uses- the details will be discussed later. It seemed to be corresponding to the changes in transcriptome profiles.

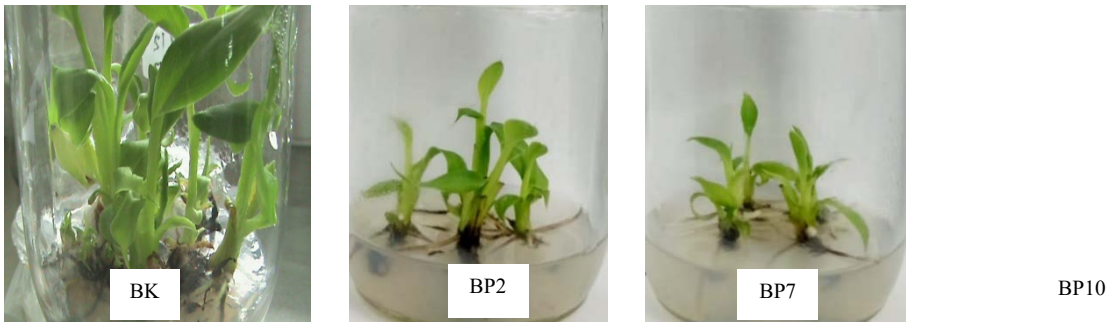

Figure 2. (A) Banana plantlets of the control (BK), (B) treatments with PEG 2.5% (BP2), (C) PEG 7.5% (BP7), and (D) PEG 10% (BP10) after four weeks of PEG treatments which were used as the sources of RNA samples for generating the transcriptome data.

The evaluation showed changes in shoot lengths, numbers of leaves and shoot multiplication rates of banana plantlets after four weeks of exposure to PEG in MS treatments (Figure 3 A-C). Compared to those of t he control treatment (BK), plantlets of the BP2, BP7 and BP10 obviously decreased their growth. The averages of heights (shoot length in mm) of the BP2, BP7 and BP10 plantlets were 38 mm, 26 mm and 19 mm which were very much lower compared to those of the control ones (65 mm). The water deficiency also greatly reduced the leaf numbers of plantlets. Drought stressed plantlets had lower numbers of leaves on averages of 3.8 (BP2), 2.5 (BP7) and 2.3 (BP10) whereas the control plantlets evenly had higher numbers of enlarged leaves (6.3 per plantlet). Other than that, the lack of sufficient water seemed to suppress the growth ability of a xillary buds causing shoot multiplication rates were excessively declined, especially at 10% PEG (BP10).

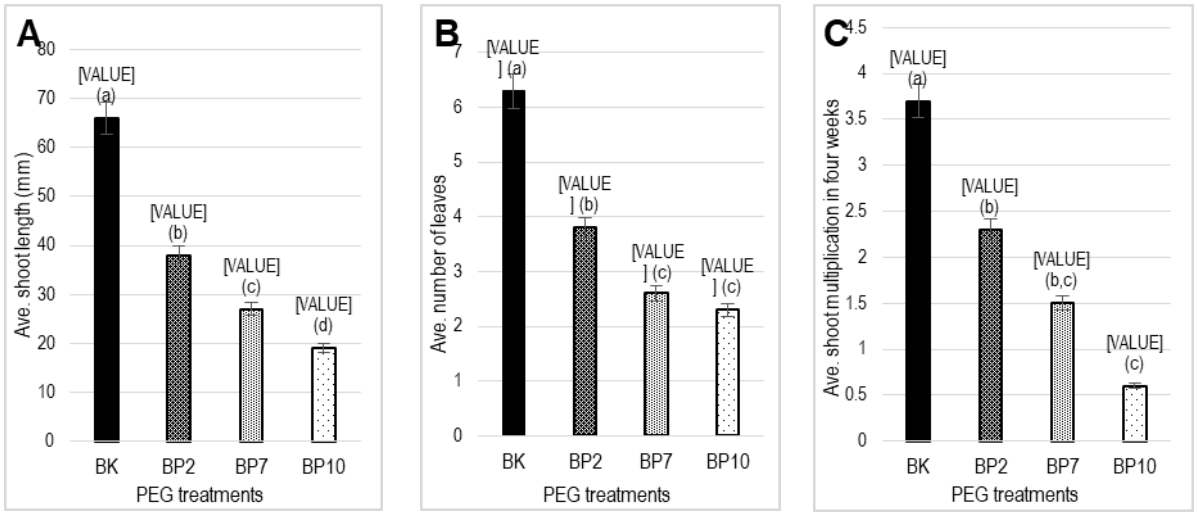

Figure 3. (A) Average of shoot lengths (mm), (B) average of leaf numbers, and (C) average of shoot multiplication rates of banana plantlets: BK, BP2, BP7 and BP10 four weeks after exposure to PEG in MS treatments. The number at top of each bar represents the mean value with error bars at p = 0.05. Values followed by the same letters are not significantly different at 0.05 level as determined by One-way ANOVA and Tukey test.

3.2. Transcriptomic Analyses

A transcriptome dataset was generated from four cDNA libraries of ba nana plantlet groups that were exposed to water stress by the addition of PEG (BP2; BP7, BP10) and the control treatment (BK). All RNA-seq data had been submitted and registered with the BioProject database NCBI (BioProject ID PRJNA970186). In these four transcriptome libraries, each one consisting of ~3,500,000 paired-end raw reads, a total of 147,811 contigs were assembled, from which 129,701 contigs were annotated with SwissProt reference and *Musa acuminata* gene model. After the redundant and low quality contigs were filtered out, a total of 101.406 high quality and non-redundant contigs were obtained for further analyses. Contigs length ranged from 200 to 1800 bp with N50 value of 998. Transcriptome assembly statistics are listed in Table 1.

Table 1. Transcriptome statistics of the assembled contigs of banana plantlets of the low quality- and redundant- contigs were omitted with the TransRate tool.

Parameters	Values
Numbers of bases	104,118,407
Numbers of contigs	147,811
Smallest contig size (in bases)	199
Largest contig size (in bases)	7,393
Percentage of fragments mapped (%)	91.8
Percentage of good mapping (%)	77.3
Percentage of contigs uncovered (%)	17.5

3.3. Differentially expressed genes (DEGs) Analysis

Genes with very low expression levels were excluded from the 101,406 high-quality contigs and resulting in

60,637 genes being used as input in the Differential Expressed Gene (DEG) analysis. Further filtered-out with the threshold of the adjusted p-value of 0.05 resulted from a total of 8,444 contigs were obtained and used in pairwise analysis. All DEGs were divided into three groups based on its PEG treatments. The total numbers of 1,564 genes, 1,556 genes, and 1,744 genes were finally identified as differentially expressed (DEGs) following the treatments of 2.5% PEG (BP2), 7.5% PEG (BP7), and 10% PEG (BP10), respectively. In Venn diagrams (Figure 4), gene numbers in a circle showed the relationships of genes among groups. The numbers in overlapped circles exhibited similar expressions, while numbers in separate circles indicated the number of genes which did not take a part in the same trait. The three groups were BP2, BP7 and BP10 groups and showed a similar ratio of two-thirds (2/3) of up-regulated and down-regulated genes. In BP2 group there were 631 genes (40.3%) up-regulated, and 933 genes (59.7%) were down-regulated. In BP7 group, 658 genes (42.2%) were up-regulated, and 898 genes (57.8%) were down regulated, while in BP10 group, 762 genes (43.7%) were up-regulated, and 982 genes (56.3%) were down regulated (Figure 4, Table 3).

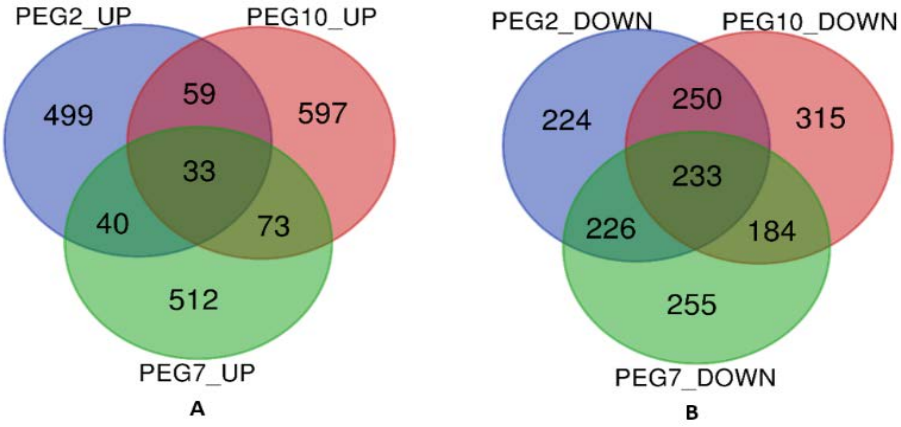

Figure 4. The Venn diagrams of the total gene counts of DEGs: (A) Upregulated genes and (B) Downregulated genes, in 2.5% PEG, 7.5%PEG, and 10% PEG.

A total of 25 annotated genes were consistently upregulated in all PEG exposed plantlets (BP2, BP7, and BP10) which consisted of genes responsible for the processes of defense to abiotic and biotic stresses, the metabolic process of the antioxidant glutathione, abscisic acid-activated signaling pathway, cell redox homeostasis, photorespiration, DNA repair and protein modifications (Table 2). The results of the DEG analysis also indicated genes that were exclusively expressed in each exposure to PEG treatment, with the biggest portion of the genes occurring in the highest PEG concentration (10% PEG). Using homology comparison with two genome references, the previously published *Musa acuminata* cv *Pahang* genome model and *Arabidopsis thaliana*, we were able to assign the functions of at least two-third of the up-regulated and down-regulated genes in each treatment group.

On the other hand, 233 genes (94 of them were annotated) were consistently down regulated in all tested concentrations of PEG (Figure 4) with the majority involved in the formation of photosynthetic machinery such as chloroplast membrane components, photosystem I and II, that play role in light harvesting during photosynthesis. In addition to that, genes related to the process of cellular ion homeostasis, amino acid transmembrane transport, ethylene- and auxin- activated pathways, fatty acid biosynthesis, cell wall biogenesis, plant organ morphogenesis, oxidoreductase activity, phenylpropanoid metabolic process, and response to abiotic and biotic stimulus- were also appeared to be consistently down-regulated in all treatments (Supplementary Table S.2).

Out of 762 up-regulated genes, 100 genes were selected as genes with the highest expression levels enhanced by at least a thousand times. Among the genes are early nodule-like protein, L-ascorbate peroxidase, acidic endochitinase, protein disulfide isomerase-like, superoxide dismutase, prolyl 4-hydroxylase, nucleolin 2, gibberellin-regulated protein, tubulin alpha-1 chain, flavonoid 3'-monooxygenase, small nuclear ribonucleoprotein G, and stearoyl-[acyl-carrier-protein] 9-desaturase (Supplementary Table S.3). Interestingly, the top 100 up-regulated genes represented quite a large variety in function. Based on their functions, these genes can be classified into eight major roles i.e., (1) photosynthesis, (2) cellular redox balance; (3) cellular components stability; (4) cellular energy preservation; (5) metal ion homeostasis; (6) hormonal-activated signaling pathways; (7) production of transcription factors; and (8) organ development.

Table 2. A total of 25 annotated genes were consistently upregulated in all PEG exposed plantlets (BP2, BP7, and BP10).

Contigs ID	Biological process	Cellular components	Molecular function
MaB_DN812_c1_g1	DNA repair; response to salt stress	cytosolic small ribosomal subunit	damaged DNA binding
MaB_DN94_c0_g2	Protein sumoylation	cytoplasm; nucleus	protein tag ubiquitin-like protein
MaB_DN1392_c1_g1	Protein refolding root development	chloroplast; endoplasmic reticulum	peptidyl-prolyl cis-trans isomerase
MaB_DN75017_c0_g1	Polar nudeus fusion; rRNA pseudo	box H/ACA snoRNP complex; box H/ACA telomerase RNP	box H/ACA snoRNA binding telomerase RNA

	uridine synthesis	comp.	binding
MaB_DN180_c0_g3	Spliceosomal snRNP assembly	U12-type spliceosomal complex	mRNA binding
MaB_DNS2396_co_g1	.	endoplasmic reticulum membrane	.
MaB_DN6130_c1_g4	.	endosome; plasma membrane;	peptidyl-prolyl cis-trans isomerase
MaB_DN16107_c0_g1	.	plasma membrane	.
MaB_DN999_c1 g1	.	eukaryotic translation initiation	mRNA binding; ribosome binding;
MaB_DN10_c1_g1	.	cytoplasm, nudeus	.
MaB_DN8775_c3_g1	Defense response to bacterium	plasma membrane	magnesium-dependent protein
MaB_DN767_c1_g2	.	nucleosome; nucleus	protein heterodimerization activity
MaB_DN31726_c0_g1	Cytokinin metabolic process extracellular space	extracellular space	cytokinin dehydrogenase activity;
MaB_DN3960_c1_g1	Glutathione metabolic process,GO:0009407 toxin catabolic cytoplasm,GO:0005829	cytoplasm,GO:0005829 cytosol	Glutathione transferase activity
MaB DN3032_c1_g1	Hydrogen peroxide catabolic	cell wall; plasmodesma; vacuole cytoplasm	heme binding; metal ion binding;
MaB_DN39392_c1_g1	.	cytoplasm	metal ion binding; superoxide
MaB_DN17680_c0_g1	Intracellular protein transport;	chloroplast, clathrin coat of trans-	clathrin light chain binding; structural
MaB_DN3027_c0_g1	Chromatin-mediated maintenance	transcription elongation factor	metal ion binding; RNA polymerase
MaB DN6388_c0_g1	Cell cycle arrest; cellular response to DNA damage stimulus	cytoplasmic ribonucleoprotein granule; ubiquitin ligase complex	kinase binding; metal ion binding; protein heterodimerization activity
MaB_DN2680_c0_g2	GO:0005412_translation	cell wall; cytosolic small ribosomal	structural constituent of ribosome
MaB DN16624_c0_g1	Abscisic acid-activated signaling	cytosol; nucleus	magnesium-dependent protein serine/threonine phosphatase
MaB_DN138_c0_g2	Defense response	cell wall; extracellular region	.
MaB DN7483 c0 g1	Glutathione metabolic process;	chloroplast: cytoplasm; cytosol	Glutathione binding; glutathione
MaB DN20701_c0_g1	Cell redox homeostasis	endoplasmic reticulum lumen	protein disulfide isomerase activity
MaB_DN47361_c0_g2	Photorespiration	mitochondrial respiratory chain	NADH dehydrogenase (ubiquinone)

Table 3. Summary of the contig annotation and differentially expressed genes (DEGs) analysis. Numbers presented in each column are total gene counts resulting from each step described in the column title.

Sample	Assembled contigs	Total annotated	Numbers of DEGs	Upregulated	Downregulated
BK (Control)	147,811	129,701	-	-	-
BP2 (2.5% PEG)			1,564	631 (40.3%)	933 (59.7%)
BP7 (7.5% PEG)			1,556	658 (42.2%)	898 (57.8%)
BP10 (10% PEG)			1,744	762 (43.7%)	982 (56.3%)

3.4. Functional Cluster Analysis of DEGs

Using *A. thaliana* genome model as a reference, all differentially expressed genes were clustered in 26 functional groups with the largest being constituted by genes playing roles in transmembrane-transports (1,307 genes), photosynthesis (1,303 genes), transcription factor (TFs) production (1,013 genes), protein phosphorylation (747 genes), cellular secretions and detoxifications (468 genes), and cell redox homeostasis (449 g enes). Other functional groups that were also overrepresented by the DEGs are those related to cellular respiration, RNA processing and translation, protein interactions, cell wall re-organization, cellular components and organelles, lipids- and amino acids- biosynthesis and transports, secondary metabolite biosynthesis, and DNA modifications and repairs (Figure 5).

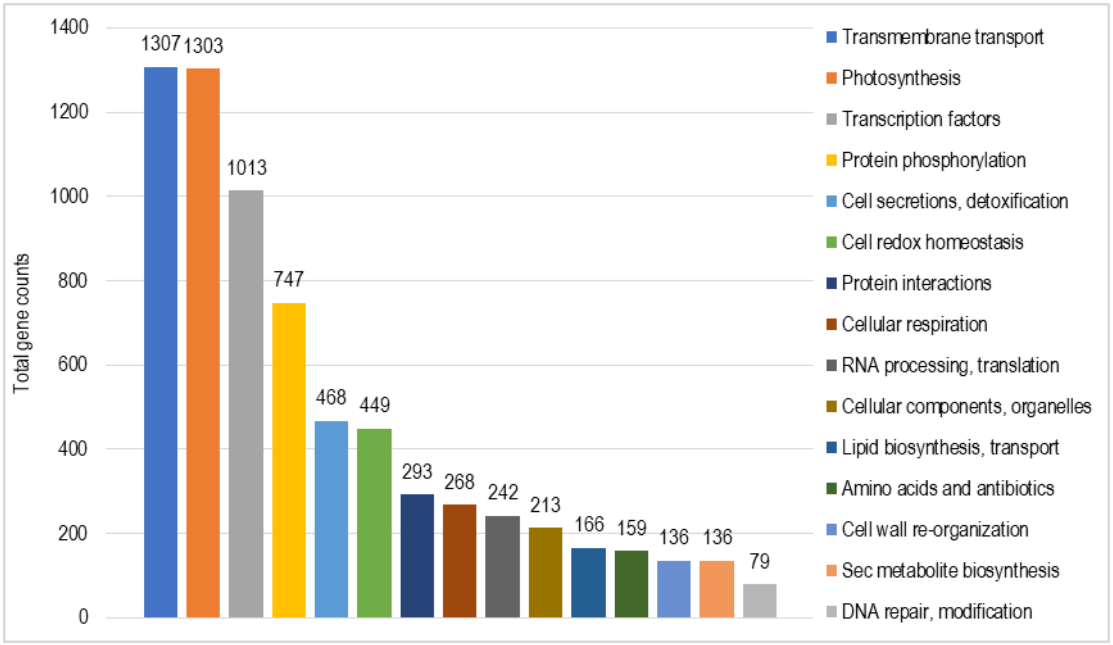

Figure 5. Gene functional cluster analysis of DEGs using DAVID bioinformatics tools.

Further GO enrichment analysis was achieved in detail for the 10% PEG treatment only. Based on DAVID, GO enrichment results of the BP10 plantlets indicated systemic changes that occur upon stress in banana involving large numbers of biological processes, i.e. the cellular process, metabolic process, response to stimulus, developmental process, and multicellular organismal process. The most significantly enriched biological processes are the cellular metabolic process, primary and secondary metabolic process, cellular catabolic process, carbohydrate metabolic process, alcohol catabolic process, the stress response to abiotic stimulus, response to chemical stimulus, cellular process, anatomical structure development, multicellular organismal development, post-embryonic development, and pollen development (Table 4). Through statistical analysis, a total of 1,744 genes were identified as differentially expressed genes (DEGs) under PEG treatment, and 1,046 genes (67%) of them were mapped to the reference genomes (Figure 5). It is important to note that the gene members can be overlapped between clusters, which means a gene can contribute to more than one functional cluster. A big portion of genes were represented in the clusters of transmembrane transport, photosynthesis, transcription factors, and protein phosphorylation. A great majority of genes responsible for photosynthetic apparatus, such as chloroplast thylakoid membrane and plastid envelope, were remarkably downregulated upon the drought stress. The suppression effect appeared to be highly exclusive in chloroplast, but not as much in other cellular structures. Downregulation effects on the macromolecular complex, especially the protein-complex composing the light harvesting complex, photosystem I- and photosystem II- reaction center, were strongly suggested in our study. Unlike other cell components, genes responsible for mitochondria structure were majorly upregulated during water stress. The GO enrichment analysis results showed the 100 highest upregulated and 100 lowest down-regulated genes under 10% PEG treatment (Supplementary Table S.3 and S.4).

Table 4. Highly-enriched GO terms in the transcriptome of the three PEG treatments. The colors represent a level of upregulation and downregulation (see the legend).

Enriched GO term_ general	Enriched GO term_ specified	Stress level					
		PEG 2.5		PEG 7.5		PEG 10	
		U	D	U	D	U	D
Photosynhesis	Light reaction						
	Electron transport chain						
	Light harvesting						
Responses to stimulus	Response to stress						
	Response to abiotic stimulus						
	Response to radiation						
	Response to temperature						
	Response to light stimulus						
	Response to chemical stimulus						
	Response to hypoxia						
Secondary metabolic process	Phenylpropanoid biosynthesis						
	Toxin metabolic process						
Carbohydrate metabolism	Carbohydrate metabolic process						
	Carbohydrate catabolic process						
Cellular process	Cellular metabolic process						
	Cellular biosynthesis process						
	Cell growth						
Developmental process	Anatomical structure development						
	Cell differentiation						
	Organ (fruits, seeds) development						
Multicellular organismal development	Pollen develoment						
	Post-embryonic development						
Establishment of localization	Transport						
	Intracellular transport						
Post-translational protein modification	Cellular protein metabolic process						
	Cellular macromolecule metabolic process						
Cell surface receptor-linked signaling pathway	Transmembrane receptor tyrosine kinase signaling						
Cellular respiration	Respiratoty chain						
	Glycolysis						
	Electron transport chain						
	Electron carrier activity						
Lipid localizaton							
Chemical homeostasis	Cellular cation homeostasis						
	Cellular metal ion homeostasis						
Regulation	Regulation of cellular structures						
	Regulation of primary metabolic						
	Regulation cellular biosynthetis						

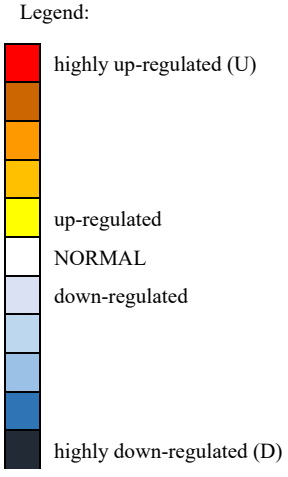

3.5. Enriched Transcription Factors Following the exposure with PEG Treatment

The increase of transcription factors (TFs) is the event that leads to the up-regulation of various stress responsive genes. From the list of down-regulated genes of BP 10 plantlet sample (with 10% PEG treatment) a total of 47 genes encoding for transcription factor (TF) that belong to at least 26 TF families were identified, including five families that are typical for stress-responsive genes families such as *MYB, WRKY, bZIP, ABF, DRE*, auxin- and ethylene-activated TFs and WUSCHEL-related homeobox (WOX). In addition to the major responses, there were other interesting biological processes. The high activation of 13 genes in phenyl-propanoid biosynthesis pathway and 5 genes in the flavonoid biosynthesis pathway, which identity and roles require further studies. Analysis results revealed there were 47 genes in 'PBM' banana plantlets that were likely encoded for Transcription Factors (TFs) which were all down-regulated following the drought treatment (Table 5). At least 26 TF families were identified in this study- with the majority are the members of zinc-finger super family protein (10 genes) followed by the *Ethylene Response Factor (ERF)* (4 genes), *MYB* and *MYB*-like TF family protein (3 genes), homeobox-leucine zipper family protein (bZIP) (3 genes), and *WRKY- DNA binding protein* (3 genes). Other TF families are listed in Table 5.

Table 5. Enriched transcription factors of banana plantlets after a four-week exposure to the 10% PEG treatment**.**

M. acuminata cv Barangan_ID	Transcription factors (TFs)
MaB_DN44306_c0_g1	GATA type zinc finger transcription factor family protein (GNC)
MaB_DN74488_c0_g1	Myb domain protein 4 (MYB4)
MaB_DN98776_c0_g1	Basic helix-loop-helix DNA-binding superfamily protein (BIM1)
MaB_DN4733_c0_g1	B-box type zinc finger protein with CCT domain-containing protein
MaB_DN10455_c0_g1	Myb domain protein 16 (MYB16)
MaB_DN41764_c0_g1	Homeobox-leucine zipper family protein/lipid-binding START domain-containing protein (ANL2)
MaB_DN41811_c0_g1	Indole-3-acetic acid 7(IAA7)
MaB_DN76283_c0_g1	Transducin/WD40 repeat-like superfamily protein (SAP)
MaB_DN19921_c1_g1	WRKY DNA-binding protein 34(WRKY34)
MaB_DN72367_c0_g1	GRAS family transcription factor (HAM1)
MaB_DN48622_c0_g1	Basic helix-loop-helix DNA-binding superfamily protein (AT2G41130)
MaB_DN73622_c0_g1	Sigma factor E(SIGE)
MaB_DN17935_c0_g1	GOLDEN2-like 2 (GLK2)
MaB_DN1504_c0_g2	Myb-like transcription factor family protein (AT3G25790)
MaB_DN11588_c0_g1	C2H2 and C2HC zinc fingers superfamily protein (AT3G49930)
MaB_DN65671_c0_g1	B-box type zinc finger family protein (BBX28)
MaB_DN11415_c0_g1	Dehydration response element B1A(DREB1A)
MaB_DN16139_c0_g1	Zinc finger (CCCH-type) family protein (AT5G58620)
MaB_DN81329_c0_g1	Ethylene response factor 1(ERF1)
MaB_DN64112_c0_g1	WUSCHEL related homeobox 4(WOX4)
MaB_DN76923_c0_g1	Abscisic acid responsive elements-binding factor 3(ABF3)
MaB_DN18967_c0_g1	Indeterminate (ID)-domain 5(IDD5)
MaB_DN1857_c3_g1	Squamosa promoter-binding protein-like (SBP domain) transcription factor family protein (AT1G76580)
MaB_DN7159_c0_g1	WRKY DNA-binding protein 15(WRKY15)
MaB_DN83106_c0_g1	Homeobox protein ATH1(ATH1)
MaB_DN2764_c1_g8	Homeobox-leucine zipper protein 4 (HB-4) / HD-ZIP protein (HAT2)
MaB_DN91310_c0_g1	B-box type zinc finger family protein (BBX31)
MaB_DN40655_c0_g1	Homeodomain-like superfamily protein (MYR2)
MaB_DN313_c0_g2	High mobility group B2(HMGB2)
MaB_DN97433_c0_g1	NAC domain containing protein 73(NAC073)
MaB_DN1150_c0_g3	Integrase-type DNA-binding superfamily protein (AT5G51190)
MaB_DN1416_c1_g3	Integrase-type DNA-binding superfamily protein (AT5G51190)
MaB_DN2208_c0_g1	Subgroup of HMGB (high mobility group B) proteins that have a distinctive DNA-binding motif, the HMG-box domain.

MaB_DN23742_c0_g1	Salt-inducible zinc finger 1;(source: Araport11)
MaB_DN17080_c0_g2	C2H2 zinc finger transcription factor that coordinately activates phytochelatin-synthesis related gene expression
MaB_DN45281_c0_g1	Early auxin-induced (IAA16)
MaB_DN65589_c0_g1	Pathogen-induced transcription factor. Forms protein complexes with itself and with WRKY40.
MaB_DN3939_c0_g4	Homeobox protein similar to GL2
MaB_DN60885_c0_g1	Nuclear factor Y, subunit C13;(source: Araport11)
MaB_DN58665_c0_g1	Member of the RAV family of DNA binding proteins. Contains B3 domain. Recognizes 5'-CACCTG-'3 motif.
MaB_DN38283_c0_g1	TCP family transcription factor. Regulated by miR319. Involved in heterchronic regulation of leaf differentiation.
MaB_DN1713_c0_g2	Basic leucine zipper transcription factor involved in the activation of SA-responsive genes.
MaB_DN11711_c1_g2	Member of the GATA factor family of zinc finger transcription factors.
MaB_DN99807_c0_g1	C2H2-like zinc finger protein
MaB_DN10167_c0_g2	Member of the ERF (ethylene response factor) subfamily B-1 of ERF/AP2 transcription factor family (ATERF-9)
MaB_DN64256_c0_g1	Member of the ERF (ethylene response factor) subfamily B-1 of ERF/AP2 transcription factor family (ATERF-9).
MaB_DN17076_c0_g1	Member of the ERF (ethylene response factor) subfamily B-1 of ERF/AP2 transcription factor family (ATERF-9).

3.6. Validation of the DEG genes by qRT-PCR

The qRT-PCR for randomly selected 15 DEGs was tested to check their expression profiles. This independent experimental validation using qRT-PCR was carried out with cDNA synthesized from shoot parts of the BP10 (10% PEG) plantlets, and the BK was used as the control treatment. The qRT-PCR results showed expressions of selected genes (Figure 6). In several points, the results showed similar trends between qRT-PCR data and RNA-seq data. The discrepancy might be due to the different RNA sources, for validation, the RNA samples for qRT-PCR were collected from shoot parts while for RNA-seq (transcriptome) the RNA samples originated from the whole part of plantlets (shoots and roots).

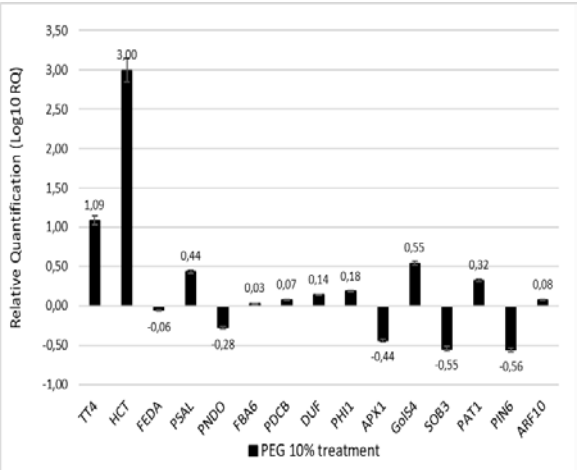

Figure 6. The expression analysis results of fifteen selected DEGs by qRT-PCR and using the *MaACT* and *MaBT* as housekeeping genes.

4. Discussion

Water stress has become a critical factor for the growth of banana plants, and caused substantial changes in their growth, morphological features, and biochemistry reactions (Surendar *et al.,* 2013). Chlorosis in shoots or leaves are indicated with the loss of their green color and turned into pale (Ahmed and El-Sayed, 2021). In banana plantlets the chlorosis in leaves seemed to have occurred as a result of the deterioration of chlorophyll and other photosynthetic pigments (Vergeiner *et al*., 2013). It was reported that lack of sufficient water supply decreased the total chlorophyll content and declined yield of banana production in the field (Ramos *et al*., 2019, and Uwimana *et al*, 2021). The transcriptomic analysis would be able to discover the reason (Bashir *et al.*, 2021).

The results of transcriptomic profiling showed that 78% (101,962 genes) of the assembled contigs were mapped to the gene model of the banana genome reference available in CIRAD library. It was indicated that the transcriptome profile was quite unique between different cultivars of banana. There are about 22% (45,849 genes) of the *M. acuminata* cv Barangan Merah that did not match any gene in the previously published *M. acuminata* cv 'DH Pahang' at CIRAD. The difference, however, could also be contributed by the different sample types where the RNA was resourced (Wang *et al*., 2020). The quite large functional variety of the top 100 up regulated genes indicated that once challenged with water deficit conditions, the banana plantlets simultaneously activated many 'strategies' to maintain all the cellular basic functions by protecting cellular components from damage while minimizing further water loss and detoxifying the cells from the free radicals (Muthusamy *et al.*, 2016).

The 10% PEG treatment evidently enhanced expression of genes related with biosynthesis of amino acids including proline, glutamine, glutathione, and anthocyanin. The result indicated that one of the primary responses of the drought-stressed Barangan Merah banana cells was to actively produce those amino acids to maintain cellular osmotic balance as well as to chelate the reactive oxygen species (ROS) and other free radicals (Mahdid *et al.*, 2020). The increase of amino acid production and protein formation is known to be related with the biosynthesis of signaling proteins, which play significant roles in response to abiotic stresses, including drought (Bashir *et al*., 2021). Furthermore, signaling proteins are involved in various biological functions of growth and development of plants cells of bananas (Mattos-Moreira *et al*., 2018). Similar results were also reported (Xu *et al*., 2019). The PEG-induced water stress also affected the contents of soluble proteins and gave an impact on increasing the biosynthesis

of proline, and free amino acid in banana plantlets (Amnan *et al*., 2021).

Our data showed a drastic turndown in the expression of genes responsible for the biosynthesis of both the photosynthesis apparatus and the enzymes that catalyzed the process. When water, as one of the primary components in photosynthesis, was diminished, the plant adjusted by down-regulating the relevant genes for photosynthesis, preserving energy for other primary functions. Similarly, previous studies reported a large turndown of photosynthetic genes in tangor (Xiao *et al*., 2017), bermudagrass (Yuan *et al*, 2021), and several okra varieties (Ahmed and El-Sayed., 2021) when the plants are under drought stress. It was also reported in rice plants that a major reduction in photosynthesis rates was related to the decrease in photosynthesis enzyme activities and oxidative damage to the chloroplast (Wada *et al.* 2019). A reduction in photosynthesis rate as a response to drought stress was reportedly occurred through the stomatal- and non-stomatal-routes in potato (Chen *et al*., 2020). In the lower level of drought, the stomatal conductance was lowered down upon the sensing of water deficit, resulting in stomatal closure, and causing the decrease of photosynthesis rate (Yuan *et al*., 2021). In a higher drought stress, the free radicals accumulate to a level that exceeds the capacity of cellular antioxidants to neutralize. This signals the cell to repress the production of a core protein of photosystem II, causing further reduction in photosynthesis (Wang *et al*., 2020).

In the present study, it was indicated that the plant perceives the 10% PEG treatment as severe water stress due to at least two reasons: first, the massive downregulation of chloroplast structural genes following drought exposure; second, the high expression of the stress-marker genes, such as *superoxide dismutase (SOD)* and *ascorbate peroxidase (APX)*, as well as the antioxidant genes. In addition to photosynthesis reduction, a large amount of stress responding genes was highly increased upon drought treatment. Interestingly, the genes that were activated upon drought stress were the genes that are also responsive to other kinds of abiotic stimuli, such as light, radiation, temperature (Yang *et al*., 2015), chemicals (Xu *et al*., 2019) and hypoxia (Ilyas *et al*., 2021). These stress-responsive gene families produce two types of products. The first types are proteins that are involved in the protection of the cells and in the regulation of signal transduction of stress-related-pathways, such as *heat shock proteins (HSP)*, *chaperons, late-embryogenesis abundant (LEA)* proteins (Oguz *et al*., 2022). Second products are proteins that involve in further regulation of signal transduction and stress-responsive gene expression (Kimotho *et al*., 2019), such as *Transcription Factors (TFs)* and *dehydration responsive elements (DRE)*. Our DEG results also identified 1 *heat shock proteins (HSP)* genes, 5 chaperon genes, 4 reactive oxygen species (ROS)-responsive genes, and 47 transcription factors. In fact, water shortage signals the cells, through activation of abscisic acid (ABA)-dependent and ABA-independent regulatory systems, to activate the expressions of various drought related genes. Similar results were reported in various plants when the plants were exposed to a water stress condition (Seleiman *et al*., 2021).

The reduction in photosynthesis rate consequently reduced the production of cellular energy resources. In addition, water-deficit stress causes large energy consumption. Many studies showed that plants compensate for this energy-demanding condition by increasing their cellular respiration (Yuan *et al.,* 2021). It demonstrated upregulation of genes encodes for mitochondrial components as well as the genes playing a role in glycolysis, electron transport chain, and electron carrier activity. Eight genes related to 'mitochondrial structures', four genes were assigned to 'mitochondrial respiratory chain complex', three genes of 'cytochrome c, and nine genes related to 'glycolytic activity' were identified in this study, which demonstrated a substantial raise in oxidative respiration process following water-deficit stress. In addition to oxidative respiration, plant under drought stress also reportedly exhibited alternative respiration through fermentation in order to survive the harsh condition (Hu *et al*., 2017). In line with this, four pyruvate kinase genes and eight alcohol dehydrogenase genes were identified, both are important enzymes in the anaerobic respiration pathway. This may imply that the stressed-banana employs the anaerobic respiration, in addition to the aerobic respiration, to cope with the water scarcity (Mahdid *et al*., 2020). Our data showed that there are so many changes in other processes in banana plant that consistently occurred in all PEG treatment groups, such as polysaccharide metabolic and catabolic processes, multicellular organismal development, intracellular and transmembrane transports, post-translational protein modification, cell surface receptor-linked signaling pathway, and regulation of cellular chemical homeostasis (Ahmed and El-Sayed, 2021).

Plants are known to produce a wide array of secondary metabolites as a defense mechanism against environmental stresses. Drought is also able to influence the biosynthesis of secondary metabolites, that are positively correlated with the increments of antioxidants (Al-Gabbiesh *et al.*, 2015). Phenylpropanoid biosynthesis pathway, in particular, has been reported to be highly activated, following harsh abiotic stresses including heavy metal, salinity, heat, cold, UV radiations, and drought, leading to the accumulation of polyphenolic compounds including flavonoids (Šamec *et al*., 2021). Anthocyanin, carotenoid, flavonoid, and phenolic compounds are known as the antioxidants, which are important in protecting water-stressed cells from the damage caused by the ROS (Ahad *et al.,* 2018). Among others, flavonoids have been suggested to contribute in protecting plants from abiotic disturbances, such as drought, root zone salinity, UV-radiation, and scavenging the harmful ROS (Xu *et al*., 2020). Biochemical and molecular mechanisms of flavonoid and phenyl-propanoid accumulation in response to abiotic stress have been well reviewed in various plants (Bashir *et al*., 2021).

The DEG result identified 47 transcription factors which were affected by the 10% PEG-induced water stress. The central role of transcription factors (TF) in regulating the transcription of stress-responsive genes following environmental stresses has been widely reported and reviewed (Joshi *et al*., 2016). The identification of those TF families in our studies indicated that, like many other plants, *Musa acuminata* also uses both ABA-dependent and ABA-dependent routes to activate the expression of stress-responsive genes (Hrmova and Hussain 2021). Involvement of TF families, such as

WRKY, MYB, bZIP, ABF, ABRE, and *DRE*, in response to abiotic stresses had been reported in bananas. García-Laynes *et al.* (2022) identified the *MaWRKY* family genes from the wild banana *Musa acuminata* ssp. *malaccensis*, which is known as a progenitor of most banana cultivars, and resistant to several diseases and environmental disturbances. Their study discovered that those *MaWRKY* genes showed distinctive expressions in banana plants in response to environmental stresses. The *WRKY* transcription factors (TFs) has been known to encode functional transcription factors (Chen *et al.*, 2015), and play a part in plant defense responses through phytohormone the signaling pathways (Yang *et al*., 2015). Moreover, there had been many identified TF families from *Musa acuminata* that were highly affected by the drought conditions. Interestingly, hormone-activated TFs, such as ethylene response factor (ERF, 4 genes) and auxin-induced TFs (2 genes), were among the TF families induced by water-deficit. The result implied that banana plantlets also used auxin and ethylene, in addition to abscisic acid, to signal the activation of stress responses genes (Hu *et al.*, 2015). Our GO analysis results also showed enriched numbers of genes that take parts in post-embryonic- and plant organ development. Another finding that we found intriguing was the identification of a gene encodes for WUSCHEL-related homeobox (WOX), a TF family that is known to play important roles in determining cell fates during embryogenesis, and all other stages of plant development even under water stress. In this study, it was discovered that, like other plants, banana plantlets responded to water stress through a complex metabolic and signaling networks (Oguz *et al.*, 2022).

As shown in Figure 6, in general, the confirmation of gene expressions of 15 selected annotated DEGs showed similar trends of expressions between qRT-PCR data and RNA-seq data. These 15 DEGs were selected for their potentially key roles in some important bioprocesses, which were affected by water stress. Those genes are identified and known to be involved in photosynthesis (*MaFEDA, MaPSAL*, and *MaPNDO*), biosynthesis of flavonoid and antioxidants (*MaTT4* and *MaHCT*), glycolysis (*MaFBA6* and *MaPDCB*), respond to osmotic stress (*MaDUF*, *MaPHI1*, *MaAPX1,* and *MaGolS4*), organ development (*MaSOB3, MaPAT1*and *MaPIN6*), and as a transcription factor (*MaARF10*). Gene functions of the 15 selected DEG are listed in Supplementary Data Table S.1. In several points, there were some dissimilarities between expression results based on the transcriptome analysis and the qRT-PCR assay, for instance the *MaGolS4*, *MaSOB3,* and *MaPAT1* genes. A similar research result was reported in banana transcriptomic analysis by Hu *et al.* (2017). They suggested that there were some possible reasons for discrepancies. The first possibility might be due to the fact that genes have different alternative forms, where the RNA-seq might be able to capture the expression of all alternative forms for a gene, while the qRT-PCR assay might capture the expression of only one alternative form. Secondly, the RNA-seq and qRT-PCR seemed to exhibit consistent results for genes with high significance expressions and might not be persistent for genes with low expressions (Hu *et al.*, 2017). Taken together, because of the important functions of these genes in banana defense mechanism, further studies are still needed.

5. Conclusion

Morphological changes occurred in plantlets after four weeks of PEG exposure. The addition of PEG caused a lack of sufficient water and seemed to be corresponding to the changes in transcriptome profiles. A transcriptome library of 129,701 annotated genes, and the expression profile, of banana (*Musa acuminata* cv 'Barangan Merah') has been established. Transcriptomic analysis revealed eight major biological processes were highly affected by the drought stress in banana plantlets, those are: 1) photosynthesis, 2) cellular redox balance; 3) cellular components stability; 4) cellular energy preservation; 5) metal ion homeostasis; 6) hormonal-activated signaling pathways; 7) production of transcription factors; and 8) organ development. This study found that exposure to water stress highly influenced primary and secondary metabolism in banana plantlets. In a relatively smaller extent, other processes that seemed to be affected are cell wall re-organization, plant hormone production, transmembrane signaling pathways and secondary metabolite biosynthesis. The high induced phenylpropanoid biosynthesis and flavonoid pathways suggest that banana produce flavonoid compounds in response to water stress, which evident and identities need to be further investigated. A total of 47 genes encode for transcription factor (TF) were identified. They belong to at least 26 TF families, including five families that are typical for stress-responsive genes families (MYB, WRKY, bZIP, ABF, DRE), auxin- and ethylene-activated TFs and WUSCHEL-related homeobox (WOX). Further transcriptomic analyses are still needed to reveal the effect of water stress on major bioprocesses in detail.

Acknowledgements

This research was supported by several parties i.e., the visiting scholars from The Schatz Center for Tree Molecular Genetics, the Department of Ecosystem Science and Management, Pennsylvania State University (PSU), University Park, PA 16802, USA (2013); The ITB World Class University (WCU) in house post-doctoral program (2019) and ITB-WCU International collaboration research program (2020). We also thank the technical staffs of the Directorate of Information System and Technology (DIST)-ITB, Bandung for their assistance in providing the computing space and consultation during the transcriptome data analysis.

Conflict of interest

The authors declare that they have no conflicts of interest in the research.

References

Ahad A, Yaqoob A, Nawaz R, Gul A, Shahid N, Rehman sami ullah T, Rao AQ, Shahid AA and Hasnain T. 2018. Multidimensional roles of flavonoids in background of *Gossypium hirsutum*. *Cogent food agric*, **4(1)**: 1510754. https://doi.org/10.1080/23311932.2018.1510754

Al-Gabbiesh A, Kleinwächter M and Selmar D. 2015. Influencing the contents of secondary metabolites in spice and medicinal plants by deliberately applying drought stress during their cultivation. *Jordan J Biol Sci.*, **8(1)**: 1-10. http://jjbs.hu.edu.jo

Ahmed ZG and El-Sayed MA. 2021. Influence of drought stress on physiological traits of crossed okra varieties. *Jordan J Biol Sci*., **14(2)**: 253-260. https://doi.org/10.54319/jjbs/ 140208

Amalia L, Taufikurahman and Widiyanto SNB. 2016. *Catalase (CAT)* and *ascorbate peroxidase (APX)* genes expression level in growth of banana plantlets *(Musa acuminata)* cv. Ambon Lumut under chromium stress condition. *Plant Sci.*, **11(4)**: 69-74. https://doi.org/ 0.3923/jps.2016.69.74

Amnan MAM, Pua T, Lau S, Tan BC, Yamaguchi H, Hitachi K, Tsuchida K and Komatsu S. 2021. Osmotic stress in banana is relieved by exogenous nitric oxide. *PeerJ.*, **9**: e10879. https://doi.org/10.7717/peerj.10879

Backiyarani S, Uma S, Saraswathi MS, Saravanakumar AS and Chandrasekar A. 2015. Transcriptome analysis of banana (*Musa balbisiana*) based on next-generation sequencing technology. *Turk J Agric For.,* **39(5)**: 705-717. https://doi.org/10.3906/tar-1406-171

Bashir SS, Hussain A, Hussain SJ, Wani OA, Nabi SZ, Dar NA, Baloch FS and Mansoor S. 2021. Plant drought stress tolerance: Understanding its physiological, biochemical and molecular mechanisms. *Biotechnol Biotechnol Equip.,* **35(1)**: 1912-1925. https://doi.org/ 10.1080/13102818.2021.2020161

Bharati K, Prasad M, Mir H and Pal AK . 2018. In vitro regeneration and acclimatization of banana cv. Malbhog. *CJAST*, **31(4)**: 1-6. http://dx.doi.org/10.9734/CJAST/2018/45985

Bhattacharjee S and Saha AK. 2014. Plant water-stress response mechanisms. In: Gaur RK and Sharma P. (Eds.), **Approaches to Plant Stress and their Management**. Springer, India, pp. 149-172. https://doi.org/ 10.1007/978-81-322-1620-9_8

Chen T, Li W, Hu X, Guo J, Liu A and Zhang B. 2015. A cotton *MYB* transcription factor, *GbMYB5*, is positively involved in plant adaptive response to drought stress. *Plant Cell Physiol*, **56(5)**: 917-929. https://doi.org/10.1093/pcp/pcv019

Chen Y, Li C, Yi J, Yang Y, Lei C and Gong M. 2020. Transcriptome response to drought, rehydration and re-dehydration in potato. *Int J Mol Sci.,* **21(1):** 159. https://doi.org/10.3390/ ijms21010159

Davey MW, Gudimella R, Harikrishna JA, Sin LW, Khalid N and Keulemans J. 2013. A draft *Musa balbisiana* genome sequence for molecular genetics in polyploid, inter-and intra-specific *Musa* hybrids. *BMC genomics*, **14**: 1-20. https://doi.org/10.1186/ 1471-2164-14-683

Diningrat DS, Widiyanto SM, Pancoro A, Iriawati, Shim D, Panchangam B, Zembower N, and Carlson JE. 2015. Transcriptome of teak (*Tectona grandis*, L.f) in vegetative to generative stages development. *J Plant Sci,* **10(1)**: 1-14. https://doi.org/10.3923/jps.2015.1.14

El-Gebali S, Mistry J, Bateman A, Eddy SR, Luciani A, Potter SC, Qureshi M, Richardson LJ, Salazar GA, Smart A and Sonnhammer ELL. 2019. The Pfam protein families database in 2019. *Nucleic Acids Res.,* **47(D1)**: D427-D432. https://doi.org/10.1093/nar/gky995

García-Laynes S, Herrera-Valencia VA, Tamayo-Torres LG, Limones-Briones V, Barredo-Pool FA, Baas-Espinola FM, Alpuche-Solís AG, Puch-Hau C and Peraza-Echeverria S. 2022. The banana *MaWRKY18, MaWRKY45, MaWRKY60* and *MaWRKY70* genes encode functional transcription factors and display differential expression in response to defense phytohormones. *Genes*, **13**: 1891. https://doi.org/10.3390/genes13101891

Haas BJ, Papanicolaou A, Yassour M, Grabherr M, Blood PD, Bowden J, Couger MB, Eccles D, Li B, Lieber M and MacManes MD. 2013. De novo transcript sequence reconstruction from RNA-seq using the Trinity platform for reference generation and analysis. *Nat Protoc.,* **8(8)**: 1494-1512. https://doi.org/10.1038/nprot.2013.084

Harb AM, AL-Hadid KJ and Sharab AS. 2020. Molecular and biochemical changes of indole-3-acetic acid in the expanding leaves of barley (*Hordeum vulgare* L.) under salinity stress. *Jordan J Biol Sci.*, **13(1):** 93-100.

Hrmova M and Hussain SS. 2021. Plant transcription factors involved in drought and associated stresses. *Int J Mol Sci*., **22(11):** 5662. https://doi.org/10.3390/ijms22115662

Hu W, Zuo J, Hou X, Yan Y, Wei Y, Liu J, Li M, Xu B and Jin Z. 2015. The auxin response factor gene family in banana: genome-wide identification and expression analyses during development, ripening, and abiotic stress. *Front Plant Sci.,* **6**:742. https://doi.org/10.3389/ fpls.2015.00742

Hu W, Ding Z, Tie W, Yan Y, Liu Y, Wu C, Liu J, Wang J, Peng M, Xu B and Jin Z. 2017. Comparative physiological and transcriptomic analyses provide integrated insight into osmotic, cold, and salt stress tolerance mechanisms in banana. *Sci Rep*., **7(1)**: p.43007. https://doi.org/10.1038/srep43007

Ilyas M, Nisar M, Khan N, Hazrat A, Khan AH, Hayat K, Fahad S, Khan A and Ullah A. 2021. Drought tolerance strategies in plants: A mechanistic approach. *J Plant Growth Regul.,* **40**: 926–944. https://doi.org/10.1007/s00344-020-10174-5

Joshi R, Wani SH, Singh B, Bohra A, Dar ZA, Lone AA, Pareek A and Singla-Pareek SL. 2016. Transcription factors and plants response to drought stress: Current understanding and future directions. *Front Plant Sci.,* **7**:1029. https://doi.org/10.3389/fpls.2016.01029

Kimotho RN, Baillo EH and Zhang Z. 2019. Transcription factors involved in abiotic stress responses in maize (*Zea mays* L.) and their roles in enhanced productivity in the post genomics era. *PeerJ*, **7**: e7211. https://doi.org/10.7717/peerj.7211

Kusdianti DS, Diningrat DS, Iriawati and Widiyanto SN. 2016. P5CS and HSP 8 1-2 gene expression profile of banana (*Musa acuminata*) in vitro culture under salt stress condition. *J. Plant Sci.,* **11(4)**: 91-95. https://doi.org/10.3923/jps.2016.91.95

Langmead B and Salzberg SL. 2012. Fast gapped-read alignment with Bowtie 2. *Nat Methods*, **9(4)**: 357-359. https://doi.org/10.1038/nmeth.1923

Li B and Dewey CN. 2011. RSEM: accurate transcript quantification from RNA-Seq data with or without a reference genome. *BMC Bioinform.*, **12**: 1-16. https://doi.org/10.1186/1471-2105-12-323

Livak KJ and Schmittgen TD. 2001. Analysis of relative gene expression data using real-time quantitative PCR and the $2^{-\Delta\Delta CT}$ method. *Methods*, **25(4)**: 402-408. https://doi.org/10.1006/ meth.2001.1262

Love M I, Huber W and Anders S. 2014. Moderated estimation of fold change and dispersion for RNA-seq data with DESeq2. *Genome Biol.*, **15(12)**: 1-21. https://doi.org/10.1186/s13059-014-0550-8

Lowe R, Shirley N, Bleackley M, Dolan S, and Shafee T. 2017. Transcriptomics technologies. *PLoS Comput Biol*. **13(5)**: e1005457. https://doi.org/10.1371/journal.pcbi. 1005457

Mahdid M, Kameli A and Simonneau T. 2021. Rapid osmotic adjustment in leaf elongation zone during polyethylene glycol application: Evaluation of the imbalance between assimilation and utilization of carbohydrates. *Jordan J Biol Sci.*, **14(1)**: 147-155. https://doi.org/10.54319/ jjbs/140119

Martin G, Baurens FC, Droc G, Rouard M, Cenci A, Kilian A, Hastie A, Doležel J, Aury JM, Alberti A and Carreel F. 2016. Improvement of the banana *Musa acuminata* reference sequence using NGS data and semi-automated bioinformatics methods. *BMC Genom.*, **17(1)**: 1-12. https://doi.org/10.1186/s12864-016-2579-4

Mattos-Moreira LA, Ferreira CF, Amorim EP, Pirovani CP, de Andrade EM, MAC Filho and Ledo CAS. 2018. Differentially expressed proteins associated with drought tolerance in bananas (*Musa* spp.) *Acta Physiol Plant.,* **40**(60): 1-14. https://doi.org/10.1007/s11738-018-2638-3

Michel BE and Kaufmann MR. 1973. The osmotic potential of polyethylene glycol 6000. *Plant Physiol.*, **51(5)**: 914-916. https://doi.org/10.1104/pp.51.5.914

Murashige T and Skoog F. 1962. A revised medium for rapid growth and bioassays with tobacco tissue cultures. *Physiol Plant.,* **15**: 473-497. https://doi.org/10.1111/j.13993054.1962. tb08052.x

Muthusamy M, Uma S, Backiyarani S and Saraswathi MS. 2014. Computational prediction, identification, and expression profiling of microRNAs in banana (*Musa* spp.) during soil moisture deficit stress. *J Hortic Sci Biotechnol*., **89(2)**: 208-214. https://doi.org/10.1080/ 14620316.2014.11513070

Muthusamy M, Uma S, Backiyarani S and Saraswathi MS. 2015. Genome-wide screening for novel, drought stress-responsive long non-coding RNAs in drought-stressed leaf transcriptome of drought-tolerant and-susceptible banana (*Musa* spp) cultivars using Illumina high-throughput sequencing. *Plant Biotechnol Rep*., **9**: 279-286. https://doi.org/10.1007/ s11816-015-0363-6

Muthusamy M, Uma S, Backiyarani S, Saraswathi MS and Chandrasekar A. 2016. Transcriptomic changes of drought-tolerant and sensitive banana cultivars exposed to drought stress *Front Plant Sci.*, **7**: 1609. https://doi.org/10.3389/fpls.2016. 01609.

Nansamba M, Sibiya J, Tumuhimbise R, Karamura D, Kubiriba J and Karamura E. 2020. Breeding banana (*Musa* spp.) for drought tolerance: A review. *Plant Breed.*, **139(4)**: 685-696. https://doi.org/10.1111/pbr.12812

Nayar NM. 2010. The Bananas: Botany, Origin, Dispersal. *In:* Janick J (Ed.), **Horticultural Reviews** Vol. 36. Wiley-Blackwell, India, pp. 117-164. https://doi.org/10.1002/ 9780470527238.ch2

Oguz, MC, Aycan M, Oguz E, Poyraz I and Yildiz M. 2022. Drought stress tolerance in plants: Interplay of molecular, biochemical and physiological responses in important development stages. *Physiologia,* **2**: 180–197. https://doi.org/10.3390/physiologia2040015

Omprakash, Gobu R, Bisen P, Baghel M and Chourasia KN. 2017. Resistance/tolerance mechanism under water deficit (drought) condition in plants. *Int J Curr Microbiol App Sci*., **6(4)**: 66-78. https://doi.org/10.20546/ ijcmas.2017.604.009

Rani B and Sharm VK. 2017. Transcriptome profiling: methods and applications- A review. *Agric Rev*., **38(4)**: 271-281. http://dx.doi.org/10.18805/ag.R-1549

Ramos LM, PI Meneses, FO Reis, Silva BV and Reis IS. 2019. Ecophysiology of banana seedlings grown in different water regimes. *Rev Bras Cienc Agrar*., **42(2)**: 440-447. h ttps:// doi.org/10.19084/rca.17174

Šamec D, Karalija E, Šola I, Bok VV and Salopek-Sondi B. 2021. The role of polyphenols in abiotic stress response: The influence of molecular structure. *Plants*, **10(1):** 118. https:// doi.org/10.3390/plants10010118

Santos AS, Amorim EP, Ferreira CF and Pirovani CP. 2018. Water stress in *Musa* spp.: A s ystematic review. *PLoS One*, **13(12)**: e0208052. https://doi.org/10.1371/journal.pone. 0208052

Sebayang NS, Puspita DE and Basri S. 2018. Different planting media in Barangan banana (*Musa Acuminata* Colla) breeding in Southeast Aceh. *Indonesian J Agric Res*., **1(3)**: 307-316. https://doi.org/10.32734/injar.v1i3.473

Seleiman MF, Al-Suhaibani N, Ali N, Akmal M, Alotaibi M, Refay Y, Dindaroglu T, Abdul-Wajid HH and Battaglia ML. 2021. Drought stress impacts on plants and different approaches to alleviate its adverse effects. *Plants,* **10**: 259. https://doi.org/10.3390/plants 10020259

Smith-Unna R, Boursnell C, Patro R, Hibberd JM and Kelly S. 2016. TransRate: reference-free quality assessment of de novo transcriptome assemblies. *Genome Res*., **26(8):** 1134-1144. https://doi.org/10.1101/gr.196469.115

Surendar KK, Devi DD, Ravi I, Krishnakumar S, Kumar SR and Velayudham K. 2013. Water stress in banana-A review. *Bull Env Pharmacol Life Sci*., **2(6)**: 1-18. https://bepls.com/may_ 2013/1.pdf

Song H, Liu Y, Hu G, Qin Y an d Lin S. 2011. An improved method for total RNA isolation from recalcitrant loquat (*Eriobotrya japonica* Lindl.) buds. *Pak J Bot*., **43(2)**: 1163-1171. http://www.pakbs.org/pjbot/

Uwimana B, Zorrilla-Fontanesi Y, van Wesemael J, Mduma H, Brown A, Carpentier S and Swennen R. 2021. Effect of seasonal drought on the agronomic performance of four banana genotypes (*Musa* spp.) in the East African highlands. *Agronomy,* **11(4)**: 1-23. https://dx.doi. org/10.3390/agronomy11010004

Vergeiner C, Banala S an d Krautler B. 2013. Chlorophyll breakdown in senescent banana leaves: Catabolism reprogrammed for biosynthesis of persistent blue, fluorescent tetrapyrroles. *Chem Eur J.,* **19**: 12294-12305. https://doi.org/10.1002/chem.201301907

Wada S, Takagi D, Miyake C, Makino A and Suzuki Y. 2019. Responses of the photosynthetic electron transport reactions stimulate the oxidation of the reaction center chlorophyll of photosystem I, P700, under drought and high temperatures in rice. *Int J Mol Sci*., **20(9)**: 2068. https://doi.org/10.3390/ ijms20092068

Wang R, Xu Y, Li XG, Shen Y, Wang LX and Xie ZS. 2020. Comparison of drought tolerance of banana genotypes. *GMR*, **19(2)**: 1-14. http://dx.doi.org/10.4238/gmr18544

Xiao JP, Zhang LL, Zhang HQ and Miao LX. 2017. Identification of genes involved in the responses of tangor (*C. reticulata* × *C. sinensis*) to drought stress. *Biomed Res Int.,* **(2017)** ID 8068725: 1-15. https://doi.org/10.1155/2017/8068725

Xu M, Zeng CB, He R, Yan Z, Qi Z, Xiong R, Cheng Y, Wei SS and Tang H. 2019. Transcriptome analysis of banana (*Musa acuminate* L.) in response to low-potassium stress. *Agronomy*, **9(4):** 169. https://doi.org/10.3390/agronomy9040169

Xu N, Liu S, Lu Z, Pang S, Wang L, Wang L and Li W. 2020. Gene expression profiles and flavonoid accumulation during salt stress in Ginkgo biloba seedlings. *Plants*, **9(9)**: 1162. https://doi.org/10.3390/plants9091162

Yang QS, Gao J, He W D, Dou1 TX, Ding LJ, Wu JH, Li CY, Peng XX, Zhang S and Yi GJ. 2015. Comparative transcriptomics analysis reveals the difference of key gene expression between banana and plantain in response to cold stress. *BMC Genom,* **16:** 446. https://doi.org/ 10.1186/s12864-015-1551-z

Yuan Z, Ni X, Arif M, Dong Z, Zhang L, Tan X, Li J and Li C. 2021. Transcriptomic analysis of the photosynthetic, respiration, and aerenchyma adaptation strategies in Bermuda-grass *(Cynodon dactylon)* under different submergence stress. *Int J Mol Sci.,* **22(15)**: 7905. https://doi.org/10.3390/ijms22157905

SUPPLEMENTARY TABLES

Table S.1. List of 17 selected gene primers used for validation using qRT-PCR assay including housekeeping genes.

Gene Symbol	Function	Primer Sequence (Forward)	Primer Sequence (Reverse)	Product Size (bp)
MaACT	Actin histone-lysine N-methyltransferase setd3	CTGACTGGCAGCAGGACATA	CCAAATCGTGCCTTTGAACT	162
MaBT	Beta tubulin (housekeeping)	AGTCCGGAGCTTCAACCTTT	ACGCTGACGATGGAGAAGAC	221
MaTT4	Chalcone and stilbene synthase	CTCCCAACCTCTACGAGCAG	GGGTCCATGTAGGAGCACAT	267
MaHCT	Hydroxycinnamoyl-CoA shikimate transferase	ATGGTGGAAGTGGTGGAATC	TTGAGCAGCTGTACGGAGAA	167
MaFEDA	2-Fe-2S ferredoxin	TTGCCATCTCTCCCTGTCTT	GGCATTCGATCACCTTCTCT	214
MaPSAL	Photosystem I subunit l	GCATCTCACGAACACCATTG	GATGGGCTGAATCACTTGGT	196
MaPNDO	Pyridine nucleotide-disulfide oxidoreductase	GCTTTCTCCAGCATCAAAGG	CCCATTCCTCCTTCGACATA	216
MaFBA6	Aldolase superfamily protein 6	CTCAGGAGGGCAGAGTGAAG	CTCGCCTTCTCGACATTCTC	162
MaPDCB	Thiamine pyrophosphate dependent pyruvate decarboxylase family protein B	TGTGCTTCATCGAGGTCATC	AGTCTCGGACGCAAGAACAT	215
MaDUF	2-Aminoethanethiol dioxygenase, putative	TCCAGGCATGACGGTATTCAC	TGAGGCACATTGACCCAGTC	78
MaPHI1	Phosphate-responsive 1 family protein	TAACACGAACCCAAGAAGCG	CCCACCACCATATTCTGCTAAG	95
MaAPX1	Ascorbate peroxidase 1	ACGATGTGGTGTCAAAGACG	GTATGTCAAGATGGGGAACTGC	140
MaGolS4	Galactinol synthase 4	TCGAAGAAGGTAAGCAGGTCTC	CACTGGAAAGGAAGCTAACATGG	140
MaSOB3	Putative AT-hook DNA-binding family protein	TCGCAGCCACATTCTTGAAC	GCAATCCTTCTGTGACCAATCG	96
MaPAT1	GRAS family transcription factor	ATCGTCAATCCCTGTGATCCG	TGACTTCCAGATTGCTCAAGGG	103
MaPIN6	Auxin efflux carrier family protein	GGATCTCACAGTTTCCTTCGTTG	ACATCACGGTGTAGAAGTCCTC	71
MaARF10	Auxin response factor 10	AATGTGAACCGTGTGAACCC	AGAAGGGAGCAAGATGGATAGC	73

Table S.2. List of the 94 annotated genes, out of 233 genes, that were consistently downregulated in all levels of PEG treatments (PEG 2.5, PEG7, and PEG10).

Contig ID *M.acuminata* 'Barangan'	GO annotation		
	Biological process	Cellular components	Molecular function
MaB_DN55073_c0_g1	regulation of endosperm development; regulation of starch biosynthetic process	chloroplast	amylopectin binding; maltoheptaose binding; starch binding
MaB_DN54882_c0_g1	actin filament-based movement; cell division; fruit development; Golgi localization; gynoecium development; mitochondrion localization; post-embryonic development; root hair elongation; trichome morphogenesis	myosin complex; plasmodesma; root hair tip; transport vesicle	actin binding; ATP binding; calmodulin binding; motor activity
MaB_DN84725_c0_g1	leaf-, floral-, fruit- morphogenesis; microtubule cytoskeleton organization; oxidation-reduction process; regulation of cell shape; regulation of epidermal cell division and differentiation; regulation of trichome morphogenesis; response to osmotic stress; response to salt stress	cytoplasmic stress granule; cytosol; microtubule; trans-Golgi network	identical protein binding; NAD binding; protein homodimerization activity
MaB_DN71017_c0_g1	cation transport; cellular metal ion homeostasis; cellular response to phosphate starvation; meristem maintenance; pollen germination; pollen maturation; stem cell fate determination	endoplasmic reticulum membrane; integral component of membrane; plasma membrane	ATP binding; ATPase activity; metal ion binding
MaB_DN8953_c0_g2	defense response to bacterium; negative regulation of translation; nuclear-transcribed mRNA poly(A) tail shortening	CCR4-NOT core complex; nucleus; P-body	3'-5' exonuclease activity; metal ion binding; poly(A)-specific ribonuclease activity; RNA binding
MaB_DN36213_c0_g1	lysyl-tRNA aminoacylation	cytosol	ATP binding; lysine-tRNA ligase activity; tRNA binding
MaB_DN27607_c0_g4	carbon utilization	chloroplast stroma	carbonate dehydratase activity; zinc ion binding
MaB_DN6111_c0_g2	photosynthesis	chloroplast thylakoid membrane; integral component of membrane; photosystem I reaction center	.
MaB_DN31557_c0_g1	signal transduction	.	ATP binding; protein serine/threonine kinase activity
MaB_DN75200_c0_g1	endocytosis; lipid transport; viral process	endoplasmic reticulum; endosome membrane; integral component of membrane; plasma membrane	lipid binding; metal ion binding
MaB_DN3084_c0_g1	protein ubiquitination; response to cadmium ion; response to chitin	.	metal ion binding; ubiquitin-protein transferase activity
MaB_DN5666_c0_g1	photosynthesis, light harvesting in photosystem I; protein-chromophore linkage; response to light stimulus	chloroplast envelope; chloroplast thylakoid membrane; photosystem I; photosystem II	chlorophyll binding; metal ion binding
MaB_DN62333_c0_g1	phosphatidylinositol phosphorylation; phosphatidylinositol-mediated signaling	chloroplast; cytoplasm; membrane; plasma membrane	1-phosphatidylinositol 4-kinase activity
MaB_DN344_c0_g4	photosynthesis, light harvesting; protein-chromophore linkage	chloroplast thylakoid membrane; integral component of membrane; photosystem I; photosystem II	chlorophyll binding; metal ion binding

MaB_DN7600_c0_g1	amino acid transmembrane transport; amino acid transport	integral component of membrane; plasma membrane	amino acid transmembrane transporter activity; primary active transmembrane transporter activity; symporter activity
MaB_DN345_c0_g2	.	.	ATP binding; ubiquitin conjugating enzyme activity
MaB_DN16594_c1_g1	cellular copper ion homeostasis; response to light intensity; zinc ion homeostasis	chloroplast; chloroplast envelope; chloroplast inner membrane	ATP binding; ATPase activity; cadmium transmembrane transporter activity, phosphorylative mechanism; metal ion binding; ATPase-coupled zinc transmembrane transporter activity
MaB_DN17080_c0_g2		nucleus	DNA binding; metal ion binding
MaB_DN6425_c0_g1	transport of virus in host, cell to cell; viral entry into host cell; viral penetration into host nucleus	host cell	aspartic-type endopeptidase activity; nucleic acid binding; RNA-directed DNA polymerase activity; RNA-DNA hybrid ribonuclease activity; zinc ion binding
MaB_DN82953_c0_g1	histone H3-K4 methylation	histone methyltransferase complex	histone binding
MaB_DN26630_c0_g1	intracellular signal transduction; protein phosphorylation	cytoplasm; nucleus	ATP binding; protein serine/threonine kinase activity
MaB_DN904_c0_g1	.	chloroplast stroma	ATP binding
MaB_DN68858_c0_g1	iron ion homeostasis	integral component of membrane	cadmium ion transmembrane transporter activity; manganese ion transmembrane transporter activity
MaB_DN95436_c0_g1	long-day photoperiodism; flowering; regulation of timing of transition from vegetative to reproductive phase	cytoplasm; nucleus; perinuclear region of cytoplasm; plasma membrane	transcription factor binding
MaB_DN72306_c0_g1	unsaturated fatty acid biosynthetic process	integral component of membrane	oxidoreductase activity, acting on paired donors, with oxidation of a pair of donors resulting in the reduction of molecular oxygen to two molecules of water
MaB_DN81905_c0_g1	.	integral component of membrane; plasma membrane	ATP binding; protein serine/threonine kinase activity
MaB_DN78426_c0_g1	peptidyl-L-cysteine S-palmitoylation; protein targeting to membrane	endoplasmic reticulum; Golgi apparatus; integral component of membrane; plasma membrane	protein-cysteine S-palmitoyltransferase activity
MaB_DN7935_c0_g1	photosynthesis, light harvesting; protein-chromophore linkage	chloroplast thylakoid membrane; integral component of membrane; photosystem I; photosystem II	chlorophyll binding; metal ion binding
MaB_DN58280_c0_g1	.	integral component of membrane; plasma membrane	ATP binding; protein serine/threonine kinase activity
MaB_DN904_c0_g2	.	chloroplast stroma	ATP binding
MaB_DN8360_c0_g1	.	.	ATP binding; helicase activity; RNA binding
MaB_DN14270_c0_g1	polar nucleus fusion; rRNA pseudouridine synthesis; snRNA pseudouridine synthesis	box H/ACA snoRNP complex; box H/ACA telomerase RNP complex; Cajal body; nucleolus	box H/ACA snoRNA binding; telomerase RNA binding
MaB_DN10259_c0_g2	.	nucleus	AT DNA binding; DNA-binding transcription factor activity
MaB_DN78376_c0_g1	defense response to Gram-negative bacterium; floral organ abscission; lateral root morphogenesis; leaf abscission; pectin catabolic process; protein autophosphorylation; regulation of gene expression	integral component of membrane; plasma membrane	ATP binding; protein serine/threonine kinase activity; transmembrane receptor protein tyrosine kinase activity

MaB_DN65589_c0_g1	defense response to bacterium, fungus; regulation of defense response; response to salicylic acid	nucleus	DNA-binding transcription factor activity; sequence-specific DNA binding
MaB_DN7935_c1_g1	photosynthesis, light harvesting in photosystem I; protein-chromophore linkage; response to light stimulus	chloroplast envelope; chloroplast thylakoid membrane; integral component of membrane; photosystem I; photosystem II; plastoglobule	chlorophyll binding; metal ion binding
MaB_DN43104_c0_g1	amino acid transmembrane transport; gamma-aminobutyric acid transport	integral component of membrane; plasma membrane	amino acid transmembrane transporter activity; gamma-aminobutyric acid transmembrane transporter activity
MaB_DN67987_c0_g1	trichome branching	.	calcium ion binding
MaB_DN12891_c0_g1	.	chloroplast stroma	ATP binding
MaB_DN7159_c0_g1	response to chitin	nucleus	calmodulin binding; DNA-binding transcription factor activity; transcription regulatory region DNA binding
MaB_DN78578_c0_g1	peptidyl-pyroglutamic acid biosynthetic process, using glutaminyl-peptide cyclotransferase	endoplasmic reticulum membrane; integral component of membrane; plasma membrane	glutaminyl-peptide cyclotransferase activity
MaB_DN1568_c0_g2	chlorophyll biosynthetic process; photosynthesis	chloroplast	protochlorophyllide reductase activity
MaB_DN58553_c0_g1	.	.	transferase activity, transferring hexosyl groups
MaB_DN7935_c2_g1	photosynthesis, light harvesting in photosystem I; protein-chromophore linkage; response to light stimulus	chloroplast envelope; chloroplast thylakoid membrane; integral component of membrane; photosystem; photosystem II; plastoglobule	chlorophyll binding; metal ion binding
MaB_DN89859_c0_g1	cell cycle; multicellular organism development; response to abscisic acid	cytoplasm	.
MaB_DN99671_c0_g1	cellular response to phosphate starvation; phosphate ion transport	Golgi apparatus; integral component of membrane; plasma membrane; trans-Golgi network	inositol hexakisphosphate binding; phosphate ion transmembrane transporter activity
MaB_DN62890_c0_g1	cytokinin-activated signaling pathway; phosphorelay signal transduction system; phosphorylation	cytoplasm; nucleus	histidine phosphotransfer kinase activity; protein histidine kinase binding
MaB_DN47361_c0_g1	photorespiration	integral component of membrane; mitochondrial membrane; mitochondrial respiratory chain complex I; respiratory chain complex I	NADH dehydrogenase (ubiquinone) activity
MaB_DN12562_c0_g2	.	.	serine-type carboxypeptidase activity
MaB_DN36962_c0_g1	photosynthesis, light harvesting in photosystem I; protein-chromophore linkage; response to light stimulus	chloroplast thylakoid membrane; integral component of membrane; photosystem I; photosystem II; plastoglobule	chlorophyll binding; metal ion binding
MaB_DN66931_c0_g1	.	integral component of membrane; plasma membrane	transmembrane transporter activity
MaB_DN75006_c0_g1	clathrin coat assembly; clathrin-dependent endocytosis; pollen tube growth; protein localization to plasma membrane; vesicle budding from membrane	clathrin-coated pit; clathrin-coated vesicle; Golgi apparatus; plasma membrane; pollen tube	1-phosphatidylinositol binding; clathrin heavy chain binding; phosphatidylinositol-4,5-bisphosphate binding; SNARE binding
MaB_DN1777_c1_g1	translation	cytosolic large ribosomal subunit; plasma membrane	mRNA binding; structural constituent of ribosome

MaB_DN63_c1_g1	.	.	calcium ion binding
MaB_DN10464_c0_g3	autophagosome assembly; protein autophosphorylation; protein transport; regulation of autophagy	autophagosome; cytoplasmic vesicle; cytosol; membrane; phagophore assembly site	ATP binding; protein serine/threonine kinase activity
MaB_DN12135_c0_g1	defense response signaling pathway; detection of bacterium; immune response-regulating signaling pathway; plant-type hypersensitive response; regulation of anion channel activity	endomembrane system; integral component of membrane; plasma membrane	ATP binding; protein serine/threonine kinase activity; transmembrane receptor protein kinase activity
MaB_DN39798_c0_g1	transmembrane transport	integral component of membrane; plasma membrane	ATP binding; ATPase-coupled transmembrane transporter activity
MaB_DN7546_c0_g2	pollen tube growth	.	carboxylic ester hydrolase activity; methyl indole-3-acetate esterase activity
MaB_DN11415_c0_g1	abscisic acid-activated signaling pathway; glucosinolate metabolic process	nucleus	DNA-binding transcription factor activity; sequence-specific DNA binding
MaB_DN6765_c0_g3	photosynthesis; light harvesting in photosystem I, photosystem II; protein-chromophore linkage; regulation of stomatal movement; response to abscisic acid; response to high light stimulus	chloroplast envelope; chloroplast thylakoid membrane; integral component of membrane; photosystem I; photosystem II; plastoglobule; thylakoid membrane	chlorophyll binding; metal ion binding; protein domain specific binding
MaB_DN344_c0_g3	photosynthesis, light harvesting in photosystem; protein-chromophore linkage; response to light stimulus	chloroplast envelope; chloroplast thylakoid membrane; integral component of membrane; photosystem I; photosystem II; plastoglobule	chlorophyll binding; metal ion binding
MaB_DN27607_c0_g1	carbon utilization	chloroplast stroma	carbonate dehydratase activity; zinc ion binding
MaB_DN8953_c0_g1	defense response to bacterium; negative regulation of translation; nuclear-transcribed mRNA poly(A) tail shortening	CCR4-NOT core complex; nucleus; P-body	3'-5' exonuclease activity; metal ion binding; poly(A)-specific ribonuclease activity; RNA binding
MaB_DN36120_c0_g1	pentose-phosphate shunt; reductive pentose-phosphate cycle	chloroplast thylakoid membrane; cytosol	calcium ion binding; cobalt ion binding; manganese ion binding; transketolase activity
MaB_DN59498_c0_g1	.	anchored component of membrane; anchored component of plasma membrane	electron transfer activity; metal ion binding
MaB_DN13736_c0_g1	.	integral component of membrane	carbon-sulfur lyase activity; transaminase activity
MaB_DN2207_c0_g3	photosynthetic electron transport in photosystem I; photosynthetic NADP+ reduction; photosystem I stabilization	chloroplast envelope; chloroplast membrane; photosystem I; chloroplast thylakoid membrane; integral component of membrane	.
MaB_DN76923_c0_g1	abscisic acid-activated signaling pathway; response to abscisic acid; response to salt stress; response to water deprivation	nucleus	DNA-binding transcription factor activity; transcription regulatory region sequence-specific DNA binding
MaB_DN45814_c0_g1	.	cell wall; extracellular region	.
MaB_DN59396_c0_g1	.	extracellular space	copper ion binding; oxidoreductase activity
MaB_DN13250_c0_g1	.	chloroplast thylakoid membrane; integral component of membrane	.
MaB_DN2764_c1_g8	auxin-activated signaling pathway, negative regulation of transcription	nucleus	DNA-binding transcription factor activity; sequence-specific DNA binding

MaB_DN80742_c0_g1	.	membrane	heme binding; iron ion binding; oxidoreductase activity, acting on paired donors, with incorporation or reduction of molecular oxygen, NAD(P)H as one donor, and incorporation of one atom of oxygen
MaB_DN64755_c0_g1	hydrogen peroxide catabolic process; response to oxidative stress	extracellular region	heme binding; metal ion binding; peroxidase activity
MaB_DN34665_c0_g1	photosynthesis; pyruvate metabolic process	chloroplast	ATP binding; kinase activity; metal ion binding; pyruvate, phosphate dikinase activity
MaB_DN67584_c0_g1	amyloplast organization; cell division; embryo development ending in seed dormancy; embryonic axis specification; late endosome to vacuole transport, receptor-mediated endocytosis	endoplasmic reticulum; endosome membrane; Golgi apparatus; intracellular membrane-bounded organelle; late endosome membrane; trans-Golgi network; vacuolar membrane	.
MaB_DN7510_c0_g1	.	cytoplasm	5'-nucleotidase activity; metal ion binding; nucleotide binding
MaB_DN82130_c0_g1	defense response; response to biotic stimulus	extracellular region; vacuole	.
MaB_DN7968_c0_g2	ribosomal large subunit assembly	preribosome, large subunit precursor	.
MaB_DN22837_c0_g1	cell wall biogenesis; cell wall organization; xyloglucan metabolic process	apoplast, cell wall	hydrolase activity, hydrolyzing O-glycosyl compounds; xyloglucan: xyloglucosyl transferase activity
MaB_DN16139_c0_g1	regulation of transcription	.	DNA-binding transcription factor activity; metal ion binding
MaB_DN31_c2_g1	defense response to fungus; induced systemic resistance; response to abscisic acid; response to cold; response to salt stress	chloroplast outer membrane; endoplasmic reticulum; extracellular region; plant-type cell wall; plasmodesma	.
MaB_DN77256_c0_g1	defense response to fungus; response to abscisic acid; response to glucose; response to salt stress	mitochondrion	.
MaB_DN64112_c0_g1	cell division; phloem or xylem histogenesis; procambium histogenesis	nucleus	DNA binding
MaB_DN7987_c0_g1	phenylpropanoid metabolic process	.	4-coumarate-CoA ligase activity; ATP binding
MaB_DN45737_c0_g1	RNA modification	.	zinc ion binding
MaB_DN36169_c0_g1	.	.	electron transfer activity; metal ion binding
MaB_DN90833_c0_g1	copper ion transmembrane transport; photosynthetic electron transport chain	chloroplast envelope; chloroplast membrane; chloroplast stroma; integral component of membrane; plastid	ATP binding; copper chaperone activity; copper transmembrane transporter activity, phosphorylative mechanism
MaB_DN36962_c0_g2	photosynthesis, light harvesting in photosystem I; protein-chromophore linkage	chloroplast thylakoid membrane; integral component of membrane; photosystem I-II; plastoglobule	chlorophyll binding; metal ion binding
MaB_DN7935_c3_g1	photosynthesis; light harvesting; protein-chromophore linkage	chloroplast thylakoid membrane; integral component of membrane; photosystem I-II	chlorophyll binding; metal ion binding
MaB_DN7935_c4_g1	photosynthesis; light harvesting; protein-chromophore linkage	chloroplast thylakoid membrane; integral component of membrane; photosystem I-II	chlorophyll binding; metal ion binding
MaB_DN22217_c1_g2	photosynthesis	chloroplast photosystem I	protein domain specific binding
MaB_DN17076_c0_g1	defense response; ethylene-activated signaling pathway	nucleus	DNA binding; DNA-binding transcription factor activity
MaB_DN95147_c0_g1	poly(A)+ mRNA export from nucleus	cell	DNA binding; metal ion and mRNA

				binding

Table S.3. List of the 100 genes with the highest upregulation following the 10% PEG treatment.

Contig ID *M.acuminata* 'Barangan'	ID M acuminata 'Pahang'	GO annotation		
		Cellular component	Molecular function	Biological process
MaB_DN477_c0_g1	Ma06_p06180.1	integral component of membrane	.	nodulation
MaB_DN553_c0_g1	Ma06_p06180.1	integral component of membrane	.	nodulation
MaB_DN2532_c0_g2	Ma05_p07040.1	cytoplasm	L-ascorbate peroxidase activity	hydrogen peroxide catabolic process; response to oxidative stress
MaB_DN1283_c1_g1	Ma09_p30640.1	.	.	.
MaB_DN32_c0_g2	Ma08_p33280.1	.	chitinase activity	chitin catabolic process; polysaccharide catabolic process
MaB_DN37218_c0_g1	Ma09_p11800.1	.	.	.
MaB_DN2428_c0_g2	NA	.	.	.
MaB_DN955_c0_g1	Ma08_p23240.1	.	.	.
MaB_DN3418_c0_g1	Ma06_p06040.1	endoplasmic reticulum membrane	Iron ion binding; L-ascorbic acid binding; procollagen-proline 4-dioxygenase activity	peptidyl-proline hydroxylation to 4-hydroxy-L-proline
MaB_DN9130_c0_g1	Ma09_p30690.1	.	.	.
MaB_DN39392_c0_g1	Ma02_p04310.2	cytoplasm	metal ion binding; superoxide dismutase activity	.
MaB_DN176_c1_g1	Ma08_p30760.1	plasma membrane; vacuolar membrane	proton-transporting ATPase activity	.
MaB_DN1937_c0_g2	Ma04_p29690.1	.	.	.
MaB_DN4829_c0_g1	Ma05_p31910.1	.	.	.
MaB_DN20701_c0_g1	Ma01_p10230.1	endoplasmic reticulum lumen	protein disulfide isomerase activity	cell redox homeostasis
MaB_DN1912_c0_g2	Ma02_p03250.1	nucleolus; ribonucleoprotein complex	nucleosome binding; RNA binding	rRNA processing
MaB_DN138_c0_g2	Ma06_p03940.1	cell wall; extracellular region	.	defense response
MaB_DN402_c0_g1	Ma08_p20020.1	cytoplasm; microtubule; plasma membrane	GTP binding; structural constituent of cytoskeleton	microtubule cytoskeleton organization; mitotic cell cycle
MaB_DN8443_c0_g1	Ma03_p12340.1	cytoplasm; nucleus	kinase binding; metal ion binding; phosphatase binding	response to glucose; response to mannose; response to sucrose
MaB_DN2818_c0_g4	Ma11_p14250.1	endoplasmic reticulum	monooxygenase activity; oxidoreductase activity	anthocyanin-containing compound biosynthetic process
MaB_DN180_c0_g3	Ma05_p25540.1	U12-type spliceosomal complex; U5 snRNP	mRNA binding	spliceosomal snRNP assembly
MaB_DN12172_c0_g1	Ma07_p03130.1	chloroplast stroma; membrane	acyl-[acyl-carrier-protein] desaturase activity; metal ion binding; stearoyl-[acp] desaturase activity	fatty acid biosynthetic process
MaB_DN10862_c0_g1	Ma09_p24220.1	cytoplasm	pyruvate kinase activity	cellular response to insulin stimulus; glycolytic process
MaB_DN43140_c0_g1	Ma05_p26790.2	.	.	.
MaB_DN89_c0_g3	Ma08_p29910.1	cytoplasm	alcohol dehydrogenase (NAD) activity; zinc ion binding	.
MaB_DN277_c0_g2	Ma06_p11050.1	chloroplast stroma; chloroplast thylakoid	fructose-bisphosphate aldolase activity	fructose 1,6-bisphosphate metabolic process; gluconeogenesis; glycolytic process

MaB_DN7961_c0_g2	Ma09_p27320.1	.	.	.
MaB_DN21625_c0_g1	Ma08_p27150.1	.	.	.
MaB_DN9175_c0_g2	Ma07_p03130.1	chloroplast stroma; membrane	acyl-[acyl-carrier-protein] desaturase activity; metal ion binding; stearoyl-[acp] desaturase activity	fatty acid biosynthetic process
MaB_DN7723_c0_g1	Ma03_p05380.1	.	heme binding; iron ion binding; monooxygenase activity; oxidoreductase activity	.
MaB_DN767_c1_g2	Ma04_p40090.1	nucleosome; nucleus	DNA binding; protein heterodimerization activity	.
MaB_DN3032_c1_g1	Ma10_p15940.1	cell wall; extracellular region; vacuole	heme binding; metal ion binding; peroxidase activity	hydrogen peroxide catabolic process; response to oxidative stress
MaB_DN17547_c0_g1	Ma02_p09950.1	cytoplasm	alcohol dehydrogenase (NAD) activity; metal ion binding	.
MaB_DN999_c1_g1	Ma06_p07440.1	eukaryotic translation initiation factor 2B complex	mRNA binding; ribosome binding; translation initiation factor activity	.
MaB_DN1937_c0_g1	Ma04_p29690.1	.	.	.
MaB_DN2366_c0_g2	Ma08_p24610.1	cytosolic large ribosomal subunit	protein-containing complex binding; structural constituent of ribosome	response to anoxia; translational elongation
MaB_DN4517_c0_g1	Ma05_p31910.1	.	.	.
MaB_DN4934_c0_g2	Ma02_p00070.1	nucleus	DNA-binding transcription factor activity	ethylene-activated signaling pathway; regulation of root development; response to anoxia
MaB_DN4894_c0_g1	NA	.	.	.
MaB_DN3972_c0_g2	Ma06_p13180.1	cytoplasm; nucleus	metal ion binding	response to glucose; response to mannose; response to sucrose
MaB_DN75017_c0_g1	Ma01_p13850.2	box H/ACA snoRNP complex; box H/ACA telomerase RNP complex	box H/ACA snoRNA binding; telomerase RNA binding	polar nucleus fusion; rRNA pseudouridine synthesis; snRNA pseudouridine synthesis
MaB_DN9175_c0_g1	Ma07_p03130.1	chloroplast stroma; membrane	acyl-[acyl-carrier-protein] desaturase activity; metal ion binding; stearoyl-[acp] desaturase activity	fatty acid biosynthetic process
MaB_DN11566_c0_g2	Ma10_p21060.1	cytosol; nucleus	cysteine dioxygenase activity; metal ion binding	detection of hypoxia; peptidyl-cysteine oxidation; response to hypoxia
MaB_DN194_c0_g2	NA	.	.	.
MaB_DN8753_c0_g1	NA	.	.	.
MaB_DN27124_c0_g1	NA	.	.	.
MaB_DN436_c0_g3	Ma05_p28820.1	plasma membrane	FMN binding; NAD(P)H dehydrogenase (quinone) activity	cellular response to auxin stimulus; oxidation-reduction process
MaB_DN46343_c0_g1	NA	.	.	.
MaB_DN16664_c0_g1	NA	.	.	.
MaB_DN3310_c0_g1	Ma06_p21540.1	chloroplast	phosphopantetheine binding	fatty acid biosynthetic process
MaB_DN38_c0_g4	Ma05_p14530.1	cytoplasm; nucleus	protein tag	cellular protein modification process; mRNA splicing, via spliceosome
MaB_DN52337_c0_g1	NA	.	.	.
MaB_DN6388_c0_g1	Ma04_p23090.1	BRCA1-BARD1 complex; cytoplasmic ribonucleoprotein granule; ubiquitin ligase complex	kinase binding; metal ion binding; protein homodimerization activity; RNA binding; ubiquitin-protein transferase activity	cell cycle arrest; DNA repair; negative reg of mRNA 3'-end processing; negative reg of protein export from nucleus; positive reg of apoptosis; positive reg of

				protein catabolic process; protein ubiquitination
MaB_DN8337_c2_g1	Ma02_p07900.1	actin cortical patch; Arp2/3 protein complex	actin binding; ATP binding	complex-mediated actin nucleation; multicellular organism development
MaB_DN9186_c0_g1	Ma02_p22480.1	.	carbohydrate binding	.
MaB_DN5380_c2_g1	NA	.	.	.
MaB_DN95883_c0_g1	NA	.	.	.
MaB_DN3027_c0_g1	Ma10_p27760.1	transcription elongation factor complex	metal ion binding; RNA polymerase II complex binding	chromatin-mediated maintenance of transcription; transcription elongation from RNA polymerase II promoter
MaB_DN4811_c0_g2	Ma05_p20020.1	Golgi apparatus; integral component of plasma membrane; vacuolar membrane	myo-inositol:proton symporter activity	carbohydrate transport
MaB_DN10_c1_g1	Ma03_p24340.1	cytoplasm; nucleus	.	.
MaB_DN2929_c0_g2	Ma06_p29340.1	cytosol; eukaryotic translation initiation factor 3 complex	metallopeptidase activity; translation initiation factor activity	abscisic acid-activated signaling pathway; positive regulation of translational initiation; response to auxin; response to glucose, maltose, sucrose
MaB_DN39009_c0_g1	Ma02_p22100.1	cytoplasm; cytosol	ATP binding; kinase activity; magnesium ion binding; potassium ion binding; pyruvate kinase activity	cellular response to insulin stimulus; glycolytic process
MaB_DN15150_c0_g1	Ma08_p11550.1	.	.	.
MaB_DN3508_c0_g1	Ma09_p30630.1	.	.	.
MaB_DN3960_c1_g1	Ma01_p16820.1	cytoplasm; cytosol	glutathione transferase activity	glutathione metabolic process; toxin catabolic process
MaB_DN60512_c0_g1	NA	.	.	.
MaB_DN10999_c0_g2	NA	.	.	.
MaB_DN13031_c0_g1	NA	.	.	.
MaB_DN1352_c0_g1	NA	.	.	.
MaB_DN73222_c0_g1	Ma03_p19090.1	.	.	.
MaB_DN15289_c0_g1	Ma02_p18370.1	nucleus	DNA binding; metal ion binding	jasmonic acid mediated signaling pathway; leaf senescence
MaB_DN2680_c0_g2	Ma04_p37480.1	cell wall; cytosolic small ribosomal subunit	structural constituent of ribosome	translation
MaB_DN4901_c1_g2	Ma11_p05230.1	nucleus	DNA binding; DNA-binding transcription factor activity	ethylene-activated signaling pathway; regulation of root development; response to anoxia
MaB_DN6967_c0_g5	NA	.	.	.
MaB_DN13691_c0_g1	Ma02_p05260.1	chloroplast	6-phosphogluconolactonase activity	carbohydrate metabolic process; pentose-phosphate shunt
MaB_DN5380_c1_g1	NA	.	.	.
MaB_DN578_c0_g1	Ma01_p07620.1	.	.	.
MaB_DN123_c0_g1	Ma02_p03590.1	ribosome	rRNA binding; structural constituent of ribosome	translation
MaB_DN53893_c0_g1	Ma01_p05190.1	mitochondrion	metal ion binding; NADH dehydrogenase (ubiquinone) activity; quinone binding	.
MaB_DN55569_c0_g1	Ma02_p18200.1	nucleus	DNA-binding transcription factor activity; protein self-association	flower development; photomorphogenesis; vegetative to reproductive phase transition of meristem

MaB_DN25760_c0_g1	Ma09_p20790.1	.	.	.
MaB_DN8892_c0_g2	Ma09_p19760.1	nucleus	DNA-binding transcription factor activity	circadian rhythm; flower development; negative regulation of gene expression; phosphorelay signal
MaB_DN19846_c0_g1	NA	.	.	.
MaB_DN43068_c0_g1	NA	.	.	.
MaB_DN44820_c0_g1	Ma08_p29910.1	cytoplasm	alcohol dehydrogenase (NAD) activity; zinc ion binding	.
MaB_DN12210_c0_g1	NA	.	.	.
MaB_DN43870_c0_g1	Ma08_p06620.2	.	.	.
MaB_DN46215_c0_g1	Ma02_p02500.1	integral component of membrane	metal ion binding	oxidation-reduction process
MaB_DN92475_c0_g1	Ma04_p27850.1	.	.	.
MaB_DN3655_c0_g2	Ma02_p19680.1	nucleus	NAD+ ADP-ribosyltransferase activity	multicellular organism development
MaB_DN423_c0_g2	mipo3_t00160.1	mitochondrion	.	.
MaB_DN46664_c0_g1	Ma10_p03280.2	.	.	.
MaB_DN6373_c0_g1	Ma05_p27790.1	cytoplasm	fructose-bisphosphate aldolase activity	fructose 1,6-bisphosphate metabolic process; gluconeogenesis; glycolytic process
MaB_DN6458_c0_g1	Ma06_p12350.2	.	sucrose synthase activity	sucrose metabolic process
MaB_DN6560_c0_g1	Ma08_p17730.1	nucleus	sequence-specific DNA binding	negative regulation of transcription, DNA-templated
MaB_DN81145_c0_g1	Ma01_p11690.2	.	.	chromatin organization; regulation of gene expression; epigenetic
MaB_DN98221_c0_g1	NA	.	.	.
MaB_DN1361_c0_g2	Ma05_p09360.1	.	1-aminocyclopropane-1-carboxylate oxidase activity; dioxygenase activity; L-ascorbic acid binding; metal ion binding	cellular response to fatty acid; cellular response to iron ion; defense response; ethylene biosynthetic process
MaB_DN17680_c0_g1	Ma04_p17320.2	chloroplast; clathrin coat of trans-Golgi network vesicle; plasma membrane	clathrin light chain binding; structural molecule activity	intracellular protein transport; receptor-mediated endocytosis
MaB_DN25228_c0_g1	NA	.	.	.

Table S.4. List of the 100 genes with the most <u>downregulation</u> following the 10% PEG treatment.

Contig ID M.acuminata 'Barangan'	ID M acuminata 'Pahang'	GO annotation		
		Cellular component	Molecular function	Biological process
MaB_DN766_c0_g1	Ma05_p08930.1	chloroplast envelope; chloroplast thylakoid membrane; photosystem I; photosystem II; plastoglobule	chlorophyll binding; metal ion binding	photosynthesis, light harvesting in photosystem I; protein-chromophore linkage; response to light stimulus
MaB_DN1015_c0_g2	Ma03_p12880.1	apoplast, cell wall; chloroplast outer membrane; endoplasmic reticulum; plasmodesma	protein self-association	cellular response to cold; cold acclimation; defense response to fungus; induced systemic resistance; plant-type hypersensitive response; systemic acquired resistance
MaB_DN1426_c0_g1	Ma06_p05860.1	plasma membrane	calcium ion binding	innate immune response; long-day photoperiodism; regulation of flower development; regulation of nitric oxide metabolic process; response to abscisic acid; response to absence of light;

				response to auxin; response to calcium ion; response to cold; response to heat; response to hydrogen peroxide; response to mechanical stimulus; response to metal ion
MaB_DN733_c0_g2	Ma08_p20080.1	.	.	.
MaB_DN1721_c0_g1	Ma01_p08390.1	chloroplast thylakoid membrane	copper ion binding; electron transfer activity	.
MaB_DN321_c0_g1	Ma07_p20600.1	chloroplast envelope; chloroplast thylakoid membrane; integral component of membrane; photosystem II; plastoglobule	chlorophyll binding	photosynthesis, light harvesting in photosystem I; protein-chromophore linkage; response to light stimulus
MaB_DN766_c1_g1	Ma10_p15370.1	chloroplast envelope; chloroplast thylakoid membrane; integral component of membrane; photosystem I; photosystem II; plastoglobule	chlorophyll binding; metal ion binding	photosynthesis, light harvesting in photosystem I; protein-chromophore linkage; response to light stimulus
MaB_DN8953_c0_g2	Ma09_p30300.1	CCR4-NOT core complex; nucleus; P-body	3'-5' exonuclease activity; metal ion binding; poly(A)-specific ribonuclease activity; RNA binding	defense response to bacterium; exonucleolytic catabolism of deadenylated mRNA; negative regulation of translation; nuclear-transcribed mRNA poly(A) tail shortening
MaB_DN2736_c0_g1	Ma06_p26850.1	cytoplasm	metal ion binding; oxidoreductase activity acting on single donors with incorporation of molecular oxygen; incorporation of two atoms of oxygen	oxylipin biosynthetic process
MaB_DN1077_c0_g1	Ma06_p08680.2	chloroplast; chloroplast thylakoid membrane; integral component of membrane; photosystem I; thylakoid	.	photosynthesis; light harvesting in photosystem I; photosynthetic electron transport chain
MaB_DN344_c0_g1	Ma04_p39550.1	chloroplast thylakoid membrane; integral component of membrane; photosystem I; photosystem II	chlorophyll binding; metal ion binding	photosynthesis, light harvesting; protein-chromophore linkage
MaB_DN7546_c0_g2	Ma09_p07910.1	.	carboxylic ester hydrolase activity; methyl indole-3-acetate esterase activity	pollen tube growth
MaB_DN57_c0_g1	Ma05_p10690.1	.	.	.
MaB_DN8953_c0_g1	Ma06_p20750.1	CCR4-NOT core complex; nucleus; P-body	3'-5' exonuclease activity; metal ion binding; poly(A)-specific ribonuclease activity; RNA binding	defense response to bacterium; exonucleolytic catabolism of deadenylated mRNA; negative regulation of translation; nuclear-transcribed mRNA poly(A) tail shortening
MaB_DN18653_c0_g2	NA	.	.	.
MaB_DN6653_c0_g2	Ma07_p08010.1	chloroplast thylakoid membrane; extrinsic component of membrane; photosystem II oxygen evolving complex	calcium ion binding	photosynthesis
MaB_DN489_c0_g2	Ma06_p16670.1	extracellular region	mannose binding	.
MaB_DN973_c1_g1	Ma03_p24340.1	cytoplasm; nucleus	.	.
MaB_DN8204_c1_g2	Ma04_p30440.1	apoplast, chloroplast stroma; chloroplast thylakoid membrane; photosystem II oxygen evolving complex; thylakoid lumen	calcium ion binding; electron transporter, transferring electrons within the cyclic electron transport pathway of photosynthesis activity	photosynthetic electron transport chain
MaB_DN1096_c0_g1	Ma04_p39550.1	chloroplast thylakoid membrane; integral component of membrane; photosystem I; photosystem II	chlorophyll binding; metal ion binding	photosynthesis; light harvesting; protein-chromophore linkage
MaB_DN668_c0_g1	Ma08_p03860.1	chloroplast thylakoid membrane; photosystem II oxygen evolving	oxygen evolving activity	photosystem II assembly; photosystem II stabilization

		complex		
MaB_DN3084_c0_g1	Ma05_p16120.1	.	metal ion binding; ubiquitin-protein transferase activity	protein ubiquitination; response to cadmium ion; response to chitin
MaB_DN64878_c0_g1	Ma09_p24580.1	chloroplast thylakoid membrane	copper ion binding; electron transfer activity	.
MaB_DN475_c0_g3	Ma11_p01810.1	chloroplast	protochlorophyllide reductase activity	chlorophyll biosynthetic process; photosynthesis
MaB_DN3605_c0_g2	Ma09_p01450.2	chloroplast envelope; chloroplast thylakoid membrane; integral component of membrane; photosystem I; photosystem II; plastoglobule	chlorophyll binding; metal ion binding	light harvesting in photosystem I; protein-chromophore linkage; response to light stimulus
MaB_DN984_c0_g2	Ma04_p27610.1	chloroplast thylakoid membrane; integral component of membrane; photosystem II	.	photosynthesis; photosystem II stabilization
MaB_DN2188_c0_g1	Ma10_p12550.1	apoplast, chloroplast	glyceraldehyde-3-phosphate dehydrogenase (NAD+) (phosphorylating) activity; glyceraldehyde-3-phosphate dehydrogenase (NADP+) (phosphorylating) activity; NAD binding; NADP binding	glucose metabolic process; reductive pentose-phosphate cycle; response to light stimulus
MaB_DN1185_c0_g1	Ma06_p14120.2	chloroplast; chloroplast thylakoid membrane; integral component of membrane; photosystem I; photosystem II antenna complex; plastoglobule; PSII associated light-harvesting complex II; thylakoid membrane	chlorophyll binding; metal ion binding; protein domain specific binding	nonphotochemical quenching; photosynthesis, light harvesting in photosystem I; photosystem II assembly; protein-chromophore linkage; response to blue light; response to far red light; response to light stimulus
MaB_DN984_c0_g1	Ma04_p27610.1	.	.	.
MaB_DN2931_c0_g1	NA	.	.	.
MaB_DN11395_c0_g1	Ma09_p09670.1	chloroplast; chloroplast envelope; chloroplast thylakoid; thylakoid membrane; integral component of membrane; photosystem I reaction center; plastoglobule	protein domain specific binding	photosynthesis
MaB_DN489_c0_g1	Ma06_p16670.1	extracellular region	mannose binding	.
MaB_DN531_c0_g1	Ma07_p10230.1	nuclear chromatin; nucleosome	DNA binding; protein heterodimerization activity	chromatin organization
MaB_DN317_c1_g1	Ma08_p15280.1	.	.	.
MaB_DN785_c0_g2	Ma08_p03640.1	chloroplast envelope; chloroplast thylakoid; thylakoid membrane; integral component of membrane; photosystem I; photosystem II; plastoglobule	chlorophyll binding; metal ion binding	photosynthesis, light harvesting in photosystem I; protein-chromophore linkage; response to blue light; response to cytokinin; response to far red light; response to light stimulus
MaB_DN730_c0_g1	Ma04_p32230.1	.	.	.
MaB_DN7850_c0_g1	Ma05_p03450.1	chloroplast	ATP binding; phosphoribulokinase activity	reductive pentose-phosphate cycle
MaB_DN11003_c0_g1	Ma08_p12270.1	.	.	.
MaB_DN6975_c0_g4	Ma09_p22990.1	.	.	.
MaB_DN344_c0_g2	Ma10_p15370.1	chloroplast thylakoid membrane; integral component of membrane; photosystem I; photosystem II	chlorophyll binding; metal ion binding	photosynthesis, light harvesting; protein-chromophore linkage
MaB_DN7316_c1_g1	Ma08_p17130.1	.	.	.
MaB_DN16544_c0_g2	Ma06_p06320.3	.	.	.
MaB_DN8805_c0_g1	Ma08_p30830.1	nucleus; protein-containing complex	protein homodimerization activity; zinc ion binding	response to water deprivation

MaB_DN13574_c0_g1	Ma02_p01750.1	nucleus	calmodulin binding	regulation of salicylic acid metabolic process; response to salt stress; response to water deprivation
MaB_DN1150_c0_g3	Ma07_p06960.1	nucleus	DNA binding; DNA-binding transcription factor activity	defense response; ethylene-activated signaling pathway
MaB_DN6653_c0_g1	Ma07_p08010.1	chloroplast thylakoid membrane; extrinsic component of membrane; photosystem II oxygen evolving complex	calcium ion binding	photosynthesis
MaB_DN3888_c0_g1	Ma05_p11320.1	.	.	.
MaB_DN936_c1_g1	Ma08_p33260.1	amyloplast	calcium ion binding; chitinase activity	chitin catabolic process; polysaccharide catabolic process; seed germination; seedling development
MaB_DN1416_c1_g3	Ma04_p21170.1	nucleus	DNA-binding transcription factor activity	defense response; ethylene-activated signaling pathway
MaB_DN1061_c0_g2	Ma09_p09900.1	chloroplast thylakoid membrane; integral component of membrane; photosystem I	.	photosynthesis
MaB_DN16455_c0_g1	Ma07_p09650.1	.	.	.
MaB_DN32471_c0_g1	Ma05_p26840.1	.	.	.
MaB_DN9613_c0_g1	Ma09_p22170.1	.	.	.
MaB_DN344_c1_g1	Ma02_p11170.1	chloroplast thylakoid membrane; integral component of membrane; photosystem I; photosystem II	chlorophyll binding; metal ion binding	photosynthesis; light harvesting; protein-chromophore linkage
MaB_DN770_c1_g1	NA	.	.	.
MaB_DN7091_c0_g1	Ma11_p20650.1	chloroplast	glyceraldehyde-3-phosphate dehydrogenase (NADP+) (phosphorylating) activity; NAD binding; NADP binding	glucose metabolic process; reductive pentose-phosphate cycle
MaB_DN9475_c0_g1	Ma02_p16400.1	.	lipid binding	lipid transport
MaB_DN6765_c0_g2	Ma02_p11170.1	chloroplast envelope; chloroplast thylakoid membrane; integral component of membrane; photosystem I; photosystem II; plastoglobule	chlorophyll binding; metal ion binding	photosynthesis, light harvesting in photosystem I; protein-chromophore linkage; response to light stimulus
MaB_DN5894_c0_g2	Ma09_p21570.1	chloroplast; chloroplast envelope; chloroplast thylakoid membrane; integral component of membrane; photosystem I; photosystem II; plastoglobule	chlorophyll binding; metal ion binding; protein domain specific binding; structural molecule activity	photosynthesis, light harvesting in photosystem I; light harvesting in photosystem II; protein-chromophore linkage; regulation of stomatal movement; response to abscisic acid; response to herbicide; response to high light intensity: response to light stimulus
MaB_DN1419_c0_g2	Ma04_p17650.1	chloroplast thylakoid membrane; photosystem I reaction center	.	photosynthesis
MaB_DN23730_c1_g1	Ma03_p03390.1	.	heme binding; metal ion binding; peroxidase activity	hydrogen peroxide catabolic process; response to oxidative stress
MaB_DN92726_c0_g1	Ma04_p31600.1	integral component of membrane; plasma membrane	ATP binding; protein serine/threonine kinase activity	.
MaB_DN344_c0_g4	Ma04_p39550.1	chloroplast thylakoid membrane; integral component of membrane; photosystem I; photosystem II	chlorophyll binding; metal ion binding	photosynthesis; light harvesting; protein-chromophore linkage
MaB_DN17080_c0_g2	Ma09_p27170.1	nucleus	DNA binding; metal ion binding	.
MaB_DN33262_c0_g1	NA	.	.	.
MaB_DN5666_c0_g2	Ma06_p22130.1	chloroplast envelope; chloroplast thylakoid membrane; integral component of membrane;	chlorophyll binding; metal ion binding	photosynthesis, light harvesting in photosystem I; protein-chromophore

		photosystem I; photosystem II; plastoglobule		linkage; response to light stimulus
MaB_DN167_c0_g3	Ma04_p17220.1	.	lipid binding	lipid transport
MaB_DN344_c0_g5	Ma10_p15370.1	chloroplast thylakoid membrane; integral component of membrane; photosystem I; photosystem II	chlorophyll binding; metal ion binding	photosynthesis, light harvesting; protein-chromophore linkage
MaB_DN11415_c0_g1	Ma07_p06000.1	nucleus	DNA-binding transcription factor activity; sequence-specific DNA binding	abscisic acid-activated signaling pathway; glucosinolate metabolic process
MaB_DN18785_c0_g1	Ma05_p26790.2	.	.	.
MaB_DN1776_c0_g1	NA	.	.	.
MaB_DN3328_c0_g1	Ma03_p07810.1	.	.	.
MaB_DN8109_c0_g3	Ma07_p28730.1	mitochondrion	glycine hydroxy methyl-transferase activity; pyridoxal phosphate binding	glycine biosynthetic process from serine; tetrahydrofolate interconversion
MaB_DN1217_c0_g1	Ma06_p08680.2	chloroplast; chloroplast thylakoid membrane; integral component of membrane; photosystem I; thylakoid	.	photosynthesis; light harvesting in photosystem I; photosynthetic electron transport chain
MaB_DN5274_c0_g1	Ma00_p03960.1	.	magnesium ion binding; terpene synthase activity	.
MaB_DN129_c0_g2	Ma08_p33270.1	vacuole	chitinase activity; lysozyme activity	chitin catabolic process; polysaccharide catabolic process
MaB_DN9720_c0_g1	Ma01_p20450.1	.	.	.
MaB_DN1419_c0_g1	Ma05_p14680.1	chloroplast thylakoid membrane; photosystem I reaction center	.	photosynthesis
MaB_DN2315_c1_g2	Ma06_p26850.1	cytoplasm	metal ion binding; oxidoreductase activity, acting on single donors with incorporation of molecular oxygen, incorporation of two atoms of oxygen	oxylipin biosynthetic process
MaB_DN4486_c0_g2	Ma06_p30010.1	chloroplast thylakoid membrane; integral component of membrane; photosystem II	manganese ion binding	photosynthesis
MaB_DN2915_c0_g1	NA	.	.	.
MaB_DN1671_c0_g1	Ma00_p03960.1	.	magnesium ion binding; terpene synthase activity	.
MaB_DN595_c0_g1	Ma10_p05350.1	cytosol; plant-type cell wall; plasmodesma	heme binding; metal ion binding; peroxidase activity	defense response to fungus; hydrogen peroxide catabolic process; response to oxidative stress; rhythmic process
MaB_DN4968_c0_g1	Ma04_p32230.1	cell wall; extracellular region	.	plant-type cell wall organization
MaB_DN1274_c1_g1	Ma06_p38350.1	integral component of membrane; vacuolar membrane	pyrophosphate hydrolysis-driven proton transmembrane transporter activity; inorganic diphosphatase activity; metal ion binding	proton transmembrane transport
MaB_DN16140_c0_g1	Ma04_p14940.1	chloroplast thylakoid membrane; integral component of membrane; photosystem I; photosystem II	chlorophyll binding; metal ion binding	photosynthesis, light harvesting; protein-chromophore linkage
MaB_DN668_c0_g3	Ma08_p03860.1	chloroplast thylakoid membrane; photosystem II oxygen evolving complex	oxygen evolving activity	photosystem II assembly; photosystem II stabilization
MaB_DN4486_c1_g1	Ma08_p29270.1	chloroplast thylakoid membrane; integral component of membrane; photosystem II	manganese ion binding	photosynthesis
MaB_DN2687_c1_g1	Ma05_p17280.1	extracellular region	hydrolase activity; acting on	cuticle development; lipid catabolic

			ester bonds	process
MaB_DN15560_c0_g3	Ma09_p06640.1	chloroplast envelope; chloroplast thylakoid membrane; integral component of membrane; photosystem I; photosystem II; plastoglobule	chlorophyll binding; metal ion binding	photosynthesis; light harvesting in photosystem I; protein-chromophore linkage; response to light stimulus
MaB_DN10592_c0_g5	NA	.	.	.
MaB_DN9417_c0_g1	Ma03_p08980.1	chloroplast	ATP binding; glutamate-ammonia ligase activity	glutamine biosynthetic process
MaB_DN67987_c0_g1	Ma04_p23780.1	.	calcium ion binding	trichome branching
MaB_DN79356_c0_g1	Ma06_p18330.1	.	.	.
MaB_DN8358_c2_g1	Ma09_p07130.1	cytoplasm; cytosol; nuclear envelope; nucleus	Ran GTPase binding	miRNA loading onto RISC involved in gene silencing by miRNA; protein import into nucleus
MaB_DN11059_c0_g1	NA	.	.	.
MaB_DN17024_c0_g1	Ma02_p11170.1	chloroplast thylakoid membrane; integral component of membrane; photosystem I; photosystem II	chlorophyll binding; metal ion binding	photosynthesis; light harvesting; protein-chromophore linkage
MaB_DN16139_c0_g1	Ma05_p30610.1	.	DNA-binding transcription factor activity; metal ion binding	regulation of transcription, DNA-templated
MaB_DN4631_c0_g2	Ma01_p10240.1	chloroplast; chloroplast thylakoid; thylakoid membrane; integral component of membrane; photosystem II, PSII associated light-harvesting complex II	chlorophyll binding; protein domain specific binding; xanthophyll binding	nonphotochemical quenching; photosynthesis; response to karrikin; thylakoid membrane organization
MaB_DN5430_c0_g1	Ma02_p11040.1	chloroplast thylakoid membrane; integral component of membrane; photosystem I reaction center	.	photosynthesis

JJBS

Volume 17, Number 1,March 2024
ISSN 1995-6673
Pages 67 – 75
https://doi.org/10.54319/jjbs/170106

Jordan Journal of Biological Sciences

Effect of Gamma Irradiation on Morphological Biochemical and Cytological Attributes of *Salvia hispanica* L.

G. Kumar[1], Satya Pandey[1,*], Naveen Kumar Tiwari[2], Priyanka Pandey[3], Jyoti Yadav[4]

Naithani Plant Genetics Laboratory, Department of Botany, University of Allahabad, UP-211002

Received: March 1, 2023; Revised: June 26, 2023; Accepted: July 8, 2023

Abstract

The present study focuses on investigating the interaction between radiation and biological systems, specifically examining the detrimental effects of radiation. This approach has proven to be effective in determining the optimal tolerance range of radiation on plants, which can lead to the development of beneficial characteristics and help improve the narrow genetic base. The study was conducted on Salvia hispanica L., a medicinally important plant. Inbred seeds of Salvia hispanica L. were subjected to five different doses of gamma rays (50, 100, 150, 200, 250 Gy) using a Co-60 source with a gamma irradiator of 7.247 k rate. The seeds were sown in triplicate, along with a control set. Various characteristics were assessed, including germination percentage, survival percentage, presence of chlorophyll mutants, and plant height. The results indicate that lower doses of gamma irradiation (<LD50) positively influence plant growth, including plant height, inflorescence size, and productivity. However, higher doses of gamma radiation (>LD50) have detrimental effects on several plant attributes, such as seed germination, survivability, inflorescence size, and pollen fertility. Chromosomal abnormalities were also observed, with an increase in their occurrence corresponding to higher doses of gamma radiation. Germination percentage and survivability were found to decrease as the dose of gamma radiation increased. The dose of 50 Gy resulted in the highest level of genetic variability. Additionally, compared to the control group, a significant percentage of chromosomal abnormalities, particularly stickiness and scattering, was observed at a dose of 250 Gy. Lower doses of gamma radiation (specifically 50 and 100 Gy) showed statistically significant ($p>0.5$) positive responses in Salvia plants, including plant height, leaf area, leaf mutants, inflorescence axis, and seed size. On the other hand, higher doses of radiation proved to be fatal for the plants.

In summary, this study provides valuable insights into the effects of gamma radiation on Salvia hispanica L., highlighting the optimal dose range for inducing beneficial changes in plant characteristics while also emphasizing the harmful consequences associated with higher doses of radiation.

Keywords- *Salvia hispanica* L., Gamma rays, chromosomal aberrations, Genetic Variations, LD_{50}.

1. Introduction

Salvia hispanica L. most preferably referred to as "*chia*" is a medicinally important plant of the Lamiaceae family. It is native to central and southern Mexico and Guatemala and distributed over several countries of South America. Chia seeds are high in oil contents, rich in polysaccharides and fatty acids mainly omega-3 fatty acids and omega-6 fatty acids. In ancient times, "chia" was used highly by Mayan and Aztec populations as a plant of medicine.

China is merging it as a new "superfood" that offers a great source of antioxidants, dietary fiber, and omega-3 fatty acids. Seeds of plants were used as food since 3500 B.C. and functional as a commercial crop in central Mexico between 500 and 900 B.C. (De Falco *et al.,* 2017).

"Chia" also helps to enhance the satiety index and prevent nervous system disorders, inflammation, cardiovascular disease, and diabetes. Gutierrez *et al.* (2014) highlight that chia seeds contain a significant amount of alpha-linolenic acid, comprising approximately 68% of their composition. Additionally, according to Jimenez *et al.* (2013), polyunsaturated fatty acids like omega-3 and omega-6 are considered crucial for human health since they cannot be synthesized within the human body.

Black chia, a crop that has been known since pri-Cortesian times and is considered a pseudocereal, is utilized as both food and medicine due to its high content of alpha-linoleic and omega-3 acids, which hold great importance to conduct genetic improvement work on the species to enhance certain agronomic attributes (Lopez, e.d.2020).

In the study conducted on Salvia hispanica L. plants, it was observed that the irradiation dose had an impact on the composition of chia seed oil. Specifically, there was a decrease in the levels of oleic acid (18:1) and linoleic acid (18:2), while an increase in the levels of palmitic acid (16:0) and stearic acid (18:0) was observed. This shift in fatty acid composition was directly proportional to the increase in the irradiation dose. Furthermore, a reduction in the overall content of monounsaturated and polyunsaturated fatty acids was also noted (Akyol *et al.,*

* Corresponding author. e-mail: satyap.sp90@gmail.com .

2022). These findings indicate that gamma irradiation treatment influences the fatty acid profile of chia seed oil, potentially impacting its nutritional properties and applications.

Mutation breeding serves as an effective tool for plant breeders to introduce variability in crop plants without altering the original genetic makeup of the cultivar. It offers the potential to obtain desirable characteristics that may not exist in nature or have been lost during the course of evolution (Novak and Brunner, 1992). Artificial mutations can be induced using specific mutagens, including physical agents such as gamma rays, X-rays, fast and slow neutrons, and chemical substances such as ethyl methane sulphonate (EMS), methyl methane sulphonate (MMS), sodium azide, base analogs, and acridine dye. These mutagens facilitate the induction of mutations in the plant's genetic material.

Mutation induction has become a well-established and widely accepted approach in plant breeding programs. It allows for the integration of novel traits into existing germplasm and the improvement of cultivars with desired characteristics (Kiani *et al.,* 2022). By harnessing the power of mutation breeding, plant breeders can enhance the genetic diversity of crops and develop improved varieties that exhibit specific qualities.

A lot has been accomplished in crop improvement through the development and official release of thousands of crop varieties with the help of mutation breeding programs. Variation in living organisms on Earth planet was ultimately sourced from mutations. Gamma rays are the most used physical mutagens and breeders have adhered to them for crop improvement programs (Celik and Atak, 2017). The interaction between gamma rays and atoms or molecules of the biological material can be direct or indirect. In direct action, DNA was hit by the rays, thereby disrupting the molecular/genome structure while in indirect action the rays hit the water and cause radiolysis of water that eventually results in the generation of free radicles (Limoli *et al.,*2001;Desouky *et al.,* 2015).

The use of mutagenesis has been widely employed to enhance variability for crop improvement (Acharya *et al.,* 2007). The stimulatory attributes of gamma rays at lower concentrations/doses have been vigorously used by breeders for enhancing the vigorous of numerous crop varieties which were either dealing with problems of or bearing poor qualitative, polygenic, and other stress-tolerant traits (Dwivedi *et al.,*2021). Gamma radiation was the foundation for gamma spectrometry, a key technique used for analyzing radioactive materials qualitatively and quantitatively in various ambient environments. Gamma rays are the most energetic form of electromagnetic radiation and they possess an energy level from 10 keV (Kilo Electron volt) to several hundred KeV. They are considered the most penetrating radiation source compared with other sources such as alpha and beta rays. It falls into the category of ionizing radiation and interacts with atoms or molecules to produce free radicles in cells.

Here in the experimental setup, we have installed an experimental design of triplicates and sowed the seeds of gamma treatments with a control set. We have tried to get a remarkable change in the treated sets to enhance their genotypic diversity. As in previous studies, it was observed that Gamma irradiation had a stimulatory effect on primary branches, including the number of pods/plants, number of flowers per plant, seed index, etc. Gamma-irradiation treatment regulates proteins of crop plants by altering their conformation, oxidation of amino acids of the particular protein, rupture, and breakage of covalent bonds, and by the generation of protein-free radicles that can be beneficial for application in breeding programs. The use of gamma irradiation was found to be an effective method for inducing cross-linking and improving both the barrier and mechanical properties of the edible films and coatings based on proteins (Mastro *et al*., 2016).

A significant response in plants was reported to be caused by gamma irradiation compared to the control. It was found that phenolic and tocopherol levels decreased, and free fatty acid and peroxide count increased with the increase of irradiation dose, and these changes were statistically significant ($p<0.01$). The ratio of palmitic acid and steric acid increased, while the ratio of oleic acid and linoleic acid decreased with increasing irradiation dose (Akyol, 2019).

The purpose of this study was to find out and determine the harmful effects of radiation and to establish the radiation quality and dose range in which benefits, in terms of more productive or in general more suitable plant systems, would be obtained.

2. Materials and Methods

2.1. Procurement of materials

First of all, we have purchased the inbred seeds of *Salvia hispanica* L. from NutriPlanet Private Limited, Bengaluru-520068, Karnataka, India. The rest needs and requirements were fulfilled by Naithani Plant Genetics Laboratory, Department of Botany, University of Allahabad-211002, UP, India.

2.1.1. Treatment of seeds through different Doses of gamma rays

First of all, the seeds of *Salvia hispanica* L. were filled in small plastic packets and sent to NBRI, Lucknow for gamma irradiation. The doses given to the seeds were 50, 100, 50, and 200&250 Gy respectively. The irradiation process was carried out in a Cobalt-60 at a rate of 7.247k gamma irradiator.

2.1.2. Weather conditions and optimum temperature for seed sowing

After the treatment of the seeds, they were sown in earthen pots in triplicates along with control sets. Replicates were planted in a completely randomized block design (CRBD) at a temperature of 25°C±2°C and relative humidity 76% in outdoor conditions.

2.1.3. Morphological study

For the morphological study the germination percentage was calculated after seven days of sowing, survival was noted after thirty days, and plant height trend was noted after 45 days of sowing. Inflorescence size was also measured after 7 days of its emergence.

2.1.4. Meiotic study

For the meiotic analysis young floral buds of control and variant plants of *Salvia hispanica* L. with appropriate size were fixed in Carnoy's fixative (Alcohol 3: Glacial Acetic Acid 1) for 24 hrs and then transferred in 90% alcohol to preserve the buds. Anthers were teased and

stained in 2% acetocarmine, followed by squash preparation.

Further, the process of squash and the slides were observed under a Nikon phase-contrast microscope (Eclipse iE200, Japan). The observation was made to calculate the total abnormality percentage (TAB %) of treated sets and control as.

$$\text{Total Abnormality (\%)} = \times 100 \frac{\text{Total number of actively dividing cells}}{\text{Total number of aberrant cells}}$$

2.1.5. Pollen fertility

For this study, mature flowers were taken and dusted over glass slides to remove the mature pollen grains of anthers from them. After this, the pollens were stained with acetocarmine and mounted with glycerin to observe under the microscope. The pollen fertility of each treated set was calculated by staining them with acetocarmine. The darkly stained pollens are considered viable while those unstained are considered non-viable. A common method for assessing pollen viability was by staining and direct counting, as described by Heslop-Harrison in 1992.

$$\text{Pollen fertility (\%)} = \times 100 \frac{\text{Number of fertile pollen grains}}{\text{Total number of pollen grains}}$$

2.2. Biochemical Study

Fresh leaves of *Salvia* have been taken to extract Chlorophyll a, b, and carotenoids from it with 80% acetone and the amount and estimation of it were determined according to the Lichtenthaler method (1987).

$$\textit{chlorophyll a}: \frac{12.25(A_{663}) - 2.79(A_{646}) \times \textit{volume}}{\textit{weight of leaf tissue(mg)}}$$

$$\textit{Carotenoids}: \frac{[1000(A_{470}) - 1.82(\textit{Chla}) - 85.02(\textit{Chlb})]/198 \times \textit{volume(ml)}}{\textit{weight of leaf tissue(mg)}}$$

$$\textit{chlorophyll b}: \frac{21.5(A_{646}) - 5.1(_{663}) \times \textit{volume}}{\textit{weight of leaf tissue(mg)}}$$

2.3. Statistical analysis

Statistical analysis was performed using the SPSS 16.0 software. A one-way analysis of variance (ANOVA) and Duncan's Multiple Range Test (DMRT, $p < 0.05$) was conducted for mean separation and the graph was plotted by using sigma plot 10.0 software. The actual mean and standard error were calculated and the data were subjected to analysis of variance.

3. Results

3.1. Morphological Results

3.1.1. Germination and Survival

In the current study, the germination of the seeds of *Salvia hispanica* L. reduced with increasing doses of gamma rays while at low doses of treatment *viz.* 50 Gy there was an increase in germination compared to the control plant. **Figure 1(A)** depicts that initial doses of gamma (50 and 100 Gy) are causing significant effects compared to higher doses of gamma irradiation, i.e 150, 200, and 250 Gy. The germination percentage of the control seeds was 94.66±1.33and at 50 Gy recorded 96±2.30 the highest among all the treated sets, while the higher doses showed a continuous decline in the germination percentage. The control set showed the highest survivability i.e. 92.34±1.29, while the highest gamma dose (250 Gy) showed the lowest survivability percentage (i.e. 58.45±1.94) among all the treated sets.

3.1.2. Plant Height

The plant height trend of all the treated sets was taken accordingly, and after the observation it was found that the initial doses of gamma (i.e. 50 and 100 Gy) have shown a positive effect on plant height that helps enhance the vigor and production of the plants. Figure 1(B) and Figure 2 (A) depict that the plants treated with lower doses of gamma have better height and vigor in comparison to control plants and the plants treated with higher doses of gamma (i.e. 150, 200, and 250 Gy).

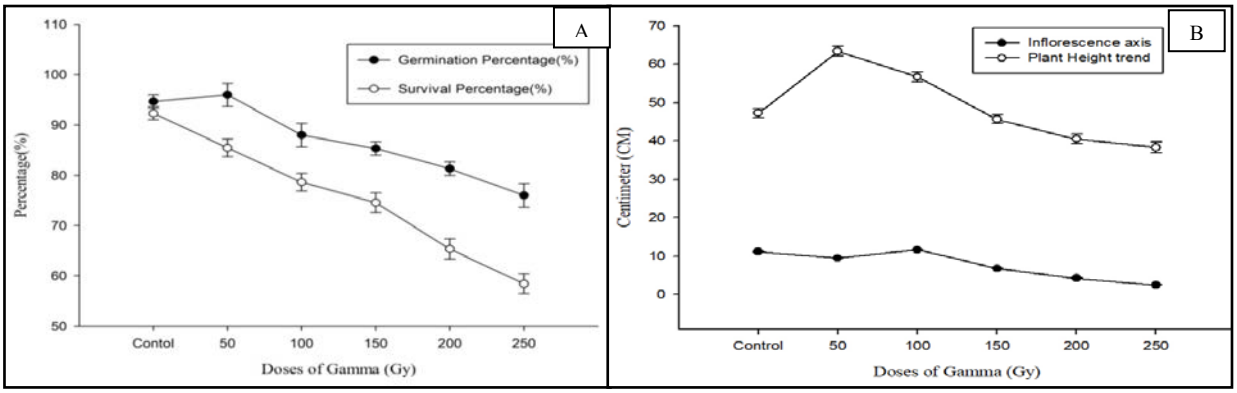

Figure 1: Graphs showing morphological parameters i.e. Germination and Survival % (A) and Inflorescence and plant height trend (B)

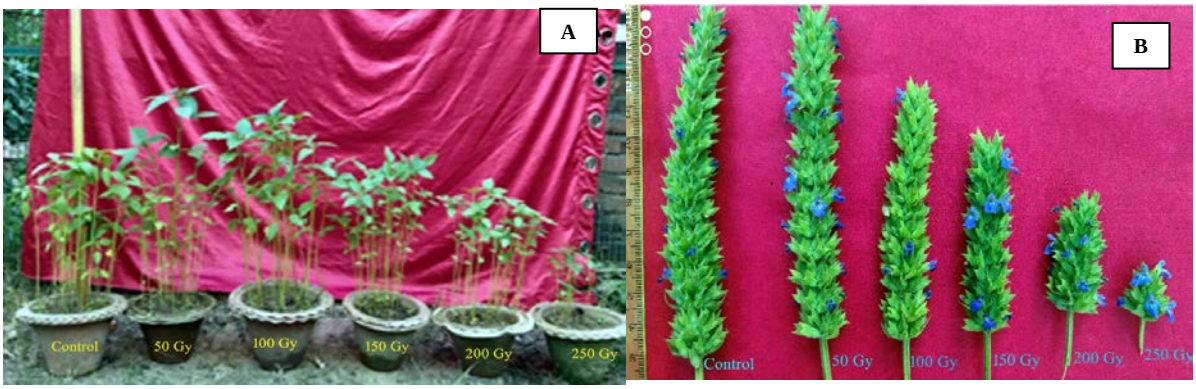

Figure 2 (A) and (B): Images showing plant height trend and inflorescence size respectively in treated sets

3.1.3. Inflorescence size

In the experimentation, variability in the inflorescence has also been observed. It was found that at initial doses of gamma, the inflorescence was larger and more vigorous in comparison to the control set, while higher doses proved disastrous to them as they are causing hindrances in the growth and development of the inflorescence. The most vigorous inflorescence was observed at 50 Gy treatments, and the frailest one was observed at a 250 Gy dose of gamma. Figure 1 (B) and 2 (B) clearly shows that the inflorescence of the 50 Gy treated set was larger and stronger than to all other sets including control plants.

3.2. Leaf variants

During the experimentation with gamma irradiation treatment, several leaf variants were observed. The treated sets exhibited abnormalities in terms of leaf color, shape, and patterns. Color variants included Xantha and Albina, representing abnormal colors compared to the control group. Shape variants comprised leaf bifurcation, rolling, and the development of leathery leaves. Additionally, pattern variants were observed in the study such as; presence of three leaves at a single node or bunches of leaves clustered at a node. Figure 3 illustrates the different types of leaf variants identified in the experimental setup, contrasting them with the control group

Figure 3: Leaf variants observed during the study: A. Control; **B.** Bifurcated leaf; **C.** Leathery leaf; **D.** Deformed leaf; **E.** Bifurcation of leaf axis; **F.** fleshy leaf; **G.** Tricotyledonous leaf; **H.** Differential development of leaf at same axis; **I.** Semi-xantha; **J.** Xantha; **K.** Semi-albina; **L.** Albina.

3.3. Cytological Results

3.3.1. Cellular abnormalities

In *Salvia hispanica* L. the haploid chromosomal set **n=6** (2n=12 in the control set, normal divisions were observed, while abnormalities were recorded in the treatment. In the cytological preparation, it was observed under the microscope that the percentage of abnormal division was increasing simultaneously with the increasing dose of gamma. In other words, the abnormality percentage was directly proportional to doses of gamma. As the dose of gamma radiation increased, there was a corresponding elevation in the total abnormality percentage (TAB%). This trend was evident from the data presented in Table 1 and illustrated in Figure 5. Specifically, the lowest TAB% (6.20±0.28) was recorded at the lowest administered dose of 50 Gy, whereas the highest TAB% (12.74±1.00) was observed at the highest dose of gamma radiation, namely 250 Gy.

Cellular abnormalities were recorded during the experiment, observed at both metaphase and anaphase stages. These abnormalities encompassed a range of irregularities, including stickiness, unorientation, scattering, forward movement, asymmetric division, and disturbed polarity. Stickiness, metaphasic scattering, precocious movement at metaphase, and stickiness at anaphase were the most frequently observed abnormalities among the recorded instances.

It was quite articulate by the contemplation of cytological preparations of the treatment that gamma irradiation treatment was injurious for the health of cellular development and it was potentially inhibiting systematic cell proliferation of the pollen mother cells (PMCs) and readily causing numerous chromosomal abnormalities mentioned in the above paragraph.

3.3.2. Pollen fertility

In the above-mentioned experimental setup, pollen fertility was also taken into account and it was observed that the fertility of pollen grains was decreased as the doses of gamma are increased. Based on the data obtained in the experiment, the pollen fertility was found to be inversely proportional to the doses of gamma (Figure 5). The rate of pollen fertility was highest (97.65%) the in control set the lowest fertility of the pollen (67.46%) was observed at the highest dose of gamma i.e.250 Gy.

According to the observation, it was pretty sure that gamma irradiation was hazardous for the health and development of potent pollen grains which fertilize the egg and play its foreknown role in the plant's life cycle.

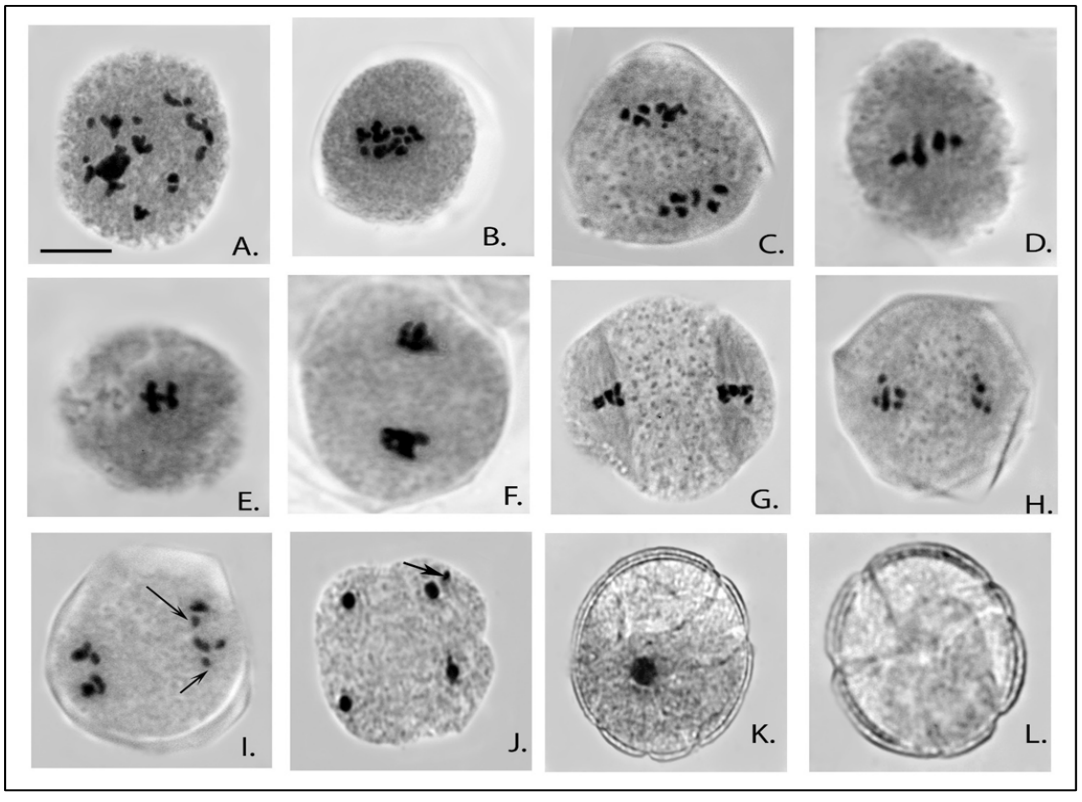

Figure 4: Cytological Observation: A. Diplotene; **B.** Normal Metaphase; **C.** Normal Anaphase; **D.** Stickiness at Metaphase I; **E.** Multivalent formation; **F.**Stickiness at Anaphase I,; **G.** Normal Metaphase II; **H.** Scattering at Metaphase II;; **I.** One laggard and one forward movement of chromosome at Anaphase II; **J.** Telophase; **K.** Fertile with (nucleus) and **L.** Sterile pollen (without nucleus). (Scale bar = 5µm)

3.4. Biochemical Results

3.4.1. Chlorophyll a

The impact of gamma irradiation treatment on the main photosynthetic pigment, chlorophyll a, was investigated in the experimental plants. The results demonstrated that gamma irradiation had a detrimental effect on the development of this crucial photosynthetic pigment. It was evident that the amount of chlorophyll a decreased progressively with increasing doses of gamma irradiation, in comparison to the control group (Figure 6). The observation clearly establishes an inverse relationship between the amount of chlorophyll a and the doses of gamma irradiation

3.4.2. Chlorophyll b

Similar to Chlorophyll a, the content of chlorophyll b also exhibited a declining trend in response to increasing treatment doses, ranging from 50 Gy to 250 Gy, as depicted in Figure (6).

3.4.3. Carotenoid

Carotenoids, which are photosensory pigments found in plants, were also important considerations, similar to treatments. In comparison to the control group, all the treated groups exhibited a declining trend (Figure 6). As the doses of gamma irradiation increased, the carotenoid content decreased in a similar manner to that observed for chlorophyll a and b.

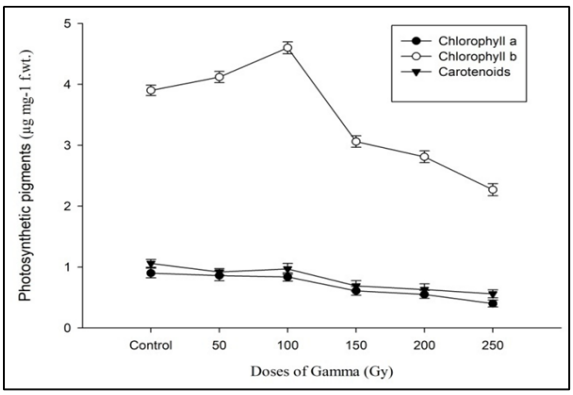

Figure 6: Graph representing photosynthetic pigments content in control as well as treated sets of Gamma

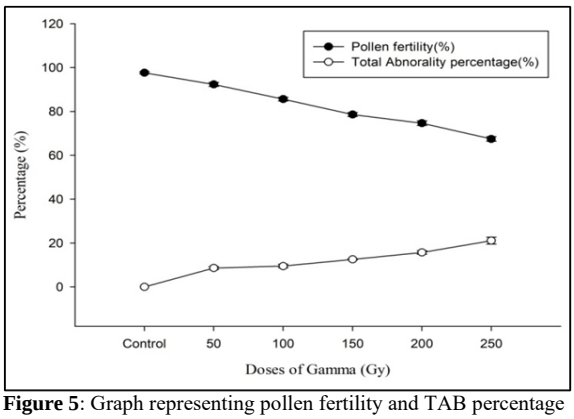

Figure 5: Graph representing pollen fertility and TAB percentage with increasing doses of irradiation.

Table 1: Gamma irradiation-inducedcytological abnormalities and their percentage in *Salvia hispanica* L.

Treatment	No of PMC's Observed	Metaphasic abnormality (%) (Mean±SE)					Anaphasic abnormality (%) (Mean±SE)					Oth	Tab	Pollen fertility %
		Sc	Pm	St	Un	Asy	St	Un	Fr	Sc	Dp			
Control	276	-	-	-	-	-	-	-	-	-	-			97.65±0.50^{a}
50 Gy	263	0.51±0.12^{a}	0.25±0.13^{a}	1.14±0.21^{a}	0.51±0.26^{a}	0.25±0.25^{a}	1.52±0.21^{a}	0.51±0.26^{a}	0.50±0.33^{a}	050±0.25^{a}	0.38±0.22^{a}	1.13±0.13^{a}	6.20±0.28	92.34±0.88^{b}
100 Gy	253	0.26±0.26^{a}	1.19±0.25^{ab}	1.45±0.14^{ab}	0.66±0.34^{a}	0.12±0.12^{ab}	1.58±0.22^{b}	0.40±0.24^{b}	0.80±0.24^{a}	0.26±0.26^{b}	0.39±0.23^{a}	0.26±0.13^{a}	7.26±0.54	85.64±0.89^{c}
50Gy	248	0.53±0.26^{a}	052±0.34^{ab}	1.71±0.13^{bc}	0.66±0.36^{a}	0.40±0.23^{ab}	1.45±0.29^{b}	0.26±0.13^{b}	0.54±0.36^{a}	0.66±0.13^{b}	0.65±0.45^{a}	0.39±0.23^{a}	7.78±0.24	78.57±0.88^{d}
200 Gy	239	0.67±0.35^{a}	0.83±0.25^{ab}	2.08±0.29^{bcd}	0.42±0.25^{a}	0.54±0.12^{b}	1.67±0.28^{b}	0.55±0.37^{b}	1.09±0.24^{a}	0.69±0.14^{b}	0.42±0.24^{a}	0.54±0.12^{a}	9.50±0.22	74.63±1.05^{e}
250 Gy	220	0.31±0.15^{a}	0.60±0.30^{b}	2.73±0.28^{cd}	1.07±0.55^{a}	0.91±0.25^{b}	2.72±0.51^{b}	1.36±0.25^{b}	0.76±0.15^{a}	1.67±0.33^{b}	0.46±0.26^{a}	0.15±0.15^{a}	12.74±1.00	67.46±1.08^{f}

Where,**PMC's-** Pollen mother cells, **SE-** Standard error,**Sc-** Scattering of chromosomes, **Pm-** Precocious movement of chromosomes, **St-** Stickiness of chromosomes, **Un-** Unorientation in chromosomal sets, **Asy-**Asynchronisation, **Fr-** forward movement in chromosomes, **Dp-** Disturbed polarity; **Oth-** Others, **Tab-** Total abnormality percentage (p= <0.5)

4. Discussion

Germination was the most important phenomenon of the life cycle of any plant to maintain the genotype in existence in the system. In the present experiment, it has been found that the germination displayed a decreasing trend as the doses of gamma increased compared to the control. A group of scientists (Raina *et al.* 2016) has also reported the delay in the initiation of metabolism following germination, resulting in a uniform delay in mitotic activity and hence seedling growth. This phenomenon may be due to the detrimental effect of high energy beams of gamma and the chromosomal aberrations, disturbance in DNA and auxin synthesis, and to impaired cell metabolism (Kirtane and Dhumal, 2004). The same results were also found in Bhringraj by Kumar and Mishra (2019). They also found a decreasing pattern of the rate of germination with increasing doses of irradiation. Rifnas *et al.* (2019) also reported a progressive reduction in the germination of *Calotropis gigantea* seeds with increasing doses of gamma. The same pattern of the rate of germination *Zea mays was* reported by Yadav *et al.* (2015).

Survivability was the second important thing for the growth and development of the plants, which showed the same pattern as of rate of germination. The survivability of the plants also decreased with increasing doses of gamma irradiation. Reduced survival rate at higher mutagenic levels has been attributed to various factors, such as chromosomal damage leading to meiotic arrest (Khursheed

et al., 2008). Kumar and Singh, 2020, also reported that at metabolic levels, higher doses of gamma rays may disrupt chloroplast membrane and metabolism, due to which photosynthesis was affected which ultimately reduces survivability and causes the death of the plants.

The trend observed in plant height indicated that lower doses of irradiation were beneficial and resulted in more favorable responses. Similar findings have been reported by Kumar and Mishra (2020) in Bhringraj and Kumar & Singh (2020) in Artemisia annua. Ali *et al.* (2016) have proposed that lower doses of gamma rays can stimulate plant growth by enhancing the antioxidative capacity of cells or by modulating hormonal signalling. Wi *et al.* (2007) put forward a hypothesis suggesting that lower doses of gamma irradiation can induce growth by influencing hormonal activities in plant cells or by bolstering antioxidant defences, enabling plants to better cope with daily stress factors such as temperature fluctuations and light intensities.

In contrast, higher doses of irradiation were found to have inhibitory effects on plant growth, potentially attributed to disturbances in hormonal balance, leaf gas exchange, water exchange, and enzyme activity (Kiong *et al.,* 2008). These factors may lead to a reduction in internodal length due to insufficient water and mineral supply to the plants. Additionally, as the radiation dose increases, the rate of DNA mutations also increases, which can disrupt bud development and interrupt cell differentiation, ultimately inhibiting plant growth (Ali et al., 2016). The increase in inflorescence size could potentially be attributed to the same underlying consequences described by Wi *et al.* (2007) and Ali et al. (2016).

Chlorophyll mutants reported (Fig-3) viz., semi-xantha, Xantha, semi-Albina, and Albina were observed in the gamma treatment. Fig-3 (I) Xantha wasstraw-coloured yellow leaves(Arul Balachandran and Mullainathan, 2009). Chlorophyll mutant, Albina (Fig. 3D) was pale dull white color and its lifespan (10-20 days) was comparatively shorter than usual leaf (Kumar *et al.* 2022). Several authors have reported the occurrence of different types of chlorophyll mutations such as Xantha, Albina, Viridis, Chlorine, etc. (Kolar *et al.,* 2011; Arisha *et al.,* 2015; Verma *et al.,* 2018). The reason behind these chlorophyll mutants and the genes and proteins involved in it was still a matter of research (Ahumada-Flores *et al.,* 2021).

In the case of cytological observations, the major abnormalities recorded were stickiness, scattering, precocious movement, unorientation, asynchronisation, etc. These chromosomal abnormalities in the PMCs are attributed to the change in their organization, imbalance in their protein signaling, and disturbance in microtubule formation and functioning. The inhibitory effect on the cell cycle of gamma irradiation at higher doses has also been reported earlier in *Hordeum vulgare* by Eroglu *et al.* (2007), *Allium cepa* by Ahirwar, (2015), and *Triticum aestivum* by Borzouei *et al.* (2010).

The abnormalities observed in the experimentation may be attributed to numerous problems related to spindle fibers, microtubules, histone proteins, and a few other chromosomal proteins. The major chromosomal anomalies viz. Stickiness (Fig. 4 D, F, H) in the chromosomes arise due to an imbalance of spindle fibres caused by mutagenic treatment (Jabee *et al.,* 2008). Gaulden (1987) predicted that the stickiness in chromosomes has been seen due to the malfunctioning of one or two types of specific non-histone proteins which are responsible for the proper organization and compaction of chromosomes. In one more study, the sticky chromosomes resulting in the cells may be due to the increased chromosomal contraction and condensation [Ahmed and Grant (1972)]. In a study, Kuras *et al.* (2006) observed that this abnormality of chromosomes was the outcome of an imbalance in histones or other proteins which can control the proper structure of nuclear chromatin.

Precocious movement (Fig. 4 I) in chromosomes at metaphase was observed because of the migration of chromosomes to the poles, which may be attributed to early chiasma terminalization in diakinesis or metaphase I (Srivastava and Kapoor, 2008) or due to disruption of spindle formation (Kumar and Dwivedi, 2015). Precocious movement noted in the cells of experimental plants may be due to early terminalization of the chromosome or due to the chemical breaking of the protein moiety of the nucleoprotein backbone. (Kumar and Pandey, 2017)

Levan (1938) studied that the scattering of chromosomes (Figure 4G) was a result of the problematic function of spindle fibers and was generated in the process due to the loss of microtubules, disruption of the spindle fibers, etc.in *Allium cepa* L.

Unorientation in the cells may be due to the disturbed microtubule orientation or disturbed polarity of the cells. Disturbed polarity (Fig. 1K) or tri polarity might be due to spindle disfunctioning (Kumar and Dwivedi, 2012).

Declinement in pollen fertility was because of the formation of sterile pollen due to the side effects of mutagens on male reproductive organs. Pollen viability was considered to be an important parameter of pollen quality (Dafni and Firmage, 2000). Pollen sterility was also a major finding reported in the study. Here it was found that the rate of pollen sterility was increasing with increasing doses of irradiation which ultimately leads to non-viable pollen formation and creates a danger over the survival of the genotypes of the plants in the system. Muthusamy &Jayabalan (2002) also reported the same in the *Gossypium* plant. They reported that the rate was directly proportional to the irradiation dose. Kumar and Singh (2020) also reported the same pattern in *Artemisia annua*. Jagtap & More (2014) have analyzed the same output on *Lablab purpureus* and concluded that sterility in the plants enhances vigorously as the dose of physical or chemical mutagen increases.

Biochemical studies revealed the same pattern of decline meant as germination, survival, and pollen fertility. Here, major photosynthetic pigments including Chl*a* & Chl*b* have shown a narrowing from the control plant's mean value of photosynthetic pigment. A sharp deterioration in the amount of both the photosynthetic pigments (Chl a &Chl b) was observed. Carotenoids, the accessory photosynthetic pigment have also shown the same phenomenon of decline, such as main photosynthetic pigments. These findings may be attributed to the hazardous nature of high-energy gamma rays. Gamma radiation alters photosynthetic apparatus by damaging the photosystem complexes, but at lower doses of gamma rays these complexes allow photosynthesis by capturing light energy, protect photo-oxidative damage of chlorophyll

from ROS, and release excess energy as heat (Kovacs and Keresztes, 2002; Kim *et al.,* 2004). Jing *et al.* (2008) also found that photosynthetic pigments decreased in gamma-treated sets compared to the control set. Kumar and Singh (2020) also proposed that gamma irradiation was detrimental to the photosynthetic pigments of Bhri ngraj and the effect was strengthened with increasing doses of gamma irradiation.

5. Conclusion

In terms of c ytology, the study revealed a clear association between increasing doses of irradiation and the occurrence of numerous cytological aberrations. It was noteworthy that the percentage of t otal abnormalities increased with higher doses of gamma radiation. However, alongside the adverse effects, lower doses of i rradiation also provided an opportunity to generate new mutant varieties of the plant with enhanced genetic variability and improved vigor compared to the parent plant. This offers the potential to broaden the narrowed genetic base of t he plant caused by continuous inbreeding depression.

Overall, these findings highlight the complex effects of gamma-ray irradiation on pl ant traits, with lower doses showing potential for be neficial changes in morphology and genetic variability, while higher doses induce detrimental effects across multiple aspects of pl ant development and productivity.

Acknowledgment

The authors would like to express their sincere gratitude to NutriPlanet Private Limited, located in Bengaluru-520068, Karnataka, India, for generously providing the seeds of *Salvia hispanica* L. for this research study. Additionally, the authors would like to extend their thanks to the Department of Bot any at the University of Allahabad for provi ding the necessary research area to carry out the experiment. The authors are also thankful to all individuals who directly or indirectly contributed to the successful completion of this work.

References

Acharya S N, ThomasJ E and Basu S K. 2007. Methods for the improvement of plant medicinal properties, with particular reference to fenugreek (Trigonella foenum-graecum L.). *J.Med.Plant Res.,* 491-512.

Ahirwar R. 2015. *Gamma radiation-induced chromosomal aberrations at mitosis in Allium cepa L* (No. RESEARCH).

Ahmed M and Grant W. F. 1972. Cytological effects of the pesticides phosdrin and bladex on *Tradescantia* and *Vicia faba*. *Can J Genet Cytol.,***14(1):**157-165.

Ahumada-Flores S, Pando L R G, Cota, F I P, de la Cruz Torres E Sarsu F and de los Santos Villalobos, S. (2021). Gamma irradiation induces changes of phenotypic and agronomic traits in wheat (Triticum turgidum ssp. durum). *Applied Radiation andwasotopes.*, **167:**109490.

Akyol E. 2019. *Işınlamaişleminin chia (salvia hispanica l.) tohumuyağlarınınkimyasalözelliklerüzerineetkisi* (Master's thesis, Namık Kemal Üniversitesi).

Akyol E, Geçgel Ü, and Apaydın D. 2022. Quality characteristics of oils extracted from ɣ-irradiated chia (Salvia hispanica L.) seeds. *J Am Oil Chem Soc.,***99(10):**891-898.

Ali H, Ghori Z, Sheikh S, & GulA. 2016. Crop Production and Global Environmentalwassues. *Cham, Switzerland:* **Springer International Publishing**.

Arisha M. H, Shah S N, Gong Z H, Jing, H Li, C, & Zhang, H X. 2015. Ethyl methane sulfonate induced mutations in M2 generation and physiological variations in M1 generation of peppers (Capsicum annuum L.). *Front Plant Sci.*, ***6*:**399.

Arulbalachandran D, andMullainathan L. 2009. Chlorophyll and morphological mutants of black gram (Vigna mungo (L.) Hepper) derived by gamma rays and EMS. *Journal of Phytology*, **1(4).**

Ayerza R. 1995. Oil co ntent and fatty acid composition of chia (*Salvia hispanica* L.) from five northwestern locations in Argentina. *J Am Oil Chem Soc.*, **72(9):**1079-1081.

Basu, S K, Acharya S N , and Thomas J E. 2008. Genetic improvement of fenugreek (*Trigonella foenum-graecum* L.) through EMS-induced mutation breeding for higher seed yield under western Canada prairie conditions. *Euphytica.*, **160(2);** 249-258.

Borzouei A, Kafi M, Khazaei H, Naseriyan B, and Majdabadi A. 2010. Effects of gamma radiation on germination and physiological aspects of wheat (*Triticum aestivum* L.) seedlings. *Pak. J. Bot.*, **42(4):**2281-2290.

Coates W. 1996. Production potential of chia in northwestern Argentina. *Industrial crops and products.*, ***5*(3):**229-233.

Dafni A, and Firmage D. 2000. Pollen viability and longevity: practical, ecological and evolutionary implications. *Pollen and pollination.*, 113-132.

De Falco B, Amato M, and Lanzotti V. 2017. Chia seeds products: an overview. *Phytochem Rev.,***16(4):** 745-760.

del Mastro, N L. 2016. Radiation influence on edible materials. In *Radiation Effects in Materials*. IntechOpen.

Dwivedi K, Kumar K, and Kumar G. 2021. Studies on Gamma Rays Induced Cyto-Morphological Variations and Procurement of Some Induced Novel Mutants inKalmegh [*Andrographis paniculata* (Burm. f.) Nees]. *Cytol.gent.*, **55(4):**379-387.

Eroğlu Y, Eroğlu E, and İlbaş A L İ. 2007. Gamma ray reduces mitotic index in embryonic roots of *Hordeum vulgare* L. *Adv.Ecol.Res,* **1(2).**

Firmage D H, and Dafni A. 2000. Field tests for pollen viability; a comparative approach. In *VIII International Symposium on Pollination-Pollination: Integrator of Crops and Native Plant Systems.,***561**: (87-94).

Gaulden M E. 1987. Hypothesis: Some mutagens directly alter specific chromosomal proteins to produce chromosome stickiness. *Mutagenesis.*, ***2*:** 357-365.

Gutiérrez Tolentino, R, Ramírez Vega M L, Vega y León, S, Fontecha J, Rodríguez L M, and Escobar Medina A. 2014. Fatty acid content in chia (Salvia hispanica L.) seeds grown in four Mexican states. Rev.Cuba.Plantas Med, **19(3):** 199-207.

Heslop-Harrison, J. S. 1992. Cytological techniques to assess pollen quality. ***Sexual plant reproduction***, **41-48**.

Jabee F, ANSARI M Y K, and Shahab D. 2008. Studies on the effect of maleic hydrazide on root tip cells and pollen fertility in *Trigonella foenum-graecum* L., **32(5):** 337-344.

Jagtap S S, and More A D. 2014. Effect of chemical and physical mutagens on pollen sterility in *Lablab purpureus* (L) Sweet. *Int. J. Life Scienc.*, **2(4):** 366-368.

Jiménez P, Masson S, and Quitral R. 2013. Chemical composition of chia seed, flaxseed and rosehip and its contribution in fatty acids omega-3. *Revista chilena de Nutrición*, **40(2):** 155-160.

Khursheed S, Laskar RA, Raina A, Amin R, and Khan S. 2015. Comparative analysis of cytological abnormalities induced in Vicia faba L. genotypes using physical and chemical mutagenesis. *Chromosome Sci,* **18(3-4):** 47-51.

Khursheed S, Raina A, Laskar RA, and Khan S. 2018. Effect of gamma radiation and EMS on mutation rate: their effectiveness and efficiency in faba bean (*Vicia faba* L.). *Caryologia*, **71(4):**397-404.

Kiani D, Borzouei A, Ramezanpour S, Soltanloo H, and Saadati S. 2022. Application of gamma irradiation on morphological, biochemical, and molecular aspects of wheat (*Triticum aestivum* L.) under different seed moisture contents. *Sci. Rep*, **12(1):** 11082.

Kim JH, Baek MH, Chung BY, Wi SG, and Kim JS. 2004. Alterations in the photosynthetic pigments and antioxidant machineries of red pepper (*Capsicum annuum* L.) seedlings from gamma-irradiated seeds. *Journal of Plant Biology*, **47(4):**314-321.

Kiong ALP, Lai AG, Hussein S, and Harun AR (2008). Physiological responses of *Orthosiphon stamineus* plantlets to gamma irradiation. *Am.-Eurasian J. Sustain. Agric.* **2(2):**135-149.

Kirtane S, and Dhumal KN. 2004. Studies on induced mutations in onion: Biological and cytological effects of mutagens in M2 generation. *Int J Mendel*, **21**:11-13.

Kolar F, Pawar N, and Dixit G. 2011. Induced chlorophyll mutations in *Delphinium malabaricum* (Huth) Munz. *J. Appl.Hortic.*, **13(1):** 18-24.

Kovacs E, and Keresztes A. 2002. Effect of gamma and UV-B/C radiation on plant cells. *Micron*, **33(2):**199-210.

Kumar G, and Dwivedi K. 2012. Ionizing radiation mediated cytological manifestation in microsporogenesis of *Brassica campestris* L. (Brassicaceae). *J. Cent. Eur. Agric*.

Kumar G, and Mishra R. 2019. Effect of gamma irradiation on Growth responses and Cytogenetical characterization in *Eclipta alba* (L.) Hassk. *Bull. Env. Pharmacol. Life Sci*, **9**:157-165.

Kumar G, and Pandey A. (2017). Effect of UV-B Radiation on Chromosomal Organisation and Biochemical Constituents of*Coriandrum sativum* L. *Jordan J Biol Sci*, **10(2).**

Kuraś M, Nowakowska J, Śliwińska E, Pilarski R, Ilasz R, Tykarska T, Zobel A and Gulewicz K. 2006. Changes in chromosome structure, mitotic activity, and nuclear DNA content from cells of Allium Test induced by bark water extract of *Uncaria tomentosa* (Willd.) DC. *Journal of EthnopharmacoloGy*, **107(2):**211-221.

Levan A. 1938. The effect of colchicine on root mitoses in Allium. *Hereditas*, **24(4):**471-486.

Lichtenthaler HK 1987. [34] Chlorophylls and carotenoids: pigments of photosynthetic biomembranes. In *Methods in enzymology*, **148**:(350-382). **Academic Press.**

Ling AP, Chia JY, Hussein S and Harun AR. 2008. Physiological responses of *Citrus sinensis* to gamma irradiation. *World Applied Sciences Journal*, **5(1):**12-19.

López ED. 2020. Estudio de radiosensibilidad de chía negra (Salvia hispanica L.)(Lamiaceae), bajo siete niveles de irradiación gamma. *Revista del Centro de Investigación de la Universidad la Salle*, **14(54):**37-48.

Mishra M, K umar G and Tripathi K. 2022. Cytomorphological and biochemical implications of UV-B priming in fennel (*Foeniculum vulgare* Mill.). *J. Environ. Biol.*, **43(4):** 562-570.

Muthusamy A, and Jayabalan N. (2002). Effect of mutagens on pollen fertility of cotton (*Gossypium hirsutum* L.). *Indian J. Genet*, **62(2):**187.

Novak FJ and Brunner H. 1992. Plant breeding: Induced mutation technology for crop improvement. *IAEA Bull*, **4:**25-33.

Raina A, Laskar R, Khursheed S, Amin R, Tantray Y, Parveen K and Khan S. 2016. Role of mutation breeding in crop improvement-past, present and future. *Asian Research Journal of Agriculture*, **2(2):**1-13.

Rifnas LM, Vidanapathirana NP, Silva, TD, Dahanayake N, Weerasinghe SS, and Subasinghe S. 2020. Effect of gamma radiation on the survival rate of Allamanda cathartica–An indigenous medicinal plant. *International Journal of Minor Fruits, Medicinal and Aromatic Plants*, **6(1),** 50-53.

Singh R and Kumar G. 2020. Ionizing radiation mediated effect on morphological, biochemical and microsporogenesis behavior of *Artemisia annua* L. *J. Environ. Biol.*, **41(5):**1046-1053.

Srivastava A and Kapoor K. 2008. Seed yield was not impaired by chromosome stickiness in sodium azide-treated*Trigonella foenum-graecum*. *Cytologia*, **73(2):**115-121.

Verma AK, Dhanasekar P, Choudhary S, Meena RD, and Lal G. 2018. Estimation of induced variability in M2 generation of fennel (*Foeniculum vulgare* Mill.).

Wi SG, Chung BY, Kim JS, Kim JH, Baek MH, Lee JW, and Kim YS 2007. Effects of gamma irradiation on morphological changes and biological responses in plants. *Micron,* **38:** 553-564.

Yadav A, Singh B, Sharma DK, and Ahuja S. 2015. Effects of gamma irradiation on germination and physiological parameters of maize (*Zea mays*) genotypes. *Indian J Agric Res,* **85(9):**1148-52.

JJBS

Volume 17, Number 1,March 2024
ISSN 1995-6673
Pages 77 – 87
https://doi.org/10.54319/jjbs/170107

Jordan Journal of Biological Sciences

Ethnomycological Study of Macrofungi Utilized by Pamona Community Around Lake Poso, Central Sulawesi Province, Indonesia

Yusran Yusran[1,*], Erniwati Erniwati[1], Akhmad Khumaidi[2], Rukmi Rukmi[1], Sustri Sustri[1]

[1] *Forestry Department, Forestry Faculty, Tadulako University, Jl. Soekarno-Hatta Km.8 Palu, Central Sulawesi, Indonesia 94118;*[2] *Pharmacy Department, Faculty Mathematic and Natural Sciences, Tadulako University, Jl. Soekarno-Hatta Km.8 Palu, Central Sulawesi, Indonesia 94118*

Received: December 8, 2022; Revised: May 17, 2023; Accepted: July 14, 2023

Abstract

This study was conducted around Lake Poso, which is home to several indigenous communities with unique local knowledge about nature. This region encompasses several conservation areas, including Bancea Nature Park, Pamona Nature Reserve, and Wera Nature Park. The community residing in this region include the traditional Pamona community, who are one of the ethnic groups in Central Sulawesi Province, Indonesia. Therefore, this study aimed to determine the ethnomycology and local knowledge of Pamona indigenous people in relation to utilization of wild macrofungi species for food and medicine around Lake Poso, Central Sulawesi Province, Indonesia. The results showed that 21 species of macrofungi were used by the indigenous Pamona community, which served various purposes such as a source of food, medicine, hair growth agent, animal feed mixture, and a lighting tool at night. These species include *Schizophyllum commune, Auricularia auricula-judae, Auricularia nigricans, Volvariella volvaceae, Trichaleurina javanica, Termitomyces* spp*, Tremella* sp*, Physarum polycephalum, Mycena* sp.*, Pycnoporus sanguineus, Pleurotus ostreatus, Dictyophora indusiata,* and *Russula* sp. Macrofungi species with the highest Relative Frequency of Citation (RFC) value were *Schizophyllum commune*, *Auricularia auricula-judae* (Bull.) Quel, *Termitomyces eurrhizus* (Berk.) Pegler, and *Trichaleurina javanica,* all of which had a value of 1. Meanwhile, *Tremella sp.* had the lowest RFC with a value of 0.14. The highest Informant Consensus Factor (ICF) value of 0.97 was found in the use of macrofungi as food. These results confirm the wealth of knowledge and practices within the Pamona comunnity, enabling them to effectively utilize macrofungi species for both food and medicine. These practices help to combat malnutrition and prevent and treat certain diseases in Pamona comunnity around Lake Poso, Central Sulawesi, Indonesia.

Keywords: Conservation, Edible Macrofungi, Indigenous Knowledge, Utilization

1. Introduction

There are an estimated 2.2 to 3.8 million species of fungi in the world (Hawksworth & Lűcking, 2017). Among these, more than 14,000 species of fungi have been identified and about 10% of them were macrofungi (El-Ramady et al., 2022). Based on available information, it was estimated that as many as 2189 species of macrofungi are safe for consumption and have been used worldwide (Rai et al., 2005, Li et al., 2021). Additionally, there are about 700 species of edible macrofungi that are beneficial to human health (Li et al., 2021; Lima et al., 2012). Despite the high levels of biodiversity in the tropics, the documentation of macrofungi in this region is still lacking and unclear (Hawksworth, 2001). Gandjar et al. (2006) noted that Indonesia alone may host around 200,000 species of macrofungi, but there is limited data on the number of identified species and their utilization. Generally, information on the use of edible wild macrofungi is sourced from local communities worldwide through ethnomycology. It is important to note that new macrofungi species will continue to be identified in the tropics (Douanla-Meli et al., 2007).

Ethnomycology is a branch of ethnobiology and a relatively new field of study. It is focused on the study of traditional knowledge about the use of macrofungi and the influence of the environment, culture, and its relationship with humans through space and time (Reyes-López et al., 2020). Fungi are integral to ecosystems and have historically as well as globally been recognized for the use of macrofungi in food and medicine (Živković et al., 2021). Wild edible macrofungi are known to have a long-standing and close relationship with humans, providing significant biological, economic, and nutritional contributions. They are also extensively consumed by individuals worldwide (Osarenkhoe et al., 2014; Kim & Song., 2014; Semwal et al., 2014; Alvarez-Farias et al., 2016; Kinge et al., 2011; 2017). However, in the field of

* Corresponding author. e-mail: yyusranyusran610@gmail.com.

ethnomycology, this knowledge is still limited when compared to knowledge about animals and plants.

According to Manzi et al. (1999), edible macrofungi have been traditionally used by people in Asia as food and medicine since ancient times, with a growing trend of their increased use in various parts of the world (Lu et al., 2020; Wasser, 2011). Every local community possesses unique wisdom and knowledge regarding the use of these macrofungi, influenced by culture, beliefs, perceptions, environmental conditions, and local habits. Traditional knowledge about the use of macrofungi is passed down orally from generation to generation (Albuquerque, 2006; Garibay-Orije et al., 2007; Molares et al., 2019).

Macrofungi have macroscopically filamentous fruiting bodies that can be seen with the naked eye. All macrofungi are fungi, but not all fungi are macrofungi (Mgbekem et al., 2019), and they hold significant potential as a source of food and medicine. They thrive naturally and abundantly in nature and can easily be cultivated intensively, although this is limited to only a few saprotrophic species. Edible macrofungi, depending on their species, chemical composition, and growth substrate, are considered a healthy and sustainable food source for humans (El-Ramady et al., 2022). The indigenous peoples in Indonesia have valuable local wisdom regarding utilization of macrofungi natural resources as a source of food and medicine. However, there is limited knowledge about the diversity, distribution, utilization, and cultivation techniques of potential food and medicinal macrofungi species in Indonesia. Ethnomycological studies are also still lacking, although some studies have reported the existence of several macrofungi used as food and medicine by the local community around Lore Lindu National Park, Central Sulawesi (Yusran et al., 2021; 2022a.b) and by the Baduy community in Banten, Indonesia (Khastini et al., 2018; 2019; Dewi et al., 2022).

This study aimed to determine the ethnomycology and local knowledge of the indigenous Pamona community in terms of utilization of wild macrofungi species for food and medicine around Lake Poso, Central Sulawesi Province, Indonesia

2. Materials & Methods

2.1. Study Location, Ethnography, and Climate

Ethnomycological studies on the use of wild macrofungi by the indigenous Pamona community were carried out around Lake Poso, encompassing several conservation areas such as Pamona Nature Reserve, Bancea Nature Park, and Wera Saluopa Nature Park, Central Sulawesi, Indonesia. Lake Poso is situated in the central part of Sulawesi Island, precisely in Poso Regency, Central Sulawesi Province, Indonesia (Figure 1). The population in this area was 86,366 individuals, spread across several sub-districts surrounding Lake Poso, namely Pamona Puselemba, North, West, East, Southeast, and South Pamona. The inhabitants of this area were dominated by Pamona ethnic group, who were the natives. The average temperature in this area was 27.25°C, with an average humidity of 84.56% and rainfall of 2807.8 mm/year (Badan Pusat Statistik/Central Bureau of Statistics, Poso Regency, 2020). The study was conducted within an altitude range of 38 1-572 m above sea level. Interviews were conducted in several villages spread over the six sub-districts, namely Sangira, Sulewana, Saojo, Lena, Panjoka, Wera, Owini, Taipa, Bancea, Panjo, Tampemadoro, Poleganyara, Panjoka and Tindoli. The population in these villages was predominantly Pamona individuals.

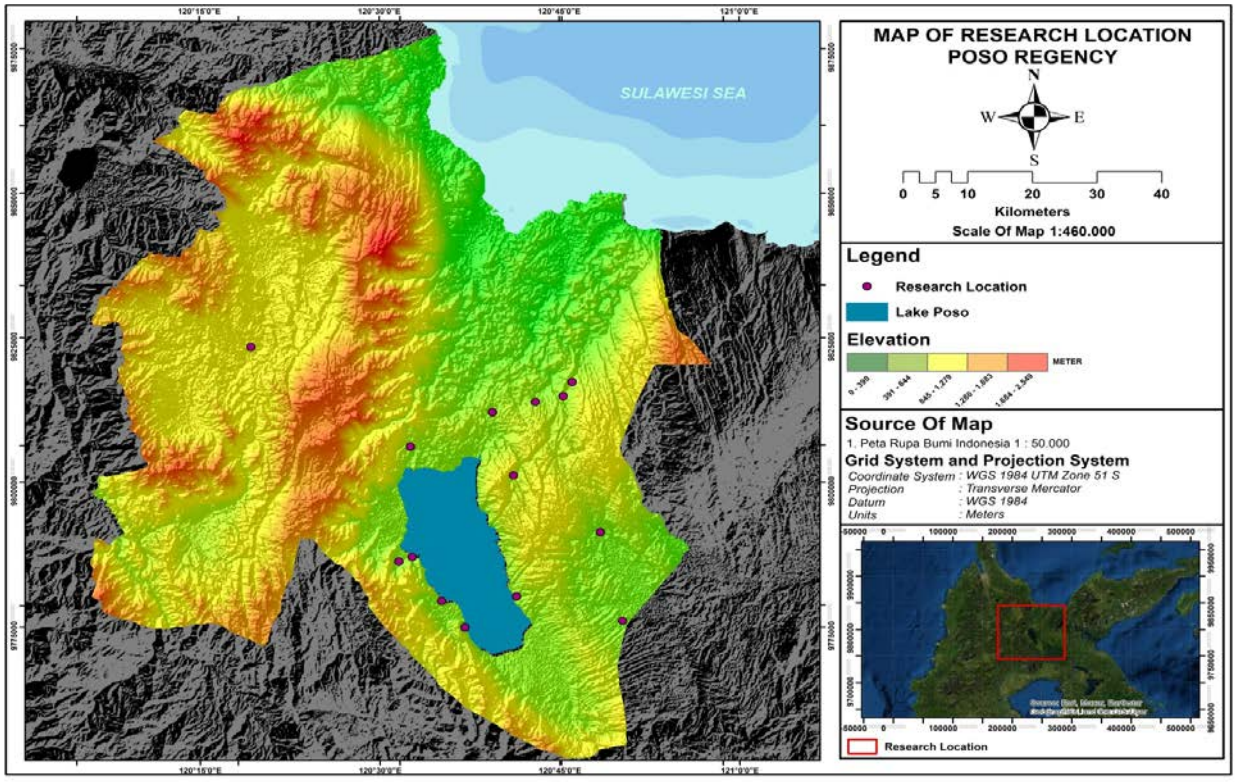

Figure 1. Study sites around Lake Poso, Central Sulawesi, Indonesia

2.2. Sampling Methods and Data Collection

In-depth interviews were conducted with resource people to obtain comprehensive information regarding ethnomycology. Sources were determined using the snowball technique. The selection of resource persons from the community involved two stages: (1) Identifying key resource persons such as traditional leaders, village heads, elders, and macrofungi sellers who were considered relevant and knowledgeable about the study; (2) selecting follow-up sources based on recommendations from previous sources to broaden the range of information and track variations in existing information.

The interviews with the community commenced by meeting with the Village Head as the initial point of contact. The Village Head was asked to provide information about individuals within the community who possessed knowledge and experience in identifying, collecting, and exploiting wild macrofungi. This included village healers, traditional community leaders, and macrofungi sellers in traditional markets who were familiar with food and medicinal macrofungi in several villages surrounding conservation areas. Questionnaires were distributed in each of these villages to selected respondents who were prepared in advance, followed by discussions between the study team and respondents. The total number of respondents in this study was 300. Questions asked included name, age, sex, occupation, education, land ownership, and number of family members. Additionally, respondents were asked about macrofungi, including local name, description, time of appearance, place of growth, method of use, part of fungi used, and the disease treated. During the interviews, photos of food and medicinal macrofungi collected from previous studies were shown to respondents for comparison. In addition to interviews, a Focus Group Discussion (FGD) was conducted to explore the commonly used species of food and medicinal macrofungi within the community and the technology for its use through pictorial percentages. The interviews were conducted in Indonesian and the local language of the local Pamona community, known as Bere'e. The interview took place at each respondent's house and in the field, and questions primarily referred to information about the species of macrofungi and their use by the local community. The collected data were then summarized and transcribed into a quantitative descriptive analysis.

The collection of samples of wild edible macrofungi was carried out over eight months within various ecosystems around the visited villages. These included primary Forest, secondary forest, agroforestry, gardens, monoculture plantations, and yards. Collection of macrofungi fruiting bodies also took place in traditional markets. Each collected fruiting body was placed in paper bags and labeled according to species, and its morphology was recorded using a digital camera. Information regarding their benefits and habitats was also recorded. The collected macrofungi samples were then brought to the laboratory for microscopic examination using a standard microscope (Andrew et al., 2013). Identification of the microfungi was based on references by Hemmes and Desjardin (2002), Desjardin et al. (2000), Desjardin et al. (2004), and online resources such as http://www.indexfungorum.org/, http://mushroomexpert.com/. Collections of dried fruit bodies were also deposited at the Laboratory of Forestry Sciences, Forestry Faculty, Tadulako University, Indonesia.

2.3. Data Analysis

The data was analyzed using qualitative and quantitative methods. Qualitative data obtained from the interviews was presented through descriptive morphological analysis. The analysis of macrofungi species was organized in a table containing information on local names and morphology. Quantitative data was obtained from the utilization value, which was analyzed by calculating the Relative Frequency of Citation (RFC) botanical index. RFC index was obtained by dividing the number of respondents who mentioned certain species of macrofungi (FC) by the number of respondents who participated in the survey (N). The value of RFC index varied from zero to one according to the informant's reference. A value of 0 indicates that no informants mentioned the species as useful macrofungi, while a value of 1 indicates unanimous agreement among all informants regarding the usefulness of the species. RFC index was calculated by using the formula proposed by Qwarse et al. (2021):

$$RFC = \frac{FC}{N}$$

where FC=Number of respondents who mentioned a particular species of macrofungi, and N is the total number of respondents interviewed

FL is the ratio of informants who mentioned the use of a particular species in the area surveyed. FL was determined using the formula

$$FL = \frac{Np}{N}$$

where Np is the number of informants who claim to use a particular species for a specific purpose and N is the total number of informants citing the species for any use.

ICF determines the homogeneity of the information provided by the respondents. It was determined by:

$$IFC = \frac{Nur - Nt}{(Nur - 1)}$$

where Nur is the number of reports on the use of informants for a particular category of macrofungi uses, and Nt represents the number of taxa or species categories of wild macrofungi species.

3. Results

3.1. Important Macrofungi Species in Ethnomycology

The results revealed that the indigenous Pamona community around Lake Poso, Central Sulawesi used 21 species of macrofungi. Macrofungi used were classified into 15 genera and 14 families. The Lyophyllaceae family had the highest number of species (4 species, 19.04%), followed by the Auriculariaceae family (3 species, 14.28%), the Pleurotaceae and Polyporaceae families (2 species, 9.52%), while the remaining 10 families were represented by one species (Table 1). Examples of macrofungi species used by the indigenous Pamona community can be seen in Figure 2.

Table 1. Species of macrofungi used by the indigenous Pamona community around Lake Poso, Central Sulawesi

No.	Vernacular name	Species	Family	Substrate	Utilization and Processing Methods	RFC	FL
1.	Tangkidi/Tangkojo	*Schizophyllum commune* Fr. 1815	Schizophyllaceae	Deadwood	The fruit bodies are used as a vegetable by mixing with coconut milk or sautéing them with other vegetables	1	1
2.	Tanggorugoru	*Auricularia auricula-judae* (Bull.) Quel 1886	Auriculariaceae	Deadwood	Fresh fruit bodies are immediately made into soup, stir-fried with vegetables, or dried, and then stored, which can be processed again at any time	1	1
3.	Tanggorugoru Talinga mbalesu	*Auricularia nigricans* (Sw.) Birkebak, Looney & Sánchez-Garcia	Auriculariaceae	Deadwood	Fresh fruit bodies are immediately made into soup, stir-fried with vegetables, or dried and then stored, which can be processed again at any time	0.56	0.83
4.	Tanggorugoru	*Auricularia* sp.	Auriculariaceae	Deadwood	Fresh fruit bodies are immediately made into soup, stir-fried with vegetables, or dried and then stored, which can be processed again at any time	0.61	0.92
5.	Tambata Mapeni	*Amauroderma* sp	Ganodermataceae	Deadwood	The fruit bodies and stalks are made into souvenirs such as masks and wall paintings by carving and varnishing/painting	0.65	0.69
6.	Tambata Buya/Toyumanu	*Lentinus* sp.	Polyporaceae	Deadwood	The fruit bodies are used like a vegetable by sautéing them with other vegetables	0.88	0.73
7.	Tambata tampopila	*Tremella* sp.	Tremellaceae	Deadwood	The fruit body is used as medicine by grinding it and then applying it directly to the wound	0.14	0.82
8.	Tambata mbega	*Phillipsia* sp.	Sarcoscyphaceae	Deadwood	The fruit body is fried or roasted and then mixed with other drinks like coffee before drinking, causing an intoxicating effect	0.24	0.73
9.	Tanouu ntana 1	*Termitomyces eurrhizus* (Berk.) R. Heim 1942	Lyophyllaceae	Soil	The fruit body is made into soup, mixed with vegetables, sautéed/fried mixed with shallots, chili, and seasonings.	1	1
10.	Tanouu ntana 2	*Termitomyces striatus* (Beeli) R. Heim 1942	Lyophyllaceae	Soil	The fruit body is made into soup, mixed with vegetables, and sautéed/fried with shallots, chili, and seasonings.	0.91	0.92
11.	Tanouu ntana 3	*Termitomyces clypeatus* R. Heim	Lyophyllaceae	Soil	The fruit body is made into soup. mixed with vegetables, and sautéed/fried with shallots, chili, and seasonings.	0.82	0.87
12.	Tanouu ntana 4	*Termitomyces* sp.	Lyophyllaceae	Soil	The fruit body is made into soup, mixed with vegetables, and sautéed/fried with shallots, chili, and seasonings.	0.80	0.82
13.	Tanouu	*Physarum polycephalum* Schwein. 1822	*Physaraceae*	Corncob	The fruit body is made into a soup mixed with other vegetables	0.56	0.81
14.	Toyu ntana	*Trichaleurina javanica* (Rehm) M.Carbone, Agnello & P. Alvarado 2013	Pyronemataceae	Soil	The liquid squeezed out of the fruit body is used as a hair tonic and the dregs of the fruit body are finely chopped and used as a mixture for pig feed.	1	1
15.	Tare'e	*Volvariella volvaceae* (BuLL.) Singer 1822	Pluteaceae	Soil	The fruit body is made into a soup mixed with other vegetables	0.22	0.82
16.	Tambata columbia	*Pycnoporus sanguineus* (L.) Murrill.	Polyporaceae	Deadwood	The fruit bodies are sautéed or boiled	0.34	0.78
17.	Tambata karyada	*Mycena* sp	Mycenaceae	Deadwood	The fruit bodies, which light up at night and are still attached to weathered wood, are used as a light source when walking in the garden/forest	1	1
18.	Tanouu ngkaju/ntua	*Pleurotus* sp.	Pleurotaceae	Deadwood	The fruit bodies are sautéed or dipped and mixed with other spices and vegetables	0.80	0.87
19.	Tamporu	*Russula* sp.	Russulaceae	Soil	The fruit bodies are sautéed or dipped and mixed with other spices and vegetables	0.49	0.63

20. Keje angga	*Dictyophora indusiata* (Vent.) Desy, 1822	Phallaceae	Soil	The stalk and the cap are used as medicine for goiter and swelling of the body by finely grinding the fruit body and then mixing it with coconut oil, then smeared on the surface of the goiter of the neck or any part of the body that is swollen or has lumps.	0.92	1
21. Arindi	*Pleurotus ostreatus* (Jacq.) P. Kumm. 1871	Pleurotaceae	Deadwood	The fruit body is made into a soup mixed with other vegetables	0.46	0.83

Note: RFC= Relative Frequency of Citation, FL= ratio of informants.

Table 2. Informant consensus factor (ICF)

User category	N_{ur}	N_t	ICF
Food	655	18	0.97
Medicine	67	7	0.91
Souvenir & Lighting	45	3	0.95
Animal Feed	33	5	0.88

N_{ur} is the number of use reports and N_t is the number of taxa

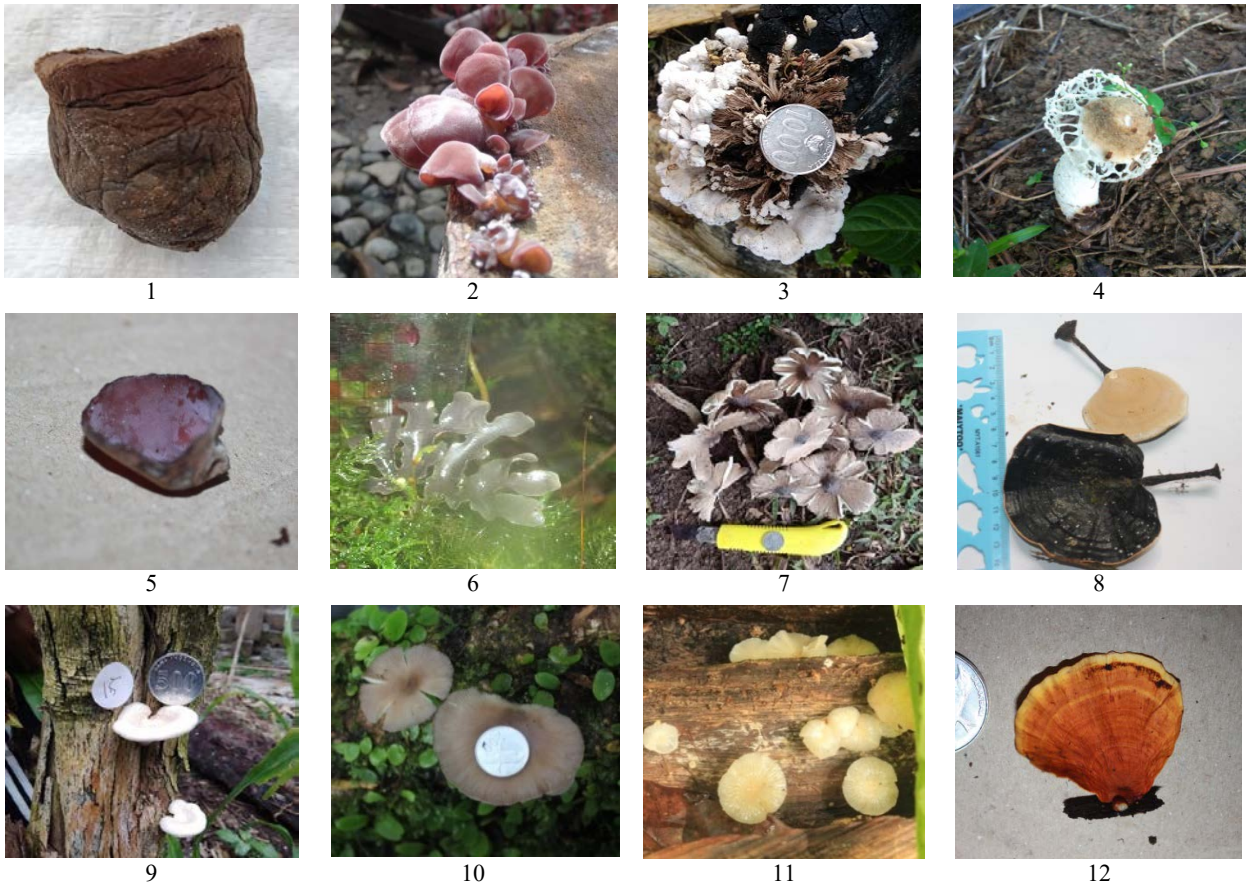

Figure 2. Examples of species of macrofungi used by the indigenous Pamona community: 1) *Trichaleurina javanica*, 2) *Auricularia auricula-judae*, 3) *Schizophyllum commune*, 4) *Dictyophora indusiata*, 5) *Auricularia nigricans*., 6) *Tremella* sp., 7) *Termitomyces eurrhizus,* 8) *Amauroderma* sp., 9) *Lentinus sp*., 10) *Termitomyces sp*., 11) *Mycena sp*., 12) *Pycnoporus sanguineus*

3.2. Preference Rating for Edible Macrofungi

Species of macrofungi with low RFC values have a greater risk of extinction than other species due to their limited recognition and utilization by the public. Increasing the awareness and introduction of these macrofungi to younger generations can help enhance their recognition value.

Table 1 shows that *Schizophyllum commune*, *Auricularia auricular-judae* (Bull.) Quel, *Termitomyces eurrhizus* (Berk.) Pegler and *Trichaleurina javanica* had the highest RFC values of 1, while *Tremella sp* had the lowest RFC value of 0.14. Macrofungi species with low RFC values require domestication to ensure their sustainable use. The highest FL value of 1 was found in *S. commune*, *A. auricula-judae* (Bull.) Quel, *T. eurrhizus* (Berk.) Pegler, *Trichaleurina javanica*, *Mycena sp.,* and *Dictyophora indusiata,* while the other species were below zero. Furthermore, the highest ICF value of 0.97 was found in the use of macrofungi as food.

3.3. Collection, Transfer of Knowledge, Market Opportunities, Utilization, and Phenology of Macrofungi

Knowledge of mycology, including species identification, naming, habitat, phenology, and preparation methods for using macrofungi as food and medicine, has been passed on by word of mouth across generations. There was also no written documentation found regarding these aspects. Furthermore, schools or other formal educational institutions, social and religious institutions, government institutions, and agricultural experts do not play a significant role in the transfer of local knowledge in this study area.

The majority of the local Pamona community trades macrofungi, particularly *Schizophyllum commune* (tanggidi) and *Auricularia auricula-judae* (Tambata talinga valesu). This mainly occurs during the rainy season when these macrofungi grow easily. Due to the abundance of these two macrofungi, they are harvested in large quantities. Some are sun-dried and then stored in jars, and at any time when required, the dried fruit bodies are soaked in water for a few minutes to rehydrate before being cooked.

Table 3. Percentage of macrofungi respondent groups involved in the food macrofungi collection

Parameters	Informant groups	Involvement in macrofungi collection		How often do you collect macrofungi?		
		Yes	No	Never	Sometimes	Always
Sex	Female	104 (34.7%)	13 (4.3%)	13 (4.3%)	17 (5.7%)	87 (29.0%)
	Male	162 (54.0%)	21 (7.0%)	21 (7.0%)	27 (9.0%)	135 (45.0%)
Age	Young (15-30 Years)	76 (25.3%)	7 (2.3%)	7 (2.3%)	27 (9.0%)	49 (16.3%)
	Senior (>30 Years)	202 (67.4%)	15 (5.0%)	15 (5.0%)	8 (2.7%)	194 (64.7%)
Literacy level	Illiterate	50 (16.7%)	6 (2.0%)	6 (2.0%)	17 (5.7%)	33 (11.0%)
	literate	230 (76.7%)	14 (4.6%)	14 (4.6%)	47 (15.7%)	183(61.0 %)
Informant category	Key	117 (39.0%)	17 (5.7%)	17 (5.7%)	32 (10.7%)	85 (28.6%)
	General	137 (45.7%)	29 (9.6%)	29 (9.6%)	51 (17.0%)	86 (51.8%)
Family income	Low (3.000.000 IDR)	218 (72.7%)	5 (1.6%)	5 (1.6%)	19 (6.3%)	199 (66.3%)
	High (>3.000.000 IDR)	68 (22.7%)	9 (3.0)	9 (3.0%)	36 (12.0%)	32 (10.6%)
Distance from forest	<5 km	162 (54.0%)	16 (5.3%)	16 (5.3%)	7 (2.3%)	155 (51.7%)
	>5 km	113 (37.7%)	9 (3.0%)	9 (3.0%)	42 (14.0%)	71 (23.6%)

IDR = Indonesian currency

The group of informants described in Table 3 exhibits differences in their involvement in the collection of macrofungi. Among the 183 male and 117 female informants, 162 men (54.0%) and 104 women (34.7%) were involved, while 21 men (7.0%) and 31 women (4.3%) were not involved in the collection of macrofungi. In terms of age, 76 youths (25.3%) of 15-30 years were involved in the collection of macrofungi, while 7 (2.3%) were not involved. Among the seniors (> 30 years), 202 individuals (67.4%) were involved in the collection of macrofungi, while the remaining 15 individuals (5.0%) were not involved. Based on their level of education, educated informants were more active in collecting macrofungi than the uneducated. Informants from households with low income were more active in collecting macrofungi than those with high income. The distance from the house to the forest where macrofungi are collected also had an effect, with informants residing closer to the forest collecting more macrofungi.

Table 3 also shows the frequency of informants in collecting macrofungi. Pamona community frequently collect macrofungi, as evidenced by percentages above 50% across all parameters except for informant income. Individuals with higher income rarely collect macrofungi, as they have the means to fulfill their family's needs and prefer to purchase them at local traditional markets.

Respondents showed understanding of the seasonal emergence of macrofungi by acknowledging the significant influence of the rainy season on the appearance of fruit bodies (Table 4). Although most species of edible macrofungi appeared during the rainy season, certain species exclusively appeared during the rainy season, such as *Termitomyces* spp. which was associated with rainy weather accompanied by lightning. There were also macrofungi species emerged during the dry season, such as *Amauroderma sp*., *Lentinus sp*., and *Picnoporus sanguineus*. *Trichaleurina javanica* was found in forests, gardens or recently cleared fields due to their preference for fertile soil. These microfungi were particularly abundant in the rainy season during months like September, October, November, and December. However, *S. commune* macrofungi were found and used by the Pamona community all year round due to their widespread growth.

Table 4. Phenology of the species of macrofungi based on the perceptions of the respondents

No.	Species	Months
1.	*Schizophyllum commune* Fr. 1815	January-December
2.	*Auricularia auricular-judae* (Bull.) Quel 1886	April – November
3.	*Auricularia nigricans* (Sw.) Birkebak, Looney & Sánchez-Garcia	January – August
4.	*Auricularia* sp.	July – December
5.	*Amauroderma* sp.	April – July
6.	*Lentinus* sp.	March – June
7.	*Tremella* sp.	January – May
8.	*Phillipsia* sp.	May – November
9.	*Termitomyces eurrhizus* (Berk.) R. Heim 1942	September – October
10.	*Termitomyces striatus* (Beeli) R. Heim 1942	September – October
11.	*Termitomyces clypeatus* R. Heim	August – September
12.	*Termitomyces* sp.	August – October
13.	*Physarum polycephalum* Schwein. 1822	June – September
14.	*Trichaleurina javanica* (Rehm) M.Carbone, Agnello & P. Alvarado 2013	January – December
15.	*Volvariella volvaceae* (BuLL.) Singer 1822	April – June
16.	*Pycnoporus sanguineus* (L.) Murrill.	May – August
17.	*Mycena* sp.	January – December
18.	*Pleurotus* sp.	June – September
19.	*Russula* sp.	September – November
20.	*Dictyophora indusiata* (Vent.) Desy, 1822	September – December
21.	*Pleurotus ostreatus* (Jacq.) P. Kumm. 1871	October – December

4. Discussion

The Pamona community categorizes macrofungi into two major groups based on where they grow. These include "Tambata" for macrofungi that grow on weathered wood or living trees (saprophytes) and "Tanouu" for those that grow on the ground. The name Tambata is also the same as that given by the Kaili community, who live in the valley of Palu and Sigi Regency, Central Sulawesi, Indonesia (Yusran et al., 2021; 2022a).

The ethnomycology study showed that all respondents had extensive knowledge of several macrofungi as being the best quality food for the Pamona community. These microfungi include *Schizophyllum commune*, *Auricularia auricula-judae* (Bull.) Quel, *Auricularia nigricans*, *Auricularia* sp., *Termitomyces eurrhizus* (Berk.) Pegler, *Termitomyces striatus* Var. annulatus R. Helm Pegler, *Termitomyces clypeatus* R. Heim, and *Termitomyces* sp. The identification and folk taxonomy of these macrofungi was easily understood by the public, as they were frequently collected for consumption and sale.

Macrofungi *Trichaleurina javanica* is called "Toyuntana" when it is young and underground and “Tanouu” when it blooms. Among the 21 macrofungi species found, macrofungi *Schizophyllum commune* (Tanggidi) was the most commonly known among the indigenous Pamona community in Poso District, Central Sulawesi. The name "Tanggidi" was also used by the Kaili community in Sigi Regency, Central Sulawesi (Yusran et al., 2022b). This species is commonly consumed due to its excellent taste and easy availability, especially during the rainy season. It is well known with different names across several provinces in Indonesia, such as Kulat Kritip in Central Kalimantan (Nion et al., 2012), Supa in Banten (Khastini et al., 2018), Tirau in Sumatera Island (Kusrinah and Kasiamdari, 2015), and Jaggery in West Papua (Nurlita et al., 2021).

Another species of macrofungi that is believed to cure goiter by the indigenous Pamona community is *Dictyophora indusiata*. The method of using it involved taking the stem (stipe) of macrofungi, growing it until smooth, mixing it with coconut oil, and then applying it to the surface of the goiter lump on the neck. *Tremella sp.* (Tambata Tampopila) is a species that is believed by the Pamona community to heal wounds on the surface of the body. The method of use involved crushing the fruit body until smooth and then sticking it directly on the wound.

According to Panda and Tayung (2015), it is very common for people in newly developing countries to use macrofungi to maintain health and prolong life. Macrofungi have high nutritional value because they are rich in protein, essential amino acids, vitamins, and fiber but low in fat and antioxidants (Rahman et al., 2021; Agrahar-Murugkar and Subbulakshmi, 2005; Balan et al., 2018; Cardwell et al., 2018; Taşkın et al., 2021). Various studies have reported on the medicinal effects of *D. indusiata* fruit bodies, including anti-obesity (Wang et al., 2019), neuroprotective effects for Alzheimer's disease (Talebi et al., 2021), and wound treatment (Nazir et al., 2021). Similarly, the microfungi *Tremella fuciformis* Berk., known for its snow-like appearance, has been used for thousands of years in China due to its traditional therapeutic effects, particularly in skin care, immune repair, and disease prevention (Ma et al., 2021). In this study, it was found that there were 21 macrofungi used by the indigenous Pamona community around Lake Poso. This number is higher compared to a study by Sharma et al. (2022) which identified 14 species of edible macrofungi in the Jammu district, India. However, the results were lower than several previous studies, as reported by Kamalebo et al. (2018), who discovered 68 species of macrofungi used as food and medicine in Thsopo Province, the Democratic Republic of Congo. It was also lower than the 46 species in San Mateo Huexoyucan, Tlaxcala, Mexico (Alonso-Aguilar et al., 2014), 47 species

of edible macrofungi by five communities in Ocoyoacac, Mexico (Romero et al., 2015), 25 species in Sabah, Malaysia (Fui et al., 2018), and 91 species of food and medicinal macrofungi found through a market survey in Southwest Yunnan, China (Wang et al., 2022).

The Pamona community primarily obtain macrofungi for household consumption and rarely for sale in the local market, resulting in minimal impact on their income levels. The most commonly found macrofungi was *Termitomyces,* which was consistent with the results of previous studies (Sharma et al., 2022; Teke et al., 2018; Sitotaw et al., 2020; Tibuhwa et al., 2012). Among macrofungi species, *Schizophyllum commune* is the most frequently consumed due to its delicious taste and easy availability. Based on previous reports, it has been used traditionally in Southeast Asian countries and India (Singh, 2017; Waktola and Temesgen, 2018; Valverde et al., 2015; Sánchez, 2017; Sande et al., 2019; Srikram and Supapvanich, 2016).

According to Dapar et al. (2020), a high FL value validates the traditional potential of macrofungi for specific uses, while a low FL value indicates a wide range of uses with disagreement over the specific uses of certain species. An FL value of 1 for a particular macrofungi species suggests that all usage reports mention the same macrofungi for specific uses in the study area (Khastini et al., 2018).

Preferences for macrofungi species vary among communities in different parts of the world. In this study, the most preferred was the *Schizophyllum commune* species, which aligned with the preferences of the local people in Tshopo Province, the Democratic Republic of the Congo (Kamalebo et al., 2018), and the Gaddang community in Nueva Vizcaya, Philippines (Lazo et al., 2015). However, in the Selous-Niassa Corridor in the Ruvuma Region, Tanzania, the most preferred macrofungi species was *Agaricus* (Qwarse et al., 2021). Different countries also have their preferences, such as the genus *Termitomyces* in the Meng district, Asossa Zone, Benshangul Gumuz Region, Ethiopia, (Sitotaw et al., 2020), *Cantharelus* in ethnicities in India, Cameroon, Burundi, and Congo (Kamalebo and Kesel., 2020), and the genus *Lactarius* in India (Kumar et al., 2017). These species are well known and liked by the public because they taste good and have high nutritional content. In addition, *Schizophylllum commune*, *Auricularia* sp., and *Termitomyces* sp. had sufficient nutritional content before and after cooking (Yusran et al., 2022a).

These results are consistent with a previous study conducted by Sharma et al. (2022) in a community in Jammu district, India, where macrofungi were primarily used as food. Similarly, the local community in The Selous-Niassa Corridor, Ruvuma Region, Tanzania, obtained the highest ICF values for macrofungi used as food (Qwarse et al., 2021). According to Uddin and Hassan (2014), ICF value for macrofungi species was used to determine agreement among informants residing around Lake Poso regarding customary knowledge about edible and inedible wild macrofungi or other uses such as medicine. ICF score reflects the homogeneity, reliability, and level of knowledge among informants on the use of macrofungi species for food, medicine, and those considered inedible in the community.

Pamona community collected macrofungi mainly for food and medicine, and this was also practiced by local people in the Selous-Niassa Corridor, Ruvuma Region, Tanzania (Qwarse et al., 2021), and several communities in Tanzania (Haäkönen et al., 2003). It was prepared by boiling, frying/stir-frying, or cooking with coconut milk (curry) mixed with fish or other species of vegetables. The same method was also practiced by the Khasi people in India (De Leon et al., 2012) and the Gaddang people in Nueva Vizcaya, Philippines (Lazo et al., 2015). A similar phenomenon was also observed among the local community in Meng district, Asossa zone, Benshangul Gumuz Region, Ethiopia (Sitotaw et al., 2020) and also a community in Jammu district, J&K (UT), India (Sharma et al. 2022). This differs from local people in the Meng district, Asossa Zone, Benshangul Gumuz Region, Ethiopia (Sitotaw et al. 2020), where family income does not affect the frequency of macrofungi collection.

5. Conclusions

In conclusion, the consumption of macrofungi was based on knowledge of the informants. Pamona community was rich in traditional knowledge and practices in utilizing various macrofungi species for both food and medicine and could distinguish between edible and poisonous macrofungi. Therefore, the results of this study provide valuable information about edible macrofungi, which can improve nutritional status, reduce malnutrition and prevent and treat certain diseases within the Pamona community residing around Lake Poso, Central Sulawesi, Indonesia. The results also showed that a total of 21 macrofungi species were used by Pamona indigenous people as food, medicine, souvenirs, lighting in the dark, hair growth agents, and a mixture for making livestock rations. Among these, *Schizophyllum commune*, *Auricularia auricula-judae* (Bull.) Quel, *Termitomyces eurrhizus* (Berk.) Pegler, and *Trichaleurina javanica* had the highest RFC of 1, while *Tremella sp* had the lowest RFC of 0.14. The highest ICF value of 0.97 was associated with the use of macrofungi as food. It is worth emphasizing that saprotrophic macrofungi species that have low RFC values require domestication to ensure their availability and promote sustainability. These macrofungi have the potential for further development in the domestication stage through cultivation and future analysis of nutrients and bioactive compounds.

Acknowledgments

The authors are grateful to the Rector of Tadulako University for funding this study through the Faculty DIPA, Postgraduate, PSDKU Tojo Una-Una University, The Ministry of Education and Culture, Tadulako University, No. 3654/UN28.2/KP/2022, April 11, 2022. The authors are also grateful to Pamona community who participated in the interviews during the study.

Conflict of interest

All the authors declare that there is no conflict of interest.

References

Agrahar-Murugkar D, Subbulakshmi GJ. 2005. Nutritional value of edible wild macrofungicollected from the Khasi hills of Meghalaya. *Food Chem.*, **89(4)**:599-603.

Alonso-Aguilar LE, Montoya A, Kong A, Estrada-Torres A, Garibay-Orije R.2014. The cultural significance of wild mushrooms in San Mateo Huexoyucan, Tlaxcala, Mexico. *J. Ethnobiol Ethnomed.*, 10:27. doi:10.1186/1746-4269-10-27.

Álvarez-Farias Z, Diaz-Godinez G, Teller-Tellez M, Villegas E, Acosta-Urdapilleta ML. 2016. E thnomycological knowledge of wild edible macrofungiin Tlayacapan, Morelos. *Mycosphere.*, **7(10)**:1491–1499. http://dx.doi.org/10.5943/mycosphere/si/3b/1.

Albuquerque UP, Lucena RFP, Monteiro JM, Florentino ATN, Almeida C. 2006. Evaluating two quantitative ethnobotanical techniques. *Ethnobot. Res, Appl.*, **4**:51–60.

Andrew EE, Kinge TR, Tabi EM, Thiobal N, Mih AM. 2013. Diversity and distribution of macrofungal (macrofungis) in the Mount Cameroon Region. *J. Ecol. Nat. Environ.*, **5(10)**:318-334.

Badan Pusat Statistik, Kabupaten Poso (Central Bureau of Statistics, Poso Regency). 2020. Kabupaten Poso Dalam Angka.

Balan V, Munafo JP, Pattathil S, Merritt BB, Venketachalam S, Ng WO. 2018. Protocols to Evaluate the Nutritional and Potential Health Benefits of Edible Macrofungis. *CBIOT.*, **7**:34–58.

Cardwell G, Bornman J, James A, Black L. 2018. A Review of Macrofungias a Potential Source of Dietary Vitamin D. *Nutrients.*, **10**:1498

Chen WY, Yang T, Yang J, Qiu ZC, Ding XY, Wang YH, Wang YH. 2021. Wlid plants used by the Lhoba people in Douyu Village, characterized by high mountains and valleys, in Southeastern Tibet, China. *J. Ethnobiol Ethnomed.*. 17-46.

Dapar MLG, Alejandro GID, Meve U, Liede-Schumann S. 2020. Quantitative ethnopharmacological documentation and molecular confirmation of medicinal plants used by the Manobo tribe of Agusan del Sur, Philippines. BMC. *J. Ethnobiol Ethnomed*., **16(14)**:1-60.

De Leon AM, Reyes RG, Dela Cruz TEE. 2012. An ethnomycological survey of macrofungi utilized by Aeta communities in Central Luzon, Philippines. *Mycosphere*., **3(2)**:251–259, Doi 10.5943/mycosphere/3/2/9.

Desjardin DE, Flegel TW, Boonpratuang T. 2004. Basidiomycetes. In: EGB Jones, M Tanticharoen and KD Hyde (eds.). **Thai Fungal Diversity**, Biotech Publishing, Thailand, 37-49.

Desjardin DE, Retnowati A, Horak E. 2000. Agaricales of Indonesia 2. A Preliminary monograph of Marasmius from Java and Bali. *Sydovia.*, **52(2)**:92-193.

Dewi RF, Ummah NR, Hidaya N. 2022. Ethnomycology studies of edible and medicinal macroskopis fungi in Jember Indonesia. *J. Biotik.*, **2** eds. 218-229.

Douanla-Meli C, Ryvarden L, Langer E. 2007. Studies of tropical African pore fungi (Basidiomycota, Aphyllophorales): three new species from Cameroon. *Nova Hedwigia*., **84**: 3-4 409-420.

El-Ramady H, Abdalla N, Badgar K, Llanaj X, Törős G, Hajdú P, Eid Y, Prokisch J. 2022. Edible Macrofungifor Sustainable and Healthy Human Food: Nutritional and Medicinal Attributes. *Sustainability*., **14**:4941. https:// doi.org/10.3390/su14094941

Fui FS, Saikim FF, Kulip J, Seelan JSS. 2018. Distribution and ethnomycological knowledge of wild edible macrofungiin Sabah (Northern Borneo), Malaysia. *Journal of Tropical Biology and Conservation (JTBC).*, **15**:203-222.

Gandjar I, Sjamsuridzal W, Oetari A. 2006. **Mikologi Dasar dan Terapan**. Yayasan Obor Indonesia. Jakarta.

Garibay-Orijel R, Caballero J, Estrada-Torres A, Cifuentes J. 2007. Understanding cultural significance, the edible macrofungicase. *J Ethnobiol Ethnomed.*, **3**:4. https://doi.org/10.1186/1746-4269-3-4.

Haäkönen M, Niemela T, Mwansumbi. 2003. **Tanzanian macrofungi edible, harmful and other fungi**. Botanical Museum, Museum of Natural History, Helsinki, Finland.

Hawksworth DL, Lűcking R. 2017. Fungal diversity revisited: 2.2 to 3.8 Million species. *Microbiol Spectr*., **5(4)**:FUNK-0052-2016.doi:10.1128/microbiolspec:FUNK-0052-2016.

Hawksworth DL. 2001. The magnitude of Fungal Diversity: the 1.5 million species estimate revisited. *Mycol. Res.*, **105**:1422-1432. https://doi.org/10.1017/S0953756201004725

Hemmes DE, Desjardin DE. 2002. **Macrofungiof Hawai'I (An identification guide)**. Ten speed press. Berkeley, California. 212.

Index Fungorum. 2022. Available from: http://www.indexFungorum.org/names. (accessed 14 July 2022).

Kamalebo HM, Kesel AD. 2020. Wild edible ectomycorrhizal fungi an underutilized food resources from the rainforests of Tshoop province of Democratic Republic of Congo. BMC, *J. Ethnobiol Ethnomed.*, **16(8)**:1-13.

Kamalebo HM, Malale HNSW, Ndabaga CM, Degreef J, De Kesel A. 2018. Uses and impotance of wild fungi: traditional knowledge from the Tshopo province in the Democratic Republic of the Congo. *J. Ethnobiol Ethnomed.*, **14**:13. DOI 10.1186/s13002-017-0203-6

Khastini RO, Wahyuni I, Saraswati I. 2018. Ethnomycology of bracket fungi in Baduy Tribe Indonesia. Biosaintifika. *Journal of Biology & Biology Education.*, **10(2)**:424-432.

Khastini RO, Wahyuni I, Lista L, Saraswati I. 2019. Inventory and utilization of macrofungi species for food in Cikartawana inner Baduy Banten. Biodidaktika, *Wahana-Bio*., **14(1)**:7-13. http://dx.doi.org/10.30870/biodidaktika.v14i1.4838

Kim H, Song MJ. 2014. Analysis of traditional knowledge for wild edible macrofungiconsumed by residents living in Jirisan National Park (Korea). *J. Ethnopharmacol*., **153(1)**: 90-97.

Kinge TR, Tabi EM, Mih AM, Enow EA, Njouonkou L, Nji TM. 2011. Etnomycological studies of edible and medicinal macrofungiin the mount Cameroon region (Cameroon, Africa). *Int. J. Med. Mushrooms*., **13(3)**:299-305.

Kinge TR, Apalah NA, Nji T M, Acha AN, Mih AM. 2017. Species richness and traditional knowledge of macrofungi (Macrofungis) in the Aing Forest Reserve and communities, Nortwest Region, Cameroon. *J. Mycol.*, 17:1-9.

Kumar M, Harsh NSK, Prasad R, Pandey VV. 2017. An ethnomycological survey of Jansar, Chakrata and Dehradum, *India. J. Threat. Taxa*., **9(9)**:10717-10725.

Kusrinah and Kasiamdari RS. 2015 - Morphological Characteristics and Kinship Relationship of Macrofungi *Schizophyllum commune* Fr. *J. Nat. Sci. Math. Res*., **1(2)**:65-71. DOI: 10.21580/jnsmr.2015.1.2.1620.

Lazo CRM, Kalaw SP, De Leon AM. 2015. Ethnomycological survey of macrofungi utilized by Gaddang communities in Nueva Vizcaya, Philippines. *Curr. Res. Environ. Appl. Mycol.*, **5(3)**:256-262.

Li H, Tian Y, Menolli NJr, Ye L, Karunarathna SC, Perez-Moreno J, Rahman MM, Rashid MH, Phengsintham P, Rizal L, Kasuya T, Lim YW, Dutta AK, Khalid AN, Huyen LT, Balolong MP, Baruah G, Madawala S, Thongklang N, Hyde KD, Kirk PM, Xu J, Sheng J, Boa E, Mortimer PE. 2021. Reviewing the world's edible macrofungi species: a n ew evidence-based classification system. *Compr Rev Food Sci Food Saf.*, **20**:1982–2014. https://doi.org/10.1111/1541-4337.12708.

Li M, Yu L, Zhao J, Zhang H, Chen W, Zhai Q, Tian F. 2021. Role of Dietary Edible Macrofungiin the Modulation of Gut Microbiota. *J. Funct. Foods.*, **83**:104538

Lima AD, Costa FR, Carvalho G, Novaes MR, Percário S. 2012. Poisonous macrofungis: a r eview of the most common intoxications. *Nutr. Hosp*., **27(2)**:402-408. DOI:10.1590/s0212-16112012000200009.

Lu H, Lou H, Hu J, Liu Z, Chen Q. 2020. Macrofungi: A review of cultivation strategies, bioactivity, and application of mushrooms. Compr Rev Food Sci Food Saf., **19**:2333–2356. https://doi.org/10.1111/1541-4337.12602

Ma X, Yang M, He Y, Zhai C, Li C. 2021. A r eview on the production, structure, bioactivities and applications of *Tremella polysaccharides*. *Int. J. Immunopathol. Pharmacol.*, **35**:1–14. DOI: 10.1177/20587384211000541

Manzi P, Gambelli L, Marconi S, Vivanti V, Pizzoferrato L. 1999. Nutrients in edible macrofungis: an interspecies comparative study. *Food Chem.*, **65**:477-468.

Mgbekem MA, Lukpata F, Ndukaku N, Armon M, Uka VK, Udosen GN, Pricilla AB. 2019. Knowledge and Utilization of Macrofungi as a Food Supplement among Families in Selected Local Government Areas of Cross River State, Nigeria. *Food. Nutr. Sciences.*, **10**: 1287-1299. https://doi.org/10.4236/fns.2019.1011093

Molares S, Toledo CV, Stecher G, Barroetavena C. 2019. Traditional mycological knowledge and processes of change in Mapuche communities from Patagonia, Argentina: A s tudy on wild edible fungi in Nothofagaceae forests. *Mycologia*., **112(1)**:1-16.

Mushroom Expert. 2022. Available from https://www.mushroomexpert.com/. (Accessed 20 July 2022)

Nazir Y, Linsaenkart P, Khantham C, Chaitep T, Jantrawut P, Chittasupho C, Rachtanapun P, Jantanasakulwong K, Phimolsiripol Y, Sommano SR, Tocharus J, Mingmalairak A, Wongsa A, Arjin C, Sringarm K, Berrada H, Barba F.J, Ruksiriwanich W. 2021. High Efficiency In Vitro Wound Healing of Dictyophora indusiata Extracts via Anti-Inflammatory and Collagen Stimulating (MMP-2 Inhibition) Mechanisms. *J. Fungi*,, **7**: 1100. https://doi.org/10.3390/jof7121100

Nion YS, Djaya AA, Kadie EM, Lune. Sumarlan. Wijaya CH. 2012. Siklus Hidup Jamur Konsumsi Lokal Kulat Kritip (*Schizophyllum commune*) Pada Daerah Bergambut dan Daerah Bertanah Mineral serta Potensi Nutrisinya (Cycles life of local edible macrofungi Kulat Kritip (*Schizophyllum commune*) on peat soil and mineral soil also its nutrition potency). *J. Biologi Indonesia*., **8(20)**:399-406. DOI 10.14203/jbi.v8i2.3060.

Nurlita AI. Putra IP. Ikhsan M. 2021. Catatan Pemanfaatan *Schizophyllum commune* di Kampung Udapi Hilir, Papua Barat. *Integrated Lab J*., **9(1)**:18-28. DOI: https://doi.org/10.14421/ilj.2021.090104.

Osarenkhoe OO, John OA, Theophilus DA. 2014. Ethnomycological Conspectus of West African Macrofungis: An Awareness Document. *Adv. Microbiol.*, **4(1)**:39–54. http://dx.doi.org/10.4236/aim.2014.41008.

Panda MK, Tayung K. 2015. Documentation and ethnomedical knowledge on w ild edible macrofungiamong ethnic tribes of Northem Odisha, India. *Asian J Pharm Clin Res*., **8(4)**:139-143.

Qwarse M, Moshi M, Mihale MJ, Marealle AI, Se mpombe J, Mugoyela V. 2021. Knowledge on utilization of wild macrofungiby the local communities in the Selous-Niassa Corridor in Ruvuma Region, Tanzania. *J. Yeast and Fungal Res.*, **12(1)**:8-19. DOI: 10.5897/JYFR2020.0203

Rahman MA, Rahman T, Rahman M, Arif M. 2021. Usage of Macrofungiin Culinary and Medicinal. *Virol Mycol*., **10** Iss.5 No:1000216

Rai M, Tidke G, Wasser SP. 2005. Therapeutic potentials of macrofungis. *Nat Prod Radiance.*, **4(4)**: 246–57.

Reyes-López RC, Montoya A, Kong A, Cruz-Campuzano EA. Caballero-Nieto J. 2020. Folk classification of wild macrofungifrom San Isidro Buensuceso, Tlaxcala, Central Mexico. *J. Ethnobiol. Ethnomed*., **16**:53. https://doi.org/10.1186/s13002-020-00408-x

Romero DD, Reyes JIA, Valdés CV, Popoca NPR. 2015. Uso Y Manejo de Hongos Silvestres en Cinco Comunidades del Municipio de Ocoyoacac, Estado de Mexico [Use and Management of wild macrofungiin five communities in the Municipality of Ocoyoacac, State of Mexico]. *Trop. Subtrop. Agroecosystems*., **18**:133 – 143

Sande D, de Oliveira GP, Moura MA., Martins BA, Lima MTNS, Takahashi JA, 2019. Edible macrofungias a ubiquitous source of essential fatty acids. *Food Res. Int*., **125**. https://doi.org/10.1016/j.foodres.2019.108524

Sánchez C. 2017. Reactive oxygen species and antioxidant properties from macrofungis. *Synth. Syst. Biotechnol.*, **2(1)**:13–22. https://doi.org/https://doi.org/10.1016/j.synbio.2016.12.001**.**

Semwal KC. Stephenson SL. Bhatt VK. Bhatt RP. 2014. Edible macrofungiof the North Western Himalaya, India: a study of indigenous knowledge, distribution and diversity. *Mycosphere*., **5(3)**:440–461. http://dx.doi.org/10.5943/mycosphere/5/3/7.

Sharma R. Sharma YP. Hashmi SAJ. Kumar S. Manhas RK. 2022. Ethnomycological study of wild edible and medicinal macrofungiin district Jammu, J & K (UT), India. *J Ethnobiol Ethnomed*., **18(23)**.

Singh R. 2017. A Review on Different Benefits of Macrofungi. *J. Pharm. Biol. Sci*., **12(1)**:107-111. DOI: 10.9790/3008-120102107111.

Sitotaw R, Lulekal E, Abate D. 2020. Ethnomycological study of edible and medicinal macrofungiin Menge District, Asossa Zone, Benshangul Gumuz Region, Ethiopia. *J Ethnobiol Ethnomed*., **16**:11.

Srikarm A, and Supapvanich S. 2016. Proximate compositions and bioactive compounds of edible wild andcultivated macrofungifrom Northeast Thailand. *Agric. Nat. Resour*., **50**:432-436. https://doi.org/10.1016/j.anres.2016.08.001.

Talebi M, Kakouri E, Talebi M, Tarantilis PA, Farkhondeh T, İlgün S, Pourbagher-Shahri AM, Samarghandian S. 2021. Nutraceuticals-based therapeutic approach: Recent advances to combat pathogenesis of Alzheimer's disease. *Expert Rev. Neurother*., **21**:625–642.

Tardío J, Pardo-de-Santayana M. 2008. Cultural importance indices: A comparative analysis based on the useful wild plants of Southern Cantabria (Northern Spain). *Economic Botany*., **62(1)**: 24–39

Taşkın H, Süfer Ö, Attar ŞH, Bozok F, Baktemur G, Büyükalaca S, Kafkas NE. 2021. Total Phenolics, Antioxidant Activities and Fatty Acid Profiles of Six Morchella Species. *J. Food Sci., Technol*., **58**:692–700.

Teke NA, Kinge TR, Bechem E, Nji TM, Ndam LM, Mih AM. 2018. Ethnomycological study in the Kilum-Ijim mountain forest, Northwest Region, Cameroon. *J Ethnobiol Ethnomed*., **14**: 25.

Tibuhwa DD. 2012. *Termitomyces* species from Tanzania, their cultural properties and unequalled basidiospores. *J Biol Life Sci*., **3(1)**:140–59.

Uddin ZM, Hassan MA. 2014, Determination of informant consensus factor of ethnomedicinal plants used in Kalenga forest. Bangladesh. *Bangladesh J. Plant Taxon*., **21(1)**: 83–91.

Valverde ME, Hernández-Pérez T, Paredes-López O. 2015. Edible macrofungis: Improving Human Health and Promoting Quality Life. *Int. J. Microbiol.*, 1-14. https://doi.org/10.1155/2015/376387.

Waktola G, Temesgen T, 2018. Application of macrofungias food and medicine. *Adv. Biotechnol. Microbiol.*, **11(4)**:555817. DOI: 10.19080/ AIBM.2018.11.555817.

Wang W, Song X, Zhang J, Li H, Liu M, Gao Z, Wang X, Jia L. 2019. Antioxidation, hepatic-and renal-protection of water-extractable polysaccharides by *Dictyophora indusiata* on obese mice. *Int. J. Biol. Macromol*., **134**:290–301.

Wang R, Herrera M, Xu W, Zhang P, Moreno JP, Colinas CYF. 2022. Ethnomycological study on wild macrofungiin Pu'er prefecture, Southwest Yunan, China. *J. Ethnobiol. Ethnomed*., **18**:55. https://doi.org/10.1186/s13002-022-00551-7

Wasser, S. P. 2011. Current findings, future trends, and unsolved problems in studies of medicinal mushrooms. *Appl. Microbiol. Biotechnol*., **89(5)**, 1323–1332. https://doi.org/10.1007/ s00253-010-3067-4

Yusran Y, Erniwati E, Wahyuni D, Ramadhanil R, Khumaidi A. 2021. Diversity of macro fungus across three altitudinal ranges in Lore Lindu National Park, Central Sulawesi, Indonesia and their utilization by local residents. *Biodiversitas.*, **22(1)**:199-210. https://doi.org/10.13057/biodiv/d220126

Yusran Y, Erniwati E, Khumaidi A, Setiarto RHB. 2022a. Effect of cooking on the proximate composition and minerals content of wild edible macro fungi from Lore lindu National Park, Central Sulawesi, Indonesia. *African. J. Food Agric. Nutr. Dev*., **22(5)**:20523-20541. https://doi.org/10.18697/ajfand.110.21660

Yusran Y, Erniwati E, Khumaidi A, Pitopang R, Rahmawati R, Korja I.N, Labiro E, Rukmi R, Muthmainnah M, Maksum H, Setyawati R. 2022b. Diversity of Macro Fungus Species in Several Speciess of Land Use Around Lore Lindu National Park, Central Sulawesi, Indonesia. *Int. J. Des. Nat. Ecodyn*., **17(3)**:341-351. https://doi.org/10.18280/ijdne.170303

Živković J, Ivanov M, Stojković D, Glamočlija J. 2021. Ethnomycological Investigation in Serbia: Astonishing Realm of Mycomedicines and Mycofood. *J. Fungi*., **7**:349. https://doi.org/ 10.3390/jof7050349

JJBS

Volume 17, Number 1,March 2024
ISSN 1995-6673
Pages 89 – 98
https://doi.org/10.54319/jjbs/170108

Jordan Journal of Biological Sciences

Novel Thiazolidinedione Linked 1,3,4-Oxadiazole Derivatives as AXL Inhibitors Targeting Breast Cancer: *In-Silico* Design, ADMET Screening, and MM-GBSA Binding Free Energy

Mahendra Gowdru Srinivasa[1], Ananya Dinesh Rao[1], Ancilla Laveena Dsouza[1], Gauthami R[1], Jackson Loy Monteiro[1], Shridhar Deshpande N[1], Natasha Naval Aggarwa1[1], Banylla Felicity Dkha rGatphoh[1], Revanasiddappa B.C[1]

[1]*Department of Pharmaceutical Chemistry, NGSM Institute of Pharmaceutical Sciences (NGSMIPS), Nitte (Deemed to be University), Mangalore-575018, (Karnataka) India ;*

Received: May 4, 2023; Revised: July 17, 2023; Accepted: July 20, 2023

Abstract

A new series of thiazolidinedione linked 1,3,4oxadiazole hybrid analogs (T1-25) were designed by In-silico approach for their AXL inhibitor activity against breast cancer. Molecular docking studies were performed with binding pocket of AXLinhibitor (PDB ID: 5TD2) by using Schrodinger suit 2020- to elucidate the binding interactions of the newly designed targets. The docking studies were performed for all the designed molecules by Prime-MMGBSA module to determine free energy, In-silico ADMET screening by QikProp and Glide module. Based on the Glide score, the binding affinity of all the designed molecules towards AXL was chosen. AXL was inhibited by the designed molecules that have good hydrogen bonding interactions. The molecules (T1-25) have significant Glide scores in the range of -3.847 to -9.181 when compared with the standard Cyclophosphamide (-3.847) and 5-fluorouracil (-6.233). The In-silico molecular docking, ADMET properties were found within the suggested values. The MM-GBSA binding free energy results displayed very promising activity with the selected AXL inhibitor. The compounds T15, T19, T21 and T22 with highest Glide scores were found to be significant for anti-breast cancer activity.

Keywords: 2,4-thiazolidinone, 1,3,4-oxadiazoles, In-silico analysis, MM-GBSA, AXL inhibitor, Breast cancer.

1. Introduction

In the United States, breast cancer is the second most common cancer among women and the second largest cause of cancer death (Musetti et al.,2021; Savitri et al., 2023). Malignancies are including lung, breast, prostate, gastric, ovarian, and thyroid, have high levels of AXLkinase (Ito et al.,1999). Hepatocellular leukemia and acute myeloid leukemia have also been shown to be over expressed (Heet al., 2021). In 2020, 2,79,100 new cases are expected to be diagnosed in the United States, with over 42,000 deaths due to this kind of cancer (Siegel et al.,2016). Cancer molecular targeted therapy has become a research priority in recent years. Tyrosine kinase inhibitors (TKIs) that are targeting the platelet-derived growth factor receptor (PDGFR), vascular endothelial growth factor (VEGF), and epidermal growth factor receptor (EGFR),(Jänne et al.,2015)have shown promise in clinical studies, prompting researchers to investigate for additional diagnostic and prognostic markers (Subbiah et al.,2017;Gay et al.,2017).

In chronic myeloid leukemia (CML) sufferers, the AXL gene on chromosome 19q13.2 was found (Feneyrolles et al., 2014). The Greek term "anexelekto" means "uncontrollable." The AXL gene produces the protein AXL (UFO, ARK, Tyro7, or JTK11). Compared to normal tissues, the level of AXL expression in cancer tissues is higher (Narukawa et al.,2020). By activating AXL kinase, several signaling pathways involved in cell proliferation, metastasis (Paccez et al., 2015), and apoptosis inhibition (Gjerdrum et al 2010; Nazreen et al.,2014) are activated. Due to its strong correlation with tumour growth, metastasis, inadequate survival, and drug resistance, AXL has become a desirable target for cancer therapy. AXL signalling supports the immunosuppressive and pro-tumorigenic phenotypes in the tumour microenvironment where it is expressed in cellular components. Preclinical investigations have shown that a range of AXL inhibitors are effective.

Insulin sensitizers known as thiazolidinediones (glitazones) are used to treat type 2 diabetes. They are having high-affinity towards Peroxisome proliferator-activated receptor (PPARc) ligands that reduce insulin resistance and effectively lower plasma glucose levels (Chen et al., 2015; Hu et al 2020). Thiazolidinedione derivatives have also been found to be anti-inflammatory, antibacterial, and anticancer drugs (Shankar et al.,2020; Tokala et al.,2018). Compounds that activate PPAR-c have been suggested to induce cancer cell differentiation (Trotsko et al.,2018). For example, the TZD analogue efatutazone (CS-7017) is a strong PPAR-c agonist and cancer differentiation inducer (Shimazaki et al., 2008). By inhibiting the insulin growth factor 1 (IG F1) pathway's constituent parts and changing the activity of the AMP-activated protein kinase (AMPK) pathway, PPAR-c

agonists have been proven to reduce cancer risk (Smallridge et al.,2013; Belfiore et al.,2009). Thiazolidinedione derivatives have anticancer effects through various mechanisms, including Blockade of t he PI3K/Aktand Raf/MEK/ERK signaling pathways by inhibiting PI3K-a (Lee et al.,2008).

The wide range of a pplications for 1, 3,4-oxadiazoles, on the other hand, renders them an interesting potential in medicinal chemistry. The pharmacophore 1,3,4-oxadiazole derivative has a potential antineoplastic impact in the treatment of several malignancies (Knight et al.,2010; Liu et al.,2012). Recently, new 1,3,4-oxadiazole containing thiazolidinedione derivatives have been identified as possible AXLinhibitors(Shen et al.,2019).Combining substantial bioactive pharmacophores into a complex measure is critical in medicinal chemistry for producing physiologically active molecules with distinct properties(Xu et al.,2020). To our knowledge, no studies on the anticancer effects of thiazolidinedione derivatives as AXL inhibitors have been reported. To discover possible AXL inhibitors, we tried to combine thiazolidinedione and 1,3,4- oxadiazole under one design. In silico analysis of AXL inhibitory actions were described in this paper. All the designed molecules were subjected to docking investigations in order to better understand the molecular mechanisms interactions (Alzhrani et al.,2020).

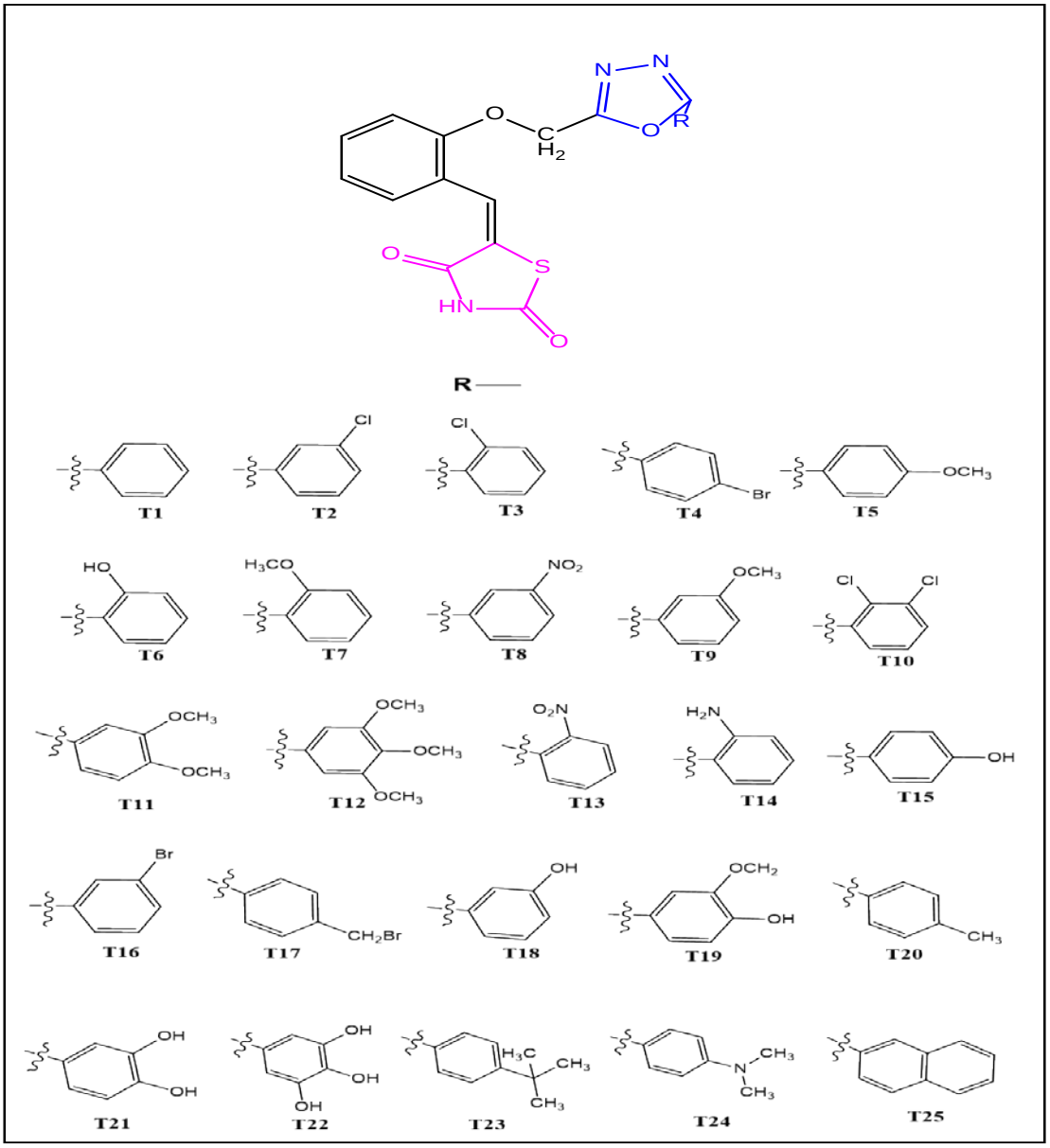

Figure 1. Design of Thiazolidinedione linked 1,3,4-oxadiazole molecules (T1-T25)

2. Materials and Methods

2.1. Molecular Docking

In-silico computer simulations were used to better understand the binding manner of the designed molecules with the target. The binding properties of the molecules were carried out with the Maestro 11.4 of S chrodinger suite 2020-3version (Batra et.al., 2021).

2.2. Ligand Preparation

A new series of designed thiazolidinedione linked 1,3,4 oxadiazole molecules(T1-T25) were constructed by using chemdraw software (figure-1). The chemical library was converted from 2D to 3D formats; geometry optimisation, bond orde r selection, and ligand ionisation state creation (through Epik) were done using the Ligprep module of t he Schrodinger suite-2020-3. The OPLS-3E forcefield was utilized to reduce the energy of the ligands' 3D structures. Optimized ligands were further taken for docking studies. The docking structures should be a good representation of actual ligand structures as they appear in a protein-ligand complex to get better docking scores. Because the docking tools will only change the ligand's torsional coordinates, the reset of the geometric patterns should be optimized first, implying that the structures placed into the docking system should match all required standard conditions. The ligands that had been optimized to fit all the criteria were then used for docking experiments.

2.3. Protein Preparation

The protein data bank was used to obtain crystal structures with precise PDB IDs. Protein Preparation Wizard was used to optimize the chain. Assigning bond order, adding hydrogens, and handling disulfide are all part of the protein's preprocessing. Water molecules that were 5 Å distant from the hetero groups were eliminated entirely. The remaining water molecules' orientation was corrected, and hydrogen bonding was allocated. A and B chains were found in the crystal structure of 5TD2 with a resolution of 2.68Å. Chain A was favored because it was complete, with no missing residues.

Chain A was taken up for further studies to achieve a better binding approach. The preferred chains of t he crystal structures were pre-processed using Schrodinger 2020-3 module. Generation of Het states was done using Epik at pH 7. Refinement of the protein was carried out by optimization by using PROPK, including sample water orientation. Waters with less than 3 H-bonds to non-waters were removed. OPLS-3E reduced the protein's size. Finally, the energy of t he protein structure was decreased to energy Root Mean Square Deviation (RMSD) 0.30 Å utilizing the OPLS-3E force field. This is important to avoid steric conflicts by reorienting the hydroxyl groups in the side chains. The docking of the ligand against the protein was done in the first pocket of t he protein molecule. The Figure 2 showed phi and phi scattering of amino acid residues, which were visualized by plotting the protein using the Ramachandran method.

2.4. Receptor grid generation

The 5TD2 crystal structures have been picked. The default parameters of the Receptor grid generation tool were utilized for gri d generation by the Schrodinger 2020-3 suite. The ligand was contained within the box that encloses the centroid. The grid created could help the ligands in the same manner as the conventional derivatives.

2.5. Docking

Generation of conformers and orientation in the binding pocket take place in the presence of grid potentials (Al-Khayyat et. al., 2021). To exclude the ligand poses which do not correspond to a well-docked result, Hierarchical filters are used. The extra precision (XP) model was used to conduct a flexible ligand docking study of the designed compounds by the OPLS-3E force field. The ligands were prepared, and a specific grid was used for the analysis. Confirmations for e very ligand were generated automatically by the docking process. Hierarchical filters are applied to the obtained ligand poses to estimate the ligand-receptor interaction. A penalty for the state of Epik was added to the docking score. Docking was used to expose ligands. To soften the potential of non-polar parts of t he ligand, the partial charge cut-off was kept at 0.15 and the Van der Waal radii of the ligand atoms were scaled to 0.8. For all dockings, the default settings of the Glide module were kept. The co-crystallized ligand was first removed from the generated protein and redocked at the binding site to check the RMSD and other properties of the docking programme. To compare the docked and reference conformations, the RMSD value is employed. RMSD value will be less (Ideally less than 1 Å) when redocking or cross-docking is performed. RMSD is primarily used to verify the method used for docking studies. In m olecular docking, RMSD was calculated to compare the docked conformation of t he reference ligand with the original conformation of the reference ligand and validate the protein-bound ligand, which is docked in the same pocket check the deviation. The RMSD values were 0.1293Å for 5TD2. These were the most negligible RMSD value and are selected for further studies. At the ligand-binding site, all of the proposed ligands were docked with the protein. The dock score results from XP docking were summarized and studied.

2.6. MM-GBSA Assay

It is a post-docking experiment for de termining the relative binding affinity of l igands that stands for Molecular mechanics with generalized Born a nd surface area solvation. A lower number indicates a stronger binding because the MM-GBSA binding energies are near to binding free energies. Prime MM-GBSA refines binding energy calculations using the VSGB solvation model, which uses the variable dielectric generalized Born model, water as a solvent, and the OPLS-3E force field. The docked molecules were selected, and Prime MM-GBSA binding free energy calculations were performed with respect to the desired minimized protein. After XP docking, the protein complexes and the designed ligands were further taken for energy calculations. The minimized protein was included, the desired ligands with better docking scores were selected, and the MM-GBSA job was run using the Prime MM-GBSA tool. This module aims to facilitate calculations of ligand binding energies and ligand strain energies, using prime technology.

2.7. ADMET studies

All the designed molecules were subjected for ADMET descriptors approach by using Schrodinger's Suite and Qikprop toxicity prediction procedure, and the ADMETSAR dataset (freely available at http://www.admetexp.org) was employed.

3. Results and Discussion

3.1. Molecular docking studies

Molecular Docking of the designed molecules (T1-T25) was performed in the groove of the target binding site, which played an essential role as a signal transducer in breast cancer and targeted to AXL receptor (Dey et al.,2021). In terms of G score, the binding affinity of all the derivatives is shown in Table-1. It is found that the binding free energy of all these derivatives ranged from -9.181 to -3.847 kcal/mol. Compounds T22, T21, and T19 are having the most refined binding energies with a binding score of -9.181, -8.503, and -7.556, respectively (Fig-2, 3, and 4). Compound T22 showed the highest binding affinity towards a target with binding free energies of -9.181. In compound T22, hydrogen bonding interactions of hydroxyl and carbonyl group substitution on the thiazolidinedione and phenyl ring were observed with Leu593 and Glu595, respectively. The interaction is observed in Figure-2. The other interactions with the amino acids are Gly594, Gly596, Val601, Ala617, Lys619, Met650, Leu671, Pro672, Phe673, Met674, Lys675, Gly677, Asp678, Asp728, Met730, Ala740, and Asp741 were observed. In compound T21, carbonyl and hydroxyl groups have hydrogen bond interaction and are observed with Leu593 and Glu595, respectively (Figure -3). Val601, Ala617, Met650, Leu671, Pro672, Phe673, Met674, Lys675, Gly677, Asp678, Asp728, Met730, Ala740, and Asp741 interaction were observed. In compound T19, hydrogen bonding interactions of carbonyl group substitution on the Thiazolidinedione ring were observed with Glu595. Gly594, Gly596, Val601, Ala617, Lys619, Met650, Leu671, Pro672, Phe673, Met674, Lys675, Gly677, Asp678, Asp728, Met730, Ala740, and Asp741.

In standard compound Methotrexate, hydrogen bonding interactions of nitro group in the ring structure are observed with amino acid Met674, the salt bridge was observed with carboxyl group with Lys591. (Figure-5). The other interactions with the amino acids are Lys591, Leu593, Gly594, Val601, Glu603, Asn605, Lys615, Ala617, Met650, Pro672, Phe673, Met674, Lys675, Tyr676, Gly677 and Met730 were observed. Based on the docking scores, the selected candidates were found to be suitable for AXL receptor activity.

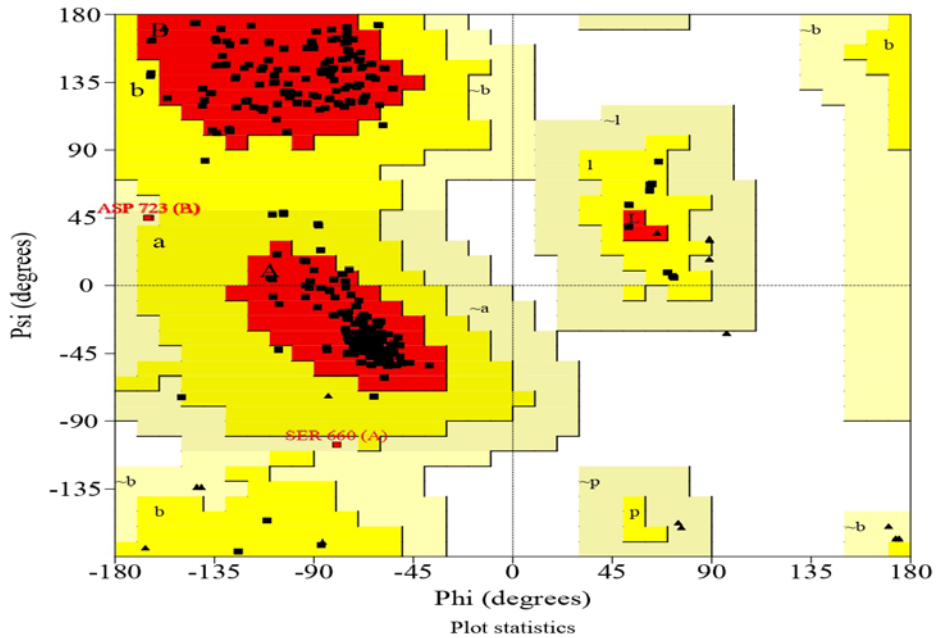

Figure-2: Ramachandran plot

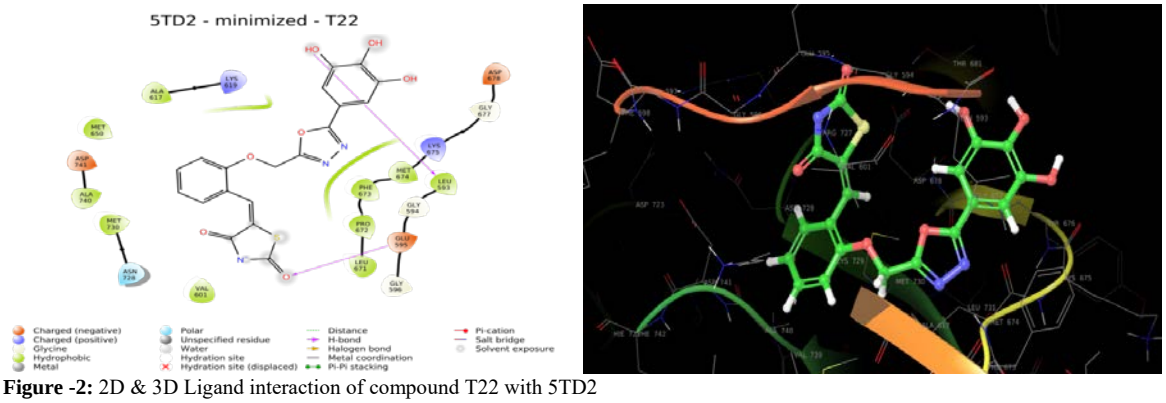

Figure -2: 2D & 3D Ligand interaction of compound T22 with 5TD2

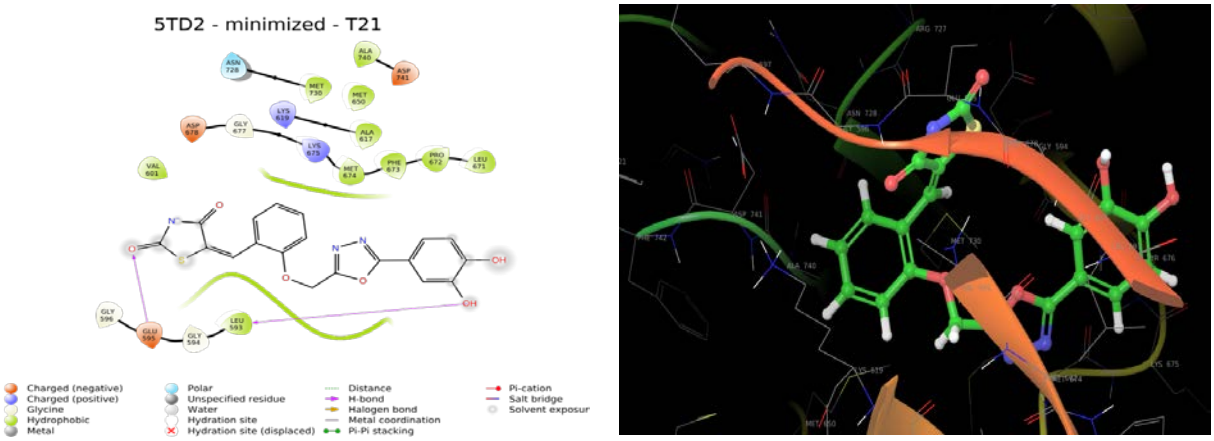

Figure-3: 2D & 3D Ligand interaction of compound T21 with 5TD2

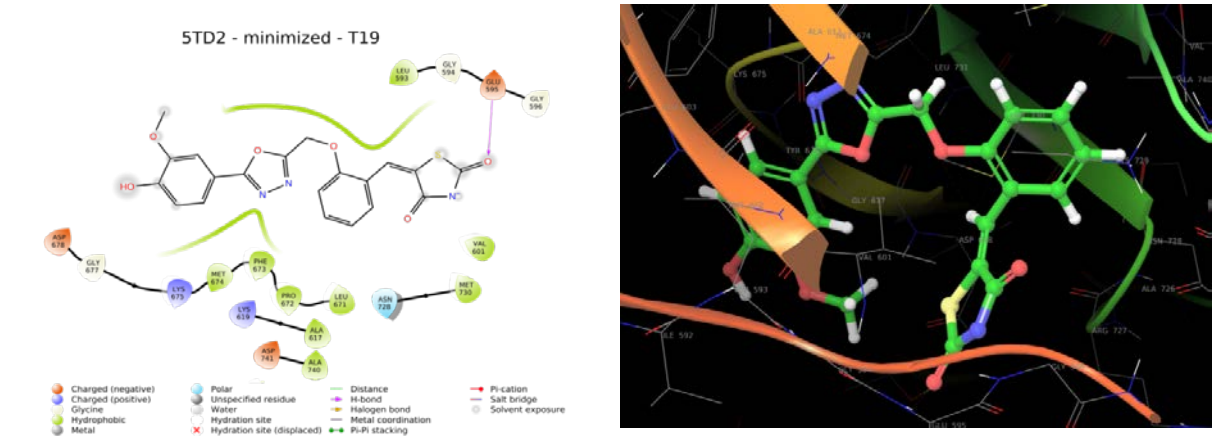

Figure 4: 2D & 3D Ligand interaction of compound T19 with 5TD2

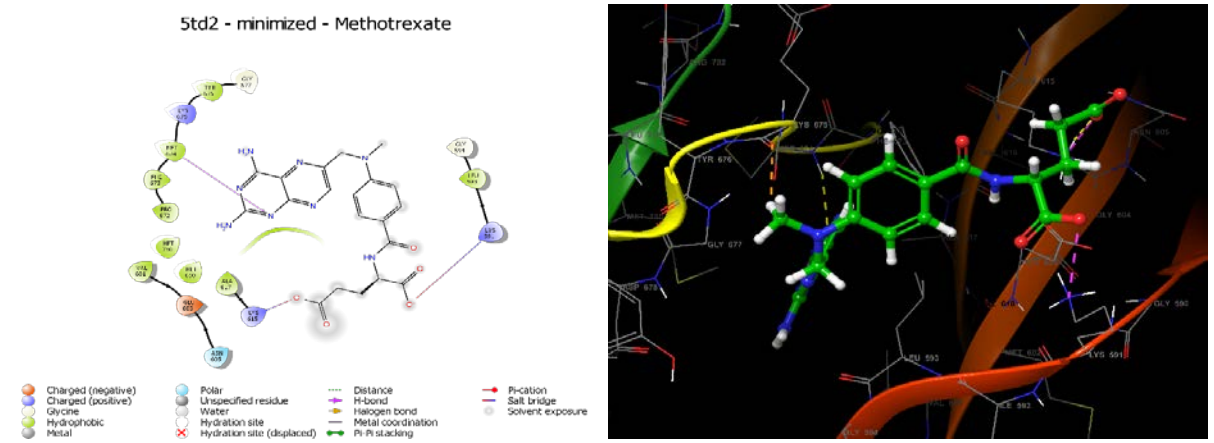

Figure -5: 2D & 3D Ligand interaction of compound Methotrexate with 5TD2

Table 1: Docking studies for compounds (T1-T25) with AXL inhibitor (5TD2)

Compounds	Glide score	Glide EvdW	XP H Bond	Glide emodel	G Rotab bonds	Glide ecoul
T1	-5.448	-42.524	0	-62.614	5	-4.192
T2	-6.945	-44.396	-1.032	-73.108	5	-6.354
T3	-6.29	-43.454	-0.172	-68.057	5	-6.681
T4	-5.505	-44.702	-0.198	-62.813	5	-8.932
T5	-6.942	-43.732	-1.084	-73.359	6	-9.132
T6	-6.621	-45.067	-0.742	-77.338	5	-3.284
T7	-5.61	-45.486	-0.199	-69.048	6	-7.367
T8	-6.115	-46.142	-0.399	-71.168	6	-5.988
T9	-6.2	-43.071	-0.51	-65.386	6	-6.023
T10	-6.727	-46.7	-0.938	-76.418	5	-7.493
T11	-6.057	-43.882	-0.203	-67.537	7	-5.96
T12	-6.267	-47.765	-0.302	-67.522	8	-5.044
T13	-6.028	-43.699	-0.358	-68.888	5	-6.211
T14	-6.187	-41.55	-0.199	-66.333	5	-6.804
T15	-7.004*	-43.728	-1.038	-74.21	6	-6.113
T16	-6.996	-45.167	-1.033	-77.154	5	-5.696
T17	-5.702	-42.606	-0.424	-65.653	6	-6.884
T18	-6.117	-42.077	-0.47	-66.217	6	-6.121
T19	-7.556*	-45.815	-1.512	-76.106	7	-6.372
T20	-6.054	-40.812	-0.208	-63.784	5	-6.616
T21	-8.503*	-43.252	-2.002	-76.886	7	-13.021
T22	-9.181*	-40.463	-2.076	-81.517	8	-18.769
T23	-6.528	-45.972	-0.625	-76.683	6	-5.918
T24	-6.025	-42.294	-0.41	-66.144	6	-6.593
T25	-6.729	-46.827	-0.35	-81.337	5	-6.661
Methotrexate (Std)	-8.485	-43.149	-1.212	-60.083	10	-4.359
5-fluorouracil (Std)	-6.233	-14.544	-1.086	-27.3	0	-2.36
Cyclophosphamid (Std)	-3.847	-21.907	0	-29.144	5	-5.692

Glide score: glide score; Glide EvdW: glide van der Waals energy; XP H Bond: extra precision hydrogen bonding;Glideemodel: glide model energy; G Rotatable bonds: Glide Rotatable bonds; Glide Ecoul: glide Coulomb energy

Table 2: Binding free energy calculation using Prime/MM-GBSA approach of compounds (T1-T25)

Comp	ΔG bind (Kcal/ mol)	ΔG bind Coulomb	ΔG bind covalent	ΔG bind Vander	ΔG bind H Bond	ΔG bind Lipophilic
T1	-79.88	-0.24	-0.83	-43.58	-0.71	-36.4
T2	-81.59	-0.05	-2.23	-39.81	-0.9	-42.54
T3	-79.32	-1.39	-2.87	-35.97	-0.94	-41.22
T4	-92.44	-21.33	-3.02	-45.23	-0.72	-41.57
T5	-92.46	-23.07	-2.27	-46.09	-0.93	-40.3
T6	-90.94	-21.97	-0.9	-46.82	-1.05	-39.41
T7	-90.72	-20.61	-0.73	-47.77	-0.9	-42.54
T8	-83.83	3.7	-0.64	-47.37	-0.72	-40.76
T9	-81.77	1.69	-2.12	-40.95	-0.71	-40.49
T10	-81.04	1.16	-2.94	-36.88	-0.71	-44.44
T11	-80.7	-1.02	3.09	-45.77	-0.72	-43.65
T12	-82.66	5.17	0.86	-44.91	-1.34	-40.25
T13	-79.43	0.25	0.69	-45.82	-1.13	-41.2
T14	-75.62	-1.6	-3.02	-36.5	-0.71	-39.69

T15	-79.8	-0.26	0.72	-40.69	-0.79	-41.47
T16	-82.16	-0.23	-2.17	-40.23	-0.72	-41.16
T17	-91.43	-21.7	-5.77	-45.97	-0.92	-38.14
T18	-81.25	-7.77	2.05	-42.42	-0.95	-40.62
T19	-79.07	-1.28	1.98	-44.19	-0.72	-42.71
T20	-78.46	0.89	-2.48	-39.83	-0.72	-39.72
T21	-92.51	-31.59	0.77	-43.85	-1.18	-39.36
T22	-75.14	9.58	2.61	-45.2	-3.42	-30.23
T23	-68.45	-4.02	-3.8	-33.71	-0.93	-38.94
T24	-81.73	2.37	-6.73	-44.25	-0.93	-39.57
T25	-81.48	-0.36	-2.39	-41.68	-0.93	-37.6
Methotrexate (Std)	-55.04	78.51	7.07	-51.06	-4.23	-30.59
5-fluorouracil (Std)	-21.78	-1.7	0.12	-17.34	-0.48	-7.36
Cyclophosphamid (Std)	-49.32	-8.82	6.31	-23.6	-0.8	-37

Δ G bind:free energy of binding; ΔG bind Coulomb:Coulomb energy; ΔG bind covalent: covalent energy (internal energy); ΔG bind Vander:van der Waals energy; ΔG bind H Bond:hydrogen bonding energy; ΔG bindLipophilic:hydrophobic energy (non-polar contribution estimated by solvent accessible surface area).

Table 3: Compliance of active thiazolidinedione linked 1,3,4oxadiazole derivatives (T1-T25) to electronic parameters of drug likeness and toxicity

Compounds	ADME descriptors and their probabilities											
	BBB+	HIA+	$Caco_2$	CYP	CYPIP	HERGI	Non AMES toxicity	Non carcinogens	Fish toxicity	Aqueous solubility (LogS)	Caco-2 permeability	Rat acute toxicity
T1	0.8186	1.000	0.6024	0.5430	0.5606	0.9778	0.5114	0.8268	0.8312	-3.3285	0.9878	2.3033
T2	0.8248	1.000	0.5893	0.5787	0.9203	0.9687	0.5687	0.7510	0.7756	-4.0323	1.0609	2.3299
T3	0.8248	1.000	0.5893	0.5787	0.9203	0.9687	0.5687	0.7510	0.7756	-4.0323	1.0609	2.3299
T4	0.8219	1.000	0.5939	0.6216	0.9395	0.9799	0.5660	0.7846	0.8299	-3.9035	1.0333	2.3730
T5	0.6151	1.000	0.5762	0.8638	0.8850	0.9744	0.5029	0.8491	0.8383	-3.1650	1.0702	2.3473
T6	0.5844	0.9965	0.6664	0.7039	0.6055	0.9850	0.5520	0.8143	0.9753	-3.1369	0.6442	2.2804
T7	0.6151	1.0000	0.5762	0.8638	0.8850	0.9744	0.9092	0.8491	0.8383	-3.1675	1.7072	2.3473
T8	0.6951	0.9947	0.5898	0.6649	0.9603	0.9277	0.7566	0.7588	1.0979	-3.6576	1.9017	2.4672
T9	0.6151	1.0000	0.5762	0.8638	0.8850	0.9744	0.5092	0.8491	0.8383	-3.1675	1.0702	2.3473
T10	0.8248	1.0000	0.5893	0.8665	0.9203	0.9687	0.5687	0.7510	0.7756	-4.0323	1.0609	2.3299
T11	0.5427	1.0000	0.5733	0.8466	0.8522	0.9809	0.5284	0.8300	0.8048	-3.2153	1.1021	2.3750
T12	0.5117	1.0000	0.5660	0.8456	0.8391	0.9793	0.5424	0.8116	0.7938	-3.3533	1.1938	2.3696
T13	0.7288	1.0000	0.6358	0.7590	0.7620	0.9857	0.5076	0.8072	0.9515	-3.3204	0.9443	2.2810
T14	0.7184	1.0000	0.5896	0.8756	0.9121	0.9746	0.5066	0.8122	0.8115	-3.3648	1.0635	2.2860
T15	0.5844	0.9956	0.6664	0.7039	0.6055	0.9850	0.5520	0.8143	0.9753	-3.1369	0.6442	2.2804
T16	0.8219	1.0000	0.5939	0.8475	0.9395	0.9799	0.5660	0.7876	0.8299	-3.9035	1.0333	2.3730
T17	0.7967	1.0000	0.5910	0.8240	0.9397	0.9787	0.5164	0.7846	0.8070	-3.5368	1.0638	2.4108
T18	0.5844	0.9956	0.6664	0.8589	0.6055	0.9850	0.5520	0.8143	0.9753	-3.1369	0.6442	2.2804
T19	0.8212	0.9953	0.6474	0.7533	0.6224	0.9827	0.5487	0.8411	0.9853	-3.0050	0.7298	2.3198
T20	0.7184	1.0000	0.5896	0.8756	0.9121	0.9746	0.5066	0.8122	0.8151	-3.3548	1.0635	2.2860
T21	0.7060	0.9891	0.6730	0.6340	0.5167	0.9840	0.5717	0.8260	0.9874	-3.0264	0.4770	2.3065
T22	0.7615	0.9774	0.6764	0.5969	0.5381	0.9845	0.5799	0.8394	1.0347	-2.9691	0.3577	2.3214
T23	0.5190	1.0000	0.5799	0.7389	0.8588	0.9935	0.5966	0.7418	0.6703	-3.8643	1.2083	2.4377
T24	0.5989	1.0000	0.5480	0.6371	0.6053	0.9696	0.5557	0.7435	0.7998	-3.3714	1.1102	2.4220
T25	0.8150	1.0000	0.6007	0.8328	0.8918	0.9741	0.5088	0.8402	0.7561	-3.7114	0.9726	2.3191

Table 5: Calculation of electronic parameters of drug likeness or oral bioavailability of the thiazolidinedione linked 1,3,4oxadiazole derivatives (T1-T25) by using Qikprop

Compounds	Mol. MW	HB donor	HB acceptor	QPPCaco	QPlogBB	QPPMDCK	Percent human oral absorption	PSA	Rule of five
Acceptable ranges	130-750	< 5	<10	2.0 – 20.0	–3.0 – 1.2	<25 Poor >500 greater	>80%is high <25% is poor	7.0-200.00	Max 4
T1	379.389	1	6.25	235.872	-1.387	187.022	87.582	116.128	0
T2	413.834	1	6.25	238.955	-1.221	451.031	90.728	115.726	0
T3	413.834	1	6.25	259.568	-1.162	419.28	90.731	116.137	0
T4	458.285	1	6.25	242.132	-1.206	491.13	91.293	115.733	0
T5	409.416	1	7	235.991	-1.473	182.53	88.5	124.443	0
T6	395.389	2	7	99.451	-1.869	72.939	77.363	135.726	0
T7	409.416	1	7	259.162	-1.429	205.782	89.274	121.51	0
T8	424.387	1	7.25	28.812	-2.517	19.132	67.155	160.963	0
T9	409.416	1	7	233.696	-1.515	183.758	88.222	124.193	0
T10	448.28	1	6.25	258.525	-1.048	858.024	93.149	115.619	0
T11	439.442	1	7.75	411.558	-1.08	290.245	96.37	125.374	0
T12	469.468	1	8.5	418.27	-1.166	294.288	92.571	136.57	0
T13	394.404	2.5	7.25	95.51	-1.869	70.566	75.749	139.144	0
T14	393.416	1	6.25	298.236	-1.282	238.972	91.296	114.986	0
T15	393.416	1	6.25	70.854	-2.015	49.277	74.36	138.703	0
T16	458.285	1	6.25	236.362	-1.229	487.908	90.958	115.735	0
T17	472.312	1	6.25	245.378	-1.326	503.338	93.49	116.134	0
T18	395.389	2	7	70.743	-2.066	50.528	74.288	138.608	0
T19	425.415	2	7.75	81.8	-2.073	59.684	75.865	143.728	0
T20	393.416	1	6.25	235.279	-1.426	182.574	89.694	116.192	0
T21	411.388	3	7.75	26.236	-2.59	17.277	62.513	160.138	0
T22	427.388	4	8.5	9.392	-3.172	5.692	50.181	181.667	0
T23	435.497	1	6.25	232.7	-1.576	182.837	94.804	116.130	0
T24	422.458	1	7.25	235.375	-1.498	175.099	90.525	119.538	0
T25	429.449	1	6.25	234.157	-1.493	184.087	93.253	115.986	0
Methotrexate (Std)	454.444	6.25	11.75	0.06	-4.671	0.022	0	233.239	2
5-fluorouracil (Std)	130.078	2	3.5	187.736	-0.673	142.642	65.585	87.585	0
Cyclophosphamide (Std)	261.087	1	8.5	3262.693	0.319	10000	94.796	40.602	0

3.2. MM-GBSA Assay

The target protein and the relevant protein were made in accordance with the structure as shown in Fig-1. All of these suggested analogues had strong free binding energies and will match the AXL receptor well. The binding free energies of the Compound T21 have the highest ΔG binding energy to 5TD2 with a value of -92.51 kcal/mol compared to the known standard drug, and Cyclophosphamide having ΔG binding energy of -49.32 kcal/mol.

3.3. ADMET studies

Many drugs fail mostly during the drug di scovery process owing to toxicity, blood-brain permeation failure, and low efficacy. Because most anticancer medicines have poor pharmacokinetic qualities, were designed molecules and their properties were studied. In t herapeutic development, the properties of a bsorption, distribution, metabolism, excretion, and toxicity (ADMET) are critical. Failures in drug discovery are mainly related to lack of efficacy and severe toxicity. The ability of medications to traverse membranes and cytosol to reach their target is dependent on t heir lipophilic properties. ADMET-related parameters such as water solubility, CYP450, human intestine absorption, plasma protein binding, oral bioavailability, volume of di stribution, blood-brain barrier penetration, transporter, and safety are used to refine drug similarity features (Life and software package, version 3.5 2008). The ADMET characteristics of t he linked 1,3,4oxadiazolederivatives were anticipated in this study using the ADMETSAR dataset, which is an open source. Several ADMET related factors, such as oral bioavailability, water solubility, human intestine absorption, blood-brain barrier penetration renal, organic cation transporter, CYP450 substrates, P-glycoprotein substrate and inhibitor, inhibition (CYP1A2, 2C9, 2C19, 2D6, and 3A4), the volume of distribution, plasma protein

binding, human Ether-ago-go-Related gene (hERG) inhibition, rat acute toxicity, drug-induced liver injury skin sensitivity, carcinogens, AMES mutagenicity, the Tetrahymenapyriformis toxicity, and fish toxicity have been predicted. The probabilities of thiazolidinedione linked 1,3,4 oxadiazole being blood-brain barrier penetration, CYP450 substrates and inhibition, human intestinal absorption, AMES mutagenicity, and human Ether-a-go-goRelated gene (hERG) inhibition, fish toxicity, carcinogenicity, Caco-2 Permeability, aqueous solubility (LogS), and rat acute toxicity range from 0.5190-0.8248. The comprehensive anticipated properties of other investigated compounds in relation to thiazolidinedione analogs are shown in (Table- 4).

Blood-brain barrier penetration probabilities of compounds T1, T2, T3, T4, T10, T16, T19, and T25 are higher than the standard. Probabilities of human intestinal absorption range from 0.9774 to 1.0000. Proposed compounds have stronger ADME characteristics and so have a higher likelihood of becoming lead compounds. In addition, pharmaceutically important features of thiazolidinedione analogs were examined using QikProp software (Table-5) and distinguished to reference medications Methotrexate, 5-fluorouracil, and Cyclophosphamide. The QikProp results revealed the discovery of compounds (T1-T25) with good ADME properties. Molecular weight (mol MW) (150–500), aqueous solubility (QPlogS) (-6.5 to 0.5), apparent MDCK cell permeability (QPPMDCK) (500 great), percent human oral absorption and brain/blood partition coefficient (QPlogBB) (-3.0 to 1.2) are the primary descriptors presented in QikProp (Schrodinger) software (C80 percent is high, B25 percent is deficient). All substances examined have an oral absorption rate of 80–100% in humans (Table-5). The first three properties, molecular weight (mol MW) less than 650, solubility (QPlogS) greater than -7, and partition coefficient between octanol and water (logPo/w) between -2 and 6.5, are based on the Lipinski rule of five. The brain/blood partition coefficient (QPlogBB) measure determines a drug's capacity to pass the blood-brain barrier, which is important in ADME druggability studies. A drug-likeness test is performed using Lipinski's rule of five pharmacokinetics filter. According to this criterion, orally administered medications must have a molecular weight (MW) of 500 or less, ten or fewer hydrogen bond acceptor sites (N and O atoms), a logP of five or less, and five or few hydrogen bonds donor sites. All compounds in this study have H donor sites of less than five and H acceptor sites of less than ten. T1-T25 is estimated to have a molecular weight of less than 500. In addition, topological polar surface area analysis was used to determine the bioavailability of all the designed analogs. Using topological PSA, the polar surface area (PSA) was estimated. This descriptor has been connected to drug bioavailability and has been correlated well with passive molecular transport through membranes. As an outcome, it can be used to predict drug transport qualities. Any molecule having a PSA value of less than 100 A° 2 is thought to be capable of sound absorption. Oral bioavailability is anticipated to be limited for passively absorbed compounds with a PSA 140 A° 2. All of the developed molecules have a PSA value that is within the limit (Table-5)

4. Conclusion

Thiazolidinedione has gained medicinal importance due to its various pharmacological and biological profiles, making it a unique molecule for multiple studies. Likewise, 1,3,4-oxadiazoles are well-known substances in the realm of organic chemistry. In-silico investigations were used to examine the hybrids of these moieties for potential anticancerous action. According to the investigation, the 1,3,4-oxadiazole moiety-linked thiazolidinedione exhibited outstanding binding energy and G score. The choice of the AXL receptor has shown that these hybrid compounds have a promising level of activity. To validate its enhanced SAR, the work still needs more in vitro and in vivo investigations. The developed compounds have impressively displayed anticancer activities in the in-silico investigations. The compounds T22, T21, T19, and T15 have shown strong anti-breast cancer action, and these analogues are recognized as promising molecules and still need to undergo structural modifications by the wet lab procedure in order to produce the lead molecules.

Acknowledgements

The authors express sincere thanks to NGSM Institute of Pharmaceutical Science and Nitte (Deemed to be University) Mangalore, Karnataka and NGSM-CADD Lab for providing all the necessary facilities required to carry out this research work.

References

Al-Khayyat MZ.2021. *In silico* screening for inhibitors targeting 4-diphosphocytidyl-2- c-methyl-d-erythritol kinase in *salmonella typhimurium. Jordan J Bio Sci.***14(1):** 75-82.

doi.org/10.54319/jjbs/140110

Alzhrani, Z. M. M., Alam, M. M., Neamatallah, T., and Nazreen, S. 2020.Design, synthesis and in vitro antiproliferative activity of new thiazolidinedione-1, 3, 4-oxadiazole hybrids as thymidylate synthase inhibitors. *J Enzyme Inhib Med Chem.* **35(1):** 1116-23. doi: 10.1080/14756366.2020.175958

Batra B, SudanSS, PantM, PantK, Lal A and Gusain T. 2022. Molecular docking and tlc analysis of candidate compounds from lesser used medicinal plants against diabetes mellitus targets. *Jordan J Bio Sci.***15(2):**339-346. doi.org/10.54319/jjbs/150221

Belfiore, A., Genua, M., and Malaguarnera, R. 2009. PPAR-agonists and their effects on IGF-I receptor signaling: implications for cancer. *PPAR Research*. 2009: 830501.
doi: 10.1155/2009/830501

Chen, R., Yan, J., Liu, P., and Wang, Z. 2 015. Effects of thiazolidinedione therapy on inflammatory markers of type 2 diabetes: a meta-analysis of randomized controlled trials. *PloSOne*. **10(4):** e0123703.
doi: 10.1371/journal.pone.0123703.

Dey S, KaushikG, Mahanta Sand Chakraborty A.2021. Homology modeling of apoprotein Opsin and covalent docking of 11-cis retinal and 11-cis 3, 4-didehyroretinal to obtain structures of Rhodopsin and Porphyropsin from Zebra danio, *Danio rerio* (Hamilton, 1822). *Jordan J Bio Sci.***14(4):** 727-732.
doi.org/10.54319/jjbs/140413

Feneyrolles, C., Spenlinhauer, A., Guiet, L., Fauvel, B., Daydé-Cazals, B., Warnault, P., .and Yasri, A. 2014. AXL kinase as a key target for oncology: focus on small molecule inhibitors. *Mol Cancer Ther*. **13(9):** 2141-48. doi: 10.1158/1535-7163

Gay, C. M., Balaji, K., and Byers, L. A. 2017. Giving AXL the axe: targeting AXL in human malignancy. *Br J Cancer*. **116(4)**: 415-23. doi: 10.1038/bjc.2016.428

Gjerdrum, C., Tiron, C., Høiby, T., Stefansson, I., H augen, H., Sandal, T., ...and Lorens, J. B. 2010. AXL is an essential epithelial-to-mesenchymal transition-induced regulator of breast cancer metastasis and patient survival. Proc Natl Acad Sci USA. **107(3):** 1124-29. doi: 10.1073/pnas.0909333107

He, L., Zhang, J., Jiang, L., Jin, C., Zhao, Y., Yang, G., and Jia, L. 2010. Differential expression of AXL in hepatocellular carcinoma and correlation with tumor lymphatic metastasis. *Mol Carcinog*. **49(10):** 882-91. doi.org/10.1002/mc.20664

Hu, C. F., Zhang, P. L., Sui, Y. F., Lv, J. S., Ansari, M. F., Battini, N., and Geng, R. X. 2020. Ethylenic conjugated coumarin thiazolidinediones as new efficient antimicrobial modulators against clinical methicillin-resistant Staphylococcus aureus. *Bioorg Chem.* **94:** 103434. doi: 10.1016/j.bioorg.2019.10343

Ito, T., Ito, M., Naito, S., Ohtsuru, A., Nagayama, Y., Kanematsu, T., and Sekine, I. 1999.Expression of the AXL receptor tyrosine kinase in human thyroid carcinoma. *Thyroid.* **9(6):** 563-67. doi: 10.1089/thy.1999.9.563.

Jänne, P. A., Yang, J. C. H., Kim, D. W., Planchard, D., Ohe, Y., Ramalingam, S. S., and Ranson, M. (2015). AZD9291 in EGFR inhibitor–resistant non–small-cell lung cancer. *N Engl J Med*. **372(18):** 1689-99. doi: 10.1056/NEJMoa1411817.

Knight, S. D., Adams, N. D., Burgess, J. L., Chaudhari, A. M., Darcy, M. G., Donatelli, C. A., and Dhanak, D. 2010. Discovery of GSK2126458, a highly potent inhibitor of PI3K and the mammalian target of rapamycin. *ACS Med Chem Lett*. **191(1):** 39-43. doi: 10.1021/ml900028r

Lee, W.H., and Kim, S.G. 2010.AMPK-dependent metabolic regulation by PPAR agonists. *PPAR Res.* **2010.** : 2010:549101. doi: 10.1155/2010/549101.

Liu, K., Rao, W., Parikh, H., Li, Q., Guo, T. L., Grant, S.,and Zhang, S. 2012. 3, 5-Disubstituted-thiazolidine-2, 4-dione analogs as anticancer agents: design, synthesis and biological characterization. *Eur J Med Chem***47**: 125-37. doi: 10.1016/j.ejmech.2011.10.031

Musetti, S. N., and Huang, L. 2021. Tinagl1 gene therapy suppresses growth and remodels the microenvironment of triple negative breast cancer. *Mol Pharm.* **18(5):** 2032-38. doi: 10.1021/acs.molpharmaceut.1c00008.

Narukawa, T., Hongo, F., Fujihara, A., Ueno, A., Matsugasumi, T., and Ukimura, O. 2020. Pazopanib after Nivolumab-Induced Tumor Lysis Syndrome in a Patien t with Metastatic Clear-Cell Renal Cell Carcinoma. *Case Rep Oncol.* **13(1):** 249-54. doi: 10.1159/000506196

Nazreen, S., Alam, M. S., Hamid, H., Yar, M. S., Shafi, S., Dhulap, A., and Pillai, K. K. 2014. Design, synthesis, in silico molecular docking and biological evaluation of novel oxadiazole based thiazolidine-2, 4-diones bis-heterocycles as PPAR-γ agonists. *Eur J Med Chem*. **87:** 175-85. doi: 10.1016/j.ejmech.2014.09.010

Paccez, J.D., Vasques, G.J., Correa, R.G., Vasconcellos, J.F., Duncan, K., Gu, X., Bhasin, M., L ibermann, T.A, and Zerbini L.F. 2013.The receptor tyrosine kinase AXL is an essential regulator of prostate cancer proliferation and tumor growth and represents a n ew therapeutic target. *Oncogene*.**32(6):**689-98. doi: 10.1038/onc.2012.89.

Savitri AD, Hidayati HB, Veterini L, Widyaswari MS, Muhammad AR, Fairus A, Zulfikar MQB, Astri M, Ramasima NA, Anggraeni DP, Nainatika RSA and Juliana.2023. An in-silico study on allicin compound in garlic (allium sativum) as a potential inhibitor of human epidermal growth factor receptor (her)-2 positive breast cancer. *Jordan J Bio Sci*.**16(1)**:7-12. doi.org/10.54319/jjbs/160102

Shankar, S., and Vuppu, S. 2020.In vitro drug metabolism and pharmacokinetics of a n ovel thiazolidinedione derivative, a potential anticancer compound. *J Pharm Biomed Anal*. **179**: 113000. doi: 10.1016/j.jpba.2019.113000

Shen, W., Xi, H., Li, C., Bian, S., Cheng, H., Cui, J.and Chen, L. 2019. Endothelin-A receptor in gastric cancer and enhanced antitumor activity of trastuzumab in combination with the endothelin-A receptor antagonist ZD4054. *Ann N Y Acad Sci.* **1448(1):** 30-41. doi: 10.1111/nyas.14053

Shimazaki, N., Togashi, N., Hanai, M., Isoyama, T., Wada, K., Fujita, T.,andKurakata, S. 2008. Anti-tumour activity of CS-7017, a selective peroxisome proliferator-activated receptor gamma agonist of thiazolidinedione class, in human tumour xenografts and a s yngeneic tumour implant model. *Eur J Cancer*. **44(12):** 1734-43. doi:10.1016/j.ejca.2008.04.016

Siegel, R. L., Miller, K. D., and Jemal, A. 2016.Cancer statistics, 2016. *CA: Cancer J Clin*. **66(1):** 7-30. doi: 10.3322/caac.21332

Smallridge, R. C., Copland, J. A., Brose, M. S., Wadsworth, J. T., Houvras, Y., Menefee, M. E ., and Von Roemeling, R..2013. Efatutazone, an oral PPAR-γ agonist, in combination with paclitaxel in anaplastic thyroid cancer: results of a multicenter phase 1 trial. *J Clin Endocrinol Metab*. **98(6):** 2392-2400. doi: 10.1210/jc.2013-1106.

Subbiah, V., Meyer, C., Zinner, R., Meric-Bernstam, F., Zahurak, M. L., O'Connor, A., and Azad, N. A. 2017. Phase Ib/II study of the safety and efficacy of combination therapy with multikinase VEGF inhibitor pazopanib and MEK inhibitor trametinib in advanced soft tissue sarcoma. *Clin Cancer Res.* **23(15):** 4027-34. doi: 10.1158/1078-0432.CCR-17-0272.

Tokala, R., Thatikonda, S., Sana, S., Regur, P., Godugu, C., and Shankaraiah, N. 2018. Synthesis and in vitro cytotoxicity evaluation of β-carboline-linked 2, 4-thiazolidinedione hybrids: potential DNA in tercalation and apoptosis-inducing studies. *New J Chem*. **42(19):** 16226-36. https://doi.org/10.1039/C8NJ03248C

Trotsko, N., Przekora, A., Zalewska, J., Ginalska, G., Paneth, A., and Wujec, M. 2018. Synthesis and in vitro antiproliferative and antibacterial activity of new thiazolidine-2, 4-dione derivatives. *J Enzyme Inhib Med Chem*. **33(1):** 17-24. doi: 10.1080/14756366.2017.1387543

Xu, C., Han, Y., Xu, S., Wang, R., Yue, M., Tian, Y. and Gong, P. 2020. Design, synthesis and biological evaluation of new AXL kinase inhibitors containing 1, 3, 4-oxadiazole acetamide moiety as novel linker. *Eur J Med Chem*. **186:** 111867. doi: 10.1016/j.ejmech.2019.111867.

JJBS

Volume 17, Number 1,March 2024
ISSN 1995-6673
Pages 99 – 108
https://doi.org/10.54319/jjbs/170109

Jordan Journal of Biological Sciences

The Salivary Glands of the Camel: An Element of Adaptation to Desert Conditions and Mitigation of Climate Change Impacts

Mansour Almansour[1], Bashir Jarrar[2,*], Bernard Faye[3], Amin Al-Doaiss[4], Ali Shati[4], and Djamila Meriane[5]

[1]Zoology Department, College of Science, King Saud University, Saudi Arabia, [2]Climate Change Unit, College of Sciences, Jerash University, Jordan; [3]Cirad-La recherche agronomique pour le développement, Département Scientifique Environnements et Sociétés, Montpellier, France; [4]Department of Biology, College of Science, King Khalid University, Saudi Arabia; [5]Department of Plant Biology and Ecology, Faculty of Natural and Life Sciences, Ferhat Abbas Setif 1 University, Algeria

Received: March 5, 2023; Revised: June 29, 2023; Accepted: July 26, 2023

Abstract

The one-humped camel is well-adapted to low nutritive resources, arid environments and desert ecosystems. Salivary glands have an essential role in moistening and swallowing the ingested food and forestomach digestion regulation and in water body homeostasis. The present study aims to find out the morphological, histological and histochemical characterization of the salivary glands of the dromedary camel concerning the salivation process's role in challenging the arid conditions and to mitigate the climate change impacts. Representative samples of the salivary glands of healthy 16 adult one-humped camel **(**Camelus dromedaries) of both sexes were tested including mandibular glands, parotid glands, sublingual glands, buccal glands, lingual glands, labial glands and palatine ones. The samples were processed according to the following handling: gross examination, fixation, dehydration, clearing, wax impregnation, embedding, trimming, sectioning, slide mounting, hematoxylin-eosin (H&E) and a battery of histological and histochemical staining. The salivary glands demonstrated variable types of tubule-acinar and tubule-alveolar secretory portions surrounded by numerous myoepithelial cells and armed with interlobular and intralobular ducts rich with goblet cells. In addition, the glands showed variable secretory cells (mucous, serous, mucoserous and mixed seromucous) with variable secretory products mainly mucusubstances, neutral mucin, acidic mucosubstances, sialomucins, sulphomucins, and glycoproteins. Moreover, the glands collectively demonstrated activities for the following enzymes: dehydrogenases, phosphatases, esterases, carboxylases, aminopeptidases, peroxidases, cytochrome oxidases and carbonic anhydrases. furthermore, the glands exhibited alcianophilia and metachromasia. The findings of the present study indicate that the structure and the secretion of the salivary glands of the camel support an efficient salivation process and represent a strong challenge to growing water scarcity and expansion of xerophytes as the main pastoral resources for camels. In that sense, salivary glands in camels are one of the elements of his panoply adaptation to arid conditions and to mitigate the climate change impacts.

Keywords: Camel, salivary glands, histochemistry, mucosubstances, mitigation, adaptation, climate change

1. Introduction

The one-humped camel is living in a specific environment characterized notably by the low nutritive value of the pastoral resources and the aridity of the ecosystems. Many studies showed that the dromedary camel is physiologically adapted to such conditions (Yagil, 1985; Wilson, 1989; Bengoumi and Faye, 2002). The ability of the camel to survive in such environments is based on his unique anatomical and physiological particularities including salivation which could play an eminent role in the current context of climatic changes (Faye et al., 2012). Indeed, due to the arid environment, the plants grazed by camels are mainly xerophytes, characterized by small leaves often covered by wax, more or less spinous and usually rich in lignin (Fahn and Cutler, 1992). To consume such vegetation, the camel had to develop mastication, salivation and swallowing mechanisms based anatomically on tough and mobile lips together with a unique tongue able to pick desert plants small leaves (Taib and Jarrar, 1989). In addition, the dromedary has buccal internal dermis lined by compound keratinized epithelium covering a loose connective dense fibrous connective tissue (Tayeb 1950; Al-Asgah et al., 1990). Moreover, the cheek of this animal is lined by crowded thick papillae, together with sharp teeth, muscular esophagus and efficient salivary glands (Nadipour et al., 2001). These unique anatomical features, enable the camel to ingest and feed on xerophytes that require a large amount of saliva as a lubricant and on grasses that are not eatable by other animals of the same arid environment.

Camel saliva plays an essential role in moistening and swallowing the ingested food, and in oral hygiene maintaining the gastrointestinal canal regulation of digestion and absorption (Jarrar and Faye, 2012). In addition, camel saliva demonstrates buffer power in the

* Corresponding author. e-mail: bashirjarrar@yahoo.com.

stomach due to the specific richness of camel saliva by bicarbonates (Al-Razaiki et al., 2023).

The camel lives in an environment characterized by the scarcity of water and suffering from being irregularly watered. The dromedary camel can produce daily about 12-21 liters of saliva with respect to diet components and can be 150 liters under the toughest conditions (Kay et al., 1980; Kay and Maloiy, 1989). The dromedary camel relies on well-sophisticated salivary glands scattered around the oral cavity enabling him to produce large quantities of saliva. The salivary glands battery includes large parotid glands and well-developed mandibular glands located obliquely to the parotid ones and having less than half of their size (Nawar and Khaligi, 1977). The mandibular glands of the one-humped camel could produce rapid saliva secretion during feeding with a slower rate of salivation during rumination (Hoppe et al., 1975). Moreover, the camel possesses a well-developed pair of polystomatic sublingual glands covered by the mylohyoid muscle and situated under the epithelial lining of the tongue root. In addition, the camel has a set of minor salivary glands that support the process of salivation. Of these are scattered buccal glands situated in the buccinators where the ventral buccal salivary glands are embedded anterior to the masseter muscle in the lateral sides of the mandibular epithelium (Jarrar and Faye, 2012). Moreover, the camel possesses scattered lingual Von Ebner's salivary glands open in the trench surrounding the lingual circumvallate papillae (Jarrar and Taib, 1989). Furthermore, labial glands are situated in the lamina propria of the inner labial epithelial lining located just above the labial muscularis together with palatine salivary glands embedded in the palatine epithelial lining (Jarrar and Taib, 1989).

Some morphometric studies, and to a lesser extent histological ones, investigated the major salivary glands of the one-humped camel (Nassar, 1971; Nawar & Khaligi, 1975; Nawar and Khaligi, 1977, Abdalla, 1979, Mosallam et al., 1983), and to lesser extent the minor ones (Fahmy and Dellman, 1968; Jarrar and Taib, 2005, Taib and Jarrar, 1998). However, beyond the anatomical dispersion of the salivary glands, their performance in terms of quantity and quality of saliva production is related to their anatomic-physiological structure. The present work was undertaken to provide morphometric, histological and histochemical description and characterization for the salivation battery of the dromedary camel as a tool of adaptation to arid environments.

2. Materials and Methods

Representative biopsies of major (mandibular, parotid and sublingual) and minor (buccal, lingual, labial and palatine) salivary glands were collected from 16 healthy adult one-humped camels of both sexes with the age of 5-6 years old (body weigh 470-560 kg) of Majaheem breed obtained from the main slaughterhouse in Skaka city of Saudi Arabia. The tissue blocks were subjected to detailed anatomical, histological and histochemical investigations including gross anatomy, fixation by buffered neutral formalin (BNF), dehydration by ascending concentration of ethanol, clearing in chloroform, impregnation and embedding by paraffin wax (melting point 58 C).

Paraffin sections (4-5 πm thickness) of all samples under study were subjected to hematoxylin and eosin (H&E) and trichrome stains (Jarrar and Taib, 2018). In addition, paraffin and frozen sections (8-10 πm thickness) were subjected to the following battery of histochemistry techniques (Pearse, 1992; Jarrar and Taib, 2016 and 2018; Survarna et al., 2019): Periodic acid Schiff (PAS) reaction, amylase digestion-PAS for glycogen and neutral mucosubstances characterization, alcian blue (AB) at pH 2.5 and 1.0 for acid mucosubstances, PAS-AB (pH 2.5) and PAS-AB (pH 1.0) for distinction between neutral and acid mucosubstances, aldehyde fuchsin (AF) and AF-AB (pH 2.5 and 1.0) for the distinction between sulphomucins and sialomucins. Other paraffin sections were exposed to the following enzymatic digestion tests: amylase-PAS, neuraminidase-AB (pH 2.5), hyaluronidase-AB (pH 2.5), neuraminidase-TB (pH 3.7) and hyaluronidase-TB (pH 2.0). In addition, proteins were detected by ninhydrin-Schiff, mercuric bromophenol blue (MBP) and trypsin digestion-PAS. Moreover, the enzyme histochemical activity was determined for the following enzymes: alkaline phosphatase, acid phosphatase, mitochondrial adenosine triphosphatase, non-specific esterases, succinic dehydrogenase, carbonic anhydrase and aminopeptidase.

All conducted experimental procedures were approved by the Ethics Committee for the use of experimental animals at Jerash University (approval number JU/17/05/2019).

3. Results and Discussion

The dromedary camel has a thick upper lip divided by a fissure of two mobile parts. This fissure is continuous with a lateral nose external wing. On the other hand, the lower lip demonstrates hanging with an apparent chin and becomes more pointed. However, both lips are covered by hairy skin with long tactile hairs covering the external superficial surface (Figure 1a-c). A previous study reported that both lips have scattered labial glands in grey-blue labial epithelial lining (Taib and Jarrar, 1987).

The lips guard the entrance of the oral activity and each consists anatomically of three anatomical zones: cutaneous, transitional and mucosal zone (Figure 2a). Histologically, the cutaneous of the lip consists of two layers, an outer epidermis and deeper dermis. The dermis is embedded with scattered sweat and sebaceous glans together with the roots of the tactile hairs (Figure 2b). The labial transitional area is covered by a thin skin and extends up to the oral mucosa. This zone lacks sweat glands and hair roots. The labial mucosal zone includes three sublayers: Mucosa, submucosa and muscularis. The mucosa consists of compound squamous epithelium while the submucosa is formed of connective tissue rich in blood vessels and collagenous fibers together with tubule-alveolar labial glands (Figure 2c). The muscularis of the mucosal zone consists of skeletal muscle fibers making the core of the mucosal sublayer (Figure 2d).

The one-humped camel has an elongated mobile tongue consisting mainly of obliquely arranged skeletal muscle bulk (Figure 3b-c). The tongue is about 40 cm long and is attached to the hyoid bone. Filiform, fungiform and circumvallate papillae cover the upper surface of the dorsum of the tongue and its lateral edges. Some studies reported that the tongue of the camel is highly innervated

containing numerous ganglia and nerve fibers (Qayyum et al., 1991). In addition, the tongue of the one-humped camel is covered with a variable thickness of cornified compound squamous epithelium. The lingual lamina propria is narrow and continuous with the muscularis mucosa lining the submucosa sublayer (Figure 4a). The dorsal lingual epithelium of this animal demonstrates filiform, fungiform, circumvallate papillae together with wart-like papillae (Figure 4b). Bundles of thick connective tissue are seen along the ventral lingual surface. The filiform papillae are conical in shape with variable thickness and height and are scattered mainly in the dorsum and the lateral edges of the tongue. On the other hand, the rounded fungiform papillae together with the taste pores are seen in the anterior lingual surface. However, the circumvallate papillae are restricted to the posterior portion of the tongue (Figure 3c).

The inferior lingual surface lacks cornification and is lined with squamous epithelium. Two types of minor salivary glands are situated in the lamina propria: Von Ebner's glands and Weber's glands which are superficially embedded amongst dense connective tissues and surrounded by bundles of lingual striated muscle. The lingual core exhibits a bundle of skeletal muscles arranged variably in transverse and oblique arrangements (Figure 4c). The stroma of the tongue contains numerous ganglia and nerve fibers.

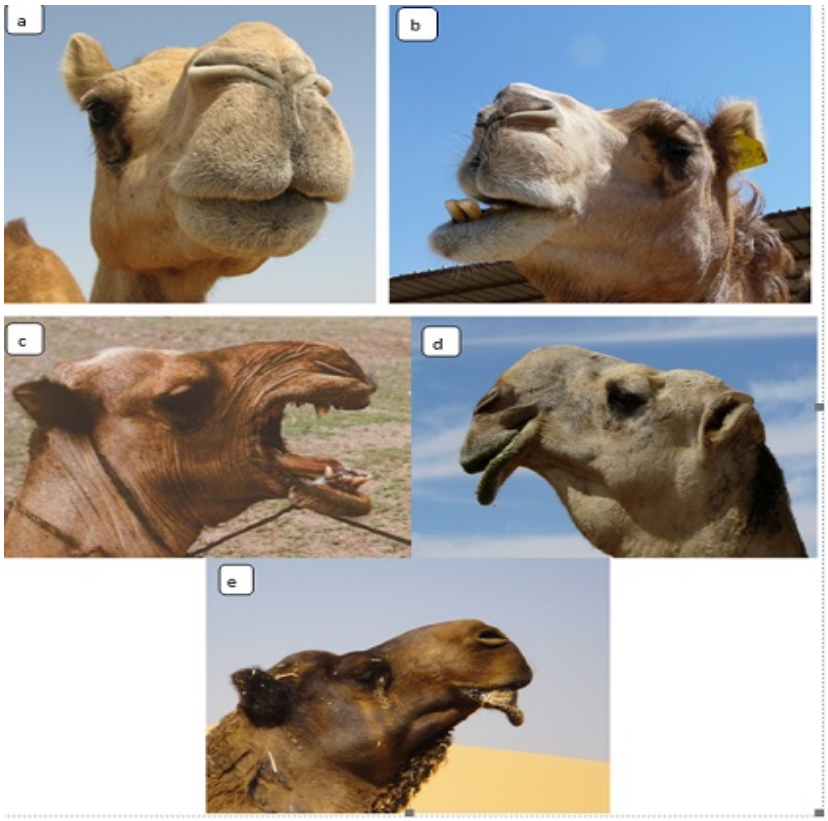

Figure 1. Photographs on libs of the one-humped camel demonstrating: (a) The external surface of the lip covered by long tactile hairy skin, (b) Tactile hairs covering both libs, (c) Sharp teeth, (d) Mobile rubbery lip (e) Hanging lip in an old camel

 © 2023 Jordan Journal of Biological Sciences. All rights reserved - Volume 16, Number 1

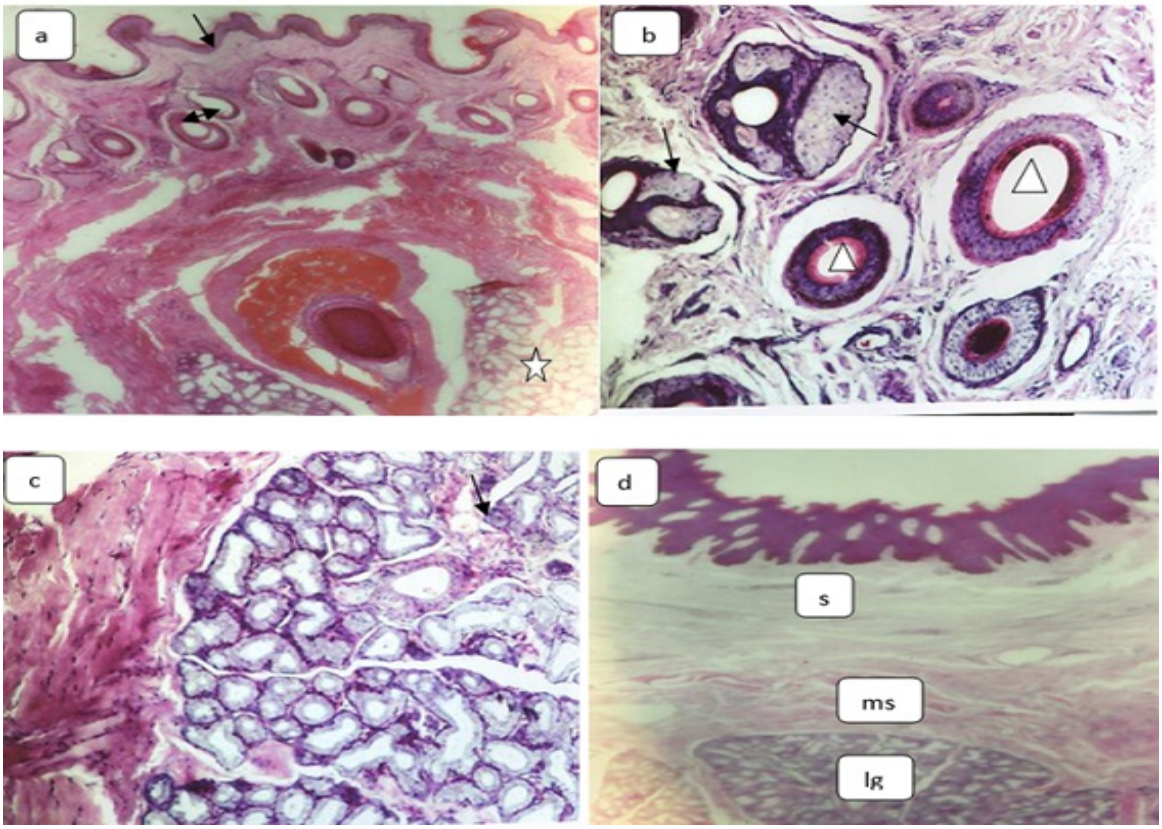

Figure 2(a-d). Micrographs through in the cutaneous zone of the camel lip demonstrating (a) The epidermis (arrow), hair roots (double arrow) and labial glands (star), (b) Sebaceous glands (arrows) and hair follicles (triangles), (c) The tubule-alveolar nature of the labial salivary glands, (d**)** The mucosal zone sublayers: submucosa (s), muscularis (ms) and labial glands (lg).

Figure 3(a-c). Photographs showing (a) The muscle mass of the camel tongue, (b)The hole-elongated tongue. Note the situation of the papillae at the base of the tongue, (c) The circumvallate and wart-like papillae.

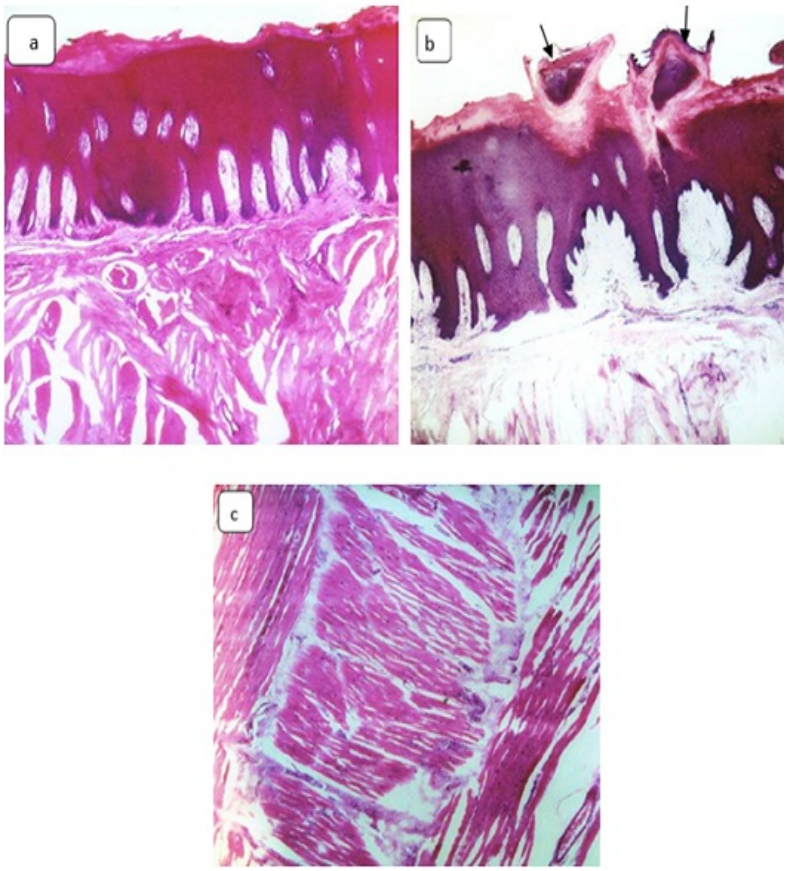

Figure 4(a-c). Micrographs in the tongue of the one-humped camel demonstrate (a) The lingual dorsum with the lamina propria, (b) The lingual dorsum with two fungiform papillae (arrows), (c) Muscle bundles of the lingual core.

3.1. The parotid glands

This major salivary gland is the largest in the dromedary camel with a four-sided shape and brown-red color, located between the ramus of the mandible and the atlas wing (Figure 5a). It demonstrates an average weight of 0.005% of live body weight and up to 145 gm in the adult animal (Kay et al., 1980). Also, this gland shows an average dimension of 13. 8 cm x 5. 7 cm x 2. 5 cm. The parotid gland of the camel has a ductal system lined by cuboidal epithelium with occasional goblet cells and ambulated narrow intercalated ducts can. This gland can produce up to 21 liters of saliva depending on the type of diet (Nawar and El-Khaligi, 1975; Kay and Maloiy, 1989).

The parotid gland of the camel is of serous compound tubule-acinar type, covered by a capsule of fibrous and connective tissue. This gland demonstrates three variable end pieces of storage, secretory and exhaustion but lacks glycogen. The parotid gland of a one-humped camel has a large duct with folded lumen lined by compouned columnar epithelium with a large number of goblet cells (Figure 5b).

3.2. The mandibular glands

The mandibular gland of the camel is oval in shape and located obliquely under the parotid gland and covered by a layer of fi brous connective tissue surrounded by a collagenous capsule (Figure 5c). This gland demonstrates an average dimensions of 9.5 cm x 3.6 cm x 1.9 cm and an average weight of 52 gm (Nawar and Khaligi, 1977). Moreover, the salivation of the mandibular glands of the camel is rapid during ingestion and slow during rumination (Hoppe et al., 1975).

The secretory portion of the mandibular glands of the camel is tubuloacinar type consisting of mucous and seromucous cells with seromucous cells embedded between the mucous ones. The former cells are made of the secretory tubules and acini, while the seromucous one form acini and demilunes filled with variable types of secretory granules (Figure 5e). In addition, the duct of this gland has folded lumen lined by stratified columnar epithelium rich in goblet cells. However, goblet cells are also seen in the epithelium of the interlobular ducts.

3.3. The inferior molar glands

These glands are also called the ventral buccal glands and are embedded in the buccinators anterior to the masseter muscle and lateral to the mandibles (Taib and Jarrar, 1989). The dorsal part of this gland consists of large lobules while the ventral part demonstrates a dark brown layer in the form of a pyramid. The ventral portion of this gland consists of serous acini surrounded by numerous myoepithelial cells, while the dorsal part of the gland is composed of mucoserous acini. The serous acini of the ventral buccal gland are devoid of mucosubstances of any type while mucouserous ones demonstrate carboxylated mucosubstances and glycoproteins but are devoid of glycogen and sulphated mucosubstances. Moreover, this gland shows enzymatic activity for adenosine triphosphatase, nonspecific esterase, α-amylase, succinic dehydrogenase and alkaline phosphatase. However, the ventral buccal gland of the dromedary does not have enzymatic activity for lipase, aminopeptidase, beta-glucuronidase and cholinesterase.

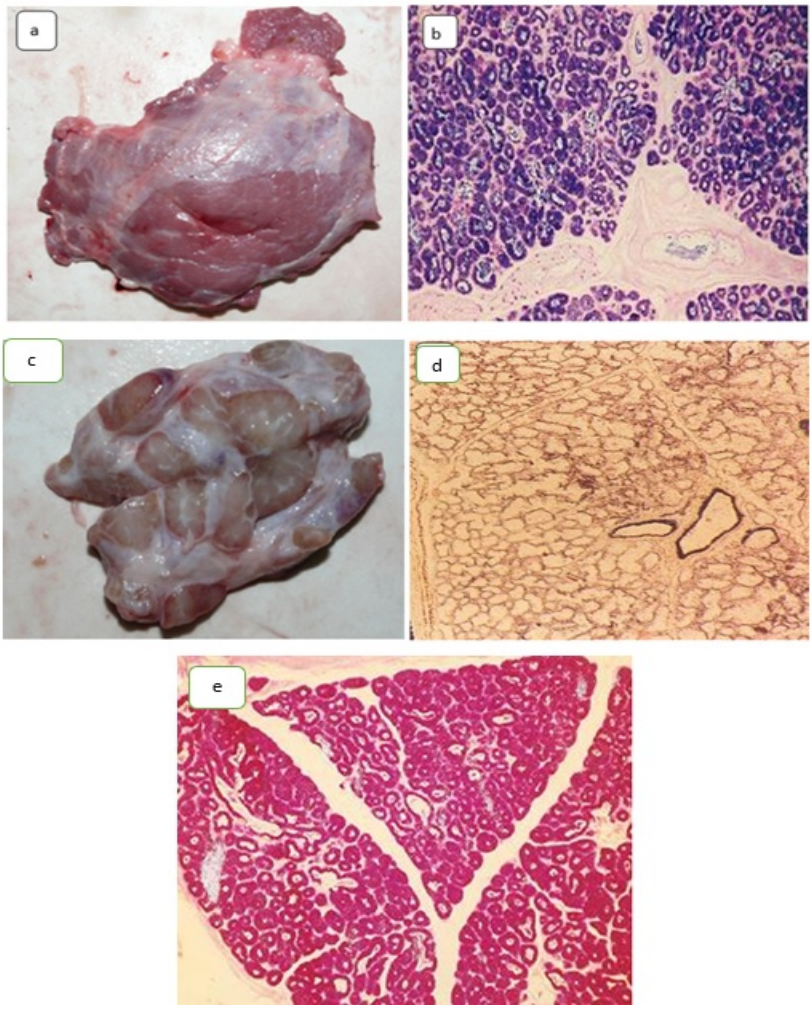

Figure 5(a-f). Micrographs show (a) Gross view of the parotid gland, (b) Parotid gland section stained with alcain blue-Aldehyde fuchsin stain demonstrating acid mucosubstances. (c) Gross examination of the mandibular gland demonstrates lobulation of the gland, (d) Section through the mandibular salivary gland demonstrates succinate dehydrogenase activity, (e) Section through the mandibular salivary glands stained with PAS method.

3.4. The sublingual glands

The sublingual glands of the camel are located along the root of the tongue under the mucous membrane (Jarrar and Faye, 2012). These glands are polystomatic in nature, small in size, pale yellow in color, flat in shape and covered by the mylohyoid muscle. These glands open separately in the floor of the buccal cavity via 16-20 excretory ducts and are embedded in dense fibrous connective tissue rich with adipose tissue and scattered in between smooth muscle bundles. The sublingual glands have numerous excretory ducts that open on the floor of the cavum oris proprium in both sides.

These glands are compound tubulo-acinar ones composed of many lobules made of two types of cells: seromucous and mucoserous (Figure 6a). The mucoserous cells constitute the main secretory portion of the glands and to a lesser extent the seromucous part. However, the mucoserous portion is distributed in the surrounding connective tissue while the seromucous excretory cells are seen embedded between the mucoserous ones. The mucoserous cells secrete neutral mucosubstances, sialomucins and to less extent sulphomucins (Figure 6b). On the other hand, the seromucous cells elaborate moderate quantity of neutral and acid mucosubstances but lack glycogen (Figure 6c).

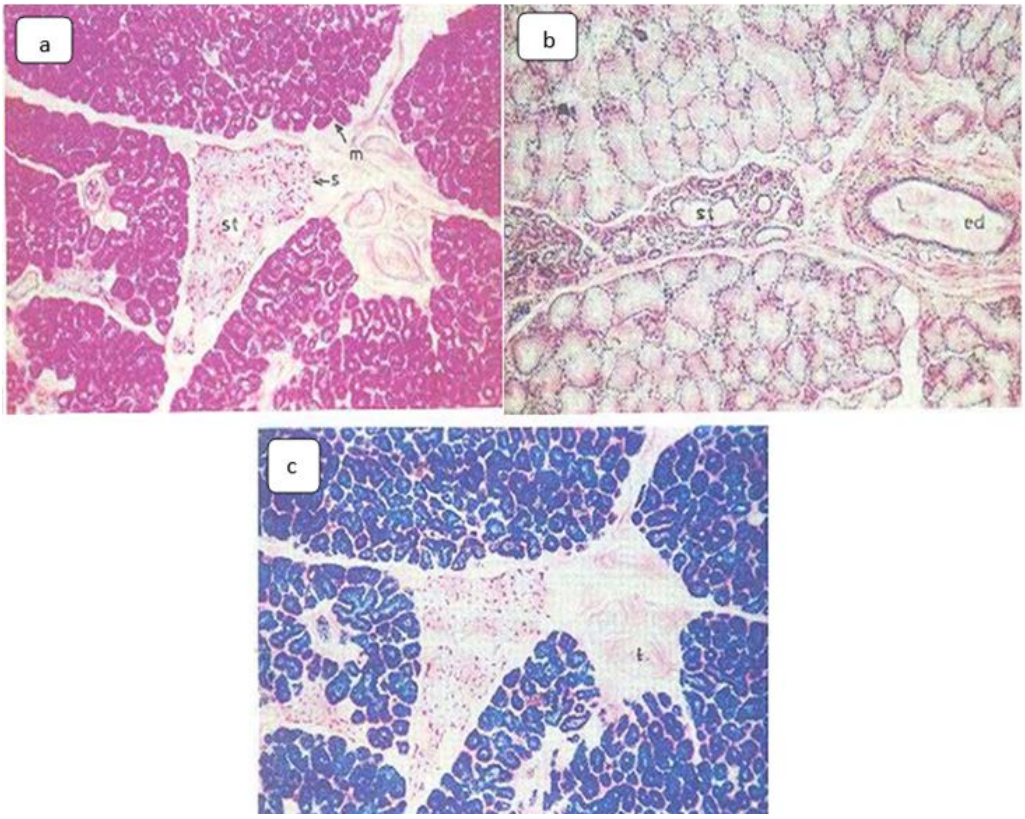

Figure 6(a-c). Micrographs show sections in the sublingual salivary gland of a camel demonstrating (a) Sublingual gland lobulation, (b) The sublingual salivary gland stained with PAS demonstrating neutral mucosubstances, (c) The sublingual salivary gland stained with alcian blue.

The sublingual glands of the dromedary camel glands demonstrate the activity of succinic dehydrogenase, alkaline phosphatase, non-specific esterase and aminopeptidase and to lesser extent activities of peroxidase and cytochrome oxidase with no beta-glucoronidase, lipase and amylase activities. The intralobular and striated ducts are lined with simple cuboidal cells with flattened epithelium seen in the intercalated ducts with no goblet cells.

3.5. The lingual salivary glands

The dromedary camel has two groups of lingual salivary glands, the Von Ebner's and Weber's glands with the following anatomical presentation:

3.5.1. The Von Ebner's lingual glands

These glands are situated in the lingual connective tissue under the circumvallate papillae. Studies indicated that these glands open mainly in the trench that surrounds the circumvallate papillae and are deeply located in the lingual adipose tissues (Jarrar and Taib, 1989). The Von Ebner's glands are a holocrine tubuloalveolar type and seromucous in nature with a branch of intercalated ducts (Figure 7a). The endpieces of these lingual glands rest on a delicate thin basement membrane. The striated ducts are lined by simple cuboidal epithelium while the cells of the secretory portion have prominent large nuclei and are filled with eosinophilic granules in their apical. Moreover, the histochemical characterization reveals that Von Ebner's glands contain a mixture of neutral mucosubstances, carboxylated and sulphated acidic mucosubstances together with orthochromatic materials. In addition, these glands demonstrate activity for the following enzymes: acid phosphatases, alkaline phosphatase, carbonic anhydrase, adenosine triphosphatase, amylase, succinic dehydrogenase and non-specific esterase (Figure 7b).

3.5.2. The Weber's lingual glands

The Weber's glands of the camel are located under the scattered thin papillae located at the tongue base. These glands consist of branched secretory tubules lined by a simple columnar epithelium with cells having alveolar cytoplasm and elongated nuclei located at the base of the cells (Figure 7c). These glands have conspicuous interlobular excretory and striated ducts lined by pseudostratified epithelium. These glands are embedded in vascularized dense connective tissue in between the bundles of muscles. However, Weber's glands demonstrate neutral mucosubstances, carboxylated and sulphated mucosubstances together with the activity of dehydrogenases and phosphatases (Figure 7d).

3.6. The labial glands

The lips of the dromedary camel are covered with hairs except for the contact area between the skin and the epithelial lining of the oral cavity which constitutes a keratinized stratified squamous epithelium covering the orbicularis muscle and the underneath collagenous connective tissues.

The labial glands of the dromedary camel are situated deeply in the lamina propria and in between the labial striated muscles. These glands are tubule-alveolar mucoserous ones in both the infra- and supra-labial libs (Figure 8a). The acini of these glands are capped by serous demilunes separated from each other by interlobular ducts and to a lesser extent in the intertubular ones. The secretory cells of the labial glands demonstrate variable

shapes containing cytoplasmic granules with eosinophilic granules filling the cytoplasm of the demilunar cells. Moreover, these glands exhibit neutral mucosubstances, alcianophilia and metachromasia (Figure 8b). In addition, the mucoserous cells of these glands reveal enzymatic activity mainly for acid phosphatase, ATPase, alkaline phosphatase, succinic dehydrogenase, non-specific esterase, carbonic anhydrase, aminopeptidase and amylase (Figure 8c).

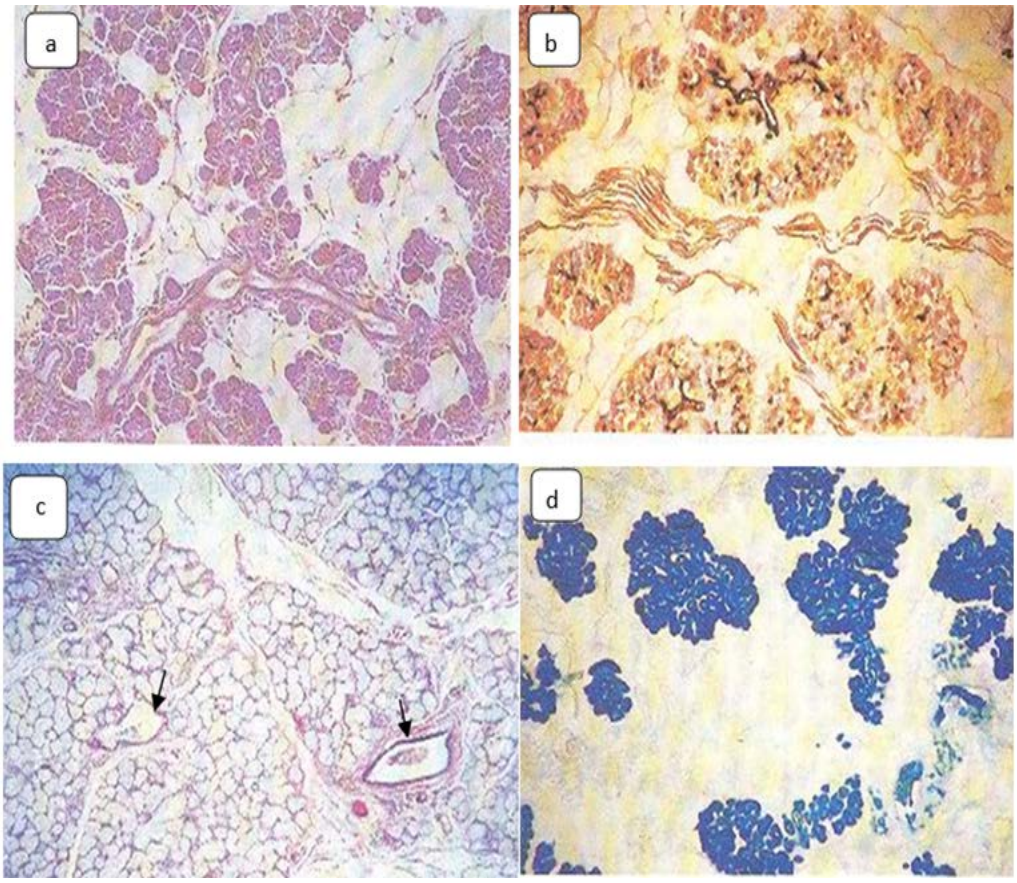

Figure 7(a-d). Micrographs illustrate sections demonstrated in the tongue of the one-humped camel: (a) The secretory portion of Von Ebner's glands, (b) Von Ebner's glands demonstrating alkaline phosphatase activity, (c) Secretory portion and the striated duct of the Weber's glands, (d) The Weber's lingual salivary gland stained with alcian blue (pH = 1.0) demonstrating sulphated mucosubstances

3.7. The palatine glands

These glands are located mainly in the soft palate but not in the hard one. The lining of the plate consists of stratified squamous epithelium forming ridges in the hard palate but not in the soft one. The stroma of the palatine glands is rich in muscle fibers, fat cells and interlobular ducts (Figure 8d). The lining of both the interlobular and intralobular ducts consists of simple cuboidal epithelium with secretory cells open in the striated ducts. However, the palatine glands of the camel are devoid of intercalated ducts. Moreover, these glands elaborate sialomucins, sulfomucins and neutral mucosubstances (Figure 8e). In addition, these glands demonstrate activity for dehydrogenases, phosphatases, and carboxyhdrases.

Thus, salivary glands in camels are characterized by their wide physiological functions, not only acting as a lubricant of the alimentary bowl in dry conditions), but also in many enzymatic activities contributing to the better valorization of a diet characterized in desert conditions by its dryness, poor nutritive value and low-absorbable components. In a context of climatic changes and living in an ecosystem facing one major hot spot of the interaction livestock-environment (i.e. desertification), the camel is showing his remarkable ability to not only survive but to valorize such a growing ecosystem (Steinfeld et al., 2003; Faye et al., 2012). The one-humped camel demonstrates anatomical, physiological and behavioral features adaptable for desert ecosystems that are not seen among other livestock (Yagil, 1985; Bengoumi and Faye, 2002; Jarrar 2006; Jarrar and Faye, 2012). The salivation function based on the specific structure of salivary glands is one element of the expected ability of the camel to be adapted to this transitional period toward a warmer and dryer world as we can experience with the growing presence of large camelids over the world (Faye, 2022). Notably, the expansion of dromedary camels in Africa following the recent droughts that have affected the margin of Sahara supports this evidence (Thornton et al., 2009). Moreover, the implementation of camel farming in desert areas of Southern Africa and North America (Faye, 2020) could be indirectly considered as a consequence of the ability of camels to occupy and valorize all arid lands of the world. Furthermore, in more favorable environments as in Western Europe, the newly implemented camels showed their ability to clear the ground by consuming nettles, brambles or rumex, plants that are neglected by other herbivores.

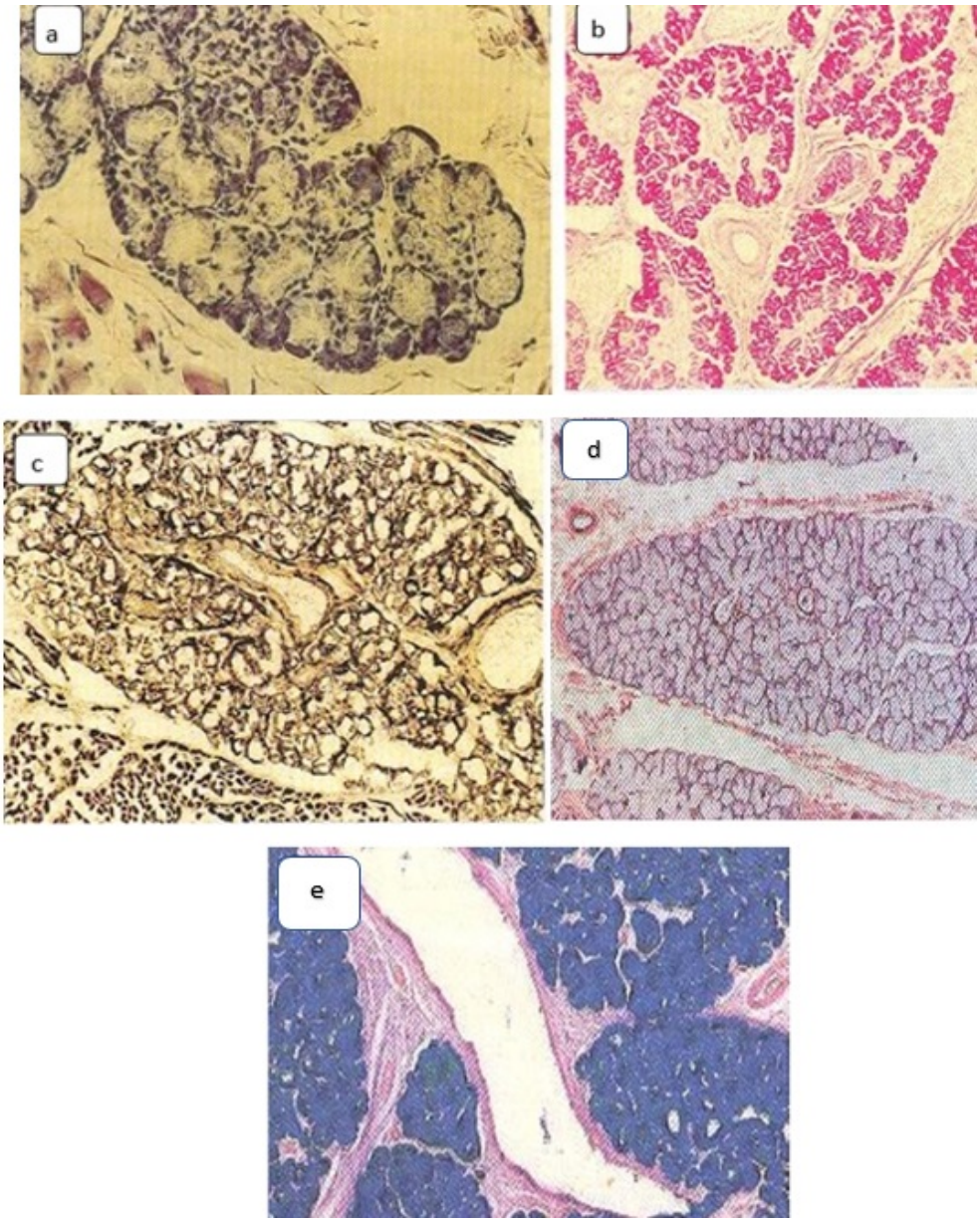

Figure 8(a-e). Micrograph sections in the labial salivary glands of the dromedary camel demonstrating: (a) Cluster of the labial gland acini, (b) Labial neutral mucosubstances, PAS stain, (c) Labial ATPase activity, (d) Palatine salivary glands stained with H&E stain, (e) Palatine salivary glands stained with PAS-alcian blue-(pH = 2.5).

The findings of the present work showed that camels have a complex salivary gland system consisting of three pairs of major salivary glands and several minor salivary glands. Adult camels can produce up to 150 liters of saliva per day, which is significantly more than other ruminants (cattle, ≥ 100 liters; sheep, ≥ 10 liters) (Al Razaiki et al., 2023). In addition, the findings indicate that camels' saliva contains a variety of proteins, electrolytes and enzymes. The sticky viscous saliva of camels helps them to retain mouth water, moist the food, prevent excessive water loss through evaporation and to reduce the amount of water needed for digestion. Moreover, the high concentration of electrolytes in camels' saliva helps to keep electrolytes homeostasis and prevent dehydration. Furthermore, the variable proteins and enzymes content of the camels' saliva have been found to offer antimicrobial and antifungal properties protecting the digestive system from harmful pathogens (Kay and Maloiy, 1989).

Collectively, the structure and the secretory contents of the camel salivary glands play an essential role in preventing dehydration and in breaking the tough fibrous plants they consume. Saliva helps to moisten the food, retain water in the mouth, moisten the nasal passage and enhance water reabsorption in the intestine. In addition, camels' saliva plays a vital role in their body's thermal regulation through panting where saliva evaporates to cool the inside of the mouth.

4. Conclusion

One may conclude from the findings that camels demonstrate an efficient salivation system contributing to better efficiency in the valorization of pastoral resources marked by the specific characteristics of the desert plants. The structure and the secretions of the salivary glands of the camel support an efficient salivation process and represent a strong challenge to the growing scarcity of

water and the expansion of xerophytes as the main pastoral resources for camels. In t hat sense, salivary glands in camels are one of the elements of their panoply to resist harsh conditions and to mitigate the climate change impacts.

Acknowledgments

This project was supported by Researchers Supporting Project number (RSPD2024R900) King Saud University, Riyadh, Saudi Arabia. In a ddition, the authors greatly appreciate the help they got from Jerash University. The authors are thankful for t he support they received from King Sau University and Jerash University.

Conflict of interest

The authors declare that they have no c onflict of interests of any type.

References

Abdalla AB. 1979. Structure of the secretory cells of the salivary glands of the dromedary camel. Sudan J Vet Sci An im Husb, **20**: 65-16.

AL-Asgah NA, Taib, NT, Jarrar, BM. 1990. Structure and histochemistry of the sublingual gland of the one- humped camel (Camelus dromedarius). Rev Elev Med Vet P ays Trop, **43(4)**:519-527.

Al Razaiki K, Al Khaldi K, Al Harthy N, Al Wahaibi A, Qutieshat A. 2023. Evaluating the role of inorganic elements of Camelus dromedarius saliva in protecting enamel against tooth surface loss. J Vet Dentist, https://doi.org/10.1177/08987564231177575

Bengoumi M, Faye B. 2002. Adaptation du dromadaire à la déshydratation. Sécheresse.**13**: 121-129.

Fahmy MF, Dellman H D. 1968. Studies on t he microscopic anatomy of the oral cavity of Camelus dromedarius. J Vet Sci UAR, **5(1)**: 45-51.

Fahn A, Cutler DF. 1992. Xerophytes. Gebrüder Borntraeger Publ., Stuttgart, Germany.

Faye B, Chaibou M, Vias G. 2012. Integrated Impact of climate change and socioeconomic development on the evolution of camel farming systems. Brit J Environ Clim Chan, **23**: 227-244.

Faye B., 2020. How many large camelids in the world? A synthetic analysis of the world camel demographic changes. Pastoralism: Res Pol Pract, **10**: 25; https://doi.org/10.1186/s13570-020-00176-z

Faye B. 2022. Is the camel conquering the world?, Anim Front, **12(4)**: 8–16, https://doi.org/10.1093/af/vfac034

Hoppe P, Kay RB, Maloiy GO. 1975. Salivary secretion in the camel. J Physiol, **244**: 32-33.

Jarrar BM, Taib NT. 2005. Histochemical characterization of dehydrogenases in the nephron of the one-humped camel (Camelus dromedaries). Pakistan J Biol Sci, **8(7)**: 1055-1059.

Jarrar BM, Taib NT. 1989. Histochemical distribution of mucrosubstances and enzyme activity in the lingual salivary glands of the one-humped camel (Camelus dromedarius). Rev Elev Med Vet Pays Trop, **42(1)**: 63-71.

Jarrar B, Faye B. 2012. Normal Pattern of Camel Histology. Camel Breeding, Protection and Improvement Center, Saudi Arabia, FAO Publish., Riyadh

Jarrar BM, Taib, NT. 2016. Histocytotechnology. King Saud University Press, Riyadh, Saudi Arabia

Jarrar BM, Taib NT. 2018. Histochemistry: Techniques and Horizon. King Saud University Press, Riyadh, Saudi Arabia

Jarrar BM. 2006. Renal phosphatases histochemistry in the nephron of the dromedary camel (Camelus dromedaries). Proceeding of the International Scientific Conference on Camel, College of Agriculture & Veternary Medicine, Qassim University, Volume **3**: 1332-1342.

Kay RB, Engelhardt WV, White RG. 1980. The Digestive Physiology of Wild Ruminants. In: "Digestive Physiology and Metabolism in Ruminants" (eds. Y. Ruckebusch & P. Thivend), MTP Press, Lancaster (UK), 743-761.

Kay RN, Maloiy MO. 1989. Digestive secretions in camels. Options méditerranéennes, Série Seminaries, **2**: 83-87.

Khaligi GE. 1975. Morphological, micromorphological and histochemical studies on the parotid salivary glands of the one-humped camel (Camelus dromedarius). Gegenbaurs Morphol Jahrb. **121(4)**: 430-449.

Mosallam ES, Gharib N, Mousa M. 1983. A h isto-enzymatic study of the mandibular salivary glands of the one-humped came1 (Camelus dromedarius). Egypt Vet Med, **43**: 183-196.

Nadipour A, Khanzadi S, Gaasemi MJ. 2001. Anatomical and histological studies of esophagus of one-humped camel. J Fac Vet Med Tehran Univ, **56(4)**: 113-117

Nassar SM. 1971. Digestion in Camels. Thesis, Fac. Vet. Med., Cairo University.

Nawar SM, El-Khaligi GE. 1975. Morphological, micromorphological and histochemical studies on the parotid salivary glands of the one-humped camel (Camelus dromedarius). Gegenbaurs morphologisches Jahrbuch, Leipzig, **4**: 430-449.

Nawar SM, Khaligi GE. 1977. Morphological and histochemical studies on the mandibular salivary glands of the one-humped camel (Camelus dromedarius). Anat Anz, **142**: 346-362.

Pearse AV. 1992. Histochemistry: Theoretical and Applied, Enzyme Histochemistry. 4th edition, Churchill Livingstone

Qayyum MA, Fatani JA, Mehta L. 1991. Anatomical and histological observations on t he tongue of one-humped camel, *Camelus dromedarius*. *Funct Dev Morphol*, **1(3)**: 23-26.

Steinfeld H, De Haan C, Blackburn H. 2003. Livestock - Environment Interactions: issues and options. FAO publ.

Suvarna SK, Layton C, Bancroft, JD. 2019. *Bancroft's Theory and Practice of Histological Techniques*. 8th edition, 40-557, Elsevier Ltd.

Taib NT, Jarrar BM. 1987. Histochemistry of the labial salivary glands of the one-humped camel, Camelus dormedarius. Boll Zool **54(1)**: 19-25.

Taib NT, Jarrar BM. 1989. Morphology, histology and histochemistry of the ventral buccal glands of the one- humped camel (Camelus dromdarius). J Zool London, **219**: 423-434.

Taib NT, Jarrar BM. 1998. Histochemical characterization of the palatine salivary glands of the one-humped camel. J Camel Prac Res, **5(1)**: 39-4.

Thornton PK., van de Steeg J, Notenbaert A., Herrero M. 2009. The impacts of climate change on livestock and livestock systems in developing countries: a review of what we know and what we need to know. Agric Syst, **101**: 113–127

Wilson RT. 1989. Ecophysiology of the camelidae and desert ruminants. Ed. Springer- Verlag, New-York (USA), 120

Yagil R. 1985. The Desert Camel: Comparative Physiological Adaptation. Ed. Karger, Basel (Switzerland)

JJBS

Volume 17, Number 1,March 2024
ISSN 1995-6673
Pages 109 – 122
https://doi.org/10.54319/jjbs/170110

Jordan Journal of Biological Sciences

Review: Shilajit (Mumie) A natural Product with Anti-hyperglycemic, Anti-obesity, Anti-oxidant, and Anti-Inflammatory properties for a potential treatment of diabetes mellitus

Abd Al-Rahman S Al-Shudiefat[1,*], Jihad A. M. Alzyoud[2]

[1]The Hashemite University - Faculty of Applied Medical Sciences- Department of Medical Laboratory Sciences, Zarqa 13133, Jordan;[2]The Hashemite University -Faculty of Medicine- Department of Anatomy, Histology, Physiology and Biochemistry, Zarqa 13133, Jordan.

Received: June 22, 2023; Revised: July 21, 2023; Accepted: July 31, 2023

Abstract

Diabetes is a major health problem worldwide that hinders normal life. Diabetes is a leading cause of death with high prevalence across the globe. Many drugs are used for the management of type 2 diabetes, unfortunately with some side effects including abdominal pain, kidney, liver, heart complications, and most commonly life-threatening hypoglycemia. Furthermore, these medications mitigate hyperglycemia symptoms and do not address the root cause, which is lipid accumulation in the pancreas, liver, and muscles. Therefore, there is a need for a safe natural product that manages diabetes and reduces obesity with fewer side effects. Shilajit, which is an exudate from many rock layers of mountains, especially the Himalayas, is made up of plant and microbial metabolites, including a mixture of organic humus, humic acid, fulvic acid, and minerals. It was used for many ailments in old traditional medicine and in current human and animal studies, in which its safety and fewer side effects were affirmed. Shilajit has anti-diabetic properties that include anti-hyperglycemia, anti-obesity, anti-oxidant, anti-inflammatory effects, increased metabolism, and important minerals. Anti-hyperglycemia of shilajit could be due to decreasing oxidative stress, decreasing inflammation, and increasing metabolism that leads to the burning of fat and decreasing obesity; all of these are implicated in insulin resistance and diabetes. Other uses of Shilajit include treatment of cancer, allergy, and increased immunity. More clinical studies are required to explore the mechanisms and benefits of Shilajit, as recent research is promising.

Keywords: Shilajit (Mumie); Diabetes mellitus; Anti-hyperglycemia; Anti-inflammatory; Anti-oxidant; Anti-obesity; Insulin sensitivity.

1. Introduction

Diabetes is an alarming health problem worldwide; it caused 1.5 million deaths in 2019 alone, with a prevalence of 8.5% for ages 18 and older and 422 million cases in 2014 (World Health Organization, 2019). Diabetes is a chronic, endocrinological, metabolic disorder (Trivedi et al., 2004) characterized mainly by hyperglycemia. Other symptoms include frequent urination, thirst, hunger, fatigue, blurred vision, and restlessness (Ramachandran, 2014; World Health Organization, 2019). Elevation of blood glucose levels in diabetes mellitus is due to insufficient pancreatic insulin secretion or insulin resistance by target cells (Piero et al., 2015). There are many types of diabetes: type 1 diabetes, type 2 diabetes, and gestational diabetes (Piero et al., 2015). Type 1 diabetes is an autoimmune disease against beta-pancreatic cells, and therefore is associated with insulin deficiency (DiMeglio et al., 2018). Type 2 diabetes is characterized by insulin resistance and beta cell dysfunction in the pancreas (Hameed et al., 2015). Most diabetes cases (around 90%) are of type 2 diabetes, and it was estimated in 2018 with 500 million cases worldwide (Kaiser et al., 2018; World Health Organization, 2016). According to the International Diabetes Federation (IDF), it is estimated that there will be 582 million adults living with diabetes worldwide in 2022. Of these, approximately 90% will have type 2 diabetes (Atlas, 2019).

There are many risk factors associated with diabetes, such as age, genetic factor or family history, lifestyle, physical inactivity, smoking, as well as obesity, and being overweight, which increase the risk of diabetes mellitus (World Health Organization, 2016). Furthermore, inflammation (Halim & Halim, 2019; Oguntibeju, 2019) and oxidative stress (Asmat et al., 2016; CHANDRA et al., 2019) are risk factors for the development of diabetes mellitus.

Chronic diabetes can lead to dangerous and life-threatening complications including hypertension, coronary heart disease, stroke, neuropathy, renal failure, cancer, retinopathy, obesity, proteinuria, hypertriglyceridemia, amputations, and foot ulcers (Basit et al., 2004; Harding et al., 2019; Stolar, 2010). The 5-year total cause mortality rate for diabetes type 1 and type 2 was estimated at 5.5 and 18.9%, respectively (Cusick et al., 2005). The diagnosis of diabetes includes a fasting plasma glucose test, random plasma glucose test, oral

* Corresponding author. e-mail: abdsalem29@hu.edu.jo.

glucose tolerance test, and HbA1C test (Cox & Edelman, 2009).

Diabetes mellitus must be managed to prevent the progression of complications, mainly in type 1 diabetes mellitus, by using insulin replacement therapy, while diet, lifestyle changes, increased exercise, weight loss, and oral medication are considered for the treatment and management of type 2 diabetes mellitus (Bastaki, 2005). Insulin is also important in type 2 diabetes mellitus when blood glucose levels cannot be controlled; herbal supplements can also be useful in the management and treatment of diabetes (Bastaki, 2005). Medications used for diabetes include metformin, sulfonylurea, Glinides, thiazolidinediones, GLP-1 receptor agonists, DPP-4 inhibitors, and SGLT2 inhibitors (Hu & Jia, 2019). Unfortunately, these medications have some side effects, and some of them have dangerous consequences, such as hypoglycemia, which could be fatal. Therefore, there is an urgent need for natural products to be safe and have no dangerous side effects.

2. Diabetes medications side effects

Insulin is used as the first choice of treatment in type 1 diabetes and in some cases for type 2 diabetes, it has some side effects such as hypoglycemia, hyperinsulinemia, weight gain, and ketoacidosis (Chantelau et al., 1989; Wong et al., 2016). Metformin, which is used as a first-line drug to treat type 2 diabetes (Holman, 2007), has some side effects, including lactic acidosis (DeFronzo et al., 2016), diarrhea (Takemori et al., 2020), abdominal cramps (Li et al., 2011), nausea (Zheng et al., 2015), vomiting (Duong et al., 2013), flatulence (Saluja et al., 2020), and abdominal pain (Bolen et al., 2007). Furthermore, metformin is associated with vitamin B12 deficiency (Kumthekar et al., 2012). Sulfonylurea is associated with hypoglycemia (Middleton et al., 2017), weight gain (Hemmingsen et al., 2014), and digestive disorders (Confederat et al., 2016). It is also associated with higher mortality rates and cardiovascular events (Azoulay & Suissa, 2017). Glinides have some side effects similar to sulfonylurea, including hypoglycemia (Wei et al., 2019), weight gain (Kroon & Zhou, 2021), and cardiovascular disease (Lv et al., 2020). The use of thiazolidinediones was related to some undesirable effects such as hypoglycemia (Rizos et al., 2009), edema (Idris et al., 2012), weight gain (Wilding, 2006) , increased bone fracture (Billington et al., 2015), liver failure (Farley-Hills et al., 2004; Floyd et al., 2009), and heart failure (Hernandez et al., 2011). The GLP-1 receptor agonist has some unwanted effects such as hypoglycemia (Iorga et al., 2020), nausea, vomiting (Hayes et al., 2021), and diarrhea (Gilbert & Pratley, 2020). DPP-4 inhibitors are also implicated with some negative effects, such as the increased risk of heart failure (Scirica et al., 2013), hypoglycemia (Salvo et al., 2016), pancreatitis (Zheng et al., 2018), headache and nausea (Salvo et al., 2016). SGLT2 inhibitors have also accompanied some unwanted side effects such as hypoglycemia (Horii et al., 2020), genital infections (Scheen, 2019), urinary tract infections (Donnan et al., 2019), and ketoacidosis (FDA, 2015). These side effects of diabetes medications are summarized in table 1. Therefore, there is a need for safe and natural medication with fewer side effects to manage diabetes such as herbs.

Table 1. Some commonly used diabetes drugs and their possible side effects.

Diabetes drug	Side effects	References
Insulin	Hypoglycemia, hyperinsulinemia, weight gain, ketoacidosis.	(Chantelau et al., 1989; Wong et al., 2016)
Metformin	Lactic acidosis, diarrhea, abdominal cramps, nausea, vomiting, flatulence, vitamin B12 deficiency.	(Holman, 2007) (Takemori et al., 2020) (Li et al., 2011) (Zheng et al., 2015) (Duong et al., 2013) (Saluja et al., 2020) (DeFronzo et al., 2016) (Kumthekar et al., 2012)
Sulfonylurea	Hypoglycemia, cardiovascular events, weight gain, digestive disorders.	(Middleton et al., 2017) (Hemmingsen et al., 2014) (Confederat et al., 2016) (Azoulay & Suissa, 2017)
Glinides	Hypoglycemia, cardiovascular disease, weight gain.	(Wei et al., 2019) (Kroon & Zhou, 2021) (Lv et al., 2020)
Thiazolidinediones	Hypoglycemia, heart failure, edema, weight gain, increased bone fracture, liver failure.	(Rizos et al., 2009) (Idris et al., 2012) (Wilding, 2006) (Billington et al., 2015) (Farley-Hills et al., 2004; Floyd et al., 2009) (Hernandez et al., 2011)
GLP-1 receptor agonist	Hypoglycemia, nausea, vomiting, diarrhea.	(Iorga et al., 2020) (Hayes et al., 2021) (Gilbert & Pratley, 2020)
DPP-4 inhibitors	Hypoglycemia, increased risk of heart failure, pancreatitis, headache, nausea.	(Scirica et al., 2013) (Salvo et al., 2016) (Zheng et al., 2018)
SGLT2 inhibitors	Hypoglycemia, genital infections, urinary tract infections, ketoacidosis.	(Horii et al., 2020) (Scheen, 2019) (Donnan et al., 2019) (FDA, 2015)

Please note that these studies were done on human and animals in different situations

There has been increasing interest in herbal remedies among researchers in recent years in both human and animal studies, due in part to concerns about the safety and efficacy of synthetic drugs (Al-Shudiefat et al., 2022; Newman & Cragg, 2020; Payab et al., 2020). Herbs can be used as anti-hyperglycemic and anti-hypertensive agents, due to biological actions and chemical composition (Eff et al., 2020). Shilajit is one of the herbomineral supplements that could be used for the treatment of diabetes in both humans and animals (Kanikkannan et al., 1995; Saxena et al., 2003).

3. Shilajit's physical properties and safety

Shilajit has many names (mumie; *Asphaltum Punjabianum* (scientific name), shilajatu, mumijo, mumiyo, mineral pitch, momiai, tasmayi, salajit, Hajar-ul-musa, Arakul dshibal, and mimie) (Ghosal et al., 1991; Khakimov, 1974; Kizaibek, 2013; Mishra et al., 2019; Stohs, 2014). The use of these different names of Shilajit in Google Scholar, PubMed database, and commercially on Ebay are shown in Figures (1 + 2), with Shilajit being the most common name used in all. Three famous online websites were initially assigned to search for shilajit products, these are (Amazon, Alibaba, and Ebay). After searching for s hilajit products on t hese online websites, Ebay online website was chosen, because the number of shilajit products was much higher on Ebay than the others.

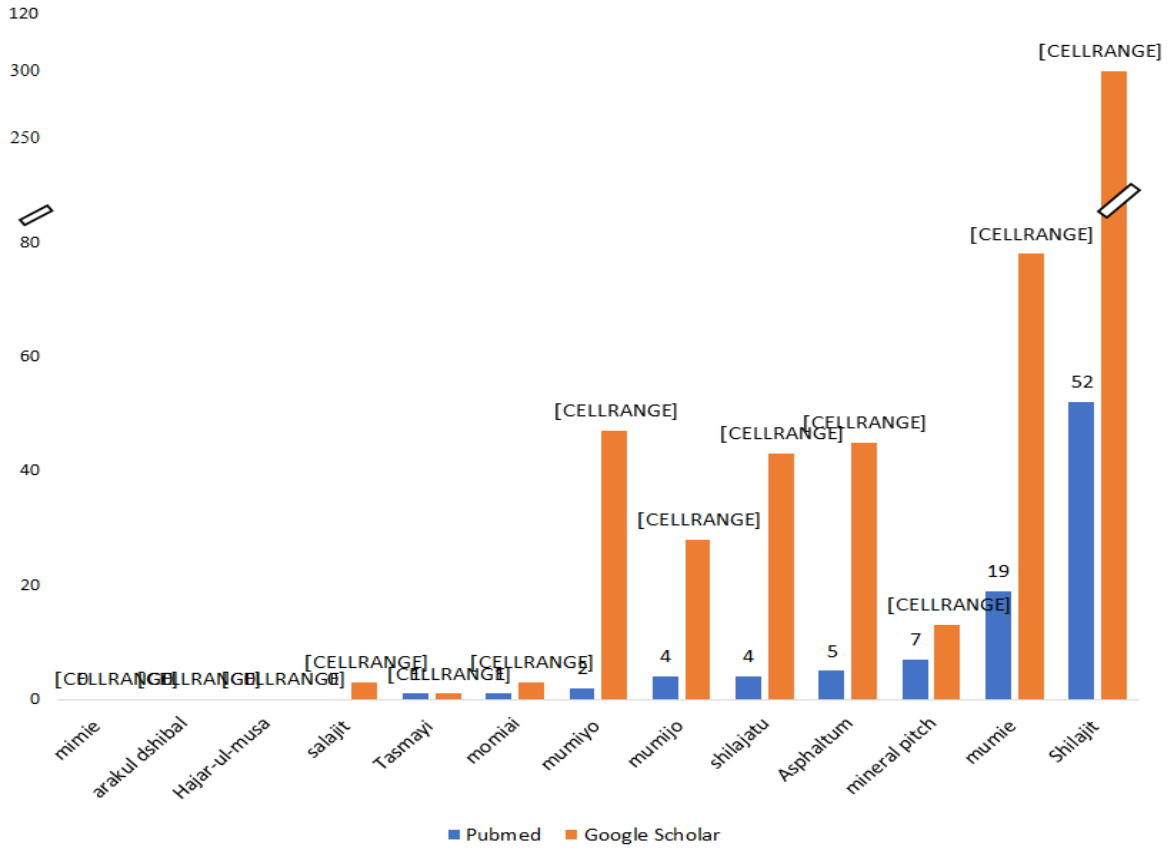

Figure 1. Shilajit with its alternative names used in publications in PubMed and Google Scholar revealed Shilajit as the most used name between 1963 and 2022. The number of publications for each name is shown on bars.

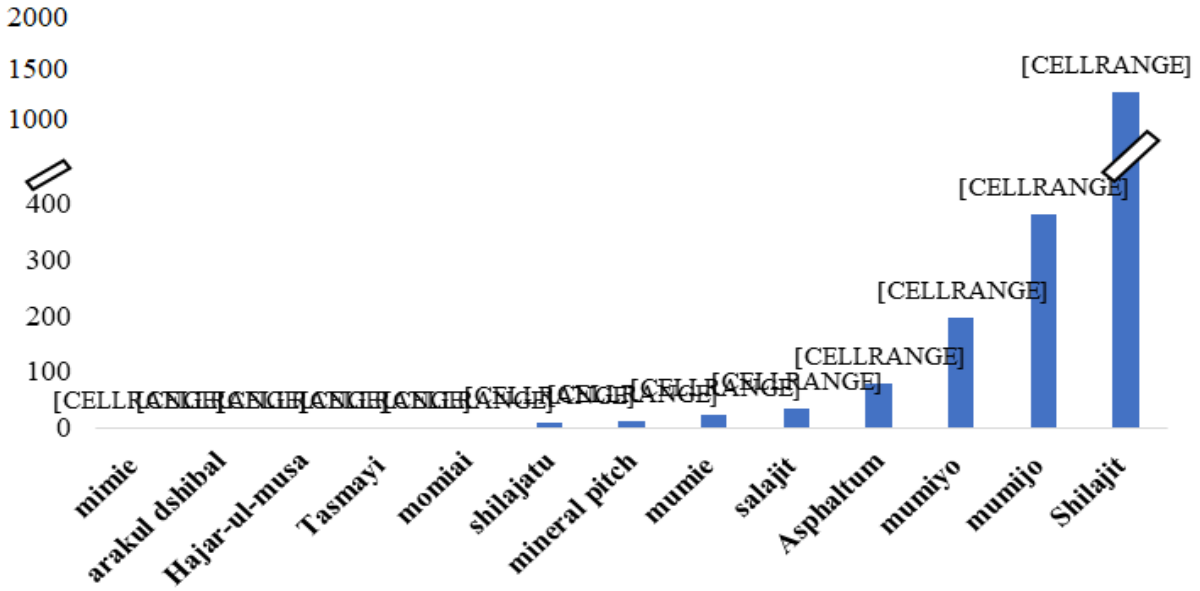

Figure 2. Shilajit with its alternative names in the description of products offered on 1-1-2023 on the online shopping site Ebay.com.

Shilajit is a black brown herbo-mineral material (Kanikkannan et al., 1995) extracted from rocks from the Himalaya mountains (C Velmurugan et al., 2012), different regions of the formerly Union of Soviet Socialist Republics, Nepal, Pakistan, Tibet, Afghanistan, and China, at altitudes of 1 t o 5 ki lometers (Ghosal et al., 1991; Khakimov, 1974). Shilajit is derived from Sanskrit, which means destroyer of weakness (Agarwal et al., 2007). It is a strong and very safe component, capable of managing several diseases (Carrasco-Gallardo et al., 2012). Its major pharmacological effects are attributed to its content of fulvic acid, humic acid, dibenzo-alpha-pyrones, and minerals (Mishra et al., 2019).

Shilajit is formed by the decomposition of pl ants by microorganisms, and it is rich in fulvic acid 60-80% (Carrasco-Gallardo et al., 2012), carotenoids (Wilson et al., 2011), potassium, calcium, and magnesium make up over 90% of t he total mineral content in Shilajit, sulfur, and sodium being the next most common minerals (Trivedi et al., 2004). According to its origin, it is classified as petroleum, animal, and plant, and it could be mixed (animal feces and plants) (Ding et al., 2020; Khakimov, 1974). Shilajit acts as an anti-oxidant, and anti-inflammatory (Stohs, 2014) due to its components; humic acid, fulvic acid, and fat-soluble components such as taxol, verbenol, α-pinene; therefore, it plays an important role in the management of diabetes (Ding et al., 2020). Many varieties of shilajit differ in their composition according to the geological nature of rocks, humidity, altitude, plant species involved, and local temperature. For example, Shilajit from India-Kumaon contains 21.4% of fulvic acid, while shilajit from Nepal contains 15.4%, Pakistan 15.5%, and Russia (19%). Also, they have different percentages of humic acid and other elements (Agarwal et al., 2007). There is an increase in interest in Shilajit's properties to heal different diseases worldwide with time, which is shown by many Shilajit publications in Google Scholar and PubMed database figures (3+4).

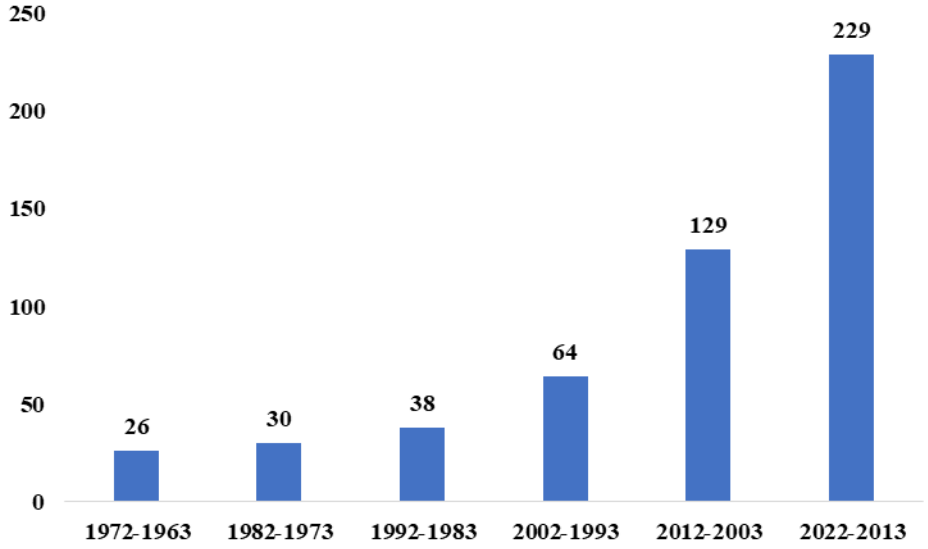

Figure 3. Increased interest in Shilajit healing properties for different diseases with time in publications in Google Scholar including academic and non-academic 516 publications between 1963 and 2022.

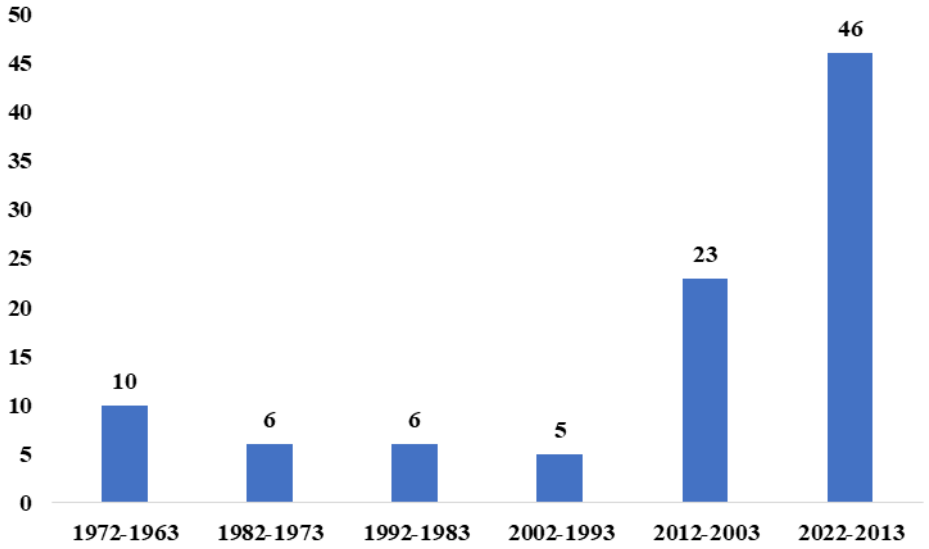

Figure 4. Increased interest in Shilajit healing properties for different diseases with time in published research papers in the PubMed database with 96 total publications between 1963-2022.

Shilajit has been used for both preventing and treating many ailments (such as diabetes, allergies, hypertension, loss of memory, immune dysfunction, arthritis, loss of libido, etc.) for more than 3000 years, indicating its powerful benefits and safety for its use in humans (Lawley et al., 2013). Diabetes involves the disruption of trace elements in the body, which can lead to increased oxidative stress, increased insulin resistance, and diabetes complications, in which Shilajit could be the richest natural product that contains these trace elements (Chandran et al., 2016). Shilajit should be used after purification and not exceed the daily recommended dose to prevent the toxicity of some molds (mycotoxins), heavy metals, polymeric quinones, and free radicals (Chopra & Chopra, 1994). Shilajit heavy metals (iron, zinc, chromium, manganese, cobalt, and lead) were determined and were at the allowed level as indicated by the World Health Organization (WHO) (Rahim et al., 2016). Purified Shilajit can be used safely in clinical research and practice (Agarwal et al., 2007; Stohs, 2014). It is used in clinical trials with 500 mg given daily for 56 days and with 1000 mg given daily for 30 days without any safety problems (Mishra et al., 2019). In another study, 20 healthy individuals received 2000 mg Shilajit capsules for 45 days without any systemic toxicity, with no significant effect on body weight, heart rate, blood pressure, glucose, urea, creatinine, uric acid, total protein albumin, and liver enzymes (Sharma et al., 2003). Shilajit safety in the long term as a dietary supplement was also revealed in animal studies, in which 24 Wistar rats (12 males and 12 females) were given 5000 mg/kg with water once daily for 91 days without any significant toxicity (C. Velmurugan et al., 2012). There are seventeen clinical trials registered in the World Health Organization on Shilajit with different diseases, three of them on diabetes between 2012-2021 without posting their results on their website (World Health Organization, 2023). In addition, there are six clinical trials registered in USA/National Institute of Health NIH/National Library of Medicine/Clinical Trials on Shilajit for different diseases, one of them on diabetes, without posting its results on their website (NIH, 2023).

Shilajit can be used commercially in many forms: resins, capsules, paste, tablets, drops, liquid, powder, oil, gummy, gel, balm, lotion, grains, and ointments. The most popular formulation offered commercially on the Ebay.com online shopping site on 1-1-2023 was resin form, as shown in figure 5.

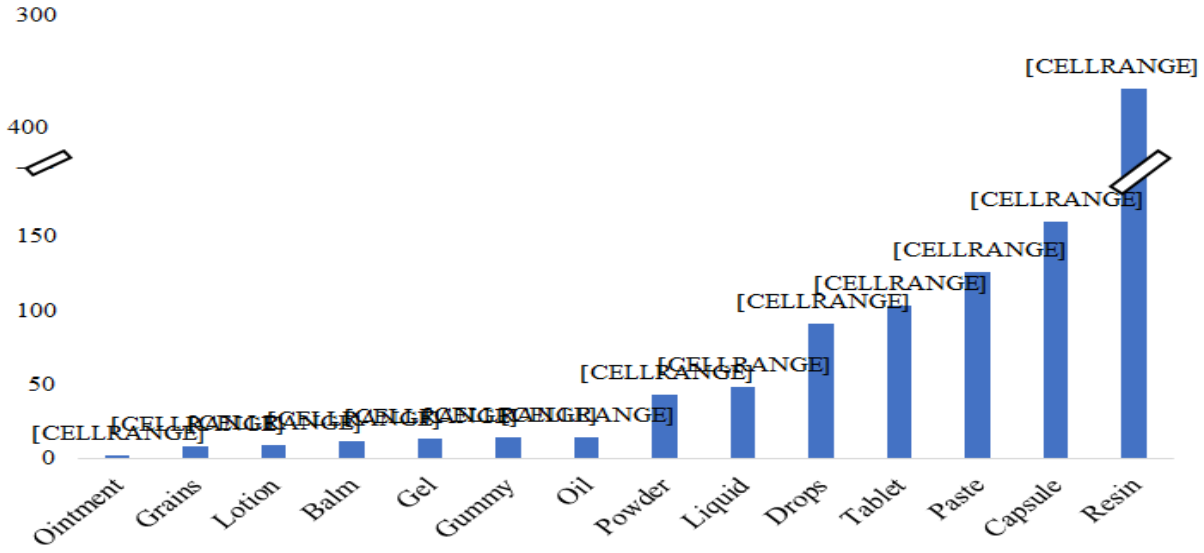

Figure 5. Different available formulations of Shilajit on Ebay.com. The most available formulation of Shilajit was the resin form offered in 1-1-2023.

4. Shilajit Studies

4.1. Shilajit studies on diabetes

Shilajit is a natural herbo-mineral product that offers a new promising approach to the long-term management of mature-onset diabetes because it appears to be beneficial and completely safe for Madhumeha treatment (type 2 diabetes mellitus) (Bihari et al., 2016). Although a variety of antidiabetic medications, such as oral hypoglycemic medications and various insulin preparations, are available for the treatment of diabetes, their long-term usage has several side effects, specifically hypoglycemia, which may lead to death. In addition, these drugs mitigate the hyperglycemia symptoms of diabetes and do not correct the underlying cause, which is the accumulation of lipids in the pancreas, liver, and muscles (Donath & Shoelson, 2011; Mirmiran et al., 2014). Besides its safety, Shilajit includes a wide range of components that reduce obesity, which is implicated in many diseases such as diabetes (Patil et al., 2022; Pattonder et al., 2011). In 2017, a clinical study of giving 500 mg of Shilajit capsule twice daily to forty-five patients for 3 months improved their hyperglycemia symptoms and significantly reduced their fasting glucose levels. There was a significant reduction in fast blood sugar and postprandial blood sugar by 24.01% and 20.23%, respectively. More than 75% of the patients had relief from polyuria, polyphagia, polydipsia, general weakness, and reduced libido (Gupta et al., 2016). In another study, 48 patients with type 2 diabetes received Vamana & Virechana (for 30 days) and 1000 mg Shilajit capsule twice a day before food with practicing Yoga for 60 days, showed that 29.1% of them improved markedly in hyperglycemia symptoms (polyuria, thirst, sweating,

constipation, tingling sensation, dyspnea, weakness, increased sleep, and appetite) with improvement in body weight, body mass index (BMI), cholesterol, LDL, triglycerides and decrease of 26-50 mg/dL in fast blood sugar (FBS) and postprandial blood sugar (PPBS). 20.8% of patients got moderate improvement in symptoms, body weight, BMI, and lipids and a decrease of 10-25 mg/dL in FBS and PPBS, and the rest were just like the control group (Raju & Sharma, 2016). Forty patients with type 2 diabetes received 250 mg Shilajit capsules twice a day for 12 weeks showed significant improvement in lipid profile, endothelial function, and cardiovascular parameters (Niranjan et al., 2016). In another study, thirty patients who received Shilajit showed a significant improvement in hyperglycemia symptoms (polyuria, polyphagia, polydipsia, weakness, FBS, PPBS) (Bihari et al., 2016). Capsules containing 250 mg of Shilajit extract and 250 mg of Ashwagandha (Withania somnifera) were administered with type 2 diabetes mellitus twice in the morning and evening to thirty-two patients significantly improved fasting blood sugar and lipid profile. Furthermore, in 18 of them (56%) hyperglycemia symptoms were improved (Upadhyay et al., 2009). In a study done in 2014, eighty-four diabetic patients, whereby a third of them received 500 mg Shilajit capsule twice a day with water after meal for three months, showed improved hyperglycemia symptoms (polyuria, polyphagia, polydipsia, weakness, cramps, loss of libido, joint pain, tingling sensation, hyperesthesia, numbness, hot and cold sensation, and burning sensation). Furthermore, Shilajit treatment significantly reduced their fasting blood sugar and postprandial sugar (Kumar et al., 2014).

Potassium, magnesium, and zinc are at lower concentrations in the skeletal muscles of diabetic patients compared to healthy controls (SJÖGREN et al., 1988). It has been shown in a clinical trial involving 7542 adults that potassium intake is inversely associated with abdominal obesity and fasting hyperglycemia (Shin et al., 2013). In another clinical trial, an increase in potassium intake in healthy individuals was involved in the increase of insulin secretion (Dluhy et al., 1972). Administration of magnesium in type 2 diabetes, improved insulin-mediated glucose uptake (Barbagallo et al., 2003). Zinc is important for the processing and storage of insulin (Chabosseau & Rutter, 2016). Chromium is an essential mineral for fat and carbohydrate metabolism. It has been shown in a recent metanalysis of 25 randomized controlled trials that consumption of chromium significantly reduced glycated hemoglobin (HbA1c), fasting blood sugar, triglycerides, and increased HDL levels (Suksomboon et al., 2014). Its deficiency led to diabetes in patients with long-term parenteral nutrition and the diabetes was resolved after chromium supplementation (Jeejeebhoy et al., 1977). Shilajit contains many trace elements including, chromium, potassium, magnesium, zinc, copper, iron, and many others (Mishra et al., 2019). Shilajit contains chromium, which is very important in carbohydrate and lipid metabolism and is recommended to be taken by diabetic patients; it increases insulin binding to its receptors; thus, it increases insulin sensitivity (Anderson, 2000). Taking a mixture of 12 herbs twice a day for 13 days in 10 diabetic patients, including Shilajit, significantly reduced the accumulative hemoglobin HbA1C (Pal & Shrivastav, 2020). In one of the studies, the chromium found in the average of two samples was approximately 0.005% (Rahim et al., 2016), in which a dose of 500 mg will contain 0.025 mg or 25 µg, which is considered adequate intake for healthy males and females (Russell et al., 2001).

In a recent study, fulvic acid in Shilajit acts as exercise; it increased metabolism, ATP consumption, and protection of mitochondrial membrane potential while decreasing insulin resistance, liver fat, and weight in high-fat diet-fed mice correcting glucose and insulin irregular levels. In the same study, fulvic acid increased ATP and glucose uptake in C2C12 muscle progenitor cells (Natsume et al., 2018). In another study in Wistar rats, Shilajit with a concentration of 200 mg/ kg was dissolved in normal saline administered orally for five weeks, showed considerable antioxidant capacity, and reduced the following: lipid levels, inflammation, and blood glucose by more than 50% compared to control, and even inhibited hemoglobin glycation better than insulin and the Glibenclamide drug (Vemuri et al., 2018). Furthermore, Shilajit prevented streptozotocin-induced degeneration of pancreatic beta cells. Diabetic albino rats received three doses of Shilajit (50, 100, 200 mg/kg/day orally), showed a significant reduction in blood glucose and a beneficial effect on the lipid profile (Trivedi et al., 2004). Giving 100 mg/kg Shilajit orally to streptozotocin-induced diabetic Wistar rats attenuated hyperglycemia, and significantly increased superoxide dismutase, which could protect the pancreatic beta cells from damage induced by oxidative stress (Bhattacharya, 1995). Injection of processed Shilajit (50 µg/Kg) simultaneously with insulin (0.25-1.0 U / kg) both subcutaneously, improved and extended the hypoglycemic effect of insulin on streptozotocin-induced diabetes in rats, while chronic administration of processed Shilajit (1.0 mg/kg twice a day intraperitoneally) prevented streptozotocin-induced diabetes in rats (Kanikkannan et al., 1995).

The underlying cause of diabetes is mainly associated with obesity, oxidative stress, and inflammation (Donath & Shoelson, 2011; Natsume et al., 2018). Shilajit has been shown to reduce all these factors involved in diabetes, which will be discussed below.

4.2. Shilajit studies on obesity

Obesity is one of the most prevalent public health problems associated with nutritional and clinical conditions; it is defined as the condition in which an excessive amount of fat is accumulated in the body (NICE & Care, 2006; Pattonder et al., 2011). Obesity can lead to insulin resistance, hypertension (Wilding et al., 2016). It is associated with a high risk of developing type 1 diabetes (Ferrara et al., 2017; Rewers & Ludvigsson, 2016), and type 2 diabetes (Verma & Hussain, 2017). Individuals with obesity and abdominal adiposity are at increased risk of hyperinsulinemia, insulin resistance, and diabetes (Warolin et al., 2014). Obesity is associated with an increased risk factor for several non-communicable diseases (Leitner et al., 2017). Recent evidence suggests that oxidative stress and inflammation may be the mechanistic link between obesity and related complications such as diabetes in obese patients, and antioxidant defenses are also lower in obese patients than their normal weight counterparts, and their levels inversely correlate with central adiposity (Gariballa et al., 2013). Obesity is also characterized by higher levels

of reactive oxygen or nitrogen species (Issa, 2016), while the first molecular link between obesity and inflammation, is the inflammatory cytokine tumor necrosis factor alpha (TNF-α), which is overexpressed in the adipose tissues (Ruan et al., 2002).

Shilajit increases metabolism and has an antioxidant effect on fat oxidation in various ways and can lower cholesterol levels in the blood (Saqib et al., 2016). Its main component, fulvic acid, contains supercharged antioxidants, superoxide dismutase, and free radical scavengers, all of which can aid fat metabolism (Narayanan & Kharkar, 2019). Fulvic acid and dibenzo-a-pyrones (DBP) present in Shilajit promotes cell division and increase metabolism (Stohs, 2014). Shilajit enhances and maintains cell function and its organelles, and also sustains cell energy by promoting ATP production (Bhattacharyya et al., 2009).

A mixture of Shilajit and Agnimantha (*Premna integrifolia*), a type of herb (250 mg), was given with warm Luke water orally twice a day before food to 32 patients for 45 days, significantly reduced obesity-accompanied signs (shortness of breath, sweating, overeating, heaviness in the body, thirsty, large abdomen, large breast, and weakness). Furthermore, this treatment was effective in reducing body weight, BMI, chest girth, abdomen girth, hip girth, mid-arm girth, and waist-to-hip ratio (Patil et al., 2022). Fifty-three obese patients were administered 500 mg capsule containing a mixture of Shilajit and Agnimantha (*Clerodendrum phlomidis* Linn.) twice a day for 10 weeks with Lukewarm water, significantly relieved signs accompanied obesity (pendulous movement of body parts, heaviness of the body, excessive perspiration, excessive thirst, bad body odor, excessive hunger, shortness of breath, lack of energy, hypersomnia, oily or greasy body, skin fold thickness, large organ measurements, and weakness). Furthermore, treatment significantly decreased BMI and weight (Pattonder et al., 2011). Seven patients received 500 mg of Shilajit capsule with 250 mg capsule of Khadir Ghana herb (*Acacia catechu*) and 500 mg of Kutaki herb capsule (*Picrorhiza kurroa*) for three months; significantly reduced their weight, BMI, waist circumference, hip circumference, and these parameters were reduced more when combined with regular exercise and a healthy diet in another 10 patients receiving the same herbs (Bhavna et al., 2013). Thirty-two diabetic patients with type 2 diabetes received a mixture of 250 mg Shilajit and 250 mg of Ashwagandha (*Withania somnifera*) twice a day for four weeks, significantly reduced cholesterol, LDL, VLDL, triglyceride, and increased HDL (Upadhyay et al., 2009). Two grams of purified Shilajit were administered to twenty normal medical students for 45 days, significantly reducing serum triglycerides, cholesterol, LDL, and VLDL, while improving HDL (Sharma et al., 2003).

Giving Shilajit of 200 mg/kg orally to streptozotocin-induced diabetic Wistar rats, significantly reduced triglyceride (TG), low-density lipoprotein (LDL), and very low-density lipoprotein (VLDL), while significantly increased high-density lipoprotein (HDL) (Vemuri et al., 2018). Ten male albino rats fed a high-fat diet containing 20% fat (hyperlipidemic rats) and received 200 mg/kg Shilajit orally for 8 weeks, significantly reduced their weight compared to the control (Saqib et al., 2016).

4.3. Shilajit studies on oxidative stress

Oxidative stress is defined as a ratio of highly reactive oxygen species (ROS) to antioxidants that is out of balance (Sies, 1997). Endogenous antioxidants such as glutathione (GSH) and superoxide dismutase (SOD) are outmatched when the cellular equilibrium swings towards greater ROS (Al-Shudiefat et al., 2013; Al-Shudiefat et al., 2022). Cellular dysfunction, lipid peroxidation, and cell death can lead to chronic inflammatory disorders that are associated with oxidative stress. It induces the synthesis of inflammatory mediators, which in turn increases the formation of reactive oxygen species (Giacco & Brownlee, 2010) and plays a key role in the progression of diabetes complications (Mathebula, 2018). Oxidative stress and activation of the JNK pathway are involved in the damage of pancreatic beta cells and therefore the etiology of type 1 and type 2 diabetes (Kaneto et al., 2007). Some of the consequences of oxidative stress are insulin resistance, beta-cell dysfunction, impaired glucose intolerance, and mitochondrial dysfunction which could lead to diabetes disease. Furthermore, oxidative stress can arise from lifestyle, disease, sleep deprivation, and high caloric intake (Rains & Jain, 2011).

Diabetes mellitus can contribute to increasing oxidative stress through the polyol pathway. The polyol pathway is based on a family of aldo-keto reductases that can use a wide range of carbonyl compounds as substrates and reduce them using nicotinic acid adenine dinucleotide phosphate (NADPH) to each other's sugar alcohols (polyols) (Yan, 2018). The enzyme aldose reductase converts glucose to sorbitol, which is then oxidized to fructose by the enzyme sorbitol dehydrogenase (SDH) with NAD as a cofactor (Mathebula, 2018). The original conversion of glucose to sorbitol leads to lower levels of NADPH, which is required as a cofactor for glutathione reductase to keep the levels of reduced glutathione (GSH), a key cellular antioxidant, within safe limits (Yan, 2018). Decreased GSH levels can lead to an increase in reactive oxygen species, which can contribute to oxidative stress (Jawaid et al., 2020). Fulvic acid coming from the humic substance of Shilajit helps in reducing free radicals which can protect the pancreatic beta cells that produce insulin from damage (Bastaki, 2005).

Sixty postmenopausal women received 500 mg of Shilajit extract for 48 weeks, significantly decreased oxidative stress (decreased malondialdehyde (MDA)), and significantly increased glutathione compared to placebo (Pingali & Nutalapati, 2022). Sixty-one diabetic patients received 500 mg Shilajit capsules twice a day for 30 days, significantly decreased oxidative stress (decrease in malondialdehyde), and significantly increased catalase (Saxena et al., 2003). Twenty normal volunteers received 2 grams of Shilajit for 45 days, significantly increased superoxide dismutase, vitamin E, and vitamin C (Sharma et al., 2003).

Shilajit administered at a dose of 800 mg/kg in Sprague Dawley rats for two weeks, significantly increased glutathione, glutathione peroxidase, catalase, and superoxide dismutase, while significantly decreased oxidative stress (MDA) (Derhami et al., 2022). Shilajit 250 mg/kg administration to Wistar rats ameliorated acetaminophen, increased hepatic damage parameters including alanine amino transferase, aspartate aminotransferase, gamma glutamine transferase, nitric

oxide, oxidative stress, and it significantly improved glutathione peroxidase (Atashbar et al., 2018). Shilajit increased total antioxidant capacity by 97%, superoxide radical scavenging activity, and hydroxyl radical scavenging activity, whereas, it inhibited streptozotocin-induced hemoglobin glycation in Wistar rats (Vemuri et al., 2018). Rats received processed Shilajit 50 mg/kg i.p. for 21 days, led to an increase of superoxide dismutase, catalase, and glutathione peroxidase in the frontal cortex and striatum and prevented methyl methacrylate-induced oxidative stress (Bhattacharya et al., 1995).

4.4. Shilajit studies on inflammation

Lipid accumulation, inflammation, and diabetes are intricately linked, and a growing body of evidence suggests that inflammation plays a critical role in the pathogenesis of type 2 diabetes. Lipid accumulation, particularly in adipose tissue and the liver, can trigger an inflammatory response that can contribute to the development of insulin resistance and ultimately lead to the onset of diabetes (Hotamisligil, 2017).

Adipose tissue is a key site for lipid accumulation in the body, and obesity is associated with chronic low-grade inflammation of adipose tissue, characterized by the infiltration of immune cells such as macrophages (Gregor & Hotamisligil, 2011). These immune cells produce pro-inflammatory cytokines, including tumor necrosis factor-alpha (TNF-α), interleukin-6 (IL-6), and interleukin-1 beta (IL-1β), which can activate inflammatory pathways such as the nuclear factor-kappa B (NF-κB) pathway, ultimately leading to the production of more cytokines and the recruitment of more immune cells (Shoelson, 2006). The chronic low-grade inflammation that accompanies lipid accumulation can promote insulin resistance by impairing insulin signaling and promoting the breakdown of insulin-sensitive tissues. Furthermore, inflammation can interfere with the normal functioning of adipose tissue, resulting in the release of free fatty acids into the bloodstream and the accumulation of toxic lipid metabolites in organs such as the liver, muscle, and pancreas, all of which can further exacerbate insulin resistance and ultimately lead to the onset of diabetes (Tilg & Moschen, 2008).

Several lines of evidence support the role of inflammation in the development of insulin resistance and diabetes. For example, in a study of obese and non-obese individuals, the obese group had higher levels of pro-inflammatory cytokines such as IL-6 and C-reactive protein (CRP), which were positively correlated with insulin resistance (Kern et al., 2001).

Inflammation has been shown to play an important role in the pathogenesis of diabetes through IKKβ pathway, since inhibition of this pathway by giving sodium salicylate and aspirin, which are used in rheumatic fever and rheumatoid arthritis as anti-inflammatory agents, can reverse insulin resistance and decrease hyperglycemia (Yuan et al., 2001). This was proved by administering aspirin 7 g/day to nine patients with type 2 diabetes for two weeks, which resulted in a decrease in fasting plasma, triglycerides, total cholesterol, and C-reactive protein (an indicator of inflammation) and insulin clearance (Hundal et al., 2002). In type 1 diabetes mellitus, beta cells are suggested to fail due to the response to inflammatory apoptosis resulting from the secretion of IF N-gamma controlled by the PTPN2 gene (Moore et al., 2009). Inflammatory cytokines such as IL-6 have been shown to stimulate apoptosis in beta-pancreatic cells and act as a predictor of the progression of type 2 diabetes (Pradhan et al., 2001). There is a link between the inflammatory TNF-alpha cytokine and insulin resistance, obesity, and beta cell inflammation, and its overexpression led to beta cell death and insulin resistance (Pradhan et al., 2001; Ruan et al., 2002).

Sixty postmenopausal women received 500 mg of Shilajit for 48 weeks, significantly decreased the inflammatory protein hsCRP (Pingali & Nutalapati, 2022). Shilajit was shown to protect against acetaminophen-induced liver injury in rats and significantly reduced the inflammatory cytokines IL-6, IL-1β and TNF-α (Firozsalari et al.). Shilajit administered at a dose of 200 mg/kg.bw to streptozotocin-induced diabetic rats, reduced the expression of inducible nitric oxide synthase (iNOS) proinflammatory gene in pancreatic tissue (Vemuri et al., 2018). Oxidative stress and inflammation are implicated in the pathogenesis of obesity (Savini et al., 2013). Oxidative stress stimulates the production of inflammatory mediators (Pattonder et al., 2011), while fulvic acid decreases proinflammatory markers (Giacco & Brownlee, 2010). Fulvic acid could prevent chronic inflammatory diseases, including diabetes, by reducing the release of proinflammatory mediators from cells (Koya et al., 2003). Fulvic acid acts as an immune modulator and influences the redox state (Sharma et al., 2003). Shilajit at a concentration of 50 mg/kg i.p. showed significant anti-inflammatory effects against carrageenan-induced pedal edema in rats (Goel et al., 1990).

In summary, Shilajit can reduce the risk factors (obesity, insulin resistance, inflammation, oxidative stress) that can lead to diabetes in normal people, while at the same time, it could reverse or ameliorate type 2 diabetes mellitus and prevent its progression to fatal complications, as shown in figure (6).

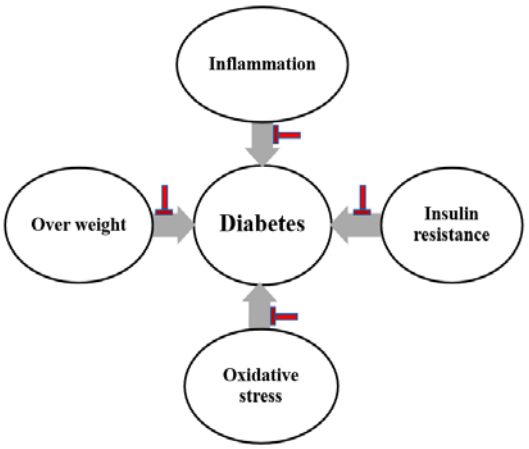

Figure 6. Possible mechanisms by which Shilajit could prevent, reverse diabetes, or ameliorate its symptoms and its complications.

4.5. Shilajit studies on other diseases and conditions

In addition to Shilajit benefits for diabetes (Gupta et al., 2016; Raju & Sharma, 2016), it can also be beneficial for other diseases and conditions, including insulin resistance (Gupta, 1966; Kanikkannan et al., 1995), obesity (Patil et al., 2022; Pattonder et al., 2011), inflammation (Firozsalari et al.; Pingali & Nutalapati, 2022), oxidative stress

(Atashbar et al., 2018; Derhami et al., 2022), arthritis (Azizi et al., 2018; Lawley et al., 2013), cancer (Kloskowski et al., 2021; Pant et al., 2012), bone health (Cesur et al., 2019; Labban, 2013), allergy (Ghosal et al., 1989; Sadeghi et al., 2020), mental health (Jaiswal & Bhattacharya, 1992; Khaksari et al., 2013), immune system (Bižanov et al., 2012; Musthafa et al., 2018), increased energy (Bhattacharyya et al., 2009; Stohs et al., 2017), adaptogenic (Agarwal et al., 2007; Bansal & Banerjee, 2016), antiaging and rejuvenating (Ghosal, 1990; Wilson et al., 2011), and for sexual health (Ikram-ul-Haq et al., 2016; NİZAM & SELÇUK, 2021). These benefits are shown in table 2.

Table 2. Some diseases/ conditions in which Shilajit used.

Diseases/conditions	Research Reference/(s)
Diabetes	(Gupta et al., 2016; Raju & Sharma, 2016)
Insulin resistance	(Ghezelbash et al., 2022; Kanikkannan et al., 1995)
Obesity	(Patil et al., 2022; Pattonder et al., 2011)
Inflammation	(Firozsalari et al.; Pingali & Nutalapati, 2022)
Oxidative stress	(Atashbar et al., 2018; Derhami et al., 2022)
Arthritis	(Azizi et al., 2018; Lawley et al., 2013)
Cancer	(Kloskowski et al., 2021; Pant et al., 2012)
Bone health	(Cesur et al., 2019; Labban, 2013)
Allergy	(Ghosal et al., 1989)
Mental health	(Jaiswal & Bhattacharya, 1992)
Immune system	(Bižanov et al., 2012; Musthafa et al., 2018)
Increase Energy	(Bhattacharyya et al., 2009; Stohs et al., 2017)
Adaptogenic (adapt to stress)	(Agarwal et al., 2007; Bansal & Banerjee, 2016)
Anti-aging and rejuvenator	(Ghosal, 1990; Wilson et al., 2011)
Sexual health	(Ikram-ul-Haq et al., 2016; NİZAM & SELÇUK, 2021)

* Please note that studies include animals and humans

5. Discussion

Diabetes is a major problem worldwide with high mortality and morbidity rates. Although there are many medications developed for the management of diabetes, they have many side effects, and the most common one is hypoglycemia which could be life-threatening. Some diabetes medications' side effects are shown in table 1. In addition to their side effects, these medications only treat hypoglycemia symptoms and do not address the root cause of diabetes, which is obesity and the accumulation of lipids in vital organs such as the pancreas, liver, and muscles (Donath & Shoelson, 2011; Natsume et al., 2018). Therefore, there is a need for a natural remedy for diabetes, which is safe for the long term and with fewer side effects. Shilajit is a natural exudate that occurs by the decomposition of residues of plants and animals in high-altitude rock mountains and has been used for thousands of years in traditional medicine for several diseases including diabetes (Lawley et al., 2013). Furthermore, several studies in humans and animals revealed its safety as a nutritional supplement for a long period (Mishra et al., 2019). There is an increase in interest in Shilajit research and in the commercial use of it for different diseases over time, which is obvious form the number of publications in Google Scholar, the PubMed database, and the Shilajit products offered in E-bay.com figures (1-4). For commercial use, we first looked at three big online companies including www.E-bay.com, www.Amazon.com, and www.Alibaba.com; because they are large online retailers, and it was easy to search for certain products on their websites. Because the products of Shilajit offered were the largest on E-bay.com compared to the other two companies, we decided to use E-bay website to reveal people interest in Shilajit products. Commercially, Shilajit is used in many formulations, in which resin is the most formulation offered in Ebay as shown in figure 5.

It is suggested that Shilajit's antidiabetic activity is through increasing numbers of beta cells in the pancreas (Gupta, 1966), increasing insulin sensitivity, increasing metabolism, or could be through decreasing hyperglycemia, obesity, oxidative stress, and inflammation (Natsume et al., 2018; Winkler & Ghosh, 2018), Therefore, Shilajit can reverse, heal, and ameliorate diabetes root cause (Figure 6). Moreover, Shilajit contains chromium and can decrease the glycation of hemoglobin, which is important for combatting diabetes (Jeejeebhoy et al., 1977; Pal & Shrivastav, 2020). Besides that, fulvic acid of Shilajit acts as exercise by increasing metabolism and ATP consumption, and protecting mitochondrial membrane potential, which is important for correcting levels of insulin and glucose in the blood (Natsume et al., 2018). Shilajit also acts as an exercise by increasing metabolism, and it contains minerals essential for glucose metabolism such as chromium. Shilajit is used for other conditions other than diabetes; it is used for insulin resistance, obesity, inflammation, oxidative stress, arthritis, cancer, allergy, mental health, immune system, increased energy, adaptogenic, antiaging, and for sexual health as shown in (table 2).

The most challenging part of this investigation was that Shilajit has more than twenty names according to different languages (Wilson et al., 2011), and we searched for the most popular names to obtain this review. Another difficulty was that one of the Shilajit names (mumie) had the meaning of mummy in some languages and other languages means mom; therefore, translation of different articles was a big obstacle and to filtrate these results manually was a big headache. We also faced some difficulties dealing with some Ayurvedic (using natural products as medicine) terms that have either Sanskrit or Hindi language origin regarding herbs and symptoms in Indian Shilajit publications.

6. Conclusions

Although there are many medications used for diabetes mellitus, they have many side effects; the most common one is hypoglycemia which could threaten life. In addition, they are not addressing the root cause of diabetes, which is obesity. Shilajit is a natural product that is proved to be safe with fewer side effects and with anti-hyperglycemic, anti-obesity, anti-oxidative stress, and anti-inflammatory effects that may reverse or ameliorate diabetes and its

complications. Therefore, Shilajit could be used as an alternative to anti-diabetic drugs, which have some negative side effects. Moreover, Shilajit acts as an exercise effect by increasing metabolism, and it contains minerals important for gl ucose metabolism such as chromium, potassium, magnesium, and zinc. Furthermore, Shilajit is used for many diseases and conditions other than diabetes such as insulin resistance, obesity, inflammation, bone health, Allergy, mental health, immune system, increase energy, adaptogenic, antiaging, rejuvenator, and for sexual health, and many others.

Since the current Shilajit research on di abetes has promising results, more animals and clinical trials are warranted to explore Shilajit mechanisms and benefits in diabetic patients. From these studies, exact recommendations on t he doses that could be taken for patients within the permissible level could be achieved with the most beneficial outcomes.

Author Contributions

writing - original draft preparation A.A.; writing—review and editing, A.A., J.A. All authors have read and agreed to the published version of the manuscript.

Funding

This research received no external funding.

Institutional Review Board Statement

Not applicable.

Informed Consent Statement

Not applicable.

Data Availability Statement

Data is contained within this review manuscript.

Conflicts of Interest

The authors declare no conflict of interest.

References

Agarwal, S. P., Khanna, R., Karmarkar, R., Anwer, M. K ., & Khar, R. K. (2007). Shilajit: a review. *Phytother. Res.*, *21*(5), 401-405.

Al-Shudiefat, A. A.-R. S., Alzyoud, J. A., Al Najjar, S. A., Talat, S., Bustanji, Y., & Abu-Irmaileh, B. (2022). The effects of some natural products compared to synthetic products on the metabolic activity, proliferation, viability, migration, and wound healing in sheep tenocytes. *Saudi J. Biol. Sci.*, *29*(9), 103391.

Al-Shudiefat, A. A. R., Sharma, A. K., Bagchi, A. K., Dhingra, S., & Singal, P. K. (2013). Oleic acid mitigates TNF-α-induced oxidative stress in rat cardiomyocytes. *Mol. Cell. Biochem.*, *372*(1), 75-82.

Al-Shudiefat, A. A. R., Ludke, A., Malik, A., Jassal, D. S., Bagchi, A. K., & Singal, P. K. (2022). Olive oil protects against progression of heart failure by inhibiting remodeling of heart subsequent to myocardial infarction in rats. *Physiol. Rep.*, *10*(15), e15379.

Anderson, R. A. (2000). Chromium in the prevention and control of diabetes. *Diabetes Metab.*, *26*(1), 22-28.

Asmat, U., Abad, K., & Ismail, K. (2016). Diabetes mellitus and oxidative stress—A concise review. *Saudi Pharm J., 24*(5), 547-553.

Atashbar, J., Shahrokhi, N., Khaksari Haddad, M., Asadi Karam, G., Shahrokhi, N., & Ghazi, F. (2018). Mumijo Protection gainst Acetaminophen-Induced Acute Hepatic Injury: Role of Oxidative Stress. *J Kerman Uni Med Sci*, *25*(1), 44-56.

Atlas, D. (2019). IDF diabetes atlas. *International Diabetes Federation (9th editio). Retrieved from http://www. idf. org/about-diabetes/facts-figures*.

Azizi, S., Kheirandiah, R., Azari, O., & Torabi, N. (2018). Potential pharmaceutic effect of Shilajit (mumie) on experimental osteoarthritis in rat. *Comp Clin Path.*, *27*(3), 755-764.

Azoulay, L., & Suissa, S. (2017). Sulfonylureas and the risks of cardiovascular events and death: a methodological meta-regression analysis of the observational studies. *Diabetes Care*, *40*(5), 706-714.

Bansal, P., & Banerjee, S. (2016). Effect of withinia somnifera and shilajit on alcohol addiction in mice. *Pharmacogn Mag.*, *12*(Suppl 2), S121.

Barbagallo, M., Dominguez, L. J., Galioto, A., Ferlisi, A., Cani, C., Malfa, L., Pineo, A., & Paolisso, G. (2003). Role of magnesium in insulin action, diabetes and cardio-metabolic syndrome X. *Mol. Aspects Med.*, *24*(1-3), 39-52.

Basit, A., Hydrie, M. Z. I ., Hakeem, R., Ahmedani, M. Y ., & Masood, Q. (2004). Frequency of chronic complications of type 2 diabetes. *J. Coll. Physicians Surg. Pak.*, *14*(2), 79-83.

Bastaki, A. (2005). Diabetes mellitus and its treatment. *Int. J. Diabetes Metab., 13*(3), 111.

Bhattacharya, S. K. (1995). Shilajit attenuates streptozotocin induced diabetes mellitus and decrease in pancreatic islet superoxide dismutase activity in rats. *Phytother. Res.*, *9*(1), 41-44.

Bhattacharya, S. K., Sen, A. P., & Ghosal, S. (1995). Effects of shilajit on biogenic free radicals. *Phytother. Res.*, *9*(1), 56-59.

Bhattacharyya, S., Pal, D., Gupta, A. K., Ganguly, P., Majumder, U. K., & Ghosal, S. (2009). Beneficial effect of processed shilajit on swimming exercise induced impaired energy status of mice. *Pharmacologyonline*, *1*, 817-825.

Bhavna, S., Sujatha, N., Sharma, M., & Upadhyaya, S. (2013). Clinical evaluation of Shilajatu (Asphaltum punjabinum), Kutaki (Picrorhiza kurroa) and Khadir (Acacia catechu) in the management of Sthaulya (obesity). *Int. J. Ayurveda Pharma Res. (IJRAP)*, *4*(4), 503-506.

Bihari, T. A., Nitin, M., Nikhil, M., & Poonam, G. (2016). ROLE OF SHILAJIT IN THE MANAGEMENT OF MADHUMEHA wsr to DIABETES MELLITUS. *Int. Ayurvedic Med. J.*, *4*(4).

Billington, E. O., Grey, A., & Bolland, M. J. (2015). The effect of thiazolidinediones on bone mineral density and bone turnover: systematic review and meta-analysis. *Diabetologia*, *58*(10), 2238-2246.

Bižanov, G., Barinova, N., & Jonauskienė, I. (2012). Experimental immunology Adjuvant effect of Shilajit and plant extracts on the immune responses to bovine serum albumin in hens. *Cent Eur J Immunol.*, *37*(2), 91-95.

Bolen, S., Feldman, L., V assy, J., Wilson, L., Yeh, H.-C., Marinopoulos, S., Wiley, C., Selvin, E., Wilson, R., & Bass, E. B. (2007). Systematic review: comparative effectiveness and safety of oral medications for type 2 diabetes mellitus. *Ann. Intern. Med.*, *147*(6), 386-399.

Carrasco-Gallardo, C., Guzmán, L., & Maccioni, R. B. (2012). Shilajit: a n atural phytocomplex with potential procognitive activity. *Int J Alzheimers Dis*, *2012*. 2012: 674142.

Cesur, M. G., Ogrenim, G., Gulle, K., Sirin, F. B., Akpolat, M., & Cesur, G. (2019). Does Shilajit Have An Effect On New B one Remodelling In The Rapid Maxillary Expansion Treatment? A Biochemical, Histopathological And Immunohistochemical Study. *Sdü Tıp Fakültesi Dergisi*, *26*(1), 96-103.

Chabosseau, P., & Rutter, G. A. (2016). Zinc and diabetes. *Arch. Biochem. Biophys.*, *611*, 79-85.

CHANDRA, K., SINGH, P., DWIVEDI, S., & Jain, S. (2019). Diabetes Mellitus and Oxidative Stress: A C o-relative and Therapeutic Approach. *J. Clin. Diagnostic Res., 13*(5).

Chandran, S., Patgiri, B., & Dharmarajan, P. (2016). Shilajatu and Swarna Makshika–A promising ayurvedic combination in the management of Madumeha (Diabetes). *J. Ayurvedic Herb. Med.*, *2*(3), 96-99.

Chantelau, E., S praul, M., Mühlhauser, I., Gause, R., & Berger, M. (1989). Long-term safety, efficacy and side-effects of continuous subcutaneous insulin infusion treatment for type 1 (insulin-dependent) diabetes mellitus: a o ne centre experience. *Diabetologia*, *32*(7), 421-426.

Chopra, R. N., & Chopra, I. C . (1994). *Indig. drugs of India*. Academic publishers.

Confederat, L., Ștefan, R., Lupașcu, F., Constantin, S., Avram, I., Doloca, A., & Profire, L. (2016). Side effects induced by hypoglycaemic sulfonylureas to diabetic patients-a retrospective study. *Farmacia*, *64*(5), 674-679.

Cox, M. E., & Edelman, D. (2009). Tests for screening and diagnosis of type 2 diabetes. *Clin. Diabetes*, *27*(4), 132-138.

Cusick, M., Meleth, A. D., Agrón, E., Fisher, M. R., Reed, G. F., Knatterud, G. L., Barton, F. B., Davis, M. D., Ferris III, F. L., & Chew, E. Y. (2005). Associations of mortality and diabetes complications in patients with type 1 and type 2 diabetes: early treatment diabetic retinopathy study report no. 27. *Diabetes Care*, *28*(3), 617-625.

DeFronzo, R., Fleming, G. A., Chen, K., & Bicsak, T. A. (2016). Metformin-associated lactic acidosis: Current perspectives on causes and risk. *Metab.*, *65*(2), 20-29.

Derhami, A., Rajabi, S., Rad, G. H., & Jafari, F. (2022). The Effect of Shilajit on Carboplatin-induced Thrombocytopenia and Oxidative Stress in Rats. *J. Pharm. Negat.*, 621-625.

DiMeglio, L. A., Evans-Molina, C., & Oram, R. A. (2018). Type 1 diabetes. *The Lancet*, *391*(10138), 2449-2462.

Ding, R., Zhao, M., Fan, J., Hu, X., Wang, M., Zhong, S., & Gu, R. (2020). Mechanisms of generation and exudation of Tibetan medicine Shilajit (Zhaxun). *Chin. Med.*, *15*(1), 1-15.

Dluhy, R. G., Axelrod, L., & Williams, G. H. (1972). Serum immunoreactive insulin and growth hormone response to potassium infusion in normal man. *J. Appl. Physiol.*, *33*(1), 22-26.

Donath, M. Y., & Shoelson, S. E. (2011). Type 2 diabetes as an inflammatory disease. *Nat. Rev. Immunol.*

, *11*(2), 98-107.

Donnan, J. R., Grandy, C. A., Chibrikov, E., Marra, C. A., Aubrey-Bassler, K., Johnston, K., Swab, M., Hache, J., Curnew, D., & Nguyen, H. (2019). Comparative safety of the sodium glucose co-transporter 2 (SGLT2) inhibitors: a systematic review and meta-analysis. *BMJ open*, *9*(1), e022577.

Duong, J. K., Furlong, T. J ., Roberts, D. M., Graham, G. G., Greenfield, J. R., Williams, K. M., & Day, R. O. (2013). The role of metformin in metformin-associated lactic acid osis (MALA): case series and formulation of a model of pathogenesis. *Drug Saf.*, *36*(9), 733-746.

Eff, A. R. Y., Rahayu, S. T., WM, P. G. M., & Lena, A. P. (2020). Antihypertensive, Antidiabetic and CytotoxicActivities of Indonesian Traditional Medicine. *Curr. trends. biotechnol. pharm.* 12(6)Suppl: 1623-1629.

Farley-Hills, E., Sivasankar, R., & Martin, M. (2004). Fatal liver failure associated with pioglitazone. *Bmj*, *329*(7463), 429.

FDA. (2015). *FDA revises labels of SGLT2 inhibitors for diabetes to include warnings about too much acid in the blood and serious urinary tract infections*. FDA. Retrieved 7-12-2022 from https://www.fda.gov/drugs/drug-safety-and-availability/fda-revises-labels-sglt2-inhibitors-diabetes-include-warnings-about-too-much-acid-blood-and-serious

Ferrara, C. T., Geyer, S. M., Liu, Y.-F., Evans-Molina, C., Libman, I. M., Besser, R., Becker, D. J., Rodriguez, H., Moran, A., & Gitelman, S. E. (2017). Excess BMI in childhood: a modifiable risk factor for type 1 diabetes development? *Diabetes Care*, *40*(5), 698-701.

Firozsalari, F. G., Shahrokhi, N., Hadad, M. K., Asadikaram, G., & Atashbar, J. (2018). Effect of Shilajit on the Levels of Pro-inflammatory and Anti-inflammation Cytokines in Hepatic Injury in Male Rats. *J Mazandaran Univ Med Sci;* 28 (159) :1-13.

Floyd, J. S., Barbehenn, E., Lu rie, P., & Wolfe, S. M. (2009). Case series of liver failure associated with rosiglitazone and pioglitazone. *Pharmacoepidemiol. Drug Saf.*, *18*(12), 1238-1243.

Gariballa, S., Afandi, B., AbuHaltem, M., Yassin, J., Habib, H., & Ibrahim, W. (2013). Oxidative damage and inflammation in obese diabetic Emirati subjects supplemented with antioxidants and B-vitamins: a r andomized placebo-controlled trail. *Nutr. Metab.*, *10*(1), 1-7.

Ghezelbash, B., Shahrokhi, N., Khaksari, M., Asadikaram, G., Shahrokhi, M., & Shirazpour, S. (2022). Protective Roles of Shilajit in Modulating Resistin, Adiponectin, and Cytokines in Rats with Non-alcoholic Fatty Liver Disease. *Chin. J. Integr. Med.*, *28*(6), 531-537.

Ghosal, S. (1990). Chemistry of shilajit, an immunomodulatory Ayurvedic rasayan. *Pure Appl. Chem.*, *62*(7), 1285-1288.

Ghosal, S., Lal, J., Singh, S. K., Dasgupta, G., Bhaduri, J., Mukhopadhyay, M., & Bhattacharya, S. K. (1989). Mast cell protecting effects of shilajit and its constituents. *Phytother. Res.*, *3*(6), 249-252.

Ghosal, S., Lal, J., Singh, S. K., Goel, R. K., Jaiswal, A. K., & Bhattacharya, S. K. (1991). The need for formulation of Shilajit by its isolated active constituents. *Phytother. Res.*, *5*(5), 211-216.

Giacco, F., & Brownlee, M. (2010). Oxidative stress and diabetic complications. *Circ Res.*, *107*(9), 1058-1070.

Gilbert, M. P., & Pratley, R. E. (2020). GLP-1 analogs and DPP-4 inhibitors in type 2 diabetes therapy: review of head-to-head clinical trials. *Front. Endocrinol.*, *11*, 178.

Goel, R., Banerjee, R., & Acharya, S. (1990). Antiulcerogenic and antiinflammatory studies with shilajit. *J. Ethnopharmacol.*, *29*(1), 95-103.

Gregor, M. F., & Hotamisligil, G. S. (2011). Inflammatory mechanisms in obesity. *Annu. Rev. Immunol.*, *29*, 415-445.

Gupta, S. (1966). Experimental Studies On Pituitary Diabetes. V. Effects Of Shilajit Ficus Bengalensis And Anterior Pituitary Extract On Glucose Tolerance In Rats. *Indian J. Med. Res.*, *54*(4), 354-&.

Gupta, V., Keshari, B. B., Tiwari, S., & Murthy, K. N. (2016). A comparative study of Shilajatu and Asanadi Ghana Vati in the management of Madhumeha wsr to type-2 diabetes mellitus. *Ayu*, *37*(2), 120.

Halim, M., & Halim, A. (2019). The effects of inflammation, aging and oxidative stress on the pathogenesis of diabetes mellitus (type 2 diabetes). *Diabetes Metab Syndr.*, *13*(2), 1165-1172.

Hameed, I., Masoodi, S. R., Mir, S. A., Nabi, M., Ghazanfar, K., & Ganai, B. A. (2015). Type 2 diabetes mellitus: from a metabolic disorder to an inflammatory condition. *World J. Diabetes*, *6*(4), 598.

Harding, J. L., Pavkov, M. E., Magliano, D. J., Shaw, J. E., & Gregg, E. W. (2019). Global trends in diabetes complications: a review of current evidence. *Diabetologia*, *62*(1), 3-16.

Hayes, M. R., Borner, T., & De Jonghe, B. C. (2021). The Role of GIP in the Regulation of GLP-1 Satiety and Nausea. *Diabetes*, *70*(9), 1956-1961.

Hemmingsen, B., Schroll, J. B., Wetterslev, J., Gluud, C., Vaag, A., Sonne, D. P., Lundstrøm, L. H., & Almdal, T. (2 014). Sulfonylurea versus metformin monotherapy in patients with type 2 diabetes: a C ochrane systematic review and meta-analysis of randomized clinical trials and trial sequential analysis. *Can. Med. Assoc. J.*, *2*(3), E162-E175.

Hernandez, A. V., Usmani, A., Rajamanickam, A., & Moheet, A. (2011). Thiazolidinediones and risk of heart failure in patients with or at high risk of type 2 diabetes mellitus. *Am. J. Cardiovasc. Drugs*, *11*(2), 115-128.

Holman, R. (2007). Metformin as first choice in oral diabetes treatment: the UKPDS experience. *Journ. Annu. Diabetol. Hotel Dieu*, 13-20.

Horii, T., Oikawa, Y., Kunisada, N., Shimada, A., & Atsuda, K. (2020). Real-world risk of hypoglycemia-related hospitalization in Japanese patients with type 2 diabetes using SGLT2 inhibitors: a nationwide cohort study. *BMJ Open Diabetes Res. and Care*, *8*(2), e001856.

Hotamisligil, G. S. (2017). Inflammation, metaflammation and immunometabolic disorders. *Nature*, *542*(7640), 177-185.

Hu, C., & Jia, W. (2019). Therapeutic medications against diabetes: what we have and what we expect. *Adv. Drug Del. Rev.*, *139*, 3-15.

Hundal, R. S., Petersen, K. F., Mayerson, A. B., Randhawa, P. S., Inzucchi, S., Shoelson, S. E., & Shulman, G. I. (2002). Mechanism by which high-dose aspirin improves glucose metabolism in type 2 diabetes. *J. Clin. Invest.*, *109*(10), 1321-1326.

Idris, I., Warren, G., & Donnelly, R. (2012). Association between thiazolidinedione treatment and risk of macular edema among patients with type 2 diabetes. *Arch. Intern. Med.*, *172*(13), 1005-1011.

Ikram-ul-Haq, M., Ahmad, M., Zubair, M., Gul, S. T., & Bashir, M. I. (2016). Effects of asphaltum (Shilajit) on scrotal circumference and semen quality parameters of adult Lohi rams. *J. Entomol. Zool. Stud.*, 4(2), 559-563

Iorga, R. A., Bacalbasa, N., Carsote, M., Bratu, O. G., Stanescu, A. M. A., Bungau, S., Pantis, C., & Diaconu, C. C. (2020). Metabolic and cardiovascular benefits of GLP-1 agonists, besides the hypoglycemic effect. *Exp. Ther. Med.*, *20*(3), 2396-2400.

Issa, N. (2016). Role of inflammation in the pathogenesis of insulin resistance in obesity: specific role of reactive oxygen and reactive nitrogen species. Ph.D. dissertation. Université Laval, Quebec, Canada.

Jaiswal, A. K., & Bhattacharya, S. (1992). Effects of Shilajit on memory, anxiety and brain monoamines in rats. *Indian J Pharmacol*, *24*(1), 12-17.

Jawaid, P., Rehman, M. U ., Zhao, Q.-L., Misawa, M., Ishikawa, K., Hori, M., Shimizu, T., Saitoh, J.-i., Noguchi, K., & Kondo, T. (2020). Small size gold nanoparticles enhance apoptosis-induced by cold atmospheric plasma via depletion of intracellular GSH and modification of oxidative stress. *Cell Death Discov.*, *6*(1), 83.

Jeejeebhoy, K., Chu, R., Marliss, E., Greenberg, G., & Bruce-Robertson, A. (1977). Chromium deficiency, glucose intolerance, and neuropathy reversed by chromium supplementation, in a patient receiving long-term total parenteral nutrition. *Am. J. Clin. Nutr.*, *30*(4), 531-538.

Kaiser, A. B., Zhang, N., & DER PLUIJM, W. V. (2018). Global prevalence of type 2 diabetes over the next ten years (2018-2028). *Diabetes*, *67*(Supplement_1).

Kaneto, H., Katakami, N., Kawamori, D., Miyatsuka, T., Sakamoto, K. y., Matsuoka, T.-A., Matsuhisa, M., & Yamasaki, Y. (2007). Involvement of oxidative stress in the pathogenesis of diabetes. *Antioxid. Redox Signal.*, *9*(3), 355-366.

Kanikkannan, N., Ramarao, P., & Ghosal, S. (1995). Shilajit-induced potentiation of the hypoglycaemic action of insulin and inhibition of streptozotocin induced diabetes in rat. *Phytother. Res.*, *9*(7), 478-481.

Kern, P. A., Ranganathan, S., Li, C., Wood, L., & Ranganathan, G. (2001). Adipose tissue tumor necrosis factor and interleukin-6 expression in human obesity and insulin resistance. *Am. J. Physiol. Endocrinol. Metabol.* 280 (5), E745-E751

Khakimov, Z. (1974). Mumie as a kind of natural resources and its signs. PhD dissertation. *Tashkent University. Tashkent,* Uzbekistan.

Khaksari, M., Mahmmodi, R., Shahrokhi, N., Shabani, M., Joukar, S., & Aqapour, M. (2013). The effects of shilajit on brain edema, intracranial pressure and neurologic outcomes following the traumatic brain injury in rat. *Iran. J. Basic Med. Sci.*, *16*(7), 858.

Kizaibek, M. (2013). [Research advances of Tasmayi]. *Zhongguo Zhong Yao Za Zhi*, *38*(3), 443-448.

Kloskowski, T., Szeliski, K., Krzeszowiak, K., Fekner, Z., Kazimierski, Ł., Jundziłł, A., Drewa, T., & Pokrywczyńska, M. (2021). Mumio (Shilajit) as a potential chemotherapeutic for the urinary bladder cancer treatment. Sci. Rep, *11*(1), 1-12.

Koya, D., Hayashi, K., Kitada, M., Kashiwagi, A., Kikkawa, R., & Haneda, M. (2003). Effects of antioxidants in diabetes-induced oxidative stress in the glomeruli of diabetic rats. *J. Am. Soc. Nephrol.*, *14*(suppl 3), S250-S253.

Kroon, L., & Zhou, C. (2021). Glinides. In: White, J. (Jr.) (Ed.),. **The 2021-22 Guide to Medications for the Treatment of Diabetes Mellitus.** American Diabetes Association. USA, pp.280-300.

Kumar, S., Singh, G., Pandey, A. K., & Singh, R. H. (2014). A clinical study on the Naimittika Rasayana effect of Silajatu and Mamajjaka in type-2 Diabetes Mellitus. *Ayu*, *35*(4), 404.

Kumthekar, A. A., Gidwani, H. V., & Kumthekar, A. B. (2012). Metformin associated B12 deficiency. *J. Assoc. Physicians India*, *60*(3), 58-59.

Labban, N. Y. (2013). Shilajit, a novel regulator of bone/cartilage healing. Ph.D. dissertation. Indiana University, Bloomington, USA.

Lawley, S., Gupta, R., Goad, J., Canerdy, T., & Kalidindi, S. (2013). Anti-inflammatory and anti-arthritic efficacy and safety of purified shilajit in moderately arthritic dogs. *J Vet Sci Anim Husb*, *1*(3), 302.

Leitner, D. R., Frühbeck, G., Yumuk, V., Schindler, K., Micic, D., Woodward, E., & Toplak, H. (2017). Obesity and type 2 diabetes: two diseases with a need for combined treatment strategies-EASO can lead the way. *Obes. Facts*, *10*(5), 483-492.

Li, X. J., Yu, Y. X., Liu, C. Q., Zhang, W., Zhang, H. J., Yan, B., Wang, L. Y., Yang, S. Y., & Zhang, S. H. (2011). Metformin vs thiazolidinediones for treatment of clinical, hormonal and metabolic characteristics of polycystic ovary syndrome: a meta-analysis. *Clin. Endocrinol. (Oxf.)*, *74*(3), 332-339.

Lv, W., Wang, X., Xu, Q., & Lu, W. (2020). Mechanisms and characteristics of sulfonylureas and glinides. *Curr. Top. Med. Chem.*, *20*(1), 37-56.

Mathebula, S. D. (2018). Biochemical changes in diabetic retinopathy triggered by hyperglycaemia: A review. *Afr. Vis. Eye Health.*, *77*(1), 1-7.

Middleton, T. L., Wong, J., Molyneaux, L., Brooks, B. A., Yue, D. K., Twigg, S. M., & Wu, T. (2017). Cardiac effects of sulfonylurea-related hypoglycemia. *Diabetes Care*, *40*(5), 663-670.

Mirmiran, P., Bahadoran, Z., & Azizi, F. (2014). Lipid accumulation product is associated with insulin resistance, lipid peroxidation, and systemic inflammation in type 2 diabetic patients. *Endocrinol. Metab.*, *29*(4), 443-449.

Mishra, T., Dhaliwal, H. S., Singh, K., & Singh, N. (2019). Shilajit (Mumie): Current Status of Biochemical, Therapeutic and Clinical Advances. *Curr. Nutr. Food Sci*., *15*(2), 104-120.

Moore, F., Colli, M. L., Cnop, M., Esteve, M. I., Cardozo, A. K., Cunha, D. A., Bugliani, M., Marchetti, P., & Eizirik, D. L. (2009). PTPN2, a candidate gene for type 1 diabetes, modulates interferon-γ–induced pancreatic β-cell apoptosis. *Diabetes*, *58*(6), 1283-1291.

Musthafa, M. S., Asgari, S. M., Elumalai, P., Hoseinifar, S. H., & Van Doan, H. (2018). Protective efficacy of Shilajit enriched diet on growth performance and immune resistance against Aeromonas hydrophila in Oreochromis mossambicus. *Fish Shellfish Immunol.*, *82*, 147-152.

Narayanan, V., & Kharkar, R. (2019). Fulvic acid–A natural and multifaceted approach to the management of inflammatory dermatosis. *Indian Pract.*, *72*, 28-31.

Natsume, C., Takanishi, M., Mizuno, K., Tei, Y., Tsujimura, S., Tanaka, K., & Fujita, T. 2018. Fulvic acid-induced mitochondrial membrane potential improves diabetic symptoms in mice. Proceedings for Annual Meeting of The Japanese Pharmacological Society WCP2018 (The 18th World Congress of Basic and Clinical Pharmacology), American Society for Pharmacology and Experimental Therapeutics. Kyoto, Japan.

Newman, D. J., & Cragg, G. M. (2020). Natural products as sources of new drugs over the nearly four decades from 01/1981 to 09/2019. *J. Nat. Prod*., *83*(3), 770-803.

NICE Centre for Public Health Excellence at NI CE (UK); National Collaborating Centre for Primary Care (UK). Obesity: The Prevention, Identification, Assessment and Management of Overweight and Obesity in Adults and Children [Internet]. London: National Institute for Health and Clinical Excellence (UK); 2006 Dec. PMID: 22497033.

NIH. (2023). *NIH U.S National Library of Medicine ClinicalTrial.gov*. Retrieved 1-1-2023 from https://www.clinicaltrials.gov/ct2/results?cond=&term=Shilajit&cntry=&state=&city=&dist=

Niranjan, K., Ramakanth, G., Fatima, N., & Usharani, P. (2016). Evaluation of the effect of purified aqueous extract of shilajit in modifying cardiovascular risk with special reference to endothelial dysfunction in patients with type 2 diabetes mellitus. *Int J Ayurveda Pharma Res*. 4(4):1-7.

NİZAM, M. Y., & SELÇUK, M. (2021). Evaluation of Rooster Semen Frozen With Shilajit Containing Extender. EDUVET International Veterinary Sciences Congress. *PROCEEDINGS BOOK*, pages 103-108. Istanbul, Turkey.

Oguntibeju, O. O. (2019). Type 2 diabetes mellitus, oxidative stress and inflammation: examining the links. *Int. J. Physiol. Pathophysiol. Pharmacol*., *11*(3), 45.

Pal, S., & Shrivastav, V. (2020). Yagya Therapy Treatment Reduced Blood Glucose Level in Diabetic Patients in 2 weeks-a Single Arm Study. *Interdiscip. j. yagya res*., *3*(1), 30-36.

Pant, K., Singh, B., & Thakur, N. (2012). Shilajit: a humic matter panacea for cancer. *Int. J. Toxicol. Pharmacol. Res.*.; 4(2): 17-25

Patil, R. S., Varghese, J., Pawar, J. P., Kurbet, R. G., & Pote, A. R. (2022). A Comparative Clinical Study to Evaluate the Efficacy of Gomutra Arka Bhavita Shilajatu and Agnimantha Bhavita Shilajatu in Sthaulya WSR To Obesity. *Res J Pharm Technol*., *15*(11), 5245-5249.

Pattonder, R. K., Chandola, H., & Vyas, S. (2011). Clinical efficacy of Shilajatu (Asphaltum) processed with Agnimantha (Clerodendrum phlomidis Linn.) in Sthaulya (obesity). *Ayu*, *32*(4), 526.

Payab, M., Hasani-Ranjbar, S., Shahbal, N., Qorbani, M., Aletaha, A., Haghi-Aminjan, H., Soltani, A., Khatami, F., Nikfar, S., & Hassani, S. (2020). Effect of the herbal medicines in obesity and metabolic syndrome: a systematic review and meta-analysis of clinical trials. *Phytother. Res.*, *34*(3), 526-545.

Piero, M., Nzaro, G., & Njagi, J. (2015). Diabetes mellitus-a devastating metabolic disorder. *Asian J. Biomed. Pharm. Sci.*, *5*(40), 1.

Pingali, U., & Nutalapati, C. (2022). Shilajit extract reduces oxidative stress, inflammation, and bone loss to dose-dependently preserve bone mineral density in postmenopausal women with osteopenia: A randomized, double-blind, placebo-controlled trial. *Phytomedicine*, *105*, 154334.

Pradhan, A. D., Manson, J. E., Rifai, N., Buring, J. E., & Ridker, P. M. (2001). C-reactive protein, interleukin 6, and risk of developing type 2 diabetes mellitus. *JAMA*, *286*(3), 327-334.

Rahim, M., Mohammadzai, I., Hassan, W., & Ahmad, N. (2016). Heavy metal profile of shilajit samples obtained from Gilgit and Chellas. *Pakistan. J. Phys. Sci*., *27*(2), 139.

Rains, J. L., & Jain, S. K. (2011). Oxidative stress, insulin signaling, and diabetes. Free Radic. Biol. Med., *50*(5), 567-575.

Raju, K. N., & Sharma, R. S. (2016). A Comparative Clinical Study of Vamana & Virechana with and without Shilajit Yoga in the Management of Madhumeha wsr to Type-2 Diabetes Mellitus. *AYUSHDHARA*., 3(4): 749763.

Ramachandran, A. (2014). Know the signs and symptoms of diabetes. *Indian J Med Res*, *140*(5), 579.

Rewers, M., & Ludvigsson, J. (2016). Environmental risk factors for type 1 diabetes. *The Lancet*, *387*(10035), 2340-2348.

Rizos, C. V., Elisaf, M., Mikhailidis, D. P., & Liberopoulos, E. N. (2009). How safe is the use of thiazolidinediones in clinical practice? *Expert Opin. Drug Saf.*, *8*(1), 15-32.

Ruan, H., Miles, P. D., Ladd, C. M., Ross, K., Golub, T. R., Olefsky, J. M., & Lodish, H. F. (2002). Profiling gene transcription in vivo reveals adipose tissue as an immediate target of tumor necrosis factor-α: implications for insulin resistance. *Diabetes*, *51*(11), 3176-3188.

Russell, R., Beard, J. L., Cousins, R. J., Dunn, J. T., Ferland, G., Hambidge, K., Lynch, S., Penland, J., Ross, A., & Stoecker, B. (2001). **Dietary reference intakes for vitamin A, vitamin K, arsenic, boron, chromium, copper, iodine, iron, manganese, molybdenum, nickel, silicon, vanadium, and zinc**. A report of the panel on micronutrients, subcommittees on upper reference levels of nutrients and of interpretation and uses of dietary reference intakes, and the standing committee on the scientific evaluation of dietary reference intakes food and nutrition board Institute of medicine,. Washington (DC): National Academies Press Washington DC.

Sadeghi, S. M. H., Hosseini Khameneh, S. M., Khodadoost, M., Hosseini Kasnavieh, S. M., Kamalinejad, M., Gachkar, L., Rampp, T., & Pasalar, M. (2020). Efficacy of momiai in tibia fracture repair: a randomized double-blinded placebo-controlled clinical trial. *J. Altern. Complement. Med.*, *26*(6), 521-528.

Saluja, M., Pareek, K., & Swami, Y. K. (2020). Study of Diversity of Metformin Related Gastrointestinal Side Effects. *J Assoc Physicians India. 68*(8), 36-38.

Salvo, F., Moore, N., Arnaud, M., Robinson, P., Raschi, E., De Ponti, F., Bégaud, B., & Pariente, A. (2016). Addition of dipeptidyl peptidase-4 inhibitors to sulphonylureas and risk of hypoglycaemia: systematic review and meta-analysis. *Bmj*, *353*.

Saqib, M., Malik, R., & Kausar, S. (2016). Effect of Shilajit on Obesity in Hyperlipidemic Albino Rats. *Pakistan J. Medical Health Sci*., *10*, 1019-1023.

Savini, I., Catani, M. V., Evangelista, D., Gasperi, V., & Avigliano, L. (2013). Obesity-associated oxidative stress: strategies finalized to improve redox state. *Int. J. Mol. Sci.*, *14*(5), 10497-10538.

Saxena, N., Dwivedi, U. N., Singh, R. K., Kumar, A., Saxena, C., Saxena, R. C., & Saxena, M. (2003). Modulation of oxidative and antioxidative status in diabetes by Asphaltum panjabinum. *Diabetes Care*, *26*(8), 2469-2470.

Scheen, A. J. (2019). An update on the safety of SGLT2 inhibitors. *Expert Opin. Drug Saf.*, *18*(4), 295-311.

Scirica, B. M., Bhatt, D. L., Braunwald, E., Steg, P. G., Davidson, J., Hirshberg, B., Ohman, P., Frederich, R., Wiviott, S. D., & Hoffman, E. B. (2013). Saxagliptin and cardiovascular outcomes in patients with type 2 diabetes mellitus. *N. Engl. J. Med.*, *369*(14), 1317-1326.

Sharma, P., Jha, J., Shrinivas, V., Dwivedi, L., S uresh, P., & Sinha, M. (2003). Shilajit: evalution of its effects on blood chemistry of normal human subjects. *Anc. Sci. Life*, *23*(2), 114.

Shin, D., Joh, H.-K., Kim, K. H., & Park, S. M. (2013). Benefits of potassium intake on metabolic syndrome: The fourth Korean National Health and Nutrition Examination Survey (KNHANES IV). *Atherosclerosis*, *230*(1), 80-85.

Shoelson, S. (2006). Lee j, Goldfine AB. *Inflammation and insulin resistance. J Clin Invest*, *116*(7), 1793-1801.

Sies, H. (1997). Oxidative stress: oxidants and antioxidants. *Exp. Physiol.: Trans. Integr.*, *82*(2), 291-295.

SJÖGREN, A., FLORÉN, C. H., & Nilsson, A. (1988). Magnesium, potassium and zinc deficiency in subjects with type II diabetes mellitus. *Acta Med. Scand.*, *224*(5), 461-466.

Stohs, S. J. (2014). Safety and efficacy of shilajit (mumie, moomiyo). *Phytother. Res.*, *28*(4), 475-479.

Stohs, S. J., Singh, K., Das, A., Roy, S., & Sen, C. K. (2017). Energy and Health Benefits of Shilajit. In: Bagchi, D., (Ed), **Sustained Energy for Enhanced Human Functions and Activity.** Elsevier. Academic Press. USA**.** (pp. 187-204).

Stolar, M. (2010). Glycemic control and complications in type 2 diabetes mellitus. *Am J Med*, *123*(3), S3-S11.

Suksomboon, N., Poolsup, N., & Yuwanakorn, A. (2014). Systematic review and meta-analysis of the efficacy and safety of chromium supplementation in diabetes. *J Clin Pharm Ther*., *39*(3), 292-306.

Takemori, H., Hamamoto, A., Isogawa, K., Ito, M., Takagi, M., Morino, H., Miura, T., Oshida, K., & Shibata, T. (2020). Mouse model of metformin-induced diarrhea. *BMJ Open Diabetes Res. Care*., *8*(1), e000898.

Tilg, H., & Moschen, A. R. (2008). Inflammatory mechanisms in the regulation of insulin resistance. *Mol. Med.*, *14*, 222-231.

Trivedi, N., Mazumdar, B., Bhatt, J., & Hemavathi, K. (2004). Effect of shilajit on blood glucose and lipid profile in alloxan-induced diabetic rats. *Indian J. Pharmacol.*, *36*(6), 373.

Upadhyay, A., Kumar, K., & Mishra, H. (2009). Effects of combination of Shilajit extract and Ashwagandha (Withania somnifera) on fasting blood sugar and lipid profile. *J. Pharm. Res.*, *2*(5), 897-899.

Velmurugan, C., Vivek, B., Wilson, E., Bharathi, T., & Sundaram, T. (2012). Evaluation of safety profile of black shilajit after 91 days repeated administration in rats. *Asian Pac J Trop Biomed*, *2*(3), 210-214. https://doi.org/10.1016/s2221-1691(12)60043-4

Vemuri, S. K., Banala, R. R., Katragunta, K., Madhuri, V., Raju, K., Annapareddy, V. G. R., & Goli, P. V. S. (2018). Antioxidant, anti-inflammatory and anti-diabetic efficiency of Indian medicinal plants against streptozotocin induced diabetes in male Wistar rats. *Free radic. antioxid.*, *8*(2), 141-148.

Verma, S., & Hussain, M. E. (2017). Obesity and diabetes: an update. *Diabetes Metab. Syndr.*, *11*(1), 73-79.

Warolin, J., Coenen, K. R., Kantor, J. L., Whitaker, L. E., Wang, L., Acra, S. A., Roberts, L. J., & Buchowski, M. S. (2014). The relationship of oxidative stress, adiposity and metabolic risk factors in healthy Black and White American youth. *Pediatr. Obes.*, *9*(1), 43-52.

Wei, Y., Lin, F. J., Lin, S. Y., & Wang, C. C. (2019). Risk of Hypoglycemia and Concomitant Use of Repaglinide and Clopidogrel: A Population-Based Nested Case-Control Study. *Clin Pharmacol Ther.*, *106*(6), 1346-1352.

Wilding, J. (2006). Thiazolidinediones, insulin resistance and obesity: finding a balance. *Int. J. Clin. Pract.*, *60*(10), 1272-1280.

Wilding, J., Bailey, C., Rigney, U., Blak, B., Beekman, W., & Emmas, C. (2016). Glycated hemoglobin, body weight and blood pressure in type 2 diabetes patients initiating dapagliflozin treatment in primary care: a retrospective study. *Diabetes Ther.*, *7*(4), 695-711.

Wilson, E., Rajamanickam, G. V., Dubey, G. P., Klose, P., Musial, F., Saha, F. J., Rampp, T., Michalsen, A., & Dobos, G. J. (2011). Review on shilajit used in traditional Indian medicine. *J. Ethnopharmacol.*, *136*(1), 1-9.

Winkler, J., & Ghosh, S. (2018). Therapeutic potential of fulvic acid in chronic inflammatory diseases and diabetes. *J. Diabetes Res.*, *2018*.

Wong, C. Y., Martinez, J., & Dass, C. R. (2016). Oral delivery of insulin for treatment of diabetes: status quo, challenges and opportunities. *J. Pharm. Pharmacol.*, *68*(9), 1093-1108.

World Health Organization. (2016). *Global report on diabetes*. WHO. Retrieved 19-9-2022 from https://www.who.int/publications/i/item/9789241565257

World Health Organization. (2019). *Diabetes key facts*. https://www.who.int/news-room/fact-sheets/detail/diabetes

World Health Organization. (2023). *International Clinical Trials Registry Platform Search Portal: Shilajit*. WHO. Retrieved 1-1-2023 from https://trialsearch.who.int/

Yan, L. j. (2018). Redox imbalance stress in diabetes mellitus: Role of the polyol pathway. *Anim Models Exp Med.*, *1*(1), 7-13.

Yuan, M., Konstantopoulos, N., Lee, J., Hansen, L., Li, Z.-W., Karin, M., & Shoelson, S. E. (2001). Reversal of obesity-and diet-induced insulin resistance with salicylates or targeted disruption of Ikkβ. *Science*, *293*(5535), 1673-1677.

Zheng, S. L., Roddick, A. J., Aghar-Jaffar, R., Shun-Shin, M. J., Francis, D., Oliver, N., & Meeran, K. (2018). Association between use of sodium-glucose cotransporter 2 inhibitors, glucagon-like peptide 1 agonists, and dipeptidyl peptidase 4 inhibitors with all-cause mortality in patients with type 2 diabetes: a systematic review and meta-analysis. *JAMA*, *319*(15), 1580-1591.

Zheng, W., Li, X.-B., Tang, Y.-L., Xiang, Y.-Q., Wang, C.-Y., & de Leon, J. (2015). Metformin for weight gain and metabolic abnormalities associated with antipsychotic treatment: meta-analysis of randomized placebo-controlled trials. *J. Clin. Psychopharmacol.*, *35*(5), 499-509.

JJBS

Volume 17, Number 1,March 2024
ISSN 1995-6673
Pages 123 – 128
https://doi.org/10.54319/jjbs/170111

Jordan Journal of Biological Sciences

Evaluation of Genetic Diversity in Jordanian *Solanum nigrum* Plants and Genetic Stability of *invitro* Grown Plant using (AFLP) Technique

Mu'ad AL-Kiyyam [1], Rida A. Shibli[2,3,*], Ahmad Zatimeh[4], Reham W. Tahtamouni[5], Tamara S. AlQudah[3], Shireen Hassan[3]

[1] *Department of Plant Production and Protection, Faculty of Agriculture, Jerash University, Jordan.* [2]*Department of Agricultural Biotechnology and Genetic Engineering, Faculty of Agriculture Technology, Al-Ahliyya Amman University, Amman 19328, Jordan;* [3]*Hamdi Mango Center for Scientific Research (HMCSR), University of Jordan, Amman, Jordan.* [4]*Department of Applied Sciences, Huson College, Al Balqa-Applied University, Irbid 19117, Jordan;* [5]*Department of Social and Applied Sciences, Princess Alia University College, Al-Balqa Applied University, Jordan.:*

Received: March 15, 2023; Revised: July 19, 2023; Accepted: August 4, 2023

Abstract

Solanum nigrum is an herbal plant that is reported for its healing powers against many ailments. In Jordan *S. nigrum* grows wild as a toxic weed in neglected fields and without any consideration of its medicinal value. This research aimed to collect and examine the genetic relationships of *S. nigrum* from different sites in Jordan. The *in vitro-grown S. nigrum* was established from the collected wild populations. Results of wild populations of *S. nigrum.* were arranged in two clusters (A & B) at the top range of hierarchy (genetic similarity of 0.13). Cluster A separated Bergesh Reserve population into its own group, while cluster B contained the remaining populations which were divided into two sub-clusters at a genetic similarity of 0.65, B1 contained Deer Alla and Jerash (2014 + 2015) po pulations at genetic similarity of 0.69 and B2 contained Almojeb Valley and Salt populations at genetic similarity of 0.71. However, the highest genetic similarity (0.87) was obtained between Jerash 2014 and Jerash 2015 from the same location. This dissimilarity might be due to the probability of cross-pollination AFLP (Amplified Fragment Length Polymorphism) molecular analysis gave no genetic variations between *in vitro* grown *S. nigrum* before and after micropropagation compared with wild- type mother plants collected from the Jerash site in 2014. A solid conclusion needs more research on the genetic diversity of Jordanian wild-grown *S. nigrum*. This can be achieved by extending the collection scale to include all sites where this valuable plant grows.

Keywords: AFLP, Callus, Cell suspension culture, Genetic diversity, Genetic stability, *In vitro*, microshoots, *Solanum nigrum.*

1. Introduction

Plant biodiversity is vital for all living as they comprise the main source of food be sides being the prominent source of medicine (Ochoa-Villarreal et al., 2016; Shibli et al., 2018; Tahtamouni et al., 2021). Nowadays, folk medicine is getting a universal attention, especially in developing countries, as it represents an affordable approach for t heir medications (Aware et al., 2022; El-Saadony et al., 2023).Secondary metabolites extracted from plants have a long history as row resources of remedies for fol k and modern systems of medicine (Pedrosa et al., 2023; Al-Qura'n, 2011, Wang et al., 2022).

Jordan is reputable for its huge plant biodiversity due to the nature of its multifarious geography and ecology (Oran, 2014). Unfortunately, Jordanian plant biodiversity has been exposed to extensive drops as a result of uncontrolled collection, urbanization, and climate change (Al-Eisawi et al., 2000; Oran 2014, Shibli et al., 2016). Many threatened Jordanian plant species have remarkable curative values, but are sadly still neglected and left without any collection, characterization, or documentation.

Solanum nigrum is one of the Solanaceae family members and is known as the black nightshade (Mandal et al., 2023). *S. nigrum* is considered as a weed and can be found in neglected areas and waste lands (Al- Kiyyam et al., 2019). According to Jordan's red list (Taifour, 2016), *S. nigrum* grows wild in different parts of Jordan in the north, such as Jerash and Ajloun, until reaching the south parts such as Aqaba and Petra. Till now, there is no adequate data about its population in Jordan.

Like most members of the Solanaceae family, *S. nigrum* was reported to contain many medically important compounds like glycoalkaloids (solasodine and solanine), glycoproteins, polysaccharides, polyphenolic compounds alkaloids and flavonoids (Churiyah et al., 2020.). Consequently, this plant was prescribed against bacteria, fungi, cancer and cytotoxic activities, and prescribed to heal cardiac ailments, skin cancer, and kidney diseases (Mahajan and Shaikh 2023).

We investigate the genetic relationships and diversity in this study for *S. nigrum* samples collected from five locations throughout Jordan using (AFLP) technique. Furthermore, we conduct an assessment of t he genetic

* Corresponding author. e-mail: shibli@ammanu.edu.jo.

stability of the samples taken from selected treatments of tissue culture experiments (micro shoots, callus, and cell suspension), and compare them with the mother wild plant that was used for in vitro propagation part (taken from the Jerash site in 2014). The overall goal of this research is to provide comprehensive conservation strategies for *S. nigrum* by assessing the genetic diversity of *S. nigrum* populations in five locations and then validating the genome stability for t he tissue culture plant samples (a conservation method) and comparing them with wild mother plants.

2. Materials and Methods

2.1. Genetic diversity and stability of S. nigrum

Seeds from wild grown plant samples were collected randomly from different five locations throughout Jordan (Table 1), planted in greenhouse- School of Agriculture at Jordan University, and then we investigated the genetic diversity or t hese samples using (AFLP) technique. The samples were taken from germinated seeds that were taken from each location. About one hundred seeds were collected from different plants in each location and were used for germination in the greenhouse. About ten samples of these germinated plants were taken from each location and were assessed using AFLP.

Also, mature seeds were collected from a mother plant grown at Jerash - Jordan (N: 32.27372, S: 35.89464) and *in vitro* propagated plants were established from mother plants that are grown in Jerash- Jordan location according to Al-Kiyyam et al. (2019). The microshoots were developed in MS media (Murashige and Skoog, 1962) plus 1.2 mg.L^{-1}Thidiazuron (TDZ), while the callus and cell suspension were established on MS media plus2.0 mg.$L^{-1}$of 2,4-Dichlorophenoxyacetic acid (2,4- D) and1.5 mg.L^{-1}TDZ. Then, the samples from the three types of plant material were tested for t heir genetic stability by comparing their results to data taken from their mother plant collected from Jerash using (AFLP) technique. All chemicals in this part were purchased from sigma Aldrich company.

In vitro propagation system was only applied to the Jerash population. The in vitro propagation protocol was mentioned in detail previously in (Al-Kiyyam et al., 2019). The establishment of the in vitro material was from seeds collected from the Jerash population. After seed germination; micro shoots were established from in vitro germinated seeds and further callus and cell suspension cultures were produced from microshoots according to (Al-Kiyyam et al., 2019); and each culture was maintained in the determined media for four weeks.

Table (1): Coordination of the locations of collected *S. nigrum* in Jordan

No.	Govornorate	Population	Coordinate		
			Altitude (m)	Latitude (N)	Longitude (E)
1	Jerash	Jerash	505	32.27372	35.89464
2	Irbid	Bergesh Reserve	865	32.41532	35.75775
3	Madaba	Almojeb Valley	400	31.44506	35.81405
4	AL- Balqaa'	Salt	962	32.05115	35.71655
5	AL-Balqaa'	Deer Alla	-210	32.12677	35.60668

2.2. The extractionof DNA

The extraction of DNA was done using Cetyltrimethyl ammonium bromide (CTAB) from collected plants according to Saghai Maroof et al.(1994) protocol with slight modifications. Leaves from each collected sample were merged and mashed in LN (Liquid Nitrogen). About 200 mg of young plant tissues was added to 2 ml tube has600 µL of CTAB (2% CTAB, 3 M sodium chloride,20 mM EDTA at pH: 8.0, 100 mM Tris at pH: 8.0 with 0.2% Beta-Mercaptoethanol (BME)). The tested plant samples were put under 65 °C for ha lf of hour a nd were mixed every 10 m inutes. Next, 800 µL Chloroform isoamylalcohol was applied at the concentration 24:1. After that, samples were put in centrifuge at the maximum speed (10 min at 13800 rpm). About 600µLof the aqueous phase was removed, the liquid phase was transferred into new tubes, and1µL RNase was put in fora quarter hour at 37°C. The precipitation method was applied to nucleic acids using 700 µL of pre-chilled isopropanol, and then the centrifugation was done with 13000 rpm for up to ten minutes. Ethanol of 70% concentration was used for DNA washing and samples were then air dried for 15 m inutes. The DNA was suspended again in 75 µl 0.1X TE and left at -20°C. Stock solution concentration is 10 ng.$\mu L^{-1}$and 3 ng were added to each sample. The quality DNA was tested by 1% a garose using gel electrophoresis (Intron, Bio-tek, Korea). Genomic DNA was then inspected using a spectrophotometer (BIO-RAD, Smart spec Tm plus USA).

2.3. AFLP analysis:

The digestion of DNA was done using 30 ng of D NA, adaptor ligation, and amplification. About ten plants from germinated seeds were used for each location to conduct the AFLP analysis. The genetic diversity was applied only to five locations and not to the in vitro grown plants. In-vitro grown plants were only assessed for t heir genetic stability in comparison to their mother plants (Jerash location) using AFLP technique.

To determine the genetic variation between the samples, 8 primers were used (Table 2). AFLP procedure was applied according to Vos et al. (1995) with few alterations. AFLP protocol for digestion of DNA was done with*Eco*RI and *Mse*I enzymes, while the *Eco* RI and *Mse* I adaptors were used for ligation, pre-amplification with E-A and M-C primers, and selective AFLP amplification using labeled E-AAC IRDye 700 and E-ACT IRDye 800 primers and unlabeled M-CTA, M-CTT, M-CTG and M-CAG primers (Table 2).

Table 2. Adapters and primers used for AFLP analysis

Primer/Adapter	The Sequence (3'-5')
Eco RI adapter (top strand)	CTCGTAGACTGCGTACC
(bottom strand)	AATTGGTACGCAGTC
Mse I adapter (top strand)	GACGATGAGTCCTGAG
(bottom strand)	TACTCAGGACTCAT
E-A	GACTGCGTACCAATTCA
M-C	GATGAGTCCTGAGTAAC
E-AAC	GACTGCGTACCAATTCAAC
E-AGC	GACTGCGTACCAATTCACT
M-CTA	GATGAGTCCTGAGTAACTA
M-CTT	GATGAGTCCTGAGTAACTT
M-CTG	GATGAGTCCTGAGTAACTG
M-CAG	GATGAGTCCTGAGTAACAG

Selective amplification was conducted using the program of touchdown at 65 ºC with13 cycles. Other 23 cycles were performed at 94 ºC for 30 seconds. LI-COR Bioscience 4300 DNA Analyzer was used to perform AFLP markers

The genetic diversity was assessed using AFLP bands which were scored at 1 for presence, and 0 means for absence. Data were analyzed using (NTSys- PC) program (version 2.02) according to (Dice, 1945; Rohlf, 2000). After that, the cluster was analyzed using (UPGMA) the unweighted pair group method with arithmetic average.

3. Results and Discussions

3.1. Genetic diversity analysis

Genetic variation among *S. nigrum* plants collected from the five locations (Jerash 2014 and 2015, Almojeb Valley, Deer Alla, Barges Reserve and Salt) was analyzed using AFLP technique (Fig. 1), and generated polymorphic bands and their number from eight primer combinations were recorded (Table 3).The polymorphic bands are marked with arrows as shown in Fig. 1. Genetic diversity was evaluated previously for *Solanum elaeagnifolium* using AFLP and SSR which showed high genetic diversity in collected *Solanum elaeagnifolium* samples (Qasem et al., 2019). Qasem et al., (2019) found that a sixth of AFLP bands used were polymorphic with (PIC) of 38. 0% in *Solanum elaeagnifolium*. Besides that, the genetic relationship was analyzed for *S. nigrum* populations in Kenya by SSR method (Mafuta et al., 2023). Furthermore, another method of (S NP) Markers was used also in *S. nigrum* to evaluate population structure and genetic diversity in China (Li et al., 2023).

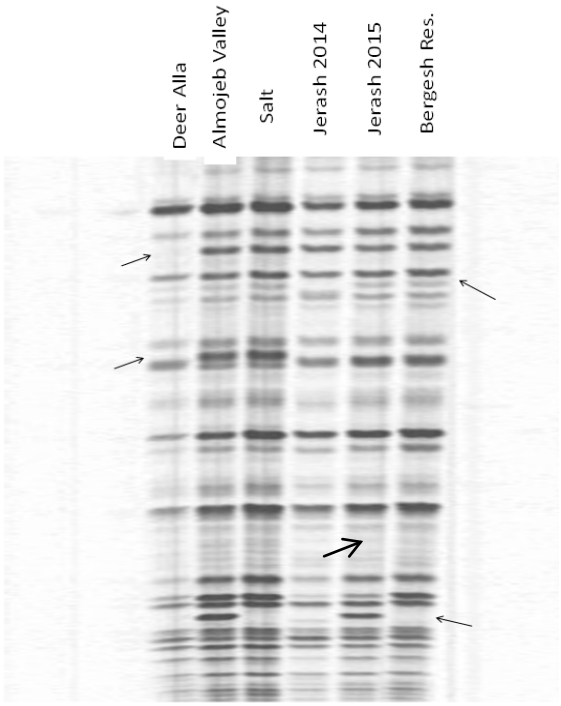

Figure 1 Amplified DNA patterns using AFLP primers for *S. nigrum* gathered from different sites. The primer combinations are (M-CTG with E-AGC), and arrows indicate the polymorphic bands.

Table 3. Number of generated polymorphic bands from eight primer combinations in *Solanum nigrum*.

Primer combinations	Selective nucleotides		Number polymorphic of bands
	*Mse*l	*Eco*RI	
1	CTA	AAC	5
2	CTA	AGC	4
3	CTT	AAC	7
4	CTT	AGC	5
5	CTG	AAC	5
6	CTG	AGC	7
7	CAG	AAC	3
8	CAG	AGC	1
Total			37

A genetic similarity matrix was constructed to investigate genetic diversity among the populations. Results showed that the genetic distances (1 minus Dice coefficient) between the studied populations were distributed as close as 0.13 to those genetically different as 0.63.In contrast, the overall mean of genetic dissimilarity was 0.585 (Table 4). The distance between the DNA of different species was measured and a good diversity was found between while the relationship between them was close (Jacoby, 2003).*S. nigrum* from Kenya and Germany was characterized using AFLP and the distance between the markers were correlated morphological characters (Matasyoh et al., 2015).

Table 4: Dice (1945) coefficient of genetic similarity matrix among *S. nigrum* wild populations using eight AFLP primers.

	Almojeb Valley	Salt	Jerash 2014	Jerash 2015	Deer Alla	Bergesh Reserve
Almojeb Valley	1					
Salt	0.7108511	1				
Jerash 2014	0.7058824	0.7179487	1			
Jerash 2015	0.6868421	0.6511628	0.8789474	1		
Deer Alla	0.6500000	0.6818182	0.6945946	0.6780488	1	
Bergesh Reserve	0.4000000	0.5263158	0.3703704	0.4516129	0.4375000	1
Means	0.6307152	0.6443113	0.6479708	0.5648305	0.4375	
Over all means	0.585					

From the dendrogram (Fig. 2) of t he six *S. nigrum* plants were two clusters in two main groups (cluster A and cluster B) (F ig. 1) a t the maximum level of hierarchy (genetic similarity of 0. 13) (Fig. 1 a nd 2). Cluster A separated Bergesh Reserve population into its own group, while cluster B contained the remaining populations which were divided into 2 c lusters with a 0.65 similarity index; B1 contained Deer Alla and Jerash (2014 + 2015) populations at genetic similarity of 0.69 and B2 contained Almojeb Valley and Salt populations at genetic similarity of 0.71. However, the similarity of (0.87) was the highest obtained between Jerash 2014 and Jerash 2015 which were collected from the same location, but in different years, and this dissimilarity might be due to the probability of cross-pollination occurrence (citation). Genetic dissimilarity (0.585) between the six collected samples increases the possibility of cross-pollination occurrence as a causal agent behind these genetic dissimilarities, taking into account that *S. nigrum* is a self-pollinated plant with little chance of cross-pollination occurrence. Similarly, Kapesa et al. (2021) found t hat the molecular analysis of *Solanum nigrum* collected from Congo was separated into two distinct groups. Additionally, Mafuta et al., (2022) found that the genetic diversity of *Solanum nigrum* from Western Kenya gave a dendrogram that was grouped into three clusters. These clusters gave high variety which was attributed to cross ability between accessions (Mafuta et al., 2022).

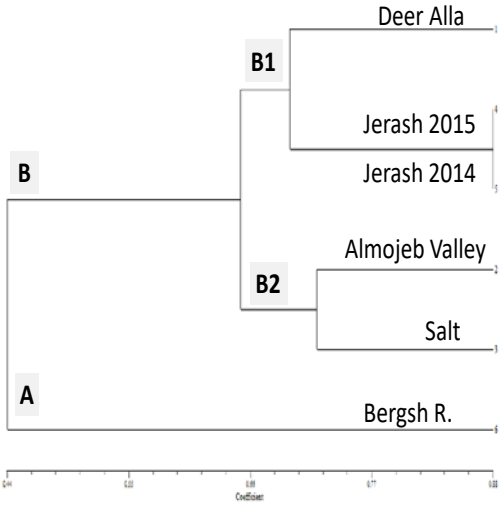

Figure 2. Unweighted pairwise group method with UPGMA (arithmetic mean)- clustering 6 wild *S. nigrum* plants, according to AFLP markers.

3.2. Effect of in vitro propagation on genetic stability of S. nigrum L. explants (microshoots, callus, and cell suspension)

The results obtained after AFLP molecular analysis indicated that there were no genetic variations between *S. nigrum* (microshoots) before and after micropropagation in comparison to the mother plant (Fig.3 and 4). These results were expected due to the fact that microshoots are differentiated tissues that are known (like any other differentiated tissue) for t heir ability to remain true type even after being undergone tissue culturing systems (Tikendra et al., 2019; Zhang et al., 2023; Biswas et al., 2023). Luo *et al.* (2023) confirmed the genetic stability in their study on *Manglietiastrum sinicum* when RAPD or ISSR markers were used after *in vitro* propagation. Our results are similar to Parzymies *et al.* (2023) study on the effects of m icropropagation on the genetic stability of *Salix myrtilloides*, as they found no di fferences between microshoots and mother plants.

Although plant genetic stability was put under validation in cases where undifferentiated explants like cell suspension or callus were used as plant material due to some tissue culture protocols and in vitro preservation (Tahtamouni et al., 2017; Qahtan et al., 2022), our results revealed that genetic makeup was unaltered in callus and cell suspension cultures (Fig. 3 a nd 4). However, genetic alterations in tissue-cultured plant materials reported in some studies were rare and referred to personal error rather than the tissue culture technique itself and described to be epigenetic as the original DNA was not altered (Smulders and Klerk, 2011;Biswas et al., 2023).The tissue culture of plants could be affected by somaclonal variation and other factors like the type of plant hormones used, the time of in vitro propagation, direct- versus indirect regeneration, etc (Biswas et al., 2023; Bulbarela et al., 2023). However, most reports found a low percentage of s oma clonal variation occurrences in tissue-cultured plants (Taji et al., 2002; Duta-Cornescu et al., 2023). Finally, this is a primary study on tissue-cultured plants because the major aim was genetic diversity as a tool of conservation and the other aim was to show if there is any genetic variation after tissue culture. Soma clonal variation analysis needs deeper studies and may be used as recommendations for further studies of the genetic stability of the tissue cultured samples.

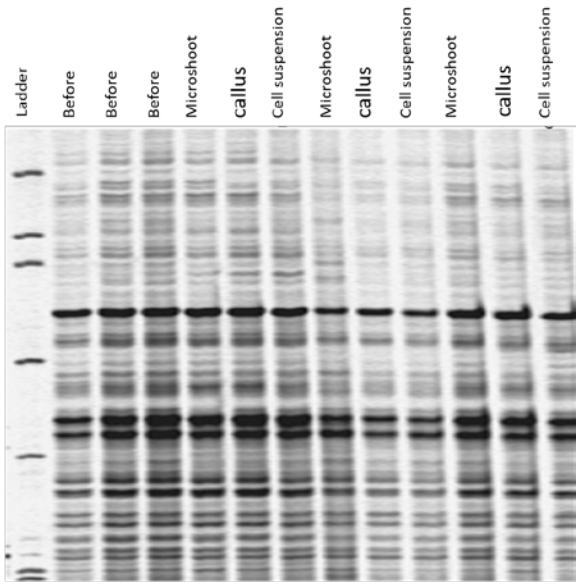

Figure3. DNA banding patterns using AFLP for *S. nigrum.* Pre-amplified DNA p roducts were selectively amplified using four *Eco*RI+*MseI* primer combinations (M-CTA IR Dye 700 with E-AAC and E-AGC). The panel labeling includes three replicates for each label (before: refers to the plant before tissue culture, micro shoot, callus, and cell suspension).

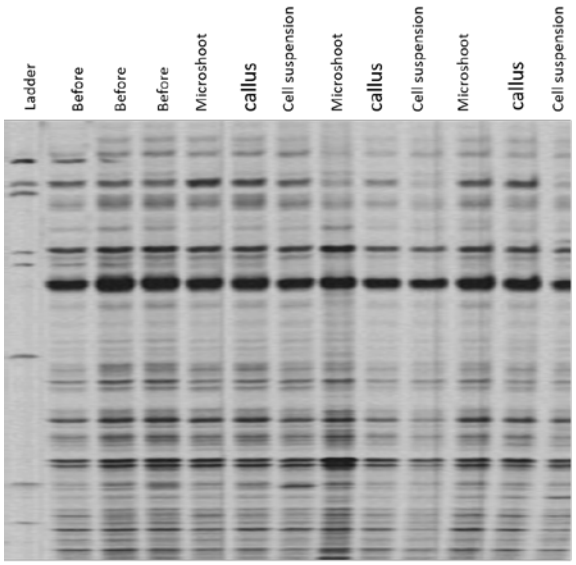

Figure 4. Bands of DNA via AFLP technique for *S. nigrum,* using four *Eco*RI+*MseI* primer combinations (M-CTT IR Dye 800 with E-AAC and E-AGC). The panel labeling includes three replicates for each label (before: refers to the plant before tissue culture, micro shoot, callus, and cell suspension).

4. Conclusion

The results obtained after AFLP molecular analysis indicated that six *S.nigrum* wild populations separated and prated in two clusters (A & B) at the highest level of hierarchy (genetic similarity of 0.13). Cluster A separated into Bergesh Reserve population into its own group, while Cluster B contained the remaining populations which were divided into 2 clusters with 0.65 similarities, B1 contained Deer Alla and Jerash (2014 + 2015) popul ations at the genetic similarity of 0 .69 and B2 c ontained Almojeb Valley and Salt populations at the genetic similarity of 0.71.

Also, AFLP molecular analysis indicated that there were no ge netic variations between *S. nigrum* (microshoots) before and after micropropagation in comparison to the mother plant (taken from the Jerash sitesite in 2014), which proved the ability of *S. nigrum* to be micropropagated without any change in genetic makeup.Conducting more research is necessary to make a solid conclusion about the genetic diversity of *S. nigrum* which grows wild in Jordan.This can be achieved by extending the collection scale to include all sites where this valuable plant grows.

5. References

AL- Kiyyam M., Shibli R., Tahtamouni R., AlQudah T., Abu-Iramaileh B. 2019. Manipulating Some Culturing Conditions, Enhances Production of Solanine in Microshoots, Callus and Cell suspension Cultures of *Solanum nigrum* L.: A Wild Medicinal Plant. J. Agric. Mar. Sci. *[JAMS]*., **24**: 51-62

AL-Eisawi DM, EL-Oqlah A, Oran SA, Lahham J . 2000. Jordan Country Study on Biological Diversity, Plant Biodiversity and Taxonomy. United Nations Environment Program.

Al-Qura'n S. 2011. Conservation of medicinal plants in Ajlun woodland Jordan. *J. Med. Plant Res*., **5**: 5857-5862.

Aware, C. B., Patil, D. N., Suryawanshi, S. S., Mali, P. R., Rane, M. R., Gurav, R. G., & Jadhav, J. P. 2022. Natural bioactive products as promising therapeutics: A review of natural product-based drug development. *S. Afr. J. Bot*., **151**: 512-528.

Biswas, P., & Kumar, N. 2023. Application of Molecular Markers for the Assessment of Genetic Fidelity of In Vitro Raised Plants: Current Status and Future Prospects. Molecular Marker Techniques: A Po tential Approach of Crop Improvement, 233-256.

Bulbarela-Marini, J. E., Gómez-Merino, F. C., Galindo-Tovar, M. E., Pastelín-Solano, M. C ., Murguía-González, J., Núñez-Pastrana, R., & Castañeda-Castro, O. 2023. Ratio of Somaclonal Variation and the Phytohormonal Content of Citrus× latifolia in Three In Vitro Culture Systems. *J. Plant Growth Regul*., **42(6)**: 3356-3364.

Churiyah, C., Ningsih, S., & Firdayani, F. 2020. The cytotoxic, apoptotic induction, and cell c ycle arrest activities of *Solanum nigrum* L. ethanolic extract on MCF-7 human breast cancer cell. Asian Pac J Cancer Prev*: APJCP*., **21(12)**: 3735.

Duta-Cornescu, G., Constantin, N., Pojoga, D. M., Nicuta, D., & Simon-Gruita, A. (2023). Somaclonal variation—Advantage or disadvantage in micropropagation of the medicinal plants. *Int. J. Mol. Sci*., **24(1):** 838.

El-Saadony, M. T., Zabermawi, N. M., Zabermawi, N. M., Burollus, M. A ., Shafi, M. E ., Alagawany, M., & Abd El-Hack, M. E. 2023. Nutritional aspects and health benefits of bioactive plant compounds against infectious diseases: a review. *Food Rev. Int.*,**39(4)**: 2138-2160.

Jacoby, A. 2003. Genetic variability in the *Solanum nigrum* L. complex and related species in South Africa (Doctoral dissertation, University of the Free State).

Kapesa, B. B., Sosef, M., Janssens, S., Le Péchon, T., & Luyeye, F. L. 2021. Preliminary Study on t he *Solanum nigrum* L.(Solanaceae) Complex in the Democratic Republic of the Congo. *European j. biol.* biotechnol., ***2*(5):** 9-18.

Li, J., Wei, S., Huang, Z., Zhu, Y., Li, L., Zhang, Y., ... & Huang, H. 2023. Genetic Diversity and Population Structure in *Solanum nigrum* Based on Single-Nucleotide Polymorphism (SNP) Markers. *Agronomy*, **13(3)**: 832.

Luo, Y., Zheng, K., Liu, X., Tao, J., Sun, X., Deng, Y., & Deng, X.2023. In Vitro Propagation and Genetic Uniformity Assessment of *Manglietiastrum sinicum*: A Critically Endangered Magnoliaceae Species. *Plants*, **12(13)**: 2500.

Mafuta, J. N., Chepkoech, E., O namu, R., Shibairo, S. I., & Wamocho, L. S. 2022. Genetic Diversity of African Nightshade (*Solanum nigrum* L.) Complex Accessions from Western Kenya. *Afr. Env. Rev. J*., **5(1):** 224-232.

Mahajan, V. D., & Shaikh, H. S. 2023. *Solanum nigram*-A Potential Medicinal Herb. *Res. J. Sci. Technol*., **15(1)**: 27-34.

Mandal, S., Vishvakarma, P., Verma, M., Alam, M. S., Agrawal, A., & Mishra, A. 2023. *Solanum nigrum* Linn: An Analysis Of The Medicinal Properties Of The Plant. *J Pharm Negat Results*., 1595-1600.

Matasyoh, L. G., Abel, S., Budahn, H., & Klocke, E. 2015. Characterization of the *Solanum nigrum* complex of Kenya by AFLP markers. *Int. J. Agric Sci. and Techn*.,**3(1):** 10-21.

Murashige, T., Skoog, F. 1962. A revised medium for rapid growth and bioassays with tobacco tissue cultures. *Physiol Plant*.,**15:** 473-479.

Ochoa-Villarreal M., Howat S, Hong S., Jang M., Jin Y., Lee E., Loake G. 2016. Plant cell culture strategies for the production of natural products. *Review BMB Rep.,* **49(3)**:149-58. doi: 10.5483/bmbrep.2016. 49.3.264.

Oran, S. A. 2014. A list of flowering wild plants in Tafila Province, Jordan. Int. J. Biodivers. *Conserv.,* **6(1)**: 28-40.

Pedrosa, M. C ., Lima, L., Aloso-Esteban, J. I., Roriz, C. L., Barros, L., Ferreira, I. C., & Carocho, M. 2023. History of Secondary Metabolites: From Ancient Myths to Modern Scientific Validation. In Natural Secondary Metabolites*:* From Nature, Through Science, to Industry (pp. 3-18). Cham: Springer International Publishing.

Qahtan, A. A., Faisal, M., Alatar, A. A., & Abdel-Salam, E. M. 2022. Callus-Mediated High-Frequency Plant Regeneration, Phytochemical Profiling, Antioxidant Activity and Genetic Stability in *Ruta chalepensis* L. *Plants*, **11(12)**: 1614.

Shibli, R. A., Hawmdeh, F. A., Duwayri, M., Hadidi, N., Al-Qudah, T. S., Tahtamouni, R. W., & Zateemeh, A. 2016. Experimenting Two Cryopreservation Techniques (Vitrification and Encapsulation-Dehydration) as Approaches for Long-term Conservation of in vitro Grown Shoot Tips of Wild Fennel. *Jordan J. Biol. Sci. (JJBS)*, **9(3).**

Shibli, R. A., Sharaf, S. A., Kasrawi, M. A ., & Al-Qudah, T. S . 2018. In Vitro Multiplication of the White Wormwood, *Artemisia herba-alba* asso. *Jordan J. Biol. Sci., (JJBS)*, **11(3)**.

Smulders , M. J. M., Klerk, G. J. 2011. Epigenetics in plant tissue culture. *J. Plant Growth Regul*., **63**:137–146

Tahtamouni R, Shibli R, Al Qu dah T, Saifan S, Khawldeh R. 2021. A n Outlook on J ordan Efforts in Conservation of Plant Biodiversity during the First Hundred Years of the Country's Founding. *Jordan J. Agri. Sci. (JJAS)*, **17(3)**: 195-206

Tahtamouni, R. W., Shibli, R. A., Al-Abdallat, A. M., Al-Qudah, T. S., Younis, L., Al-Baba, H., & Al-Ruwaiei, H. 2017. Cryopreservation of *Thymbra spicata* L. var. spicata and genetic stability assessment of the cryopreserved shoot tips after conservation. *Jordan J. Biol. Sci. (JJBS)*, **10(1)**, 19-28.

Taifour H., A. El-Oqlah. 2016. Jordan Plant Red List (2 ed.). Volume 2 Royal Botanic Garden- Jordan (pp. 78, 572).

Taji, A., Prakash, N., & Lakshmanan, P. (2002). In vitro plant breeding. food products Press.

Tikendra, L., Koijam, A. S., & Nongdam, P. 2019. Molecular markers based genetic fidelity assessment of micropropagated *Dendrobium chrysotoxum* Lindl. *Meta Gene*, **20**: 100562.

Vos P., Hogers R., Bleeker M., Reijans M., Van d. L., Hornes T. M., Frijters A. P., Peleman J. J., Kuiper M., Za beau, M. l 995. AFLP: a n ew technique for DNA f ingerprinting. *Nucleic Acids Res*., **23**:4407–4414

Wang, L., Kong, D., Tian, J., Zhao, W., Chen, Y., An, Y., Zhou, H. 2022. Tapinanthus species: A r eview of botany and biology, secondary metabolites, ethnomedical uses, current pharmacology and toxicology. *J. Ethnopharmacol*., **296:** 115462.

Zhang, Y., Cao, Y., Wang, Y., & Cai, X. 2023. Somatic embryogenesis induction and genetic stability assessment of plants regenerated from immature seeds of *Akebia trifoliate* (Thunb.) Koidz. *Forests*, ***14*(3):** 473.

JJBS

Volume 17, Number 1,March 2024
ISSN 1995-6673
Pages 129 – 134
https://doi.org/10.54319/jjbs/170112

Jordan Journal of Biological Sciences

Oxaloacetate: Transmitter Function, Contribution to the Neurophysiological Processes of the Body, Prospects for Therapeutic Application. Experimental data

Nataliya Kolotyeva[1], Irina Gorbacheva[2,*], Oksana Gusyakova[2], Olga Baldina[2], Frida Gilmiyarova[2]

[1]Research Center of Neurology, 125367, Moscow, Russia;[2]Samara State Medical University, 443099 Samara, Russia

Received: April 13, 2023; Revised: August 15, 2023; Accepted: August 18, 2023

Abstract

The focus of our attention is directed towards the small molecule of oxaloacetate. This work is dedicated to the investigation of the role played by natural intermediates as metabolism switches in intermolecular interactions. The full range of biological activity for oxaloacetate has been unveiled through the utilization of computer modeling methods. Furthermore, the interaction partner proteins have been characterized. It has been demonstrated that small molecules act as metabolic intermediates, serving as points of intersection for numerous metabolic pathways encompassing protein, carbohydrate, and lipid metabolism. Concurrently, a coordinating role is assumed by these molecules in the execution and modulation of mediator, hormonal, receptor responses, immunological, inflammatory, antibacterial, and antiviral reactions, thus manifesting anticarcinogenic properties. Through the application of differential scanning fluorimetry and microcapillary thermophoresis, the interaction between lactate dehydrogenase and ligands of endogenous origin has been established. The calculated Kd value obtained for the interaction between oxaloacetate and lactate dehydrogenase was determined to be 0.5±0.01 μM. The thermalstability of LDH is enhanced by final concentrations of oxaloacetate ranging from 0.5 to 1 μM, whereas a concentration of 16 μM of the metabolite diminishes its thermostable characteristics. In intermolecular processes in in vitro cell culture, the stimulating effect of oxaloacetate 33,8 % (p= 0.028) on the primary culture of human dermal fibroblasts was shown.

Keywords: protein-metabolite interactions, oxaloacetate, computer modelling, differential scanning fluorimetry, microcapillary thermophoresis, human dermal fibroblasts

1. Introduction

Currently, it is important to study the role of metabolites in the systems of intercellular interaction. In particular, protein - metabolite interactions can regulate and control a variety of cellular processes: transport of substances, signaling, playing a role in maintaining cellular homeostasis (Zhao *et al.* 2021). The small molecule of oxaloacetate is the focus of our attention. It is a linking compound of carbohydrate and protein exchanges. Oxaloacetate quantitatively determines the intensity of the tricarboxylic acid cycle. It is necessary to constantly regenerate oxaloacetate to ensure that the citric acid cycle and the electron transfer process in the mitochondrial respiratory chain are not interrupted (Campos *et al.* 2012; Pesi *et al.*2018). Scientific research has shown that oxaloacetate affects lifespan. It activates FOXO/DAF-16 transcription factors and protein kinase activity. These processes are required in adenosine monophosphate (Williams *et al.* 2009; Al-Homsi *et al.* 2012; Edwards *et al.* 2013). In addition, oxaloacetate stimulates the growth of neurons of the hippocampal gyrus, which leads to a decrease in the intensity of cell division. Active cell division in this area has a beneficial effect on cognitive processes and mnemonic functions (Wilkins *et al.*2014). Intermediate effects play a crucial role in several vital functions - it has a general promitochondrial effect. Which is expressed by in increasing the content of mitochondrial markers COX4|1 and PGC1α. Along with preventing neuroinflammation and neurodegeneration (Lu *et al.* 2018; New M. 2019; Zerr *et al.* 2019). Oxaloacetate can penetrate through the blood-brain barrier into the central nervous system. This finding became a prerequisite for preclinical trials of drugs against Alzheimer's disease and therapy in ischemic stroke neurodegeneration (Vidoni *et al.* 2021; Shahouzehi *et al.* 2023).

Experimentally assessing the intermolecular interaction of millions of chemical compounds with thousands of ligands is difficult both from an economic and practical point of view; therefore, it is advisable to conduct a preliminary assessment of the biological activity of specific chemicals *in silico* (Chakraborty *et al.* 2019). The use of computer simulation can reduce the amount of necessary experiments by a factor of ten compared to blind search (Filimonov *et al.* 2018). The study of structure-functional features of small molecules includes the

* Corresponding author. e-mail: i.v.gorbacheva@samsmu.ru.

following stages of research: determination of predicted spectrum of biological activity using computer technologies; identification of potential protein partners to confirm the scientific hypothesis; setting up *in vitro* and *in vivo* model experiments revealing these or those properties of the studied molecule.

The study aims to predict *in silico* biological properties, determine potential protein partners of the interaction of oxaloacetate, and study its effect on the conformation and thermolability of lactate dehydrogenase (LDH) and on the viability of human dermal fibroblasts. An important step in studying the effect of low molecular weight ligands on protein structures is to conduct experiments involving individual proteins. The monocatalytic protein lactate dehydrogenase (lactate dehydrogenase catalytic system) was chosen as the object of our further study, and oxaloacetate was chosen as a low molecular weight ligand. In its structure, this metabolite is similar to one of the substrates of the lactate dehydrogenase reaction, pyruvate, differing in the presence of an additional carboxyl group. Fibroblast culture is an adequate experimental model for assessing the metabolic profile, exo- and endometabolome variability associated with changes in the incubation environment during the study (Stunova, Vistejnova, 2018).

2. Materials and Methods

2.1. Computer modeling of the biological activity of oxaloacetate using PASS

The software PASS version 1.917 (Prediction of Activity Spectra for Substances) is intended for prediction of the biological activity spectrum of a compound by its structural formula based on the analysis of structure-activity relationships. The spectrum of biological activity predicted by PASS includes molecular mechanisms of action, pharmacological effects, specific toxicity, side effects, effect of molecules on metabolism, molecular transport, gene expression, and identification of undesirable targets. The prediction result is presented as Pa "to be active" and Pi "to be inactive" probabilities with values from 0 to 1. We took Pa over 0.5 as the optimal probability value for the presence of activity. The prediction of the biological activity spectrum was obtained as an ordered list of Pa and Pi probability estimates.

2.2. Evaluation of probable partner proteins for oxaloacetate in STITCH

Potential protein interaction partners for small molecules were identified using Search Tool for Interactions Chemicals (STITCH) version 5.0. http://stitch.embl.de. The standard SMILES entry was used to search for identifiers and common names of chemicals that are stored in the small molecule information database. The program calculates the parameter p - the probability of small molecule-protein interaction. In STITCH, the interaction network can be displayed and adjusted using different settings: by degree of evidence, confidence, molecular action or bond affinity. In our work, we used the bond affinity score. The program predicts intermolecular interactions in a confidence threshold from 0 to 1 (low, medium, high, highest); we used a medium confidence threshold of p>0.4

2.3. Method for evaluation by microcapillary thermophoresis of LDH interaction with oxaloacetate

Experiments on the influence of oxaloacetate (Sigma, product number O4126) on the conformation and thermostability of lactate dehydrogenase (Sigma, product number L1254) were carried out in the laboratory of molecular and radiation biophysics at the Kurchatov Institute (Russia). We used reagents Sigma-Aldrich, USA: lactate dehydrogenase, oxaloacetate, Tris-HCl buffer 50mM, pH 7.5. We measured the pH value before and after adding the oxaloacetate solution to the samples using a Mettler Toledo (USA) pH-meter. The pH variation of the medium had fluctuations within the range of 0.01-0.02.

Experiments using the method of microcapillary thermophoresis to establish the fact of ligand-protein interaction, as well as to calculate the dissociation constant. The procedures were performed using Monolith NT.115 equipment (NanoTemper Technologies GmbH). Lactate dehydrogenase labeling was performed using a standard L001 protein labeling kit "Monolith NT Protein Labeling Kit RED-NHS". The unreacted "free" dye was removed by gel filtration. To calculate the dissociation constant (Kd) by microthermophoresis, a series of dilutions were prepared, where the final concentration of LDH was chosen empirically to be 1.65 μM, and the amount of added lactate varied from 40 μM to 0.0012 μM.

2.4. Study of the influence of oxaloacetate on the conformational structure of LDH using differential scanning fluorimetry

Determination of changes in the conformational structure of lactate dehydrogenase under the influence of oxaloacetate was performed using differential scanning fluorimetry based on changes in intrinsic fluorescence of protein tryptophan and tyrosine at 330 and 350 nm. Prometheus NT.48 device (NanoTemper Technologies, Germany) was used. Protein conformational stability was described by its average denaturation temperature Tm (°C), which is the point where half of the protein unfolds. Six dilutions were prepared. In which the final concentration of LDH was constant - 1 μM. The final concentration of oxaloacetate varied, 0.5 μM, 1 μM, 2 μM, 4 μM, 8 μM, 16 μM. Capillaries were scanned at 30% laser intensity, heating range from 20°C to 95°C, 1°C/min step. The effect of oxaloacetate concentration range on the lactate dehydrogenase fluorescence ratio (350/330 nm) in the physiological temperature range (36.5-37.5°C) was analyzed. The pH value was monitored before and after adding the solutions of the studied small molecules to the samples using a Mettler Toledo pH-meter (USA). The pH variation ranged from 0.01-0.02.

2.5. Determination of viability of human dermal fibroblasts

The effect of oxaloacetate on viability of human dermal fibroblasts was assessed at the Institute of Experimental Medicine and Biotechnology of Samara State Medical University, Ministry of Health of Russia, using reagents for cultivation of human cells produced by Biolot LLC (Russia) with MTT-test using a Tecan Infinite M200 PRO multirider (Tecan Austria GmbH, Austria) at 570 nm. Statistical analysis of the obtained parameters was performed using SPSS 25.

3. Results and discussion

3.1. Biological activity of oxaloacetate determined by the PASS

We have revealed the influence of oxaloacetate on the regulation of metabolism using the PASS computer environment (Table1).

Table 1. The interaction of oxaloacetate with target enzymes

Target enzymes	Enzyme code number	Pa oxaloacetate
Alanine transaminase inhibitor	EC 2.6.1.2	0.916
Oxaloacetate tautomerase inhibitor	EC 5.3.2.2	0.895
Oxaloacetate tautomerase inhibitor	EC 5.3.2.2	0.895
Glutamine-phenylpyruvate transaminase inhibitor	EC 2.6.1.64	0.856
Malate dehydrogenase acceptor inhibitor	EC 2.7.3.9	0.851
Pyruvate decarboxylase inhibitor	EC 4.1.1.1	0.827
Aspartate-phenylpyruvate transaminase inhibitor	EC 2.6.1.70	0.818
Oxaloacetate decarboxylase inhibitor	EC 4.1.1.3.	0.815
Phenylpyruvate decarboxylase inhibitor	EC 4.1.1.43	0.807
Pyruvate dehydrogenase inhibitor	EC 1.2.4.1.	0.802
L-lactate dehydrogenase (cytochrome) inhibitor	EC 1.1.2.3	0.794
L-lactate dehydrogenase (cytochrome) inhibitor	EC 1.1.2.3	0.794
Phosphoenolpyruvate carboxykinase inhibitor	EC 4.1.1.38	0.786
D-lactate dehydrogenase (cytochrome) inhibitor	EC 1.1.2.4	0.783
D-lactate dehydrogenase (cytochrome) inhibitor	EC 1.1.2.4	0.783
Succinate dehydrogenase inhibitor	EC 1.3.5.1	0.755
Serine-3-dehydrogenase inhibitor	EC1.1.1.276	0.733
Malate dehydrogenase inhibitor	EC 1.1.1.37	0.708
Malate dehydrogenase inhibitor	EC 1.1.1.37	0.708
Glycerol-3-phosphate dehydrogenase (NAD+) inhibitor	EC 1.1.1.8	0.675
Tryptophan transaminase inhibitor	EC 2.6.1.27	0.647
Glycerol-3-phosphate oxidase inhibitor	EC 1.1.3.21	0.628

Pa - probability of presence

Oxaloacetate inhibits enzymes of protein metabolism: alanine transaminase, serine-3-dehydrogenase, tryptophantransaminase. It is known that the realization of oxaloacetate action on carbohydrate metabolism is carried out by inhibiting effect on a number of key enzymes: lactate dehydrogenase, malate dehydrogenase, malatoxidase, pyruvate dehydrogenase. It was revealed that oxaloacetate is involved in the regulation of lipid metabolism. It reduces the activity of enzymes: trans-2-enoyl-CoA reductase, acylcarnitine hydrolase, glycerol-3-phosphate dehydrogenase, cytochrome-b5 reductase.

It should be emphasized that oxaloacetate has an inhibitory effect on succinate dehydrogenase, which is not only a part of the Krebs cycle but also an important element in the electron transfer chain. At the same time, it has been determined that impaired succinate dehydrogenase function accompanies a number of pathological conditions, such as Lee syndrome (Finisterer, 2008), familial paraganglioma syndrome (Her, 2015), and neuroendocrine tumors (Armstrong, 2009).

The effects of oxaloacetate on gene expression are noteworthy (Table 2): the increase in expression of the HMOX1 gene encoding the hemoxygenase-1 protein and the JAK2 gene, which regulate the viability, proliferation, and differentiation of many cell types. There is an interesting fact that oxaloacetate enhances the expression of the TP53 gene. The p53 protein acts as a suppressor of malignant tumor formation, so the TP53 gene is an anti-oncogene (Chavez-Perez et al., 2011). The inhibitory effect of oxaloacetate on the expression of the MMP9 gene, a protein of matrix metalloproteinase family, was predicted. In addition, oxaloacetate was shown to reduce the expression of the gene for tumor necrosis factor (TNF), which encodes a multifunctional proinflammatory cytokine that is mainly secreted by macrophages and is involved in the regulation of a wide range of biological processes. In addition, oxaloacetate was modeled to inhibit HIF1A factor, which functions as the main regulator of transcription of the adaptive response to hypoxia.

Table 2. Effect of oxaloacetate on gene expression

Effect on gene expression	Pa	Pi
BRAF expression inhibitor	0.683	0.004
JAK2 expression inhibitor	0.661	0.022
MMP9 expression inhibitor	0.601	0.015
TP53 expression enhancer	0.599	0.05
HMOX1 expression enhancer	0.574	0.023
EIF4E expression inhibitor	0.518	0.008
TNF expression inhibitor	0.514	0.026
HIF1A expression inhibitor	0.506	0.055
APOA1 expression enhancer	0.483	0.032

Pa - probability of presence; Pi - probability of absence

3.2. Predicted proteins of interaction with oxaloacetate

We used the STITCH v.5.0 to study intermolecular interactions between proteins and oxaloacetate. It is a well-known fact that oxaloacetate interacts as substrates with malate dehydrogenase and its various isoforms (Halestrap and Wilson, 2012). Oxaloacetate with a high degree of probability interacts with proteins of the Solute Carrier Family (SLC25). The data that coincide with those from the PASS system on the relationship of oxaloacetate with the succinate dehydrogenase complex are interesting; oxaloacetate has been shown to mediate the ADP-dependent inhibition of mitochondrial Complex II-induced respiration (Fink *et al*., 2018) (Table 3).

Table 3. Predicted proteins - partners of interaction with oxaloacetate

Proteins as partners		p
ACLY	ATP citrate lyase	0.992
CS	Citrate synthase	0.985
PCK1	Phosphoenolpyruvate carboxykinase 1	0.985
PC	Pyruvate carboxylase	0.984
MDH2	Malate dehydrogenase 2, mitochondrial	0.979
MDH1	Malate dehydrogenase 1	0.976
FH	Fumarate hydratase	0.937
ACACA	Acetyl-CoA carboxylase alpha	0.923
SLC25A10	Solute carrier family 25 (dicarboxylate transporter), member 10	0.916
SLC25A11	Solute carrier family 25 (oxoglutarate transporter), member 11	0.916
SLC25A1	Solute carrier family 25 (citrate transporter), member 1	0.911
ME3	Malic enzyme 3, NADP(+)-dependent	0.864
ME1	Malic enzyme 1, NADP(+)-dependent, cytosolic	0.859
ME2	Malic enzyme 2, NAD(+)-dependent	0.848
SDHB	Succinate dehydrogenase complex, subunit B	0.834
SDHA	Succinate dehydrogenase complex, subunit A	0.818
SDHC	Succinate dehydrogenase complex, subunit C	0.811
SDHD	Succinate dehydrogenase complex, subunit D	0.765
OGDH	Oxoglutarate dehydrogenase (lipoamide)	0.611

p - the probability of interaction between a small molecule and a protein

It was noted that oxaloacetate can be a partner in the interaction of aspartate transaminases of types 1 and 2, providing a neuroprotective effect (Martin *et al*., 2014). Oxaloacetate can bind to interleukin 4; alpha-subunit of hypoxia-inducible factor (HIF1). This allows it to indirectly influence gene expression. Which are responsible for cell adaptation to hypoxic conditions (Semenza, 2004), which is consistent with the PASS data. Determination of the interaction between oxaloacetate and lactate dehydrogenase by microcapillary thermophoresis

The next step was a series of *in vitro* experiments designed to determine the interaction of oxaloacetate with lactate dehydrogenase by microcapillary thermophoresis. We prepared a series of experiments of 16 dilutions in which the final concentration of dye-labeled LDH remained unchanged at 1.65 μM and the final concentration of oxaloacetate varied from 0.0012 to 40μM. The software automatically plots the fluorescence as a function of time (Fig. 1). Then, the software calculates the degree of lactate dehydrogenase binding to oxaloacetate by plotting the ratio between fluorescence before and after switching on the laser as a function of oxaloacetate concentration.

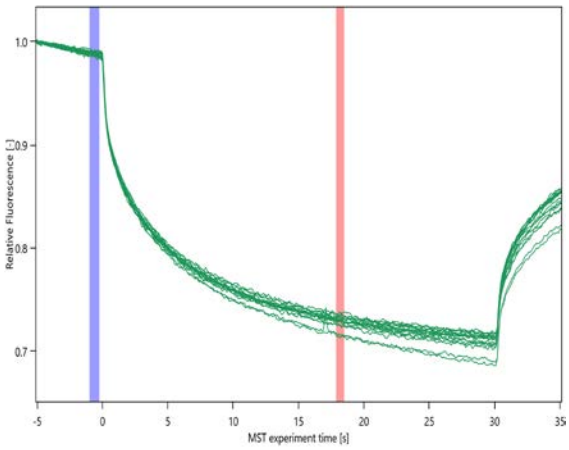

Figure 1. Analysis of the interaction between LDH (at a constant concentration (1.65 μM) and oxaloacetate at varying concentrations.

To estimate the degree of affinity, we used a stoichiometric parameter, the dissociation constant (Kd), numerically equal to the ligand concentration at which the free and bound partner molecules are equal. The calculated Kd value obtained for oxaloacetate with lactate dehydrogenase was 0.5±0.01 μM. It should be noted that in most cases the equilibrium dissociation constant numerically corresponds to the Michaelis-Menten constant, which is used to describe the affinity of the protein-ligand bond and is applicable only at the steady state (Lasseter, 2019).

3.3. Assessment of the influence of oxaloacetate on the thermostability of lactate dehydrogenase by differential scanning fluorimetry

Differential scanning fluorometry (DSF) is one of the methods for assessing the thermostability of proteins under various conditions, including after binding to small ligand molecules. It is used to determine the melting point (Tm) (transition temperature) of a protein. This is when half of the protein is in a folded conformation and the other half has undergone thermal denaturation.

We performed an experiment to evaluate the formation of the spatial structure of lactate dehydrogenase under the influence of oxaloacetate using differential scanning fluorimetry (Table 4).

Table 4. Melting initiation temperature and temperature inflection points of LDH upon addition of oxaloacetate.

Ligand concentration, μM	Melting point,°C	Inflection point, °C
16	48.3	56.0
8	51.1	56.4
4	51.7	56.5
2	51.5	56.6
1	50.8	56.6
0.5	51.1	56.6

LDH control: Melting point = 50.5°C, Inflection point = 56.3°C

It is remarkable that with a small difference in the melting temperature of LDH a different state of LDH-oxaloacetate complexes is observed, which is manifested by a different depth of the peak. The melting temperature of LDH with different concentrations of oxaloacetate

corresponds to the deepest point of the formed peak on the first derivative curve. The observed change in the depth of the formed peaks can be explained by the different influence of oxaloacetate concentrations on the thermal stability of the molecule.

3.4. Mathematical Modelling

After a visual analysis of the original scattergrams, mathematical modeling of the fluorescence values obtained during the experiment on heating the protein molecule was performed.

We performed a more detailed simulation of the lactate dehydrogenase melting curve functioning under the influence of different concentrations of oxaloacetate in the physiological temperature range of 36.5-37.5°C (Fig.3, Table 5).

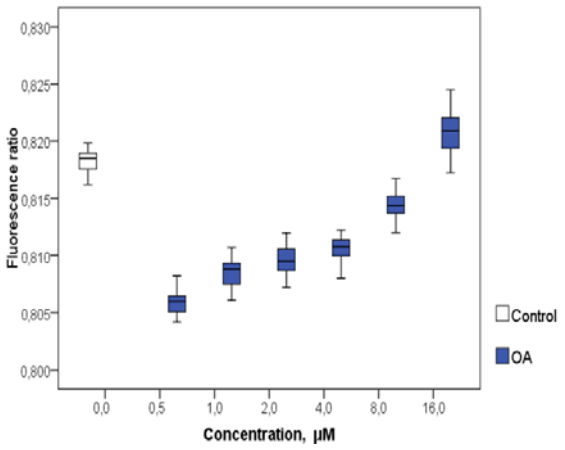

Figure 2 .Comparison of the effect of different oxaloacetate concentrations on LDH thermostability at 36.5-37.5°C.

We analyzed 29 measurements of fluorescence ratios at different temperature points of the stated temperature corridor. The effect of oxaloacetate concentration on LDH conformation was found to be statistically significant ($p < 0.005$), as manifested by changes in fluorescence intensity (table 5). No statistically significant dependence was found for oxaloacetate concentrations of 2 and 4 µM. Oxaloacetate in concentration range from 0.5-2 µM causes decrease of fluorescence ratio in comparison with control ($p < 0.001$). In this case, the most pronounced effect is exerted by the lowest ligand concentration studied - 0.5 µM. At a concentration of 8 µM, the fluorescence ratios are at the control level, while the oxaloacetate concentration of 16 µM leads to an increase in the fluorescence ratio significantly higher than the control ($p < 0.001$).

Table 5. Comparison of the effect of oxaloacetate on LDH thermostability at 36.5-37.5°C

Ligand concentration, µM	OA M±SD
Control (LDH)	0.818±0.0011
0.5	0.806±0.0009
1	0.809±0.0013
2	0.810±0.0011
4	0.811±0.0012
8	0.814±0.0012
16	0.821±0.0018
Comparison of different ligand concentrations, p_{ANOVA}	
$p_{K-0,5}$	<0.001
p_{K-1}	<0.001
p_{K-2}	<0.001
p_{K-4}	<0.001
p_{K-8}	<0.001
p_{K-16}	<0.001

High content 16 µM of oxaloacetate is reflected in decrease of thermostability of protein: decrease of the melting onset temperature and faster onset of temperature inflection point. The content of minimum concentrations of oxaloacetate is 0.5-2 µM. As a result, the melting point and the inflection point of the protein molecule are increased. It is interesting to note the ability of low concentrations of oxaloacetate to have a thermostabilizing effect, which is manifested not only by a general shift of the melting temperature in the direction of increasing its value, but also by the manifestation of the protective effect on the section of the curve corresponding to the normal temperature of the human body.

3.5. The influence of oxaloacetate on the viability of human dermal fibroblast

There is a variety of possible interactions of natural metabolites with intra- and extracellular structures *in vivo* poorly studied. The next stage of our work is to evaluate the effect of oxaloacetate on the viability of human dermal fibroblast cell culture. It was found that the differences in LDH-test values between the control and experimental samples are not significant, which suggests the absence of cytotoxicity or protective effect of oxaloacetate in this test. The value of the MTT test in culture after the addition of oxaloacetate was 0.74±0.09 compared to control cells 0.55±0.03. Oxaloacetate was shown to have a 33,8 % ($p=0.028$) stimulating effect on the primary culture of human dermal fibroblasts, which was expressed in an increase in cell viability parameters in the MTT-test. Being a natural cell component, oxaloacetate has a low cytotoxicity profile, which indicates the ability to play a regulatory role and effectively modulate cell energy flows, maintaining internal homeostasis and even optimizing metabolism under the influence of external factors.

4. Conclusion

We revealed the full range of biological activity of oxaloacetate *in silico*. We characterized the interaction partner proteins. It has been shown that it serves as points of intersection of many metabolic pathways of protein, carbohydrate, and lipid metabolism. At the same time, it is playing a coordinating role in functioning and modulating mediator, hormonal, receptor responses, immunological, inflammatory, antibacterial and antiviral reactions, having anticarcinogenic action. We established the interaction of lactate dehydrogenase with oxaloacetate using microcapillary thermophoresis and calculated dissociation constant for interacting substances. The change in protein melting point temperature at different concentrations of oxaloacetate reflects the presence of changes in the conformational stability of the enzyme during protein-metabolite interactions. The degree of change is proportional to the affinity of the bond between the protein and the ligand. A change in the conformational structure of lactate dehydrogenase under the influence of oxaloacetate in the temperature range was revealed. Final concentrations of oxaloacetate 0.5-1 μM increase the thermal stability of the protein, while the concentration of 16 μM of the metabolite reduces the thermostable properties. The effect of oxaloacetate on the proliferative properties of human dermal fibroblasts was shown. Oxaloacetate increased the viability of dermal fibroblast cell culture.

It is interesting to use the knowledge about the activating effect of low doses of oxaloacetate in the development of "mitochondrial" and "bioenergetic" medicine approaches. It is possible to influence the metabolic processes of the cell by changing the direction of energy flows by controlling the content of intracellular and, in particular, mitochondrial metabolites. In conclusion, the fundamental research carried out has provided evidence for the participation of oxaloacetate in intra- and intercellular interactions.

References

Al-Homsi L., Assaad J.M., Kweider M., Al-Okla S., Abbady A.Q. 2012. Construction of pRSET-sfGFP Plasmid for Fusion-Protein Expression, Purification and Detection. *Jordan J Biol Sci.*, **5(4)**: 279-288

Armstrong R., Greenhalgh K.L., Rattenberry E., [et al.]. 2009. Succinate dehydrogenase subunit B (SDHB) gene deletion associated with a composite paraganglioma/neuroblastoma. *Med. Genet.* **46(3):** 215–216.

Campos F., Sobrino T., Ramos-Cabrer P., Castillo J.2012. Oxaloacetate: A novel neuroprotective for acute ischemic stroke. *Int. J. Biochem. Cell Biol* **44**:262–265

Chakraborty I., Chakraborty S., 2019. Next Generation Approach of Biological Data Analysis through in silico Prediction and Analysis of Small ncRNA-RNA Interactions in Human Tissues. *Jordan J Biol Sci.*,**12(4)**: 477 – 485.

Chavez-Perez V.A., Strasberg-Rieber M., Rieber M. 2011. Metabolic utilization of exogenous pyruvate by mutant p53 (R175H) human melanoma cells promotes survival under glucose depletion. *Cancer Biol. Ther.* **12(7):** 647–656.

Edwards C.B., Copes N., Brito A.G., Canfield J., Bradshaw P.C.2013. Malate and Fumarate Extend Lifespan in Caenorhabditis elegans. *PLoS ONE* **8(3):** 58345.

Filimonov D.A., Druzhilovskij D.S., Lagunin A.A., Gloriozova T.A., Rudik A.V., Dmitriev A.V., Pogodin P.V., Porojkov V.V. 2018. Computer prediction of biological activity spectra of chemical compounds: possibilities and limitations. *Biomed. Chem.: Res. Methods.* **1(1)**:e00004

Finisterer J.2008. Leigh and Leigh-like syndrome in children and adults. *Pediatr. Neurol.* **39(4):** 223–235.

Fink B.D., Bai F., Yu L. [et al.] 2018. Oxaloacetic acid mediates ADP-dependent inhibition of mitochondrial complex II-driven respiration. *J. Biol. Chem.* **293(51):** 19932–19941.

Halestrap A.P., Wilson MC. 2012. The monocarboxylate transporter family--role and regulation. *IUBMB Life.* **64(2):** 101–109.

Her Y.F. 2015. Succinate Dehydrogenase Loss in Familial Paraganglioma: Biochemistry, Genetics, and Epigenetics. *Int. J. Endocrinol.* **1:** 296167.

Lasseter B.F. 2019. Biochemistry in the Lab: A Manual for Undergraduates. *Boca Raton* :188.

Lu Y.X., Ju H.Q., Liu Z.X., [et al.].2018. Cancer Res. 15;**78(8):**1972-1985.

Martin L., Schwarz S., Breitsprecher D. 2014. Analyzing Thermal Unfolding of Proteins: The Prometheus NT.48. *NanoTemper Technologies GmbH* :1-8.

New M., Van Acker T., Sakamaki J.I., Jiang M., Saunders R.E., Long J., Wang V.M, Behrens A., Cerveira J., Sudhakar P., Korcsmaros T., Jefferies H.B.J., Ryan K.M., Howell M., Tooze S.A.2019. The Role of Autophagy in Pancreatic Cancer—Recent Advances. *Cancer Res.* 15;**79(8):**1884-1898.

Pesi R., Balestri F., Ipata P.L.2018. Metabolic interaction between urea cycle and citric acid cycle shunt: A guided approach. *Biochem. Mol. Biol. Educ*. **46(2):**182–185.

Semenza G.L.2004. Hydroxylation of HIF-1: Oxygen Sensing at the Molecular Level. *Physiol.* **19(4):** 176 –182.

Shahouzehi B., Masoumi-Ardakani Y., Fallah H., Aminizadeh S. 2023. Concomitant Administration of L-carnitine and Performing High-Intensity Interval Training Effects on the Genes Involved in Mitochondrial Fusion and Apoptosis in Rat Liver. *Jordan J Biol Sci.*,**16(1)**: 21-26

Stunova A, Vistejnova L. 2018. Dermal fibroblasts-A heterogeneous population with regulatory function in wound healing. *Cytokine Growth Factor Rev.*; **39**:137–150.

Vidoni E.D., Choi I.Y., Lee P., Reed G., Zhang N., Pleen J., Mahnken J.D., Clutton J., Becker A., Sherry E., Bothwell R., Anderson H., Harris R.A., Brooks W., Wilkins H.M., Mosconi L., Burns J.M., Swerdlow R.H.2021. Safety and target engagement profile of two oxaloacetate doses in Alzheimer's patients. *Alzheimers. Dement.* **17(1):**7-17.

Wilkins H.M., Harris J.L., Carl S.M., Lu J., Selfridge J. Eva, Roy N., Hutfles L., Koppel S., Morris J., Burns J.M., Michaelis M.L., Michaelis E.K., Brooks W.M., Swerdlow R.H., Genet H. M. 2014. Oxaloacetate activates brain mitochondrial biogenesis, enhances the insulin pathway, reduces inflammation and stimulates neurogenesis. *Hum Mol Genet*. **23(24):**6528-41.

Williams D.S, Cash A., Hamadani L., Die mer T.2009. Oxaloacetate supplementation increases lifespan in Caenorhabditis elegans through an AMPK/FOXO-dependent pathway. *Aging Cell* **8**:765-768.

Zerr I., Villar-Piqué A., Schmitz V.E., Poleggi A., Pocchiari M., Sánchez-Valle R., Calero M., Calero O., Baldeiras I., Santana I., Kovacs G.G., Llorens F., Schmitz M.2019. Evaluation of Human Cerebrospinal Fluid Malate Dehydrogenase 1 as a Marker in Genetic Prion Disease Patients. *Biomolecules*. **28;9(12):**800.

Zhao T., Liu J., Zeng X., Wang W., Li S., Zang T., Peng J., Yang Y. 2021. Prediction and collection of protein-metabolite interactions. *Brief. Bioinformatics*. **22(5)**:bbab014.

JJBS

Volume 17, Number 1,March 2024
ISSN 1995-6673
Pages 135 – 140
https://doi.org/10.54319/jjbs/170113

Jordan Journal of Biological Sciences

Allicin (diallylthiosulfinate) Restores the Altered Lipid Profile, Erythrocyte Fragility and Permeability in 7,12-dimethylbenz(a)anthracene-induced Hamster Buccal Pouch Carcinogenesis

Sasikumar Dhanarasu*

Department of Pharmaceutical Chemistry, College of Pharmacy, University of Hafr Al Batin, Kingdom of Saudi Arabia

Received: April 15, 2023; Revised: August 8, 2023; Accepted: August 21, 2023

Abstract

To investigate the effect of the restoring effects of allicin (diallylthiosulfinate, *DADS*) on the altered lipid profile, osmotic fragility and membrane-bound enzymes in 7,12-dimethylbenz(a)anthracene (DMBA) – induced hamster buccal pouch carcinogenesis. 1 week after receiving *DADS* (20 mg/kg body weight) orally, the buccal pouches of hamsters were painted daily with 0.5% DMBA in liquid paraffin for 14 weeks. The experiment was terminated at the end of 16 weeks. The restoring effects of *DADS* were evaluated by measuring the lipid profile, osmotic fragility and membrane-bound enzymes were analyzed by using specific colorimetric methods. The modified levels of lipid profiles (total cholesterol, triglycerides, phospholipids, HDL, LDL and VLDL) in plasma, RBC-membrane and buccal mucosa tissues in DMBA-administered hamsters were normalized in *DADS*-treated animals. We observed an altered activity of erythrocyte membrane-bound enzyme (Na^+K^+-ATPase) and disturbed extracellular Na^+ and intracellular K^+ cation in the plasma tumor bearing animals, which suggests that the membrane permeability is affected during DMBA-induced oral carcinogenesis. The membrane stabilizing effects of *DADS* were confirmed by erythrocytes' osmotic fragility and the levels of sodium, potassium and the activity of Na^+K^+-ATPase were restored in DMBA-treated animals after treatment with the *DADS*. Increased erythrocyte fragility and permeability in cancer animals are probably due to their altered lipids, osmotic fragility and membrane-bound enzymes. Oral administration of *DADS* to cancer animals prevented the alterations in red cell fragility and the activity of membrane-bound Na^+K^+-ATPase, which indicates the role of *DADS* in maintaining the structural integrity of erythrocytes during carcinogenesis.

Keywords: Oral cancer, 7,12-dimethylbenz(a)anthracene, lipid profile, osmotic fragility, membrane-bound enzymes, allicin, diallylthiosulfinate

1. Introduction

Cancer is one of the most common causes of morbidity and mortality today (Cogliano V *et al*., 2004); it constitutes around 2.1% of all cancer (Alkhadar H *et al*., 2021). Oral cancer refers to a subset of head and neck cancers that arise in the lips, tongue, salivary glands, gingiva, mouth floor, oropharynx, buccal surfaces and other intra-oral areas (Conway DI *et al*., 2018). It is due to alcohol consumption, betel nut chewing, tobacco use, diet, lifestyle habits and infection (Sung H *et al*., 2021). Alterations in circulating lipoproteins are found to be associated with breast cancer and colorectal cancer (Forones NM *et al*., 1998). The mechanisms underlying cancer cachexia are poorly understood, but it was suggested that increased lipolysis might play a role. The changes in lipid profiles have long been associated with cancer because lipids play a key role in the maintenance of cell integrity (Glaus A, 1998). The abnormalities in lipid and lipoprotein patterns produce several pathological diseases including cancer (Manoharan S *et al*., 1995). Many cohort studies have shown in recent years that total cholesterol was associated with the risk of several different cancers (Kitahara CM *et al*., 2011; Strasak AM *et al*., 2009; Iso H *et al*., 2009). Lipoproteins are responsible for the transport of lipids through the vascular and extracellular tissue from their site of synthesis or absorption to peripheral tissues. Altered levels of HDL, VLDL and LDL have been implicated in the pathogenesis of several diseases, including cancer (Alaupovic P, 1996). Measurement of mean corpuscular fragility of erythrocyte membranes is useful to assess the alterations in the integrity of cell structure and function. Alteration in membrane fragility has been documented in hemolytic diseases, diabetes mellitus and cancer (Jain SK *et al*., 1983). The sodium pump (Na^+K^+-ATPase) has been implicated in the regulation of many cellular functions, including cell volume regulation. Na^+K^+-ATPase has an important role in regulating the osmotic balance of the red blood cells and maintains a high concentration of intracellular potassium (Mayne PD, 1994). Raman spectroscopy of serum in DMBA-induced oral carcinogenesis hamster model reveals early changes,

* Corresponding author. e-mail: drdskumar31@yahoo.com, sdhanarasu@uhb.edu.sa.

suggesting serum RS (SRS) potential for early diagnosis and introducing a novel *ex vivo* sequential approach for understanding cancer (Priyanka A *et al*., 2023).

Several medicinal plants and their constituents have been reported to prevent experimentally induced squamous cell carcinomas (Dhanarasu S *et al*., 2010; Sasikumar D *et al*., 2010; Manoharan S *et al*., 2006). Our previous studies indicated that medicinal plants modulate the effect of circulatory antioxidants against oral carcinogenesis (Dhanarasu S *et al*., 2010). Various phytoconstituents such as carotenoids, vitamin C and phenolic acids present in medicinal plants possess protective effects (Samir Q *et al*., 2015). Allicin, (diallylthiosulfinate, *DADS*), is the main biologically active compound derived from garlic (*Allium sativum* L.). It became an object of interest due to its potential to confer a vast spectrum of health benefits including antimicrobial, antifungal and antiparasitic (Koch HP and Lawson LD, 199), cardioprotective (Gonen A *et al*., 2005), anti-inflammatory (Lang A *et al*., 2004) and anticancer activities (Hirsch K *et al*., 2000). However, no evidence is available on the ability of allicin to have ameliorative effects associated with altered lipid profile, osmotic fragility and membrane-bound enzymes in 7,12-dimethylbenz(a)anthracene (DMBA)-induced hamster buccal pouch carcinogenesis. Hence, the present study was designed to focus on the restorative role of allicin on the status of lipid profile, osmotic fragility and membrane-bound enzymes of DMBA-induced oral carcinogenesis.

2. 2. Materials and Methods

2.1. Chemicals

7,12-dimethylben(a)anthracene (DMBA) was obtained from Sigma Aldrich Chemical Limited (St. Louis, MO, USA) while allicin was purchased from Shanghai Harvest Pharmaceutical Co., Ltd. (Shanghai, China). All other chemicals utilized in the present study were of analytical grade.

2.2. Animals

The animals were obtained from Central Animal House, King Saud University, Riyadh, KSA. 8-10 weeks old, male golden Syrian hamsters (*Mesocricetus auratus,* 80-120 g) were used for the experiments. The animals were housed in polypropylene cages at room temperatures (22±2ºC) and relative humidity of 55± 5% with a 12 hr light/dark cycle in an experimental room. They were provided with Purina chow diet pellets (Manufactured by Grain Silos and Flour Mills Organization, Riyadh, KSA) and tap water *ad libitum*. Animals were acclimatized for a week before the study. All the experimental protocols were approved by the Institutional Animal Care and Use Committee of the University of Hail, KSA.

2.3. Experimental protocol

The Golden Syrian hamsters were randomized into four groups of 10 animals each as illustrated in the experimental protocol in Figure 1. The left buccal pouches of animals allocated in group I were painted with liquid paraffin thrice a week for 14 weeks and used as negative control animals. Similarly, the left buccal pouches of animals ingroups II and III were painted with 0.5 % DMBA in liquid paraffin thrice a week for 14 weeks (Morris AL, 1961).While the animals in group II received no other treatment, those in group III received oral administration of allicin (20 mg of powder/kg body weight), starting one week before exposure to the carcinogen and continued every other day(once in 2 days), until each animal was sacrificed. Group IV animals received oral administration of allicin (20 mg/kg body weight) alone throughout the experimental period. The experiment was terminated at the end of 16weeks and all animals after being given anesthesia were euthanized by cervical dislocation. The experiments were designed according to our previous studies (Dhanarasu S *et al*., 2010; Sasikumar D *et al*., 2010; Manoharan S *et al*., 2006).

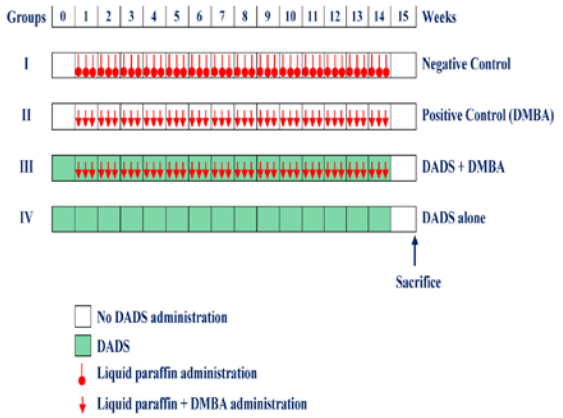

Figure 1. Experimental protocol for restoring effects of allicin against DMBA-induced carcinogenesis.

2.4. Blood and tissues samples

2.4.1. Preparation of serum and plasma

Plasma was separated from heparinized blood by centrifugation at 1000g for 15 min and stored at –20ºC for biochemical assays.

2.4.2. Preparation of Hemolysate

The erythrocytes remaining after the removal of plasma were washed three times with 310mM isotonic Tris-HCl buffer (pH 7.4). Hemolysis was carried out by pipetting out the washed erythrocyte suspension into polypropylene centrifuge tubes, which contained 20mM hypotonic Tris-HCl buffer (pH 7.2). The hemolysate was separated by centrifugation at 3500g for 15min at 20°C.

2.4.3. Isolation of Erythrocyte Membrane

The erythrocyte membrane was prepared by the method of Dodge JT *et al*. (1963) and modified by Quist EE (1980).

2.4.4. Preparation of buccal pouch tissues homogenate

Tissue samples from animals were washed with ice-cold saline and dried between folds of filter paper, weighed and homogenized using an appropriate buffer in an all-glass homogenizer with Teflon pestle. The homogenate was centrifuged at 1000g for 5 minutes and the supernatant was then used for the biochemical estimations.

2.5. Biochemical estimations

Biochemical estimations were carried out in blood and tissue samples of control and experimental animals in each group.

2.5.1. Estimation of lipid and lipoproteins

Lipid extraction was done from plasma, erythrocyte membrane and tissue by the method of Folch J *et al*., (1957). The lipid extractions were used to estimate lipid profile of plasma. Total cholesterol was estimated by the method of Parekh AC and Jung DH (1970). Phospholipids were estimated by the method of Zilversmit DB and Davis AK (1950). Triglycerides were estimated by the method of Foster LB and Dunn RT (1973). The HDL cholesterol was estimated by the heparin-manganese chloride precipitation method (Sperry WM and Webb M. 1950), whereas LDL-Cholesterol and VLDL-Cholesterol were calculated according to Friedewald WT *et al*. (1972). The *in vitro* erythrocyte osmotic fragility was evaluated in all the animals in each group using the method described by Faulknet WR and King JW (1970).

2.6. Statistical analysis

The values are expressed as mean±SD. The statistical comparisons were performed by one-way analysis of variance (ANOVA) followed by Duncan's multiple range test (DMRT), using SPSS version 16.0 for windows (SPSS Inc. Chicago; http://www.spss.com). The values are considered statistically significant if the *p*-value was less than 0.05.

3. Results

The total cholesterol, LDL-cholesterol and FFA were increased, whereas the HDL-cholesterol, phospholipids and triglycerides levels were decreased in the plasma of tumor-bearing animals as compared to negative control animals (Table 1). The total cholesterol was significantly increased whereas phospholipids were slightly decreased in the RBC membrane of tumor-bearing hamsters as compared to control animals (group I, Table 2). The level of total cholesterol was significantly increased whereas the phospholipids and FFA were decreased in buccal mucosa tissues of DMBA-painted (group II) animals as compared to control (group I) animals (Table 3). Increased c/p ratio was observed in plasma, RBC membrane and in tumor tissues. Oral administration of *DADS* normalized the altered levels of lipids and significantly prevented hyperlipidemia in tumor-bearing animals. Hamsters treated with *DADS* alone showed (group IV) no significant difference in the levels of lipid and lipoproteins as compared to control animals (group I). The fragility curve of tumor-bearing animals was shifted to the right for the control animals (group I, Fig. 2).

Table 1. Shows the levels of plasma lipid profiles in control and experimental animals in each group.

Parameters	Group I Negative Control	Group II Positive Control (DMBA)	Group III *DADS* + DMBA	Group IV DADS alone
Total Cholesterol (mg / dl)	81.61±5.64^{a}	138.5±12.86^{b}	91.73±6.92^{c}	81.01±6.20^{a}
HDL-Cholesterol (mg/dL)	21.55±1.69^{a}	16.52±1.33^{b}	23.40±1.72^{ac}	21.03±1.54^{d}
LDL-Cholesterol (mg/dL)	49.7±3.81^{a}	136.52±11.32^{b}	57.00±4.30^{c}	51.10±3.78^{ac}
VLDL-Cholesterol (mg/dL)	9.68±0.75^{a}	16.41±1.34^{b}	11.74±0.84^{c}	7.71±0.68^{a}
Phospholipids (mg/dL)	91.61±7.51^{a}	81.22±5.41^{b}	87.82±7.42^{ab}	91.42±6.88^{a}
Triglycerides (mg/dL)	48.47±3.68^{a}	83.41±6.34^{b}	53.61±4.10^{c}	41.61±3.14^{d}
Free Fatty Acids (mg/dL)	6.10±0.46^{a}	11.30±0.82^{b}	6.66±0.51^{a}	5.84±0.44^{a}
C/p ratio	0.89±0.07^{a}	1.71±0.12^{b}	1.05±0.09^{c}	0.89±0.06^{a}

Values are expressed as mean ± SD for 10 animals in each group.
Values not sharing a common superscript letter differ significantly at $p<0.05$ (DMRT).

Table 2. The table shows the levels of RBC membrane lipid profiles in control and experimental animals in each group.

Parameters	Group I Negative Control	Group II Positive Control (DMBA)	Group III *DADS*+DMBA	Group IV DADS alone
Total Cholesterol (µg / mg protein)	128.42±9.75^{a}	198.01±13.236^{b}	137.41±11.43^{a}	127.02 ±9.67^{a}
Phospholipids (µg / mg protein)	277.62±21.12^{a}	241.35±18.40^{b}	266.75±21.14^{abc}	274.75±21.90^{ac}
C/p ratio	0.46±0.03^{a}	0.82±0.07^{b}	0.52±0.03^{a}	0.46±0.03^{a}

Values are expressed as mean ± SD for 10 animals in each group.
Values not sharing a common superscript letter differ significantly at $p<0.05$ (DMRT).

Table 3. The table shows the lipid profile in the buccal mucosa tissues of control and experimental animals in each group.

Parameters	Group I Negative Control	Group II Positive Control (DMBA)	Group III *DADS* + DMBA	Group IV DADS alone
Total Cholesterol (mg / g tissue)	3.88±0.28^{a}	8.61±0.66^{e}	4.21±0.33^{a}	4.01±0.32^{a}
Phospholipids (mg / g tissue)	12.60±0.94^{ab}	7.91±0.61^{e}	12.30±0.87^{bc}	13.65±0.95^{a}
Free Fatty Acids (mg / g tissue)	8.91±0.66^{a}	5.51±0.42^{e}	8.44±0.65^{ab}	8.73±0.67^{ab}
C/p ratio	0.31±0.01^{a}	1.09±0.07^{e}	0.34±0.04^{a}	0.29±0.03^{a}

Values are expressed as mean±SD for 10 animals in each group.
Values not sharing a common superscript letter differ significantly at $p<0.05$ (DMRT).

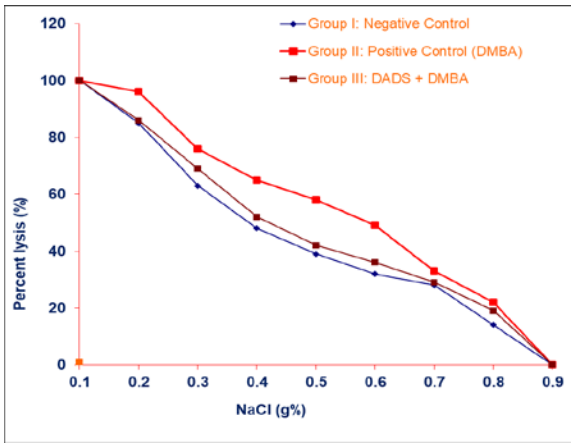

Figure 2. Shows the osmotic fragility curves for control and experimental animals in each group.

The mean corpuscular fragility was also significantly higher in cancer (group II) a nimals as compared to controls (Table 4). The administration of DADS to tumor-bearing animals led to a leftward shift in the osmotic fragility curve, particularly evident in animals with cancer within group III. Mean corpuscular fragility values did not differ significantly in animals treated with *DADS* alone (group IV) as compared to control animals (group I). In table 4, the activity of m embrane-bound $Na^{+}K^{+}$-ATPase was significantly decreased in the RBC m embrane of DMBA-induced buccal mucosa cancer animals (group II) as compared to control group a nimals (group I). The plasma sodium level was decreased whereas potassium level was increased in DMBA-induced oral carcinogenesis. The levels of s odium, potassium and the activity of $Na^{+}K^{+}$-ATPase were restored in DMBA-treated animals after treatment with the *DADS*. No significant differences were noticed between the control and animals treated with the *DADS* alone (group IV).

Table 4. The table shows the levels of plasma sodium and potassium and the activity of erythrocyte membrane $Na^{+}K^{+}$-ATPase and mean corpuscular fragility in control and experimental animals in each group.

Parameters	Group I Negative Control	Group II Positive Control (DMBA)	Group III *DADS* + DMBA	Group IV DADS alone
Plasma Sodium (meq / l)	121.81±9.19^{a}	104.93±8.15^{b}	116.42±8.71^{ab}	121.62±8.51^{a}
Plasma Potassium (meq / l)	3.64±0.35^{a}	5.39±0.35^{b}	3.96±0.31^{a}	3.65±0.28^{a}
Erythrocyte membrane $Na^{+}K^{+}$-ATPase (Units*)	0.42±0.03^{a}	0.24±0.02^{b}	0.45±0.02^{c}	0.40±0.04^{ac}
Mean Corpuscular Fragility**	0.35±0.04^{a}	0.56±0.05^{b}	0.41±0.03^{a}	0.39±0.03$^{a\#}$

Values are expressed as mean ± SD for 10 animals in each group.
The graphical representation for these values is not shown in figure 2.
Values not sharing a common superscript letter differ significantly at $p<0.05$ (DMRT).
* µ moles of inorganic phosphorus liberated/hour/mg protein.
** Concentration of NaCl solution (g %) at 50 % hemolysis.

4. Discussion

Lipids are important for various biological functions in the cell membrane of t he human body including maintaining cell integrity, cell growth and division of normal and malignant tissues (Chawda JG *et al*., 2011). Changes in the lipid profiles have been observed in group II DMBA-induced oral cancer hamsters (Neerupakam M *et al*., 2014). The increased levels of plasma triglycerides (TGs), LDL-Cholesterol and VLDL-Cholesterol (Laisupasin P *et al*., 2013, Kapil U *et al*., 2013) were observed in cancer animals compared with group I animals. Cholesterol can facilitate metastasis via the induction of e strogen-receptor-positive cancer cells (Cedó L *et al*., 2019). However, the conflicting findings regarding dyslipidemia and cancer, as documented by Ma HQ *et al* (2016) and Li X *et al* (2018), underscore the intricate and multifaceted nature of this disease relationship. The levels of total cholesterol, free fatty acids and LDL-cholesterol were significantly increased whereas phospholipids and HDL-cholesterol were decreased in the plasma of D MBA-treated animals. The level of total cholesterol was increased whereas phospholipids were moderately decreased in the erythrocyte membrane of DMBA-painted animals. The level of cholesterol was increased whereas phospholipids and free fatty acids were decreased in tumor tissues of cancer-bearing animals as compared to control animals. Oral administration of *DADS* brought back the values to near normal range in DMBA-painted hamsters. It has been reported that cancer subjects showed weight loss accompanied by hyperlipidemia at advanced stages of the tumor. The increase in plasma cholesterol in cancer animals can be related to increased circulatory free fatty acids, which in turn leads to increased VLDL-Cholesterol secretion by the liver, resulting in an increase in cholesterol output into circulation. Increased plasma FFA is attributed to the hypermetabolic state of

cancers (Legaspi A *et al*., 1987). Cholesterol is an essential constituent of lipoprotein fractions like LDL, HDL and VLDL. Seventy-five percent of the plasma cholesterol is transported in the form of LDL cholesterol. Body cells sequester cholesterol from the LDL fraction of lipoproteins (Kesaniemi YA *et al*., 1983). In the present study, a significant decrease in plasma HDL-cholesterol and an increase in LDL-cholesterol were observed in cancer animals (Budd D and Ginsberg H, 1986, Dessi S *et al*., 1992). The increase in plasma cholesterol in cancer subjects can therefore be related to a decrease in HDL fraction or increase in LDL-cholesterol. Cholesterol is essential for the maintenance of the structural and functional integrity of biological membranes. It is also involved in the activity of membrane-bound enzymes (Sabine JR, 1977). The observed increase in cholesterol and c/p ratio (group II animals) indicates the loss of membrane fluidity in cervical cancer patients (Cooper RA, 1977). Alterations in the erythrocyte lipid composition may be a reflection of altered plasma lipid, due to an ineffective exchange mechanism with plasma. An increase in cholesterol in tumor tissues is due to the sequestration of cholesterol from circulation for the biogenesis of new bio-membrane in tumor tissues. Lowered fatty acids in tumor tissues are responsible for decreased phospholipids levels and are partly responsible for lowered lipid peroxidation in tumor tissues. Oral administration of *DADS* to DMBA painted animals reversed the lipids levels to near normal range, which indicates their lipids regulatory effects in tumor-bearing animals.

Erythrocytes of tumor-bearing animals were more fragile than those from control animals (Abou-Seif MA *et al*., 2000). Erythrocytes and erythrocyte membranes are more vulnerable to lipid peroxidation due to constant exposure to high oxygen tension and richness in polyunsaturated fatty acids respectively (Eritsland J, 2000). Increased osmotic fragility in cancer animals can be due to the increased oxidative stress in erythrocytes (Dhanarasu S *et al*., 2010, Sasikumar D *et al*., 2010and Manoharan S *et al*., 2006). Overproduction of reactive oxygen species has been implicated in the alterations of membrane structure and function. Increased lipid peroxidation is therefore responsible for the increase in osmotic fragility (Hebbel RP, 1986). The decline in red blood cell reduced glutathione observed in tumor-bearing animals is partly responsible for the increased osmotic fragility of erythrocytes (McLellan LI and Wolf CR, 1999).We observed an altered activity of erythrocyte membrane-bound enzyme (Na^+K^+-ATPase) and disturbed extracellular (Na^+) and intracellular (K^+) cation in the plasma tumor-bearing animals, which suggests that the membrane permeability was affected during DMBA-induced oral carcinogenesis. Free radical-induced oxidative damage to membrane ATPase has been assumed to be crucial for cell lysis (Brovelli A *et al*., 1977). Increased erythrocyte fragility and permeability in cancer animals are probably due to their altered lipids, lipid peroxidation and antioxidant status. Oral administration of *DADS* to these cancer animals prevented the alterations in red cell fragility and the activity of membrane-bound Na^+K^+-ATPase, which indicates the role of *DADS* in maintaining the structural integrity of erythrocytes during carcinogenesis.

5. Conclusion

The *DADS* protected the alteration seen in membrane fragility and permeability. It also reversed the lipids levels to near normal range, which indicates their lipids regulatory effects in tumor-bearing animals. The present study thus concludes that allicin has potent restoring effects on altered lipids and red cell fragility in DMBA-induced oral carcinogenesis.

Acknowledgment

We are grateful to the authority of the College of Medicine, the University of Hail, for providing facilities to carry out the research study.

References

Abou-Seif MA, Rabia A and Nasr M. 2000. Antioxidant status, erythrocyte membrane lipid peroxidation and osmotic fragility in malignant lymphoma patients. *Clin Chem Lab Med*, **38(8)**: 737-42.

Alaupovic P. 1996. Significance of apolipoproteins for structure, function and classification of plasma lipoproteins. *Methods Enzymol*, **263**: 32-60.

Alkhadar H, Macluskey M, White S, Ellis I and Gardner A. 2021. Comparison of machine learning algorithms for the prediction of five-year survival in oral squamous cell carcinoma. *J Oral Pathol Med*, **50**: 378-84.

Brovelli A, Suhail M, Pallavicini G, Sinigaglia F and Balduini C. 1977. Self-digestion of human erythrocyte membranes. Role of adenosine triphosphate and glutathione. *Biochem J*, **164(2)**: 469-72.

Budd D and Ginsberg H. 1986. Hypocholesterolemia and acute myelogenous leukemia. Association between disease activity and plasma low-density lipoprotein cholesterol concentrations. *Cancer*, **58(6)**: 1361-5.

Cedó L, Reddy ST, Mato E, Blanco-Vaca F and Escolà-Gil JC. 2019. HDL and LDL: Potential New Players in Breast Cancer Development. *J Clin Med*, **8(6)**: 853.

Chawda JG, Jain SS, Patel HR, Chaduvula N and Patel K. 2011. The relationship between serum lipid levels and the risk of oral cancer. *Indian J Med PaediatrOncol,* **32(1)**: 34-7.

Cogliano V, Straif K, Baan R, Grosse Y, Secretan B, El Ghissassi F. 2004. WHO International Agency for Research on Cancer. Smokeless tobacco and tobacco-related nitrosamines. *Lancet Oncol*. **5(12)**: 708.

Conway DI, Purkayastha M and Chestnutt IG. 2018. The changing epidemiology of oral cancer: definitions, trends and risk factors. *Br Dent J*, **225(9)**: 867-873.

Cooper RA. 1977. Abnormalities of cell-membrane fluidity in the pathogenesis of disease. *N Engl J Med*, **297(7)**: 371-7.

Dessi S, Batetta B, Pulisci D, Spano O, Cherchi R, Lanfranco G, Tessitore L, Costelli P, Baccino FM, Anchisi C, Pani P. 1992. Altered pattern of lipid metabolism in patients with lung cancer. *Oncology*, **49(6)**: 436-41.

Dhanarasu S, Selvam M, Salama SM, Shanmugam M and Sethuraman P. 2010. *Terminalia Arjuna* (Roxb.) Modulates Circulatory Antioxidants on 7, 12-dimethylbenz(a)anthracene-induced Hamster Buccal Pouch Carcinogenesis. *Oman Med J,* **25(4)**: 276-81.

Dodge JT, Mitchell C and Hanahan DJ. 1963. The preparation and chemical characteristics of hemoglobin-free ghosts of human erythrocytes. *Arch BiochemBiophys*, **100**: 119-30.

Eritsland J. 2000. Safety considerations of polyunsaturated fatty acids. *Am J ClinNutr*, **71(1)**: 197S-201S.

Faulknet WR and King JW. 1970. Manual of Clinical Laboratory Procedures. Clevland OH: Chemical Rubber Company, 345.

Folch J, Lees M and Sloane Stanely GH. 1957. A simple method for the isolation and purification of total lipides from animal tissues. *J Biol Chem*,**226**: 497-509.

Forones NM, Falcao JB, Mattos D an d Barone B. 1998. Cholesterolemia in colorectal cancer. *Hepatogastroenterology*, **45(23)**: 1531-4.

Foster LB and Dunn RT. 1973. Stable reagents for determination of serum triglycerides by a co lorimetric Hantzsch condensation method. *Clin Chem*, **19(3)**: 338-340.

Friedewald WT, Levy RI and Fredrickson DS. 1972. Estimation of the concentration of low-density lipoprotein cholesterol in plasma, without use of the preparative ultracentrifuge. *Clin Chem*, **18(6)**: 499-502.

Glaus A. 1998. Fatigue and cachexia in Cancer patients. *Support Care Cancer*, **6**: 77-78.

Gonen A, Harats D, Rabinkov A, Miron T, Mirelman D, Wilchek M, Weiner L, Ulman E, Levkovitz H, Ben-Shushan D and Shaish A. 2005. The antiatherogenic effect of allicin: possible mode of action. *Pathobiology*, **72(6)**: 325-34.

Hebbel RP. 1986. Erythrocyte antioxidants and membrane vulnerability. *J Lab Clin Med*, **107(5)**: 401-4.

Hirsch K, Danilenko M, Giat J, Miron T, Rabinkov A, Wilchek M, Mirelman D, Levy J and Sharoni Y. 2000. Effect of purified allicin, the major ingredient of freshly crushed garlic, on cancer cell proliferation. *Nutr Cancer*, **38(2)**: 245-54.

Iso H, Ikeda A, Inoue M, Sato S, Tsugane S an d JPHC Study Group. 2009. Serum cholesterol levels in relation to the incidence of cancer: the JPHC study cohorts. *Int J Cancer*, **125(11)**: 2679-86.

Jain SK, Mohandas N, Clark MR and Shohet SB. 1983. The effect of malonyldialdehyde, a product of lipid peroxidation, on t he deformability, dehydration and 51Cr-survival of erythrocytes. *Br J Haematol*, **53(2)**: 247-55.

Kapil U, Bhadoria AS, Sareen N, Singh P and Dwivedi SN. 2013. Total cholesterol and triglyceride levels in patients with breast cancer. *J Breast Cancer*, **16(1)**: 129-30.

Kesaniemi YA, Witztum JL and Steinbrecher UP. 1983. Receptor-mediated catabolism of low density lipoprotein in man. Quantitation using glucosylated low density lipoprotein. *J Clin Invest*, **71(4)**: 950-9.

Kitahara CM, Berrington de González A, Freedman ND, Huxley R, Mok Y, Jee SH and Samet JM. 2011. Total cholesterol and cancer risk in a lar ge prospective study in Korea. *J Clin Oncol*, **29(12)**: 1592-8.

Koch HP an d Lawson LD. 1996. Garlic: the Science and therapeutic application of *Allium sativum* L. and related species. 2nd ed. Baltimore: Williams & Wilkins.

Laisupasin P, Thompat W, Sukarayodhin S, Sornprom A an d Sudjaroen Y. 2013. Comparison of Serum Lipid Profiles between Normal Controls and Breast Cancer Patients. *J Lab Physicians,***5(1)**: 38-41.

Lang A, Lahav M, Sakhnini E, Barshack I, Fidder HH, Avidan B, Bardan E, Hershkoviz R, Bar-Meir S and Chowers Y. 2004. Allicin inhibits spontaneous and TNF-alpha induced secretion of proinflammatory cytokines and chemokines from intestinal epithelial cells. *ClinNutr*, **23(5)**: 1199-208.

Legaspi A, Jeevanandam M, Starnes HF J r and Brennan MF. 1987. Whole body lipid and energy metabolism in the cancer patient. *Metabolism*, **36(10)**: 958-63.

Li X, Liu ZL, Wu YT, Wu H, Dai W, Arshad B, Xu Z, Li H, Wu KN and Kong LQ. 2018. Status of lipid and lipoprotein in female breast cancer patients at in itial diagnosis and during chemotherapy. *Lipids Health Dis*, **17(1)**: 91.

Ma HQ, Cui LH, Li CC, Yu Z and Piao JM. 2016. Effects of Serum Triglycerides on Prostate Cancer and Breast Cancer Risk: A Meta-Analysis of Prospective Studies. *Nutr Cancer*, **68(7)**: 1073-1082.

Manoharan S, Panjamurthy K, Vasudevan K an d Sasikumar D. 2006. Protective effect of *Jasminum grandiflorum* Linn. On DMBA-induced chromosomal aberrations in bone marrow of wister rats. *Int J Pharmacol*, **2(4)**: 406-410.

Manoharan S, Ramachandran CR and Nagini S. 1995. The altered lipid profile in oral cancer patients is related to life-style. *Medical science research*, **23(7)**: 493-495.

Mayne PD. 1994. Sodium, water and potassium metabolism. In Mayne PD, editor. Clinical chemistry in diagnosis and treatment. 6th ed. London: Edward Arnold; 25-78.

McLellan LI and Wolf CR. 1999. Glutathione and glutathione-dependent enzymes in cancer drug resistance. *Drug Resist Updat*, **2(3)**: 153-164.

Morris AL. 1961. Factors influencing experimental carcinogenesis in the hamster cheek pouch. *J Dent Res*, **40**: 3-15.

Neerupakam M, Alaparthi RK, Sathish S, Katta SA, Polisetty N, Damera S. 2014. Alterations in plasma lipid profile patterns in oral cancer. *J Indian Acad Oral Med Radiol*, **26(3)**: 274-8.

Parekh AC and Jung DH. 1970. Cholesterol determination with ferric acetate-uranium acetate and sulfuric acid-ferrous sulfate reagents. *Anal Chem*. **42**: 1423-1427.

Priyanka A. Jadhav, Kshama Pansare, Arti Hole, Arvind Ingle, Rukmini Govekar, C. Murali Krishna. 2023. Serum Raman spectroscopy in experimental carcinogenesis hamster buccal pouch model: Exploring early diagnostic capability. *J Raman Spectrosc*, **54(1)**, 37-46.

Qiblawi S, Dhanarasu S, Faris MA. 2015. Chemopreventive Effect of Cardamom (*Elettaria cardamomum* L.) Against Benzo(α)Pyrene-Induced Forestomach Papillomagenesis in Swiss Albino Mice. *J Environ PatholTox*, **34(2)**: 95-104.

Quist EE. 1980. Regulation of erythrocyte membrane shape by Ca^{2+}. *BiochemBiophys Res Commun*, **92(2)**: 631-7.

Sabine JR. 1977. Cholesterol. Marcel Dekker, Inc. New York, 80-103.

Sasikumar D, Awdah H, Prema S an d Mathi S. 2010. Chemopreventive and Antilipidperoxidative Potential of *Thespesiapopulnea* (L.) on Experimental Buccal Pouch Carcinogenesis, *Ibnosina J Med BS*, **2(6)**: 269-277.

Sperry WM and Webb M. 1950. A revision of the Schoenheimer-Sperry method for cholesterol determination. *J Biol Chem*, **187(1)**:97-106.

Strasak AM, Pfeiffer RM, Brant LJ, Rapp K, Hilbe W, Oberaigner W, Lang S, Borena W, Concin H, Diem G, Ruttmann E, Glodny B, Pfeiffer KP, Ulmer H an d VHM&PP Study Group. 2009. Time-dependent association of total serum cholesterol and cancer incidence in a cohort of 172,210 men and women: a p rospective 19-year follow-up study. *Ann Oncol*, **20(6)**: 1113-20.

Sung H, Ferlay J, Siegel RL, Laversanne M, Soerjomataram I, Jemal A, Bray F. 2021.Global Cancer Statistics 2020: GLOBOCAN Estimates of Incidence and Mortality Worldwide for 36 Cancers in 185 Countries. *CA Cancer J Clin*, **71(3)**: 209-249.

Zilversmit DB and Davis AK. 1950. Microdetermination of plasma phospholipids by trichloroacetic acid precipitation. *J Lab Clin Med*, **35(1)**: 155-160.

JJBS

Volume 17, Number 1,March 2024
ISSN 1995-6673
Pages 141 – 151
https://doi.org/10.54319/jjbs/170114

Jordan Journal of Biological Sciences

Synergistic Antineoplastic and Immunomodulatory Effects of Hesperidin in Ehrlich Ascites Carcinoma Tumor Model Treated with Cisplatin

Heba M. Abd El Latif* , Asmaa M. El-Morsy , Hany M. Ibrahim , Dalia S. Morsi

Zoology Department, Faculty of Science, Menoufia University, Shebin El-Kom (postal code: 32511), Egypt.

Received: March 16, 2023; Revised: August 21, 2023; Accepted: August 25, 2023

Abstract

Despite substantial advancements in cancer research in recent years, the treatment of cancer remains fraught with difficulties. Cisplatin is a strong chemotherapeutic drug used to treat a variety of cancers, but its efficacy is limited by drug resistance and toxic effects on non-tumor tissues. The flavonoid hesperidin was reviewed to have anticancer properties. In the present study, a tumor model was established, cisplatin plus hesperidin synergism was conducted, antineoplastic and immunomodulatory effects were evaluated; oxidative stress markers and liver and kidney function tests were measured after mono and combined treatments. The mechanisms of hesperidin synergistic role with cisplatin chemotherapy were explored using ninety mice divided equally into nine groups. The findings indicated that hesperidin treatment alone, or in combination with cisplatin, inhibited tumor growth by causing cell cycle arrest, stimulating apoptosis, and reducing tumor cell proliferation. Furthermore, it stimulated anti-tumor immunity by increasing the proportion of T cytotoxic ($CD3^+CD8^+$) and T helper ($CD3^+CD4^+$) cells in the spleen with modulating effect on $CD4^+CD25^+$ regulatory cells accompanied by improving spleen cells proliferation. Moreover, a significant increase in IFN-γ and granzyme B levels of tumorized mice co-treated with 100 or 200 mg/kg hesperidin plus cisplatin was demonstrated. Interestingly, the use of hesperidin in combined treatment succeeded to counteract toxic effects induced by cisplatin on normal healthy tissues. In conclusion, the combined use of hesperidin and cisplatin has a synergistic effect that enhances the efficacy of cancer treatment by inducing apoptosis and regulating the immune response against cancer cells. Additionally, this combination therapy reduces the harmful effects of cisplatin on healthy tissues.

Keywords: Hesperidin; Antineoplastic; Immunomodulatory; antitoxic; Cisplatin; Tumor model.

1. Introduction

The malignant nature of cancer is a great challenge in modern medicine and scientific research. Despite the tremendous efforts dedicated to discovering methods for treating cancer and overcoming its poor prognosis and recurrence, it remains the most common cause of global mortality accounting for approximately ten million deaths in 2020 (Garcia et al., 2020; Sung et al., 2021). Chemotherapeutics are the most common and powerful drugs used in elimination of rapidly proliferating tumor cells even in sites far from their primary origin (Schirrmacher, 2019; Sarbaz et al., 2022). The use of chemotherapeutics is clinically limited due to their severe side and toxic effects in recipient body during treatment of malignant tumors (Liu et al., 2016; Brown et al., 2019; Aliwaini et al., 2020; Zavattaro et al., 2021; Fouad et al., 2022).

Cisplatin (Cis) is an inorganic compound comprising two chlorine atoms and two ammonia groups surrounding a central platinum atom (Pourmadadi et al., 2022). It is considered as a potent chemotherapeutic drug used for treating various human cancers, such as ovarian, breast, bladder, esophageal, cervical, head and neck, brain, and lung cancer, alone or combined with other medications (Sleijfer et al., 1985; Pourmadadi et al., 2022). The cytotoxic effect of Cis stands on its ability to inhibit the replication of rapidly proliferating cells through the formation of Cis-DNA adducts and induction of apoptosis (Siddik, 2003). Unfortunately, there are many challenges facing Cis in treating cancer including drug resistance and the potential for toxic effects on non-tumor tissues (Al-Kharusi et al., 2013; Dasari and Tchounwou, 2014; Dasari et al., 2022). Therefore, many studies aimed to develop strategies to overcome the chemotherapy drawbacks using natural products or drugs to modulate one or more mechanisms of chemoresistance, enhance their antineoplastic efficiency, and prevent toxic effects on non-tumor tissue (Osman et al., 2015; Liu et al., 2016; Donia et al., 2018; Schirrmacher, 2019; Xu et al., 2023).

Flavonoids are one of the fundamental subtypes of dietary polyphenols present in plants, vegetables, and fruits (Liu et al., 2014; Rodríguez-García et al., 2019). These are regarded as the most crucial phytochemical compounds that exhibit beneficial effects on various cancerous tissues (Spatafora and Tringali, 2012; Darband et al., 2018; Sudhakaran et al., 2019). Hesperidin (HDN) is one of the most remarkable flavonoids abundant in

* Corresponding author. e-mail: heba.abdellatif@science.menofia.edu.eg.

numerous citrus fruits such as oranges and lemons (Devi et al., 2015). There have been reports indicating that HDN exhibits a broad spectrum of biological characteristics, functioning as a strong anti-inflammatory, antioxidant, cardioprotective, neuroprotective, antimicrobial, immunomodulatory, antiviral, antiallergic, antiatherosclerotic, and anticancer compound (Aishatwi et al., 2013; Hassouna et al., 2015; Roohbakhsh et al., 2015; Ahmadi and Shadboorestan, 2016; Barreca et al., 2017). More importantly, Aggarwal et al. (2020) stated that HDN can reverse cancer cells resistance against antineoplastic drugs when used in combination with them, which makes it a promising anticancer candidate. Thus, the aim of our study was to investigate the potential anticancer properties and immunomodulatory effects of two doses of HDN supplementation in mice inoculated with Ehrlich ascites carcinoma (EAC) tumor cells and subsequently treated with Cis.

2. Material and methods

2.1. Chemicals:

Hesperidin was purchased from Sigma-Aldrich (St. Louis, MO, USA) and was dissolved in a solution of 0.9% sodium chloride. Cisplatin was purchased from Mylan SAS pharmaceutical company (Saint-Priest, France).

2.2. Tumor cell line preparation:

The EAC cell line was generously supplied by the National Cancer Institute (NCI), Cairo University, Egypt. To maintain the cell line, we performed successive intraperitoneal (i.p.) injections of 2.5×10^5 viable tumor cells in 200 µL saline, carried out every two weeks, as outlined in Ibrahim et al. (2018). These injections were administered into healthy naïve mice within our laboratory.

2.3. Animals:

Adult female Swiss albino mice (*Mus musculus*), with an age range of 6 to 8 weeks and a weight of 25-30 g, were purchased from NCI, Cairo University, Egypt. The animals were adapted for two weeks before the experiment in standard cages under optimum housing conditions, with free and unlimited access to both food and water. The study was performed after the consent of the institutional Animal Ethical Committee, Menoufia University, with approval ID: (MUFS/ F / PH /1/23).

2.4. Experimental design:

For the intended protocol, nine experimental groups were established each comprising ten randomly chosen female mice. Mice in all groups were i.p. inoculated with 2.5×10^5 EAC cells at day (d0) except in group I, II & III.

Group I: control group, injected with 0.2mL saline i.p. at d0.

Group II and III: HDN 100mg and 200mg groups, received 14 consecutive oral doses of HDN (100mg/kg b.w./day) and (200mg/kg b.w./day), respectively, from d1 to d14 according to (Berköz et al., 2021).

Group IV: EAC group, inoculated i.p. with 2.5×10^5 EAC cells at d0 (Ibrahim et al., 2018).

Group V: EAC+Cis group, EAC bearing mice injected i.p. with Cis (2mg/kg b.w.) at d3, d5 & d7 according to El-Bolkiny et al. (2021).

Group VI and VII: EAC+HDN 100mg and EAC+HDN 200mg groups, EAC bearing mice orally administrated with 14 consecutive doses of HDN as in group II and III, respectively.

Group VIII and IX: EAC+Cis+HDN 100mg and EAC+Cis+HDN 200mg groups, treated with Cis as in group V in addition to the 14 oral doses of HDN as in group II and III, respectively.

2.5. Sampling:

On the 15th day following the i.p. injection of EAC cells, samples of blood were assembled from retro-orbital sinuses of each mouse. The collected blood was divided into two tubes one mixed with EDTA for CBC analysis, and the other was allowed to coagulate for serum separation. The obtained serum was stored at -80°C for future use. Subsequently, mice were sacrificed with cervical dislocation and dissected to harvest ascitic fluid from the peritoneal cavity. In addition, the spleen was extracted from each mouse for further analysis.

2.6. EAC growth response:

Tumor growth was evaluated by changes in the total count of EAC cells, the count of viable and nonviable EAC cells, using trypan blue dye exclusion assay and the rate of tumor growth inhibition as detailed in Ibrahim et al. (2018).

2.7. Blood count analysis:

Hematological parameters, platelet count, total and differential white blood cell counts, red blood cell count, hemoglobin concentration, and hematocrit value, were manually assessed in EDTA-treated blood samples from each mouse. The methodology followed was in accordance with Dacie and Lewis (1984).

2.8. Apoptosis detection in EAC cells:

Using flow cytometer (BD Accuri C6, San Jose, CA, USA) along with appropriate software (San Jose, CA, USA), tumor early and late apoptotic cells were discriminated as mentioned previously by Ibrahim et al. (2018). Shortly, tumor cells were harvested, washed, and incubated in PBS at 4°C for thirty minutes before staining them with annexin-V (FITC)/propidium iodide (PI) at 25°C for fifteen minutes according to the manufacturing instructions of the commercial kit (Abcam, Canada).

2.9. EAC cell cycle detection:

The percentage of EAC cells in different phases of cell cycle was measured using MODFIT DNA analysis program (Verity Software House, Topsham, ME, USA, version: 2.0). A BD Accuri C6 flow cytometer and the suitable software (San Jose, CA, USA) were used for phase distribution analysis. After fixation and washing of tumor cells, they were treated with RNAase A and stained finally with PI according to Morsi et al. (2022).

2.10. Preparation of spleen cell suspension and its phenotypic analysis:

A single-cell suspension of splenocytes was prepared according to Ibrahim et al. (2010). After cell counting, using hemocytometer and viability exclusion method by trypan blue dye, T helper ($CD3^+CD4^+$), T cytotoxic ($CD3^+CD8^+$), and T regulatory ($CD4^+CD25^+$) cells were detected using anti-mouse monoclonal antibodies including Fluorescein isothiocyanate (FITC)-labelled CD3

(clone: 17A2), Phycoerythrin (PE)-labelled CD25 (clone: PC61), Allophycocyanin (APC)-labelled CD4 (clone: RM4-5), and Phycoerythrin-cyanine 5 (PE.Cy5)-labelled CD8 (clone: 53-6.7) according to their manufacturing instructions. The monoclonal antibodies were purchased through BD Bioscience Company (BD Bioscience CO, USA), and the assessments were conducted using flow cytometer (BD Accuri C6, San Jose, CA, USA) with the suitable software (San Jose, CA, USA).

2.11. Proliferation marker Ki67:

Flowcytometric analysis to detect the Ki67 nuclear protein in both tumor and spleen cells was conducted using BD Accuri C6 flow cytometer and the suitable software (San Jose, CA, USA). Cells were suspended in PBS at a concentration of one million cells per milliliter, and flowcytometric analysis was carried out using mouse Ki67 antibody (Santa Cruz Biotechnology, Inc., Texas, USA) according to manufacturer's instructions.

2.12. Granzyme B and interferon γ (IFN- γ) detection:

Sandwich enzyme linked immunosorbent assay (ELISA) was used to detect serum granzyme B (CUSABIO, CSB-E08720m, USA) and IFN-γ (CUSABIO, CSB-E04578m, USA). The ELISA procedure was conducted in accordance with the instructions outlined in the manufacturer's kit.

2.13. Biochemical analysis:

Serum samples were utilized for the assessment of oxidative stress biomarkers, including the levels of malondialdehyde (MDA; Elabscience, E-BC-K025-M, USA) and reduced glutathione (GSH; Elabscience, E-BC-K030-M, USA). The colorimetric assays were conducted in accordance with the instructions furnished by the manufacturer's kit. Moreover, the collected serum was employed to determine further biochemical parameters, including the activity of alanine aminotransferase (ALT; Linear Chemicals, REF 1105000, Spain), aspartate aminotransferase (AST; Linear Chemicals, REF 1109000, Spain), as well as the levels of total protein (SPINREACT, Ref: 1001291, Spain), albumin (SPINREACT, Ref: MX1001020, Spain), urea (SPINREACT, Ref: 1001333, Spain), and creatinine (SPINREACT, Ref: MD1001111, Spain).

2.14. Statistical analysis:

Data are expressed as mean ± standard error of mean (SEM). Statistical disparities among the groups were assessed through a one-way analysis of variance (ANOVA) test using the IBM SPSS Statistics software for Windows, Version 22 (IBM Corp., Armonk, NY USA) followed by least significant differences (LSD) post hoc test for multiple comparisons. $P<0.05$ was considered to be statistically significant.

3. Results

3.1. Hesperidin and cisplatin synergistic effect on tumor burden:

Mono-treatment of EAC-bearing mice with Cis or with the two different doses of HDN and dual treatment of EAC-bearing mice with Cis and each dose of HDN led to a highly significant ($P<0.001$) reductions in ascitic fluid volume, total tumor cell count, and tumor cell viability in comparison to the untreated EAC group(Table 1) with the greatest tumor scavenging effect induced by combined treatment with 200 mg/kg HDN and Cis, while comparison with Cis treated group showed that tumorized mice co-treated with Cis and 100 mg/kg of HDN had no significant ($P>0.05$) effect on ascitic fluid volume, total tumor cell count or tumor cell viability. On the contrary, co-treatment with 200 mg/kg HDN (in EAC+Cis+HDN 200mg/kg group) exerted a significant ($P<0.05$) reduction in the volume of ascitic fluid ($P<0.05$), total tumor cell count ($P<0.001$), and their viability ($P<0.05$). Moreover, our study clarified that the highest rate of tumor inhibition was achieved by dual-treatment of animals bearing EAC with Cis and 200 mg/kg of HDN to be 77.88%, while the rate of tumor inhibition was nearly similar in EAC+Cis group (54.07%) and EAC+Cis+HDN100 mg/kg group (57.76%) as shown in Table 1.

Table 1. Anti-tumor effects of mono- or combined-treatments in EAC-bearing mice

	Ascitic fluid volume (mL)	Tumor cells count (10^6/mL)	Tumor cells viability (%)	Tumor inhibition rate (%)
EAC	18.5±0.44	75.30±1.25	99.33±0.04	0
EAC+Cis	2.13±0.21 **	34.58±0.98 **	68.90±2.05 **	54.07
EAC+HDN 100 mg	13.16±0.40 **$^{\#\#}$	66.13±2.15 **$^{\#\#}$	92.78±1.23 *$^{\#\#}$	12.17
EAC+HDN 200 mg	10.00±0.36 **$^{\#\#}$	63.78±1.75 **$^{\#\#}$	76.79±0.60 **$^{\#}$	15.29
EAC+Cis+HDN100 mg	1.71±0.10 **	31.80±0.82 **	69.93±3.01 **	57.76
EAC+Cis+HDN200 mg	1.21±0.08 **$^{\#}$	16.65±0.57 **$^{\#\#}$	59.72±2.80 **$^{\#}$	77.88

Values are displayed as mean ± standard error of mean (SEM), n = 6. * $P<0.05$ significantly different from EAC group. ** $P<0.001$ significantly different from EAC group. $^{\#}$ $P<0.05$ significantly different from Cis-treated mice. $^{\#\#}$ $P<0.001$ significantly different from Cis-treated mice. EAC: Ehrlich ascites carcinoma, HDN: hesperidin, Cis: cisplatin.

3.2. Hesperidin and cisplatin synergistic effect on tumor cell apoptosis:

To determine the mechanism of action of HDN and/or Cis on EAC tumor cells, flowcytometric analysis of annexin-V/PI (apoptotic marker) expression was evaluated. The influence of Cis and/or HDN on tumor cell apoptosis was demonstrated in Fig. 1. The percentage of total apoptotic cells (annexin-V^+ plus annexin-V^+/PI^+) increased significantly ($P<0.001$) after mono and dual treatments of EAC mice when compared with EAC untreated group. Furthermore, dual treatment with Cis and 100 or 200 mg/kg HDN significantly ($P<0.05$) raised the rate of tumor cell apoptosis being nearly doubled in EAC+Cis+HDN 200mg/kg (42.45±1.18%) when compared with EAC+Cis group which recorded an apoptosis rate of 23.65±0.89%.

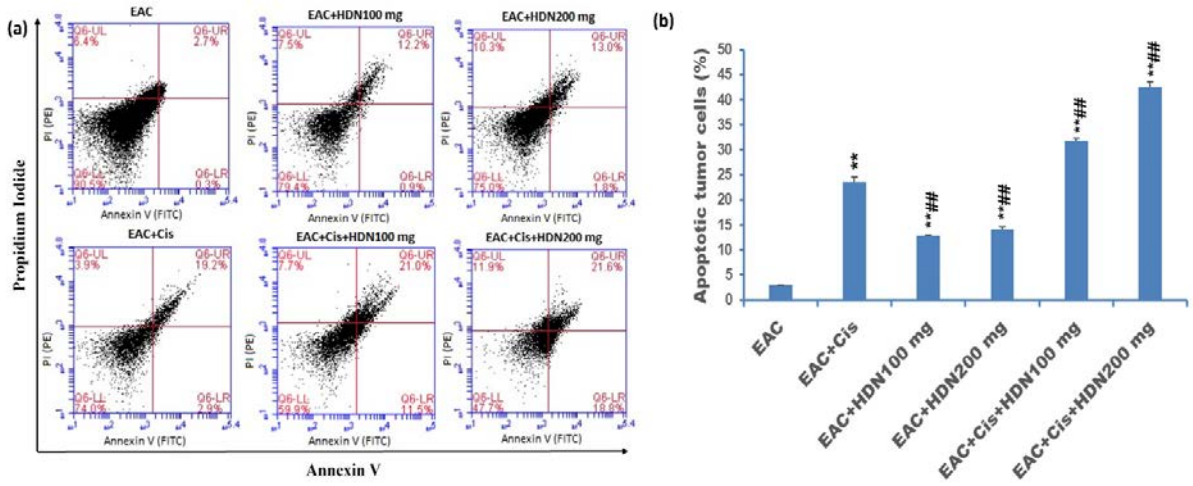

Figure 1. Hesperidin and cisplatin synergistically induced tumor cells apoptosis. Apoptotic EAC cells were distinguished by flow cytometry based on their PI/Annexin-V staining patterns. (a) The presented dot plot is representative of one trial from a total of six conducted independently. (b) Pooled data from the six experiments are presented as mean % of apoptotic tumor cells (annexin-V^+ plus annexin-V^+PI^+) ± SEM. ** P<0.001 significantly different from EAC group. $^{\#\#}$ P<0.001 significantly different from Cis-treated mice. EAC: Ehrlich ascites carcinoma, HDN: hesperidin, Cis: cisplatin, PI: propidium iodide.

3.3. Hesperidin and cisplatin synergistic effect on cell cycle and proliferation of EAC cells:

Using flowcytometry, it was possible to investigate the percentage of tumor cells across different phases of cell cycle depending on their DNA content. Results demonstrated in Fig. 2 showed appreciable changes in cell cycle after treating EAC bearing mice with Cis with or without HDN. In comparison with EAC non-treated group, there was highly significant (P<0.001) increase in G0/G1 cell population after mono-treatment with Cis (73.43±0.49%) or HDN 200mg/kg (62.10±1.09%) and co-treatment with Cis and HDN 100mg/kg (73.50±1.44%) or Cis and HDN 200mg/kg (82.45±1.41%). Simultaneously, these treatments led to a highly significant (P<0.001) decrease in cell fractions at S and G2/M phases except the effect of EAC+HDN 200 mg/kg on G2/M that was not significant (P>0.05). Co-treatment with Cis and 200 mg/kg HDN achieved a significant (P<0.05) arrest or increase of tumor cell fraction at G0/G1 phase and significant (P<0.01) decline of cell fraction in S phase and non-significant (P>0.05) decrease at G2/M phase, when compared with EAC+Cis. Thus, the influence of combined treatment with Cis and 200 mg/kg of HDN produced noticeable cell cycle specificity that highlights the synergetic role of high dose of HDN with Cis.

Furthermore, flowcytometric analysis of Ki67, a marker for cell proliferation, expression in tumor cells was evaluated. Compared with non-treated EAC group, where percentage of $Ki67^+$ tumor cells was 80.38±1.60 %, all treated groups achieved highly significant (P<0.001) reduction in the percentage of $Ki67^+$ tumor cells and the greatest rate of reduction was recorded in EAC+Cis+HDN 200mg/kg group to be 11.06±0.21% (Fig. 3). Moreover, combined treatment with Cis and 100 or 200 mg/kg of HDN showed a significant (P<0.001) decrease in $Ki67^+$ tumor cells % when compared with EAC+Cis group.

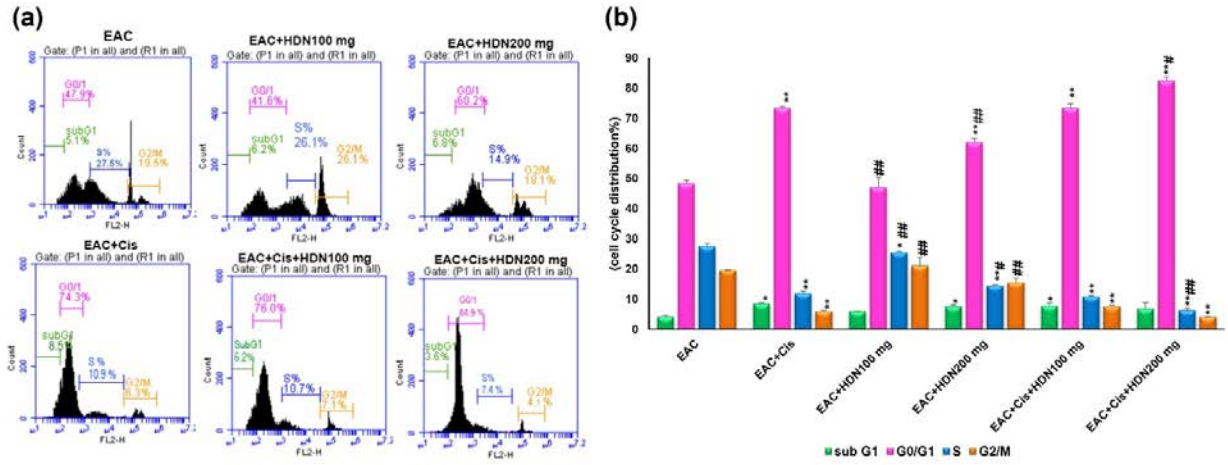

Figure 2. Hesperidin and cisplatin synergistically arrest tumor cells' cell cycle. (a) The presented histogram is representative of one trial from a total of six conducted independently showing distribution of tumor cells in different phases of cell cycle. (b) Pooled data showing percentage of EAC cells in different phases of cell cycle. Data are displayed as mean ± SEM of six mice. * P<0.05 significantly different from EAC group. ** P<0.001 significantly different from EAC group. $^{\#}$ P<0.05 significantly different from Cis-treated mice. $^{\#\#}$ P<0.001 significantly different from Cis-treated mice. EAC: Ehrlich ascites carcinoma, HDN: hesperidin, Cis: cisplatin.

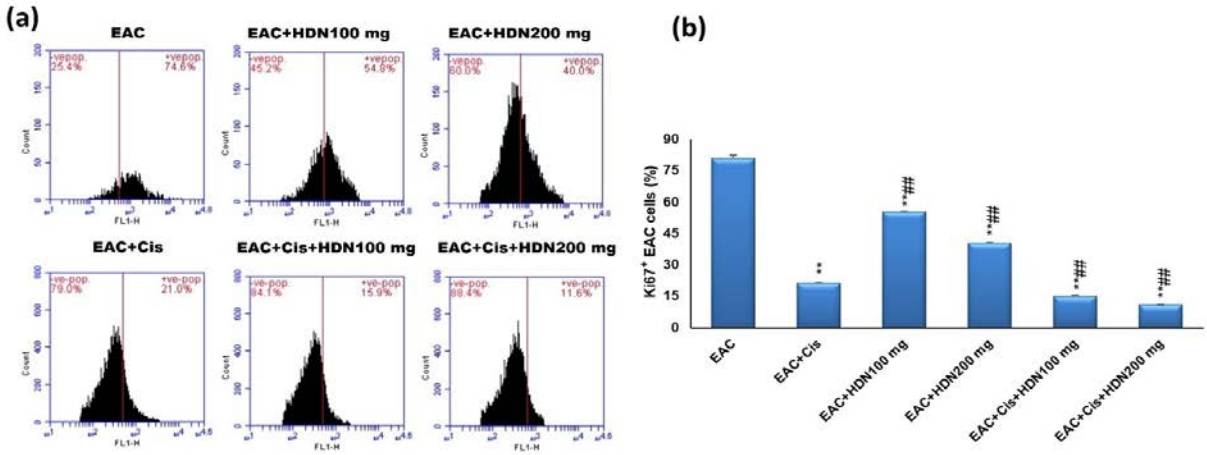

Figure 3. Hesperidin and cisplatin synergistically inhibit tumor cells' proliferation. Tumor cells proliferation was evaluated using flow cytometry depending on their Ki67 protein staining patterns. (a) The presented histogram is representative of one trial from a total of six conducted independently. (b) Pooled data from the six experiments are presented as mean % of $Ki67^+$ cells ± SEM. ** P<0.001 significantly different from EAC group. $^{\#\#}$ P<0.001 significantly different from Cis-treated mice. EAC: Ehrlich ascites carcinoma, HDN: hesperidin, Cis: cisplatin.

3.4. Hesperidin and cisplatin synergistically affect splenic proliferation and immunophenotyping in EAC bearing mice:

In comparison with EAC group, the percentage of $Ki67^+$ spleen cells exhibited a significant (P<0.001) decrease after mono treatment with Cis. On the other hand, mono treatments with both doses of H DN significantly (P<0.001) succeeded in increasing its percentage. Remarkably, mono treatments (100 or 200 m g/kg HDN) and combined treatments (Cis with 100 or 200 mg/kg HDN) exerted a significant (P<0.001) improvement in splenic proliferation when compared with Cis mono treated group (Fig. 4).

To investigate the effect of C is and/or HDN on the alterations of s plenocytes immunophenotyping, the expressions of CD 3^+CD4^+, $CD3^+CD8^+$, and $CD4^+CD25^+$ immune cells were presented in Table 2. Tabular data shows that, $CD3^+CD4^+$, and $CD3^+CD8^+$ cell percentages declined significantly (P<0.001) in untreated EAC group, parallel with the significant rise in $CD4^+CD25^+$ cells as compared with normal control group. Chemotherapeutic treatment with Cis alone resulted in highly significant (P<0.001) decrease in $CD3^+CD4^+$, $CD3^+CD8^+$, and $CD4^+CD25^+$ cells percentage compared to untreated EAC group. In comparison with Cis mono-treated group, mono and combined treatments achieved a significant (P<0.001) improvement in the % of CD 3^+CD4^+, $CD3^+CD8^+$, and $CD4^+CD25^+$ spleen cells. Importantly, the demonstrated results proved the strong modulatory role of HDN doses in conjunction with Cis to alter the immune response against tumor.

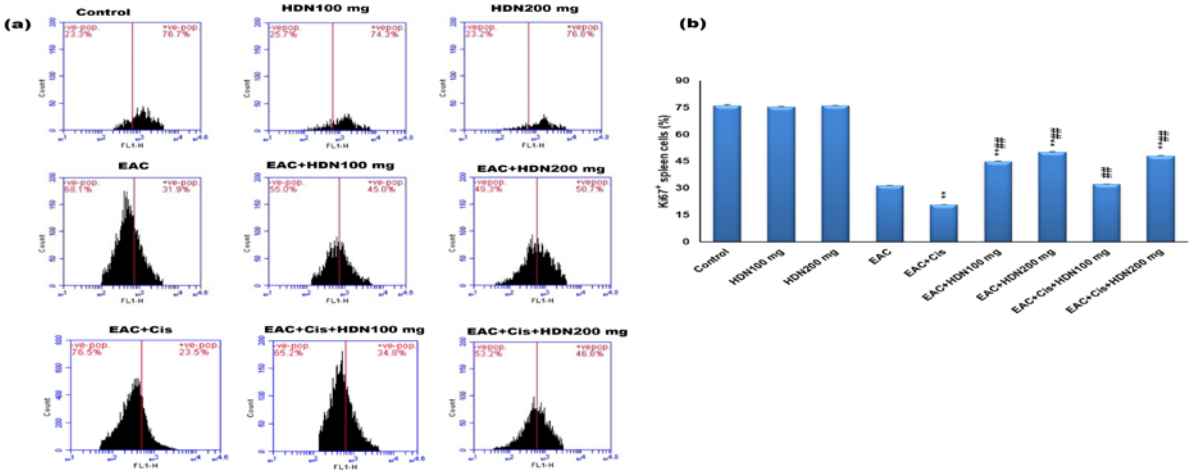

Figure 4. Hesperidin and cisplatin synergistically improve spleen cells proliferation. Spleen cells proliferation was evaluated by flow cytometry depending on their Ki67 protein staining patterns. (a) The presented histogram is representative of one trial from a total of six conducted independently. (b) Pooled data from six experiments are presented as mean % of $Ki67^+$ cells ± SEM. ** P<0.001 significantly different from EAC group. $^{\#\#}$ P<0.001 significantly different from Cis-treated mice. EAC: Ehrlich ascites carcinoma, HDN: hesperidin, Cis: cisplatin.

Table 2. Hesperidin and cisplatin synergistically improve splenocytes phenotypic analysis in tumor-bearing mice.

	$CD3^+$ $CD4^+$(%)	$CD3^+CD8^+$(%)	$CD4^+CD25^+$(%)
Control	51.15±0.81	36.96±0.36	17.68±0.25
HDN100 mg	50.96±0.93	35.95±0.55	17.15±0.32
HDN200 mg	51.23±0.86	37.03±0.92	17.18±0.39
EAC	15.33±0.13 $^{\$\$}$	26.15±0.21 $^{\$\$}$	39.31±0.27$^{\$\$}$
EAC+Cis	10.11±0.19 **	19.95±0.29 **	4.80±0.11 **
EAC+HDN 100 mg	18.95±0.30 **$^{\#\#}$	30.20±0.19 **$^{\#\#}$	32.51±0.16**$^{\#\#}$
EAC+HDN 200 mg	37.10±0.34 **$^{\#\#}$	33.13±0.20 **$^{\#\#}$	22.11±0.09**$^{\#\#}$
EAC+Cis+HDN 100 mg	22.31±0.18 **$^{\#\#}$	25.61±0.19 $^{\#\#}$	11.63±0.21**$^{\#\#}$
EAC+Cis+HDN 200 mg	45.65±0.21 **$^{\#\#}$	41.78±0.16 **$^{\#\#}$	23.88±0.18**$^{\#\#}$

Data are displayed as mean ± SEM, n = 6. $^{\$\$}$ P<0.001 significantly different from control group. ** P<0.001 significantly different from EAC group. $^{\#\#}$ P<0.001 significantly different from Cis-treated mice. EAC: Ehrlich ascites carcinoma, HDN: hesperidin, Cis: cisplatin.

3.5. Hesperidin and cisplatin synergistic effect on IFN-γ and granzyme B levels in EAC bearing mice:

The impacts of HDN and Cis mono or dual treatments on serum IFN- γ and granzyme B levels are depicted in Fig. 5. The data showed that there was highly significant (P<0.001) decrease in their levels in untreated EAC group compared with control group. Additionally, a significant (P<0.001) decline in the level of IFN- γ and granzyme B was recorded after chemotherapeutic treatment with Cis alone when compared with EAC group. Conversely, mono-treatment of mice bearing EAC with 200mg of HDN, as well as co-treatment with Cis plus 200mg of HDN, exerted highly significant (P<0.001) increase as compared to EAC group. Moreover, there was significant (P<0.001) increase in IFN- γ and granzyme B levels after different mono and combined HDN treatments when compared to Cis treated group.

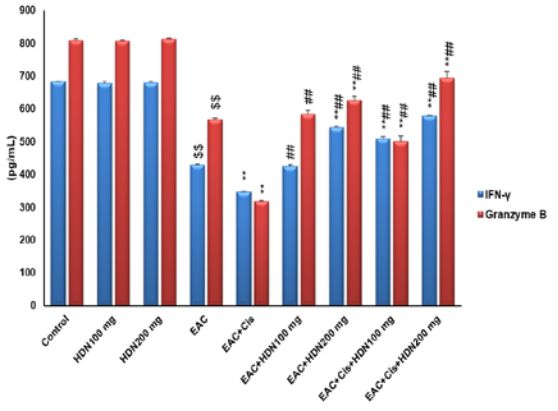

Figure 5. Hesperidin and cisplatin synergistically improve serum IFN- γ and granzyme B levels. Data are displayed as the mean ± SEM (n=6). $^{\$\$}$ P<0.001 significantly different from control group. ** P<0.001 significantly different from EAC group. $^{\#\#}$ P<0.001 significantly different from Cis-treated mice. EAC: Ehrlich ascites carcinoma, HDN: hesperidin, Cis: cisplatin.

3.6. Hesperidin combination with cisplatin ameliorated hematological changes in EAC bearing mice:

Oral administration of HDN alone, at doses of 100 or 200 mg/kg, did not induce significant (P>0.05) changes in the whole set of hematological parameters (Table 3 and 4) when compared with normal control group. However, inoculation of 2.5×10^5 cell of EAC cell line led to a significant (P<0.05) decrease in Hb content (11.76±0.30), RBCs count (6.05±0.24), and Ht value (29.05±0.51) accompanied by a significant increase in platelet count (835.00±10.24) as compared with normal control group (14.24±0.10), (8.08±0.34), (42.80±1.06), and (673.33±9.58), respectively. Chemotherapeutic treatment of EAC bearing mice with Cis caused a significant (P<0.001) reduction in Hb content, RBCs count (P<0.05), Ht value (P<0.001), and platelets count (P<0.001) as compared to EAC untreated group. In comparison with Cis treated group, mono treatment of EAC bearing mice with 100 or 200 mg/kg HDN or combined treatment with Cis and 100 or 200 mg/kg HDN recovered these changes significantly (P<0.001) toward normal values, except the impact of combined treatment with 100 mg/kg HDN and Cis on thrombocytes that was not significant (P>0.05) (Table 3).

Total and relative differential counts of leukocytes were around normal range of control group following treatments of non-tumorized mice with 100 or 200 mg/kg HDN alone as demonstrated in Table 4, although a significant (P<0.05) variation in total and differential leukocyte counts was observed in the untreated EAC group with respect to control group. Treatment with Cis alone resulted in a significant (P<0.001) decrease in total leukocyte count and relative lymphocytes, which was associated with a significant (P<0.001) rise in relative granulocyte count when compared to EAC group. Mono treatment with 100 or 200 mg/kg HDN and combined treatment with Cis and 100 or 200 mg/kg HDN revealed a significant (P<0.05) dose dependent recovery in total and relative differential WBC counts almost toward normal count as compared to Cis treated group. However, the effect on relative monocytes was not significant (P>0.05) when compared to the Cis mono-treated mice.

Table 3 Alterations in erythrogram of EAC bearing mice upon treatment with cisplatin and/or hesperidin.

	Hb (g/dL)	RBCs (10^6/mm^3)	Ht (%)	Platelets (10^3/mm^3)
Control	14.24±0.10	8.08±0.34	42.80±1.06	673.33±9.58
HDN100 mg	14.23±0.10	7.99±0.15	42.41±0.44	668.16±6.52
HDN200 mg	14.40±0.10	8.23±0.14	42.60±0.28	662.00±7.69
EAC	11.76±0.30 $^{\$\$}$	6.05±0.24 $^{\$\$}$	29.05±0.51 $^{\$\$}$	835.00±10.24 $^{\$\$}$
EAC+Cis	9.03±0.14 **	5.20±0.07 *	22.88±0.15 **	564.33±7.98 **
EAC+HDN 100 mg	12.28±0.22 $^{\#\#}$	6.53±0.15 $^{\#\#}$	32.83±0.65 *$^{\#\#}$	796.00±10.44 *$^{\#\#}$
EAC+HDN 200 mg	13.66±0.26 **$^{\#\#}$	7.21±0.09 **$^{\#\#}$	39.98±1.67 **$^{\#\#}$	668.50±6.27 **$^{\#\#}$
EAC+Cis+HDN100 mg	11.02±0.25 *$^{\#\#}$	6.45±0.15 $^{\#\#}$	30.41±0.81 $^{\#\#}$	576.00±10.44 **
EAC+Cis+HDN200 mg	13.78±0.30 **$^{\#\#}$	7.65±0.06 **$^{\#\#}$	43.45±0.46 **$^{\#\#}$	620.33±9.60 **$^{\#\#}$

Data are displayed as mean ± SEM, n = 6. $^{\$\$}$ P<0.001 significantly different from control group. * P<0.05 significantly different from EAC group. ** P<0.001 significantly different from EAC group. $^{\#\#}$ P<0.001 significantly different from Cis-treated mice. EAC: Ehrlich ascites carcinoma, HDN: hesperidin, Cis: cisplatin, Hb: hemoglobin, RBCs: red blood cells, Ht: hematocrit.

Table 4. Alterations in total and differential leukocytic counts of EAC bearing mice upon treatment with cisplatin and/or hesperidin.

	Leukocytes (10^3/mm^3)	Granulocytes (%)	Lymphocytes (%)	Monocytes (%)
Control	8.35±0.13	32.50±0.61	63.16±0.47	4.33±0.21
HDN100 mg	8.23±0.11	32.83±0.47	62.66±0.55	4.50±0.22
HDN200 mg	8.28±0.11	32.66±0.55	63.16±0.70	4.16±0.30
EAC	10.90±0.15 $^{\$\$}$	51.83±1.07 $^{\$\$}$	42.83±1.19 $^{\$\$}$	5.33±0.21
EAC+Cis	5.35±0.06 **	65.66±0.42 **	29.66±0.33 **	4.66±0.21
EAC+HDN100 mg	9.85±0.25 *$^{\#\#}$	51.50±0.42 $^{\#\#}$	44.00±0.93 $^{\#\#}$	4.50±0.76
EAC+HDN200 mg	8.91±0.13 **$^{\#\#}$	40.16±0.30 **$^{\#\#}$	56.00±0.57 **$^{\#\#}$	3.83±0.30 *
EAC+Cis+HDN100 mg	6.13±0.13 **$^{\#}$	47.00±0.68 **$^{\#\#}$	48.50±0.61 **$^{\#\#}$	4.50±0.42
EAC+Cis+HDN200 mg	7.91±0.25 **$^{\#\#}$	33.83±0.47 **$^{\#\#}$	61.00±0.36 **$^{\#\#}$	5.16±0.30

Data are presented as mean ± SEM, n = 6. $^{\$\$}$ P<0.001 significantly different from control group. * P<0.05 significantly different from EAC group. ** P<0.001 significantly different from EAC group. $^{\#}$ P<0.05 significantly different from Cis-treated mice. $^{\#\#}$ P<0.001 significantly different from Cis-treated mice. EAC: Ehrlich ascites carcinoma, HDN: hesperidin, Cis: cisplatin.

3.7. Effect of hesperidin combination with cisplatin on oxidative stress markers in EAC-bearing mice

Mice that received HDN alone showed no significant (P>0.05) change in serum MDA and GSH levels in respect to normal group. On the other hand, EAC bearing mice revealed a significant (P<0.001) rise in MDA levels accompanied with a significant (P<0.001) decline in GSH levels as compared to normal mice; this negative effect was nearly duplicated significantly (P<0.001) after treating EAC mice with Cis alone as compared to EAC untreated mice. On contrary, mono- or combined treatment with HDN or HDN with Cis was able to ameliorate induced oxidative stress through a significant (P<0.001) decline in MDA levels and a rise in GSH levels in a dose dependent manner when compared with Cis treated group (Fig. 6A & Fig. 6B).

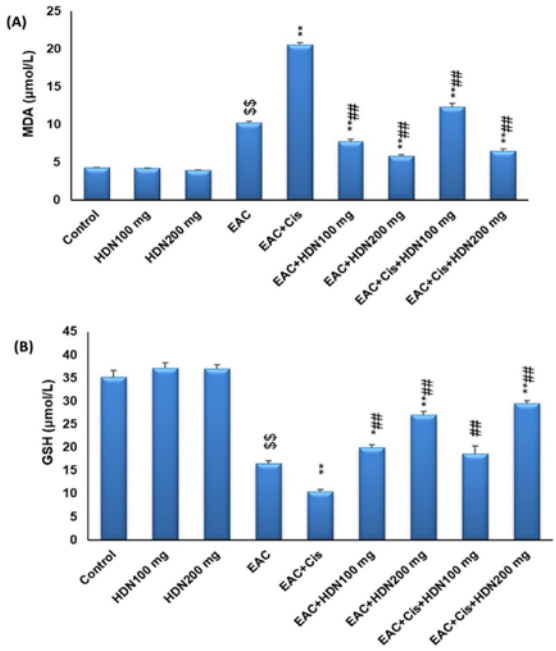

Figure 6. Hesperidin and cisplatin enhancing effect on serum concentrations of oxidative stress marker MDA (**A**) and the antioxidant GSH (**B**). Data are displayed as mean ± SEM, n = 6. $$ P<0.001 significantly different from control group. * P<0.05 significantly different from EAC group. ** P<0.001 significantly different from EAC group. $^{\#\#}$ P<0.001 significantly different from Cis-treated mice. EAC: Ehrlich ascites carcinoma, HDN: hesperidin, Cis: cisplatin, MDA: malonaldehyde, GSH: reduced glutathione.

3.8. Hesperidin and cisplatin enhancing effect on other biochemical parameters in EAC bearing mice:

The data presented in Table 5 demonstrates that EAC bearing mice revealed a significant (P<0.001) increase in ALT, AST, urea, and creatinine levels associated with a significant (P<0.001) decrease in total protein and albumin levels as compared to normal control group. Moreover, mono-treatment with Cis resulted in a significant (P<0.05) increase in these hepato-renal toxicity parameters in comparison with the EAC untreated group. Interestingly, treatment of EAC bearing mice with HDN alone or combined with Cis significantly (P<0.001) relieve the negative biochemical effects upon HDN mono-treatment when compared to EAC group and decreased toxic effects induced by Cis on these biochemical parameters when compared to Cis treated group. This positive effect exhibited a dose-dependent trend with HDN treatment, moving the values toward the normal range.

Table 5. Hesperidin and cisplatin enhancing effect on biochemical changes in EAC bearing mice.

	ALT (U/L)	AST (U/L)	Total protein (g/dL)	Albumin (g/dL)	Urea (mg/dL)	Creatinine (mg/dL)
Control	26.00±4.61	60.66±0.66	6.68±0.06	4.14±0.03	41.83±0.54	0.16±0.005
HDN100 mg	27.50±0.99	58.50±0.99	6.55±0.09	4.05±0.04	40.50±0.42	0.14±0.009
HDN200 mg	24.16±0.74	58.33±0.84	6.56±0.07	4.03±0.07	39.00±0.51	0.12±0.006
EAC	89.83±0.54 $^{\$\$}$	103.33±1.30 $^{\$\$}$	5.13±0.08 $^{\$\$}$	2.61±0.12 $^{\$\$}$	53.83±0.60 $^{\$\$}$	0.30±0.019 $^{\$\$}$
EAC+Cis	118.33±2.78 **	130.33±2.26 **	4.17±0.04**	2.25±0.09 *	81.66±1.99 **	1.14±0.039 **
EAC+HDN100 mg	49.33±1.60 **$^{\#\#}$	89.16±1.60 **$^{\#\#}$	5.58±0.09 **$^{\#\#}$	2.98±0.06 *$^{\#\#}$	50.00±1.36 *$^{\#\#}$	0.26±0.007 $^{\#\#}$
EAC+HDN200 mg	36.16±1.19 **$^{\#\#}$	76.33±2.02 **$^{\#\#}$	6.03±0.07 **$^{\#\#}$	3.35±0.09 **$^{\#\#}$	45.66±0.91 **$^{\#\#}$	0.20±0.011**$^{\#\#}$
EAC+Cis+HDN100 mg	56.66±1.45 **$^{\#\#}$	111.33±1.85 *$^{\#\#}$	4.83±0.05 *$^{\#\#}$	2.78±0.07##	71.83±1.07**$^{\#\#}$	0.96±0.017**$^{\#\#}$
EAC+Cis+HDN200 mg	42.16±0.83 **$^{\#\#}$	76.50±1.23 **$^{\#\#}$	6.03±0.06 **$^{\#\#}$	3.53±0.12 **$^{\#\#}$	51.50±0.84 $^{\#\#}$	0.46±0.018**$^{\#\#}$

Data are displayed as mean ± SEM, n = 6. $^{\$\$}$ P<0.001 significantly different from control group. * P<0.05 significantly different from EAC group. ** P<0.001 significantly different from EAC group. $^{\#\#}$ P<0.001 significantly different from Cis-treated mice. EAC: Ehrlich ascites carcinoma, HDN: hesperidin, Cis: cisplatin, ALT: alanine aminotransferase, AST: aspartate aminotransferase.

4. Discussion

Despite substantial advancements in cancer research in recent years, the treatment of cancer remains fraught with difficulties (Du and Shim, 2016; Xu et al., 2023). One of the main reasons for the failure of chemotherapy and radiotherapy to effectively treat cancer in clinics is due to tumor resistance (Bhosle et al., 2005). Therefore, innovative approaches to cancer treatment are crucial. Recently, combining multiple anti-cancer agents has emerged as a promising method in cancer therapies, known as the synergistic effect (Zhong et al., 2019; Kubota et al., 2023). In this investigation, the role of HDN in enhancing the sensitivity of Ehrlich cancer cells to Cis chemotherapy while reducing its side effects on the normal healthy tissues was demonstrated. In the present study, EAC tumor model of albino mice was established, Cis chemotherapy plus HDN synergism were conducted, antineoplastic and immunomodulatory effects were evaluated, oxidative stress markers and liver and kidney function tests were measured after mono and combined treatments and mechanism of HDN synergistic role with Cis chemotherapy were explored.

The results showed that the combination of HDN with Cis effectively suppressed tumor burden through decreasing ascitic fluid volume, tumor cell count and viability, resulting in the highest tumor inhibition rate observed. This means that when cancer cells are treated with both chemotherapy drug and HDN, the response to chemotherapy is improved. This enhanced chemosensitivity has been attributed to various mechanisms, including the induction of apoptosis, cell cycle arrest of cancer cells, and the suppression of tumor cell proliferation as demonstrated in our results. The anticancer properties of HDN have been previously documented (Donia et al., 2018; Du et al., 2018; Aggarwal et al., 2020; Jeong et al., 2022).

Interestingly, Wang et al. (2015) documented that HDN was discovered to halt the cell cycle at the G0/G1 phase by decreasing cyclin D1 and increasing p21 and p53 expression. It was also found to activate the endoplasmic reticulum stress pathway, leading to apoptosis in HeLa cells (a type of immortal cervical cancer cells). This process is achieved by decreasing the protein levels of cyclin D1, cyclin E1, and cyclin-dependent kinase 2, which are involved in the cell cycle regulation. In the same line, Pandey et al. (2019) reported that HDN induced ROS-mediated apoptosis in human gall bladder carcinoma, but they found cell cycle arrest at G2/M phase.

Undoubtedly, the immune system plays a crucial role in defending against cancer (Vesely et al., 2011). It has the ability to recognize and destroy abnormal cells, such as cancer cells that are potentially harmful to the body. The process is known as immunosurveillance and involves the activation of immune cells, such as T cells and natural killer cells, to identify and destroy cancer cells. In some cases, the immune system may also stimulate an immune response that directly targets cancer cells, such as the production of cytokines and the activation of an immune response (Pandya et al., 2016).

Within the scope of this study, flow cytometric analysis showed that HDN combined treatment with Cis induced an antitumor immune response by increasing the percentage of splenic T helper ($CD3^+CD4^+$) and T cytotoxic ($CD3^+CD8^+$) cells, while concurrently orchestrating a modulatory effect on $CD4^+CD25^+$ regulatory cells accompanied by improving spleen proliferation, which regulate the immune response against tumor. Similarly, earlier investigations revealed the synergistic role of combined treatments with Cis on antitumor immunity (Ye et al., 2018; El-Bolkiny et al., 2021; Wang et al., 2022). Hassouna et al. (2015) and Berköz et al. (2021) documented that HDN can improve the immunosuppressive impact of diazinon and cyclophosphamide, respectively. This was achieved by enhancing both adaptive and innate immune responses, and so it is considered as a useful immunomodulatory agent during cancer chemotherapy; these findings strongly support results of the current study.

Cytotoxic $CD8^+$ T cells are the final executors of antitumor immune action due to their direct cytotoxicity on

cancer cells via secreting IFN-γ, triggering Fas-mediated cytotoxicity or perforin induced cell lysis (Martinez-Lostao et al., 2015). IFN-γ consistently orchestrates both pro-tumorigenic and antitumor immunity within the tumor microenvironment. It plays a role as a cytotoxic cytokine combined with granzyme B and perforin to initiate tumor cells apoptosis (Tau et al., 2001; Maimela et al., 2018). Interestingly, Jorgovanovic et al. (2020) reviewed the fundamental role of IFN-γ in activating cellular immunity and subsequently induction of anti-tumor immune response. The present study revealed a significant increase in IFN-γ and granzyme B serum levels of tumorized mice mono-treated with 200 mg/kg HDN and co-treated with 100 or 200 mg/kg HDN plus Cis chemotherapy. These observations collectively suggest that HDN treatment promotes the efficacy of $CD8^+$ T cells in combating tumors and strengthens their role in anti-tumor immunity. Additionally, these findings shed light on one of the mechanisms through which HDN triggers apoptosis in tumor cells.

The previous results demonstrated the potential of HDN as a standalone agent in cancer treatment, although its effect was enhanced when used in combination with Cis chemotherapy. Thus, while HDN alone may have some potential in treating cancer, its true strength lies in its ability to enhance the efficacy of chemotherapy drugs, making it a promising complementary therapy for cancer treatment.

Chemotherapy exerts severe and long-lasting side effects on normal, healthy cells and tissues. These side effects can significantly impact the quality of life for patients undergoing chemotherapy, and in some cases, they may even be more harmful than the cancer itself. For example, studies have shown that cardiotoxicity induced by chemotherapy can reach to heart failure and death, even in patients with no prior history of heart disease (CadedduDessalvi et al., 2018). Therefore, it is important for healthcare providers to closely monitor patients receiving chemotherapy and take steps to minimize and manage these harmful effects.

In the current study, tumorized animals treated only with Cis exhibited severe anaemia characterized by a notable reduction in RBCs count, Hb content, and Ht value. This anemic condition was accompanied by a sharp decrease in total leukocytes, relative lymphocyte count, and total platelet count. Moreover, in this study chemotherapeutic treatment resulted in oxidative stress that was detected by elevated serum MDA levels and reduced serum GSH levels and, induced liver and kidney toxicity. On the contrary, combined treatment with (HDN and Cis) improved these hematological alterations, hepato-renal toxicity, and oxidative stress toward normal values. Previous studies have reported toxic effects of Cis on bone marrow cell colonies that substantially affect blood cells and induce hematotoxicity (Das et al., 2003; Aldossary 2019; Ibrahim et al., 2020; El-Bolkiny et al., 2021).

The review article by Aldossary (2019) on the toxic effects of Cis highlights several major toxicities associated with the use of this chemotherapy drug which include nephrotoxicity, hepatotoxicity, cardiotoxicity, and neurotoxicity. Recent investigations have demonstrated that hesperidin and other flavonoids can be utilized safely to counter the harmful cytotoxic effects brought on by chemotherapy drugs. This is due to their antioxidant, anti-tumor, and immunostimulant properties (Korga et al., 2019; Rodríguez-García 2019; Berköz et al., 2021).

5. Conclusion

The synergistic effect between hesperidin and cisplatin chemotherapy augments the effectiveness of cancer treatment through inducing apoptosis, suppressing the proliferation of tumor cells, and regulating the immune response. Hesperidin not only successfully enhanced chemosensitivity of cancer cells but also reduced the severity of cisplatin toxic effects on normal tissues. Despite these promising current results, further investigations are required to fully comprehend the molecular mechanisms underneath the current role of hesperidin in enhancing chemosensitivity and to determine the optimal dosing and administration strategies.

Funding

This research did not receive any funding.

Declaration of competing interests

The authors declare that they have no known competing financial interests or personal relationships that could have appeared to influence the work reported in this paper.

Reference

Aggarwal V, Tuli HS,Thakral F, Singhal P, Aggarwal D, Srivastava S, Pandey A, Sak K, Varol M, Khan MA and Sethi G. 2020. Molecular mechanisms of action of hesperidin in cancer: Recent trends and advancements. Exp Biol Med,245(5):486–497. doi: 10.1177/1535370220903671.

Ahmadi A and Shadboorestan A. 2016. Oxidative stress and cancer; the role of hesperidin, a citrus natural bioflavonoid, as a cancer chemoprotective agent. Nutr Cancer,68:29–39.

Aishatwi AA, Ramesh E, Periasamy VS and Subash-Babu P. 2013. The apoptotic effect of hesperetin on human cervical cancer cells is mediated through cell cycle arrest, death receptor, and mitochondrial pathways. Fundam Clin Pharmacol, 27:581–92.

Aldossary SA. 2019. Review on pharmacology of cisplatin: clinical use, toxicity and mechanism of resistance of cisplatin. Biomed Pharmacol J,12(1):doi: 10.13005/bpj/1608.

Aliwaini SH., El-Bashiti TA and Mortaja KM. 2020. Pitavastatin enhances doxorubicin-induced apoptosis in MCF7 breast cancer cells. JJBS, 13(1): 101–105.

Al-Kharusi N, Babiker H, Al-Salam S, Waly M, Nemmar A, Al-Lawati I, Yasin J, Beegam S and Ali B . 2013. Ellagic acid protects against cisplatin-induced nephrotoxicity in rats: a dose-dependent study. Eur Rev Med Pharmacol Sci, 17: 299–310.

Barreca D, Gattuso G, Bellocco E, Calderaro A, Trombetta D, Smeriglio A, Lagana G, Daglia M,Meneghini S and Nabavi SM. 2017. Flavanones: citrus phytochemical with health-promoting properties. Biofactors,43:495–506.

Berköz M, Yalın S, Özkan-Yılmaz F, Özlüer-Hunt A, Krośniak M, Francik R, Yunusoğlu O, Adıyaman A, Gezici H, Yiğit A, Ünal S, Volkan D and Yıldırım M. 2021. Protective effect of myricetin, apigenin, and hesperidin pretreatments on cyclophosphamide-induced immunosuppression. Immunopharmacol Immunotoxicol, 43(3):353–369. doi: 10.1080/08923973.2021.1916525.

Bhosle SM, Huilgol NG and Mishra KP. 2005. Enhancement of radiation-induced oxidative stress and cytotoxicity in tumor cells by ellagic acid. Clin Chim Acta, 359: 89–100.

Brown A, Kumar S and Tchounwou PB. 2019. Cisplatin-based chemotherapy of human cancers. J Cancer Sci Ther, 11: 97.

CadedduDessalvi C, Deidda M, Mele D, Bassareo PP, Esposito R, Santoro C, Lembo M, Galderisi M and Mercuro G. 2018. Chemotherapy-induced cardiotoxicity: new insights into mechanisms, monitoring, and prevention. J Cardiovasc Med (Hagerstown), 19(7): 315–323. doi: 10.2459/JCM.0000000000000667.

Dacie SJV andlewis SM. 1984. Practical Hematology,sixth ed. Churchill Livingstone, UK. 24–45.

Darband SG, Kaviani M,Yousefi B, Sadighparvar S, Pakdel FG, Attari JA, Mohebbi I, Naderi S and Majidinia M. 2018. Quercetin: A functional dietary flavonoid with potential chemo-preventive properties in colorectal cancer. J Cell Physiol, 233: 6544–6560.

Das B, Yeger H, Baruchel H, Freedman MH, Koren G and Baruchel S. 2003. In vitro cytoprotective activity of squalene on a bone marrow versus neuroblastoma model of cisplatin-induced toxicity: implications in cancer chemotherapy. Eur J Cancer, 39(17): 2556–2565. doi: 10.1016/j.ejca.2003.07.002.

Dasari S and Tchounwou PB. 2014. Cisplatin in cancer therapy: Molecular mechanisms of action. Eur J Pharmacol, 740: 364–378. doi: 10.1016/j.ejphar.2014.07.025.

Dasari S, Njiki S, Mbemi A, Yedjou CG and Tchounwou PB. 2022. Pharmacological effects of cisplatin combination with natural products in cancer chemotherapy. Int J Mol Sci, 23: 1532. doi: 10.3390/ijms23031532.

Devi KP, Rajavel T, Nabavi SF, Setzer WN, Ahmadi A, Mansouri K and Nabavi SM. 2015. Hesperidin: A promising anticancer agent from nature. Ind Crops Prod, 76: 582–589. doi: 10.1016/j.indcrop.2015.07.051.

Donia TIK, Gerges MN and Mohamed TM.2018. Amelioration effect of Egyptian sweet orange hesperidin on Ehrlich ascites carcinoma (EAC) bearing mice. Chem Biol Interact, 285:76–84. doi: 10.1016/j.cbi.2018.02.029.

Du GY, He SW, Zhang L, Sun CX, Mi LD and Sun ZG. 2018. Hesperidin exhibits *in vitro* and *in vivo* antitumor effects in human osteosarcoma MG-63 cells and xenograft mice models via inhibition of cell migration and invasion, cell cycle arrest and induction of mitochondrial-mediated apoptosis. Oncol Lett,16(5):6299–6306. doi: 10.3892/ol.2018.9439.

Du B and Shim JS. 2016. Targeting epithelial-mesenchymal transition (EMT) to overcome drug resistance in cancer. Molecules, 21(7): 965.doi: 10.3390/molecules21070965.

El-Bolkiny YE, Salem ML, El-Naggar SA and El-Sharkawy FR.2021. Ameliorating effects of rosemary and costus on blood-associated toxicity in Ehrlich-bearing mice treated with cisplatin. Int J cancer Biomed Res (IJCBR), 5(4): 85–98. doi:10.21608/jcbr.2021.84374.1219.

Fouad GI, El-Sayed SAM, Mabrouk M, Ahmed KA andBeherei HH. 2022. Neuroprotective potential of intranasally delivered sulforaphane-loaded iron oxide nanoparticles against cisplatin-induced neurotoxicity. Neurotox Res, 40(5):1479–1498.doi: 10.1007/s12640-022-00555-x.

Garcia J, Hurwitz HI, Sandler AB, Miles D, Coleman RL, Deurloo R and Chinot OL. 2020. Bevacizumab (Avastin®) in cancer treatment: A review of 15 years of clinical experience and future outlook.Cancer Treat Rev, 86:102017. doi: 10.1016/j.ctrv.2020.102017.

Hassouna I, Ibrahim H, Abdel Gaffar F, El-Elaimy I and Abdel Latif H. 2015. Simultaneous administration of hesperidin or garlic oil modulates diazinon-induced hemato- and immunotoxicity in rats. Immunopharmacol Immunotoxicol, 37(5): 442–449.doi: 10.3109/08923973.2015.1081932.

Ibrahim HM, Xuan X and Nishikawa Y.2010. Toxoplasma gondii cyclophilin 18 regulates the proliferation and migration of murine macrophages and spleen cells. Clin Vaccine Immunol, 17(9): 1322–1329.doi: 10.1128/CVI.00128-10.

Ibrahim HM, Abdel Ghaffar FR, El-Elaimy IA, Gouida MS and Abd El Latif HM. 2018. Antitumor and immune-modulatory efficacy of dual-treatment based on levamisole and/or taurine in Ehrlich ascites carcinoma-bearing mice. Biomed Pharmacother, 106:43–49. doi: 10.1016/j.biopha.2018.06.113.

Ibrahim HM, Mohamed AH, Salem ML, Osman GY and Morsi DS. 2020. Anti-neoplastic and immunomodulatory potency of co-treatment based on bovine lactoferrin and/or muramyl dipeptide in tumor-bearing mice. Toxicol Res(Camb), 9(2):137–147. doi: 10.1093/toxres/tfaa012.

Jeong SA, Yang C, Song J, Song G, Jeong W and Lim W. 2022. Hesperidin suppresses the proliferation of prostate cancer cells by inducing oxidative stress and disrupting $Ca2^{+}$homeostasis. Antioxidants, 11(9):1633. doi: 10.3390/antiox11091633.

Jorgovanovic D, Song M, Wang L and Zhang Y. 2020. Roles of IFN-γ in tumor progression and regression: a review. Biomark Res, 8: 49.doi: 10.1186/s40364-020-00228-x.

Korga A, Ostrowska M, Jozefczyk A, Iwan M, Wojcik R, Zgorka G, Herbet M, Vilarrubla GG and Dudka J. 2019. Apigenin and hesperidin augment the toxic effect of doxorubicin against HepG2 cells. BMC Pharmacol Toxicol, 20(1):22.doi: 10.1186/s40360-019-0301-2.

Kubota Y, Han Q, Aoki Y, Masaki N, Obara K, Hamada K, Hozumi C, Wong ACW, Bouvet M, Tsunoda T and Hoffman RM. 2023. Synergy of combining methionine restriction and chemotherapy: the disruptive next generation of cancer treatment. Cancer Diagn Progn, 3(3): 272–281. doi: 10.21873/cdp.10212.

Liu CM, Ma JQ, Liu SS, Zheng GH, Feng ZJ and Sun JM. 2014. Proanthocyanidins improves lead-induced cognitive impairments by blocking endoplasmic reticulum stress and nuclear factor-κB-mediated inflammatory pathways in rats. Food Chem Toxicol,72:295–302. doi: 10.1016/j.fct.2014.07.033.

Liu L, Zhao Y, Han W, Chen T, Hou G and Tong X. 2016. Protective effect of antioxidant on renal damage caused by doxorubicin chemotherapy in mice with hepatic cancer. Asian Pac J Trop Med, 9(11): 1101–1104. doi: 10.1016/j.apjtm.2016.08.003.

Maimela NR, Liu S and Zhang Y. 2018. Fates of $CD8^{+}$ T cells in Tumor Microenvironment. Comput Struct Biotechnol J,17:1–13. doi: 10.1016/j.csbj.2018.11.004.

Martinez-Lostao L, Anel A and Pardo J. 2015. How do cytotoxic lymphocytes kill cancer cells? Clin Cancer Res, 21(22): 5047–5056. doi: 10.1158/1078-0432.CCR-15-0685.

Morsi DS, El-Nabi SH, Elmaghraby MA, Abu Ali OA, Fayad E, Khalifa SAM, El-Seedi HR and El-Garawani IM. 2022. Anti-proliferative and immunomodulatory potencies of cinnamon oil on Ehrlich ascites carcinoma bearing mice. Sci Rep,12(1):11839. doi: 10.1038/s41598-022-14770-1.

Osman AM, Alqahtani AA, Damanhouri ZA, Al-Harthy SE, Elshal MF, Ramadan WS, Kamel F, Osman MA and Khan LM. 2015. Dimethylsulfoxideexcerbates cisplatin-induced cytotoxicity in Ehrlich ascites carcinoma cells. Cancer Cell Int, 15: 104. doi: 10.1186/s12935-015-0258-1.

Pandey P, Sayyed U, Tiwari RK, Siddiqui MH, Pathak N and Bajpai P. 2019. Hesperidin induces ROS-mediated apoptosis along with cell cycle arrest at G2/M phase in human gall bladder carcinoma. Nutr Cancer,71(4):676–687. doi: 10.1080/01635581.2018.1508732.

Pandya PH, Murray ME, Pollok KE and Renbarger JL. 2016. The immune system in cancer pathogenesis: potential therapeutic approaches. J Immunol Res, 2016:4273943. doi: 10.1155/2016/4273943.

Pourmadadi M, Eshaghi MM, Rahmani E, Ajalli N, Bakhshi S, Mirkhaef H, Lasemi MV, Rahdar A, Behzadmehr R and Díez-Pascual AM. 2022. Cisplatin-loaded nanoformulations for cancer therapy: A comprehensive review. J Drug Deliv Sci Technol,77: 103928. doi: 10.1016/j.jddst.2022.103928.

Rodríguez-García C, Sánchez-Quesada C andGaforio JJ. 2019. Dietary flavonoids as cancer chemopreventiveagents: an updated review of human studies. Antioxidants, 8(5): 137. doi: 10.3390/antiox8050137.

Roohbakhsh A, Parhiz H, Soltani F, Rezaee R and Iranshahi M. 2015. Molecular mechanisms behind the biological effects of hesperidin and hesperetin for the prevention of cancer and cardiovascular diseases. Life Sci, 124:64–74. doi: 10.1016/j.lfs.2014.12.030.

Sarbaz M, ManouchehriMonazah F, Eslami S, Kimiafar K and Mousavi Baigi SF. 2022. Effect of mobile health interventions for side effects management in patients undergoing chemotherapy: A systematic review. Health Policy Technol, 11: 100680. doi:10.1016/j.hlpt.2022.100680.

Schirrmacher V. 2019. From chemotherapy to biological therapy: A review of novel concepts to reduce the side effects of systemic cancer treatment (Review). Int J Oncol, 54(2): 407–419.doi: 10.3892/ijo.2018.4661.

Siddik ZH. 2003. Cisplatin: mode of cytotoxic action and molecular basis of resistance. Oncogene,22(47):7265–7279. doi: 10.1038/sj.onc.1206933.

Sleijfer DT, Meijer S and Mulder NH. 1985. Cisplatin: a review of clinical applications and renal toxicity. Pharm Weekbl Sci,7(6):237–244. doi: 10.1007/BF01959196.

Spatafora C and Tringali C. 2012. Natural-derived polyphenols as potential anticancer agents. Anti-Cancer Agents Med Chem, 12(8): 902–918. doi: 10.2174/187152012802649996.

Sudhakaran M, Sardesai S and Doseff AI. 2019. Flavonoids: new frontier for immuno-regulation and breast cancer control. Antioxidants, 8(4): 103.doi: 10.3390/antiox8040103.

Sung H, Ferlay J, Siegel RL, Laversanne M, Soerjomataram I, Jemal A and Bray F. 2021. Global cancer statistics 2020: GLOBOCAN estimates of incidence and mortality worldwide for 36 cancers in 185 countries. CA Cancer J Clin. doi: 10.3322/caac.21660.

Tau GZ, Cowan SN, Weisburg J, Braunstein NS and Rothman PB. 2001. Regulation of IFN-γ signaling is essential for the cytotoxic activity of $CD8^+$ T cells. J Immunol, 167(10):5574–5582.doi: 10.4049/jimmunol.167.10.5574.

Vesely MD, Kershaw MH, Schreiber RD and Smyth MJ. 2011. Natural innate and adaptive immunity to cancer. Annu Rev Immunol, 29: 235–271.doi: 10.1146/annurev-immunol-031210-101324.

Wang SC, Yen CY, Shiau JP, Chang MY, Hou MF, Jeng JH, Tang JY and Chang HW. 2022. Synergistic antiproliferation of cisplatin and nitrated [6,6,6] tricycle derivative (SK2) for a combined treatment of oral cancer cells. Antioxidants, 11: 926. doi: 10.3390/antiox11050926.

Wang Y, Yu H, Zhang J, Gao J, Ge X and Lou G. 2015. Hesperidin inhibits Hela cell proliferation through apoptosis mediated by endoplasmic reticulum stress pathways and cell cycle arrest. BMC Cancer,15:682.doi: 10.1186/s12885-015-1706-y.

Xu Y, Du H, Chen Y, Ma C, Zhang Q, Li H, Xie Z and Hong Y. 2023. Targeting the gut microbiota to alleviate chemotherapy-induced toxicity in cancer. Crit Rev Microbiol, 13:1-17. doi: 10.1080/1040841X.2023.2233605.

Ye J, Zou MM, Li P, Lin XJ, Jiang QW, Yang Y, Huang JR, Yuan ML, Xing ZH, Wei MN, Li Y, Shi Z and Liu H. 2018. Oxymatrine and cisplatin synergistically enhance anti-tumor immunity of $CD8^+$ T cells in non-small cell lung cancer. Front Oncol, 8:631. doi: 10.3389/fonc.2018.00631.

Zavattaro M, Lanfranco F, Salvagno F, Motta G, Sestero M, Marinelli L, Canosa S and Revelli A. 2021. Gonadal failure and infertility in cancer survivors: Clinical management and strategies for prevention. Front Horm Res,54: 58–68. doi: 10.1159/000515460.

Zhong C, Qiu S, Li J, Shen J, Zu Y, Shi J and Sui G. 2019. Ellagic acid synergistically potentiates inhibitory activities of chemotherapeutic agents to human hepatocellular carcinoma. Phytomedicine, 59: 152921.doi: 10.1016/j.phymed.2019.152921.

JJBS

Volume 17, Number 1,March 2024
ISSN 1995-6673
Pages 153 – 161
https://doi.org/10.54319/jjbs/170115

Jordan Journal of Biological Sciences

Potential Active Compounds of Propolis as Breast Anticancer Candidates: *In Silico* Study

Ruswanto Ruswanto[1], Tita Nofianti[1], Tresna Lestari[1], Ade Dwi Septian[1], Agung Purnama Firmansyah[2], Richa Mardianingrum[2,*]

[1]*Faculty of Pharmacy, Universitas Bakti Tunas Husada, Tasikmalaya, West Java, Indonesia;* [2]*Department of Pharmacy, Universitas Perjuangan, Tasikmalaya, West Java, Indonesia;*

Received: March 23, 2023; Revised: August 13, 2023; Accepted: August 26, 2023

Abstract

Breast cancer is the most common cancer in Indonesian women. A number of drugs derived from native ingredients have been widely developed and researched for the treatment of breast cancer, one of which is propolis from Indonesia. This study aims to determine the interaction of propolis bioactive compounds on the breast cancer receptor ERα and to establish its pharmacokinetic and toxicity properties *in silico*. The methods used include virtual screening toxicity, pharmacokinetics, docking, and molecular dynamic simulation of 111 bioactive compounds of propolis from was collected from database and compared with 4-hydroxytamoxifen (4-OHT). The results of virtual screening showed that propolis bioactive compounds had good pharmacokinetics, were not toxic and had the best Gibbs free energy (ΔG) and inhibition constant (Ki). Molecular dynamics simulations were continued for three compounds with the best virtual screening values, namely 4-OHT, PRO9 and PRO62. The conclusion of the molecular mechanics-Generalised Born surface area (MM-GBSA) calculation showed that PRO62 has the smallest ΔG_{total} value (-48.469 Kcal/mol) compared to 4-OHT and PRO9. The bioactive compound propolis, namely PRO62 or lanosterol (3-beta), has a more stable interaction than 4-OHT against ERα.

Keywords: anticancer, breast cancer, ERα, in silico, propolis

1. Introduction

Breast cancer is a type of cancer that occurs due to uncontrolled cell growth around the breast. According to statistical data released by the International Agency for Research on Cancer (IARC) in December 2020, the number of breast cancer cases has surpassed lung cancer as the most frequently diagnosed cancer in the world (World Health Organization, 2020). Of the 19.3 million new cancer cases, an estimated 2.3 million were new cases of breast cancer (11.7%), followed by lung cancer (11.4%), colorectal cancer (10.0%), prostate cancer (7.3%) and stomach cancer (5.6%) (Bray et al., 2018). Breast cancer is the most common type of cancer in Indonesian women, with 42.1 cases per 100,000 population and an average mortality rate of 17 per 100.000 population (Riskesdas, 2018). As many as 75% of cases are oestrogen receptor alpha breast cancer (Miah et al., 2019).

The high cost of cancer treatment and the ineffectiveness of treatment encourages people to choose treatment derived from native ingredients (Hasanah and Widowati, 2016). A number of drugs derived from native ingredients have been widely developed and researched for the treatment of breast cancer, one of which is propolis (Kustiawan et al., 2015). More than 300 compounds have been found in propolis scattered in various regions of the world. In general, the bioactive compounds of propolis are influenced by the bee species, the geographical origin of the beehive, and the source of the plant origin (Amalia et al., 2020).

Propolis from the tropics, especially in Southeast Asia, has become an interesting subject because it has various bioactive compounds that are not well known, but published data on propolis from Indonesia is very limited and has received little attention (Fikri et al., 2020). The propolis extract produced by *Trigona insica* bees from East Kalimantan had cytotoxic and apoptotic activity against cancer cells, with an IC_{50} value of 4.28±0.14 g/mL (Kustiawan et al., 2015). Another study conducted showed that propolis extract from Indonesia was able to inhibit the growth of MCF-7 cancer cells, with an IC_{50} value of 18.6±0.03 mg/mL (Amalia et al., 2020). Propolis originating from Indonesia is spread over several areas, including Java (Fikri et al., 2020), Sulawesi (Amalia et al., 2020; Miyata et al., 2019), Kalimantan (Kustiawan et al., 2015) and Sumatra (Kalsum et al., 2016).

In silico studies are widely used in drug research and development as a fast and inexpensive technique that can be applied in both academia and industry. This study aims to determine the interaction of propolis bioactive compounds on the breast cancer receptor ERα and to establish its pharmacokinetic and toxicity properties *in silico.*

* Corresponding author. e-mail: richamardianingrum@unper.ac.id.

2. Material and Methods

2.1. Materials

A personal computer with specification Intel(R) Core(TM) i5-8265U CPU @ 1.60GHz (8 CPUs) x 8.00 GB *of Ram 64-Bit Operating System of Windows 10* was used. The autodockTools 1.5.6 was used for preparation receptor and docking simulation, the *MarvinSketch* version 21.17.0 was used for preparation the compounds, *Discovery Studio Version* 20.1 was used for visualization 2D/3D, and *pkCSM* web-based programs for pharmacokinetics and toxicity prediction. The breast cancer receptor was downloaded from the PDB with codes 3ERT (https://www.rcsb.org/structure/3ERT).

2.2. Methods

2.2.1. Preparation of the structure of the Ligand

A total of 111 structures of propolis bioactive compounds (The detailed structures can be seen in Supplementary Table S1) and comparison compounds were collected and downloaded from database in http://pubchem.ncbi.nih.gov (Batra et al., 2022). Ligands were prepared using the *MarvinSketch 5.2.5.1* program; two-dimensional structural drawings were converted into three dimensions and then geometric estimation and ligand protonation at pH 7.4 were carried out, as well as a *conformational search*, which was subsequently saved in *.pdb* format (Ruswanto et al., 2023).

2.2.2. Receptor Analysis and Receptor Preparation

The receptors used were cancer receptors downloaded from the PDB on the http://rcsb.org/pdb website (Abuhamdah et al., 2020). Receptor analysis was performed at http://www.ebi.ac.uk/databases/cgi-bin/pdbsum/, with the requirement that the most favoured regions value > 90% and the disallowed regions value < 0.8% on the Ramachandran plot (Ho and Brasseur, 2005; Pratami et al., 2022). This was followed by protein preparations, which were carried out by removing water and charge on receptors with the help of the 2017 BIOVIA Discovery Studio program. Receptors and native ligand were stored in .pdb format.

Before the test ligand selection process was carried out in this study, receptor validation was first performed using the AutoDock 1.5.6 program (Al-Khayyat, 2021) by re-docking native ligands at the original receptor. The parameter used was RMSD (root mean square deviation), and the docking method was said to be valid if it had an RMSD value of ≤ 2Å (Bajda et al., 2014).

2.2.3. Molecular Docking & Virtual Screening Simulation

The study aimed to determine the best energy value (ΔG) and inhibition constant (Ki) of ligands as breast anticancer agents. Virtual screening was conducted with the PyRx 0.9.8 program on 111 test ligands and one comparison ligand. The results were visualized using BIOVIA Discovery Studio 2017 program, and the interaction between ligands and receptors was analysed using Discovery Studio software (Dallakyan and Olson, 2015; Tripathi et al., 2019).

2.2.4. Pharmacokinetics and Toxicity Prediction

The prediction of pharmacokinetic parameters (ADME) and toxicity was carried out with the help of pkCSM online tool. Compounds drawn using MarvinSketch 5.2.5.1 were converted into SMILES molecular format and then uploaded to http://biosig.unimelb.edu.au/pkcsm/prediction. The pharmacokinetic parameters used were Caco-2, human intestinal absorption (HIA), VDss, blood brain barrier (BBB) permeability, total clearance, and renal organic cation transporter 2 (OCT2) substrate. The toxicity parameters used were Ames toxicity, LD 50 and hepatotoxicity (Pires et al., 2015).

2.2.5. Molecular Dynamic Simulation

Simulations were carried out on test ligands that had the best value and compared using the *AMBER 16* program. The parameters used in the *molecular dynamics* were *root mean square fluctuation (RMSF), RMSD* and *molecular mechanics-Generalised Born surface area* (*MM-GBSA).*(Mardianingrum et al., 2020) The simulation was carried out with several stages, namely parameterisation, system minimisation, equilibration, *heating* and production (Mardianingrum et al., 2022) .

3. Results

3.1. Receptor Analysis and Preparation

The receptor used was the breast cancer receptor (ERα) with PDB code 3ERT (Shiau et al., 1998). The receptor was downloaded from the site http://rcsb.org/pdb. The x-ray diffraction protein crystal structure was obtained from the human oestrogen receptor with a resolution of 1.90. This receptor has the native ligand 4-hydroxytamoxifen (4-OHT) bound to 247 amino acid residues. Receptor analysis was carried out by looking at the statistics of the Ramachandran plot via the website http://www.ebi.ac.uk/pdbsum. This Ramachandran plot was used to see the stability and quality of the protein, with the requirements for the most favoured regions > 90% indicated by the red area, and the disallowed regions < 0.8% value indicated by the white area (Ho and Brasseur, 2005). Based on the results of the 3ERT receptor analysis, the number of amino acids distributed in the most favoured regions is 91.2%, and the amino acids in the disallowed regions are 0.0%; so, it can be stated that the protein structure of the 3ERT receptor is stable and has met the requirements. The structure of the 3ERT receptor protein and Ramachandran plot can be seen in Figure 1.

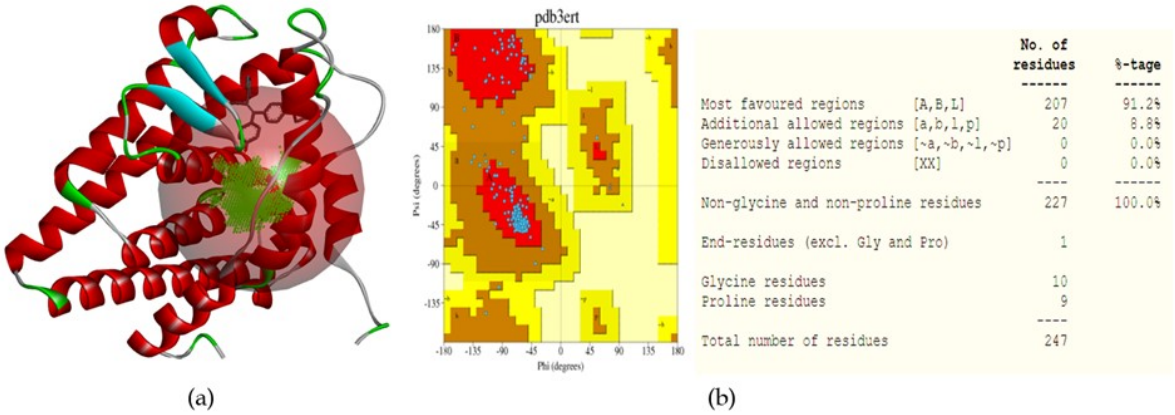

Figure 1. The structure of the 3ERT receptor protein (a) and Ramachandran plot (b).

3.2. Validation Docking

Receptor validation or re-docking was carried out by docking native ligand (4-OHT) to the prepared receptor using the AutoDock 1.5.6 program. The RMSD value is used as a parameter to determine the accuracy of the docking method. A small RMSD value indicates that the conformation of the ligand is close to the original position before re-docking; this value can be obtained by adjusting the coordinates of the grid box (x, y, z) where the interaction between the receptor and the ligand occurs. The Lamarckian Genetic Algorithm calculation system was chosen, with GA_run 100. The docking validation method was said to be valid if it had an RMSD value of 2Å (Bajda et al., 2014; Ruswanto et al., 2020). The overlay of native ligand poses with re-docked ligands and the position of the ligands in the grid box can be seen in Figure 2.

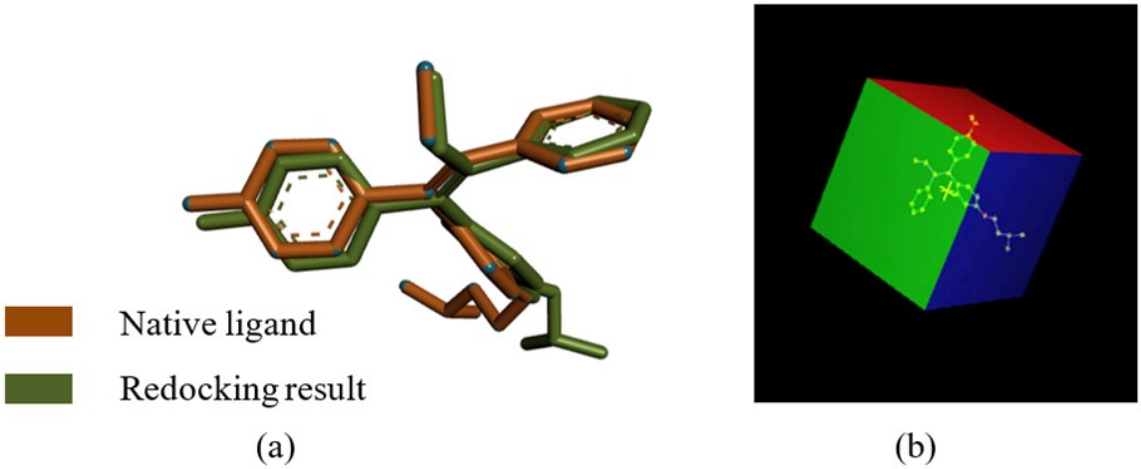

Figure 2. Overlay native ligand pose (4-OHT) crystallographic results with re-docking results (a) and ligand position in grid box (b).

Table 1 Docking Method Validation Results

Protein Data Bank (PDB) Code	*Centre Grid Box*	*Box Dimension*	*Space*	RMSD (Å)	*Binding Affinity* (kcal/mol)
3ERT	x = 30.191 y = -1.913 z = 24.207	x = 40 y = 40 z = 40	0.375	1.09	-11.52

Based on Table 1, the docking validation can be said to meet the requirements, with an RMSD value of 1.09Å, so the grid box coordinates (x, y, z) and box dimensions can be used as a reference for conducting a virtual screening process using the PyRx 9.8 program.

3.3. Simulation Molecular Docking & Virtual Screening

Virtual screening was conducted to select propolis bioactive compounds that have the most stable interaction with the 3ERT receptor in terms of binding energy (ΔG) and inhibition constant (Ki) values using the PyRx 0.9.8 program. A total of 111 structures of propolis bioactive compounds were downloaded from http://pubchem.ncbi.nih.gov, and the ligands were then screened by activating the docking menu in the PyRx 0.9.8 program. The comparison compound used was 4-OHT, which also acts as a native ligand found in the 3ERT receptor. The coordinates of the grid box from the validation of the docking method (Table 1) were used as a reference for screening. The results of virtual screening can be seen in Table 2.

The structure of the three compounds with the best virtual screening values can be seen in Figure 3.

Table 2 Virtual screening results of ligands with the best binding affinities

Code	Compound	ΔG (Kcal/mol)	Ki (μM)
4-OHT	4-hydroxytamoxifen (native ligand)	-11.21	0.006
PRO9	7-{2-[(2E)-3,7-dimethylocta-2,6-dien-1-yl]-3,4-dihydroxyphenyl}-4-hydroxy-3-(3-methylbut-2-en-1-yl)-5-oxo-5,6,7,8-tetrahydronaphthalen-2-olate	-10.73	0.013
PRO62	(1S,2R,5S,10R,11S,14R,15R)-2,6,6,11,15-pentamethyl-14-[(2R)-6-methylheptan-2-yl]tetracyclo[8.7.0.0^{2,7}.0^{11,15}]heptadec-7-en-5-ol	-10.42	0.022
PRO61	(1S,2R,5R,10R,11S,14R,15R)-2,6,6,11,15-pentamethyl-14-[(2R)-6-methylheptan-2-yl]tetracyclo[8.7.0.0^{2,7}.0^{11,15}]heptadec-7-en-5-ol	-10.29	0.028
PRO64	(2S,5S,7R,11S,14S,15S)-2,6,6,11,15-pentamethyl-14-[(2S)-6-methylhept-5-en-2-yl]tetracyclo[8.7.0.0^{2,7}.0^{11,15}]heptadec-1(10)-en-5-ol	-10.15	0.036
PRO63	(1S,2R,10R,11S,14R,15R)-2,6,6,11,15-pentamethyl-14-[(2R)-6-methylheptan-2-yl]tetracyclo[8.7.0.0^{2,7}.0^{11,15}]heptadec-7-en-5-yl acetate	-9.95	0.050
PRO67	(1S,3R,6S,8R,12S,15R,16R)-7,7,12,16-tetramethyl-15-[(2R)-6-methyl-5-methylideneheptan-2-yl]pentacyclo[9.7.0.0^{1,3}.0^{3,8}.0^{12,16}]octadecan-6-ol	-9.82	0.063
PRO6	3-{2-[(2E)-3,7-dimethylocta-2,6-dien-1-yl]-3,4-dihydroxyphenyl}-6,8-dihydroxy-1,2,3,4-tetrahydronaphthalen-1-one	-9.75	0.082
PRO8	3-{3-[(3E)-4,8-dimethylnona-3,7-dien-1-yl]-4,5-dihydroxyphenyl}-6,8-dihydroxy-1,2,3,4-tetrahydronaphthalen-1-one	-9.55	0.099
PRO66	(3S,6aR,6bS,8aR,12aS,14bR)-4,4,6a,6b,8a,11,11,14b-octamethyl-1,2,3,4,4a,5,6,6a,6b,7,8,8a,9,10,11,12,12a,14,14a,14b-icosahydropicen-3-yl acetate	-9.32	0.148
PRO83	6-{6-hydroxy-7,7,12,16-tetramethylpentacyclo[9.7.0.0^{1,3}.0^{3,8}.0^{12,16}] octadecan-15-yl}-2-methyl-3-methylideneheptanoate	-9.13	0.202
PRO47	(1R,2S,5R,8S,9S,10S,13R,14R,17S,19R)-1,2,5,9,10,14,18,18-octamethyl-8-(prop-1-en-2-yl)pentacyclo[11.8.0.0^{2,10}.0^{5,9}.0^{14,19}]henico san-17-o	-8.82	0.340
PRO82	2-methyl-3-methylidene-6-{7,7,12,16-tetramethyl-6-oxopentacyclo[9.7.0.0^{1,3}.0^{3,8}.0^{12,16}]octadecan-15-yl}heptanoate	-8.64	0.462
PRO7	3-(3,4-dihydroxyphenyl)-7-[(3E)-4,8-dimethylnona-3,7-dien-1-yl]-6,8-dihydroxy-1,2,3,4-tetrahydronaphthalen-1-one	-8.63	0.475
PRO78	5-hydroxy-2-(4-hydroxyphenyl)-8-(3-methylbut-2-en-1-yl)-4-oxo-4H-chromene-3,7-bis(olate)	-8.59	0.501
PRO21	1-(3-cyclohexyl-3-hydroxy-3-phenylpropyl)piperidin-1-ium	-8.31	0.810
PRO85	(1S,3R,6S,8R,11S,12S,15R,16R)-15-[(2R,5Z)-hept-5-en-2-yl]-7,7,12,16-tetramethylpentacyclo[9.7.0.0^{1,3}.0^{3,8}.0^{12,16}] octadecan-6-ol	-8.3	0.828
PRO69	(11S,15S,16R)-2-methoxy-16-(7-methoxy-2H-1,3-benzodioxol-5-yl)-4,6,13-trioxatetracyclo[7.7.0.0^{3,7}.0^{11,15}]hexadeca- 1(9),2,7-triene	-8.09	1.18
PRO68	(3S,4aR,6aR,6bS,8aR,11R,12S,12aR,14aR,14bR)-4,4,6a,6b,8a,11,12,14b-octamethyl-1,2,3,4,4a,5,6,6a,6b,7,8,8a,9,10,11,12,12a,14,14a,14b-icosahydropicen-3-yl acetate	-7.96	1.46
PRO77	5,7,8-trihydroxy-2-[4-hydroxy-3-(3-methylbut-2-en-1-yl)phenyl]-6-(3-methylbut-2-en-1-yl)-4-oxo-4H-chromen-3-olate	-7.89	1.65
PRO48	(4aS,6aS,8aS,9R,12bR,14aR)-2,2,4a,6a,8a,9,12b,14a-octamethyl-docosahydropicene	-7.88	1.67

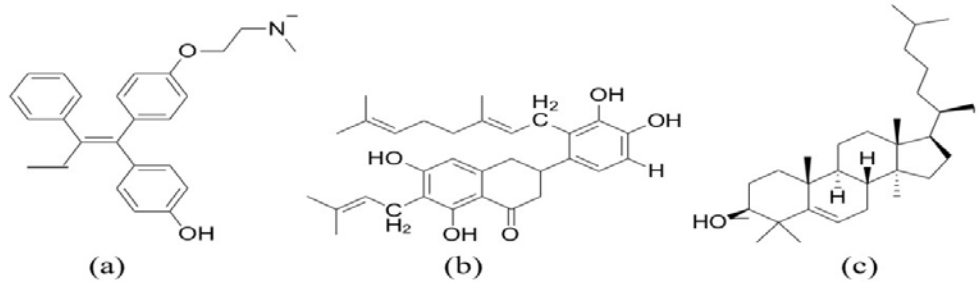

Figure 3. The structure of the compounds having the best virtual screening value 4-OHT (a), PRO9 (b), PRO63 (c).

3.4. Docking Result Visualisation Analysis

The BIOVIA Discovery Studio 2017 program was used to visualize the interaction between ligands and amino acid residues from the 3ERT receptor. The structure of a n amino acid consists of a C a tom covalently bonded to a carboxyl group, amine group, H atom, and side chain or R group. Hydrogen bonding is an important bond be tween the ligand and the receptor, affecting the molecule's affinity to the target protein. Hydrophobic bonds, non-covalent bonds, determine the ligand's stability with the

target protein, forming groups on t he polar side of t he protein structure due to the merging of non-polar chains (Harti, 2014); (Herschlag and Pinney, 2018; Siswandono, 2020); (Gouda and Almalki, 2019). The docking interaction results can be seen in Table 3.

Table 3 Interaction with amino acids

No.	Compound	Bond Type			
		Hydrogen	Pi-sigma Pi-sulphur Amide	Pi-alkyl/alkyl	van der Waals
1	4-OHT	Glu353, Arg394	-	Ala350, Leu387, Leu391, Phe404, Met421, Leu428, Leu525	Met343, Leu346, Thr347, Leu349, Asp351, Glu353, Leu354, Trp383, Leu384, Met388, Glu419, Gly420, Ile424, Gly521, His524, Met528, Leu536
2	PRO9	Leu387, Arg394, Met343	Met343, Leu346, Leu525	Ala350, Leu391, Phe404, Met421, Leu428, His524, Met528	Thr347, Leu349, Glu353, Trp383, Met388, Gly420, Ile424, Gly521, Lys529
3	PRO62	Asp351	-	Leu346, Leu349, Ala350, Leu384, Leu387, Leu391, Phe404, Leu525	Met343, Thr347, Glu353, Met388, Arg394, Met528

From the binding site prediction, it can be seen that the amino acids present in the binding site area are Met342, Leu345, Leu346, Leu349, Asp351, Arg352, Ala382, Trp383, Ile 386, Leu403, Val418, Glue419, Gly420, Met427, Lys520 and His524. And it can be seen that there are amino acids in the binding site area of 3 ERT that interact with ligands, for e xample the PRO9 compound (Leu346, His524, Leu349, Trp383 dan Gly420). Visualisation of the interaction of the ligand to the 3ERT receptor can be seen in Figure 4.

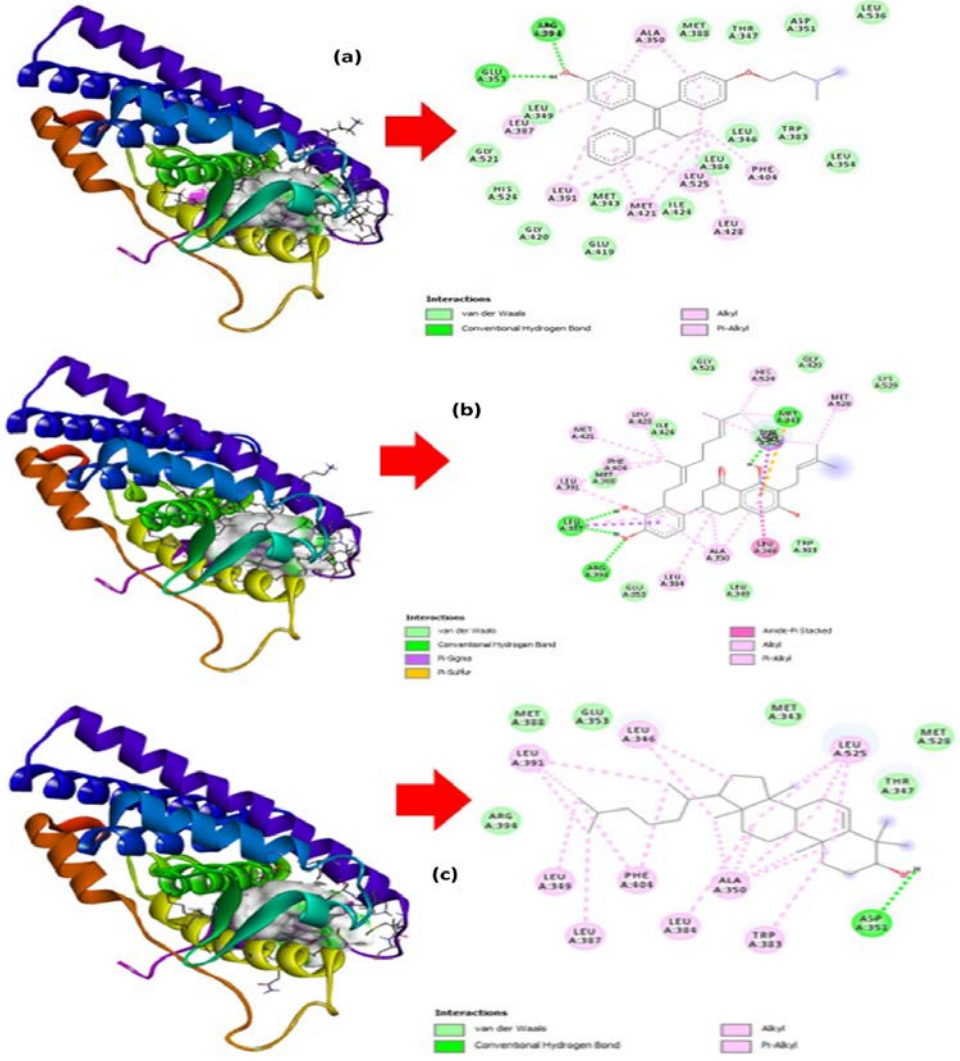

Figure 4. The 2D and 3D visualisation of the interaction of the ligand to the 3ERT receptor (a) native.

3.5.

3.6. Pharmacokinetics and Toxicity Prediction

Two propolis bioactive compounds and a comparison compound (4-OHT) with the best virtual screening values were selected to predict pharmacokinetic and toxicological properties. The pharmacokinetic parameters used were the Caco-2, HIA, VDss, BBB permeability, total clearance and renal OCT2 substrate, while the toxicity parameters used were Ames toxicity, LD 50 and hepatotoxicity (Pires et al., 2015). The Pharmacokinetic result can be seen in Table 4.

Table 4 Pharmacokinetics Parameters

		Pharmacokinetics Parameters					
		Absorption		Distribution		Metabolism	Excretion
No	Compounds	Caco-2 (Log cm/s)	HIA (%)	VDss (Log L/Kg)	BBB (Log BB)	CYP3A4 Substrate	Renal OCT2 substrate
1	4-OHT	1.120	95.378	0.156	-0.288	Yes	No
2	PRO9	0.941	86.731	-0.165	-1.091	Yes	No
3	PRO62	1.284	97.308	0.196	0.769	Yes	No

Note: HIA – human intestinal absorbance; BBB – blood brain barrier.

Based on Table 4, the CaCo-2 is used to predict the permeability of drug compounds. A drug is said to have high permeability if the CaCo-2 value is > 0.90 Log cm/s (Pires et al., 2015). Based on Table 4, several compounds met the requirements. HIA is used to predict drug absorption in the intestine. A drug has good absorption if it has an HIA value > 80% and poor absorption if the HIA value is < 30% (Chander et al., 2017). Based on the data from Table 4, propolis bioactive compounds and comparison compounds had good absorption (> 80%).

VDss is used to predict the drug concentration in blood plasma. The higher the VDss value, the higher the drug distribution to the tissues (Pires et al., 2015). The VDss value is said to be low if < -0.5 and high if > 0.45. Based on Table 4, several compounds had good drug distribution values.

BBB permeability is used to predict the ability of drugs to penetrate the blood brain barrier. This parameter is important to reduce the toxic effects and side effects of a drug. A BBB value > 0.3 is estimated to be able to penetrate the blood brain barrier well, while a BBB value < -1 is estimated to have a poor ability to penetrate the blood brain barrier (Pires et al., 2015). Based on Table 4, several compounds have good BBB values and can be predicted to have few side effects and low toxicity.

CYP3A4 substrate is used to predict drug metabolism, which generally occurs in the liver by involving brain cytochrome P450 enzymes (Pires et al., 2015). Based on Table 4, most of the compounds were metabolised by cytochrome P450 enzymes. OCT2 was used to predict drug excretion. The substrate of OCT2 has the potential to cause side interactions. Based on Table 4, several compounds are not substrates of OCT2.

Table 5 The Toxicity Parameters

		Toxicity Parameters		
No	Compounds	Ames Toxicity	LD 50 (mol/kg)	Hepatotoxicity (Yes/No)
1	4-OHT	Yes	2.069	No
2	PRO9	No	2.144	No
3	PRO62	No	3.598	No

The toxicity parameters are given in Table 5. Ames toxicity was used to predict the mutagenic potential of the compound. Positive test results indicate the ability of the compound to act as a carcinogen (Pires et al., 2015). The mutagenic ability of 4-OHT is in line with the theory that the use of tamoxifen has the potential to cause uterine cancer (Lorizio et al., 2012). The LD50 was used as a reference standard for acute toxicity measurements.

3.7. Molecular Dynamics

Molecular dynamic simulations were conducted using the AMBER 16 program to analyze the interaction, flexibility, and stability of propolis bioactive compounds, such as PRO9 and PRO62, compared to 4-OHT. The simulation involved preparing receptors and ligands, parameterizing the system, and constructing complex topology coordinates. The general amber force field (GAFF) was used to construct the topology on the ligands, and the ff14SB force field was used for the protein. The system was neutralized by adding Na+ ions or Cl- ions, and energy minimisation was performed. The system was heated at 0-310 K, and equilibration was performed six times to maintain constant volume, pressure, and temperature. The final stage involved production for 20 ns. The RMSD value was used to determine molecular conformation shifts, with stable values up to 0.1 nm indicating protein stability (Desheng et al., 2011; Muttaqin, 2019).

The RMSD graph of the 4-OHT, PRO9 and PRO62 systems can be seen in Figure 5.

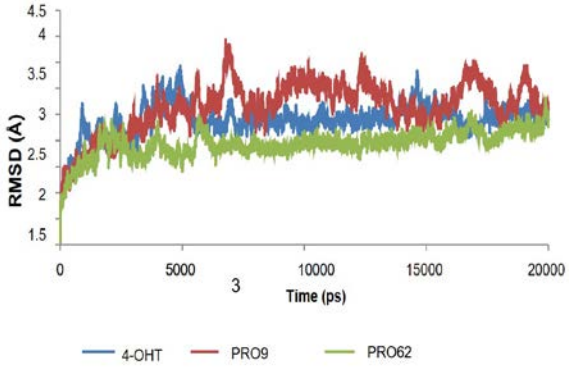

Figure 5. The RMSD for 4-OHT, PRO9 and PRO62

RMSF is used to see fluctuations in the shift of amino acid residues that make up proteins that interact with ligands. The RMSF value shows the size of the deviation between the particle position and several reference positions to describe the conformational shift of each amino acid residue that gives flexibility to the protein. The RMSF graph of the 4-OHT, PRO9 and PRO62 systems against the 3ERT receptor can be seen in Figure 6.

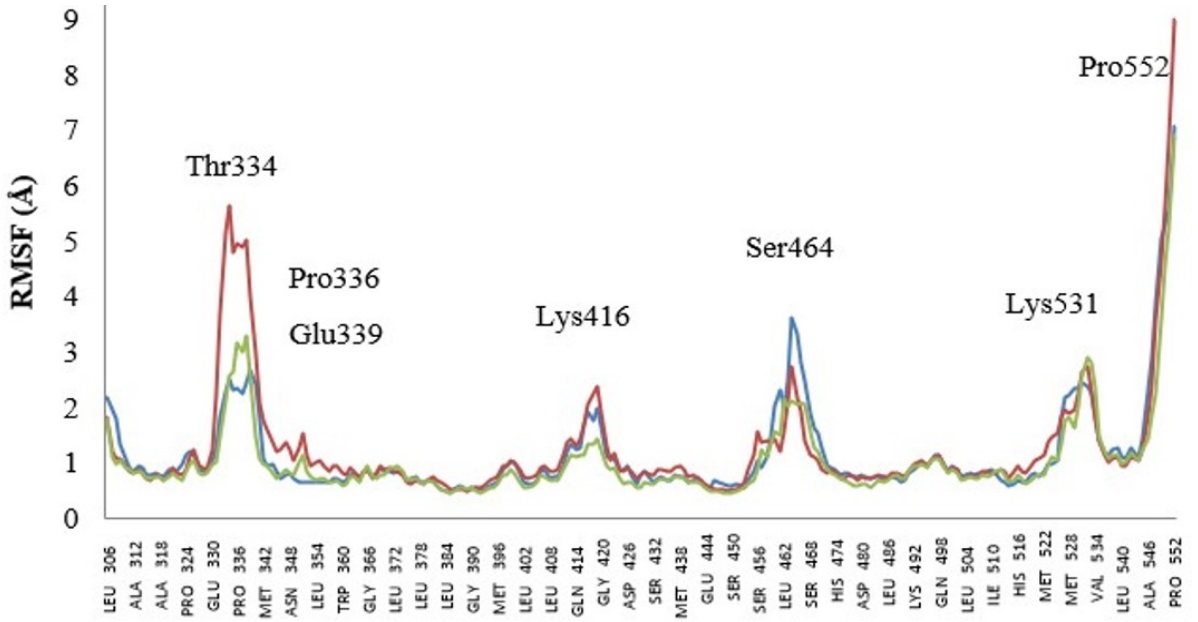

Figure 6. The RMSF for 4-OHT, PRO9 and PRO62.

The MM-GBSA was used to calculate the total bond energy (ΔG_{Total}) that occurred in the ligand-receptor system during the simulation. The smaller the value of free energy (ΔG) is, the more stable the interaction produced by the ligand-receptor system will be. The MMGBSA results can be seen in Table 6.

Table 6 Values of Molecular Mechanics-Generalised Born Surface Area (MM-GBSA) System 4-OHT, PRO9 and PRO62 against 3ERT

Parameters (Kcal/mol)	System		
	4-OHT	PRO9	PRO62
Interaction van der Waals (vdW)	-49.450	-47.141	-41.225
Electrostatic Energy (EEL)	111.070	125.898	87.489
Electrostatic contribution to solvation free energy (EGB)	-90.978	-103.303	-88.822
Non-polar contribution to solvation free energy (ESURF)	-7.169	-65.389	-5.912
ΔG_{Gas} (vdW+ EEL)	61.621	78.757	46.265
ΔG_{Solv} (EGB+ ESURF)	-98.147	-109.842	-9.473
ΔG_{Total} (vdW+EEL+EGB+ SURF)	-36.527	-31.085	-48.469

4. Discussion

Based on Table 2, the 20 compounds with the best virtual screening values were selected from 111 bioactive compounds of propolis. The Gibbs free energy (ΔG) was used to measure the ability of the ligand to bind to the receptor, while the value of the inhibitory constant (Ki) was used to measure the inhibitory activity. The smaller the ΔG value is, the higher are the bond affinity and the inhibitory activity, and the smaller is the Ki value, so that the ligands can form stronger and more stable bonds (Mardianingrum et al., 2021). It is known that the compounds with the best ΔG and Ki values, respectively, are 4-OHT (-11.21 Kcal/mol; 0.06 M), PRO9 (-10.73 Kcal/mol; 0.013 M) and PRO62 (-10.42 Kcal/mol; 0.022 M), so it can be said that the comparison compound 4-OHT has the most stable binding to the ERα receptor.

Based on Table 3, it can be seen that the 4-OHT compound has two hydrogen bonds to Glu353 and Arg394, while PRO9 has three hydrogen bonds to Met343, Leu387, Arg394, and PRO62 has one hydrogen bond with the Asp351 residue. PRO9 has a hydrogen bond equation with 4-OHT bonded to Arg394, which indicates a similarity in forming a stable bond with ERα. The ERα has hydrogen bonds with amino acid residues of His524, so the ligand can be an agonist if it has hydrogen bonds with His524, which causes helix-12 to open (Muchtaridi et al., 2014). Based on Table 3, 4-OHT, PRO9 and PRO62 do not have hydrogen bonds with His524, so they are predicted to have antagonistic properties that can block the binding of coactivators to the ERα receptor.

4-OHT has 17 hydrophobic bonds with Met343, Leu346, Thr347, Leu349, Asp351, Glu353, Leu354, Trp383, Leu384, Met388, Glu419, Gly420, Ile424, Gly521, His524, Met528 and Leu536. PRO9 has 13 hydrophobic bonds with 4-OHT, namely Thr347, Leu349, Ala350, Glu353, Trp383, Met388, Leu391, Phe404, Gly420, Met421, Ile424, Leu428 and Gly521, while PRO62 has the same 10 hydrophobic bonds: Met343, Thr34, Ala350, Glu353, Leu387, Met388, Leu391, Phe404, Leu525 and Met528. The existence of a hydrophobic bond equation indicates the similarity of the drug's ability to penetrate biological membranes so that it is predicted to bind well to Erα, and the number of pi-sigma interactions (pi-alkyl and pi-sulphur), which mostly involve charge transfer, helps in the drug interactions at the receptor binding site (Gouda and Almalki, 2019).

From the matching interaction of amino acid residues of PRO9 and PRO62 with the comparison compound (4-OHT), it can be predicted that both compounds have the same activity, and the number of interactions with amino acid residues can affect the bond energy that occurs between the ligand and the 3ERT receptor.

Based on Figure 5, it can be seen that there was an increase in the RMSD value during the molecular dynamic simulation, indicating that the ligand was ready to form bonds with the open protein structure. The highest RMSD value of the comparison compound 4-OHT was ± 3.5 at 5

ns, whilst the highest RMSD values of PRO9 and PRO62 were ± 4 at 7 ns and ± 2.5 at 19 ns, respectively. In this study, it can be seen that the PRO62 system can maintain its structure until the simulation ends and has a good level of stability compared to 4-OHT and PRO9; it can therefore be predicted to have a stable interaction with the 3ERT receptor, but all systems had not reached a completely stable conformation at the end of the simulations, so additional simulation time is needed.

Based on Figure 6, it can be seen that the RMSF value of the system is determined by fluctuations that occur in the amino acid residues. The highest fluctuation in the 4-OHT system occurred in Pro552, Lys531, Ser464, Lys416 and Glu334, while the residues that experienced the lowest fluctuations were Glu385, Ile389 and Leu384. The highest fluctuations in the PRO9 system occurred in Pro552, Thr334, Lys416, Ser464 and Lys531, while the residues that experienced the lowest fluctuations were Glu385, Ile389 and Leu384. The highest fluctuations in the PRO62 system occurred in Pro552, Lys531, Ser464 and Pro336, while the residues that experienced the lowest fluctuations were Glu385, Ile389 and Leu384.

The protein structure of ERα has hydrogen bonds attached to amino acid residues formed between Glu19 and His52, and between Glu19 and Lys531. Thus, if there is a significant fluctuation in the amino acid residue, the ligand can be predicted to have antagonistic properties to Erα.(Muchtaridi et al., 2014) The three systems, 4-OHT, PRO9 and PRO62, had increased fluctuations in lys531, which disrupted the hydrogen bonding of ERα so that 4-OHT, PRO9 and PRO62 could all be predicted to have potential as antagonists to ER.

Based on Table 6, it can be seen that the PRO62 system has the smallest ΔG_{Total} (-48.469 Kcal/mol) compared to 4-OHT (-36.527 Kcal/mol) and PRO9 (-31.085 Kcal/mol). Electrostatic energy has a great influence on the system. This shows that the PRO62 compound has a better affinity for the ERα breast cancer receptor (3ERT), so the compound can be predicted to have better potential as a breast cancer drug than the 4-OHT comparison drug by forming a more stable bond. The results of this study are also directly equivalent to several studies that reveal that lanosterol compounds have the potential to be developed as anticancer drugs.(Lasunción et al., 2012; Chung et al., 2010; Sanora et al., 2019).

5. Conclusion

A bioactive compound of propolis from was collected from database, namely PRO62 or lanosterol (3-beta) from Java and Kalimantan, has a more stable interaction than tamoxifen on breast cancer receptors (ERα), with a ΔG_{Total} value of -48.469 Kcal/mol. This compound met the pharmacokinetic requirements and had lower toxicity than tamoxifen.

Acknowledgments

The authors thank Universitas Bakti Tunas Husada and Universitas Perjuangan for the equipment provided for the research.

Disclosure

The authors report no conflicts of interest in this work.

References

Abuhamdah S, Abuhamdah R, Howes M J and Chazot P L. 2020. A Molecular Docking Study of Aloysia citrodora Palau. Leaf Essential Oil Constituents towards Human Acetylcholinesterase: Implications for Alzheimer's disease. *Jordan J Biol Sci*., **13(Supp. Issue)**: 575–580.

Al-Khayyat M Z. 2021. In Silico Screening for Inhibitors Targeting 4-diphosphocytidyl-2-C-methyl-D-erythritol Kinase in Salmonella typhimurium. *Jordan J. Biol. Sci*., **14(1)**: 75–82. https://doi.org/10.54319/140110.

Amalia E, Diantini A and Subarnas A. 2020. Water-soluble propolis and bee pollen of Trigona spp. from South Sulawesi Indonesia induce apoptosis in the human breast cancer MCF-7 cell line. *Oncol. Lett*., **20(5)**: 1–1. https://doi.org/10.3892/ol.2020.12137.

Bajda M, Jończyk J, Malawska B and Filipek S. 2014. Application of Computational Methods for the Design of BACE-1 Inhibitors: Validation of in Silico Modelling. *Int. J. Mol. Sci*., **15(3)**: 5128–5139. https://doi.org/10.3390/ijms15035128.

Batra B, Sudan S S, Pant M, Pant K, Lal A and Gusain T. 2022. Molecular docking and TLC analysis of candidate compounds from lesser used medicinal plants against diabetes mellitus targets. *Jordan J. Biol. Sci*., **15(2)**: 339–346. https://doi.org/10.54319/jjbs/150221.

Bray F, Ferlay J, Soerjomataram I, Siegel R L, Torre L A and Jemal A. 2018. Global cancer statistics 2018: GLOBOCAN estimates of incidence and mortality worldwide for 36 cancers in 185 countries. *CA. Cancer J. Clin*., **68(6)**: 394–424. https://doi.org/10.3322/caac.21492.

Chander S, Tang C R, Al-Maqtari H M, Jamalis J, Penta A, Hadda T B, Sirat H M, Zheng Y T and Sankaranarayanan M. 2017. Synthesis and study of anti-HIV-1 RT activity of 5-benzoyl-4-methyl-1,3,4,5-tetrahydro- 2H -1,5-benzodiazepin-2-one derivatives. *Bioorganic Chem*., **72(6)**: 74–79. https://doi.org/10.1016/j.bioorg.2017.03.013.

Chung M J, Chung C K, Jeong Y and Ham S S. 2010. Anticancer activity of subfractions containing pure compounds of chaga mushroom (Inonotus obliquus) extract in human cancer cells and in balbc/c mice bearing sarcoma-180 cells. *Nutr Res Pract*., **4(3)**: 177-182. https://doi.org/10.4162/nrp.2010.4.3.177.

Dallakyan S and Olson AJ. 2015. Small-Molecule Library Screening by Docking with PyRx, in: Hempel JE, Williams CH and Hong CC (Eds), **Methods in Molecular Biology**. Springer New York, New York, pp. 243–250. https://doi.org/10.1007/978-1-4939-2269-7_19.

Desheng L, Jian G, Yuanhua C, Wei C, Huai Z and Mingjuan J. 2011. Molecular dynamics simulations and MM/GBSA methods to investigate binding mechanisms of aminomethylpyrimidine inhibitors with DPP-IV. Bioorg. Med. Chem. Lett., **21(22)**: 6630–6635. https://doi.org/10.1016/j.bmcl.2011.09.093.

Fikri A M, Popova M, Sulaeman A and Bankova V. 2020. Stingless bees and Mangifera indica: A close relationship? Indian J. Nat. Prod. Resour., **11(2)**: 130–134. https://doi.org/10.56042/ijnpr.v11i2.25682.

Gouda A M and Almalki F A. 2019. Carprofen: a theoretical mechanistic study to investigate the impact of hydrophobic interactions of alkyl groups on modulation of COX-1/2 binding selectivity. *SN Appl. Sci*., **1(4)**: 332. https://doi.org/10.1007/s42452-019-0335-5.

Harti. 2014. **Health Biochemistry (Biokimia Kesehatan)**, Nuha Medika, Yogyakarta.

Hasanah S N and Widowati L. 2016. Jamu in tumor/cancer patients as complementary therapy. *J. Kefarmasian Indones*., **6(1)**: 49–59. https://doi.org/10.22435/jki.v6i1.5469.49-59.

Herschlag D and Pinney M M. 2018. Hydrogen bonds: simple after all? *Biochemistry*., **57(24)**: 3338–3352. https://doi.org/10.1021/acs.biochem.8b00217.

Ho B K and Brasseur R. 2005. The Ramachandran plots of glycine and pre-proline. *BMC Struct. Biol*., **5(1)**: 14. https://doi.org/10.1186/1472-6807-5-14.

Kalsum N, Setiawan B and Wirawati C U. 2016. Phytochemical studies and GC-MS analysis of propolis trigona spp. from two region in Lampung Province of Indonesia. Int. J. Sci. Eng. Res., **7(10)**: 173–180.

Kustiawan P M, Phuwapraisirisan P, Puthong S, Palaga T, Arung E T and Chanchao C. 2015. Propolis from the stingless bee trigona incisa from East Kalimantan, Indonesia, induces in vitro cytotoxicity and apoptosis in cancer cell lin es. *Asian Pac. J. Cancer Prev*., **16(15)**: 6581–6589. https://doi.org/10.7314/APJCP.2015.16.15.6581.

Lasunción M A, Martín-Sánchez C, Canfrán-Duque A and Busto R. 2012. Post-lanosterol biosynthesis of cholesterol and cancer. *Curr. Opin. Pharmacol*., **12(6)**: 717–723. https://doi.org/10.1016/j.coph.2012.07.001.

Lorizio W, Wu A H B , Beattie M S, Rugo H, Tchu S, Kerlikowske K an d Ziv E. 2012. Clinical and biomarker predictors of side effects from tamoxifen. Breast Cancer Res. Treat., **132(3)**: 1107–1118. https://doi.org/10.1007/s10549-011-1893-4.

Mardianingrum R, Endah S R N, Suhardiana E, Ruswanto R and Siswandono S. 2021. Docking and molecular dynamic study of isoniazid derivatives as anti-tuberculosis drug candidate. *Chem. Data Collect*., **32(4)**: 100647. https://doi.org/10.1016/j.cdc.2021.100647.

Mardianingrum R, Hariono M, Ruswanto R, Yusuf M and Muchtaridi M. 2022. Synthesis, Anticancer Activity, Structure–Activity Relationship, and Molecular Modeling Studies of α-Mangostin Derivatives as hERα Inhibitor. *J. Chem. Inf. Model*., **62(21)**: 5305–5316. https://doi.org/10.1021/acs.jcim.1c00926.

Mardianingrum R, Yusuf M, Hariono M, Mohd Gazzali A an d Muchtaridi M. 2020. α-Mangostin and its derivatives against estrogen receptor alpha. *J. Biomol. Struct. Dyn*., **40(6)**: 2621-2634. https://doi.org/10.1080/07391102.2020.1841031.

Miah S, Bagu E, Goel R, Ogunbolude Y, Dai C , Ward A, Vizeacoumar F S, Davies G, Vizeacoumar F J, Anderson D an d Lukong K E. 2019. Estrogen receptor signaling regulates the expression of the breast tumor kinase in breast cancer cells. *BMC Cancer*., **19(1)**: 78. https://doi.org/10.1186/s12885-018-5186-8

Miyata R, Sahlan M, Ishikawa Y, Hashimoto H, Honda S an d Kumazawa S. 2019. Propolis components from stingless bees collected on South Sulawesi, Indonesia, and their xanthine oxidase inhibitory activity. *J. Nat. Prod*., **82(2)**: 205–210. https://doi.org/10.1021/acs.jnatprod.8b00541.

Muchtaridi M, Yusuf M. Diantini A, Choi S, Al-Najjar B, Manurung J. Subarnas A, Achmad T, Wardhani S and Wahab H. 2014. Potential Activity of Fevicordin-A from Phaleria macrocarpa (Scheff) Boerl. Seeds as Estrogen Receptor Antagonist Based on Cytotoxicity and Molecular Modelling Studies. *Int. J. Mol. Sci*., **15(5)**: 7225–7249. https://doi.org/10.3390/ijms15057225.

Muttaqin F Z. 2019. Study of molecular docking, molecular dynamic, and toxicity prediction of naphthyridine alkaloid derivatives as protein casein kinase 2-α inhibitor in leukemic cancer. *Pharmacoscript*., **2(1)**: 49–64. https://doi.org/10.36423/pharmacoscript.v2i1.241.

Pires D E , Blundell T L and Ascher D B . 2015. pkCSM: predicting small-molecule pharmacokinetic and toxicity properties using graph-based signatures. *J. Med. Chem*., **58(9)**: 4066–4072.

Pratami M P, Fendiyanto M H, Satrio R D, Nikmah I A, Awwanah M, Farah N, Sari N I P and Nurhadiyanta, N., 2022. In-silico Genome Editing Identification and Functional Protein Change of Chlamydomonas reinhardtii Acetyl-CoA Carboxylase (CrACCase). *Jordan J. Biol. Sci*., **15(3)**: 431–440. https://doi.org/10.54319/jjbs/150312.

Riskesdas K. 2018. Key Results of Basic Health Research (RISKESDAS). *J. Phys. Math. Theor*., **44(8)**: 1–200. https://doi.org/10.1088/1751-8113/44/8/085201.

Ruswanto R, Mardianingrum R, Nofianti T, Fizriani R and Siswandono S. 2023. Computational Study of Bis-(1-(Benzoyl)-3-Methyl Thiourea) Platinum (II) Complex Derivatives as Anticancer Candidates. *Adv. Appl. Bioinforma. Chem*., Volume **16(2023)**: 15–36. https://doi.org/10.2147/AABC.S392068.

Ruswanto R, Mardianingrum R, Siswandono S an d Kesuma D. 2020. Reverse Docking, Molecular Docking, Absorption, Distribution, and Toxicity Prediction of Artemisinin as an Anti-diabetic Candidate. *Molekul*., **15(2)**: 88. https://doi.org/10.20884/1.jm.2020.15.2.579.

Sanora G D, Mastura E Y, Handoyo M O M and Purnama E R. 2019. Identification of Anticancer Active Compound from GC-MS Test Results of Zodia Leaves (Evodia suaveolens) Ethanol Extract. *J. Biota*., **5(2)**: 89–95. https://doi.org/10.19109/Biota.v5i2.3374.

Shiau A K, Barstad D, Loria P M, Cheng L, Kushner P J, Agard D A and Greene G L. 1998. The Structural Basis of Estrogen Receptor/Coactivator Recognition and the Antagonism of This Interaction by Tamoxifen. *Cell*., **95(7)**: 927–937. https://doi.org/10.1016/S0092-8674(00)81717-1

Siswandono. 2020**. Medicinal Chemistry I (Kimia Medisinal I)**, second ed. Airlangga Press, Surabaya.

Tripathi A, Shrinet K, Singh V K and Kumar A. 2019. Molecular modelling and docking of Mus musculus HMGB1 inflammatory protein with CGA. *Bioinformation*., **15(7)**: 456–466. https://doi.org/10.6026/97320630015456.

World Health Organization. 2020. **World case report: cancer research for cancer development**, IARC, France

.

JJBS

Volume 17, Number 1,March 2024
ISSN 1995-6673
Pages 163 – 171
https://doi.org/10.54319/jjbs/170116

Jordan Journal of Biological Sciences

Genetic Diversity and Relationship among and within the Bird of Paradise Plants of Strelitziaceae and Heliconiaceae

Siti Faiqotul Kholqiyah[1,*], Didik Wahyudi[2], Lia Hapsari[3]

[1]*Magister Program, Biology Faculty, Universitas Gadjah Mada, Yogyakarta, 55281, Indonesia;* [2]*Biology Department, Science and Technology Faculty, State Islamic University of Maulana Malik Ibrahim, Malang, 65144, Indonesia;* [3]*Research Center for Applied Botany, National Research and Innovation Agency, Cibinong, Bogor, 16911, Indonesia*

Received: June 17, 2023; Revised: August 9, 2023; Accepted: August 26, 2023

Abstract

Bird of paradise plants belong to families Strelitziaceae and Heliconiaceae, two close-related families in the Zingiberales order. This study aimed to study the genetic diversity and relationship of species among and within Strelitziaceae and Heliconiaceae using molecular RAPD markers and compare them to morphological characters. Samples used comprised two species from Strelitziaceae and eight species from Heliconiaceae. Twenty OPA primers showed that 17 out of 20 OPA primers were successfully amplified. Primer OPA-10 was the most informative and recommended, followed by OPA-5, OPA-7, OPA-9, OPA-11, OPA-17, OPA-18, OPA-19, and OPA-20. Heliconiaceae and Strelitziaceae were high genetic diversity (P=100%, I=0.388±0.016, He=0.237±0.013) with low similarities (0.09-0.39). Heliconiaceae was more genetically diverse than Strelitziaceae. Heliconiaceae produced P=98.88%, I=0.409±0.017, and He=0.254±0.014. Strelitziaceae produced P=60.53%, I=0.366±0.049, and He=0.251±0.033. The tree topology based on the RAPD marker differs slightly from morphology. However, the morphological characteristics are important to support and complement it. Strelitziaceae was strongly separated from Heliconiaceae, which supports the monophyly of both families. Heliconiaceae was separated into two subclusters and paraphyletic. Subcluster 1 comprises subgenera *Heliconia* and *Stenochlamys*. Subcluster 2 comprises subgenera *Griggsia* and *Stenochlamys*. In conclusion, the molecular RAPD marker proved the powerful of classification at the family level but moderate at subgenus, section, and species levels. Nonetheless, it is considered a simple and valuable method to provide a primary reference for taxonomic delimitation, conservation and breeding efforts of the bird of paradise plants in the future.

Keywords: RAPD, Phylogenetic, Polymorphism, Molecular taxonomy, Variability

1. Introduction

Strelitziaceae and Heliconiaceae are close-related families belonging to the order Zingiberales (Simpson, 2006; Malakar et al., 2022) and are known as the bird of paradise plants. Strelitziaceae originated in South Africa. This plant was introduced to Europe in 1770, with distribution in Africa, Madagascar and South America (Prince and Kress, 2002; Vieira et al., 2012). Meanwhile, Heliconiaceae originated in Tropical America and Melanesia (Andersson, 1998). The diversity centers of *Heliconia* are located in tropic and subtropic regions of South America and Central America (Cronquist, 1981). However, the current distribution of *Heliconia* is found in many tropical countries in the world, including Brazil (Marouelli et al., 2010), Colombia (Isaza et al., 2012), Mexico (Avendaño-Arrazate et al., 2017), Indonesia (Hapsari et al., 2019). Several species of both families are used as ornamental plants for garden landscapes and cut flowers. They are utilized commonly for unique inflorescence and leaf characteristics; including size, shape, arrangement and color (Malakar et al., 2022).

The species member of Strelitziaceae is limited, consisting of three genera *Strelitzia*, *Phenakospermum* and *Ravenala*. The genus *Strelitzia* has five species of *S. alba*, *S. nicolai*, *S. caudata*, *S. reginae* and *S. juncea* (Cron et al., 2012). The genera *Phenakospermum* and *Ravenala* have only one species, i.e., *P. guyanense* and *R. madagascariensis*, respectively (Santos et al., 2009). Heliconiaceae has a single genus (monotypic), namely *Heliconia*, and has many species of approximately 250-300 (Kress, 1990). Furthermore, a cladistic morphological analysis divided *Heliconia* into five subgenera, i.e. *Heliconia*, *Taeniostrobus*, *Heliconiopsis*, *Stenochlamys* and *Griggsia*, and 23 sections (Kress, 1984; Kress, 1990).

Strelitziaceae and Heliconiaceae are flowering perennial herbaceous plants. They share many common morphological characteristics such as sympodial rhizomes, banana-shaped leaves and distichous inflorescences (Marouelli et al., 2010; Santos et al., 2009). However, the plant size of Strelitziaceae is larger than Heliconiacae, ranging from perennial herbs to trees. Strelitziaceae flowers enclose in a bract which is a leaf-like structure with two sheaths. Most species have large paddle-shaped leaves (Vieira et al., 2012). Likewise, the inflorescences of Heliconiaceae have the shape of boat-like or dangling

* Corresponding author. e-mail: kholqiyahsitifaiqotul@gmail.com.

bract. Previous morphology character analysis showed that both families were clearly distinguished. Strelitziaceae is differentiated due to its palm-like trunk and leaves with the appearance of a fan. The separation within Heliconiaceae was paraphyletic with overlapping morphology characteristics (Kholqiyah et al., 2022). Morphology approaches are considered less accurate due to subjectivity and environmental influences (Probojati et al., 2019; Amer et al., 2022). Therefore, molecular applications are very significant techniques to get more information about their genetic diversity and relationship to confirm the morphology result.

Previous genetic and diversity studies have been reported on Heliconiaceae and Strelitziaceae using some molecular applications. Isaza et al. (2012), using Amplified Fragment Length Polymorphism (AFLP), revealed 170 bands with an overall average of polymorphism was 34.34%. Two well-defined groups of *Heliconia* were produced, with *S. reginae* serving as an outgroup. Meléndez-Ackerman et al. (2005), focusing on the genetic population of *H. bihai* in the Caribbean islands, showed high levels of AFLP polymorphism. About 244 loci were detected, with an average polymorphic percentage up to 73%. Meanwhile, Kumar et al. (1998) was reported using Random Amplified Polymorphic DNA (RAPD) for phylogenetic and identification studies of 16 *Heliconia* cultivars. The results showed they were closely related and suggested that some accessions were the same genotype. Likewise, Sheela et al. (2006) and Marouelli et al. (2010) reported the high RAPD polymorphism and demonstrated the monophyletic of Heliconiaceae separated from Strelitziaceae and other families in the Zingiberales. Molecular applications using DNA sequencing methods also have been reported, including Kress et al. (2002), Cron et al. (2012); Iles et al. (2017), Hapsari et al. (2019), and others..

Nevertheless, the RAPD method is considered more economical and simple, yet accurate enough to study the genetic diversity and relationship of closely related families compared to other molecular methods (Probojati et al. 2019; Trimanto et al. 2023). RAPD is considered adequate genotype identification and analysis of genetic differences among induced mutants (Wahyudi et al. 2020). In addition to Heliconiaceae and Streltiziceae, RAPD has been popularly applied at inter- and intra- specific levels of various plant species, such as wheat and barley (Ghabeish et al., 2021), rice (Sholikhah et al., 2019), ramie (Mayerni et al., 2019), legumes (Purwanti et al., 2021), pea (Osman and Ali, 2021), orchid (Hartati and Samanhudi, 2022), kalanchoe (Al-Khayri et al., 2022), banana (Probojati et al., 2019; Wiguna and Pharmawati, 2021), ginger (Trimanto et al. 2023), and many more. RAPD is a DNA amplification technique based on PCR using random primers and generally consists of 10 arbitrary base sequences with a minimum content of G and C bases of 60%. The RAPD is an easy technique, a fast process, with no need for prior genomic information, and uses a small DNA quantity (approximately 0.5-50 ng). In contrast, the RAPD is a low repetition rate. It can be overcome with the appropriate consistency of PCR conditions, especially the temperature when the primer attaches to the DNA template (Agisimanto and Supriyanto, 2007; Probojati et al., 2019; Zulfahmi et al., 2023).

Hence, the objective of this present study was to study the genetic diversity and relationship of species among and within the bird of paradise plants of Strelitziaceae and Heliconiaceae using RAPD markers. In addition, this study also aimed to compare the genetic relationship tree between molecular RAPD and morphology from Kholqiyah et al. (2022). Understanding genetic diversity and the relationship of close-related plant species is essential for taxonomic purposes and also contributes to the conservation strategy setting and further breeding efforts (Trimanto et al., 2023). Meanwhile, studies on the genetic diversity, genetic relationship, and genetic distance among and within Strelitziaceae and Heliconiaceae from Asian countries using RAPD markers are still limited. The findings of this study would benefit as a primary reference in taxonomic delimitation, setting priority for genetic conservation and germplasm breeding, and support for further related research and development of the bird of paradise plants.

2. Material and Methods

2.1. Plant materials

Ten species of the bird of paradise plants belonging to Strelitziaceae (two species) and Heliconiaceae (eight species) were used, as presented in Figure (1) and Table (1). The plant's specimens were derived from the ex-situ living collection of Purwodadi Botanic Garden, National Research and Innovation Agency located in Pasuruan Regency, East Java Province, Indonesia. The plant collections had been obtained from exploration and collecting missions, material exchanges, and donations from other botanic gardens, communities, or personals (Lestarini et al., 2012). The species identification referred to books identification guides of Heliconiaceae and Strelitziaceae (Arnold 2013; Hintze 2014); protologues of some type species, including Flora Peruviana , Flora de Brasilia, Flora of Guatemala, Flora of Java, and Flora Mesoamericana; scientific journals, and online databases including *Heliconia* Society Puerto Rico (http://www.heliconiasocietypr.org/), Plants of the world online of Kew Science (http://www.plantsoftheworldonline.org), Smithsonian Tropical Research Institute (https://biogeodb.stri.si.edu/), Centre for Agriculture and Bioscience International (https://www.cabi.org/), and Fairchild Botanic Garden (https://www.fairchildgarden.org/).

Figure 1. Plant specimens of Strelitziaceae and Heliconiaceae examined. S1=R. madagascariensis, S2=P. guyannense, H1=H. bihai, H2=H. wagneriana, H3=H. collinsiana, H4=H. chartacea, H5=H. rostrata, H6=H. metallica, H7=H. hirsuta, H8=H. psittacorum.

Table 1. Species list of Strelitziaceae and Heliconiaceae examined

Code	Species name	Subgenus	Section	Collection source
S1	*Ravenala madagascariensis* Sonn.	-	-	Malagasy
S2	*Phenakospermum guyannense* (A.Rich.) Endl. ex Miq.	-	-	Brazil
H1	*Heliconia bihai* (L.) L.	*Heliconia*	*Heliconia*	East Java
H2	*Heliconia wagneriana* Petersen	*Heliconia*	*Heliconia*	East Java
H3	*Heliconia collinsiana* Griggs	*Griggsia*	*Pendulae*	Guatemala
H4	*Heliconia chartacea* Lane ex Barreiros	*Griggsia*	*Pendulae*	Brazil
H5	*Heliconia rostrata* Ruiz & Pav.	*Griggsia*	*Rostratae*	Trop. America
H6	*Heliconia metallica* Planch. & Linden ex Hook.	*Stenochlamys*	*Cannastrum*	Brazil, Venezuela
H7	*Heliconia hirsuta* L. f	*Stenochlamys*	*Zingiberastrum*	Seram Island, Mollucas
H8	*Heliconia psittacorum* L.f.	*Stenochlamys*	*Stenochlamys*	Malagasy

2.2. DNA extraction

The fresh leaf shoot of each species was mashed using a mortar and pestle in liquid nitrogen. The whole genome DNA was isolated using a DNA isolation kit (Promega Wizard®) following the guidelines for pl ants. The extracted DNA was patterned qualitatively using electrophoresis agarose gel 0.8% in TBE buffer and quantitatively to check the concentration and purity level using a spectrophotometer Nano-drop (ND-1000) at 260 and 280 nm of wavelengths.

2.3. RAPD-PCR

Twenty OPA primers from Operon Technologies were used, as presented in Table (2). The reaction mixture was carried out in a PCR tube with a 10 µ L total volume consisting of 1 µ L (25 ng) DNA sample, 1 µ L (10 µ M) primer, 5 µL DreamTaq DNA polymerase (2x DreamTaq Green Buffers; 0.4 mM dNTPs and 4 mM MgCl2), and 3 µL nuclease-free water. The thermal cycle protocol comprised 40 cycles of denaturation at 92ºC for 1 minute, followed by annealing temperature of each RAPD primer (Probojati et al., 2019), extension at 72°C for 2 minutes and post extension at 72°C for 7 m inutes. The PCR products were confirmed using electrophoresis agarose gel 1% in TBE buffer and visualized on a Gel Doc/UV trans-illuminator (BioRAD) using a 100 bp DNA ladder marker.

Table 2. List of the RAPD primers used in this study

Primer	Sequence (5'-3')	MT(°C)	AT(°C)	GC Composition (%)
OPA 1	CAG GCC CTT C	36.40	41	70
OPA 2	TGC CGA GCT G	40.70	45	70
OPA 3	AGT CAG CCA C	34.30	39	60
OPA 4	AAT CGG GCT G	35.10	40	60
OPA 5	AGG GGT CTT G	32.60	37	60
OPA 6	GGT CCC TGA C	35.20	40	60
OPA 7	GAA ACG GGT G	33.20	38	60
OPA 8	GTG ACG TAG G	31.10	36	60
OPA 9	GGG TAA CGC C	37.40	42	70
OPA 10	GTG ATC GCA G	33.10	38	60
OPA 11	CAA TCG CCG T	36.70	41	60
OPA 12	TCG GCG ATA G	34.00	39	60
OPA 13	CAG CAC CCA C	37.70	42	70
OPA 14	TCT GTG CTG G	34.30	39	60
OPA 15	TTC CGA ACC C	34.20	39	60
OPA 16	AGC CAG CGA A	38.30	43	60
OPA 17	GAC CGC TTG T	35.70	40	60
OPA 18	AGG TGA CCG T	36.20	41	60
OPA 19	CAA ACG TCG G	34.20	39	60
OPA 20	GTT GCG ATC C	33.50	38	60

Notes: MT = Melting temperature, AT = Annealing temperature, GC = Guanine and Cytosine.

2.4. Data analysis

The amplified products of e ach primer are used to construct a binary matrix, as (0) if absent or (1) if present. They are used to estimate the level of DNA polymorphism, marker informativeness, genetic diversity, and the clustering pattern of ge netic relationship. RAPD polymorphisms were analyzed including the total number of bands (TNB), number of polymorphic bands (NPB), and percentage of pol ymorphic bands (PB). The marker informativeness of each RAPD primer was analyzed using four parameters, i.e. polymorphic information content (PIC), effective multiplex ratio (EMR), marker index (MI), and resolving power (RP). The formulas of each parameter are as follows:

$$PIC = 2f(1-f)$$

Where, f is the frequency of present bands, and 1-f is the frequency of absent bands.

$$EMR = np(\frac{np}{n})$$

Where, n is the total number of present bands, and np is the number of polymorphic bands.

$$MI = PIC\ X\ EMR$$

$$RP = 1 - [2x(0.5-p)]$$

Where, p is the proportion of species containing present bands.

The derived data were fed into GenAlEx v.6.5 (Peakall and Smouse, 2012) to estimate the genetic diversity. Other genetic parameters, including the percentage of polymorphic loci (P), Shannon's index (I), expected heterozygosity (He), and unbiased expected heterozygosity (uHe) were calculated. Hierarchical clustering was determined by a genetic relationship tree using PAST3 (Hammer et al., 2001). RAPD binary matrix was treated as a single data, using the UPGMA algorithm and Jaccard index with 1000 bootstraps. Bootstrap support (BS) was categorized as high confidence if BS >85%, moderate confidence if BS = 70-85%, low confidence if BS = 50-69%, and very low confidence if BS <50% (Kress et al., 2002).

3. Results

3.1. RAPD polymorphisms and marker informativeness

RAPD amplifications showed that seventeen primers produced 97 bands through all studied ten samples with a range of 150-1400 bp, as shown in Figure (2). The average number of polymorphic bands was about six bands. Primer OPA-10 revealed the highest polymorphic bands (13), while OPA-2 and OPA-13 produced the most minor polymorphic bands (1) (Table 3). The seventeen primers of RAPD, as a result of pr imary screening, were considered efficient for amplifying Strelitziaceae and Heliconiaceae (Figure 2, Table 3).

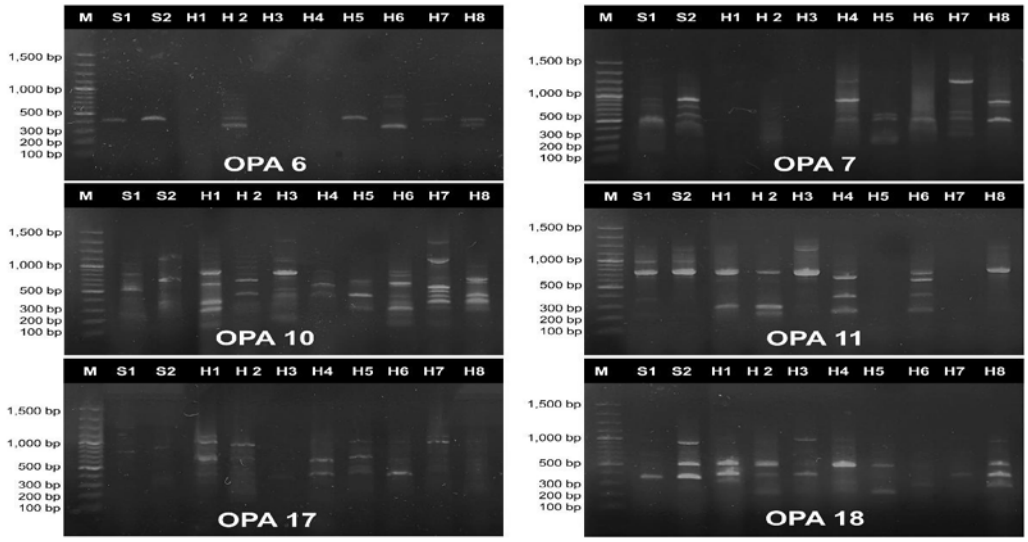

Figure 2. RAPD amplification profiles of OPA 6, OPA 7, OPA 10, OPA 11, OPA 17 and OPA 18.

PIC is a standard genetic parameter to evaluate the results of PCR amplification of genetic markers based on DNA bands (polymorphic). PIC value ranges from 0.00 to 1.00. The high value of PIC (>0.50) indicates that a primer is highly informative and discriminatory power, best for detecting the genetic variation (Anderson et al., 1993). PIC value results from this study ranged from 0.20-0.50, with an average of 0.37, which classified as moderatately informative power. The least PIC was scored 0.20 by the primer OPA-9. The highest value was 0.50 by the primer OPA-18. EMR is a genetic parameter used to determine the overall number of DNA bands formed in each primer and the number of polymorphic DNA bands (Medhi et al., 2014). The EMR values ranged from 1 to 169, with an average of 40.41 (Table 3). The primer OPA-2 and OPA-13 scored minimum EMR values (1), while the maximum EMR value scored 169 for the primer OPA-10 (Table 3). MI is a genetic parameter used to determine the index of a primer in producing polymorphic DNA bands (Varshney et al., 2007). MI values ranged from 0.32 to 76.05, with an average of 15.76. The least MI value was 0.32 for the primer OPA-2 and the highest was 7.05 by OPA-10 (Table 3). The RP is used to determine the most informative primers to differentiate DNA bands between genotypes (Prevost and Wilkinson et al., 1999). The values of RP ranged between 0.40 and 9.00, with an average of 3.16. The primer OPA-2 produced the least RP value, while the highest value was the primer OPA-10 (Table 3).

Table 3. RAPD polymorphisms and marker informativeness analysis results

Primer	TNB	NPB	PB	PIC	EMR	MI	RP
OPA 1	5	5	100	0.30	25	7.50	1.80
OPA 2	1	1	100	0.32	1	0.32	0.40
OPA 3	6	6	100	0.30	36	10.80	2.20
OPA 4	3	3	100	0.23	9	2.07	0.80
OPA 5	7	7	100	0.41	49	20.09	4.00
OPA 6	6	6	100	0.39	36	14.04	3.20
OPA 7	9	9	100	0.39	81	31.59	5.40
OPA 8	4	4	100	0.26	16	4.16	1.20
OPA 9	8	8	100	0.20	64	12.80	1.80
OPA 10	13	13	100	0.45	169	76.05	9.00
OPA 11	7	7	100	0.46	49	22.54	5.00
OPA 13	1	1	100	0.42	1	0.42	0.60
OPA 15	5	5	100	0.34	25	8.50	2.20
OPA 17	6	6	100	0.46	36	16.56	4.20
OPA 18	5	5	100	0.50	25	12.50	4.60
OPA 19	7	7	100	0.41	49	20.09	4.00
OPA 20	4	4	100	0.49	16	7.84	3.40
Total	97	97	1,700	6.33	706	275.28	53.40
Average	5.71	5.71	100	0.37	40.41	15.76	3.16

Notes: NB=Total number of present bands, NPB=Number of polymorphic bands, PB=Percentage of polymorphic bands, PIC=Polymorphic information content, EMR=Effective multiplex ratio, MI=Marker Index, and RP=Resolving Power.RAPD genetic diversity

The genetic diversity parameters analyzed from the RAPD results show that Heliconiaceae and Strelitziaceae have high genetic diversity. Heliconiaceae was more genetically diverse than Strelitziaceae in terms of polymorphic bands, Shannon index, and heterozygosity as shown in Table 4.

Table 4. RAPD genetic diversity analysis results. Data is mean value±standard error

Diversity parameters	Strelitziaceae	Heliconiaceae
No. of sample	2	8
No. of polymorphic bands	38	89
% polymorphic bands (P)	60.53	98.88
Shannon's index (I)	0.366±0.049	0.409±0.017
Expected heterozygosity (He)	0.251±0.033	0.254±0.014
Unbiased expected heterozygosity (uHe)	0.334±0.044	0.271±0.015

3.2. RAPD genetic relationship compare to morphology

Ten species of the bird of paradise plants examined in this study were clustered into two large groups following their families with low genetic similarities on both molecular RAPD and morphology methods, as shown in Figure 3. The range of genetic similarities based on RAPD was less than morphology, i.e., 0.09-0.39 and 0.11-0.74, respectively. Strelitziaceae (*R. madagascariensis* and *P. guyannense*) were separated as root (primitive relatives) at a similarity of 0.39 and supported by strong bootstrap values (100).

Furthermore, the tree topology within Heliconiaceae based on molecular RAPD (Figure 3A) was slightly different from morphology (Figure 3B). The molecular RAPD method produces two subclusters meanwhile the morphology method produces three subclusters. In the detail of RAPD genetic relationship within Heliconiaceae, cluster 1 comprised of subgenus *Griggsia* (*H. collinsiana*, *H. chartacea*, and *H. rostrata*) and subgenus *Stenochlamys* (*H. hirsuta* and *H. psittacorum*) at a similarity of 0.21; and

cluster 2 comprised of subgenus *Heliconia* (*H. bihai* and *H. wagneriana*) and subgenus *Stenochlamys* (*H. metallica*) at a similarity of 0.20. Cluster 1 of morphology clustering consisted of subgenus *Griggsia* at a similarity of 0.30; cluster 2 comprised of subgenera of *Heliconia* and *Stenochlamys* at a similarity of 0.35; and cluster 3 comprised of *H. metallica* at a similarity of 0.23 (Figures 3A-B). However, both methods revealed that the separation within the subgenera of Heliconiaceae was unclear and paraphyletic.

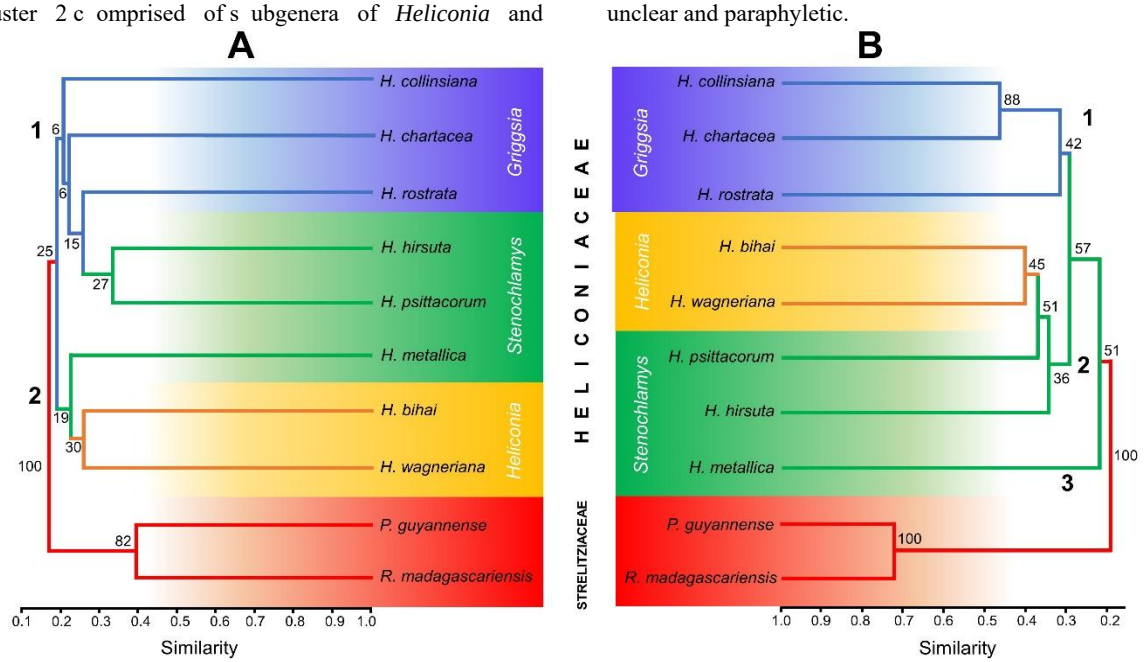

Figure 3. Dendogram relationship trees: A. based on molecular RAPD (this study); and B. based on morphology (Kholqiyah et al., 2022).

4. Discussion

The genetic diversity could be analyzed using the number of polymorphic bands. It categorizes as high if it is >50% (Hamrick and Godt, 1996). In this study, RAPD produced 100% polymorphic bands with different molecular positions across the samples. It indicates a high genetic diversity among and within species in Strelitziaceae and Heliconiaceae. Some of the species showed the absence of DNA bands (Figure 2). It may be because of a mismatch between samples and primer sequences during the annealing process. Another reason is the considerable molecular weight of the DNA fragments so that the bands fail to appear (Probojati et al., 2019; Agisimanto and Supriyanto, 2007).

A more detailed characterization of the DNA bands reveals that several primers produced unique bands at specific lengths. In this study, unique bands were found in both families. Primers OPA-4 (900 bp), OPA-11 (1000 bp) and OPA-19 (500, 600, and 1000 bp) resulted in unique bands that were only present in Strelitziaceae but absent in Heliconiaceae. Meanwhile, unique bands are found only in Heliconiaceae (subgenus *Heliconia*), namely primer OPA-3 (300 and 400 bp). The unique DNA bands from specific primers are considered as autapomorphic characters that could become a discriminant characters of that particular taxon (Assis, 2017).

Overall, RAPD marker informativeness analysis results showed that the most effective primer was OPA-10. The primer OPA-10 has high values at four parameters observed among other primers. The EMR, MI, and RP values of OPA-10 were the highest over the primers 169, 76.05, and 9.00, respectively. The PIC value of OPA-10 ranked fifth, with a high value of 0.45 (Table 3). Therefore, it could recommend the implication of OPA-10 as an effective RAPD primer for further similar genetic diversity studies on Strelitziaceae and Heliconiaceae, as well as Zingiberales in general. In addition, other effective primers recommended include OPA-5, OPA-7, OPA-9, OPA-11, OPA-17, OPA-18, OPA-19 and OPA-20.

The heterozygosity value for genetic diversity of the group of the taxon classified as high if He >0.20 (Hamrick and Godt, 1996). Shannon's information index values of Strelitziaceae (I=0.366±0.049) and Heliconiaceae (0.409±0.017) were classified as high. Hence, Heliconiaceae was more genetically diverse than Strelitziaceae. It is also supported by the fact that the species belonging to Strelitziaceae in the world are limited to only seven species (Santos et al., 2009; Cron et al. 2012), indicating that their genetic diversity is not as wide as that of Heliconiaceae which has reached 300 species. Furthermore, the genetic diversity of both families were found higher than previous studies on *Alpinia* spp. with I=0.350±0.040 (Basak et al., 2019) and *Musa* spp. with I=0.340±0.240 (Resmi et al., 2016), but lower than *Etlingera* spp. with I=0.417±0.011 (Trimanto et al., 2023) and *Curcuma* spp. with I=0.530±0.190 (Das et al., 2011).

Clustering analyses on molecular RAPD and morphology methods showed that Strelitziaceae were separated from Heliconiaceae as an outgroup and supported by strong bootstrap values of 100 (Figures 3A-B). An outgroup is important in phylogenetic inference to determine the polarity or direction of evolution (Kress et al., 2002). Therefore, this study supports the monophyly of both families, with Strelitziaceae as the primitive relative of Heliconiaceae in accordance to some previous phylogenetic studies (Sheela et al., 2006; Marouelli et al., 2010; Iles et al., 2017; Hapsari et al., 2019). Furthermore, both methods revealed that the separation within the subgenera of Heliconiaceae was unclear and paraphyletic. However, the previous study using RAPD markers showed

that subgenus *Heliconia* was monophyletic and subgenus *Stenochlamys* was polyphyletic (Marouelli et al., 2010). Compared to another AFLP marker study, Isaza et al. (2012) proved that the subgenus *Heliconia* is broadly monophyletic, while subgenus *Stenochlamys* falls in different clades and polyphyletic. Further, subgenus *Griggsia* could be paraphyletic, due to the presence of species from other subgenera in the same cluster. Thus, from this study, the RAPD application proved the power to classify at the family level (between Strelitziaceae and Heliconiaceae), but it is moderate at the subgenus, section, and species levels. Nonetheless, it is considered a simple and valuable molecular marker.

The relationship tree topology based on m olecular RAPD differs slightly with morphology. However, the morphological characteristics are significant to support and complement it. The morphological characterization from the previous study (Kholqiyah et al. 2022; Figure 1) supports the tree separation pattern of the RAPD molecular (Figure 3A). *R. madagascariensis* and *P. guyannense* of the Strelitziaceae was separated from Heliconiaceae due to several synapomorphic characters, including banana-like (musoid) and palm-like leaf growth types, light green pseudostem without blotches and wax, fan-like petiole arrangements, light green ligule color and stiff-boat shaped bracts. Within Heliconiaceae, subcluster 1 comprises subgenera *Griggsia* and *Stenochlamys*. The three species of subgenus *Griggsia* morphologically have a distinguishing character of pendant inflorescence, whereas *H. hirsuta* and *H. psittacorum* are members of s ubgenus *Stenochlamys* have several morphological similarities, including distichous bracts with shallow and narrow boat shaped, the leaf not ripped and the ligule green with brown blotches and not waxy. Subcluster 2 c omprises subgenera *Heliconia* and *Stenochlamys*. Two species of *H. bihai* and *H. wagneriana* had synapomorphic characters, including musoid leaf growth type, green pseudostem with brown blotches and waxy, oblique leaf base shape, green ligule with brown blotches, peduncle and rachis glabrous and deeply boat-shaped bracts. Meanwhile, *H. metallica* (subgenus *Stenochlamys*) was nested probably due to the presence of autapomorphic characters, namely pseudostem with brown-purplish blotches, Canna-like (cannoid) leaf growth type, the leaf blade is dark green-purplish (adaxial) and light green-purplish (abaxial), acute leaf base shape with dry and brown ligule.

The results from this study have provided important information on genetic diversity and relationship, among and within Strelitziaceae and Heliconiaceae. It could be utilized as a primary reference for t he taxonomy, conservation and breeding efforts of S trelitziaceae and Heliconiaceae germplasm. Ex-situ conservation plays a role in maintaining the existence of valuable germplasm. It includes protecting species from extinction and environmental changes (Rachmat et al., 2020). In t his study, Strelitziaceae with lower genetic diversity needs more ex-situ conservation efforts. The species member of this family is limited (only seven species recognized) (Santos et al., 2009; Cron et al., 2012) and rarely found in Indonesia (native to South Africa), thus material exchange between botanical gardens to increase the diversity of ex-situ collections is the most suitable strategy. Meanwhile, Heliconiaceae with high genetic diversity has a prioritization in conservation management. Several Heliconiaceae species comprised invasive species and weeds, including *H. bihai*, *H. wagneriana*, *H. latispatha* and *H. psittacorum*, so proper management of ex-situ collection is needed (Hapsari et al., 2019). In addition, propagation and further breeding efforts on *Heliconia* species suggested for orna mental purposes. Artificial hybridization through inter-species in *Heliconia*, particularly pairs of species with low genetic similarity as shown in Figure 3, makes it possible to produce hybrids with the desired characteristics (Malakar et al., 2022).

5. Conclusion

Molecular RAPD applications reveal that genetic diversity and relationship among and within bird of paradise plants Strelitziaceae, and Heliconiaceae had high polymorphism and low similarity. In t his study, the characterization of D NA bands led to unique bands on several primers and base length (bp) in both families. The genetic relationship was separated Strelitziaceae from Heliconiaceae. Heliconiaceae split into two subclusters, and the division of s ubgenera is paraphyletic. The tree topology based on RAPD markers was slightly different with morphology. RAPD marker was powerful in classifying at the family level between Strelitziaceae and Heliconiaceae. However, it was moderate within families, subgenus, section, and species levels. Nine RAPD primers are recommended. Further study is suggested to increase the validity and significance by using taxonomically diverse species from both Strelitziaceae and Heliconiaceae.

Acknowledgements

The authors would like to acknowledge Purwodadi Botanic Garden, National Research and Innovation Agency for the plant materials examined; also thanks go to the Griya Sains Laboratory for the molecular facilities. All authors (SFK, DW, LH) contributed equally as main authors in this manuscript including research design, field sampling and laboratory works, data compilation and analysis, data interpretation, writing the original manuscript, and the review and editing of the final manuscript.

References

Agisimanto D and Supriyanto A. 2007. Genetic diversity of Indonesian pomelo based on R andom Amplified Polymorphic DNA. *J Hort*., **17(1)**: 1-7.

Al-Khayri JM, Mahdy EMB, Taha HSA, Eldomiaty AS, Abd-Elfattah MA, Latef AAHA, Rezk AA, Shehata WF, Almaghsia MI, Shalaby TA, Sattar MN, Ghazzawy HS, Awad MF, Alali KM, Jain SM and Hassanin AA. 2022. Genetic and morphological diversity assessment of five kalanchoe genotypes by SCoT, ISSR and RAPD-PCR markers. *Plants*, **11(13)**: 1-12.

Amer WM, Shoulkamy MA, Abd El-Baset HD and Faried AM. 2022. Intraspecific identity of the wild *Brassica nigra* (L.) Koch. using morphological, cytogenetics and molecular (nuclear and chloroplast) approaches. *Jordan J Biol Sci.,* **15(3):** 489-500.

Anderson JA, Churchill GA, Autrique JE, Tanksley SD and Sorrels ME. 1993. Optimizing parental selection for genetic - linkage maps. *Genome*, **36(1)**: 181-186.

Andersson L. 1998. Heliconiaceae. In: Kubitzki K (Ed.), **Flowering Plants, Monocotyledons**. Springer-Verlag Berlin, Germany, pp. 226–230.

Arnold MA. 2013. **Landscape Plants for Texas and Environs**. Stipes Publishing Co., Illinois, USA.

Assis LCS. 2017. Patterns of character evolution in phylogenies. *J Syst Evol*., **55(3)**: 225-230.

Avendaño-Arrazate CH, Arrazate-Argueta JA, Ortiz-Curiel S, Moreno-Pérez E, Iracheta-Donjuan L, Reyes-López D, Grajales-Solis M, Martínez-Bolaños M and Cortés-Cruz M. 2017. Morphological characterization in wild species of Heliconias (*Heliconia* spp.) in Mexico. *Amer J Plant Sci*., **8(6)**: 1210–1223.

Basak S, Chakrabartty I, Hedaoo V, Shelke RG and Rangan L. 2019. Assessment of genetic variation among wild *Alpinia nigra* (Zingiberaceae) population: an approach based on molecular phylogeny. *Mol Biol Reports*, **46**: 177-189.

Cron GV, Pirone C, Bartlett M, Kress WJ and Specht C. 2012. Phylogenetic relationships and evolution in the Strelitziaceae (Zingiberales). *Syst Bot*., **37(3)**: 606-619.

Cronquist A. 1981. **An integrated system of classification of flowering plants**, Columbia University Press, New York.

Das A, Kesari V, Satyanarayana VM, Parida A and Rangan L. 2011. Genetic relationship of *Curcuma* species from Northeast India using PCR-based markers. *Mol Biotech*., **49(1)**: 65-76.

Ghabeish IH, Al-Zyoud FA and Hassawi DS. 2021. RAPD analysis and field screening of bread wheat and barley accessions for resistance to cereal leafminer *Syringopais temperatella*. *Jordan J Biol Sci.*, 14(2): 309-316.

Hammer Ø, Harper DAT and Ryan PD. 2001. PAST: Paleontological statistics software package for education and data analysis. *Palaeontol Electronic*., **4**: 1-9.

Hamrick JL and Godt MJW. 1996. Effects of life history traits on genetic diversity in plant Species. *Philosophical Transactions: Biol Sci*., **351(1345):** 1291-1298.

Hapsari L, Trimanto and Wahyudi D. 2019. Species diversity and phylogenetic analysis of *Heliconia* spp. collections of Purwodadi Botanic Garden (East Java, Indonesia) inferred by rbcL gene sequences. *Biodiversitas*, **20(5)**: 1266-1283.

Hartati S an d Samanhudi. 2022. Genetic variability analysis of *Phaius* spp orchid based on RAPD markers. *Int J Adv Sci Eng Inf Tech*., **12(4)**: 1558-1564.

Hintze J. 2014. **An Identification Picture Book for Heliconias and gingers for Cut Flower Growers**. Jungle Plant & Flower Service, Darwin NT, Australia.

Iles W, Sass C, Lagomarsino L, Benson-Martin G, Driscoll H and Specht C. 2017. The phylogeny of *Heliconia* (Heliconiaceae) and the evolution of floral presentation. Mol Phyland Evol., **117:** 150-167.

Isaza L, Marulanda ML and López AM. 2012. Genetic diversity and molecular characterization of several *Heliconia* species in Colombia. *Genet Mol Res*., **11(4):** 4552-4563.

Kholqiyah SF, Wahyudi D an d Hapsari L. 2022. Phenetic relationship of *Heliconia* spp. collection of Purwodadi Botanic Garden based on qualitative descriptors. *Bul Plasma Nutfah*, **28(1)**: 45-56.

Kress WJ, Prince LM and Williams KJ. 2002. The phylogeny and a new classification of the gingers (Zingiberaceae): Evidence from molecular data. *Amer J Bot*., **89(10)**: 1682-1696.

Kress WJ. 1984. Systematics of Central American *Heliconia* (Heliconiaceae) in Brazil. *J Arnold Arboretum*, **65(4)**: 429-532.

Kress WJ. 1990. The diversity and distribution of *Heliconia* (Heliconiaceae) in Brazil. *Acta Bot Brasilica*, **4**(1): 159–167.

Kumar PP, Yau JC and Goh CJ. 1998. Genetic analyses of *Heliconia* species and cultivars with Randomly Amplified Polymorphic DNA (RAPD) Markers. *J Amer Soc Hort Sci*., **123(1)**: 91-97.

Lestarini W, Matrani, Sulasmi, Trimanto, Fauziah and Fiqa AP. 2012. **An Alphabetical List of Plant Species Cultivated in Purwodadi Botanic Garden**, Purwodadi Botanic Garden - Indonesian Institute of Sciences. Purwodadi, Pasuruan, East Java, Indonesia.

Malakar M, Beruto M and Barba-Gonzales R. 2022. Biotechnological approaches to overcome hybridization barriers and use of micropropagation tool for further improvement in *Heliconia*: a review. *Plant Cell, Tissue and Organ Culture,* **149**: 503–522.

Marouelli LP, Inglis PW, Ferreira MA and Buso GSC. 2010. Genetic relationships among *Heliconia* (Heliconiaceae) species based on RAPD markers. *Genet Mol Res*., **9(3)**: 1377-1387.

Mayerni R, Yusniwati, Yulfa D an d Chan SROS. 2019. Genetic diversity based on RAPD marker of ramie plants (*Boehmeria nivea* (L.) Gaud) in West Sumatra. IOP Conf. Series: Earth and Environmental Science. **327.**

Medhi K, Sarmah DK, Deka M and Bhau BS. 2014. High gene flow and genetic diversity in three economically important *Zanthoxylum* spp. of Upper Brahmaputra Valley Zone of NE India using molecular markers. *Meta Gene* **2**: 706–721.

Meléndez-Ackerman EJ, Speranza P, Kress WJ, Rohena L, Toledo E, Cortés C, Treece D, Gitzendanner M, Soltis P an d Soltis D. 2005. Microevolutionary processes inferred from AFLP and morphological variation in *Heliconia bihai* (Heliconiaceae). *Int J Plant Sci* **166(5):**781-794.

Osman SA and Ali HBM. 2021. Genetic relationship of some *Pisum sativum* subspecies using different molecular markers. *Jordan J Biol Sci.*, 14(1): 65-74.

Peakall R and Smouse PE. 2012. GenALEx 6.5: Genetic analysis in Excel. Population genetic software for teaching and research-an update. *Bioinformatics* **28(19)**: 2537–2539.

Prevost A and Wilkinson MJ. 1999. A new system of comparing PCR primers applied to ISSR fingerprinting of potato cultivars. *Theor Appl Genet*., **98**: 107–112.

Prince LM and Kress WJ. 2002. **Zingiberales (Gingers and Bananas). Encyclopedia of Life Sciences.** Wiley Online Library. https://doi.org/10.1038/npg.els.0003710

Probojati RT, Wahyudi D an d Hapsari L. 2019. Clustering analysis and genome inference of Pisang Raja local cultivars (*Musa* spp.) from Java Island by Random Amplified Polymorphic DNA (RAPD) Marker. *J Trop Biodiv Biotechnol* **4(2)**: 42-53.

Purwanti E, Amin M, Zubaidah S, Maftuchah M, Hidayati SN and Fauzi A. 2021. Diversity of *Phaseolus lunatus* L. in East Java, Indonesia based on PCR-RAPD technique. *Jordan J Biol Sci.*, 14(2): 343-352.

Rachmat HH, Fambayun RA, Yulita KS and Susilowati A. 2020. Ex-situ conservation and management of Dipterocarps genetic resources through seedlings collections and nursery establishment. *Biodiversitas*, **21(2)**: 556-563.

Resmi L, Nair AR and Nair AS. 2016. Population genetic structure and diversity analysis of South Indian banana cultivars. *J Plant Breed Crop Sci*., **8(1)**: 1-12.

Santos BA, Lombera R and Benitez-Malvido J. 2009. New records of *Heliconia* (Heliconiaceae) for the region of Chajul, Southern Mexico, and their potential use in biodiversity-friendly cropping systems. *Rev Mexicana Biodiv*., **80**: 857-860.

Sheela VL, Lekshmi PRG, Nair CSJ and Rajmohan K. 2006. Molecular characterization of *Heliconia* by RAPD assay. *J Trop Agric*., **44(1-2)**: 37-41.

Sholikhah U, Parjanto, Handoyo T and Yunus A. 2019. Genetic diversity of black and aromatic rice cultivar (*Oryza sativa* L.) from various regions in Indonesia using Random Amplified Polymorphic DNA markers (RAPD). *Int J Adv Sci Eng Inf Tech*., **9(3)**: 1046-1051.

Simpson MG. 2006. **Plant Systematics.** Elsevier Academic Press, USA.

Trimanto, Probojati RT, Wahyudi D and Hapsari L. 2023. RAPD analysis to reveal the genetic diversity among closely related *Etlingera* species of *Achasma* Group, Zingiberaceae. *AIP Proceedings*. In press.

Varshney RK, Chabane K, Hendre PS, Aggarwal RK and Graner A. 2007. Comparative assessment of EST-SSR, EST-SNP and AFLP markers for evaluation of genetic diversity and conservation of genetic resources using wild, cultivated and elite barleys. *Plant Sci*., **173(6)**: 638-649.

Vieira MRS, Lima GPP, Medeiros DC, Souza A and Oliveira EC. 2012. Genus: *Strelitzia*. *J Hort For*., **4(11)**: 178-180.

Wahyudi D, Hapsari L, Sundari. 2020. RAPD analysis for genetic variability detection of mutant soybean (*Glycine max* (L.) Merr*). J Trop Biodiv Biotech*., **5(1)**: 68-77.

Wiguna IKC and Pharmawati M. 2021. Seleksi primer RAPD untuk analisis keragaman genetik tanaman pisang (*Musa* spp.). *Jurnal Biologi Universitas Andalas*, **9(2)**: 47-53.

Zulfahmi, Pertiwi SA, Rosmaina, Elfianis R, Gulnar Z, Zhaxybay T, Bekzat M and Zhaparkulova G. 2023. Molecular identification of mother trees of four matoa cultivars (*Pometia pinnata* Forst & Forst) from Pekanbaru City, Indonesia using RAPD markers. *Biodiversitas*, **24(3)**: 1524-1529.

JJBS

Volume 17, Number 1,March 2024
ISSN 1995-6673
Pages 173 – 184
https://doi.org/10.54319/jjbs/170117

Jordan Journal of Biological Sciences

Bacterial Diversity of Discarded Face Masks from Landfills, Mangroves, and Beaches, in Java, Indonesia

Anna Rakhmawati[1*], Bernadetta Octavia[1], Siti Marwati[2]

[1]*Department of Biology Education, Faculty of Mathematics and Natural Sciences, Universitas Negeri Yogyakarta, Jl. Colombo 1, Karangmalang, Yogyakarta, 55281, Indonesia Tel./Fax. +62-274-565411/+62-274-548203, email: anna_rakhmawati@uny.ac.id ;*
[2]*Department of Chemistry Education, Faculty of Mathematics and Natural Sciences, Universitas Negeri Yogyakarta, Jl. Colombo 1, Karangmalang, Yogyakarta, 55281, Indonesia*

Received: April 28, 2023; Revised: August 31, 2023; Accepted: September 6, 2023

Abstract

As the number of Covid-19 cases has increased, the production and use of face masks have also increased accordingly. This widespread use of face masks generates millions of tons of mask waste. This study analyzed the bacterial community composition of discarded masks from landfills (Piyungan, Jatibarang, Burangkeng); mangroves (Wanatirta, Tirang, Teluk Naga); and beaches (Parangtritis, Marina, Tanjung Pasir) in Yogyakarta, Semarang, Bekasi, and Tangerang, Java, Indonesia using 16S rRNA sequencing. Analyzing all samples from landfills, mangroves, and beaches revealed that the Proteobacteria phylum is the predominant. In addition, Firmicutes was the second-highest phylum in the samples from landfills and mangroves. In the meantime, Actinobacteria and Cyanobacteria dominated the phyla found in samples from beaches. Analyses at the genus level revealed that Bacillus members predominated in samples of discarded face masks from landfills. In addition, the most prevalent genus found in samples from mangroves and beaches was Vibrio. According to the findings, the distribution of bacterial communities differed among the various regions. Dissimilar bacterial communities and gradient distributions were found among discarded face masks in landfills, mangroves, and beaches. It was the first examination of bacterial distribution in discarded disposable face masks from various locations.

Keywords: bacterial communities, discarded mask, Proteobacteria, 16S amplicon sequencing.

1. Introduction

During the COVID-19 pandemic, the face mask is one of the essential fundamental equipment to prevent the spread of the Severe acute respiratory syndrome coronavirus 2 (SARS-CoV-2) from one human to another (Prata et al. 2020). The waste from disposable face masks could reach 1 million tons per month (Nghiem et al. 2021). In addition, between 0.15 and 0.39 million tons of plastic debris can accumulate annually in the world's oceans due to improper management of face masks in coastal regions (Chowdhury *et al*., 2021). Since the COVID-19 pandemic began, the widespread use of disposable face masks has become a critical ecological concern. Due to poor waste management practices and a lack of environmental consciousness, a substantial amount of untreated mask waste is dumped into the environment (Cordova *et al*., 2021). After a single use, face masks are discarded in dumpsites and landfills, although some are discarded in public places (Babaahmadi *et al*., 2021). Reports indicate that improper disposal of face masks has occurred globally. Various face masks have been discovered in urbanized areas (gardens, streets, parks), beaches, natural reserves, high mountains, and other aquatic environments (Gunasekaran *et al*., 2022).

Mishandling of face masks results in physical, physiological, and ecotoxicological harm to domestic and wild animals. Typically, face masks are composed of nonrenewable polymers derived from petroleum that are non-biodegradable and hazardous to the environment and public health. It has resulted in a great new type of pollution from improperly discarded masks, including heavy metals, volatile organic compounds (VOCs), and microfibers (Liu *et al*., 2022). Non-biodegradable face masks can cause significant problems for our ecosystem, such as microplastic pollution and increased transmission of antibiotic-resistant genes, if not properly disposed of (Pereira de Albuquerque et al. 2021). The disposable face masks are composed primarily of polypropylene (PP) and polyethylene (PE) with a high density and may also contain polyesters, polystyrene, polyurethane, and polyacrylonitrile. The slow degradation of the PP and PE fibers in face masks creates large reservoirs of microplastic pollutants that have acute and chronic effects on the physiology of aquatic organisms (Hasan *et al*., 2021; Patrício Silva *et al*., 2021; Spennemann, 2022).

In addition, the presence of discarded face masks has direct chemical effects on bacterial communities in the environment. Bioremediation of face mask-contaminated sites requires extensive knowledge of functional bacterial diversity and factors influencing bacterial functions. The role of indigenous bacteria in the biodegradation of discarded face masks is crucial. With increased discarded face mask contamination in landfills, mangroves, and beaches, the bacterial community may undergo significant changes. Due to natural selection resulting from contaminant pressure, the most dominant species in the locations are the most tolerant species (Panigrahi *et al*., 2018). Face masks discarded in the environment served as

a viable substrate for the growth of microbial biofilm and hydrocarbonoclastic microbes (Crisafi *et al*., 2022). Various bacteria, biofilm-forming bacteria, bacterial consortia, and fungi can be utilized for the biodegradation of the polymers contained in face masks. Several variables affect the biodegradation process, including microorganism type, polymer type, physicochemical properties of polymers, and environmental conditions such as pH, temperature, and UV radiation (Oliveira *et al*.,2020).

Even though the microbiome is involved in the degradation of face masks, no analysis has been conducted to compare the bacterial composition of face masks discarded in different locations. Using a culture-independent method and 16S rRNA amplicon sequencing, the primary objective of this study was to identify the bacteria from discarded face masks in landfills, mangroves, and beaches in the western, central, and southern regions of Java, Yogyakarta, Indonesia. Although the degradation of polymers by bacteria has been extensively studied, little is known about the bacteria that degrade face masks. In the future, using face mask-degrading bacteria may offer an excellent eco-friendly face mask degradation process. Therefore, it is necessary to investigate the bacterial community in discarded face masks through the analysis of bacterial diversity, with the hope that the results of this study will improve the management of face mask waste. In this study, three landfills (Piyungan, Jatibarang, Burangkeng); three mangroves (Wanatirta, Tirang, Teluk Naga); and three beaches (Parangtritis, Marina, Tanjung Pasir) in Yogyakarta, Semarang, Bekasi, and Tangerang, Java, Indonesia were chosen since these sites harbored a high abundance of discarded face masks and served as a hot spot for discovering bacterial communities for face mask degradation.

2. Materials and Methods

2.1. Discarded Face Mask Sampling

Between March and June 2022, discarded face mask samples were collected from landfills, mangroves, and beaches in Yogyakarta, Semarang, Bekasi, and Tangerang, Java, Indonesia. The discarded face mask at each location was collected with 50 mL sterile centrifuge tubes. On the island of Java, nine locations were chosen to study and represent diverse geographical conditions. The landfill site was chosen based on the size of the largest landfill in each province. The mangrove and beach were selected based on their proximity to Java Island's southern and northern tourist destinations. The sampling locations were Piyungan-Yogyakarta/A1, Jatibarang-Semarang/A2, Burangkeng-Bekasi/ A3 landfills; Wanatirta-Yogyakarta/B1, Tirang-Semarang/B2, Teluk Naga-Tangerang/B3 mangroves,and Parangtritis-Yogyakarta/C1, Marina-Semarang/C2, Tanjung pasir-Tangerang/C3 beaches as illustrated in Figure 1.

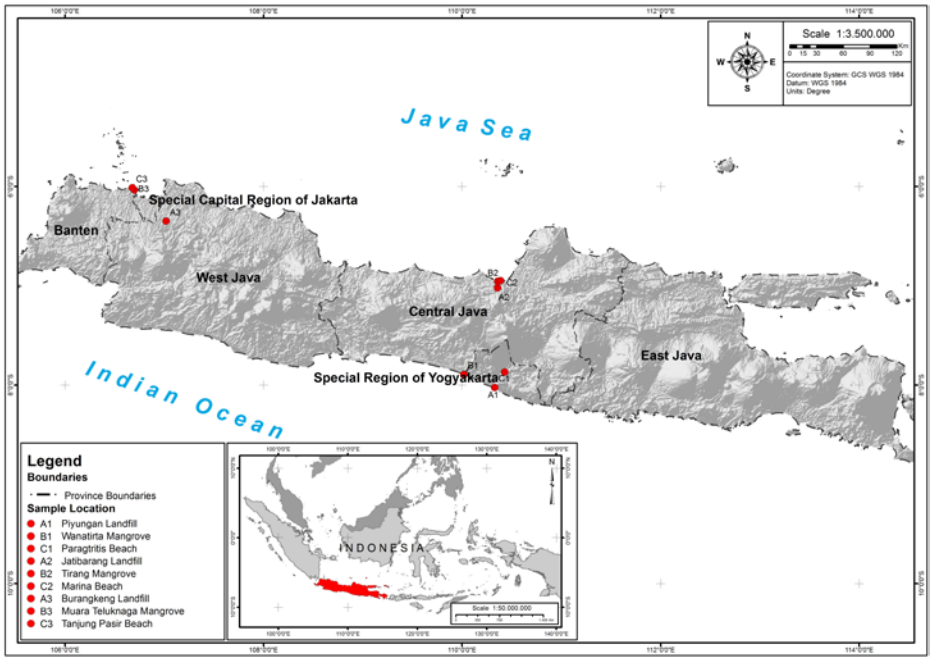

Figure 1. The location of discarded face masks sampling are landfills (A), mangroves (B), and beaches (C) in Java, Indonesia

2.2. Extraction, amplification, and sequencing of total DNA

All samples were sent for DNA extraction to PT Genetika Science Indonesia. Following the manufacturer's instructions, total DNA was extracted from each sample using a ZymoBIOMICSTM DNA Miniprep Kit (Takarina *et al*., 2022). The bacterial community was analyzed using Illumina HiSeq 2500 PE250 (Novogene, Tianjin, China). The replicated metagenomic DNA was pooled, and the hypervariable V3-V4 regions of the bacterial 16S rRNA gene were amplified using universal primers 341F (5'-CCTAYGGGRBGCASCAG-3') and (5'-GGACTACNNGGGTATCTAAT-3') primer pair (806R) to generate an amplicon library. All PCR reactions were performed with a Phusion High-Fidelity PCR master mix

(New England Biolabs). PCR amplicons were generated under the following conditions: 98 °C for 3 m inutes, followed by 35 cycles of 98 °C for 45 s , 50 °C for 60 s , and 72 °C for 9 0 s, and final elongation at 72 ° C for 10 minutes (Takahashi *et al*., 2014). We combined 2% agarose gel electrophoresis with equal volumes of 1X loading buffer (containing SYBR green) and 2 µL PCR products. Samples with a bright DNA bands of 400–450 bp were chosen for further experiments. We were mixing PCR products with equal density ratios. Qiagen Gel Extraction Kit (Qiagen, Germany) was used to purify the mixed PCR products. Using the NEBNext® UltraTM DNA Library Prep Kit for Il lumina, a sequencing library was generated, quantified using Qubit and QPCR, and analyzed using the Illumina platform. The library's quality was evaluated using a Qubit® 2.0 Fluorometer (Thermo Scientific) and an Agilent Bioanalyzer 2100 s ystem. The library was sequenced on an Illumina platform to generate 250 bp paired-end reads (Zhang *et al*., 2021).

2.3. Bioinformatics analysis

Based on t he samples' unique barcodes, paired-end reads were assigned and truncated by removing the barcode and primer sequences. The FLASH software combined the data from each paired-end sequenced reading (Magoč and Salzberg, 2011). Using the QIIME (V1.7.0) software (Kuczynski *et al*., 2011), high-quality, clean tags were obtained by performing quality filtering on the raw tags under specific filtering conditions (Bokulich *et al*., 2013). Filtering the raw tags with the UCHIME algorithm produced high-quality tags, which were then clustered into operational taxonomical units (OTUs) using a cutoff percentage of bases with a quality score > 20 and an error rate of 0.01 (Q20). Edgar *et al*. (2011) compared the clean tags to databases (Gold database) using the UCHIME algorithm to detect chimera sequences, which were then eliminated to achieve effectiveness. Using the UPARSE program (Edgar, 2013), sequenced data (effective tags) were then analyzed. Sequences with a similarity of 97% were classified as belonging to the same OTU. Each OTU was then compared to the SILVA 132 database (https://www.arb-silva.de/) to identify species at each taxonomic rank (threshold: 0.8–1). Information regarding the abundance of O TUs was normalized using the standard sequence number corresponding to the sample with the fewest sequences. Based on t hese output normalized data, subsequent alpha, and beta diversity analyses were performed. Principal coordinate analysis (PCoA) was then used to calculate the Shannon-Weiner index (relative abundance) and its effect on da ta distribution based on the annotation results. The Shannon-Weiner relative abundance and index were calculated using R (R Cor e Team, 2019) a nd Minitab 19 (Minitab, 2021) for the PCoA (Sessa *et al*., 2022).

3. Results and Discussion

The on-site collection of di scarded face masks from landfills, mangroves, and beaches in three clusters (Yogyakarta, Semarang, and Tangerang-Bekasi) revealed the presence of different types of di sposable face masks (duckbill, surgical, KF94, and KN95). During the collection of discarded face masks, it was discovered that they were mixed with other wastes in the landfill, sediments in the mangrove, and sand along the beach, as determined by a one-day sampling at each location. This study did not specify the residence time, mask type, quantity, manufacturer, or s tatus of t he physicochemical and biological processes. Illumina sequencing investigated the bacterial community structure in discarded face masks. With the advent of hi gh-throughput amplicon sequencing methods focusing on the 16S rRNA gene, a wealth of data is now available for d escribing the composition and diversity of the microbiome in natural environments. All discarded face mask samples yielded 1,020,654 effective sequences clustered into 35,612 OTUs. Our sample classified 901,664; 900,711; 885,140; 864,393; 739,319; and 278,125 sequences at the phylum, class, order, family, genus, and species levels, respectively.

In addition, differences in the microbiome's diversity and abundance between samples were compared using Chao1, ACE, Shannon, and Simpson indices (Table 1) and rarefaction curves (Figure 3). Through clustering with 97% identity on the Effective Tags of all samples, the OTUs were determined and then identified to examine each sample's bacterial community composition. Table 1 displays the bacterial community's parametric and non-parametric diversity indices in the discarded face masks. Alpha diversity indices demonstrated the abundance (observed species, Chao1 indices) and diversity (Shannon and Simpson indices) of t he microbiome within the samples. Alpha diversity indices showed the richness (observed species, Chao1 indices), and diversity (Shannon and Simpson indices) of t he microbiome in the samples. The observed alpha diversity indices for di scarded face masks from landfills were 3403 ± 387 (ob served OTUs), 8.62 ± 0.82 (Shannon), 0.99 ± 0.01 (Simpson), 4018 ± 544 (chao1), and 4126 ± 2463(ACE). The alpha diversity indices for di scarded face masks from mangroves had mean values of 3794 ± 774 (obs erved OTUs), 7.96 ± 2.00 (Shannon), 0.94 ± 0.07 (Simpson), 4442 ± 999 (chao1), and 4522 ± 989 (ACE), whereas the alpha diversity indices for discarded face masks from beaches had mean values of 3271 ± 520 (observed OTUs), 7.83 ± 0.52 (Shannon), 0.97 ± 0.01 (Simpson), 3891 ± 816 (chao1), and 4013 ± 717(ACE). These indices indicated that the species richness, evenness/abundance, number of different taxa, and phylogenetic distances of t he discarded face masks varied significantly depending on the collection location. Teluk Naga Mangrove contained the highest microbial taxa (4269), and Parangtritis Beach contained the lowest number (2861). The average number of ba cterial taxa across all nine samples was 3,489557, with mangrove, landfill, and beach samples having the highest, middle, and lowest numbers, respectively. The samples from Wanatirta Mangrove (B1) and Parangtritis Beach (C1) had the highest and lowest Chao1 non-parametric diversity indices, respectively. In a ddition, discarded face masks from the Wanatirta mangrove contained the highest bacterial diversity (Shannon's H index), while samples from the Tirang mangrove contained the least (B2).

Table 1. Normalized summary of sequence library including OTUs, diversity, and richness estimated at 97% level

Sample name	Observed species	Shannon	Simpson	Chao	ACE	Coverage
A1	3496	8.855	0.992	4467.486	4522.181	0.986
A2	3736	9.286	0.995	4174.874	4241.347	0.990
A3	2978	7.707	0.981	3412.896	3616.884	0.989
B1	4213	9.415	0.993	5115.607	5127.164	0.985
B2	2900	5.682	0.858	3294.709	3380.020	0.991
B3	4269	8.794	0.980	4918.264	5060.180	0.986
C1	2860	7.646	0.980	3286.100	3485.942	0.990
C2	3857	8.425	0.971	4819.719	4830.337	0.985
C3	3098	7.427	0.970	3568.520	3722.750	0.989

A1 (Piyungan), A2 (Jatibarang), A3 (Burangkeng) landfill; B1 (Wanatirta), B2 (Tirang), B3 (Teluk Naga) mangrove; C1(Parangtritis), C2 (Marina), C3 (Tanjung Pasir) beach

To further differentiate the three location groups, Figure 2.a displays the unique and shared OTUs, where 870 OTUs were unique to the landfill samples, 1367 OTUs were unique to the mangrove samples, and 695 OTUs were found exclusively in the beach samples out of the 3381 OTUs shared by the three location groups. In addition, based on Figure 2.b, the number of core OTUs obtained from a Venn diagram analysis was 989. It indicates that the 989 OTUs were shared by the discarded face mask in nine different locations and indicated a high degree of similarity in the bacterial community structure of all samples (Figure 2.b). This study revealed that several bacterial phyla populations in discarded face masks actively adapt to various environmental conditions.

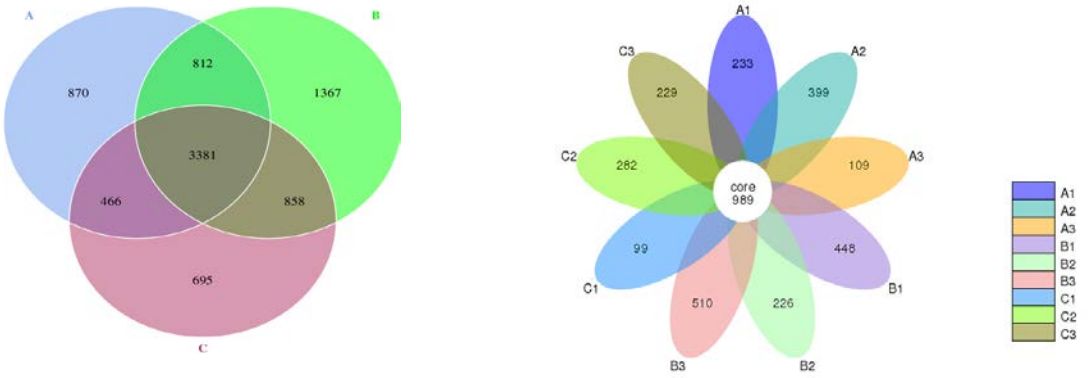

a b

Figure 2. Venn diagram showing the amount of bacterial OTUs shared among the studied discarded face mask community from A, B and C (landfill, mangrove, and beach), respectively. A1 (Piyungan), A2 (Jatibarang), A3 (Burangkeng) landfill; B1 (Wanatirta), B2 (Tirang), B3 (Teluk Naga) mangrove; C1(Parangtritis), C2 (Marina), C3 (Tanjung Pasir) beach

Figure 3 depicts the rarefaction curves generated at a threshold of 1% to compare the diversity of microbial species between sites. Environmental factors significantly impacted the abundance of bacterial groups and OTUs, as well as the appearance of some bacteria. The composition of microbial habitats can influence bacterial diversity in various environments. Notably, microbial communities are dynamic, and the results presented here represent a particular sampling time point. As observed in this study, variations in microbial diversity at various taxonomic levels in discarded face masks were related to the surrounding environment in which they originated. Considering the sampling area as a significant determinant of community composition, we can predict that the bacterial communities associated with discarded face masks will rapidly adapt to shifting environments rather than remain stable over long distances. Figure 3.a depicts that the OTUs indices of microbial communities in discarded face masks from mangroves were more significant than those from landfills and beaches. It was caused by the unique physicochemical characteristics of mangrove soil, such as oxygen, pH, salinity, and chemical compositions that were diverse for various microbial life forms and can therefore regulate the structure of mangrove microbial communities (Ceccon *et al*., 2019). The high organic carbon content of mangrove sediments results from the deposition of mangrove litter, root exudates, and phytoplankton debris. In addition, mangrove sediments support the development of taxonomically and functionally diverse microbial communities (Zhu *et al*., 2018). Changes in the physicochemical properties of mangrove soils facilitated the modification of functional microbial groups (Yang *et al*., 2022). Mangroves are transitional coastal ecosystems between terrestrial and marine environments that have been contaminated in recent decades (Cabral *et al*., 2018) and whose microbial ecosystem functions may be impacted (Cotta *et al*., 2019). Therefore, such a coastal region's sediment properties and seawater qualities result from natural and anthropogenic inputs and interactions. Physical properties, hydrological conditions, organic matter, and pollutants inputs influence microbial communities' biogeography (Su *et al*., 2018). Mangrove ecosystems are highly susceptible to the bioaccumulation of heavy metals and frequently act as metal absorbers in

coastal areas. In order to survive in environments with a high metal content, the microbial population in mangrove sediments develops various mechanisms to combat metal toxicity (Puthusseri *et al*., 2021).

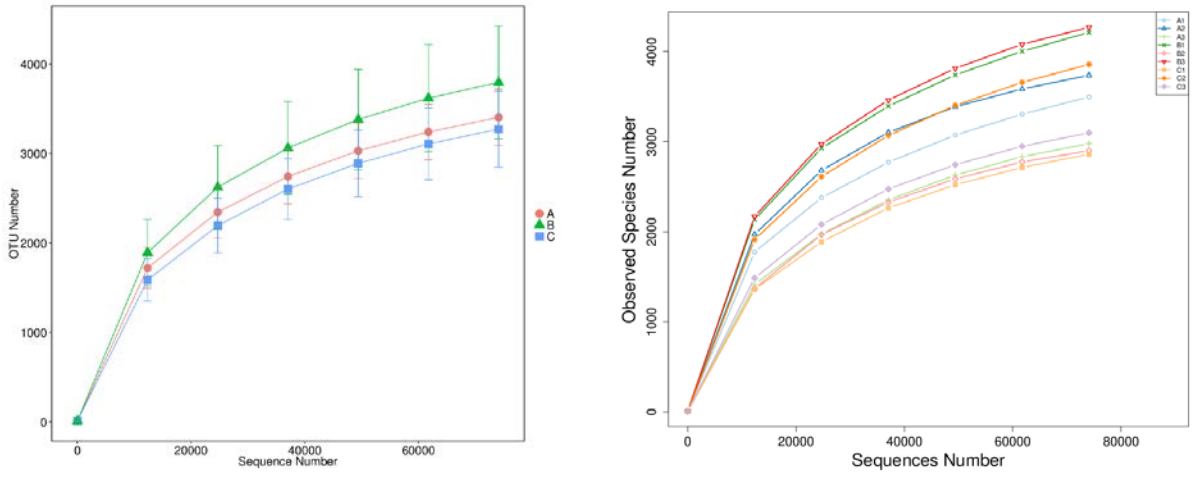

a b

Figure 3. Rarefaction curves showing the observed number of operational taxonomic units (OTUs) at 1% dissimilarity for discarded face masks.
a. The group samples of landfills A (round-redline), mangroves B (triangle-greenline), and beaches C (square-blueline).
b. A1 (Piyungan), A2 (Jatibarang), A3 (Burangkeng) landfill; B1 (Wanatirta), B2 (Tirang), B3 (Teluk Naga) mangrove; C1(Parangtritis), C2 (Marina), C3 (Tanjung Pasir) beach.

The beta diversity pattern of discarded face mask samples was depicted on a PCoA plot utilizing unweighted UniFrac based on Bray-Curtis distances. The PCoA plot reveals area-specific clustering of samples from regions A, B, and C. 38.07% (PCo1) and 19.43% (PCo2) of t he spatial variances of the bacterial community were explained by unweighted UniFrac distance (Figure 4). However, the three plots revealed dissimilarities in the structure of t he bacterial communities originating from discarded face masks (B). This difference was primarily caused by the dominance of Proteobacteria in B1 a nd Firmicutes, which were significantly more prevalent in B3 than in B2 m etagenomes. It was discovered that different bacterial communities were associated with different types of discarded face masks and collection locations. The effect of the face mask's surface on its colonization can be caused by hydrophobicity, degradability, electric charge, or roughness, or indirectly by the formation of a conditioning film on t op of t he particles. The bacterial communities are associated with the distinction between microplastics and natural particles, such as cellulose, particle-attached water fraction, and sediment (Oberbeckmann and Labrenz, 2020).

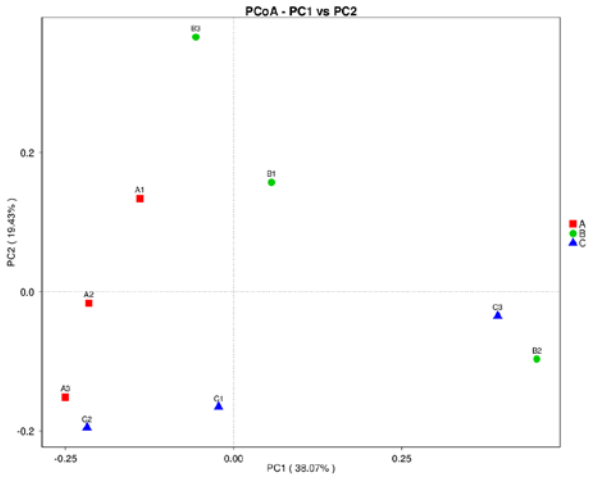

Figure 4. Beta diversity of the nine bacterial communities at studied landfills (A), mangroves (B), and C (beaches) sites. Principal coordinates analysis (PcoA) plots were constructed by applying the weighted Unifrac distance matrix on the CSS normalized OTU table data

Figure 5.a depicts Proteobacteria as the dominant phylum in all samples from landfills (33.32%), mangroves (52.22%), and beaches (53.63%). It suggests that Proteobacteria may be capable of de grading organic and inorganic materials in discarded face masks. The second dominant phylum in landfill samples was Actinobacteria (30.29%), followed by Firmicutes (17.25%). In contrast, the second dominant phylum in mangrove samples was Firmicutes (19.85%). In a ddition, the second dominant phylum in beach samples was Actinobacteria (12.62%), and the third was Cyanobacteria (11.52%). The natural environment influenced the presence of microorganisms in the face mask samples. According to previous studies, Proteobacteria is the dominant phylum in mangrove (Shah *et al*., 2022); tropical estuarine (Khandeparker *et al*., 2017); contaminated site (Kumar *et al*., 2020); and coastal waters (Li *et al*., 2021) environments. In a ddition, under various landfill conditions, Proteobacteria, Actinobacteria, and Firmicutes predominate because they can degrade complex substrates inaccessible to other microbial groups and grow with limited nutrients (Hu *et al*., 2022). Proteobacteria are the most diverse group du e to their versatile metabolism and ability to survive in various environments. They are crucial in nutrient cycling and maintenance due to their metabolic flexibility (Chakraborty *et al*., 2021). Firmicutes can constitute up to 90% of t he human gut microbiota (Quillaguamán *et al*., 2021), effectively indicating sewage contamination in mangroves. Proteobacteria and Firmicutes possess a diverse metabolic capacity for h ydrocarbon degradation. Proteobacteria and Firmicutes can tolerate and survive in a contaminated environment due to their high prevalence (Muccee and Ejaz, 2020). They were present in all samples from landfills, mangroves, and beaches, but phylum composition varied by location (Figure 5.b). It appears that environmental factors had a more significant impact on these microbial communities' structure than geographic variation (Abuzahrah *et al*., 2022). Continuous discharge of wastes can alter the physical and biological properties of the backwaters, which can have a growing impact on the ecosystem's fauna and flora (Balasubramanian *et al*., 2021). Nathan *et al*. (2020) found that bacterial communities in mangrove environments varied significantly based on t he composition and location of sediments, with each sampled mangrove ecosystem exhibiting unique environmental characteristics.

Figure 5.c depicts the diversity of bacteria at the genus level. Bacillus (5.96%), Nocardioides (3.00%), and Gardonia (2.91%) dominated the samples collected from landfills. Vibrio (19.41%), Weisella (5.49%), and Lactobacillus (3.8%) predominated in the mangrove samples. In c ontrast, Vibrio (8.34%), Coleofasciculus (5.22%), and Deinococcus (4.44%) dominated beach samples. There was also considerable variation in the occurrence (and persistence) of s ome of t he microbiome's most abundant members. For instance, Bacillus was the most prevalent group in the discarded face masks from landfills (Figure 5.d), but its prevalence varied greatly between landfills. It has been reported that Bacillus can be isolated from soil (Massadeh and Mahmoud, 2019), compost (Xie *et al*., 2021), and face masks (Delanghe *et al*., 2021). In this study, we observed that Vibrio dominated mangrove and beach samples. Nevertheless, the genus Vibrio is predominantly endemic to marine aquatic environments, ranging from the deep sea to shallow aquatic environments (Junaid *et al*., 2022); tolerant of heavy metals isolated from mangrove sediments (De Fretes *et al*., 2019), and sewage-associated plastic wastes (Metcalf *et al*., 2022).

Bacterial communities are hypothesized to have significant functional contributions to face mask degradation. The biodegradability of b acteria has been repeatedly demonstrated. However, the current research focused on di scovering new microorganisms that can degrade biodegradable and non-biodegradable face mask components. The contents of t he face mask inhibited the production of b acterial enzymes. The interaction between microplastics and dissolved organic pollutants in the environment depends on the physicochemical properties of the organic compounds. Bacillus was detected in the metagenome of discarded face masks from landfills, as determined by NGS analysis results about one of the most abundant genera in our s amples. Bacillus, which can bind heavy metals to the cell surfaces and provide bioremediation, was also responsible for degrading disposable face mask materials (Muzammil *et al*., 2021). Bacillus from various locations has been demonstrated to be an effective azo dye degrader (Guembri *et al*., 2021); plastic degrader *(Fibriarti et al*., 2021); and organometallic degrader (Tripathi *et al*., 2021). Figure 5.b illustrates the distribution of t he predominant bacterial genera in samples collected from various locations, including landfills, mangroves, and beaches. Briefly, the results demonstrated that the composition of bacterial communities differed across regions. It has been demonstrated that differences in face mask types and compositions, disposal period, and environmental factors (salinity, pH, temperature, dissolved organic carbon loading, etc.) influence bacterial community composition and dominance during degradation processes.

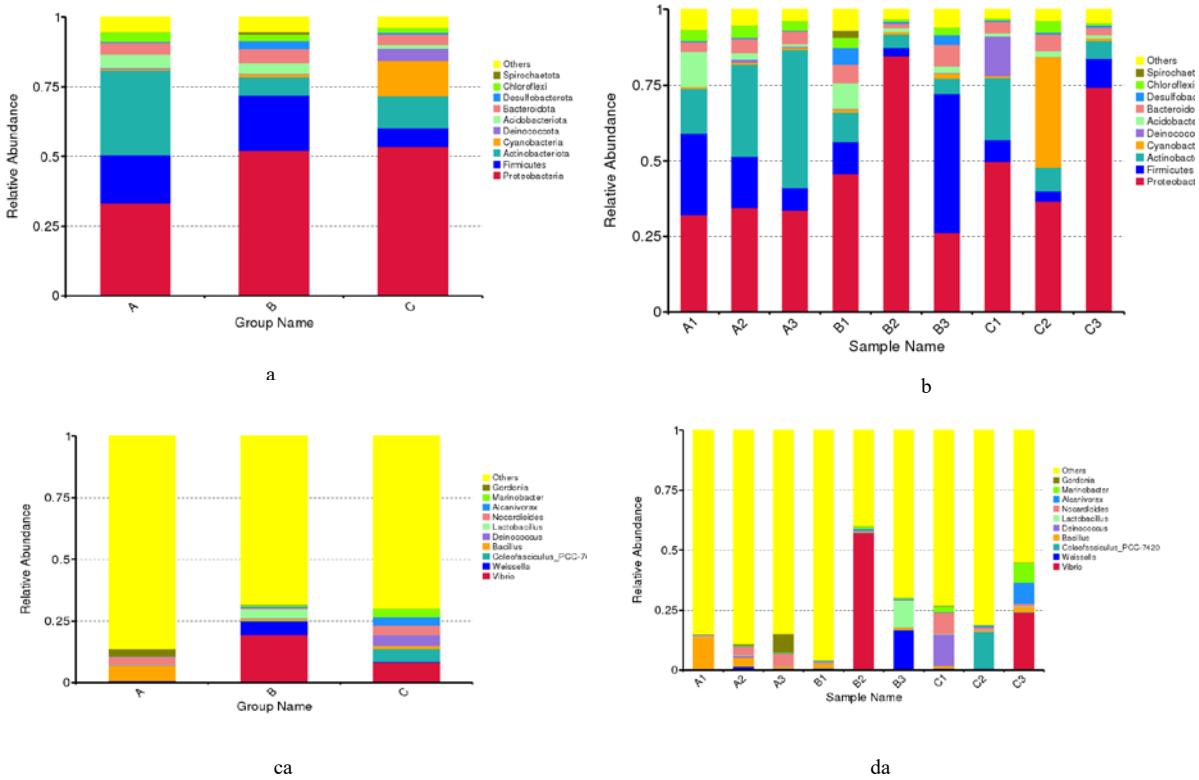

a b

ca da

Figure 5. The composition of bacterial communities at the phylum (a,b) and genus (c,d) level.

The same taxa were marked by the same color.

Based on the abundance data of the top 35 genera of all samples, a h eatmap was created to determine whether samples with similar processing were clustered or not and to observe the samples' similarities and differences (Figure 6). The bacterial communities on discarded face masks from landfills, mangroves, and beaches were distinct (Figure 6.a). Gemmatimonadota, Nitrospirota, and Eucaryarchaeota were only found in the Piyungan landfill sample, while Sumerlaota was only found in the Burangkeng landfill sample. Only the sample from Wanatirta Mangrove contained the phyla Crenarchaeota, Desulfobacterota, Methylomirabilota, Spirochaetota, Entotheonellaeota, Elusimicrobiota, and Verrucomicrobiota. In c ontrast, Campilobacterota, Halobacterota, and Latescibacterota were discovered in the Teluk Naga Mangrove sample. Only face masks from Parangtritis Beach, Marina Beach, and Tanjung Pasir Beach contained the phyla Deinoccocota, Cyanobacteria, and Thermoplasmatota.

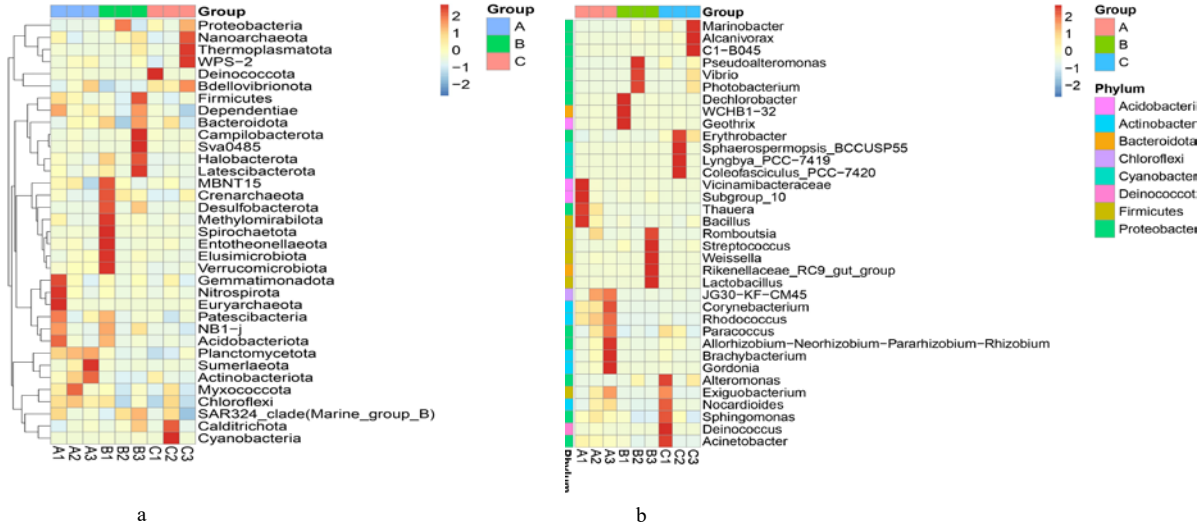

a b

Figure 6. Heatmap displaying the differences in the relative abundances of the top 35 a) phylum and b) genus.
The colors indicate the relative abundance of taxa, ranging from blue (low) to red (high).

In particular, Vicinamibacteraceae, Thauera, and Bacillus were found in the Piyungan landfill. Rhizobium, Brachybacterium, and Gordonia were found in the Burangkeng landfill sample (Figure 6.b). Regarding the activity of the bacterial community, the abundances of the six genera were relatively higher in landfills. The disposable face masks' utilization or degradation efficiency was an essential factor to consider. It showed that the microbiome in landfill can potentially degrade pollutants. Vicinamibacteraceae has the dominant genus in contaminated soils (Yi *et al*., 2022) and textile dye wastewater (Patel *et al*., 2021). Thauera is the predominant genus in leachate landfills (Saleem et al. 2018) and contaminated sediments (Y. Chen *et al*., 2018); therefore, it can be used as a bioremediation for heavy metals (Yin *et al*., 2019). Gordonia is commonly found in plastic (Adamovsky *et al*., 2021); therefore, it has the potential for polymer degradation and removal (Bhandari *et al*., 2021).

In this study, face masks found in mangroves may have been the source of the genera Dechlorobacter, Geothrix (Wanatirta mangrove); Pseudoalteromonas, Vibrio, Photobacterium (Tirang mangrove); and Rombutsia, Streptococcus, Weisella, Lactobacillus (Teluk naga mangrove), respectively (Figure 6.b). Since Dechlorobacter was discovered in waste-activated sludge in a previous study (Chen *et al*., 2021), this genus could be utilized as an organic biodegradation agent (Wang *et al*., 2020). Geothrix is prevalent in drinking water treatment residues (Wang *et al*., 2021), geothermal areas (Massello and Donati, 2021), wastewater treatment plants (Valk *et al*., 2022), and contaminated soil (Peixoto *et al*., 2022). Pseudoalteromonas can be isolated from mangroves (Alzubaidy *et al*., 2016) that can degrade hydrocarbon (Bhattacharjee *et al*., 2020). Streptococcus can be found in sediment mangroves (Chithira *et al*., 2021) that can degrade plastic *(Dang et al*., 2018), hydrocarbon (Sarkar *et al*., 2020), heavy metal biosorption (Priyadarshanee and Das, 2021), and azo dyes degradation (Slama *et al*., 2021). Weisella can be isolated from municipal solid waste (Jurado *et al*., 2020).

Considering the bacterial groups assigned at the genera level, we observed that marine bacteria dominated the predominant genera found on beach-discarded face masks. Alteromonas, Exiguobacterium, Nocardioides, Sphingomonas, Deinococcus, and Acinetobacter predominated on Parangtritis beach. However, Erythrobacter, Sphaerospermopsis, Lyngbya, and Coleofasciculus were present at Marina Beach. Figure 6.b accounts for the genera Marinobacter and Alcanivorax on Tanjung Pasir beach. Xia *et al*., (2021) demonstrated unequivocally that Alteromonas can be isolated from coastal and ocean environments. Halophilic Exiguobacterium can be isolated from arsenic-rich thermal springs and estuarine sediments (Prieto-Barajas *et al*., 2018; Cui *et al*., 2021). Sphingomonas can be isolated from marine and mangrove sediments (Al Farraj *et al*., 2021; Guo *et al*., 2011). Known as freshwater bacteria (Medeiros *et al*., 2016), Deinococcus can be isolated from lakes (Chakraborty *et al*., 2021) and antarctic soils (Ramírez-Fernández *et al*., 2021). Acinetobacter dominates in polar habitats (Ali *et al*., 2020) and urban lakes (Quillaguamán *et al*., 2021). Erythrobacter can be isolated from a marine containing microplastic (Oberbeckmann and Labrenz, 2020) has saline stress tolerance (Benidire *et al*., 2020) and can be utilized as a hydrocarbon-related pollutant degrader in oceanic and coastal environments (Ramírez *et al*., 2020). Lyngbya, also called benthic marine cyanobacteria (Narayana *et al*., 2020), can be isolated from the estuarine mangrove ecosystem (Sengupta *et al*., 2020). In addition, Marinobacter has been identified in lake ecosystems (Moopantakath *et al*., 2020), the South Atlantic Ocean (Coutinho *et al*., 2021), plastisphere bacteria (Sumithra *et al*., 2020), and hydrocarbon-degradering organisms (Hidalgo *et al*., 2021). An increased abundance of Alcanivorax sequences in oil-contaminated sand (Panigrahi *et al*., 2018) forms biofilms in marine environments. It possesses the genomic capability to degrade multiple oil-derived hydrocarbons (Roager and Sonnenschein, 2019).

A cluster tree was constructed using clustering analysis to examine similarities between various samples. Using the weighted UniFrac, the differences in microbial communities based on the occurrence and abundance of OTUs were observed. At the phylum and OTU levels, eight areas except C2 clustered together (Figure 7.a), revealing a significantly more significant distinction. In the meantime, the unweighted UniFrac calculations identified inter-community variables by determining the occurrence of OTUs. In addition, Figure 7.b demonstrates that although the samples were collected from distinct locations, they contained similar bacterial communities. To further investigate the phylogenetic relationship between the genera, the top 100 genera were chosen, and an evolutionary tree was constructed from the aligned sequences of representative species. Figure 7.c also displays the relative abundance of each genus and its genus.

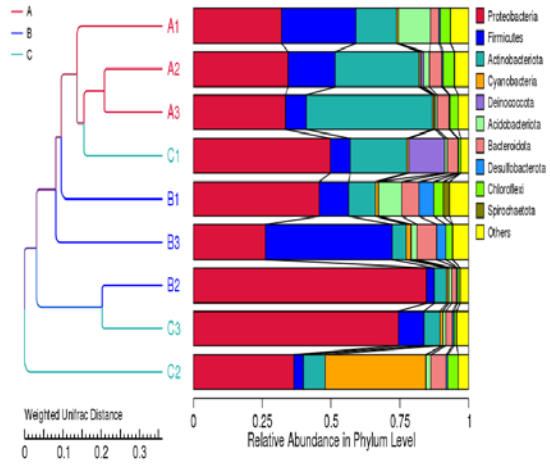

a

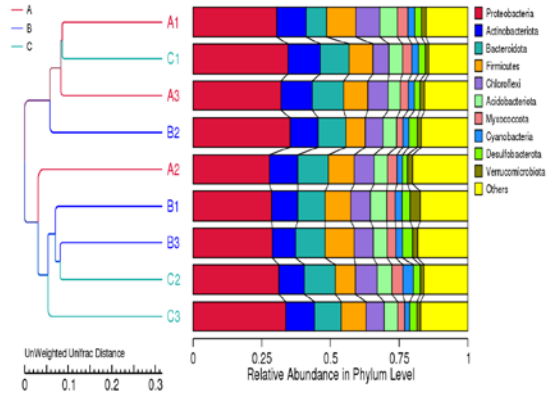

b

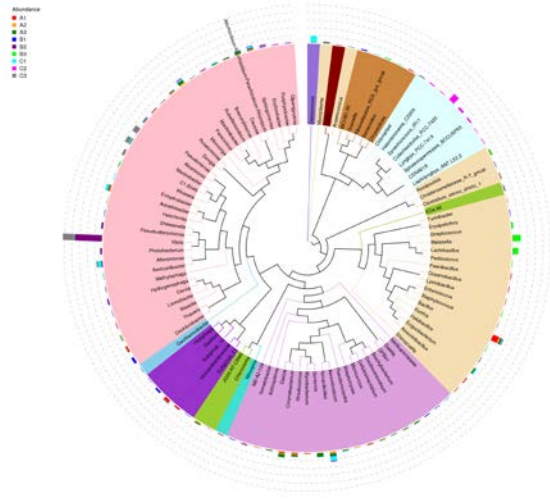

c

Figure 7. Hierarchical clustering of microbiomes from different sampling points locations. Distance matrices were created with (a) weighted and (b) unweighted UniFrac calculations. (c)16S rRNA gene-based phylogeny showing representatives of all microbial genera in discarded face masks.

In conclusion, 16S rRNA gene sequencing was used to investigate the microbial communities inhabiting discarded face masks from landfills, mangroves, and beaches on Java Island, Indonesia. The current study reported detailed investigation results regarding bacterial communities' abundance, composition, and diversity at various locations. The bacterial community composition of di scarded face masks was dynamic and susceptible to many environmental factors. This study was an essential step toward elucidating the bacterial community's potential role in modulating face mask degradation. Therefore, future research will concentrate on identifying new bacterial taxa involved in the degradation of face masks, thereby advancing the current research on this topic.

Acknowledgements

This research was supported by a Research Grant from the Ministry of Education, Culture, Research, and Technology of the Republic of Indonesia with contract number T/15.1.3 /UN34.21/PT.01.03/2022. In completing this work, the authors gratefully acknowledge Universitas Negeri Yogyakarta.

References

Abuzahrah SS, Baeshen MN, Alkaladi A, Bataweel NM, Alhejen AM, Abdelkader H. 2022. Exploring the Taxonomic and Functional Diversity of Marine Benthic Micro-Eukaryotes Along the Red Sea C oast of Jeddah City. *Saudi J. Biol. Sci*. **29(8)**: 103342.

Adamovsky O, Bisesi Jr JH, Martyniuk CJ. 2021. Plastics in Our Water: Fish Microbiomes at R isk?" *Comparative Biochem. Physiol. - Part D: Genom. Proteom*. **39**: 100834.

Al Farraj DA, Alkufeidy RM, Alkubaisi NA, Alshammari MK. 2021. Polynuclear Aromatic Anthracene Biodegradation by Psychrophilic *Sphingomonas* Sp., Cultivated with Tween-80.*Chemosphere*. **263**: 128115.

Ali B, Sajjad W, Ghimire PS, Khan S, Din G, Kang S. 2021. Culture Independent Diversity of Bacterial Communities Indigenous to Lower Altitude at L aohugou Glacial Environment.*Geomicrobiol. J*. **38(1)**: 1–13.

Alzubaidy H, Essack M, Malas TB, Bokhari A, Motwalli O, Kamanu FK, Jamhor SA, Mokhtar NA, Antunes A, Simões MF, Alam I, Bougouffa S, Lafi FF, Bajic VB, Archer JAC.. 2016. Rhizosphere Microbiome Metagenomics of Gray Mangroves (*Avicennia marina*) in the Red Sea. *Gene*. **576(2)**: 626–636.

Aragaw TA. 2020. Surgical Face Masks as a Potential Source for Microplastic Pollution in the COVID-19 Scenario *Mar. Pollut. Bull*. **159**: 111517.

Babaahmadi V, Amid H, Naeimirad M, Ramakrishna S. 2021. Biodegradable and Multifunctional Surgical Face Masks: A Brief Review on Demands during COVID-19 Pandemic, Recent Developments, and Future Perspectives. *Sci.Total Environ*. **798**: 149233.

Balasubramanian VK, Maran MIJ, Ramteke D, Vijaykumar DS, Rajendran AK, Ramachandran P, Ramachandran R. 2021. Environmental DNA Reveals Aquatic Biodiversity of an Urban Backwater Area, Southeast Coast of India. *Mar. Pollut. Bull*. **171**: 112786.

Benidire L, El Khalloufi F, Oufdou K, Barakat M, TulumelloJ, Ortet P, Heulin T, Achouak W. 2020. Phytobeneficial Bacteria Improve Saline Stress Tolerance in Vicia Faba and Modulate Microbial Interaction Network. *Sci. Total Environ*. **729:** 139020.

Bhandari S, Poudel DK, Marahatha R, Dawadi S, Khadayat K, Phuyal S, Shrestha S, Gaire S, Basnet K, Khadka U, Parajuli N. 2021. Microbial Enzymes Used in Bioremediation. *J. Chem.* 8849512: 1-17

Bhattacharjee G, Gohil N, Vaidh S, Joshi K, Vishwakarma GS, Singh V. 2020. Microbial Bioremediation of Industrial Effluents and Pesticides. **Bioremediation of Pollutants**. Elsevier Inc, New York, pp. 287-302.

Bokulich NA, Subramanian S, Faith JJ, Gevers D, Gordon JI, Knight R, Mills DA Caporaso JG. 2013. Quality-Filtering Vastly Improves Diversity Estimates from Illumina Amplicon Sequencing. *Nat Methods.* **10(11)**: 57–59.

Cabral L, de Sousaa STP, Lacerda Júniora GV, Hawley E, Andreo FD, Hess M, de Oliveira VM 2018. Microbial Functional Responses to Long-Term Anthropogenic Impact in Mangrove Soils. *Ecotoxicol. Environmen. Saf.* **160**: 231–239.

Ceccon DM, Faoro H, Lana PC, Maltempi de Souza E, Pedrosa FO 2019. Metataxonomic and Metagenomic Analysis of Mangrove Microbiomes Reveals Community Patterns Driven by Salinity and pH Gradients in Paranaguá Bay, Brazil. *Sci. Total Environ*. **694**: 133609.

Chakraborty J, Rajput V, Sapkale V, Kamble S, Dharne M. 2021. Spatio-Temporal Resolution of Taxonomic and Functional Microbiome of Lonar Soda Lake of India Reveals Metabolic Potential for Bioremediation. *Chemosphere*. **264**: 128574.

Chen S, Dai X, Yang D, Dong B. 2021. Effects of Sludge Age on Anaerobic Acidification of Waste Activated Sludge: Volatile Fatty Acids Production and Phosphorus Release. *J. Environ. Sci.* **105**: 11–21.

Chen Y, Jiang Y, HuangH, Mou L, Ru J, Zhao J, Xiao S2018. Long-Term and High-Concentration Heavy-Metal Contamination Strongly Influences the Microbiome and Functional Genes in Yellow River Sediments. *Sc. Total Environ.* **637–638**: 1400–1412.

Chowdhury H, Chowdhury T, a Sait SM. 2021. Estimating Marine Plastic Pollution from COVID-19 Face Masks in Coastal Regions. *Mar. Pollut. Bull*. **168**: 112419 .

Chun SJ, Kim YJ, Cui Y, Nam KH. 2021. Ecological Network Analysis Reveals Distinctive Microbial Modules Associated with Heavy Metal Contamination of Abandoned Mine Soils in Korea. *Environ. Pollut.* **289**: 117851.

Cordova MR,Nurhati IS, Riani E, Nurhasanah, Iswari MY. 2021. Unprecedented Plastic-Made Personal Protective Equipment (PPE) Debris in River Outlets into Jakarta Bay during COVID-19 Pandemic. *Chemosphere*. **268**: 129360.

Cotta SR,Cadete LL, van Elsas JD, Andreotea FD, Dias ACF. 2019. Exploring Bacterial Functionality in Mangrove Sediments and Its Capability to Overcome Anthropogenic Activity. *Mar. Pollut. Bull*. **141**: 586–594.

Coutinho FH, von Meijenfeldt FAB, Walter JM, Haro-Moreno JM, Lopéz-Pérez M, van Verk MC, Thompson CC, Cosenza CAN, Appolinario L, Paranhos R, Cabral A, Dutilh BE, Thompson FL2021. Ecogenomics and Metabolic Potential of the South Atlantic Ocean Microbiome. *Sci. Total Environ*. **765**: 142758.

Cui Y, C ui YW, Huang JL. 2021. A No vel Halophilic Exiguobacterium Mexicanum Strain Removes Nitrogen from Saline Wastewater via Heterotrophic Nitrification and Aerobic Denitrification. *Bioresour. Technol.* **333**: 125189.

Dang TCH, Nguyen DT, Thai H, Nguyen TC, Tran TTH, Le VH, Nguyen VH, Tran XB, Pham TPT, Nguyen TG, Nguyen QT. 2018. Plastic Degradation by Thermophilic *Bacillus* sp. BCBT21 Isolated from Composting Agricultural Residual in Vietnam. *Adv. Nat. Sci.: Nanosci. Nanotechnol.* **9**: 1-11.

De Fretes CE, Sutiknowati LI, Falahudin D. 2019. Isolasi Dan Identifikasi Bakteri Toleran Logam Berat Dari Sedimen Mangrove di Pengudang dan Tanjung Uban, Pulau Bintan, Indonesia. *Oseanologi dan Limnologi di Indonesia*. **4(2)**: 71-77.

Delanghe, L, Cauwenberghs E,Spacova I, De Boeck I, Van Beeck W, Pepermans K, Claes I,Vandenheuvel D, Verhoeven V,Lebeer S. 2021. Cotton and Surgical Face Masks in Community Settings: Bacterial Contamination and Face Mask Hygiene. *Front. Med*. **8**: 732047.

Edgar RC,Haas BJ, Clemente JC, Quince C, Knight C. 2011. UCHIME Improves Sensitivity and Speed of Chimera Detection. *Bioinform.* **27(16)**: 2194–2200.

Fibriarti BL, Feliatra, Amin B, Darwis. 2021. Biodegradation of Ldpe Plastic by Local Strain of *Bacillus* Sp. Isolated from Dump Soil of Pekanbaru, Indonesia. *Biodiversitas.* **22(12)**: 5484–5490.

Guembri M, Neifar M, Saidi M, Ferjani R, Chouchane H, Mosbah A, Cherif A, Saidi N, IOuzari HI. 2021. Decolorization of Textile Azo Dye Novacron Red Using Bacterial Monoculture and Consortium: Response Surface Methodology Optimization. *Water Environ. Res*. **93(8)**: 1346–1360.

Gunasekaran K, Mghili B, Saravanakumar A. 2022. Personal Protective Equipment (PPE) Pollution Driven by the COVID-19 Pandemic in Coastal Environment, Southeast Coast of India. *Mar. Pollut. Bull.* **180**: 113769.

Guo C, Ke L, Dang Z, Tam NF. 2011. Temporal Changes in Sphingomonas and Mycobacterium Populations in Mangrove Sediments Contaminated with Different Concentrations of Polycyclic Aromatic Hydrocarbons (PAHs). *Mar. Pollut. Bull.* **62(1)**: 133–139.

Hasan NA, Heal RD, Bashar A, Haque MM. 2021. Face Masks: Protecting the Wearer but Neglecting the Aquatic Environment? - A Perspective from Bangladesh. *Environ. Chall*. **4**: 100126.

Hidalgo KJ, Sierra-Garcia IN, Zafra G, de Oliveira VM. 2021. Genome-Resolved Meta-Analysis of the Microbiome in Oil Reservoirs Worldwide. *Microorganisms*. **9**: 1812.

Hu L, Zhang D, Qian Y, Nie Z, Long Y, Shen D, Fang C, Yao J.2022. Microbes Drive Changes in Arsenic Species Distribution during the Landfill Process. *Environ. Pollut*. **292**: 118322.

Junaid M, Liu X, Wu Y, Wang J. 2022. "Selective Enrichment of Antibiotic Resistome and Bacterial Pathogens by Aquatic Microplastics. *J. Hazard. Mater*. **7**: 100106.

Jurado MM, Camelo-Castillo AJ, Suárez-Estrella F, López MJ, López-González JA, Estrella-González MJ, Síles-Castellano AB, Joaquín M2020. Integral Approach Using Bacterial Microbiome to Stabilize Municipal Solid Waste. *J. Environ. Manage*. **265**: 110528.

Khandeparker L, Kuchi N, Kale D, Anil AC. 2017. Microbial Community Structure of Surface Sediments from a Tropical Estuarine Environment Using Next Generation Sequencing. *Ecol. Indic*. **74**: 172–181.

Khati P, Sharma A, Chaudhary P, Singh AK, Gangola S, Kumar R2019. High-Throughput Sequencing Approach to Access the Impact of Nanozeolite Treatment on Species Richness and Evenness of Soil Metagenome. *Biocatal. Agric. Biotechnol.* **20**: 101249.

Kuczynski J, Stombaugh J, Walters WA, González A, Caporaso JG, Knight R. 2011. Using QIIME to Analyze 16S Rrna Gene Sequences from Microbial Communities. *Curr. Protoc. Bioinformatics* (SUPPL.36): 1–28.

Kumar V, Thakur IS, Singh AK, Shah MP. 2020. Application of Metagenomics in Remediation of Contaminated Sites and Environmental Restoration. **Emerging Technologies in Environmental Bioremediation**. Elsevier Inc, New York, pp.197-232.

Li S, Yang B, Tan G, Ouyang L, Qiu S, Wang W, Xiang W, Zhang L.2021. Polyketide Pesticides from Actinomycetes. *Curr. Opin. Biotechnol.* **69**: 299–307..

Lin L,Yuan B, Hong H, Li H, He L, Lu H, Liu J, Yan C. 2022. Post COVID-19 Pandemic: Disposable Face Masks as a Potential Vector of Antibiotics in Freshwater and Seawater. *Sci. Total Environ.* **820**: 153049.

Liu Z, Wang J, Yang X, Huang Q, Zhu K, Sun Y, Hulle SV, Jia H. 2022. Generation of Environmental Persistent Free Radicals (EPFRs) Enhances Ecotoxicological Effects of the Disposable Face Mask Waste with the COVID-19 Pandemic. *Environ. Pollut.* **301**: 119019.

Magoč T, Salzberg SL. 2011. FLASH: Fast Length Adjustment of Short Reads to Improve Genome Assemblies. *Bioinformatics*. **27(21)**: 2957–2963.

Maroof L, Khan I, Yoo HS, Kim S, Park H, Ahmad B, Azam S. 2021. Identification and Characterization of Low Density Polyethylenedegrading Bacteria Isolated from Soils of Waste Disposal Sites. *Environ. Eng. Res.* **26(3)**: 200167.

Massadeh MI, Mahmoud SM. 2019. Antibacterial Activities of Soil Bacteria Isolated from Hashemite University Area in Jordan. *Jordan J. Biol. Sci.* **12(4)**: 503–511.

Massello FL, Donati E. 2021. Effect of Heavy Metal-Induced Stress on Two Extremophilic Microbial Communities from Caviahue-Copahue, Argentina. *Environ. Pollut.* **268**: 115709.

Medeiros JD ,Cantão ME, Cesar DE, Nicolás MF, Diniz CG, Silva VL, de Vasconcelos ATR, Coelho CM.2016. Comparative Metagenome of a Stream Impacted by the Urbanization Phenomenon. *Braz. J. Microbiol.* **47(4)**: 835–845.

Metcalf R, White HL, Moresco V, Ormsby MJ, Oliver DM, Quilliam RS. 2022. Sewage-Associated Plastic Waste Washed up on Beaches Can Act as a Reservoir for Faecal Bacteria, Potential Human Pathogens, and Genes for Antimicrobial Resistance. *Mar. Pollut. Bull.* **180**: 113766.

Moopantakath J, Imchen M, Siddhardha B, Kumavath R. 2020. 16S rRNA Metagenomic Analysis Reveals Predominance of Crtl and CruF Genes in Arabian Sea Coast of India. *Sci. Total Environ.* **743**: 140699..

Muccee F, Ejaz S. 2020. Whole Genome Shotgun Sequencing of POPs Degrading Bacterial Community Dwelling Tannery Effluents and Petrol Contaminated Soil. *Microbiol. Res.* **238**: 126504.

Muzammil, S. Siddiqueb MH, Mureed F, Andleeb R, Jabeen F, Waseem M, Zafar S, Rehman HF, Alic T, Ashraf A. 2021. Assessment of Cadmium Tolerance and Biosorptive Potential of *Bacillus cereus* GCFSD01 Isolated from Cadmium Contaminated Soil. *Braz. J. Biol.* **81(2)**: 398–405.

Narayana S, Tapase S, Thamke V, Kodam K, Mohanraju R. 2020. Primary Screening for the Toxicity of Marine Cyanobacteria *Lyngbya bouillonii* (Cyanophyceae: Oscillatoriales) Recorded for the First Time from Indian Ocean. *Reg. Stud. Mar. Sci.* **40**: 101510.

Nathan VK, Vijayan J, Ammini P. 2020. Comparison of Bacterial Diversity from Two Mangrove Ecosystems from India through Metagenomic Sequencing: Comparative Mangrove Bacterial Diversity Using Metagenomics. *Reg. Stud. Mar. Sci.* **35**: 101184..

Nghiem LD, Iqbal HFM, Zdarta J. 2021. The Shadow Pandemic of Single Use Personal Protective Equipment Plastic Waste: A Blue Print for Suppression and Eradication. *Case Stud. Chem. Environ. Eng.* **4**: 100125..

Oberbeckmann S, Labrenz M. 2020. Marine Microbial Assemblages on Microplastics: Diversity, Adaptation, and Role in Degradation. *Annu. Rev. Mar. Sci.* **12**: 209–232.

Oliveira J, Belchior A, da Silva VD, Rotter A, Petrovski Ž, Almeida PL, Lourenço ND, Gaudêncio SP 2020. Marine Environmental Plastic Pollution: Mitigation by Microorganism Degradation and Recycling Valorization.*Front. Mar. Sci.* **7**: 567126

Panigrahi S, Velraj P, Rao TS. 2018. Functional Microbial Diversity in Contaminated Environment and Application in Bioremediation. **Microbial Diversity in the Genomic Era**. Elsevier Inc, New York, pp. 359-385.

Patel D, Bapodra SL, Madamwar D, Desai C. 2021. Electroactive Bacterial Community Augmentation Enhances the Performance of a Pilot Scale Constructed Wetland Microbial Fuel Cell for Treatment of Textile Dye Wastewater. *Bioresour. Technol.* **332**: 125088..

Patrício Silva AL, Prata JC, Mouneyrac C, Barcelò D, Duarte AC, Rocha-Santos T. 2021. Risks of Covid-19 Face Masks to Wildlife: Present and Future Research Needs. *Sci. Total Environ.* **792**: 148505..

Peixoto S, Loureiro S, Henriques I. 2022. The Impact of Silver Sulfide Nanoparticles and Silver Ions in Soil Microbiome. *J. Hazard. Mater.* **422**: 126793.

Pereira de Albuquerque F, Dhadwal M, Dastyar W, Azizi SMM, Karidio I, Zaman H, Dhar BR.. 2021. Fate of Disposable Face Masks in High-Solids Anaerobic Digestion: Experimental Observations and Review of Potential Environmental Implications. *Case Stud. Chem. Environ. Eng.* **3**: 100082.

Prata JC, Silva ALP, Walker TR, Duarte AC, Santos TR. 2020. COVID-19 Pandemic Repercussions on the Use and Management of Plastics. *Environ. Sci. Technol.* **54(13)**: 7760–7765.

Prieto-Barajas CM, Valencia-Cantero E, Santoyo G. 2018. Microbial Mat Ecosystems: Structure Types, Functional Diversity, and Biotechnological Application. *Electro. J. Biotechnol.* **31**: 48–56.

Priyadarshanee M, Das S. 2021. Biosorption and Removal of Toxic Heavy Metals by Metal Tolerating Bacteria for Bioremediation of Metal Contamination: A Comprehensive Review. *J. Environ. Chem. Eng.* **9(1)**: 104686.

Puthusseri RM, Nair HP, Johny TK, Bhat SG. 2021. Insights into the Response of Mangrove Sediment Microbiomes to Heavy Metal Pollution: Ecological Risk Assessment and Metagenomics Perspectives. *J. Environ. Manage.* **298**: 113492.

Quillaguamán J, Guzman D, Campero M, Hoepfner C, Relos L, Mendieta D, Higdon SM, Eid D, Fernandez CE. 2021. The Microbiome of a Polluted Urban Lake Harbors Pathogens with Diverse Antimicrobial Resistance and Virulence Genes. *Environ. Pollut.* **273**: 116488.

Ramírez-Fernández L, Orellana LH, Johnston ER, Konstantinidis KT, Orlando J. 2021. Diversity of Microbial Communities and Genes Involved in Nitrous Oxide Emissions in Antarctic Soils Impacted by Marine Animals as Revealed by Metagenomics and 100 Metagenome-Assembled Genomes. *Sci. Total Environ.* **788**: 147693.

Ramírez D, Vega-Alvarado L, Taboada B, Estradas-Romeroc A, Soto L, Juárez K.. 2020. Bacterial Diversity in Surface Sediments from the Continental Shelf and Slope of the North West Gulf of Mexico and the Presence of Hydrocarbon Degrading Bacteria. *Mar. Pollut. Bull.* **150**: 110590.

Roager L, Sonnenschein EC. 2019. Bacterial Candidates for Colonization and Degradation of Marine Plastic Debris. *Environ. Sci. Technol.* **53(20)**: 11636–11643.

Saleem M, Lavagnolo MC, Campanaro S, Squartini A. 2018. Dynamic Membrane Bioreactor (DMBR) for the Treatment of Landfill Leachate; Bioreactor's Performance and Metagenomic Insights into Microbial Community Evolution. *Environ. Pollut.* **243**: 326–335..

Sarkar J, Roy A, Sar P, Kazy SK. 2020. Accelerated Bioremediation of Petroleum Refinery Sludge through Biostimulation and Bioaugmentation of Native Microbiome. **Emerging Technologies in Environmental Bioremediation.** Elsevier Inc, New York, pp.

Sengupta S, Pramanik A, Nag S, Roy D, Bhattacharyya A, Basak P, Bhattacharyya M. 2020. Microbial Diversity and Related Secondary Metabolite Gene Assortment at an Estuarine Mangrove Ecosystem. *Reg. Stud. Mar. Sci.* **34**: 101051..

Sessa J, Syed D, Zainab A, Al-Ghushami AH, Ahmed M. 2022. Towards Heat Tolerant Metagenome Functional Prediction, Coral Microbial Community Composition, and Enrichment Analysis. *Ecol. Inform.* **69**: 101635.

Shah R, Stephenson S, Crosswell J, Gorman D, Hillyer KE, Palombo EA, Jones OAH, Cook S, Bodrossy L, van de Kamph J, Walsh TK, Bissett A, Steven ADL, Beale DJ.2022. Omics-Based Ecosurveillance Uncovers the Influence of Estuarine Macrophytes on Sediment Microbial Function and Metabolic Redundancy in a Tropical Ecosystem. *Sci. Total Environ.* **809**: 151175.

Slama HB, Bouket CA, Pourhassan Z, Alenezi FN, Silini A, Cherif-Silini H, Oszako T; Luptakova L, Goli ´nska P, Belbahri, L. D . 2021. Diversity of Synthetic Dyes from Textile Industries, Discharge Impacts and Treatment Methods. *Appl. Sci.* **11(14)**: 1–21.

Spennemann DHR. 2022. COVID-19 Face Masks as a Long-Term Source of Microplastics in Recycled Urban Green Waste. *Sustainability*. **14:** 207.

Su Z, Daia T, Tanga Y, Taoa Y, Huang B, Mu Q, Wen D. 2018. Sediment Bacterial Community Structures and Their Predicted Functions Implied the Impacts from Natural Processes and Anthropogenic Activities in Coastal Area. *Mar. Pollut. Bull.* **131**: 481–495.

Sumithra TG, Reshma KJ, S ony M. 2020. Research on ' Plastisphere ' in Environmental Health Perspectives-A Narrative Review. *J. One Health*. **08(03)**: 70–77.

Takahashi S, Tomita J, Nishioka K, Hisada T, Nishijima M. 2014. Development of a Prokaryotic Universal Primer for Simultaneous Analysis of Bacteria and Archaea Using Next-Generation Sequencing. *PLoS ONE.* **9(8)**: e105592

Takarina ND, Sukma AM, Adiwibowo A, Sitaresmi. 2022. Water Quality and Microbial Community Assessment in Artisanal Mining- Affected Sediments of Cikidang River, Banten, Java, Indonesia. *Sains Malays.* **51(5)**: 1339–1352.

Tripathi S, Sharma P, Purchase D, Tiwari M, Chakrabarty D, Chandra R. 2021. Biodegradation of Organo-Metallic Pollutants in Distillery Wastewater Employing a Bioaugmentation Process. *Environ. Technol. Innov.* **23**: 101774.

Valk LC, Peces M, Singleton CM, Laursen MD, Andersen MH, Mielczarek AT, Nielsen PH 2022. Exploring the Microbial Influence on Seasonal Nitrous Oxide Concentration in a Full-Scale Wastewater Treatment Plant Using Metagenome Assembled Genomes. *Water Res.* **219**: 118563.

Wang C, Tian L, Wang Z, Li B, Yan Z, Bai L, Xu H, Jiang H, Yuan N 2021. Drinking Water Treatment Residue Structures Nitrogen-Cycling Microbiomes with Consequences for High Nitrogen Conversion. *J. Clean. Prod.* **320**: 128840.

Wang H, Feng C, Deng Y. 2020. Effect of Potassium on Nitrate Removal from Groundwater in Agricultural Waste-Based Heterotrophic Denitrification System. *Sci. Total Environ.* **703**: 134830.

Xia X, Zheng Q, Leung SK, Wang Y, Lee PY, Jing H, Jiao N, Liu H. 2021. Distinct Metabolic Strategies of the Dominant Heterotrophic Bacterial Groups Associated with Marine Synechococcus. *Sci. Total Environ.* **798**: 149208.

Xie G, Kong X, Kang J, Su N, Luo G, Fei J. 2021. Community-Level Dormancy Potential Regulates Bacterial Beta-Diversity Succession during the Co-Composting of Manure and Crop Residues. *Sci. Total Environ.* **772**: 145506.

Yang Z, Peng C, Cao H, Song J, Gong B, Li L, Wang L, He Y, Liang M, Lin J, Lu L 2022. Microbial Functional Assemblages Predicted by the FAPROTAX Analysis Are Impacted by Physicochemical Properties, but C, N and S Cycling Genes Are Not in Mangrove Soil in the Beibu Gulf, China. *Ecol. Indic.* **139**: 108887.

Yi M, Zhang L, Qin C, Lu P, Bai H, Han X, Yuan S 2022. Temporal Changes of Microbial Community Structure and Nitrogen Cycling Processes during the Aerobic Degradation of Phenanthrene. *Chemosphere.* **286**: 131709.

Yin K, Wang Q, Lv M, Chen L. 2019. Microorganism Remediation Strategies towards Heavy Metals. *Chem. Eng. J.* **360**: 1553-1563.

Zainun MY, Simarani K. 2018. Metagenomics Profiling for Assessing Microbial Diversity in Both Active and Closed Landfills. *Sci. Total Environ.* **616–617**: 269–278.

Zhang X, Wang P, Ma L, Guo R, Zhang Y, Wang P, Zhao J, Liu J. 2021. Differences in the Oral and Intestinal Microbiotas in Pregnant Women Varying in Periodontitis and Gestational Diabetes Mellitus Conditions. *J. Oral Microbiol.* **13(1)**: 1–11..

Zhu P, Wang Y, Shi T, Zhang X, Huang G, Gong J. 2018. Intertidal Zonation Affects Diversity and Functional Potentials of Bacteria in Surface Sediments: A Case Study of the Golden Bay Mangrove, China. *Appl. Soil Eco.* **130**: 159–168.

JJBS

Volume 17, Number 1,March 2024
ISSN 1995-6673
Pages 185 – 196
https://doi.org/10.54319/jjbs/170118

Jordan Journal of Biological Sciences

Preparation of Bioactive Oligosaccharides from Mallow Residues by Enzymes Mixture of Isolated *Aspergillus flavus* B2 and Evaluation of their Biological Activities

Shireen A.A. Saleh[1], Samia A. Ahmed[1,*] , Faten A. Mostafa[1], Asmaa A. Abd El-Galil[1], Hanan A.A. Taie[2], Walaa A. Abdel Wahab[2]

[1]*Chemistry of Natural and Microbial Products Department National Research Centre, Dokki, Cairo, Egypt ;* [2]*Plant Biochemistry Department, National Research Centre, Dokki, Cairo, Egypt*

Received: June 8, 2023; Revised: August 26, 2023; Accepted: September 12, 2023

Abstract

The preparation of biologically active oligosaccharides from the stem residues of the mallow plant (*Corchorus olitorius*) was evaluated by the enzymatic hydrolysis method. The isolated strain *Aspergillus flavus* B2 (accession number OL655454) was selected as a potential producer of the enzymes mixture. The factors affecting the hydrolysis of Mallow stems (MS) by enzyme mixture were tested using Plackett-Burman and Central Composite statistical designs. Different production conditions yielded 13 bioactive oligosaccharides (MSOS) that differed in their yield, components, monosaccharides constitution, percentage, and degree of polymerization. The optimized conditions yielded 525 milligrams of oligosaccharide per gram of dry MS using enzymes- mixture containing cellulase 4.9 U/mL, xylanase 6.8 U/mL, and pectinase 12.9 U/mL. Oligosaccharide no. 4 showed higher fibrinolytic activity than Hemoclar. All tested oligosaccharides (1 %) improved the growth of both the probiotics *Bifidobacterium lactis* and *Lactobacillus plantarum*. The antioxidant activity of the produced oligosaccharides varies depending on their characteristics and method of evaluation. Of all the samples tested, MSOS no. 11 showed the highest level of DPPH, reducing power, ABTS, and FRAP activity. Moreover, the highest reduction in tumor cell viability and the inhibited ascites were obtained by MSOS no. 11 (37.24±0.31 %).

Keywords: *A. flavus* B2, bioactivities, Jew's Mallow, enzymes-mixture, oligosaccharides, statistical method

1. Introduction

Oxidative stress caused by free radicals is one of the factors in tumor development and pathogenesis of many human diseases (Rivas *et al*., 2021). Antioxidants can act as cancer chemo-preventives substances to protect cells from oxidative stress (Xiong *et al*., 2021). Chemotherapy drugs still have significant toxicity and critical side effects on healthy cells. This pushes us to demand new treatments for this insidious disease such as natural anticancer substances (Grigalius and Petrikaite, 2017). Natural anticancer drugs are low cost, have several mechanisms of action, and are often active toward cancer cells. Recently, there is a growing demand for functional foods that have health benefits. Prebiotics as functional food components are known as selectively, non-digestible fermented components. This allows certain changes in the activity and/or composition of the intestinal flora resulting in the host's well-being and good health (Desai *et al*., 2020). Prebiotics are carbohydrates with a short chain that improve the activity and the growth of intestine probiotics (Gibson *et al*., 2004).

Oligosaccharides are polymers with short-chain (2 to 10 monosaccharide units) by glycosidic linkage with low molecular weight, which have attracted great interest for their enforcement in different fields. Oligosaccharides have some biological activities such as antioxidant, antitumor, aiding the proliferation of bifidobacteria, protecting the liver, regulating gastrointestinal functions, and reducing cardiovascular risks (Yang *et al*., 2020; Xiong *et al*., 2021). Oligosaccharides are widely and abundantly distributed and have some advantages over other natural antioxidants such as fewer side effects and better biocompatibility (Xiong *et al*., 2021).

The solubility, triple-helical chain structure, and the existence of uronic acid can affect the bioactivity of oligosaccharides (Ahmed, 2021). The biological activities of oligosaccharides appear to be related to their chemical properties. Furthermore, extraction methods may influence the composition and/or type of oligosaccharide extracted. Moreover, the end groups of oligosaccharides (OH^- of C-2 and C-6) can inhibit the oxidative process (Kang *et al*., 2014).

Currently, 37 megatons of agricultural waste are produced worldwide, causing serious economic and environmental problems related to improper disposal (Rivas *et al*., 2021). Using solid residues to produce useful compounds is a new approach to (a) valorize the great amount of the generated byproducts, (b) control the negative effects of accumulated residue on the environment, (c) benefit humans by preventing disease,

* Corresponding author. e-mail: dr_sa_ahmed@ yahoo.com; sa.sayed@nrc.sci.eg.

and (d) extending the foods shelf life through their known antimicrobial and antioxidant activity (Rivas *et al*., 2021).

Since ancient times, plants are important in pharmacology and medicine. Herbs are often used in the development of novel anticancer drugs (Grigalius and Petrikaite, 2017). Bataineh *et al*. (2023) indicated that pomegranate peel not only kills *Helicobacter pylori*, but also has protective effects on the gastric mucosa. Oligosaccharides may be gained by direct extraction or by hydrolyzation with enzymes or acids (Kang *et al*., 2014; Xiong *et al*., 2021). However, enzymatic hydrolysis is the most appealing method because of its advantages: no need for special equipment, environmentally friendly, good selectivity, and product improvement. As well as reduced production of monosaccharides and their unwanted derivatives (Li *et al*., 2016; Rivas *et al*., 2021).

Among different technologies utilized to produce valuable compounds from agricultural and industrial residues is solid-state fermentation (SSF). SSF has the characteristics of economy and sustainability, high (productivity and efficiency), low consumption (water and energy), and minimal concerns about solving disposal problems (Yazid *et al*., 2017). SSF can be utilized to produce valuable compounds because enzymes produced by microorganisms release large amounts of valuable compounds with high bioactivities (Dey and Kuhad, 2014). Sadik *et al*. (2021) used agro-industrial waste in SSF to produce value-added byproducts. In particular, filamentous fungi are suitable for SSF because this technique mimics their natural environment such as low requirements. Fungal multi-enzyme mixtures were used in the production of oligosaccharides (Li *et al*., 2016).

Corchorus olitorius L. (Jew's Mallow) is an annual herbaceous plant in Middle Eastern countries. Mallow is a highly nutritious vegetable, and its green leaves are consumed as a viscous soup (Ahmed, 2021). In addition, it contains high nutrients such as carbohydrate (44%), protein (22%), fiber and vitamins (11%), ash (16%), moisture (5%), and fat (2%) as reported by Ahmed *et al*. (2021). Hence, it is considered a suitable substrate for the production of bioactive compounds (Al-Yousef *et al*., 2017). This work aims to statistically optimize the preparation of bioactive oligosaccharides from Mallow stems residues (MSOSs) by hydrolysis with enzymes mixture from isolated fungus (*A. flavus* B2, OL655454). The prepared MSOSs were chemically characterized and their biological activities (anticoagulant, fibrinolytic, antitumor, antioxidant, and prebiotic) were estimated.

2. Materials and Methods

2.1. Materials

2,2′-azino-bis(3-ethylbenzothiazoline-6-sulfonate); 2,4,6-tripyridyl-s-triazine (TPTZ); 1,1-diphenyl-2-picrylhydrazyl (DPPH); potassium ferricyanide ($C_6N_6FeK_3$); ferrozine; Trolox; ferrous and ferric chloride [$FeCl_2$ and $FeCl_3$]; and 2,2′-azinobis-(3-ethylbenzothiazoline- 6-sulfonate) (ABTS) were obtained from Sigma Chemical Co [St. Louis, MO, USA]. Other chemicals in the present work were obtained from Sigma-Aldrich and Merck.

2.2. Methods

2.2.1. Waste material collection and preparation

Jew's Mallow stems (MS) residues were obtained from the local market (in Egypt), washed with H_2O, cut into ~1cm pieces, and dried for 1 day in an oven at 50°C. The dried sample was separated by a sieve (1 cm) and packed in airtight containers.

2.2.2. Microorganism and maintenance

The isolated strain from sugar cane bagasse *A. flavus* B2 (accession number OL655454) was selected as a potential enzymes- mixture producer as previously reported (Abdel Wahab *et al*., 2023). *A. flavus* B2 was maintained at 4°C on potato dextrose agar medium. Probiotic bacterial strains *B. lactis* and *L. plantarum* were maintained in DeMan, Rogosa, and Sharpe broth medium MRS (De Man *et al*., 1960). The strains were stored in 30 % glycerol at -80°C and then propagated for 24 h at 37°C in a suitable medium before use.

2.2.3. Utilization of MS residues for fungal enzymes and oligosaccharides (OSs) production

Fungal enzymes and oligosaccharides were produced by adding 2 g of MS to 10 mL distilled H_2O in 250 mL Erlenmeyer. After sterilization, each flask was inoculated with 1 mL of cell suspension containing 6×10^8 spores/mL of 5-day-old in 20 mL H_2O of the fungus (*A. flavus* B2). Flasks were incubated at 35°C under static conditions for 7 days. At the end of the fermentation period, the biomass was separated by adding 50 mL H_2O and centrifuged at 10,000 x*g* at 4 °C for 15 min to obtain the clear supernatant, then the enzyme activities were determined and the MSOSs were extracted.

2.2.4. Enzymes activity

2.2.4.1. Xylanase assay

Enzyme solution (0.5 mL) and 0.5 mL of 1 % xylan solution in acetate buffer (0.05 M, pH 5.0) were incubated for 0.5 h at 50°C (Warzywoda *et al*., 1983). The released reducing sugars were estimated as xylose (Neish, 1952). One unit of enzyme activity (U) was specified as the amount of enzyme releasing 1 µ mol of reducing sugars/min.

2.2.4.2. Carboxy methyl cellulase assay

The reaction mixture contained 0.5 mL enzyme solution and 0.5 mL of 1 % carboxy methyl cellulose (CMC) solution in citrate phosphate buffer (0.05 M with pH 5.0) (Hernández-Domínguez *et al*., 2014). The reaction was incubated for 0.5 h at 50°C then analyzed for the reducing sugars released as glucose (Neish, 1952). One unit (U) of enzyme activity was specified as the amount of enzyme releasing 1 µ mol of reducing sugars/min.

2.2.4.3. Pectinase assay

This was done by adding 0.2 mL of enzyme solution to 0.8 mL of 0.5 % citrus pectin in 0.05 M and pH 5.0 of acetate buffer (Silva *et al*., 2005). The reaction was incubated for 10 min at 50°C, and the released reducing sugars as galacturonic acid was estimated (Neish, 1952). One unit of pectinase activity was specified as the amount of enzyme needed to release 1 µ mol of reducing sugars/min.

2.2.5. First statistical design (Plackett-Burman PB) for MSOSs production

We tested the influence of 11 factors on the production of OSs including A is Mallow stems (MS) weight (g/flask), B is baker's yeast (g/L), C is $(NH_4)_2SO_4$ (g/L), D is glucose, E is $MgSO_4$ (g/L), F is K_2HPO_4 (g/L), G is NaCl (g/L), H is $CuSO_4$ (g/L), J is CaCl (g/L), K is Tween 80 (mL/L), and L is incubation time (day). Each of these factors was tested with high level (+1) and low level (−1) resulting in 12 runs. The statistical significance was estimated by F-value, and the proportion of variance explained by the model obtained was given by the multiple coefficients of determination, R^2.

2.2.6. Second statistical design (Central Composite CC) for MSOSs production

We tested the quantitative effect of the most 2 effective factors obtained from the PB design for OSs production including, A: $(NH_4)_2SO_4$ (g/L) and: K_2HPO_4 (g/L). Variables were investigated with 5 levels -1.414, -1, 0, and +1, +1.414 giving 13 runs. Analysis of variance (ANOVA) was used for Statistical analysis of the model.

2.2.7. Extraction of the produced oligosaccharides (OSs)

Extraction of the produced OSs was achieved by mixing fermentation broth (20 mL) with 100 mL pure ethanol, and the mixture was shaken for 1 h at 50 rpm. The collected extracts were vaporized under vacuum, weighed (designated as numbers), and presented to preparative PC on Whatman No.3 filter paper and n- butanol- acetone-water in the ratio 4: 5: 1 (v/v) as a solvent mixture (Jayme and Knolle, 1956). The developed chromatograms were air dried, and two longitudinal narrow strips (from the two sides of each chromatogram) were cut off and sprayed with aniline phthalate reagent (Partridge, 1949). The colored strips were then reassembled as markers, and areas of the unsprayed central portions, which included the individual OSs, were cut out and eluted with a suitable amount of 50 % ethanol. The eluted OSs were concentrated under vacuum.

2.2.8. Chemical characterization of the produced MSOSs

2.2.8.1. Oligosaccharides yield

After the fermentation period, the culture filtered was dried, weighed (W2), and re-dissolved in 10 ml distilled water, then treated with ethanol (3 volumes). After centrifugation, the resulting precipitate was dried, weighed (W1), and designated as numbers. The OSs yield is calculated (Dubois *et al*., 1956) as follows Eq. (1):

$$\text{Yield (\%)} = (W1/W2) \times 100 \quad (1)$$

2.2.8.2. Total carbohydrates

The total carbohydrates of the various MSOSs were determined by adopting the method of phenol-sulfuric acid (Dubois *et al*., 1956). Sample (1 mL) was added to 1 mL phenol solution (5 %), thereafter concentrated H_2SO_4 (5 mL), was added quickly. The reaction was shaken and kept at room temperature for 10 min and then at 25-30°C for 20 min in a water bath. The color density was estimated at 480-490 nm. Quantities were determined using standard curves resulting from measurements on a solution containing proper sugars in appropriate ratios for each extract of OSs.

2.2.8.3. Soluble protein

The soluble protein was estimated by the colorimetric method using pure bovine albumin as the standard curve (Lowry *et al*., 1951).

2.2.8.4. Monosaccharide constituents

For acid hydrolysis, 0.5-1.0 mg of MSOSs were heated in a sealed glass tube at 100°C with 2 mL H_2SO_4 (2 M) for 6 h followed by neutralization using $BaCO_3$ (Perila and Bishop, 1961). The hydrolysates were centrifuged, filtered, neutralized (with Dowex 50 resin H^+), concentrated under vacuum, and presented to quantitative paper chromatographic analysis (Whatman no.1) (Wilson, 1959) using n-butanol- acetone- water in the ratio 4: 5: 1 (v/v/v) as running solvent. The components of monosaccharides were clarified after spraying the chromatogram with aniline phthalate (Partridge, 1949).

2.2.8.5. Degree of Polymerization (DP)

One ml (100 µg/ mL) of each OS was added to sodium borohydride solution (0.5 mL, 1 %), and reduction was allowed at room temperature (in a dark place) for 1 h. Another similar set of samples was added to 2 N H_2SO_4 acid (0.5 mL) at the same time. Add to both groups 1mL of aqueous phenol (3 %) followed by concentrated H_2SO_4 acid (5 mL). After careful mixing, the solutions were kept at room temperature for 10 min, and then left to cool for 25 min. Absorbance measurements at 480 nm were done, and the average was used for calculating the DP of the OSs (El Azm *et al*., 2019) as follows in Eq. (2):

$$Q = A1/A2 \quad (2)$$

Where: Absorbance of the OS hydrolysate before reduction (A1) and after reduction (A2) as follows in Eq. (3):

$$DP = Q/(Q-1) \quad (3)$$

2.2.9. Biological activity of the extracted MSOSs

2.2.9.1. Anticoagulation efficiency

The anticoagulation activity of the MSOSs was estimated according to the clot formation time and compared with standard heparin sodium preparation (USA Pharmacopoeia, 1960). Glass test tubes (dimensions 31×100 mm) were cleaned by immersion for 1 day in chromic acid. To each tube add 0.8 mL of 0.01 % MSOS solution, saline solution (0.9 %), or standard Heparin solution (1.4 U/mL). Next, to each prepared tube add 1 mL of human plasma and 0.2 mL of 1 % $CaCl_2$ solution and incubate in a water bath at 37°C. Heparin (Sodium heparin) was used as a standard. For control, the experimental extract solution was replaced with the same volume of saline. The blood clot samples were then observed visually for 1 h at room temperature for any noticeable changes. The time period required for clot formation was recorded by a stopwatch by tilting the test tubes every 5 seconds. Each result is representative of at least three separate experiments. Values represent the mean of these experiments, and the results were expressed as the average of three readings.

2.2.9.2. Fibrinolytic efficiency

This was performed by exposing the plasma clot to the effect of MSOSs, an aqueous solution with proper concentration (USA Pharmacopoeia, 1960). Three glass test tubes (dimensions 31×100 mm) were cleaned by

immersion overnight in chromic acid. First, 1 mL of human plasma was mixed with 0.2 mL of 1 % $CaCl_2$ and 0.8 mL of saline solution (0.9 %) and incubated at 37°C in a water bath for fibrin clot formation. When coagulation was completed, 1 mL of Hemoclar (2 mg/tube), saline solution (0.9 %), or the MSOS (2 mg/tube) was individually added. Plasma fibrin clot with saline was used as control. Percentages (%) of plasma clots lysis at 37°C were determined with each MSOS and compared with those of standard Hemoclar (pentosane sulfuric polyester).

2.2.9.3. Prebiotic activity

The growth-enhancing effect of MSOSs on *B. lactis* and *L. plantarum* was performed by cultivating strains in MRS broth medium (10^7 CFU/ mL) fortified with filter sterilized MSOSs at different concentrations (0.1, 1, and 10 %) instead of glucose (as C-source) at 37°C for 24 h under anaerobic conditions. Then, the turbidity (bacterial growth) was determined by a spectrophotometer at 620 nm against a blank composed of an un-inoculated medium (Riaz *et al*., 2010).

2.2.9.4. Antioxidant activity (In vitro)

2.2.9.4.1. DPPH free- radical scavenging

It was estimated by adding 1 mL of methanolic DPPH solution (freshly prepared 20 µg/ mL) to 0.5 mL (2.5 mg) of the tested MSOSs (Williams *et al*., 1995). After 5 min of reaction, the color removal process was estimated at 517 nm. The ability to scavenge the DPPH radical (%) was calculated using the following Eq. (4):

DPPH (%) = [Absorbance of control − Absorbance of sample / Absorbance of control] ×100 (4)

2.2.9.4.2. Reducing power

The tested MSOS (2.5 mg/ 0.5 mL) was added to 2.5 mL of phosphate buffer (0.2 M and pH 6.6), and 2.5 mL of 1 % potassium ferricyanide. The reaction was incubated for 20 min at 50°C. 2.5 mL of aliquots of 10 % trichloroacetic acid were placed into the reaction and centrifuged at 1000 rpm for 10 min. 2.5 mL of the upper layer of solution was added to an equal volume of (0.5 mL of freshly prepared 0.1 % $FeCl_3$ solution and distilled H_2O). The intensity was estimated at 700 nm of the blue-green color (Oyaizu, 1986). According to the tested MSOS reducing power, the yellow color changes to green in the solution.

2.2.9.4.3. Metal chelating

For chelating of ferrous ions of MSOSs, 0.5 mL of each MSOSs extract (2.5 mg) was added to 0.05 mL of 2 mM $FeCl_2$ solution (Dinis *et al*., 1994). The reaction was started by adding 0.2 mL of 5 mM ferrozine, then shaking the mixture vigorously and leaving for 10 min at room temperature. The absorbance of the solution was estimated at 562 nm by spectrophotometer. The inhibition percentage (%) of the ferrozine-ferrous complex of each MSOS sample was determined as following Eq. (5):

Inhibition % = [Absorbance of control − Absorbance of sample / Absorbance of control] ×100 (5)

2.2.9.4.4. ABTS radical scavenging

ABTS radical scavenging assay was performed by the ABTS cation decolorization test with some modifications (Re *et al*., 1999). The stock solutions contained 7 mM of ABTS solution and 2.4 mM of $K_2S_2O_8$ solution. The working solution was made ready by mixing equal quantities of the two stock solutions and kept to react for 12 h in a dark place at room temperature. Then, 60 mL of methanol was added to 1 mL ABTS radical solution to obtain an absorbance of 0.706±0.001 units at 734 nm. 0.5 mL of 0.1 % tested MSOSs was reacted with 2.5 mL of ABTS reagent for 7 min and the absorbance was estimated at 734 nm using a spectrophotometer. The ABTS radical cation color removal ability of the MSOS and percentage inhibition were estimated as following Eq. (6):

ABTS (%) = [AC − AS / AC] × 100 (6)

Where: AC, absorbance of the ABTS radical cation methanol and AS, absorbance of the ABTS radical cation sample extract.

2.2.9.4.5. FRAP

The FRAP (Ferric ion Reducing Antioxidant Power) assay was done with some modifications (Benzie and Strain, 1999). The stock solutions contained 300 mM of acetate buffer pH 3.6, 10 mM of TPTZ solution in 40 mM of HCl, and 20 mM of $FeCl_3.6H_2O$ solution. The working solution was ready by mixing 25 mL of acetate buffer, 2.5 mL of TPTZ solution, and 2.5 mL of $FeCl_3.6H_2O$ solution and heating it before using it at 37°C. The tested MSOSs (2.5 g/0.5 mL) was reacted with 2.5 mL of FRAP solution in a dark place for 30 min. The produced color of the ferrous TPTZ complex was estimated at 593 nm and the results are expressed in µ mol Trolox/100 g dry matter.

2.2.9.4.6. 2.2.9.5. Antitumor activity In Vitro (Trypan blue exclusion test)

The trypan blue exclusion test was used to detect cell viability. The tumor cell suspension was obtained from peritoneal cavities of tumor-bearing mice and then diluted with phosphate-buffered saline pH 7.0, so the final preparation included 2.5×10^5 cells/ 0.1 mL. In a set of sterile test tubes, 0.1 mL/tube of the cell preparation was dispersed, followed by the addition of 0.8 mL aliquots of phosphate-buffered saline (/tube). The tested MSOSs (0.5mg) were used in tubes at 0.1 mL/ tube. The sample tubes were incubated for 2 h at 37°C under 5% CO_2 for 2 h. After that, centrifuged the tubes (5 min at 1000 rpm) the separated cells were suspended in saline. For each tube (control and examined), a new clean, dry small test tube was used, and 0.1 mL of cell suspension, 0.8 mL of saline, and 0.1 mL trypan blue were added and mixed. Then, the number of living cells was estimated by a hemocytometer slide. Viable cells appeared as unstained bodies, whereas nonviable cells appeared as blue bodies (El-Merzabani *et al*., 1979).

3. Results and discussion

Industrial applications of enzymes have been restricted by their high production cost (Ahmed *et al*., 2022). The plant cell wall structure is a complex polysaccharides composed mainly of hemicellulose, cellulose, and pectic substances. Therefore, hemicellulases, cellulases, and pectinases enzymes play an essential role in the hydrolysis of agricultural residues (Abdel Wahab *et al*., 2023). The enzymes- mixture of pectinase 3.33 U/mL, cellulase 1.74 U/mL, and xylanase 1.31 U/mL was produced by *A. flavus* B2 using MS residues as substrate under SSF as previously reported (Abdel Wahab *et al*., 2023), in addition to 150.2 mg of oligosaccharides. In the current study, the statistical

improvement of MSOSs production was evaluated by enzymes- mixture hydrolysis.

3.1. First statistical design (Plackett-Burman PB) for MSOSs production

As presented in Table 1, the interaction between the 11 factors has remarkable and different effects on oligosaccharides production.

Table 1. Plackett-Burman (PB) design for Mallow stems oligosaccharides (MSOSs) production.

Run	A MS weight , g/flask	B Baker's yeast , g/L	C $(NH_4)_2SO_4$, g/L	D Glucose, g/L	E $MgSO_4$, g/L	F K_2HPO_4, g/L	G NaCl, g/L	H $CuSO_4$, g/L	J CaCl, g/L	K Tween 80, mL/L	L Incubation time, day	MSOS weight, mg
1	1	10	10	10	0	0	0	0.2	0	1	7	349.99
2	2	0	0	0	0.5	0	2	0.2	0	1	7	205.00
3	1	0	0	0	0	0	0	0	0	0	4	115
4	2	10	10	0	0	0	2	0	0.5	1	4	405
5	1	10	0	10	0.5	0	2	0.2	0.5	0	4	190
6	1	10	10	0	0.5	5	2	0	0	0	7	408
7	2	0	10	10	0.5	0	0	0	0.5	0	7	280
8	2	10	0	0	0	5	0	0.2	0.5	0	7	284.99
9	1	0	0	10	0	5	2	0	0.5	1	7	325.00
10	2	0	10	10	0	5	2	0.2	0	0	4	350
11	1	0	10	0	0.5	5	0	0.2	0.5	1	4	410
12	2	10	0	10	0.5	5	0	0	0	1	4	295

Maximum MSOSs production was obtained in run 11 (410 mg), causing a 2.73-fold increase in production. Nine factors (B: baker's yeast, C: $(NH_4)_2SO_4$, D: glucose, F: K_2HPO_4, G: NaCl, H: $CuSO_4$, J: $CaCl_2$, K: Tween 80, L: incubation time) of t he eleven tested factors have a significant effect on OSs production. The maximum MSOSs production (run 11) is related to the action of enzymes- mixture (U/mL) pectinase 2.97, xylanase 2.33, and cellulase 0.69.

As seen in the Pareto chart (Figure 1), the other two factors (A: MS weight and E: $MgSO_4$) did not have a significant effect. The seven factors that enhanced MSOSs production included baker's yeast, $(NH_4)_2SO_4$, K_2HPO_4, NaCl, $CaCl_2$, Tween 80, and incubation time, while glucose and $CuSO_4$ showed a negative effect on MSOSs production.

Oligosaccharide weight (mg) = +303.75 +22.92 * baker's yeast +67.92 * $(NH_4)_2SO_4$ -5.42* glucose +46.25 * K_2HPO_4 +14.58 * NaCl -5.42 * $CuSO_4$ +12.08 * $CaCl_2$ +27.92* Tween 80 + 9.58 * incubation time.

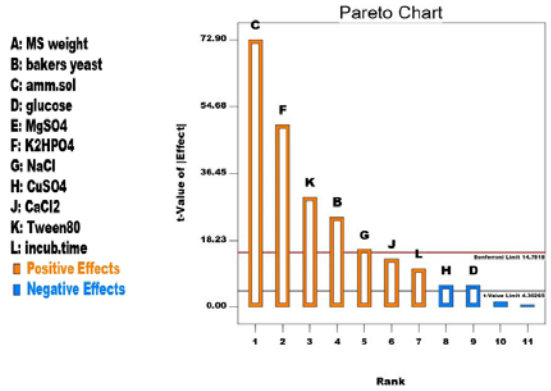

Figure 1. Pareto chart for production of Mallow stems oligosaccharides by PB design.

The enhancing effect of $(NH_4)_2SO_4$, K_2HPO_4, NaCl and $CaCl_2$ on MSOSs can be attributed to the positive significant effect of t hese factors on *A. flavus* CMCase, xylanase, pectinase production as described in previous work(Abdel Wahab *et al.*, 2023) s ince MSOSs are the hydrolyzed products of these enzymes. The negative effect of $CuSO_4$ and glucose on M SOSs production can be a result of t he more enhancing effect of t hese factors on *A. flavus* enzymes production causing more hydrolysis for MS polysaccharides producing monosaccharides not oligosaccharides.

Mallow stems are suitable residues, inexpensive, and available abundantly in Egypt and other countries (Ahmed and Mostafa, 2013). This step of fa ctorial production optimization improved MSOSs production by 2.73-fold. The significance of t he design for MSOSs production was statically analyzed by ANOVA (Table 2). Values of "Prob

> F" are <0.0500 indicating that bakers yeast, $(NH_4)_2SO_4$, glucose, K_2HPO_4, NaCl, $CuSO_4$, $CaCl_2$, tween 80 and incubation time are significant model terms. Moreover, the R2 value (0.9998) for the production of oligosaccharides, respectively, showed the significance of the model since the R2 value was very close to 1.Also, the value of predicated R^2 (0.9927) was reasonably consistent with the adjective R^2 (0.9989).

Table 2. ANOVA for PB design for Mallow stems oligosaccharides production.

Source	Sum of Squares	df	Men Square	F value	p-value Prob>F	
Model	102785.2117	9	11420.57907	1096.639	0.0009	significant
B-baker's yeast	6301.900001	1	6301.900001	605.1276	0.0016	
C-$(NH_4)_2SO_4$	55351.81167	1	55351.81167	5315.049	0.0002	
D- glucose	352.0833333	1	352.0833333	33.808113	0.0283	
F-K_2HPO_4	25668.75	1	25668.75	2464.792	0.0004	
G-NaCl	2552.200001	1	2552.200001	245.07	0.0041	
H-$CuSO_4$	352.1050003	1	352.1050003	33.81019	0.0283	
J-$CaCl_2$	1752.083333	1	1752.083333	168.2404	0.0059	
K-Tween 80	9352.195	1	9352.195	898.0262	0.0011	
L-incubation time	1102.083333	1	1102.083333	105.8254	0.0093	
Residual	20.82833367	2	10.41416683			
Cor Total	102806.04	11				

R^2 0.9998, Adj R^2 0.9989, Pred R^2 0.9927

3.2. Chemical characterization of produced MSOSs by BP design

As presented in Table 3, the chemical characterization of MSOSs indicated that the interaction between the eleven factors successfully produced 12 oligosaccharides that differed in chemical characteristics.

3.3. Monosaccharide constituents

The produced MSOSs differ in their monosaccharides constituents and percentage as illustrated in Figure 2A. I.e. some oligosaccharides composed of 4 monosaccharides constituents (galacturonic acid, galactose, glucose, and xylose), 3 monosaccharides constituents (galacturonic acid, galactose, and glucose), 2 monosaccharides constituents (galacturonic acid and glucose) or (galactose and xylose) with different percent. Differences in the composition of oligosaccharides can be attributed to the different enzymes produced during fermentation. I.e galacturonic acid as pectin monosaccharide component due to the action of pectinase enzyme, glucose as monosaccharide component of cellulose due to the action of cellulase enzyme and xylose as monosaccharide component of xylan due to the action of xylanase enzyme. Silva *et al*. (2015) reported that hydrolysis of oat spelts xylan by xylanases from by *T. inhamatum* produced larger xylooligosaccharides, xylobiose, xylotriose, and xylotetrose.

Table 3. Chemical characterization of the extracted Mallow stems oligosaccharides by PB design.

Run	Yield (%)	D.P	Analytical characteristics (%)	
			Total carbohydrate	Soluble protein
1	65.57	9	68.70	21.30
2	28.41	6	64.52	25.44
3	28.41	6	64.52	25.44
4	13.58	2	44.30	45.70
5	28.41	6	64.52	25.44
6	28.41	6	64.52	25.44
7	53.57	4	54.00	36.00
8	44.91	6	65.10	25.00
9	28.41	6	64.52	25.44
10	50.57	4	56.10	43.00
11	63.41	4	63.00	37.00
12	75.59	4	56.80	43.00

* D.P: Degree of Polymerization

3.4. Second statistical design (Central Composite CC) for MSOSs production

The quantitative effect of the most two effective factors obtained from the PB design including, (A) $(NH_4)_2SO_4$ (g/L) and (B) K_2HPO_4 (g/L) for oligosaccharides was studied. As presented in Table 4, the interaction between the quantitative effect of the highly effective factors $(NH_4)_2SO_4$ and K_2HPO_4 led to a significant variation in oligosaccharides production resulting in a 3.50-fold increase (run 4) in oligosaccharides production compared to the un-optimized medium. The highest production of MSOSs was due to the action of enzymes-mixture (pectinase 12.89 U/mL, cellulase 4.9 U/mL, and xylanase 6.76 U/mL).

Oligosaccharide weight (mg) can be calculated from the following equation:

Oligosaccharides weight (mg) = +375.00 +122.08* $(NH_4)_2SO_4$ +49.65 * K_2HPO_4 -80.73* $(NH_4)_2SO_4$ * K_2HPO_4 -21.46 * $(NH_4)_2SO_4{}^2$ -39.82 * $K_2HPO_4{}^2$

The significance of the design for oligosaccharides production was statically analyzed by ANOVA (Table 5). Values of "Prob > F" are < 0.0500 decided that A, B, AB, A^2, B^2 are significant model terms. Moreover, the value of R^2 (0.9930) indicated the significance of the model since the R^2 value was very near to 1. Also, values of predicated R^2 (0.9506) were reasonably consistent with the adjective R^2 (0.9881).

Table 4. Central Composite (CC) design for Mallow stems oligosaccharides production.

Run	Factor 1 A: $(NH_4)_2SO_4$ [g/L]	Factor 2 B: K_2HPO_4 [g/L]	Oligosaccharide Weight [mg]
1	5	2	70
2	10	6	375
3	10	6	375
4	17.071	6	525
5	10	6	375
6	10	6	375
7	5	10	322.5
8	15	2	455
9	10	6	375
10	2.929	6	150.55
11	10	11.657	377.11
12	15	10	384.6
13	10	0.343	225

3.5. Chemical characterization of MSOSs extracted by CC design

As shown in Table 6, the chemical characterization of MSOSS reported that the interaction between the highly effective factors (two) successfully produced 13 oligosaccharides that differed in their chemical characteristics.

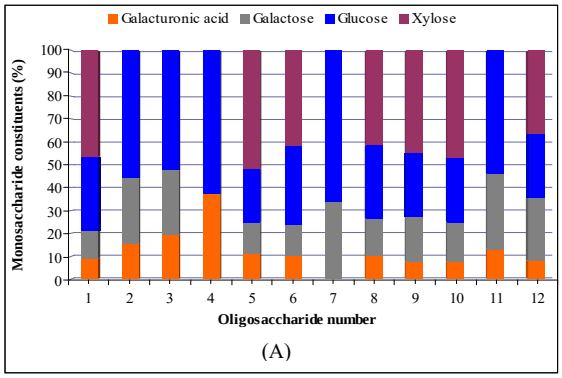

Figure 2. Monosaccharides constituents (A) in MSOSs produced by PB design **(B)** in MSOSs produced by Central Composite design.

Table 5. ANOVA for CC design for Mallow stems oligosaccharides production.

Source	Sum of Squares	df	Mean Square	F Value	p-value prob>F	
Model	177922.8	5	35584.56	199.990561	< 0.0001	significant
A-$(NH_4)_2SO_4$	119231.2	1	119231.2	670.097185	< 0.0001	
B-K_2HPO_4	19722.57	1	19722.57	110.843796	< 0.0001	
AB	26066.1	1	26066.1	146.495388	< 0.0001	
A^2	3203.698	1	3203.698	18.0052616	0.0038	
B^2	11030.49	1	11030.49	61.9929798	0.0001	
Residual	1245.519	7	177.9312			
Lack of Fit	1245.519	3	415.1728			
Pure Error	0	4	0			
Cor Total	179168.3	12				

Table 6. Chemical characterization of the extracted Mallow stems oligosaccharides by CC design.

Run	Yield (%)	D.P	Analytical characteristics (%)	
			Total carbohydrate	Soluble protein
1	1.4	9	88.38	8.75
2	7.5	2	41.72	10.27
3	7.5	2	41.72	10.27
4	10.5	4	30.6	16.73
5	7.5	2	41.72	10.27
6	7.5	2	41.72	10.27
7	3.8	2	73.62	6.08
8	9.1	3	38.7	1.52
9	7.5	2	41.72	10.27
10	4.3	3	79.38	7.98
11	10.7	3	42.3	6.46
12	5.1	2	34.38	5.32
13	4.5	2	58.5	2.28

* D.P: Degree of Polymerization

3.6. Monosaccharide constituents

The produced MSOSs differed in their monosaccharides' constituents and percentage as illustrated in Figure 2B. Some oligosaccharides were composed of 4 monosaccharides, 3 m onosaccharides, and 2 monosaccharides with different percent. The difference in oligosaccharide composition can be attributed to the different enzymes produced during fermentation. Galacturonic acid was produced as the monosaccharide component of pectin due to the action of pectinase, xylose as the monosaccharide component of xylan due to the action of xylanase, and glucose as the monosaccharide component of cellulose due to the action of cellulose. The great diversity in oligosaccharides' structure and chemical composition, as well as their safety and biodegradability, make them ideal for diverse applications (Rivas *et al.*, 2021).

3.7. Biological activity of MSOSs

3.7.1. Anticoagulation efficiency

The anticoagulation efficiency of the produced MSOSs was evaluated by estimating the coagulation times for a mixture of p lasma-standard heparin, plasma-tested samples, and plasma-saline (as control). The results in Table 7 indicated that most of the MSOSs tested exhibited either weak or even no anti-coagulation activity. The coagulation times recorded for a mixture of p lasma with each tested MSOSs ranged from 3 min and 1 sec to 13 min and 31 sec compared to 3 min (in control experiments) and 90 min for standard heparin. From the results in Table 7, MSOSs no. 8, 10, and 12 showed the highest anticoagulant activity. This result may be because MSOSs (8, 10, and 12) inhibit platelet aggregation. Chegu *et al.* (2018) reported that aqueous extract of ginger showed lower anticoagulant activity (4.15 min) than our re sult. Polysaccharides isolated from clove may have antithrombic effects as reported by Chegu *et al.* (2018). Helal *et al*. (2020) and Abd El-Galil *et al*. (2021) reported that aqueous extracts of some plants (ginger and Pea peel) had no anticoagulant activity.

3.7.2. Fibrinolytic activity

Fibrinolytic activities of the produced oligosaccharide were estimated as lysis (%) of pl asma. A commercial sample of Hemoclar, a sulfated pentosan polyester, was set for comparison in a simultaneous experiment as a standard fibrinolytic agent. Amongst the tested materials (Table 7), MSOS no. 4 exhibited fibrinolytic activity (80 % lysis) which is higher than that of Hemoclar the standard sample (50 % lysis). Also, MSOS no. 11 demonstrated fibrinolytic activity equal to that of t he standard "Hemoclar" sample. In contrast, Abd El-Galil *et al*. (2021) reported that aqueous oligosaccharide extracts from pea peel had no fibrinolytic activity. It was observed that eleven MSOS products showed lower fibrinolytic activity (Lysis ≤ 25 % of plasma clot) than the standard Hemoclar sample.

Table 7. Anticoagulation and fibrinolytic activity of the Mallow stems oligosaccharides produced by CC design.

Run	Anti-coagulation activity clotting time (min:sec)	Fibrinolytic activity lysis of plasma clot (%)
Control	03:00	< 25
1	03:01	< 25
2	10:33	25
3	10:33	25
4	06:42	80
5	10:33	25
6	10:33	25
7	11:15	< 25
8	13:26	< 25
9	10:33	25
10	13:31	< 25
11	03:12	50
12	12:40	< 25
13	03:13	< 25

***** Control: with saline

3.7.3. Prebiotic activity

The effect of MSOSs on probiotics growth (*L. plantarum* and *B. lactis*) as illustrated in Figure 3 (A and B) differed with the oligosaccharide concentration and probiotic. Firstly, all tested MSOSs had a growth-promoting effect on both probiotics with a 1 % concentration. Gobinath *et al*. (2010) and Pourabedin *et al*. (2015) reported that diets containing oligosaccharides selectively increased the population of l actobacilli and bifidobacteria. Secondly, the growth-promoting effect was higher on *B. lactis* that MSOS no. 8 caused 43 % enhancement in growth compared with 23.71 % on *L. plantarum* with MSOS no. 4 a nd 12 i n contrast to that obtained by Saleh *et al*. (2020). Finegold *et al*. (2014) showed that in the human gut microbiota, xylooligosaccharide increased bifidobacterial but not lactobacilli. Voragen (1998) reported that the difference in the effect of M SOSs on t he growth of probi otics may be due to differences in the DP, chemical structure of saccharides, water solubility, and constituent of monosaccharide units.

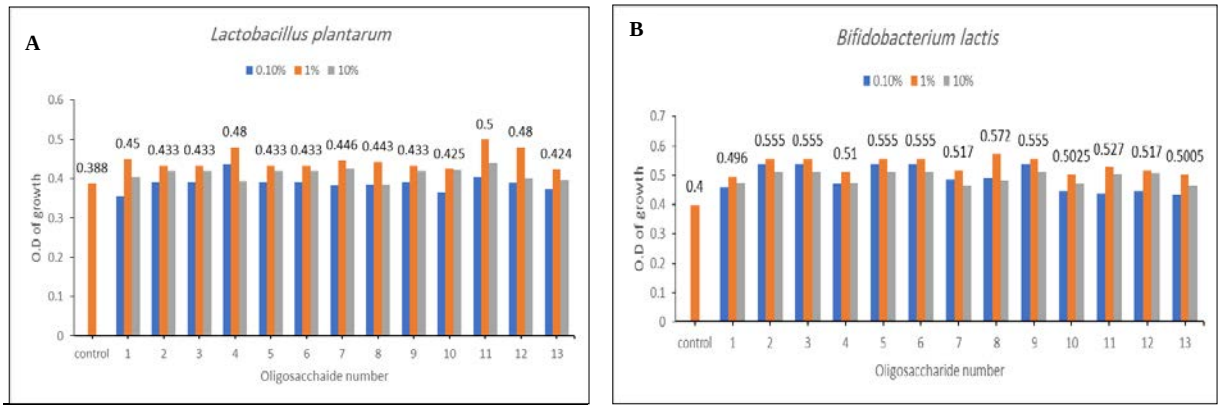

Figure 3. Prebiotic effects of Mallow stems oligosaccharides on probiotics, (A) *L. plantarum*, (B) *B. lactis.*

3.7.4. Antioxidants activity

3.7.4.1. DPPH free- radical scavenging

The antioxidant activity of ol igosaccharides attracts much attention. Xiong *et al*. (2013) reported that hydroxyl and special functional groups in the chain are the major sources of pol ysaccharides' antioxidant activities. Sun *et al*. (2004) fo und that degradation enhances the oligosaccharide antioxidant activities by increasing the number of activated hydroxyl groups. The antioxidant

ability of oligosaccharides is affected by the assay method, so it cannot be fully qualified by one method. One compounds that contains a free proton radical with an absorbent property is DPPH which is significantly reduced upon exposure to proton radical scavengers. Moreover, it is well accepted that DPPH molecules are scavenged by antioxidants due to their ability to donate hydrogen (Xiong *et al*., 2013). DPPH is a stable free radical concentrated in nitrogen, it changes color from violet by reduction to yellow (by hydrogen capture or electron donation). Results seen in Figure 4A indicate that MSOS no. 11 and 1 possess the highest DPPH at 33.24±0.24 and 29.31±0.21 %, respectively, at concentration (5mg/mL). All the other MSOSs exhibited various activities of D PPH radical scavenging ranging from 10.8±0.17 % for MSOS no. 13 to 26.36 ±0.21 % for M SOS no. 12. Abd El-Galil *et al.* (2021) reported that aqueous oligosaccharide extracts were highly antioxidant as DPPH radical scavenging.

3.7.4.2. Reducing Power

The antioxidants ability to donate electrons is evaluated by reducing power tests (Dorman *et al*., 2003). Antioxidant compounds reduce ferric to ferrous form (Fe^{3+} to Fe^{2+}) due to their reductive abilities. Prussian blue-colored complex is formed by adding $FeCl_3$ to the ferrous (Fe^{2+}) form. The presence of r eductants in the solution reduces the reduction of t he compound (ferric/ferricyanide) to the ferrous form which can be determined by estimating the formation of P erls' Prussian blue at 700 nm . All investigated MSOSs exhibited good reducing power activity specially MSOS no. 11 and 7 which recorded 1.169±0.036 and 0.97±0.012 at concentration (5 mg/mL) (Figure 4B). The reducing power ability of MSOSs in the central treatments exhibited 0.95±0.032. MSOS no. 4 re corded the least reducing power activity (0.671± 0.020). Our results are higher than those obtained from *Leucaana leucocephala* leaves extract (Mohammed *et al*., 2015).

3.7.4.3. Metal chelating

For life, iron is necessary for respiration, oxygen transport, and the activity of many enzymes. Moreover, it is a highly reactive metal and will stimulate oxidative changes in proteins, lipids, and other cellular components (Decker and Welch, 1990). Divalent transition metal ions play a pivotal role as catalysts of oxidation processes. These processes can be delayed by iron chelation and deactivation. Transition metal iron generates free radicals from peroxides by Fenton reactions and may have a role in human cardiovascular disease (Halliwell, 1997). Among all investigated MSOSs, only the central 2, 3, 5, 6, and 9 possess iron metal chelating activity (35.47±0.13 %) a t concentration (5 mg/mL) (data not shown). Xiong *et al.* (2013) reported that the antioxidant ability of xanthan oligosaccharides is useful in expanding their biomedical applications.

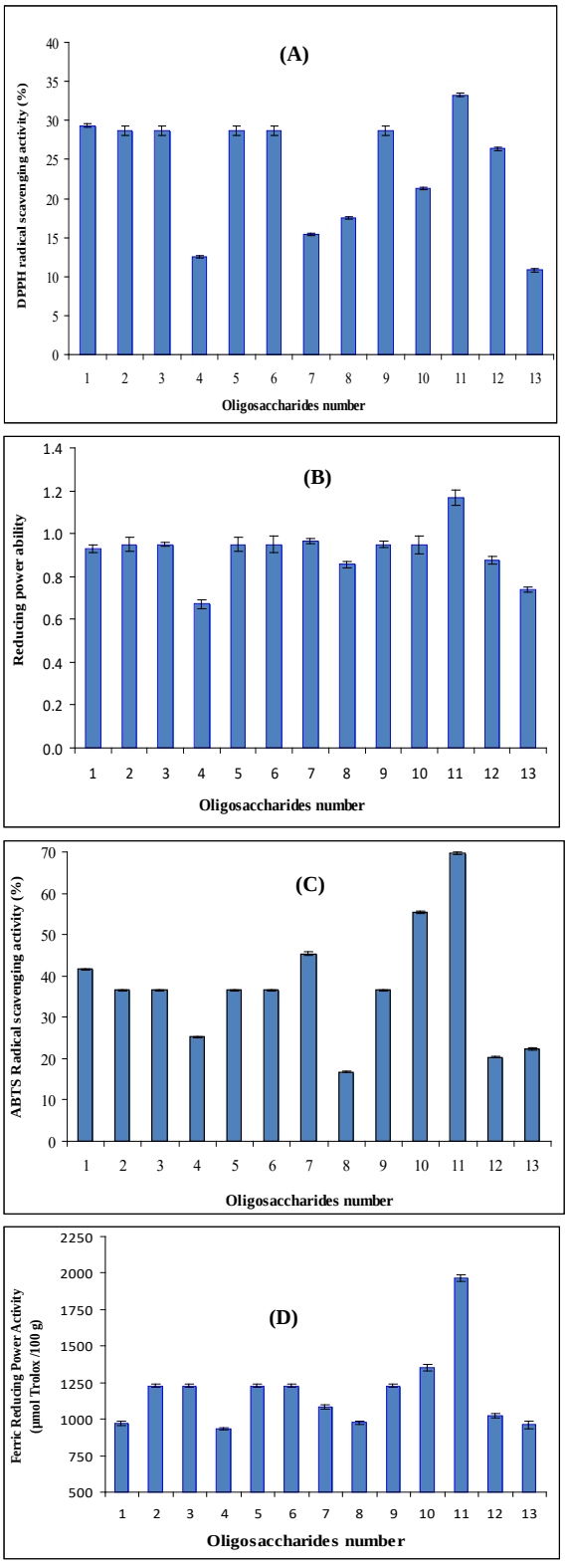

Figure 4. Antioxidant activity of Mallow stems oligosaccharides DPPH radical scavenging (A), Reducing power (B), ABTS radical scavenging (C), and FRAP (D).

3.7.4.4. ABTS radical scavenging

The ability of the MSOSs to scavenge free radicals was quantified by the ABTS test. A sample with ABTS free radical-scavenging activity confirms that it is a hydrogen donor and stopped the process of oxidation by converting the free radicals into more stable products (Suganya *et al*., 2007). Re *et al*. (1999) found that the lack of absorbance is measured after combining ABTS with the antioxidant for a few minutes, after which absorbance stabilizes. Figure 4C displays the ABTS activities of MSOSs extracts and confirms that all investigated treatments possess ABTS radical scavenging ability. As shown in the results, MSOS no. 11 followed by 10 recorded the highest ABTS activity (69.67± 0.24 and 55.41± 0.24 %, respectively). At the same concentration, MSOS no. 8 exhibited the lowest ABTS activity (16.75± 0.34 %). Thetsrimuang *et al*., (2011) reported that reducing sugar in medicinal plants is an important factor possessing antioxidant activity, and higher reducing sugar content means higher antioxidant ability.

3.7.5. Antitumor activity (In Vitro)

Ehrlich's ascites carcinoma cells are one of the most common experimental tumors used for modeling because they resembles undifferentiated human tumors and have a rapid growth rate (Ozaslan *et al*., 2011). As seen in Figure 5, a similar approach was noted in the investigated MSOSs antitumor activity using a viability test of Ehrlich ascites carcinoma cells. The viability of tumor cell was decreased and ascites was inhibited by MSOS no. 11 (37. 24±0.31 %), which is considered to have the highest effect on the viability of the cells among all investigated MSOSs, followed by MSOS no. 8 and 10 which exhibited 30.14±0.24 and 25.38±0.23 % dead cells, respectively at concentration 5mg/mL. The recorded results agreed with the hypothesis that the investigated MSOSs exert their antitumor effects as they have antioxidant activity which can be attributed to the radical activity of the substituted sugar (concentration and type).

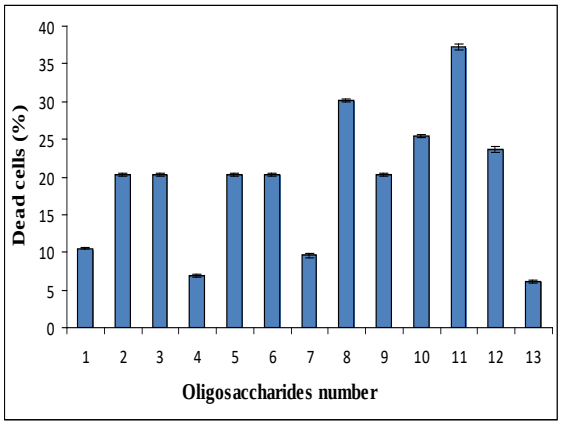

Figure 5. Effect of different Mallow stems oligosaccharides on the EACC viability.

4. Conclusion

It is an economical and eco-friendly way to use Mallow stems which are agro-industrial residues, as an inexpensive substrate for enzymes-mixture and oligosaccharides production. Thirteen oligosaccharides (with a 3.5-fold increase) were successfully obtained from MS by enzymatic hydrolysis produced by an isolated strain (*A. flavus* B2) via RSM. MSOSs extracts can represent a source of bioactive materials. All MSOSs had a growth-stimulating effect on both probiotics *B. lactis* and *L. plantarum* (highest stimulation at a concentration of 1 %), so it can be used in the food industry. In addition, anticoagulation and fibrinolytic activities were evaluated for the MSOSs. MSOS no. 4 and 11 exhibited fibrinolytic activity higher than and equal to that of Hemoclar. Furthermore, MSOSs showed antitumor activity by lowering the Tumor cell viability by 37.2% (MSOS no. 11) without side effects. Based on the results, it can be concluded that sugar content and type may have a role in the antitumor and antioxidant activities of the investigated oligosaccharide.

Declaration of competing interest

There is no conflict of interest.

Funding

This research was financially supported by Science & Technology Development Fund (STDF) Project ID: 34747.

References

Abd El-Galil AA, El-Dein AN, Awad HM, Helmy WA. 2021. Chemical composition and biological activities of aqueous extracts and their sulfated derivatives of pea peel (*Pisum sativum* L.). Biocat Agric Biotech. **35**: 102077.

Abdel Wahab WA, Mostafa FA, Ahmed SA, Saleh SAA. 2023. Statistical optimization of enzyme cocktail production using Jew's mallow stalks residues by a new isolate *Aspergillus flavus* B2 via statistical strategy and enzymes characterization. J of Biotech. **367**: 89–97.

Ahmed F. 2021. Nutraceutical potential of molokhia (*Corchorus olitorius* l.): A versatile green leafy vegetable. Pharmacogn. Res. **13**: 1-12.

Ahmed SA, Mostafa FA. 2013. Utilization of orange bagasse and molokhia stalk for production of pectinase enzyme. Braz J Chem Eng. **30**: 449–456.

Ahmed SA, Saleh SAA, Mostafa FA, Abd El Aty AA, Ammar HAM. 2016. Characterization and valuable applications of xylanase from endophytic fungus *Aspergillus terreus* KP900973 isolated from *Corchorus olitorius*. Biocat Agric Biotech. **7**: 134–144.

Ahmed SA, Abdel-Naby MA, Abdel-Fattah AF. 2.22. Kinetic, Catalytic and Thermodynamic Properties of Immobilized *B.Circulans* 25 Milk Clotting Enzyme on Activated Chitosan Polymer and Its Ability to Form Milk Curds. *Jordan J Biol Sci*, **15:** 649 – 657.

Al-Yousef HM, Amina M, Ahamad SR. 2017. Comparative study on the chemical composition of *Corchorus olitorius* leaf and stem dry oils. Biomed Res J. **28**: 4581–4587.

Antolovich M, Prenzler PD, Patsalides E, McDonald S, Robards K. 2002. Methods for testing antioxidant activity. The Analyst. **127**: 183-198.

Bataineh SMB, Abu Dalo BA, Mahawreh BS, Darmani H, Sallal AJ. 2023. Inhibitory Effect of Partially Purified Compounds from Pomegranate Peel and Licorice Extracts on Growth and Urease Activity of *Helicobacter pylori*. *Jordan J Biol Sci*, **16**: 199 – 206.

Benzie IF, Strain JJ. 1999. Ferric reducing/antioxidant power assay: direct measure of total antioxidant activity of biological fluids and modified version for simultaneous measurement of total antioxidant power and ascorbic acid concentration. Meth. Enzymol. **299**: 15–27.

Chegu K, Mounika K, Rajeswari M, Vanibala N, Sujatha P, Sridurga P, Reddy DRB. *In vitro* study of the anticoagulant activity of some plant extracts. World J Pharm Pharm Sci. **7**: 904-913.

De Man JD, Rogosa M, Sharpe ME. 1960. A medium for the cultivation of Lactobacilli. J Appl Microbiol. **23**: 130-135.

Decker EA, Welch B. 1990. Role of ferritin as a lipid oxidation catalyst in muscle food. J Agric Food Chem. **38**: 674–677.

Desai NM, Martha GS, Harohally NV, Murthy PS. 2020. Non-digestible oligosaccharides of green coffee spent and their prebiotic efficiency. LWT-Food Sci Technol. **118**: 108784.

Dey TB, Kuhad RC. 2014. Upgrading the antioxidant potential of cereals by their fungal fermentation under solid-state cultivation conditions. Lett Appl Microbiol. **59**: 493–499.

Dinis TC, Maderia VM, Almeida LM. 1994. Action of phenolic derivatives (acetaminophen, salicylate, and 5-aminosalicylate) as inhibitors of membrane lipid peroxidation and as peroxyl radical scavengers. Arch Biochem Biophys. **315**: 161–169.

Dorman HJD, Kosar M, Kahlos K, Holm Y, Hiltunen R. 2003. Antioxidant properties and composition of aqueous extracts from Mentha species, hybrids, varieties, and cultivars. J Agric Food Chem. 51: 4563–4569.

Dubois M, Gilles KA, Hamilton JK, Rebers PA, Smith F. 1956. Colorimetric method for determination of sugars and related substances. Anal Chem. **28**: 350-356.

El Azm NA, Fleita D, Rifaat D, Mpingirika EZ, Amleh A, El-Sayed MMH. 2019. Production of bioactive compounds from the sulfated polysaccharides extracts of *Ulva lactuca*: post-extraction enzymatic hydrolysis followed by ion-exchange chromatographic fractionation. Molecules. **24**: 2132.

El-Merzabani MM, El-Aaser AA, Attia MAM, El-Duweini AK, Ghazal AH. 1979. Screening system for Egyptian plants with potential antitumor activity. J Med Plant. **36**: 150–155.

Eskander MZ. 2018. Extraction of polysaccharides from the leaves of Jews-Mallow *Corchorus Olitorius L* and their potential anticoagulant activity. Bas J Vet Res. **17**: 277-290.

Finegold SM, Li Z, Summanen PH, Downes J, Thames G, Corbett K, Dowd S, Krak M, Heber D. 2014. Xylooligosaccharide increases bifidobacteria but not lactobacilli in human gut microbiota. R Soc Chem. **5**: 436–445.

Gibson GR, Probert HM, Loo JV, Rastall RA, Roberfroid MB. 2004. Dietary modulation of the human colonic micro biota: updating the concept of prebiotics. Nutr Res Rev. **17**: 259-275.

Gobinath D, Madhu AN, Prashant G, Srinivasan K, Prapulla SG. 2010. Beneficial effect of xylo-oligosaccharides and fructo-oligosaccharides in streptozotocin-induced diabetic rats. Br J Nutr. **104**: 40-47.

Grigalius I, Petrikaite V. 2017. Relationship between antioxidant and anticancer activity of trihydroxyflavones. Molecules. **22**: 2169- 2181.

Halliwell B. 1997. Antioxidants: the basics- what they are and how to evaluate them. J Adv Pharm. **38**: 3-20.

Helal MMI, Osman MY, Ghobashy MOI, Helmy WA. 2020. Study of some biological activities of aqueous extract of ginger (*Zingiber officinale*). Egypt Pharm J. **13**: 144–150.

Herández-Domínguez EM, Rios-Latorre RA, Alvarez-Cervantes J, Loera-Corral O, Roman-Gutierrez AD, Diaz-Godinez G, Mercado-Flores Y. 2014. Xylanase, cellulase, and acid protease produced by *Stenocarpella maydis* grown in solid- state and submerged fermentation. BioRes. **9**: 2341-2358.

Jayme G, Knolle H. 1956. Paper chromatography of sugar mixtures upon glass fiber paper. Angew Chem. **68**: 243-246.

Kang OL, Ghani M, Hassan O, Rahmati S, Ramli N. 2014. Novel agaro-oligosaccharide production through enzymatic hydrolysis: Physicochemical properties and antioxidant activities. Food Hydrocoll. **42**: 304-308.

Li Pj, Xia J l, Nie Zy, Shan Y. 2016. Pectic o ligosaccharides hydrolyzed from orange peel by fungal multi-enzyme complexes and their prebiotic and antibacterial potentials. LWT-Food Sci Technol. **69**: 203-210.

Lowry OH, Resebrough NJ, Farr AL, Randall RJ. 1951. Protein measurement with the folin phenol reagent. J Biol Chem. **193**: 265-275.

Mohammed RS, El Souda SS, Taie HAA, Moharam ME, Shaker KH. 2015. An tioxidant, antimicrobial activities of flavonoids glycoside from *Leucaena leucocephala* leaves. J Appl Pharm Sci. **5**: 138-147.

Neish AC. 1952**. Analytical Methods for Bacterial Fermentation**, Repor no., 46-8-3, Second Revision, National Council of Canada, 69.

Oyaizu M. 1986. S tudies on pr oducts of browning reactions: Antioxidative activities of product of browning reaction prepared from glucosamine. Jpn J Nutr. **44**: 307-315.

Ozaslan M, Karagoz ID, Kilic I H, Guldur ME. 2011. Ehrlich ascites carcinoma. Afr J Biotechnol. **10**: 2375-2378.

Partridge SM. 1949. Aniline Hydrogen phthalate as spraying reagent for chromatography of sugars. Nature. **164**: 443-446.

Perila O, Bishop PCT. 1961. Enzymatic hydrolysis of a glucomannan from that Jack Pine (*Pinus bank Siniana* LC., MP). Can J Chem. **139**: 815-826.

Pourabedin M, Guan L, Zhao X. 2015. Xylo-oligosaccharides and virginiamycin differentially modulate gut microbial composition in chickens. Microbiome. **3**: 15.

Re R, Pellegrini N, Proteggente A, Pannala A, Yang M, Rice-Evans C. 1999. Antioxidant activity applying an improved ABTS radical cation decolorization assay. Free Radic Biol Med. **26**: 1231–1237.

Riaz S, Nawaz SK, Hasnain S. 2010. Bacteriocins produced by *L. fermentum* and L. *acidophilus* can inhibit Cephalosporin resistant *E. coli*. Braz J Microbiol. **41**: 643-648.

Rivas MÁ, Casquete R, Martín A, Córdoba MdG, Aranda E, Benito MJ. 2021. Strategies to increase the biological and biotechnological value of polysaccharides from agricultural waste for application in healthy nutrition. Int J Environ Res Public Health. **18**: 5937.

Sadik MW, Zohair MM, El-Beih AA, Hamed ER, Sedik MZ.2021. Utilization of Agro-industrial wastes as carbon source in solid state fermentation processes for the production of value-added byproducts. *Jordan J Biol Sci*, **14**: 157 – 161.

Saleh SAA, Abd El-Galil AA, Sakr EAE, Taie HAA, Mostafa FA. 2020. Physiochemical, kinetic and thermodynamic studies on *Aspergillus wewitschiae* MN056175 inulinase with extraction of prebiotic and antioxidant *Cynara scolymus* leaves fructo-oligosaccharides. Int J Biol Macromol. **15**: 1026-1036.

Silva D, Tokuioshi K, Martins ES, da Silva R, Gomes E. 2005. Production of pectinase by solid state fermentation with *Penicillium viridicatum* RFC3. Process Biochem. **40**: 2885-2889.

Silva LAO, Terrasan CRF, Carmona EC. 2015. Purification and characterization of xylanases from *Trichoderma inhamatum*. Electron J Biotechnol. **18**: 307–313.

Suganya T, Siriporn O, Sombat C. 2007. Study on a ntioxidant activity of certain plants in Thailand: Mechanism of antioxidant action of guava leaf extract. Food Chem. **103**: 381–388.

Sun T, Xie WM, Xu PX. 2004. Superoxide anion scavenging activity of graft chitosan derivatives. Carbohyd Polym. **58**: 379–382.

Tezcan F, Kolayl S, Sahin H, Ulusoy E, Erim BF. 2011. Evaluation of organic acid, saccharide composition and antioxidant properties of some authentic Turkish honeys. J Food Nutr Res. **50**: 33–40.

Thetsrimuang C, Khammuang S, Sarnthima R. 2011. Antioxidant activity of crude polysaccharides from edible fresh and dry mushroom fruiting bodies of *Lentinus* sp. Strain RJ-2. Int J Pharmacol. **7**: 58–65.

USA Pharmacopoeia. Pharmacopoeia of United State o f America, 6th Revision. Mack Publishing Company; 1960. 317.

Voragen AGJ. 1998. Technological aspects of functional food-related carbohydrates. Trends Food Sci Tech. **9**: 328-335.

Warzywoda M, Ferre V, Pourquie J. 1983. Development of a culture medium for largescale production of cellulolytic enzymes by *Trichoderma reesei*. Biotechnol Bioeng. **25**: 3005–3010.

Williams WB, Cuvelier ME, Berset C. 1995. Use of a free radical method to evaluate antioxidant activity. LWT-Food Sci Technol. **28**: 25–30.

Wilson CM. 1959. Quantitative determination of sugars on paper chromatograms. Anal Chem. **31**: 1199-1201.

Xiong F, Liang HX, Zhang ZJ, Mahmud T, Chan ASC, Li X, Lan WJ. 2021. Characterization, antioxidant and antitumor activities of oligosaccharides isolated from *Evodia lepta* (Spreng) Merr. by different extraction methods. Antioxidants. **10**: 1842.

Xiong X, Li M, Xie J, Jin Q, Xue B, Sun T. 2013. Antioxidant activity of xanthan oligosaccharides prepared by different degradation methods. Carbohyd Polym. **92**: 1166-1171.

Yang C, Hu C, Zhang H, Chen W, Deng Q, Tang H, Huang F. 2020. Optimation for preparation of oligosaccharides from flaxseed gum and evaluation of antioxidant and antitumor activities *in vitro*. Int J Biol Macromol. **153**: 1107-1116.

Yazid NA, Barrena R, Komilis D, Sánchez A. 2017. Solid-State Fermentation as a novel paradigm for organic waste valorization: A review. Sustainability. **9**: 224.

Zhang ZM, Zhang YS, Liu H, Wang JH, Wang D, Deng ZW, Li TH, He Y, Yang YJ, Zhong SA. 2021. A water-soluble selenium-enriched polysaccharide produced by *Pleurotus ostreatus*: Purification, characterization, antioxidant, and antitumor activities in vitro. Int J Biol Macromol. **168**: 356–370.

JJBS

Volume 17, Number 1,March 2024
ISSN 1995-6673
Pages 197 – 205
https://doi.org/10.54319/jjbs/170119

Jordan Journal of Biological Sciences

The Effect of Anthocyanins Black Rice Bran Extract (ABRiBE) on Colorectal Cancer Cell Proliferation and ABCA1 Gene Expression in the HT-29 Cell Line

Wiza Iswanti[1], Karina Rahmadia Ekawidyani[1,2], Asmarinah[3,4], Slamet Budijanto[5], Murdani Abdullah[1,6,7,8]

[1]*Department of Nutrition, Faculty of Medicine, Universitas Indonesia,–Dr. Cipto Mangunkusumo General Hospital, Jakarta 10430, Indonesia;* [2]*Department of Community Nutrition, Faculty of Human Ecology, IPB University, Dramaga, Bogor 16680, Indonesia;* [3]*Department of Medical Biology, Faculty of Medicine, Universitas Indonesia, Jakarta 10430, Indonesia;* [4]*Molecular Biology Unit, Integrated Laboratory Faculty of Medicine, Universitas Indonesia, Jakarta 10430, Indonesia;* [5]*Department of Food Science and Technology, Faculty of Agricultural Technology, IPB University, Dramaga, Bogor 16680, Indonesia;* [6]*Human Nutrition Research Center, Indonesian Medical Education and Research Institute (IMERI), Faculty of Medicine, Universitas Indonesia, Jakarta 10430, Indonesia;* [7]*Human Cancer Research Center, Indonesian Medical Education and Research Institute (IMERI), Faculty of Medicine, Universitas Indonesia, Jakarta 10430, Indonesia;* [8]*Division of Gastroenterology, Pancreatobiliary and Gastrointestinal Endoscopy, Department of Internal Medicine, Faculty of Medicine, Universitas Indonesia,–Dr. Cipto Mangunkusumo General Hospital, Jakarta 10430, Indonesia*

Received: March 5, 2023; Revised: August 28, 2023; Accepted: September 15, 2023

Abstract

Background: Anthocyanins inhibit colorectal cancer cell proliferation and cholesterol levels regulation by interacting with the adenosine triphosphate-binding cassette subfamily A member 1 (ABCA1) protein, expressed at reduced levels in colon cancer. Anthocyanins can also increase the efflux of cholesterol from cancer cells and are present in Indonesian native black rice bran. Therefore, this study investigated the effect of Anthocyanin Black Rice Bran Extract (ABRiBE) on the mRNA expression of the ABCA1 gene and the proliferation of colorectal cancer cells in the human HT-29 cell line. The hypothesis is that ABRiBE inhibits HT-29 cell proliferation and increases ABCA1 gene expression.

Methods: This experimental study on the HT-29 cells used anthocyanins extracted from black rice bran powder through ethanol acidified with citric acid. The MTS assay measured the inhibitory concentration (IC_{50}) of 50% cell proliferation inhibition using 12 extract concentrations and control groups for 24 and 48 hours. The ABCA1 gene expression in groups above the antiproliferative IC50 value and the control group was analyzed using the quantitative Polymerase Chain Reaction (qPCR) method.

Results: The IC_{50} of black rice bran extract was 1.57 and 1.35 mg/mL for 24 and 48 hours of incubation, which decreased HT-29 cell proliferation with values of (r= 0.97, p=0.001 and r=0.95, p=0.001), respectively. Extract exposure of the 2 concentrations above the IC_{50} values of 1.7 and 2.0 mg/mL increased ABCA1 gene expression in HT-29 cells, by 1.16 and 2.32 fold compared to the control group.

Conclusion: The ABRiBE inhibited HT-29 cell proliferation and increased the ABCA1 gene expression.

Keywords: Anthocyanins; ABCA1 Gene; Black Rice Bran Extract; HT-29 Cell Line; Proliferation

1. Introduction

Colorectal cancer is among the top ten cancers contributing to cancer-related deaths. In 2020, a total of 1,931,590 incidences and 935,173 mortalities of colorectal cancer were reported (Sung *et al.*, 2021), with both increasing by 130,613 and 54,173 from 2018, respectively (Bray *et al.*, 2018). Globally, colorectal cancer ranks third and second in incidence and mortality compared to other cancers (Sung *et al.*, 2021). The increase can be influenced by changes in dietary patterns (Sung *et al.*, 2021), such as the consumption of red or processed meat, a high-fat diet, and alcohol(WCRFI, 2018).

According to Katona and Weiss (2020), chemoprevention can help reduce the incidence and mortality of colorectal cancer. The agents used for chemoprevention can either be drugs or natural substances, such as anthocyanins, which are being studied for their potential to prevent the development of colorectal cancer (Katona and Weiss, 2020). Anthocyanins are natural pigments that belong to the flavonoid family and exist in a glycosylated form (Martin *et al.*, 2017; Khoo *et al.,* 2017). Anthocyanins are natural pigments that give fruits, flowers, and whole-grain rice red, purple, blue, brown, and black coloring (Martin *et al.*, 2017; Khoo *et al.,* 2017). The high anthocyanins content is primarily found in berries, such as grapes, currants, and tropical fruits like dragon fruit skin (Khoo *et al.,* 2017). In Indonesia, one of the foodstuffs with high anthocyanins is black rice, the primary staple food of the population. The country is the largest producer of pigmented rice, especially black rice, after China and India (Prasad *et al.*, 2019). Cempo Ireng is an Indonesian black rice with the highest total anthocyanin content compared to other varieties, with 428.38 mg/100g. This is almost equivalent to the anthocyanin content of

blueberry*Vaccinium corymbosum* (CVAC5.001 cultivar) (430 mg/100g) (Kristamtini and Wiranti, 2017; Peña-Sanhueza *et al.,* 2017). Thus, black rice can be an alternative source of rich anthocyanins, particularly in areas where blueberries are not readily available.

Most in vitro studies on colorectal cancer cell lines use extracts containing anthocyanins from berries. Afrin *et al.* (2016) found that freeze-dried extract of black raspberry, administered at doses of 0.6 and 1.2 mg/mL, demonstrated anticancer activity on HT-29 cells after 48 hours of incubation. Meanwhile, this study is a novel contribution to the field due to limited in vitro examinations on human colorectal cancer cell lines using ABRiBE. Anthocyanins affect colon cancer chemopreventive through the mechanism of antioxidant, antiproliferation, induction of apoptosis, anti-invasive activity, gene demethylation, anti-inflammation, and microbiota (Shi *et al.,* 2021). In HCT 116 and HT-29 cell lines, cyanidin-3-O-glucoside and delphinidin-3-O-glucoside as anthocyanin's single compounds reduced EGFR (Shi et al., 2021; Mazewski *et al*., 2018).

The level of ABCA1 in human colorectal cancer cells is lower than the ABCA1 level in healthy cells (Lo Sasso *et al.,* 2017; Hlavata *et al.,* 2012). Previous reports have shown that anthocyanins can increase the mRNA expression of the ABCA1 gene through the Peroxisome Proliferator-Activated Receptor α (PPARα) and Liver X Receptor α (LXRα) pathways by promoting intracellular cholesterols efflux (Xia *et al.,* 2005). Intracellular cholesterols accumulation is associated with the pathogenesis of colorectal cancer (Smith and Land, 2012). According to Xia *et al.* (2005), anthocyanins can increase cholesterols efflux through the ABCA1 transporter protein. The high mRNA and protein expression of ABCA1 may reduce tumor formation in human colorectal cancer cell lines (Pasello *et al.,* 2020). Mazewski *et al.* (2018) also discovered that increased ABCA1 protein by anthocyanins exposure inhibits cancer cell proliferation. The increase of anthocyanin-modulated mRNA expression of the ABCA1 gene can enhance the elimination function of ABCA1 protein-mediated cholesterols and reduce Akt-dependent survival signaling that contributes to anticancer activity (Smith and Land, 2012). Subfamily A of ABC transporters for tumorigenesis affects the stage of cancer initiation and progression (Hlavata *et al.,* 2012; Pasello *et al.,* 2020).

The effect of ABRiBE on cell proliferation in colorectal cancer cell lines requires the determination of an IC_{50}. Although several studies have been conducted using anthocyanin-rich foods on cell lines (Afrin *et al.*, 2016), limited experiments have used black rice bran extract. Additionally, little information is available on the impact of ABRiBE on cell proliferation and ABCA1 gene expression in human colorectal cancer cell lines. Therefore, this study aimed to investigate the effects of ABRiBE on the proliferation of colorectal cancer cells and the mRNA expression of the ABCA1 gene using the HT-29 cell line.

2. Materials and Methods

The study was approved by the Health Research Ethics Committee, Ethics Number: KET−841/UN2.F1/ETIK/PPM.00.02/2020, Faculty of Medicine Universitas Indonesia and Cipto Mangunkusumo Hospital (HREC−FMUI/CMH).

2.1. Black Rice Bran Extraction

The Cempo Ireng black rice used in the study was obtained from a local farmer, Mr. Murji, located in Cigudeg, Bogor, West Java, Indonesia. The materials prepared for extraction included black rice bran powder obtained from grinding, 96% ethanol, and 20% citric acid (w/v). The procedures and reagents used for extraction have been declared safe by the National Agency of Drug and Food Control (NA-DFC) of Indonesia, as per Quality Requirements for Health Supplements No. 17 of 2019. The black rice bran and ethanol-citric acid mixture (1:10, w/v) were macerated for 24 hours at room temperature in a dark room. The black rice bran powder was homogenized in the first two hours and the last two hours of the 24 hours of maceration time. The extract was filtered using Advantec® Toyo Qualitative Filter Paper No. 5B (Advantec Toyo Kaisha, LTD., Tokyo, Japan), and the filtrate was evaporated at a temperature of 50°C using an IKA® HB10 Vacuum Rotary Evaporator (VirtualExpo Group, UK)at a speed of 30 rpm with an IKA® RV10 Digital Vacuum Rotary Evaporator (VirtualExpo Group, UK)until the ethanol had completely evaporated. Subsequently, the extract was dried using a freeze dryer for 72 hoursand stored in a freezer at -20°Cuntil used.

2.2. HT-29 Cell Line Propagation

The human colorectal cancer cell line (HT-29), on its 21st passage, was obtained from the Research Center for Virology and Cancer Pathobiology at the Faculty of Medicine, Universitas Indonesia and Dr. Cipto Mangunkusumo General Hospital. The HT-29 cell line was propagated using protocols from the Molecular Biology and Proteomics Core Facilities (MBPCF) at the Indonesia Medical Education and Research Institute (IMERI) and the Culture Unit Protocol at the Integrated Laboratory of the Faculty of Medicine, Universitas Indonesia. The cells were cultured in 90% Dulbecco's Modified Eagle Medium (DMEM) supplemented with 10% Fetal Bovine Serum (FBS), 1% penicillin-streptomycin, and 1% amphotericin. Furthermore, the cells were incubated at 37°C in 95% air/5% Carbon Dioxide (CO_2) and a water-saturated atmosphere. They were grown up to 80% confluence and divided into 72 wells using a 96-well plate for antiproliferative activity examination. Subsequently, the cells were calculated at $1x10^4$ per well. The cells for analysis of gene expression were divided into 9 wells using a 12-well plate and were calculated at $25x10^4$ per well.

2.3. Determination of the Antiproliferative Activity of HT-29 Cells

The effect of ABRiBE on colorectal cancer cell proliferation was determined using the MTS assay with CellTiter 96® AQueous Non-Radioactive Cell Proliferation Assay (MTS), catalog number selected: G5421 (Promega Corporation, Wisconsin, USA). The assay was performed following the Culture Unit Protocol established by the Integrated Laboratory of the Faculty of Medicine at Universitas Indonesia. The frozen extract of black rice bran was thawed and diluted to 12 concentrations of 0.0125, 0.025, 0.05, 0.1, 0.2, 0.4, 0.8, 1.6, 2.0, 2.4, 2.8, and 3.2 mg/mL. There were 3 groups on the antiproliferative

activity of colorectal cancer cells examination, namely the experiment, the negative control, and the blank groups. Each group was conducted in triplicate, where the experimental group consisted of plates filled with $1x10^4$ HT-29 cells per well and exposed to black rice bran extract. All groups were incubated for 24 a nd 48 hours independently after exposing the extract. The absorbances were read by spectrophotometric at wavelength 490 nm and the cell viability was calculated using the formula below

$$Cell\ viability/cell\ proliferation\ activity\ (\%) = \frac{A_E - A_B \times 100\%}{A_{NC} - A_b} \quad (1)$$

in which,

A_E= The absorbance value of the experiment group at the concentration χ

A_{NC}= The absorbance value of the negative control group

A_B= The absorbance value of the blank group

The cell viability was calculated per each extract concentration intervened to HT-29 cells.

The antiproliferative activity of colorectal cancer cells was the inhibition of colorectal cancer cell proliferation. It was determined using the result from the formula in equation (1) above.

The formula for calculating the antiproliferative activity of the colorectal cancer cells was:

Inhibition/antiproliferative activity (%)=$100\%_{NC}$–$\%_{Conc.\chi}$ cell viability at concentration χ (2)

where:

$100\%_{NC}$= 100% of cell viability resulted from the negative control group

$\%_{Conc.\chi}$ = % Cell viability at concentration χ (% the result from equation (1) calculation)

The value of the inhibition percentage was used to determine the Inhibitory Concentration (antiproliferative IC).

2.4. IC_{50} Determination

The IC_{50} value was obtained by inputting the inhibition percentage and the IC i nto the Microsoft Excel Spreadsheet Software. The antiproliferative IC_{50} value was obtained from the linear regression line equation, y = a+bχ. The determination of antiproliferative IC_{50} value referred to Culture Unit Protocol, Integrated Laboratory Faculty of Medicine, Universitas Indonesia. The linear regression line equation emanated from the linear trendline. The antiproliferative IC_{50} value was also calculated manually from y = a+bχ, which details were:

χ = Concentration of ABRiBE (mg/mL)

y = Inhibition/ antiproliferative activity (%)

$$a = Constantan\ \left(a = \frac{\Sigma y.\Sigma x^2 - \Sigma x.\Sigma xy}{n\Sigma x^2 - (\Sigma x)^2}\right)$$

$$b = Slope\ coefficint\ \left(b = \frac{n(\Sigma xy) - \Sigma x.\Sigma xy}{n\Sigma x^2 - (\Sigma x)^2}\right)$$

The antiproliferative IC_{50} value was based on 24 and 48 hours of incubation time independently after exposing the extract.

2.5. HT-29 Cell Line's Population Doubling Time (PDT)

The PDT of the HT-29 cell line used the serial culture technique to determine the current PDT of the HT-29 cell line at the 21st passage. The PDT of t he HT-29 cell line was carried out through several methods that referred to Culture Unit Protocol, Integrated Laboratory Faculty of Medicine, Universitas Indonesia. Those steps are explained below.

2.5.1. Culture of HT-29 Cells

A total of 1.2 x 10^5 HT-29 cells were inserted into a 12-well plate containing a complete DMEM, consisting of the full medium composition of 1 0% FBS, 1% penicillin-streptomycin, 1% amphotericin, and 1% ge ntamicin. This was carried out with 3 r epetitions, and the examination was conducted for 24, 48, 72, 96, 168, 192, 216, 240, and 264 hours. Cells incubation was carried out in an incubator with a temperature of 37 °C and 5% CO_2. The cells were harvested from the culture before serial culture and PDT calculation. Harvesting the culture was repeated according to the amount of examination time.

2.5.2. PDT Calculation

The PDT was calculated on the following formula:

$$PDT = \frac{\Sigma t}{n} = \frac{\Sigma t}{\frac{(logNe - log\ No)}{log\ (2)}} = \frac{\Sigma t \times 0.301}{(log\ Ne - LogNo)} \quad (3)$$

in which,

∑t= Total observation time

n= The number of doubling cells population

N_e= The number of viable cells at the end of observation

N_0= The number of viable cells at the beginning of the observation

The experiment was conducted from 3 groups , consisting of 2 gr oups using the concentration above antiproliferative IC_{50} value and the control group. Each group was conducted in triplicate.

2.6. mRNA Expression of ABCA1 Gene

2.6.1. 2.6.1 RNA Extraction and cDNA Synthesis

A total of $25x10^4$ HT-29 cells per well were prepared for mRNA expression analysis of the ABCA1 gene. HT-29 cells were treated with black rice bran extract and incubated for 48 hours. RNA was extracted from the lysate homogenate using the QIAamp® RNA Blood Mini Kit (Qiagen, Hilden, Germany). The purity and RNA concentration was determined using NanoDrop™ 2000 Spectrophotometer (ThermoFisher Scientific, UK) at wavelength 260 and 280 nm. The RNA purity at A_{260}/A_{280} of 2 and the final concentration of RNA as high as 100 ng/ 20 µL was used for cDNA synthesis. cDNA was synthesized using SensiFAST™ cDNA Synthesis Kit (Bioline Ltd, UK).

2.6.2. Relative Quantification of RT-qPCR

The primer for qPCR was designed by the Integrated Laboratory of the Faculty of Medicine, Universitas Indonesia, Dr. Cipto Mangunkusumo General Hospital, namely the human HRPT1 gene as a reference gene and the ABCA1 gene as the target gene (Table 1).

Table 1. The primer pair sequence of target and reference genes and their amplicon sizes.

Gene Name	**Accession** Number	Primary Sequence (Forward)	Primary Sequence (Reverse)	Amplicon Size
Human HRPT1	NM_024529.5	CCAGTACCAAGACCAGTTTCTC	GGTGGTAGCTGCAGGAATTAT	93 bp (base pair)
Human ABCA1	NM_005502.4	GGTGGTGTTCTTCCTCATTACT	CCGCCTCACATCTTCATCTT	112 bp

Relative quantification using RT-qPCR was performed with the QuantiTect® SYBR® Green PCR Kit (Qiagen, Hilden, Germany). The relative quantification by RT-qPCR was optimized and measured by Livak' method, i.e. 2^-(ΔΔCt) equation as fold gene expression.

The reaction mixture consisted of 2x QuantiTect® SYBR® Green PCR Master Mix, 10 µM forward primer, 10 µM reverse primer, 2.0 µL of cDNA template, and RNase-free water. The initial activation stage of PCR was carried out at a temperature of 95°C for 15 minutes. Denaturation, annealing, and extension were performed 40 times at 94°C for 15 seconds, 58°C for 30 seconds, and 72°C for 30 seconds. The final extension was carried out at 72°C for 3 minutes. A melting curve was performed after the amplification, which was obtained from a slope of 72 to 95 degrees.

2.7. Statistical Analysis

This study was analyzed descriptively and inferentially. The data were processed using Microsoft Excel Spreadsheet Software and Statistical Package for Social Science (SPSS) software version 23. The linear regression line equation was obtained from a linear trendline, available at Microsoft Word trendline layout. The r-value was obtained from the formed chart of a linear regression line equation. The p-value for the correlation of black rice bran extract and antiproliferative activity was analyzed with linear regression using SPSS software.

3. Results

3.1. ProliferativeActivityofHT-29Cells

The influence of black rice bran extract was determined through the percentage value of colorectal cancer cell proliferation activity in each concentration of ABRiBE.The freeze-dried black rice bran extract consists of 12 concentrations used to determine the percentage value of colorectal cancer cell proliferation activity: 0.0125, 0.025, 0.05, 0.1, 0.2, 0.4, 0.8, 1.6, 2.0, 2.4, 2.8, and 3.2 mg/mL. The percentage of colorectal cancer cell proliferation activity was calculated based on incubation time after exposing the extract to the cells for 24 and 48 hours, independently.

The effect of exposing various concentrations of ABRiBE into the cells tended to lower the proliferation of colorectal cancer cells. Exposing the black rice bran extract into the cells exhibited the derivation trend of colorectal cancer cell proliferation at both incubation times (Figure 1). This study found that a longer incubation time of 48 hours compared to 24 hours after administering the extract improved ABRiBE in reducing the proliferation of colorectal cancer cells, especially at higher concentrations of HT-29 cells. After 48 hours of incubation, the extract showed a significant decrease in the proliferation of colorectal cancer cells compared to the 24 hours of intervention. The difference in proliferation between the two incubation times was observed at extract concentrations above 1.5 mg/mL.

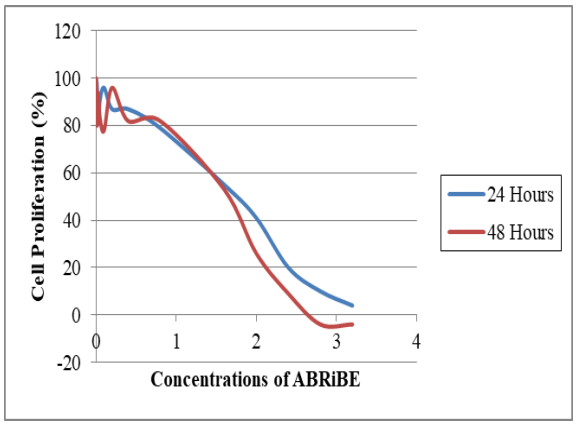

Figure 1. The trend of colorectal cancer cell proliferation activity after exposing the ABRiBE.

3.2. AntiproliferativeActivityofHT-29Cells

The percentage of colorectal cancer cell proliferation inhibition was calculated based on incubation time after independently exposing the extract to the cells for 24 and 48 hours (Table 2). The results were based on equation (2).Antiproliferative activity of HT-29 cells was determined from three groups namely the experiment group, the negative control group, and the blank group. The experiment group was the plates filled with $1x10^4$ HT-29 cells per well and exposed to black rice bran extract. Each extract concentration was intervened to well containing HT-29 cells. The negative control group was the plates filled with $1x10^4$ HT-29 cells per well and did not expose to black rice bran extract. The blank group contained only medium.

Table 2. Percentage of inhibition of colorectal cancer cell proliferation after exposing the ABRiBE.

Extract Concentrations (mg/mL)	24 Hours (%)	48 Hours (%)
Control	0	0
0.0125	3	20
0.025	19	6
0.05	9	17
0.1	4	22
0.2	13	4
0.4	13	18
0.8	21	18
1.6	45	47
2.0	59	74
2.4	80	91
2.8	90	104
3.2	96	104

3.3. Antiproliferative IC_{50}

The IC_{50} value is the extract concentration that can suppress cell proliferation by 50% of the total cells and is obtained from the linear regression line equation, y = a+bχ.This study obtained the antiproliferative IC_{50} value from the linear regression line equation for each incubation time, 24 and 48 hours independently after exposing the extract.

The antiproliferative IC_{50} value at the 24 hours of incubation time was obtained by inserting the value 50 into y in the linear regression line equation formed, y = 29,014χ + 4,4442 (Figure 2). 50 = 29.014χ + 4.4442. Therefore, the antiproliferative IC_{50} value based on 24 hours of incubation time was 1.57 mg/mL, which was the χ value from the equation calculation. The r-value was 0.95, indicating that the concentration of A BRiBE had a very strong positive correlation with antiproliferative activity. The p-value was 0.001, showing that there was an influence of the various concentrations of ABRiBE on the antiproliferative activity.

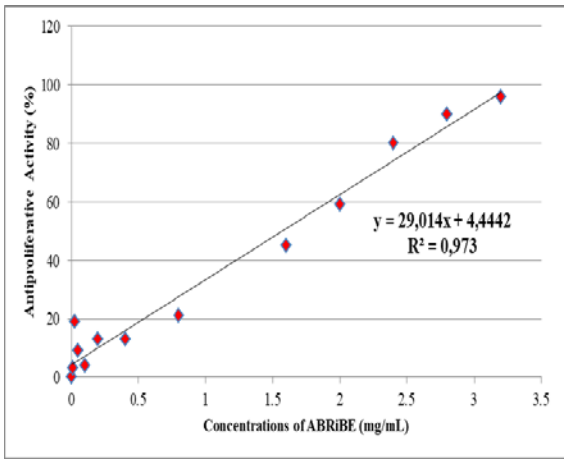

Figure 2. Antiproliferative IC_{50} is based on the incubation time of 24 hours.

The linear regression line equation of the antiproliferative IC_{50} formed at the 48 hours of incubation time was y = 31.828x + 7.1181 (Figure 3). Therefore, the antiproliferative IC_{50} was 1.35 mg/mL, which was the x value from the equation calculation. The r-value was 0.97, indicating that the concentration of A BRiBE had a very strong positive correlation with antiproliferative activity. Meanwhile, the p-value was 0.001, showing that there was an influence of the various concentrations of ABRiBE on the antiproliferative activity.

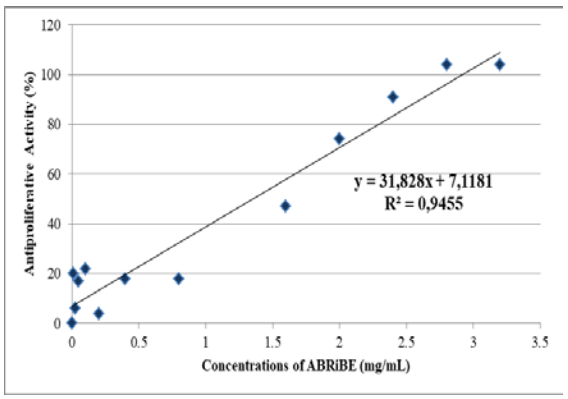

Figure 3. Antiproliferative IC_{50} is based on the incubation time of 48 hours.

3.4. PDT of HT-29 Cells

The current PDT of t he HT-29 cell line at the 21st passage was 68.74 hours (Figure 4). PDT was examined through 2 groups using the concentration above the antiproliferative IC_{50} value and the control group. PDT value resulted from $\frac{\Sigma t}{n}$ calculation.

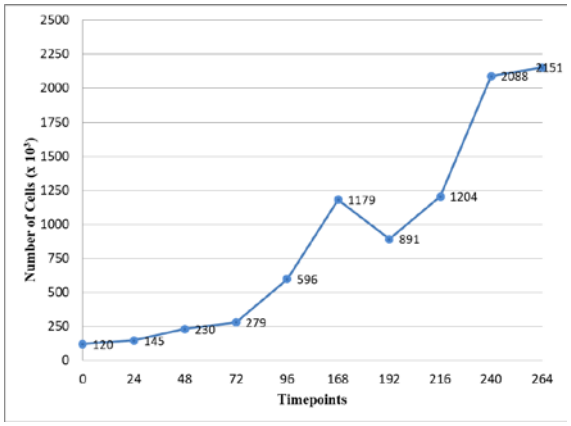

Figure 4. The HT-29 cell line growth curve at the 21st passage.

3.5. mRNA expression of ABCA1 gene

The mRNA expression analysis of t he ABCA1 gene used 2 c oncentrations above the IC_{50} value as the treatment group, namely 1.7 mg/mL and 2.0 mg/mL. HT-29 cells totaling $25x10^4$ per well were treated with black rice bran extract and incubated for 48 hours.There were 3 groups in the gene expression analysis, consisting of 2 treatments and a control group. The RNA purity of e ach group at 2 wavelengths, 260 and 280 nm, was 2. The value of 2 on RN A purity proved that it is pure. The final concentration of RNA for cDNA synthesis was 100 ng/20 µL, which indicated 100 ng RN A in 20 µL of the final total volume.

There was an increase in the mRNA relative expression of the ABCA1 gene of the HT-29 cells at both concentrations after exposing the ABRiBE compared to the control group. The results of this relative quantification are in a fold gene expression. The results showed that exposing HT-29 cells to 1.7 and 2.0 mg/mL ABRiBE led to a 1.16 and 2.32 fold increase, respectively, in the mRNA relative expression of the ABCA1 gene compared to the control group (Figure 5).

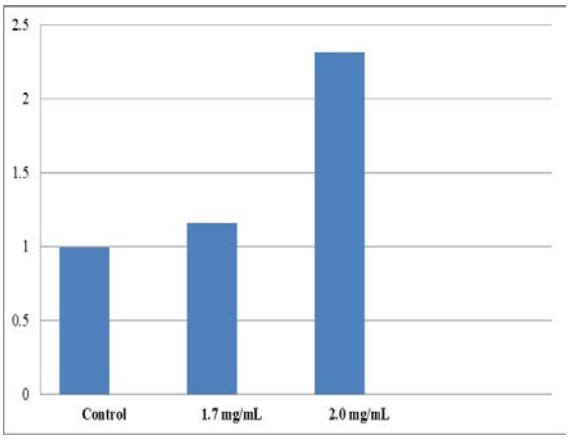

Figure 5. The mRNA relative expression of the ABCA1 gene

4. Discussion

A total of 12 concentrations of ABRiBE were dissolved in ethanol and 20% citric acid, namely 0.0125, 0.025, 0.05, 0.1, 0.2, 0.4, 0.8, 1.6, 2.0, 2.4, 2.8, and 3.2 mg/mL. Meanwhile, 8 concentration ranges, including 0.0125, 0.025, 0.05, 0.1, 0.2, 0.4, 0.6, and 0.8 mg/mL were used to obtain an IC_{50} of 0.2 mg/mL from the B16-F10 cell line after exposing the anthocyanins blueberry extract dissolved in 70% ethanol and acidified using HCl 0.1% (Wang *et al.,* 2017). Thus, if the extract in this study was acidified with HCl, the concentration range became narrower, and the IC_{50} produced was also smaller. This made the selection of black rice bran powerful and provided more satisfactory results in reducing the cell proliferation of colorectal cancer and increasing the expression of ABCA1 mRNA.

Colorectal cancer cell proliferation tended to decrease after exposing various concentrations of ABRiBE. The use of the HT-29 cell line model by Zhao *et al*. (2019) showed that anthocyanins were able to inhibit the cell proliferation of colorectal cancer. It was discovered that at 48 hours of exposing various concentrations of ABRiBE, the proliferation of colorectal cancer cells significantly reduced compared to 24 hours, with a high concentration of the extract exposed on HT-29 cells. Various concentrations of anthocyanins blueberry extract exhibited an increasing antiproliferative activity and lowered cell proliferation as well as the B16-F10 melanoma cell line with 48 hours of incubation time after exposing extract decreased than 24 hours (Wang *et al*., 2017). Indonesian Cempo Ireng black rice bran extract exhibited cell proliferation or viability decreased and antiproliferative activity increased on T47D cells (human epithelial breast cancer cell line) and HeLa cells (human cervical cancer cell line), which were incubated for 24 and 48 hours with various concentrations of extract (Pratiwi *et al*., 2019 and Pratiwi *et al*., 2015). Paudel *et al*. (2014)also reported that citric acid significantly contributed to the antiproliferative activity of the berry extract. However, the mechanism of citric acid in controlling colon cancer cell proliferation had not been elucidated. Based on previous investigations, 70% (v/v) ethanol and 5% (w/v) citric acid were found to be the most effective solutions in extracting bioactive compounds with antiproliferative effects on HCT-15 and HepG2 cancer cell lines from black sorghum bran extract as well as commercial sumac sorghum bran extract. These solutions were effective in inhibiting cancer cell proliferation in both cancer cell lines (Cox *et al.,* 2019).

The antiproliferative IC_{50} value of the extract was determined by the concentration that can suppress cell proliferation by 50% of the total cells. Based on the results, an antiproliferative IC_{50} value of 1.57 mg/mL was obtained after exposure to the ABRiBE at an incubation time of 24 hours . This is not significantly different from the study conducted by Konczak *et al*. (2012) where the IC_{50} values of quandong fruit extract, Davidson plum, rabbiteye blueberry, and southern highbush blueberry containing anthocyanins exposed to HT-29 cells were 1.88, 1.35, 1.51, and 0.93 mg/mL, respectively. Mazewski *et al*. (2018) also reported that antiproliferative IC_{50} values of black lentil, sorghum, and red grape exposed to HT-29 cells were 1.40, 1.70, and 2.00 mg/mL, respectively. According to Konczak *et al*. (2012) and Mazewski *et al*. (2018) the IC_{50} value was determined using an incubation time of 24 hours after exposing the extract. In this study, the black rice bran extract was more potent in its influence on the antiproliferation of HT-29 cells. This was shown by a lower IC_{50} value of 1.57 mg/mL compared to the other two potent extracts, namely sorghum and red grape with values of 1.70 and 2.00 mg/mL, respectively according to Mazewski and 1.88 mg/mL Quandong fruit, as stated by Konczak(Mazewski *et al.,* 2018, Konczak *et al.,* 2012).

All the 11 foodstuffs extracted by Mazewski *et al*. (2018) including black rice were exposed using a concentration of 2.5 mg/mL in HT-29 cells, which was the IC_{50} of red corn extract. Meanwhile, only 3 extracts with the highest percentage of colorectal cancer cell proliferation inhibition were examined for IC_{50}. The IC_{50} of black rice was not examined because the inhibition percentage of HT-29 cells was small, but it had the highest total anthocyanin content and Total Phenolic Content (TPC) among other extracts. The 3 essential parameters that influenced the high of colorectal cancer cells inhibition according to Mazewski *et al*. (2018) were the content of delphinidin-3-O-glucoside, TPC, and total condensed tannin. These parameters showed a strong correlation with the inhibition of colorectal cancer cells (r=0.69; r=0.87; r=0.77, respectively). Black rice contained cyanidin-3-O-glucoside and peonidin-3-O-glucoside (Yawadio *et al.,* 2007). Black rice was not the most potent foodstuff in inhibiting HT-29 cell proliferation in the study by Mazewski. This was because black rice did not have delphinidin-3-O-glucoside and high total condensed tannin, which is a family of phenolics. The high content contained in black lentil was TPC and condensed tannin. However, the IC_{50} yielded by black rice bran extract in this study was more potent than sorghum and red grape extract. These two extracts were potent among others with the highest inhibition percentage. The smaller IC_{50} value in black rice bran extract made it more potent compared to others, showing that the ABRiBE was potent. This is based on the principle that the lower the IC_{50} value, the more potent the influence of the extract on the inhibition of colorectal cancer cell proliferation.

Only pure anthocyanins such as delphinidin-3-O-glucoside had not been able to inhibit colorectal cancer cells (Mazewski *et al.,* 2018; Zhang *et al.,* 2005). However, crude extracts containing various anthocyanins and other phenolic compounds had a potential synergistic

effect in inhibiting colorectal cancer cells (Mazewski *et al.,* 2018). The inhibition process required extract with high concentration, particularly advanced colorectal cancer cells such as HT-29. HT-29 cells required higher concentration due to the resistance of the cancer cells(Mazewski *et al.,* 2018). Mazewski *et al.*(2018) used an extract concentration of 1. 0 mg/mL to intervene on HCT 116 c ells, which are early developmental colorectal cancer cells. The IC_{50} values of re d corn extract in the HCT 116 a nd HT-29 cell lines were 0.1 and 2.5 mg/mL, respectively (Mazewski *et al.,* 2018).

In this study, the antiproliferative IC_{50} value based on incubation time of 48 hours after exposing the ABRiBE was 1.35 mg/mL, and a comparative analysis was not discovered for time. The inhibition of cancer cells by 50% of the total cells, namely antiproliferative IC_{50}, can be achieved by giving a lower extract concentration of 1. 35 mg/mL. Higher IC_{50} of the extract was associated with less antiproliferative effect. Concentrations of A BRiBE were very strong positive correlation with antiproliferative activity at both incubation times of 24 a nd 48 h ours. ABRiBE exerts a greater effect on colorectal cancer cells that have had a longer (48 hour s) incubation period after being exposed to the extract. The antiproliferative IC_{50} values in colorectal cancer cells after exposing anthocyanins-rich extracts varied based on the types of human cancer cell lines, the anthocyanins sources used, and the cells' incubation time after exposing the extracts.

PDT of HT-29 cells at the first passage was approximately 23 hours, with the viable cells plated at $5x10^4/cm^2$ (ATCC, 2012). The results showed that the PDT of t he HT-29 cell line at the 21st passage was 68.74 hours. This indicated that the higher the passages of t he cell line are, the longer the PDT is. The purity of nucleic acids and proteins was determined from the ratio of t he maximum absorbance at wavelengths of 260 a nd 280 nm, respectively (Matlock, 2015). The absorbance at both wavelengths in each group was 2; therefore, the RNA was declared pure (Matlock, 2015). The final concentration for cDNA synthesis ranged from 10-100 ng from the initial total RNA concentration (Affymetrix, 2015). The final concentration for cDNA synthesis was 100 ng, with a final total volume of 20 µL (Affymetrix, 2015).

ABCA1 gene mRNA expression increased in HT-29 cells after exposing the ABRiBE. Similarly, Du *et al*. (2015) discovered that anthocyanins increased the expression of ABCA1 mRNA on H K-2 cells. The increased expression also occurred in MPM cells after exposing the anthocyanins-rich extract (Xia *et al.,* 2005). This indicated that anthocyanins exposed to cell lines can increase the expression of the ABCA1 mRNA. It had been suggested that anthocyanins activate PPARα and LXRα to increase mRNA expression of ABCA1 gene. It also reduces cholesterols accumulation by increasing intracellular cholesterols efflux through the ABCA1 transporter protein (Xia *et al.,* 2005; Du *et al.,* 2015). Generally, intracellular cholesterols levels are regulated by LXRα with mediating ABCA1 mRNA expression, which binds to the LXR element as the promoter of t he ABCA1 gene (Venkateswaran *et al.,* 2000). LXR is a member of the PPAR nuclear receptor superfamily that regulates mRNA expression of t he ABCA1 gene and plays an essential part in lipid metabolism (Schmitz and Langmann, 2005; Nakaya *et al.,* 2011). Anthocyanins-rich black rice extract of 31 .3 g/100 g de tected in rat plasma reduced triacylglycerol, LDL cholesterol, and cholesterol level (Zawistowski *et al.,* 2009; Ahuja *et al.,* 2008). An investigation conducted by Tsuda *et al*. (2006)on human adipocytes using anthocyanins also found a n increased UCP2 gene expression. Wang *et al*.(2012) demonstrated that the cyanidin-3-O-β-glucoside of pure anthocyanins was gut microbiota dependent. The gut microbiotas converted cyanidin-3-O-β-glucoside from anthocyanins to protocatechuic acids. Protocatechuic acids intervened in MPM and THP-1 cells increased mRNA expression of the ABCA1 gene by suppressing miR-10b level, thereby increasing the cholesterols efflux from macrophages (Wang *et al.,* 2012). ABCA1 mRNA and protein were also found in macrophages, which played a key role in cholesterols efflux from macrophages and the other cells (Tall *et al.,* 2002).

The expression of higher ABCA1 mRNA and protein reduced cholesterols accumulation through PPARα and LXRα pathways (Du *et al.,* 2015). Anthocyanins also increased the mRNA expression of t he ABCA1 gene through these pathways (Du *et al.,* 2015). During this process, PPAR-α functioned as the first regulator of t he reverse cholesterol transport pathway through the ABCA1 protein-mediated cholesterols efflux regulation (Pasello *et al.,* 2020). It activates LXRα, and LXRα activates LXR, which acted as a cholesterol homeostasis sensor in a heterodimeric complex with Retinoid X Receptor (RXR) (Pasello *et al.,* 2020). LXR and RXR were activated by oxysterol and 9-cis-retinoic acid, respectively (Pasello *et al.,* 2020). The direct repeat response element (DR-4) binds to the LXR receptor and the heterodimeric receptor pair, LXR, and RXR. Subsequently, DR-4, LXR, and RXR increase ABCA1 mRNA expression, which escalates the ABCA1 transporter protein. ABCA1 protein played a role in cholesterols efflux (Pasello *et al.,* 2020) and acted a transporter carrying out the cholesterols from intracellular to extracellular, which was accumulated in the tumor cells. The ABCA1 protein mediated the biogenesis of High-Density Lipoprotein (HDL) and transported cholesterols (ABCA1 protein-cholesterol binding) across the plasma membrane to Apolipoprotein A1 (ApoA1). ApoA1 is the major lipoprotein component of HDL (Attie, 2007). However, the molecular mechanism by which the ABCA1 protein mediates the cellular binding of A poA1 and nascent HDL is not well understood. Some studies proved that ApoA1 interacted directly with the extracellular domain-specific conformation of t he ABCA1 transporter protein in the early process of HDL formation (Gulshan *et al.,* 2016; Ishigami *et al.,* 2018). HDL was catalyzed by the Lecithin Cholesterol Acyltransferase (LCAT) enzyme. Cholesterols succeeded in leaving the cells grabbed by HDL to form HDL-cholesterol (HDL-C) (Lyu *et al.,* 2020). Furthermore, the cancer cell proliferation decreased due to the release of c holesterols accumulated from intracellular to extracellular through this mechanism(Xia*et al*., 2005; Du *et al*., 2015). Increased ABCA1 protein expression can inhibit colorectal cancer cell proliferation. The high ABCA1 mRNA expression increased intracellular cholesterols efflux mediated by ABCA1 transporter protein causing a decrease in colorectal cancer cell proliferation. Colorectal cancer exhibits a loss of cholesterols efflux function. The decreased or loss of cholesterols efflux function by ABCA1 transporter protein

led to tumorigenesis through high intracellular cholesterols levels(Smith and Land, 2012). Several pathways of increasing intracellular cholesterols were observed in cancer, which included low ABCA1 mRNA and protein expression. Intracellular cholesterols accumulation was associated with colorectal cancer pathogenesis (Smith and Land, 2012). The accumulation of cholesterols in tumor cells (Smith and Land, 2012) can cause an increase in the proliferation of cancer cells. The mechanism of cholesterols accumulation in cells tumor with increased cancer cell proliferation is still unknown. However, it can be associated with a risk factor for colorectal cancer is a high-fat diet (WCRFI, 2018).

The ABCA1 mRNA and protein were expressed low in colon cancer compared to healthy cells (Lo sasso *et al.,* 2013). It was found that anthocyanins-rich foodstuffs significantly increased ABCA1 mRNA and protein expression as well as suppress cholesterols accumulation in the aorta and liver (Wu *et al.,* 2013; Zern *et al.,* 2003).The mechanism of the influence of anthocyanin-rich foodstuffs on colorectal cancer in increasing the ABCA1 mRNA and protein expression still needs further investigation. The increase of ABCA1 mRNA expression modulated by anthocyanins is thought to improve cholesterols elimination function mediated by ABCA1 protein and reduce Akt-dependent survival signaling. These factors contribute to anticancer activity by the ABCA1 mRNA and protein (Smith and Land, 2012). Therefore, further study is recommended to determine the influence of anthocyanins on ABCA1 mRNA and protein to prevent colorectal cancer.

5. Conclusion

This study showed that the proliferation of colorectal cancer cells can be reduced after exposure to various concentrations of ABRiBE. The extract also increased the mRNA expression of the ABCA1 gene in HT-29 cells, suggesting that ABRiBE has an impact on the antiproliferative activity of colorectal cancer cells through ABCA1 mRNA expression. The strength of this study is a strong correlation between various concentrations of ABRiBE intervention and antiproliferative activity. Moreover, further biomolecular study is needed to determine the relationship between the ABCA1 gene and PPARα and LXRα in the HT-29 cell line with the use of ABRiBE. It is also recommended to further investigate this topic in an animal model using the extract.

Acknowledgments

The authors are grateful to Technopark, Faculty of Agricultural Technology, IPB University, Integrated Laboratory Faculty of Medicine, Universitas Indonesia, and Molecular Biology and Proteomics Core Facilities (MBPCF), Indonesia Medical Education and Research Institute (IMERI), Faculty of Medicine, Universitas Indonesia for supporting this study.

This study was supported by the Universitas Indonesia under Grant number NKB-3258/UN2.RST/HKP.05.00/ 2020 , and the National Research and Innovation Agency of Indonesia under Grant number NKB-3147/ UN2.RST/ HKP.05.00/2020.

References

Affymetrix. **Eukaryotic target preparation**. [accessed 2021 March 03]. https://www.affymetrix.com/support/technical/other/cdna_protocol_manual.pdf.

Afrin S, Giampieri F, Gasparrini M, Forbes-Hernandez TY, Varela-López A, Quiles JL, Mezzetti B and Battino M. 2016. Chemopreventive and therapeutic effects of edible berries: a focus on colon cancer prevention and treatment. *Molecules,***21(169)**:1-40. doi:10.3390/molecules21020169

Ahuja U, Ahuja SC, Thakrar R and Singh RK. 2008. Rice − a nutraceutical. *Asian Agrihist.*, **12(2)**:93-108. ISSN: 09717730. [accessed 2021 Feb 14]. https://www.asianagrihistory.org/pdf/articles/Uma-Ahuja.pdf.

American Type Culture Collection (ATCC). Thawing, propagating, and cryopreserving protocol: NCI-PBCF-HTB38 (HT-29) colon adenocarcinoma. Manassas (VA): University Blvd; 2012.

Attie AD. 2007. ABCA1: at the nexus of cholesterol, HDL and atherosclerosis. *Trends Biochem Sci.,***32(4)**:172-179. doi:10.1016/j.tibs.2007.02.001

Bray F, Ferlay J, Soerjomataram I, Siegel RL, Torre LA and Jemal A. 2018. Global cancer statistics 2018: GLOBOCAN estimates of incidence and mortality worldwide for 36 cancers in 185 countries. *CA Cancer J Clin.*, **68(6)**:394-424. doi:10.3322/caac.21492

Cox S, Noronha L, Herald T, Bean S, Lee S, Perumal R, Wang W, and Smolensky D. 2019. Evaluation of ethanol-based extraction conditions of sorghum bran bioactive compounds with downstream anti-proliferative properties in human cancer cells. *Heliyon*, **2019**:1-7.

doi:https://doi.org/10.1016/j.heliyon.2019.e01589

Du C, Shi Y, Ren Y, Wu H, Yao F, Wei J, Wu M, Hou Y and Duan H. 2015. Anthocyanins inhibit high-glucose-induced cholesterol accumulation and inflammation by activating LXRα pathway in HK-2 cells. *Drug Des Devel Ther.*, **9**:5099-50113. doi:10.2147/DDDT.S90201

Gulshan K, Brubaker G, Conger H, Wang S, Zhang R, Hazen SL and Smith JD. 2016. PI(4,5)P2 is translocated by ABCA1 to the cell surface where it mediates apolipoprotein A1 binding and nascent HDL assembly. *Circ Res.,***119(7)**:827-838. doi:10.1161/CIRCRESAHA.116.308856

Hlavata I, Mohelnikova-Duchonova B, Vaclavikova R, Liska V, Pitule P, Novak P, Bruha J, Vycital O, Holubec L, Treska V, *et al*. 2012. The role of ABC transporters in progression and clinical outcome of colorectal cancer. *Mutagenesis,* **27(2)**:187-196. doi:10.1093/mutage/ger075

Ishigami M, Ogasawara F, Nagao K, Hashimoto H, Kimura Y, Kioka N and Ueda K. 2018. Temporary sequestration of cholesterol and phosphatidylcholine within extracellular domains of ABCA1 during nascent HDL generation. *Sci Rep.***8(1)**:2-11. doi:10.1038/s41598-018-24428-6

Katona BW and Weiss JM. 2020. Chemoprevention of colorectal cancer. *Gastroenterology*, **158(2)**:368-388. doi:10.1053/j.gastro.2019.06.047

Khoo HE, Azlan A, Tang ST and Lim SM. 2017. Anthocyanidins and anthocyanins: colored pigments as food, pharmaceutical ingredients, and the potential health benefits. *Food Nutr Res.*, **61(1)**:1-21. doi:10.1080/16546628.2017.1361779

Konczak I, Sakulnarmrat K and Bull M. 2012. Potential physiological activities of selected australian herbs and fruits. **Australia (AU): Rural Industries Research and Development Corporation (RIRDC).** RIRDC Publication No. 11/097. ISBN:9781742542775

Kristamtini K and Wiranti EW. 2017. Clustering of 18 local black rice base on total anthocyanin. *Biol Med Nat Prod Chem.*, **6(2)**:47. doi:10.14421/biomedich.2017.62.47-51

Lo Sasso G, Bovenga F, Murzilli S, Salvatore L, Di Tullio G, Martelli N, D'Orazio A, Rainaldi S, Vacca M, Mangia A, *et al*. 2013. Liver X receptors inhibit proliferation of human colorectal cancer cells and growth of intestinal tumors in mice. *Gastroenterology,***144(7)**:1497-1507. doi:10.1053/j.gastro.2013.02.005

Lyu J, Imachi H, Fukunaga K, Sato S, Kobayashi T, Dong T, Saheki T, Matsumoto M, Iwama H, Zhang H, *et al*. 2020. Role of ATP-binding cassette transporter A1 in suppressing lipid accumulation by glucagon-like peptide-1 agonist in hepatocytes. *Mol Metab,* **34**:16-26. doi:10.1016/j.molmet.2019.12.015

Martín J, Navas MJ, Jiménez-Moreno AM and Asuero AG. 2017. Anthocyanin pigments: importance, sample preparation and extraction. *Intech.*, 117-152. doi:10.5772/66892

Matlock B. 2015. **Assessment of nucleic acid purity. Wilmington (MA): Thermo Fisher Scientific**. Technical Note No. 52646. [accessed 2021 Feb 13]. https://assets.thermofisher.com/TFS-Assets/CAD/Product-Bulletins/TN52646-E-0215M-NucleicAcid.pdf

Mazewski C, Liang K and Gonzalez de Mejia E. 2018. Comparison of the effect of chemical composition of anthocyanin-rich plant extracts on colon cancer cell proliferation and their potential mechanism of action using in vitro, in silico, and biochemical assays. *Food Chem.,***242**:378-388. doi:10.1016/j.foodchem.2017.09.086

Nakaya K, Tohyama J, Naik SU, Tanigawa H, MacPhee C, Billheimer JT and Rader DJ. 2011. Peroxisome proliferator-activated receptor-α activation promotes macrophage reverse cholesterol transport through a liver X receptor-dependent pathway. *Arterioscler Thromb Vasc Biol.*, **31(6)**:1276-1282. doi:10.1161/ATVBAHA.111.225383

Pasello M, Giudice AM and Scotlandi K. 2020. The ABC subfamily A transporters: multifaceted players with incipient potentialities in cancer. *Semin Cancer Biol.*, **60**:57-71. doi:10.1016/j.semcancer.2019.10.004

Paudel L, Wyzgoski FJ, Giusti MM, Johnson JL, Rinaldi PL, Scheerens JC, Chanon AM, Bomser JA, Miller AR, Hardy JK, *et al*. 2014. NMR-based metabolomic investigation of bioactivity of chemical constituents in black raspberry (*Rubus occidentalis L.*) fruit extracts. *J Agric Food Chem.,* **62(8)**:1989-1998. doi:10.1021/jf404998k

Peña-Sanhueza D, Inostroza-Blancheteau C, Ribera-Fonseca A and Reyes-Díaz M. 2017. Anthocyanins in berries and their potential use in human health. *Intech.,* 158. doi:10.1016/j.colsurfa.2011.12.014

Prasad BJ, Sharavanan PS and Sivaraj R. 2019. Health benefits of black rice – A review. *GOST*. doi:10.1016/j.gaost.2019.09.005

Pratiwi R, Amalia AR, Anindito W and Tunjung S. 2019. Active fractions of black rice bran cv Cempo Ireng inducing apoptosis and S-phase cell cycle arrest in T47D breast cancer cells. *J Math Fund Sci.*, **51(1)**:47-59. doi:10.5614/j.math.fund.sci.2019.51.1.4

Pratiwi R, Amalia AR, Anindito W and Tunjung S. 2015. Black rice bran extracts and fractions containing cyanidin 3-glucoside and peonidin 3-glucoside induce apoptosis in human cervical cancer cells. *I.J. Biotech.*,**20(1)**:69-76. doi:10.22146/ijbiotech.15271

Schmitz G and Langmann T. 2005. Transcriptional regulatory networks in lipid metabolism control ABCA1 expression. *Biochim Biophys Acta.*,**1735(1)**:1-19. doi:10.1016/j.bbalip.2005.04.004

Shi N, Chen X, Chen T. 2021. Anthocyanins in Colorectal Cancer Prevention Review. *Antioxidants.,***10(1600)**:1-20. doi:10.3390/antiox10101600

Smith B and Land H. 2012. Anticancer activity of the cholesterol exporter ABCA1 gene. *Cell Rep*., **2(3)**:580-590. doi:10.1016/j.celrep.2012.08.011

Sung H, Ferlay J, Siegel RL, Laversanne M, Soerjomataram I, Jemal A and Bray F. 2021. Global cancer statistics 2020: GLOBOCAN estimates of incidence and mortality worldwide for 36 cancers in 185 countries. *CA Cancer J Clin.,***71(3)**:209-249. doi:10.3322/caac.21660

Tall AR, Costet P, Wang N. 2002. Regulation and mechanisms of macrophage cholesterol efflux. *J. Clin. Invest.,* **110(7)**:899-904. doi:10.1172/JCI200216391

Tsuda T, Ueno Y, Yoshikawa T, Kojo H and Osawa T. 2006. Microarray profiling of gene expression in human adipocytes in response to anthocyanins. *Biochem Pharmacol.,* **71(8)**:1184-1197. doi:10.1016/j.bcp.2005.12.042

Venkateswaran A, Laffitte BA, Joseph SB, Mak PA, Wilpitz DC, Edwards PA and Tontonoz P. 2000. Control of cellular cholesterol efflux by the nuclear oxysterol receptor LXRα. *Proc Natl Acad Sci USA.* **97(22)**:12097-12102. doi:10.1073/pnas.200367697

Wang D, Xia M, Yan X, Li D, Wang L, Xu Y, Jin T and Ling W. 2012. Gut microbiota metabolism of anthocyanin promotes reverse cholesterol transport in mice via repressing miRNA10b. *Circ Res.,***111(8)**:967-981. doi:10.1161/CIRCRESAHA.112.266502

Wang E, Liu Y, Xu C and Liu J. 2017. Antiproliferative and proapoptotic activities of anthocyanin and anthocyanidin extracts from blueberry fruits on B 16-F10 melanoma cells. *Food Nutr Res.*, **61(1)**:1325308. doi:10.1080/16546628.2017.1325308

World Cancer Research Fund International (WCRFI). 2018.Diet, nutrition, physical activity, and colorectal cancer. In: **Continuous update project expert report 2018.** [accessed 2021 Feb 21]. https://www.wcrf.org/wp-content/uploads/2021/02/Colorectal-cancer-report.pdf

Wu T, Tang Q, Gao Z, Yu Z, Song H, Zheng X and Chen W. 2013. Blueberry and mulberry juice prevent obesity development in C57BL/6 mice. *PLoS One,***8(10)**:2-8. doi:10.1371/journal.pone.0077585

Xia M, Hou M, Zhu H, Ma J, Tang Z, Wang Q, Li Y, Chi D, Yu X, Zhao T, *et al*. 2005. Anthocyanins induce cholesterol efflux from mouse peritoneal macrophages: the role of the peroxisome proliferator activated receptor γ-liver X receptor α-ABCA1 pathway. *J Biol Chem.*, **280(44)**:36792-36801. doi:10.1074/jbc.M505047200

Yawadio R, Tanimori S and Morita N. 2007. Identification of phenolic compounds isolated from pigmented rices and their aldose reductase inhibitory activities. *Food Chem.,* **101(4)**:1616-1625. doi:10.1016/j.foodchem.2006.04.016

Zawistowski J, Kopec A, and Kitts DD. 2009. Effects of a black rice extract (*Oryza sativa L. indica*) on cholesterol levels and plasma lipid parameters in Wistar Kyoto rats. *J Funct Foods.* **1(1)**:50-56. doi:10.1016/j.jff.2008.09.008

Zern TL, West KL and Fernandez ML. 2003. Grape polyphenols decrease plasma triglycerides and cholesterol accumulation in the aorta of ovariectomized guinea pigs. *J Nutr*., **133(7)**:2268-2272. doi:10.1093/jn/133.7.2268)

Zhang Y, Vareed SK and Nair MG. 2005. Human tumor cell growth inhibition by nontoxic anthocyanidins, the pigments in fruits and vegetables. *Life Sciences.,* **76**:1465-1472. doi:10.1016/j.lfs.2004.08.025.

Zhao X, Feng P, He W, Du X, Chen C, Suo L, Liang M, Zhang N, Na A and Zhang Y. 2019. The prevention and inhibition effect of anthocyanins on colorectal cancer. *Curr Pharm Des.***25(46)**:4919-4927. doi:10.2174/1381612825666191212105145

JJBS

Volume 17, Number 1,March 2024
ISSN 1995-6673
Pages 207 – 216
https://doi.org/10.54319/jjbs/170120

Jordan Journal of Biological Sciences

Pentraxin-3 and Interleukin-18: Potential Biomarkers for the Early Diagnosis and Severity Prediction of Diabetic Foot Ulcer

Fatma Al-Farra[1] (MSc), Mohammed Al-Zaaneen[1] (MSc), Abeer Al-Qatati[2] (PhD), Mohammed Laqqan[1] (PhD), Mazen Alzaharna[1,*] (PhD)

[1]*Medical Laboratory Sciences Dept., Faculty of Health Sciences, Islamic University of Gaza, P.O. Box 108, Gaza City, Palestine;* [2]*Clinical Laboratory Sciences Department, Faculty of Science, The University of Jordan, Amman, Jordan;*

Received: July 9, 2023; Revised: October 3, 2023; Accepted: October 13, 2023

Abstract

Background/Aim: As the global incidence of diabetes mellitus (DM) rises, diabetic foot ulcers (DFUs) have emerged as a critical complication associated with increased lower-limb amputations, reduced quality of life, and higher mortality rates. Early detection of DFUs is crucial, sparking interest in potential biomarkers. Interleukin-18 (IL-18) and Pentraxin-3 (PTX-3) are known contributors to inflammation, and recent studies suggest their involvement in diabetic foot events. This study aims to compare IL-18 and PTX-3 levels in type 2 DM (T2DM) patients, with or without foot ulcers (FUs), and healthy controls while exploring their association with DFU diagnosis and severity.

Methods: Eighty-four males participated in the study, including 28 patients with T2DM with FUs, 28 T2DM patients without FUs, and 28 healthy controls. Individuals with type 1 DM (T1DM) or any other types of diabetes, those with infectious or other chronic diseases, and inflammation (such as chronic inflammation and autoimmune diseases), were excluded from participation. Serum IL-18 and PTX-3 were examined using the ELISA method. Enzymatic and colorimetric techniques were used to investigate fasting blood glucose (FBG), hemoglobin A1c (HbA1c), creatinine, urea, alanine transaminase (ALT), and the lipid profile.

Results: The average serum levels of IL-18 and PTX-3 were higher in cases of DFU compared to both T2DM cases and controls ($P < 0.0001$), with the highest levels observed in the DFU group. There was a statistically significant difference in FBG, HbA1c, urea, and creatinine between the different studied groups. ROC curve results showed that the IL-18 cut-off value for predicting severity in patients with DFU compared to T2DM without DFU is ≥ 124.0 pg/ml ($P < 0.0001$). Meanwhile, the PTX-3 cut-off value for predicting DFU in patients with T2DM is > 8.67 ng/ml. The level of IL-18 differed significantly across the different groups based on perfusion, extent, sensation, infection, depth, and nephropathy conditions.

Conclusion: The results indicate that PTX-3 is a promising biomarker for predicting DFU, while IL-18 is a valuable biomarker for predicting severity.

Keywords: Diabetic foot ulcer, Interleukin-18, Pentraxin-3, Type 2 diabetes mellitus, biomarkers, Gaza Strip

1. Introduction

DM is considered the most prevalent endocrine disorder worldwide. It is expected that this disease will affect 642 million individuals by 2040 (Ogurtsova *et al.*, 2017). DM is distinguished by a long-term inflammatory response with elevated blood glucose levels. The development and consequences of DM are closely tied to low-grade inflammation and immunological stimulation (Navarro-Gonzalez and Mora-Fernandez, 2008). FUs occur in 15% to 25% of patients with DM at some point in their lives (Cavanagh *et al.*, 2005). A research paper published in 2017 reported that global DFU prevalence is 6.3%, which was higher in males (4.5%) than in females (3.5%), and higher in T2DM (6.4%) than in T1DM (5.5%) (Zhang *et al.*, 2017). Unfortunately, DFU will lead to amputations in a vast majority of patients with T2DM. Neutrophils' ability to phagocytose and kill bacteria is compromised by hyperglycemia, which also causes oxidative damage and a rise in cytokines linked to inflammation. In addition, hyperglycemia triggers the production of interleukin-6, transforming growth factor-β, and tumor necrosis factor-α. These undesirable effects are connected to a tendency for infections in DFU patients (Saltoglu *et al.*, 2015).

The global prevalence of DFU was 6.3%, according to Zhang et al., (2017), with male patients with T2DM experiencing the condition more frequently than female patients. Because DM is linked to long-term complications of the microvascular and macrovascular systems, the need to identify the problems must be urgent. Hospitalization, impairment, and fatalities for T2DM patients will all decrease if risk categorization of DFU can be attained earlier (Zhang *et al.*, 2017).

When it comes to early medical diagnosis, avoiding illness, and disease course estimation, finding related biomarkers is fundamental (Atkinson *et al.*, 2001). Targets and chemicals connected to the pathogenesis of DFU can be used for early diagnosis and prognosis of the disease. Identifying the biological elements and the course of recovery of DFU has led to the discovery of some novel potential biomarkers that can be applied in the clinical field (Ozer Balin *et al.*, 2019, Chen *et al.*, 2020).

Interleukin-18 (IL-18), initially recognized as an interferon-γ (IFN-γ)-inducing factor, belongs to the IL-1 cytokine superfamily and plays a crucial role in the inflammatory process, contributing to several autoimmune diseases (Yasuda *et al.*, 2019). Recent studies have linked the increase in serum levels of IL-18 to the progression of diabetic foot disease (Chen *et al.*, 2020). However, more research is needed to determine how IL-18 affects T2DM patients with and without FUs compared to healthy controls.

Moreover, previous studies have examined the effect of cytokines other than IL-18 and different acute-phase proteins on DFU (Ozer Balin *et al.*, 2019, Chen *et al.*, 2020). An example of an acute phase protein that was investigated includes the soluble pattern recognition receptor called pentraxin-3 (PTX-3). PTX-3 is produced directly at the site of inflammation by mononuclear phagocytes, fibroblasts, myeloid dendritic cells, granulosa cells, mesangial cells, endothelial cells, smooth muscle cells, and adipocytes. A significant quantity of PTX-3 is created in the vascular wall during an inflammatory process. This substance regulates endothelial function in thrombosis and ischemic vascular disease and binds to angiogenic fibroblast growth factor-2 to prevent angiogenesis (Abu Seman *et al.*, 2013).

Therefore, this study was conducted to assess the potential to use IL-18 and PTX-3 as biomarkers for early diagnosis and severity of DFU and to explore the association between IL-18, PTX-3, and DFU.

2. Materials & methods

2.1. Study Design and Ethical Approval

The present study is a case-control one. The study was approved by the Palestinian Health Research Council, Helsinki Committee (PHRC/1096/22). The participants involved in this study signed an informed consent form before sample collection. A face-to-face interview was conducted to fill in a questionnaire with questions about personal information such as age, educational level, family history of diabetes, smoking status, and clinical data. In addition, special questions were prepared for DFU patients related to skin conditions, perfusion, nephropathy, and the existence of infections which were filled in by the physician.

2.2. Sample size and sampling

This study involved 84 participants, classified as the following: 28 people suffering from T2DM with DFU, 28 people with T2DM without DFU, and 28 healthy people. Persons with the following criteria were excluded from participation in the study: those with T1DM and any other types of diabetes (gestational diabetes & other specific types), persons having infectious or chronic diseases, or who have Alzheimer's disease, or liver disease; and persons with any conditions characterized by inflammation, such as chronic inflammation and autoimmune diseases. Persons chosen as controls were healthy persons with normal blood pressure and non-smokers.

2.3. Sample collection

A venous blood sample was obtained from each participant after an overnight fast in clot activator tubes (Dragon Med, USA) for biochemical and ELISA assays and EDTA tubes for HbA1c test. The serum samples were separated by centrifugation (Gemmy, Taiwan) at 4000 rpm for 10 minutes at room temperature. Serum samples for the analysis of IL-18 and PTX-3 were stored at -80 °C for later use.

2.4. Biochemical analysis and ELISA assay

Total cholesterol, triglycerides, high-density lipoprotein (HDL), fasting blood glucose (FBG), urea, creatinine, alanine aminotransferase (ALT), and HbA1c tests were assayed using commercial analytical kits. Low-density lipoprotein (LDL) was calculated using the Friedewald equation: LDL (mg/dl) = cholesterol - (HDL + triglycerides/5) and then converted to mmol/L. HbA1c kit from (Hipro Biotechnology, China). The cholesterol, triglycerides, and HDL kits are from (Human Diagnostics Worldwide, Germany), and with Glucose kit is from (Dialab, Austria). Urea and creatinine are from (Elitech, France), and an ALT kit is from (Diasys, Germany). IL-18 and PTX-3 levels were measured using ELISA kits (R&D Systems Inc., USA), and the results were read using an ELISA reader (Snibe, China) at 450 nm. All test analyses were performed according to the manufacturer's instructions.

2.5. Statistical analysis

Categorical variables were summarized with frequencies and percentages, and numerical variables were summarized with the mean and standard deviation (SD), median and interquartile range (quartile 1 (Q1), quartile 3 (Q3)), and minimum (Min) and maximum (Max). Differences between groups in categorical variable distributions were tested using Pearson's Chi-square test or Fisher's exact test, depending on the validity of the expected counts assumption for Pearson's Chi-square. On the other hand, differences in numerical variables between the two groups were tested using either the independent samples T-test or the Mann-Whitney U test (MW), depending on the validity of parametric assumptions. When more than two groups were compared, one-way analysis of variance ANOVA (with Tukey's HSD post hoc test) or Kruskal-Wallis rank sum test (KW) (with Dunn test post hoc testing) was employed depending on the validity of the parametric test assumptions. The Kendall rank correlation coefficient (Kendall-tau) was used to measure the ordinal association between the grade of DFU and biomarker concentration. The perfusion, extent, depth, infection, and sensation (PEDIS) Score (Chuan *et al.*, 2015), which is a severity score for DFU, was calculated by summing the stages of perfusion, extent, depth, infection, and sensation. A PEDIS score of 7 and above indicates a higher risk of adverse outcomes for ulcers, and this cut-off was used to designate the DFUs as severe or non-severe. Using the coordinates of the receiver operating characteristic (ROC) curves, the maximum Youden index was used to identify the optimal thresholds for predicting the T2DM patients (either with or without FU), and the severity of FU (severe or non-severe) based on IL-18 or PTX-3 concentrations. Since the sample size was small (N = 28 or N = 14), we could not perform multivariable analyses. All analyses and figures were produced using R version 4.2.2 (R Core Team, 2013).

3. Results

3.1. 3.1 Demographic characteristics of the study groups

The results show that T2DM patients with FU were slightly older than the other two groups (63.5 ± 6.0 vs. 62.0 ± 6.7 respectively), and they were more predominantly living in South Gaza. Furthermore, 39.3% of T2DM with or w ithout FUs were smokers or quit smoking compared to 60.7% for non-smokers. There was a significant difference between the study groups in terms of smoking status (P < 0.05), while there was no significant difference in BMI between the study groups (P = 0.362), as shown in Table 1.

Table 1: Demographic characteristics of the study groups.

	Normal (N=28)	T2DM (N=28)	T2DM with FU (N=28)	P-value
Age (years)				
Mean (SD)	60.9 (6.0)	62.0 (6.7)	63.5 (6.0)	
(Min, Max)	(50.0, 72.0)	(50.0, 72.0)	(52.0, 72.0)	0.298[#]
Median	60.5	62.0	64.0	
(Q1, Q3)	(56.5, 64.3)	(57.5, 68.3)	(59.0, 67.5)	
BMI (kg/m^2)				
Mean (SD)	24.2 (2.2)	24.5 (2.3)	24.9 (1.6)	
(Min, Max)	(21.0, 30.6)	(20.9, 29.0)	(21.9, 27.8)	0.520[#]
Median	24.2	25.0	24.9	
(Q1, Q3)	(22.5, 25.4)	(22.3, 26.2)	(24.0, 26.2)	
Smoking status				
Non-Smokers	28 (100%)	17 (60.7%)	17 (60.7%)	0.03*[$]
Quit Smoking	0 (0%)	6 (21.4%)	9 (32.1%)	
Smokers	0 (0%)	5 (17.9%)	2 (7.1%)	
Residence				
Gaza	10 (35.7%)	6 (21.4%)	5 (17.9%)	0.077[£]
Middle	3 (10.7%)	9 (32.1%)	3 (10.7%)	
South	15 (53.6%)	13 (46.4%)	20 (71.4%)	
Marital status				
Married	21 (75.0%)	20 (71.4%)	24 (85.7%)	0.413
Widowed	7 (25.0%)	8 (28.6%)	4 (14.3%)	
Education				
Illiterate	6 (21.4%)	5 (17.9%)	8 (28.6%)	
Preparatory	1 (3.6%)	2 (7.1%)	2 (7.1%)	0.922[$]
Secondary	10 (35.7%)	9 (32.1%)	10 (35.7%)	
University	11 (39.3%)	12 (42.9%)	8 (28.6%)	

BMI: Body mass index; Gaza, Middle, South: Governorates of Gaza strip. *: The test included only the T2DM patients and T2DM patients with FU groups since the normal group was chosen to be non-smokers; [#]: ANOVA test; [$]: Fisher test; [£]: Chi-square Chi-square.

3.2. Clinical characteristics and the biochemical parameters of the study groups

As illustrated in Table 2, the duration of di abetes in patients with FUs was slightly longer (8.2 ± 3.2 years) compared to T2DM patients without FUs (7.2 ± 3.4 years), but the difference was not statistically significant (P = 0.260).

Table 3 shows the levels of the different tested biochemical parameters. Both T2DM patients and T2DM patients with FUs had higher HbA1c and FBG than the normal group, and these differences were statistically significant (P < 0.0001). Cholesterol and LDL values were significantly lower in the T2DM patients with FUs group compared to the corresponding values for bot h T2DM patients without FUs and normal groups (P = 0.002 and P = 0.001, respectively). On the other hand, creatinine and urea were significantly elevated in T2DM patients with FUs compared to the other two groups (P < 0.0001).

Table 2: Clinical characteristics of the study groups.

	Normal (N=28)	T2DM (N=28)	T2DM with FU (N=28)	P value
Blood pressure				
Normal	28 (100%)	20 (71.4%)	16 (57.1%)	0.265#*
> 130 (mmHg)	0 (0%)	8 (28.6%)	12 (42.9%)	
Family history of DM				
Yes	18 (64.3%)	16 (57.1%)	17 (60.7%)	0.861#
No	10 (35.7%)	12 (42.9%)	11 (39.3%)	
Duration of diabetes (years)				
Mean (SD)	NA	7.2 (3.4)	8.2 (3.2)	0.260$
(Min, Max)	NA	(1.0, 13.0)	(4.0, 14.0)	
Median (Q1, Q3)	NA	7.0 (5.0, 9.2)	8.0 (5.8, 10.3)	

* The test included only the T2DM patients and T2DM patients with FU groups since the normal group was chosen to have normal blood pressure; # Chi square; $ T-Test.

Table 3: Comparison of the biochemical parameters among the study groups.

Parameter	Normal (N=28)	T2DM (N=28)	T2DM with FU (N=28)	P value	
				Overall	Post- hoc
HbA1c (%)					
Mean (SD)	5.7 (0.3)	9.0 (1.5)	9.8 (1.4)		<0.0001[a]
(Min, Max)	(5.2, 6.8)	(6.4, 12.2)	(7.8, 13.2)	<0.0001*	<0.0001[b]
Median (Q1, Q3)	5.7 (5.5, 5.9)	9.0 (7.9, 10.2)	9.6 (8.6, 10.5)		
FBG (mmol/L)					
Mean (SD)	5.8 (2.2)	10.3 (5.1)	11.2 (3.9)		0.0001[a]
(Min, Max)	(3.3, 13.9)	(3.6, 23.8)	(4.8, 21.4)	<0.0001*	<0.0001[b]
Median (Q1, Q3)	5.7 (4.2,6.2)	9.9 (6.7, 12.9)	10.9 (8.6, 13.7)		
Cholesterol (mmol/L)					
Mean (SD)	4.5 (0.9)	4.7 (1.0)	3.9 (0.7)		0.031[b]
(Min, Max)	(2.7, 6.1)	(2.9, 6.5)	(2.7, 5.3)	0.002#	0.002[c]
Median (Q1, Q3)	4.7 (3.8, 5.0)	5.0 (4.0, 5.4)	3.7 (3.4, 4.3)		
Triglycerides (mmol/L)					
Mean (SD)	1.8 (0.7)	1.7 (0.6)	1.8 (0.5)		
(Min, Max)	(0.7, 3.0)	(0.7, 3.1)	(0.6, 2.5)	0.669*	
Median (Q1, Q3)	1.9 (1.2, 2.2)	1.9 (1.1, 2.1)	1.8 (1.4, 2.2)		
HDL (mmol/L)					
Mean (SD)	1.1 (0.26)	1.1 (0.3)	1.0 (0.3)		
(Min, Max)	(0.7, 1.8)	(0.7, 1.6)	(0.7, 1.6)	0.884#	
Median (Q1, Q3)	1.0 (0.9, 1.2)	1.0 (0.9, 1.2)	1.0 (0.8, 1.2)		
LDL (mmol/L)					
Mean (SD)	2.6 (0.8)	2.9 (0.9)	2.0 (0.6)		0.021[b]
(Min, Max)	(1.0, 4.0)	(1.2, 4.4)	(0.9, 3.1)	0.001#	<0.001[c]
Median (Q1, Q3)	2.7 (1.9, 3.2)	2.8 (2.1, 3.6)	2.0 (1.8, 2.5)		
Creatinine (µmol/L)					
Mean (SD)	79.6 (17.7)	97.3 (26.5)	128.2 (26.5)		<0.0001[b]
(Min, Max)	(53.1, 115.0)	(61.9, 176.8)	(70.7, 176.8)	<0.0001*	<0.0001[c]
Median (Q1, Q3)	88.4 (70.7, 88.4)	88.4 (70.7, 106.1)	132.6 (115.0, 141.5)		
Urea (mmol/L)					
Mean (SD)	11.4 (2.8)	14.0 (4.7)	21.7 (10.8)		<0.0001[b]
(Min, Max)	(6.1, 16.1)	(7.1, 10.2)	(8.2, 57.1)	<0.0001*	0.001[c]
Median (Q1, Q3)	10.9 (9.6, 13.7)	13.6 (11.1, 16.4)	19.6 (15.5, 23.7)		
ALT (U/L)					
Mean (SD)	20.7 (6.19)	24.1 (11.1)	22.0 (8.9)		
(Min, Max)	(11.0, 35.0)	(10.0, 52.0)	(11.0, 41.0)	0.863*	
Median (Q1, Q3)	19.5 (16.8, 21.8)	21.0 (16.0, 29.5)	20.0 (15.0, 26.0)		

ALT: Alanine transaminase; FBG: Fasting blood glucose; HbA1c: Hemoglobin A1c; HDL: high-density lipoprotein; LDL: Low-density lipoprotein. Significant P values (P < 0.05) are in bold. [a] Diabetic vs Controls; [b] T2DM with FU vs Controls & [c] T2DM vs T2DM with FU. * Kruskal-Wallis (KW) test, # ANOVA test.

3.3. IL-18 and PTX-3 levels

As shown in Figure 1, the levels of both biochemical markers were significantly elevated in the DFU group compared to the T2DM and the normal group ($P < 0.001$). On the other hand, no significant differences have been observed in PTX-3 and IL-18 levels between the normal group and the T2DM patients.

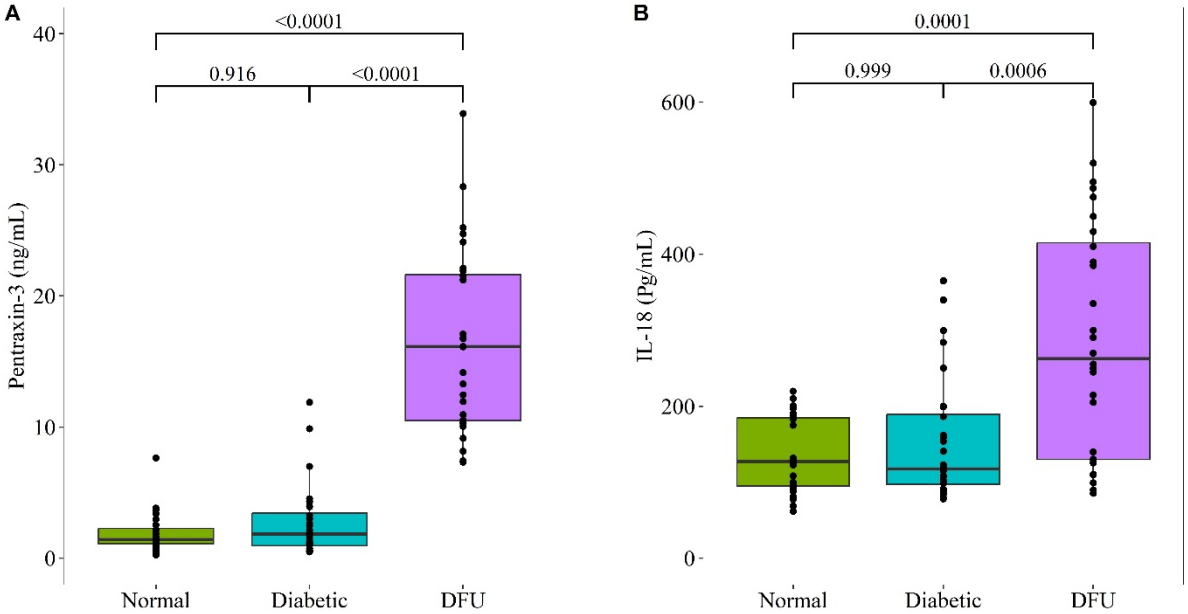

Figure 1: Boxplots of Pentraxin-3 and IL-18 levels in study groups. **A.** Pentraxin-3 levels. **B.** IL-18 levels. DFU: T2DM patients with FU. P values shown represent the Dunn test post hoc.

3.4. Association of IL-18 and PTX-3 levels with severity of FUs and stages of nephropathy

Table 4 indicates that there was a significant correlation between perfusion, extent, depth, infection, and IL-18, where IL-18 levels increased with increasing grades of these criteria (Kendall-Tau around 0.5 for all criteria and $P < 0.001$). In addition, PTX-3 and IL-18 levels were elevated in patients without sensation in their ulcers compared to those who have not lost sensation, but only the difference in IL-18 was significant ($P < 0.0001$). The sum of the grades of these five criteria represents the PEDIS score, which defines the risk for adverse outcomes (non-healing ulcer, amputation, or death). Patients with PEDIS scores of 7 and above had higher PTX-3 and IL-18 levels compared to those whose scores were lower than 7, and the difference in IL-18 was significant ($P < 0.0001$). Similarly, higher IL-18 levels were associated with an increasing stage of nephropathy (Kendall-Tau=0.576, $P = 0.04$).

Table 4: Association between concentrations of PTX-3 and IL-18 and severity of FU or stage of nephropathy in T2DM patients with FU (N=28).

Grade	n	PTX-3		IL-18	
		Median	Kendall-tau (P value)	Median	Kendall-tau (P value)
Perfusion					
0: No peripheral arterial disease	4	57.4	0.069 (0.57)	5.8	0.587 (<0.0001)
1: Peripheral arterial disease, no critical limb ischemia	14	32.9		12.8	
2: Critical limb ischemia	10	49.4		25.7	
Extent					
0: Skin intact	6	50.9		9.6	
1: <1 cm^2	4	55.0	0.069	7.2	0.479
2: 1–3 cm^2	12	35.9	(0.59)	16.4	(0.0002)
3: >3 cm^2	6	56.5		27.3	
Depth					
0: Skin intact	2	44.1*		8.7*	
1: Superficial	9	47.4	0.061	7.2	0.529
2: Fascia, muscle, tendon	11	36.8	(0.63)	16.7	(<0.0001)
3: Bone or joint	6	56.5		27.3	
Infection					
0: None	3	62.4		7.2	
1: Surface	9	35.0	0.061	7.8	0.505
2: Abscess, fasciitis, and/or septic arthritis	10	39.1	(0.63)	17.6	(<0.0001)
3: Systemic inflammatory response syndrome	6	56.2		26.0	
Sensation					
0: Sensation intact	16	37.9	0.15	7.5	<0.0001
1: Loss of sensation	12	49.4	MW	24.4	MW
PEDIS score					
< 7	14	43.2	0.430	7.5	<0.0001
≥ 7	14	48.2	T-Test	23.3	MW
Nephropathy					
0: None	9	39.1	0.167 (0.18)	7.2	0.576 (0.04)
1: stage 1	11	35.0		13.6	
2: stage 2	8	56.5		22.6	

A higher grade represents a more severe ulcer condition. PEDIS score is calculated by summing the grade of the preceding five criteria. *Median was calculated as the average of the two data points. Significant P values are in bold. The Kendall-tau P value column shows the Kendall-tau statistic and its P value except for Loss of sensation and PEDIS score.

3.5. Prediction of DFU by IL-18 and PTX-3

PTX-3 was a better predictor of group membership of T2DM patients regarding the presence or absence of FUs compared to IL-18 (AUC = 0.983 vs. 0.772; Figure 2A). The opposite was true when these biomarkers were used to classify patients with FUs into two groups based on ulcer severity, where a PEDIS score ≥ 7 was considered to be associated with a more severe case of DFU. In this regard, IL-18 was a very good predictor of ulcer severity, whereas PTX-3 was not useful in predicting ulcer severity (AUC = 0.954 vs. 0.597: Figure 2B).

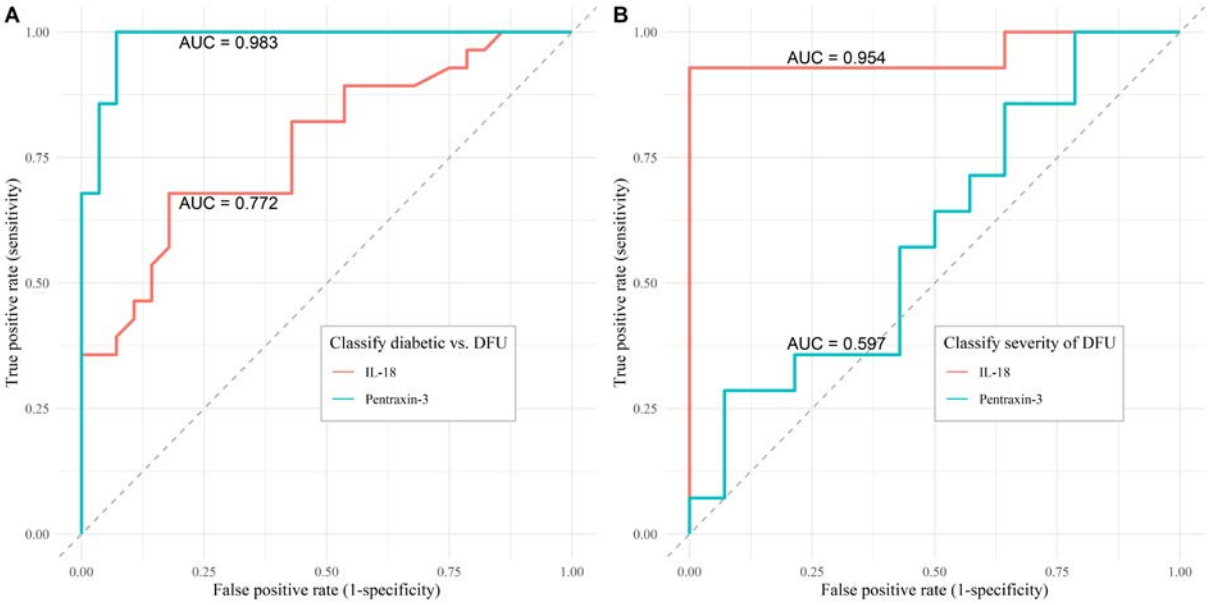

Figure 2: Receiver operating characteristic (ROC) curves of PTX-3 and IL-18 for prediction of the presence of T2DM with FU and severity of the DFU. **A.** ROC curves of the two biomarkers for prediction of T2DM patients with FUs. Each group has N=28. **B.** ROC curves of the two biomarkers for prediction of severe FUs. A PEDIS score of seven and above was taken to indicate a case of severe FU. Each group had N=14. AUC: Area under the ROC curve.

Additionally, Table 5 lists the diagnostic cut-offs and their performance for PTX-3 and IL-18 in predicting the presence of FUs in T2DM patients (Diabetic vs. DFU) and in predicting the severity of DFU. The cut-offs are based on the maximum Youden index, which gives the same weight to sensitivity and specificity. The cut-off value of 202.5 pg/ml IL-18 in classifying diabetics vs. DFU gives only 67.9% sensitivity.

Table 5. Performance of PTX-3 and IL-18 in predicting DFU group and severe FU based on maximum Youden index cut-offs.

	AUC (95% CI) P value	Cut-off	Sensitivity	Specificity	NPV	PPV	ACC
Classify Diabetic vs. DFU							
IL-18 (pg/ml)	0.772 (0.650, 0.894) <0.0001	202.5	67.9	82.1	71.9	79.2	75.0
PTX-3 (ng/ml)	0.983 (0.957, 1.000) <0.0001	7.17	100	92.9	100	93.3	96.4
Classify DFU severity							
IL-18 (pg/ml)	0.954 (0.864, 1.000) <0.0001	280	92.9	100.0	93.3	100.0	96.4
PTX-3 (ng/ml)	0.597 (0.383, 0.811) 0.383	-	-	-	-	-	-

ACC: Accuracy; AUC: Area under ROC curve; DFU: Diabetic foot ulcer; NPV: Negative predictive value; PPV: Positive predictive value. P value is the result of the statistical test between the AUC and an AUC of 0.5 (random classifier). No diagnostic criteria are shown for PTX-3 for severity classification since its AUC was not significantly different from 0.5.

3.6. Association between IL-18, PTX-3 and duration of diabetes

Since the duration of diabetes is an important factor in developing DFU, and because it affects the severity of the ulcer we also examined biomarker concentrations in the patients based on the duration of their duration of diabetes (Table 6). PTX-3 levels showed no correlation with the increasing duration of diabetes in T2DM patients with or without FUs. On the other hand, IL-18 concentration increased with increasing duration in both groups, and the correlation was strong (stronger association) in the case of T2DM patients with FUs (Kendall-Tau 0.63 vs. 0.41). None of the T2DM patients with FUs who had diabetes for longer than 10 years were in the non-severe FU group. Again, PTX-3 levels were not correlated with increasing duration of diabetes in patients with severe FUs, whereas IL-18 was significantly correlated with increasing duration in this group (although there was only one patient who had diabetes for less than 5 years).

Table 6. PTX-3 and IL-18 for T2DM patients with and without FU, and patients with severe and non-severe FU based on duration of diabetes.

Duration of diabetes (years)	Diabetic (N=28)		DFU (N=28)	
	PTX-3 (ng/ml) Median (Q1, Q3)	IL-18 (pg/ml) Median (Q1, Q3)	PTX-3 (ng/ml) Median (Q1, Q3)	IL-18 (pg/ml) Median (Q1, Q3)
<5	1.1 (0.66-2.7)	103 (82-134.5)	12.5 (11.4-14.8)	110 (97.5-117.5)
5-10	1.9 (1.0-2.7)	108 (96.5-155.3)	14.7 (10.4-22.1)	248 (132.5-323.8)
>10	2.9 (1.4-6.2)	267 (212.5-326)	16.8 (15.2-19.2)	487 (430-5.7.5)
Kendall-tau	0.20	0.41	0.11	0.63
(P value)	(0.188)	(0.007)	(0.496)	(<0.0001)
Duration of diabetes (years)	Non-severe DFU (N=14)		Severe DFU (N=14)	
	PTX-3 (ng/ml)	IL-18 (pg/ml)	PTX-3 (ng/ml)	IL-18 (pg/ml)
<5	14.5 (10.7-20.7)	120 (101.8-137.5)	12.5 (12.5-12.5)	125 (one patient)
5-10	14.7 (8.0-21.2)	210 (125-246.3)	17.5 (10.6-24.6)	387.5 (347.5-420)
>10	NA	NA	16.8 (15.2-19.2)	487 (430-507.5)
Kendall-tau	T-test	MW test	0.04	0.55
(P value)	(0.591)	(0.300)	(0.853)	(0.016)

4. Discussion

Diabetes is an illness of metabolism that affects about 9% of the global population in general. Uncontrolled DM can cause chronic problems, and a significant number of individuals already have complications when they are diagnosed (Weerasuriya *et al.*, 1998). Early diagnosis of complications is crucial since long-term microvascular and macrovascular consequences are linked to diabetes. A serious complication that affects T2DM patients is the DFU effect, which is considered a serious health issue. Lower limb amputations may result from nonhealing or slowly healing diabetic ulcers. DFU development involves numerous factors, peripheral artery disease, atherosclerotic plaque, alterations in blood circulation, and peripheral neuropathy are only a few of the intricate interactions that lead to DFU (Brownrigg *et al.*, 2013).

It is worth noting that multiple studies on potential indicators of diabetic foot are needed with the integration of diverse methodologies due to the rising incidence of diabetes and its complications worldwide. DFU biomarkers may aid in the improvement of early detection, avoidance of the disease, estimation of illness progression, and even treatment monitoring of DFU. So, we aimed to evaluate the role of some biomarkers in the early diagnosis of DFU in patients in the Gaza Strip. To the best of our knowledge, this is the first study to be done in the Gaza Strip to assess the association between IL-18, PTX-3, and DFU.

The most accurate measure of glycemic management is HbA1c. It is a crucial measure used to track blood glucose levels in people with diabetes (Diabetes Control Complications Trial Research Group, 1993). In this study, we found that both diabetic patients with and without FUs had higher HbA1c and FBG compared to the controls. These results are in agreement with what was found by (Kaleli *et al.*, 2019) in which they showed a higher level of HbA1c in T2DM patients and diabetic foot syndrome patients.

According to several reports, T2DM patients with DFU experience an increase in the frequency of cardiovascular disorders by 2-4 times (Tuttolomondo *et al.*, 2015). There is an association between inflammation and DM, as evidenced by the disparity in biochemical parameters such as LDL, triglycerides, and total cholesterol levels between normal and T2DM patients. Because of that, we decided to compare the lipid biomarkers between the study groups. We found that cholesterol and LDL values were significantly lower in diabetics with FUs group compared to the corresponding values for both diabetics without FUs and normal groups. These findings were not consistent with the study done by (Mushtaq *et al.*, 2020). Their study found that cholesterol, LDL, and triglyceride levels are significantly higher in DFU patients than in patients without DFU. These differences may be due to the limited number of participants in our work.

Furthermore, a significant increase in creatinine and urea levels was found in the DFU group when compared to the other groups. The same findings were discovered in a study conducted by (Al-karawi *et al.*, 2019). In another study, creatinine was also found to be higher in DFU patients compared to patients without FUs ($P < 0.0001$) (Aziz, 2020).

IL-18 is a pro-inflammatory cytokine that is released by dendritic cells, macrophages, and epithelial cells (Okamura *et al.*, 1995). IL-18 levels in T2DM patients were originally shown to be considerably higher than in those without diabetes (Esposito *et al.*, 2003). Moreover, increased IL-18 levels are considered a reliable indicator of T2DM and metabolic syndrome (Fischer *et al.*, 2005). IL-18 has also been demonstrated to impair insulin secretion and cause β-cell dysfunction in animal-based scientific investigations (Frigerio *et al.*, 2002). In addition, it causes endothelial cell dysfunction and plays a role in atherosclerosis (Gerdes *et al.*, 2002). In our study, we found that IL-18 was higher in the T2DM patients with FUs compared to the T2DM patients without ulcers and the healthy controls. To add to this, IL-18 was an excellent predictor of ulcer severity. Our results are consistent with (Sabuncu *et al.*, 2014) findings. Also, their study showed that IL-18 was positively correlated with high sensitivity-C reactive protein (CRP) and ESR which were the most well-known acute phase reactants. In contrast, (Weigelt *et al.*,

2009) reported that the levels of IL-18 in the serum of T2DM patients with acute FUs did not change when compared with those without DFU. When compared with the DFU group, the control group in the study by Weigelt et al. was significantly younger and had a higher HbA1c level; these variations could have affected their outcomes. Age-wise, our study's groups were closer.

We also found that IL-18 levels were elevated with increasing diabetes duration in both diabetics with and without FUs and in diabetics with severe FUs. This was in contrast with what was reported by (Aso *et al.*, 2003) where they found no significant association between IL-8 concentration and diabetes duration.

Both PTX-3 and CRP are acute-phase reactants that include five identical components collectively known as the pentraxin family. They are physically and functionally comparable molecules (Inforzato *et al.*, 2013). PTX-3 is an essential part of the innate immune system that removes dead or dying cells (Mantovani *et al.*, 2013). As it can be identified fairly early in the course of the disease, PTX-3 has been linked to the extent of several inflammatory conditions. It has been noted that bacterial and viral infections result in a considerable rise in PTX-3 levels (Muller *et al.*, 2001). Additionally, studies have demonstrated its value as a prognostic indicator in a variety of conditions, including community-acquired pneumonia (Kao *et al.*, 2013), inflammatory disorders, cardiovascular issues, and renal illnesses (Üstündağ *et al.*, 2011, Argani *et al.*, 2012). In addition, (Takashi *et al.*, 2018) reported that PTX-3 was positively linked with both the existence of diabetes and glycosylated hemoglobin.

In our study, we found that PTX-3 was very efficient in recognizing T2DM patients with FUs. Our results were compatible with what was reported by (Ozer Balin *et al.*, 2019), in which PTX-3 is an accurate indicator for the diagnosis of infectious DFU (IDFU). The subgroup analysis of IDFU in their study showed significant differences in terms of PTX-3 between mild, moderate, and severe disease subgroups.

5. Conclusion

The study of biomarkers is progressing quickly in a variety of domains. For example, various physical indicators are useful and have been taken into consideration for the diagnosis, risk classification, or monitoring of DFU. In order not to overestimate the value of the newly developed systems, it is ideal to combine the new markers with the clinical data and compare the results with the most accurate standard tests currently available for DFU. This study is the first to recommend a diagnostic application for blood IL-18 and PTX-3 levels in DFU patients in the Gaza Strip. The results show that PTX-3 is a good biomarker for the prediction of DFU, while IL-18 is a good biomarker for the prediction of the severity.

6. Limitations

However, our study has some limitations: first is the small sample size. Second, the study is cross-sectional, so it is difficult to explore the relationship between cause and effect in the correlation between systemic inflammation and FU. To further understand how inflammation affects the onset of foot ulcerations and their predictive value, longitudinal studies are required. Third, our results are valid for T2DM patients only because T1DM patients were excluded. The study of biomarkers in DFU is still in processing, and continuous attempts in this field will assist in increasing the knowledge of DFU diagnosis, prevention, and treatment.

Acknowledgment

We would like to thank Maysaa' Adnan Al-Binni for her distinguishable efforts in the statistical analysis of the study.

Conflict of interest

The authors declared that there is no conflict of interest.

Funding

The work was self-funded.

References

Abu Seman N, Witasp A, Wan Mohamud WN, Anderstam B, Brismar K, Stenvinkel P and Gu HF. 2013. Evaluation of the association of plasma pentraxin 3 levels with type 2 diabetes and diabetic nephropathy in a Malay population. *J. Diabetes Res.*, **2013**: 1-7.

Al-karawi FN, Al-Hasnawi ATN and Al-Kashwan TAJ. 2019. Role of toll-like receptor gene polymorphisms in patients with type 2 diabetes and diabetic foot ulcer. *Indian J. Public Health*, **10**(6): 1255.

Argani H, Ghorbanihaghjo A, Panahi G, Rashtchizadeh N, Safa J and Meimand SM. 2012. Serum Fetuin-A and Pentraxin3 in hemodialysis and renal transplant patients. *Clin. Biochem.*, **45**(10-11): 775-779.

Aso Y, Okumura K-i, Takebayashi K, Wakabayashi S and Inukai T. 2003. Relationships of plasma interleukin-18 concentrations to hyperhomocysteinemia and carotid intimal-media wall thickness in patients with type 2 diabetes. *Diabetes Care*, **26**(9): 2622-2627.

Atkinson AJ, Colburn WA, DeGruttola VG, DeMets DL, Downing GJ, Hoth DF, Oates JA, Peck CC and Schooley RT. 2001. Biomarkers and surrogate endpoints: preferred definitions and conceptual framework. *J Clin Pharm Ther*. **69**(3): 89-95.

Aziz KMA. 2020. Risk Factors for Developing Diabetic Foot Ulcer with Nephropathy, Diabetic Kidney Disease and Renal Failure Statistical Analysis of 10,680 Patients' Cohort. *medRxiv*: 2020.2006. 2011.20128488.

Brownrigg J, Apelqvist J, Bakker K, Schaper N and Hinchliffe R. 2013. Evidence-based management of PAD & the diabetic foot. *Eur. J. Vasc. Endovasc. Surg.*, **45**(6): 673-681.

Cavanagh PR, Lipsky BA, Bradbury AW and Botek G. 2005. Treatment for diabetic foot ulcers. *The Lancet*, **366**(9498): 1725-1735.

Chen T, Yu J, Wang J, Chang Q, and Qian C. 2020. Elevated Serum Levels of Lp-PLA2 and IL-18 are Associated with Progression of Diabetic Foot Ulcers. *Clin. Lab.*, **66**(10).

Chuan F, Tang K, Jiang P, Zhou B and He X. 2015. Reliability and validity of the perfusion, extent, depth, infection, and sensation (PEDIS) classification system and score in patients with diabetic foot ulcer. *PLoS ONE*, **10**(4): e0124739.

Diabetes Control Complications Trial Research Group. 1993. The effect of intensive treatment of diabetes on the development and progression of long-term complications in insulin-dependent diabetes mellitus. *N. Engl. J. Med.*, **329**(14): 977-986.

Esposito K, Nappo F, Giugliano F and Di Palo C. 2003. Cytokine milieu tends toward inflammation in type 2 diabetes. *Diabetes Care*, **26**(5): 1647.

Fischer CP, Perstrup LB, Berntsen A, Eskildsen P and Pedersen BK. 2005. Elevated plasma interleukin-18 is a marker of insulin resistance in type 2 di abetic and non-diabetic humans. *Clin. Immunol.*, **117**(2): 152-160.

Frigerio S, Holländer GA and Zumsteg U. 2002. Functional IL-18 is produced by primary pancreatic mouse islets and NIT-1 beta cells and participates in the progression toward destructive insulitis. *Horm Res Paediatr*, **57**(3-4): 94-104.

Gerdes N, Sukhova GK, Libby P, Reynolds RS, Young JL and Schönbeck U. 2002. E xpression of interleukin (IL)-18 and functional IL-18 receptor on human vascular endothelial cells, smooth muscle cells, and macrophages: implications for atherogenesis. *J. Exp. Med.,* **195**(2): 245-257.

Inforzato A, Reading PC, Barbati E, Bottazzi B, Garlanda C and Mantovani A. 2013. The “sweet” side of a long pentraxin: how glycosylation affects PTX3 functions in innate immunity and inflammation. *Front. immunol.*, **3**: 407.

Kaleli S, Varım C, Nalbant A and Akdoğan M. 2019. Interleukins as a marker of inflammation in diabetic foot syndrome and type 2 diabetes mellitus. *Bezmialem sci.,* **7**(1): 1-7.

Kao S-J, Yang H-W, Tsao S-M, Cheng C-W, Bien M-Y, Yu M-C, Bai K-J, Yang S-F and Chien M-H. 2013. Plasma long pentraxin 3 (PTX3) concentration is a n ovel marker of disease activity in patients with community-acquired pneumonia. *Clin. Chem. Lab. Med. CLIN CHEM LAB MED*, **51**(4): 907-913.

Mantovani A, Valentino S, Gentile S, Inforzato A, Bottazzi B and Garlanda C. 2013. T he long pentraxin PTX3: a p aradigm for humoral pattern recognition molecules. *Ann. N. Y. Acad. Sci.*, **1285**(1): 1-14.

Muller B, Peri G, Doni A, Torri V, Landmann R, Bottazzi B and Mantovani A. 2001. C irculating levels of the long pentraxin PTX3 correlate with the severity of infection in critically ill patients. *Crit. Care Med.*, **29**(7): 1404-1407.

Mushtaq S, Khan S, and Rashid MR. 2020. Study of Glycated Haemoglobin and lipid profile in patients with diabetic foot ulcer. *Int. j. contemp. med.*, **7**(6): F1-F4.

Navarro-Gonzalez JF and Mora-Fernandez C. 2008. The role of inflammatory cytokines in diabetic nephropathy. *J. Am. Soc. Nephrol.*, **19**(3): 433-442.

Ogurtsova K, da Rocha Fernandes J, Huang Y, Linnenkamp U, Guariguata L, Cho NH, Cavan D, Shaw J and Makaroff L. 2017. IDF Diabetes Atlas: Global estimates for the prevalence of diabetes for 2015 and 2040. *Diabetes Res. Clin. Pract.*, **128**: 40-50.

Okamura H, Tsutsui H, Komatsu T, Yutsudo M, Hakura A, Tanimoto T, Torigoe K, Okura T, Nukada Y and Hattori K. 1995. Cloning of a n ew cytokine that induces IFN-γ production by T cells. *Nature*, **378**(6552): 88-91.

Ozer Balin S, Sagmak Tartar A, Uğur K, Kilinç F, Telo S, Bal A, Balin M and Akbulut A. 2019. P entraxin-3: a new parameter in predicting the severity of diabetic foot infection? *Int. Wound J.*, **16**(3): 659-664.

R Core Team R. 2013. R : A language and environment for statistical computing.

Sabuncu T, Eren MA, Tabur S, Dag OF and Boduroglu O. 2014. High serum concentration of interleukin-18 in diabetic patients with foot ulcers. *J. Am. Podiatr. Med. Assoc.*, **104**(3): 222-226.

Saltoglu N, Kilicoglu O, Baktiroglu S, Osar-Siva Z, Aktas S, Altindas M, Arslan C, Aslan T, Celik S an d Engin A. 2015. Diagnosis, treatment, and prevention of diabetic foot wounds and infections: Turkish consensus report. *Klimik Journal*, **28**(1).

Takashi Y, Koga M, Matsuzawa Y, Saito J, Omura M and Nishikawa T. 2018. C irculating pentraxin 3 is positively associated with chronic hyperglycemia but negatively associated with plasma aldosterone concentration. *PLoS ONE*, **13**(5): e0196526.

Tuttolomondo A, Maida C and Pinto A. 2015. Diab etic foot syndrome: Immune-inflammatory features as possible cardiovascular markers in diabetes. *World J. Orthop*, **6**(1): 62.

Üstündağ M, Orak M, Güloğlu C, Sayhan MB, Alyan Ö and Kale E. 2011. C omparative diagnostic accuracy of serum levels of neutrophil-activating peptide-2 and pentraxin-3 versus troponin-I in acute coronary syndrome. *Anatol. J. Cardiol* **11**(7).

Weerasuriya N, Siribaddana S, Dissanayake A, Subasinghe Z, Wariyapola D and Fernando D. 1998. L ong-term complications in newly diagnosed Sri Lankan patients with type 2 diabetes mellitus. *QJM: Int. J. Med.*, **91**(6): 439-443.

Weigelt C, Rose B, Poschen U, Ziegler D, Friese G, Kempf K, Koenig W, Martin S an d Herder C. 2009. Immune mediators in patients with acute diabetic foot syndrome. *Diabetes Care*, **32**(8): 1491-1496.

Yasuda K, Nakanishi K and Tsutsui H. 2019. Interleukin-18 in health and disease. *Int. J. Mol. Sci.*, **20**(3): 649.

Zhang P, Lu J, Jing Y, Tang S, Zhu D, and Bi Y. 2017. Global epidemiology of diabetic foot ulceration: a systematic review and meta-analysis. *Ann. Med.*, **49**(2): 106-116.

Subscription

Jordan Journal of Biological Sciences

An International Peer – Reviewed Research Journal

Published by the Deanship of Scientific Research, The Hashemite University, Zarqa, Jordan

Name: ..... الاسم:

Specialty: ..... التخصص:

Address: ..... العنوان:

P.O. Box: ..... صندوق البريد:

City &Postal Code:..... المدينة: الرمز البريدي:

Country: ..... الدولة:

Phone: ..... رقم الهاتف

Fax No.: ..... رقم الفاكس:

E-mail: ..... البريد الإلكتروني:

Method of payment: ..... طريقة الدفع:

Amount Enclosed: ..... المبلغ المرفق:

Signature: ..... التوقيع:

Cheque should be paid to Deanship of Research and Graduate Studies – The Hashemite University.

I would like to subscribe to the Journal

For

- ☐ One year
- ☐ Two years
- ☐ Three years

One Year Subscription Rates

	Inside Jordan	Outside Jordan
Individuals	JD10	$70
Students	JD5	$35
Institutions	JD 20	$90

Correspondence

Subscriptions and sales:

The Hashemite University
P.O. Box 330127-Zarqa 13115 – Jordan
Telephone: 00 962 5 3903333
Fax no. : 0096253903349
E. mail: jjbs@hu.edu.jo

المجلة الأردنية للعلوم الحياتية
Jordan Journal of Biological Sciences (JJBS)

http://jjbs.hu.edu.jo

المجلة الأردنية للعلوم الحياتية: مجلة علمية عالمية محكمة ومفهرسة ومصنفة، تصدرعن الجامعة الهاشمية وبدعم من صندوق دعم البحث العلمي والإبتكار – وزراة التعليم العالي والبحث العلمي.

هيئة التحرير

رئيس التحرير

الأستاذ الدكتور محمد علي وديان
الجامعة الهاشمية، الزرقاء، الأردن

مساعد رئيس التحرير

الأستاذ الدكتور مهند عليان مساعدة
الجامعة الهاشمية، الزرقاء، الأردن

الأعضاء:

الأستاذ الدكتور خالد محمد خليفات
جامعة مؤتة

الأستاذ الدكتور ليث ناصر العيطان
جامعة العلوم و التكنولوجيا الأردنية

الأستاذة الدكتورة طارق حسن النجار
الجامعة الأردنية / العقبة

الأستاذ الدكتور وسام محمد هادي الخطيب
الجامعة اليرموك

الاستاذ الدكتور عبد اللطيف علي الغزاوي
الجامعة الهاشمية

الاستاذ الدكتور نضال احمد عودات
جامعة البلقاء التطبيقية

فريق الدعم:

المحرر اللغوي

الأستاذ الدكتور شادي نعامنة

تنفيذ وإخراج

م. مهند عقده

ترسل البحوث الى العنوان التالي:

رئيس تحرير المجلة الأردنية للعلوم الحياتية
الجامعة الهاشمية
ص.ب , 330127 , الزرقاء, 13115 , الأردن
هاتف: 0096253903333
E-mail: jjbs@hu.edu.jo, Website: www.jjbs.hu.edu.jo

المملكة الأردنية الهاشمية

المجلة الأردنية

للعلوم الحياتية

مجلة علمية عالمية محكمة

تصدر بدعم من صندوق دعم البحث العلمي و الابتكار

http://jjbs.hu.edu.jo/